LBL-26443

Lawrence Berkeley Laboratory
UNIVERSITY OF CALIFORNIA

Materials & Chemical Sciences Division

Excess Noise in the dc SQUID; 4.2 K to 20 mK

F.C. Wellstood
(Ph.D. Thesis)

October 1988

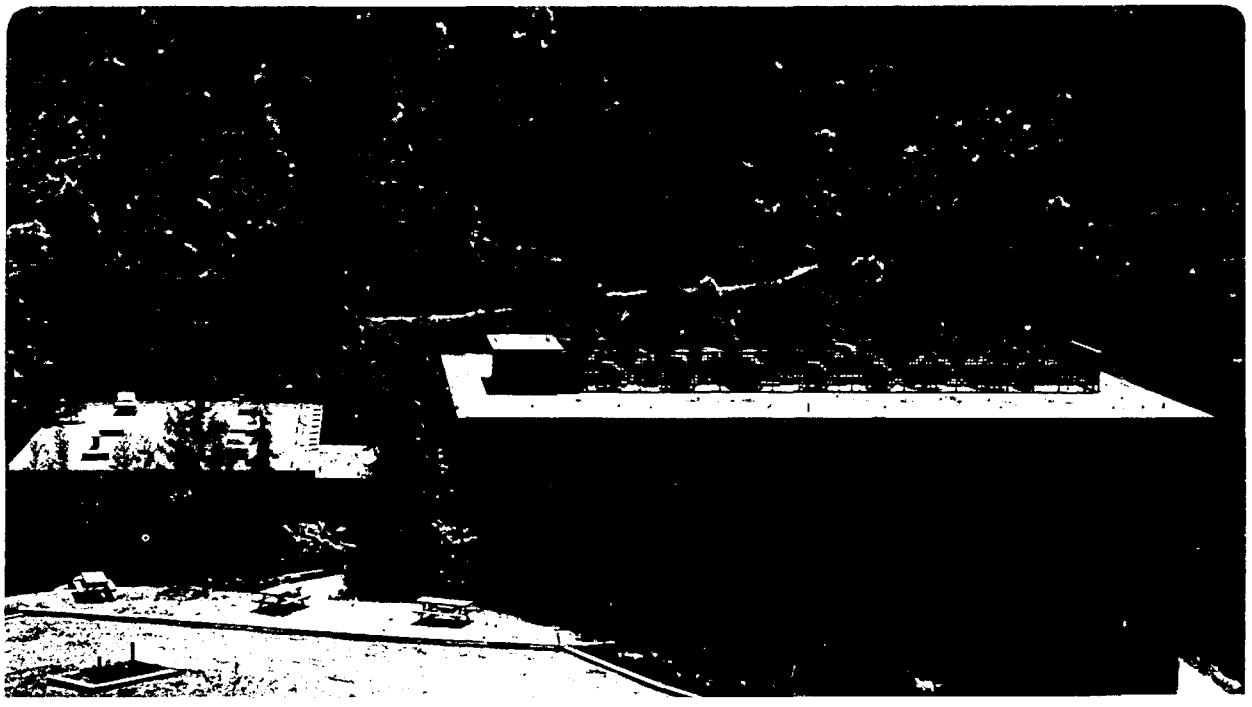

Prepared for the U.S. Department of Energy under Contract Number DE-AC03-76SF00098.

DISCLAIMER

LBL-26443

Excess Noise in the dc SQUID; 4.2 K to 20 mK

Frederick Charles Wellstood
(Ph.D. Thesis)
Materials and Chemical Sciences Division
Lawrence Berkeley Laboratory
1 Cyclotron Road
Berkeley, California 94720
USA

October 1988

Excess Noise in the dc SQUID; 4.2K to 20mK

Frederick Charles Wellstood

Excess Noise in the dc SQUID: 4.2K to 20 mK.

Frederick Charles Wellstood

Abstract

The design, construction, operation, and behavior of low noise dc SQUID measuring systems are described for temperatures from 0.020 K to 4.2 K. Evidence is presented for four different types of excess noise in dc SQUIDs operated in this temperature range. At temperatures between about 1 and 4 K, the spectral density of the low frequency flux noise of a wide variety of thin-film dc SQUIDs scales as $1/f^m$ where $m = 1.0 \pm 0.1$. The origin of this noise depends upon the construction of the SQUID. In SQUIDs with Pb or PbIn bodies the noise originates in critical current fluctuations. In SQUIDs with Nb bodies, the nature of the noise depends upon the detailed manner in which the Nb is deposited. One deposition technique produces a large level of "flux noise", while another produces only the usual level of critical current noise. When a SQUID is cooled below about 1 K, the behavior of the excess noise changes. In most of our devices, the spectral density of the excess flux noise scales as $1/f^m$, with $m = 0.66 \pm 0.1$, and the noise always originates as an apparent flux noise. The level of this excess noise depends upon the size and shape of the SQUID, but the underlying cause of the noise is not known. Devices with one unusual shape display $1/f^1$ noise at low temperatures. At the lowest temperatures, the white noise in these devices originally saturated at an effective temperature of about 150 mK. I have identified the cause of this saturation as a hot

electron effect in the resistive shunts of the SQUID, and present a theory of the effect, independent tests on thin metal films, and results on redesigned SQUIDs which minimize this source of excess noise.

Theoretical calculations are presented for the use of SQUIDs in high senstivity applications. The emphasis is on the optimal detection of pulse signals by a dc SQUID, taking into account the effect of the input circuit on the SQUID behavior, and making use of optimal filter theory.

Acknowledgements

It is important to recognize that research is a social activity. The speed with which a project is completed, or whether it is completed at all, is strongly influenced by many people in the lab who are not officially working on the project. Questions, constructive criticism, assistance, bright ideas, advice, complaints, and support are all extremely helpful, although generally greatly underappreciated. Oddly enough, I also find it very useful to think about what other people are working on in completely different areas. Most of the time, I merely come away with a better understanding of some new physics. However, I occasionally find the solution to one of my own problems or a new application for the SQUID. I think that these remarkable concurrences in apparently disparate areas are as much a result of the uderlying unity in physics as of the workings of the subconcious.

First of all, I would like to thank my adviser, Professor John Clarke, for taking me on, for allowing me to work on so many interesting things, and for providing a stimulating and exciting research environment. I would like to thank Wolf Goubau for his patience in explaining SQUID matching and the feedback electronics to a young and clueless student. I would like to thank Dan Seligson for some early, useful advice. I would like to thank Claude Hilbert for his extraordinary patience in teaching me how to make SQUIDs. I can scarcely even begin to acknowledge my debt to Cristian Urbina for his kindness, collaboration, advice, assistance, patience, and just plain hard work. Must of this thesis would have been impossible were it not for his considerable expertise, in particular, with the operation of the

dilution refrigerator. Throughout this thesis, one will frequently find me writing "we", this should almost always be taken as a shorthand version of Cristian and I. I would also like to thank Cristian for arranging a stay at Centre D'Etudes Nucleaires de Saclay (CEN), which gave me a much needed chance to work on a paper about the behavior of SQUIDs at low temperatures, and to reflect on the experimental work. I would like to thank Bonaventura Savo for his hard work and dedication in designing and operating the all Nb deposition system, without which Chapter 6 would have been impossible. I would also like to gratefully acknowledge the many helpful discussions on the construction of the SQUID cell which I had with Cristian's colleague, Michel Devoret. It should also be noted that John Martinis, Michel, Cristian, and Daniel Esteve, also from CEN, put together the dilution refrigerator system and screen room without which my own low temperature experiment would have been impossible. I would also like to acknowledge enjoyable collaborations with Bu Xin Xu and Jorn Hansen. I also thank Mark Ferrari and John Schmidt for their great care and skill in constructing a new gas handling system for the dilution refrigerator. I would especially like to thank Risto Mutikainen and Michael Cromar for providing us with dc SQUIDs from their laboratories.

I would like to thank Rita Jones for much helpful advice, and for turning many confused and illegible manuscripts into finely polished works. From the Physics Department Machine shop, I would like to thank Frank Lopez for so carefully constructing the SQUID cell, Tom Pederson for very quickly turning out a Cu replacement can that allowed us to cool to 20 mK, and Andy Brocato for many excellent stainless steel welds in both the cell and a new refrigerator vacuum can. From the Microlab, I

would like to thank Don Rodgers for his benevolent management of the microlab and for much helpful advice, and Bob Hamilton for his wide ranging knowledge and ablities. From the Physics Department Electronics shop I would especially like to thank Lavern Garner for skillfully building the many SQUID electronics boxes. I would also like to thank Ken Grove for his beneficent management of the shop, and for much helpful advice. I am grateful to the staff of the Microlab, in particular Kim Chan and Marilyn Kushner for making the SQUID masks, and Katilin Voros for providing sapphire substrates. In the Electrical Engineering and Computer Science Department, I would like to thank Professor T. Van Duzer's research group for much early assistance in the CAD mask making, in particular Paul Bradley, Herb Ko, and Greg Lee.

Enough cannot be said for the good physical insight of the Stanford Gravity Wave Group. They grasp the essence of high sensitvity measurements with the dc SQUID and have consistently steered us in the right direction, often against our seemingly better judgement. Our own program was based on trying to develop a quantum limited SQUID which they could use. This tactical choice turned out to be very fortunate for us, and I thank them and wish them good fortune in their search.

I thank David Abraham most of all for making the second basement a fun place to work, and for his patience and frienship, which I greatly missed after he left for Yorktown. I would like to thank the usual group of suspects: Andy Hasenfeld, Glen Stark, and John "Johny" Canelake for their friendship and for many cold, wet, and thoroughly enjoyable camping and sailing expeditions. I would like to thank Professor Y. Lecoz for a most unexpected and welcome visit, for several long discussions on physics and trying to have a good life while doing

science, and for writing a thesis which was almost as long as my own. I thank Andrew Cleland for sharing a lot of the hardship of operating, repairing, and maintaining the dilution refrigerator, and for many interesting discussions on small junctions. I thank H. "John" Mamin for his calm and steady approach, and his considerable knowledge of non-equilibrium superconductivity. I thank Mike Heaney for a critical reading of an early version of Chapter 12, and for many probing questions about SQUIDs and physics. I thank Nong-Qiang "Non" Fan for many heated arguments about physics and a thoroughly enjoyable driving expedition to New Orleans. I thank Tycho Sleator for various and sundry discussions about spins, SQUIDs, and just about everything else. I would also like to acknowledge his independent, earlier, and unpublished calculation of the equivalent input impedance of the SQUID, Z_{eq}, which I mention briefly in Chapter 12. I would like to thank Ning Wang for her friendship and for many useful discussions on solid state physics, electrons and phonons, and the way things are. I would like to thank Eric Ganz for many interesting discussions on physics, life and thesis writing. I would like to thank John Martinis for many useful discussions on SQUIDs, junctions, refrigerators, noise, and research. I would like to thank Johnathon Pelz for many informative discussions on $1/f^{\alpha}$ noise and thesis writing. I thank Seamus Davis for many interesting and useful discussions on refrigerators, superfluids, SQUIDs, and SQUIDs to be, and I thank Mark Johnson for many interesting discussions of spins, physics, and research.

I would like to acknowledge my debt to Zhang Xiaolei for making a summer of thesis writing the happiest of times. Finally, I would like to thank my mother, Mrs. Emily "Dr. Upton" Wellstood, for her long years of

support and confidence, and I dedicate this thesis to the loving memory of my father, Mr. Ronald Charles Wellstood.

This work was supported by the Director, Office of Energy Research, Office of Basic Energy Sciences, Materials Sciences Division of the U.S. Department of Energy under contract No. DE-AC03-76SF00098.

Excess Noise in the dc SQUID: 4.2 K to 20 mK

OUTLINE

Abstract

Acknowledgements

Outline

Chapter 0: Introduction

0.1 Development and Problems with the dc SQUID

0.2 A Useable Quantum Limited Linear Amplifier at Low Frequencies

0.3 SQUIDs at Low Temperatures: 1/f Noise Considerations

0.4 SQUIDs at Low Temperatures: Hot Electron Effects

0.5 The Detection of Gravitational Radiation

0.6 Optimization for the Detection of Pulses

0.7 Appendix A

Chapter 1: SQUID Fabrication and Design Types

1.1 Introduction

1.2 Fabrication Procedure

1.3 Junction Oxidation and Completion

1.4 The Different SQUID Types

Chapter 2 : Experimental Arrangements and Measurement Procedures

2.1 Introduction

2.2 The Refrigerator

2.3 The Cell

2.4 The Helium Fill Line

2.5 Thermometry

2.6 Cooling the Cell

2.7 Magnetic and RF Shielding

2.8 The SQUID Measuring Circuit: Construction

2.9 Circuit Operation

2.10 Data Taking

Chapter 3: The Feedback Electronics, and the Operation of an Integrated dc SQUID Magnetometer

3.1 Introduction

3.2 The SQUID and Input Circuit

3.3 The Feedback Electronics

3.4 Why Use a Two-pole Integrator?

3.5 Loop Stability Considerations

3.6 Maximum Slew Rate Considerations

3.7 Performance

3.8 Conclusions

Chapter 4: Estimation of the SQUID Parameters α, β, and L

4.1 Why is Accurate Parameter Estimation Important?

4.2 Techniques for Estimating L

4.3 Problems with the Modulation Depth Estimate of L

4.4 Calculation of the T=0, V=0 Modulation Depth Curves

4.5 Estimation of L and α

4.6 Some Measured SQUID Characteristics

4.7 Appendix A

Chapter 5: Parameter Fluctuations and Excess Noise

5.1 Introduction

5.2 Parameter Fluctuations as Sources of 1/f Noise

5.3 The Quasi-Static Solution

5.4 Parameters and the General Treatment

5.5 The Components of $\bar{\nabla}i$

5.6 The Flux Φ

5.7 The Voltage V

5.8 The Critical Currents I_{o1} and I_{o2}

5.9 The Shunt Resistances R_1 and R_2

5.10 The Parameters L_1, L_2, and M

5.11 The Parameters C_1 and C_2

Chapter 6: Critical Current Noise in Nb-Al_2O_3-Nb Junctions

6.1 Introduction

6.2 The Basic Picture: Trapped Charge

6.3 The All Nb Junctions: Preparation

6.4 Noise Measurements

6.5 Conclusions

Chapter 7: High Temperature Flux Noise and Critical Current Noise in SQUIDs

7.1 Introduction

7.2 The Magnetometer

7.3 The Pb and PbIn SQUIDs

7.4 Critique of Koch *et al.*

7.5 The New Nb SQUIDs

7.6 Conclusions

Chapter 8: Low Temperature Excess Noise in the dc SQUID

8.1 Introduction

8.2 Properties of the Low Temperature Excess Noise

8.3 Occurrence of Low Temperature Excess Noise in SQUIDs

8.4 Elimination of Likely Sources

8.5 Suggestions for Future Work

8.6 Concluding Remarks

Chapter 9: Hot Electron Effect in Normal Metals: Theory

9.1 Introduction

9.2 Simple Theory of Hot Electrons in Normal Metal: Assumptions

9.3 Calculation of Energy Loss Rate

9.4 Implications for SQUID Design

9.5 Spatial Effects and Diffusion Lengths

9.6 The Kapitza Resistance and Phonon Heating

9.7 Criticism of the Simple Heating Model

9.9 Appendices: A-E

Chapter 10: Hot Electrons in Normal Metal Thin Metal Films

10.1 Introduction

10.2 Experimental Technique

10.3 The Bias Resistor R_x

10.4 Data Analysis

10.5 The Small Resistor: Resistor 1

10.6 The Proximity Effect

10.7 Discussion of the Results: Resistor 1

10.8 The Large Resistor: Resistor 2

10.9 Discussion of Results: Resistor 2

10.10 Concluding Remarks

Chapter 11: Hot Electron Effects in the dc SQUID

11.1 Introduction

11.2 White Noise at Low Temperatures: SQUIDs with Small Shunts

11.3 White Noise in a SQUID with Large "Cooling Fins"

11.4 White Noise in a SQUID with Large Thick "Cooling Fins"

11.5 Conclusions

Chapter 12: SQUID Circuit Optimization for a Current Pulse

12.1 Introduction

12.2 Optimization of an LCR Circuit Connected to a Simple Amplifier

12.3 SQUID Circuit Optimization for Current Pulse

12.4 Input, Circuit and Noise Sources

12.5 The Input Signal

12.6 The Total Noise at the SQUID Output

12.7 The Total Noise Referred to the SQUID Input

12.8 The Best Signal-to-Noise Ratio

12.9 The Evaluation of ρ_0

12.10 The Evaluation of I_1

12.11 Optimization of Circuit Parameters for Different Sources

12.12 Figure of Merit for the SQUID

12.13 The Minimum Detectable Energy

12.14 The Minimum Detectable Energy: Optimization in the Limit $\alpha^2 << 1$

12.15 The Minimum Detectable Energy: Optimazation for Arbitrary α^2

12.16 The Minimum Detectable Energy: Optimization for Arbitrary α^2 with ω_o fixed

12.17 The Minimum Detectable Energy: How Large Should Q be: Q_{min}

12.18 The Minimum Detectable Energy: Optimization for Arbitrary α^2 with ω_o' fixed

12.19 The Minimum Detectable Energy: The Optimal Filter

12.20 The Minimum Detectable Current

12.21 The Minimum Detectable Voltage

12.22 Conclusions

12.23 Appendices A-H

CHAPTER 0: Introduction

0.1 Development and Problems with the dc SQUID

The first dc Superconducting QUantum Interference Device (SQUID) was built by R.C. Jacklevic, J. Lambe, J.E. Mercereau, and A.H. Silver in 1964.[1] This occurred shortly after B.D. Josephson's prediction of the Josephson effect[2] and its experimental verification by P.W. Anderson and J.M. Rowell.[3]

A dc SQUID consists of a superconducting loop which is broken by two Josephson junctions, see Fig. 0.1. Each junction can pass a maximum supercurrent of I_0 and is shunted by a resistor R. In normal operation, one measures the voltage V across the SQUID for fixed bias current I. When a magnetic field is applied to the SQUID, magnetic flux Φ is linked by the loop, and the voltage across the SQUID changes. The SQUID thus can be thought of as a magnetic flux to voltage transducer. The output of the SQUID is periodic in the applied flux, with periodicity given by $\Phi_0 = 2.07 \times 10^{-15}$ Tm^2. The SQUID can easily be used as an amplifier by connecting an input voltage in series with a resistance and a coil. The coil couples flux into the SQUID, producing an output voltage proportional to the input voltage for small signals. In general, the gain of such a system is rather small. A power gain of 400 might be typical for many of the SQUIDs discussed in this thesis. What makes the SQUID important is not this gain, but rather that the noise is very low, or equivalently, the SQUID's sensitivity is very high.

Early in the development of the dc SQUID, it was recognized that even very simple devices were capable of performing exquisitely senstive

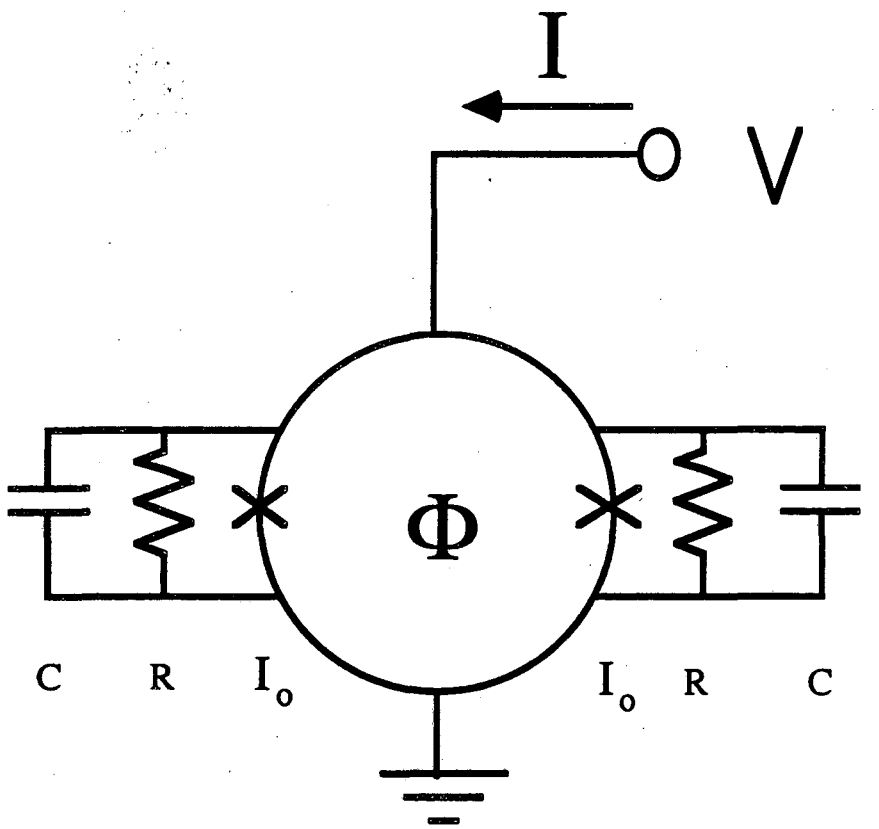

Fig. 0.1 Schematic of a dc SQUID with shunt resistance R, capacitance C, junction critical current I_o ,inductance L, and flux Φ in the loop. A current I is applied, producing a voltage V across the SQUID.

measurements.[4] For the last 20 years the SQUID has been in a constant state of improvement, which shows no signs of ending soon. The interested reader may find reviews of SQUID behavior in references (5-8), and in Appendix A of this chapter. Much progress has been made, and dc SQUIDs have been commercially available for many years now.[9]

In recent years, there have been extensive measurements of the noise of dc SQUIDs (Superconducting QUantum Interference Devices) in the liquid ^{4}He temperature range. The performance is commonly (although not completely) characterized in terms of the flux noise energy per unit bandwidth $\varepsilon_V(f) = S_\Phi(f)/ 2L$, where L is the inductance of the SQUID loop, f is the frequency and $S_\Phi(f)$ is the spectral density of the equivalent noise in the magnetic flux Φ threading the loop. In the frequency range in which the noise is white the SQUID is optimized [10] when $\beta \equiv 2LI_0/\Phi_0 \approx 1$ and $\beta_C \equiv 2\pi I_0 R^2 C/\Phi_0 \lesssim 1$, where C is the junction self-capacitance. When $\beta_C << 1$, $\beta \approx 1$, and the SQUID is in the classical thermal noise limit, computer simulations predict[10],[11]:

$$\varepsilon_V \approx (9\pm1)k_BTL/R \qquad (0.1)$$

where T is the temperature. These simulations did not actually include the effect of finite capacitance, and are therefore valid only for $\beta_C << 1$. However, one can make a qualitative prediction about the sensitivity of the SQUID for $\beta_C \approx 1$. From the conditions $\beta \approx 1$ and $\beta_C \approx 1$, one can show that $L/R = (\pi LC)^{1/2}$. Eq. (0.1) then becomes[10],[11]:

$$\varepsilon_V \approx 9\pi^{1/2}k_BT(LC)^{1/2} \approx 16k_BT(LC)^{1/2} \qquad (0.2)$$

Using an analog simulator, V. J. de Waal et al.[12] have analyzed the case of finite capacitance, and have found the best sensitivty is $\varepsilon_V \approx 12k_BT(LC)^{1/2}$ for $\beta_C \approx 1$, so that the result of Tesche and Clarke is only slightly modified by the inclusion of capacitance. Measurements on a

wide variety of thin-film SQUIDs in the ^{4}He temperature range have yielded noise energies in reasonable agreement with these predictions[8], and these simple relations have largely guided the development of ever more sensitive SQUIDs.

In light of this one might suppose that the field has matured, and relatively little interesting research remains to be done. My own opinion is that this is not at all the case, and that in fact the dc SQUID remains one of the most underutilized and poorly understood electronic devices. In my opinion, most research in Physics is directed along very well-defined lines, with a clearly limited subject area, a clear beginning, a straightforward approach, and an obvious ending. There is a lot to be said for such a state of affairs, for it is the epitome of the scientific method. In addition, ones life is not filled with uncertainties, and it is generally easier to sleep at night. Such was not the state of affairs for the research in this thesis. There was simply too little known about the SQUID, and the range of parameters we were investigating was so large, that we could never be certain of the outcome of an experiment until the experiment was complete. Many of the difficulties we found involve quite disparate subjects, but they all arose in connection with an investigation of the dc SQUID. That such divergent areas can be encountered is as much a testimony to the extreme sensitivity of the dc SQUID as it is to the large number of problems that still remain in the device. These problems may be grouped into four broad, and somewhat arbitrary, groups:

A: Problems of Use

cryogenic operation

shielding from external noise

matching to conventional electronics

achieving high frequency operation
achieving broadband operation
achieving high dynamic range

B: Parasitic and Coupling Effects

stray capacitance
input circuit resonances
junction capacitance
input circuit renormalization effects

C: Excess Noise

high temperature excess flux noise
critical current noise
low temperature excess noise
hot electron effects

D: Problems of Manufacture

irreproducibility of junction critical current I_0
stability and lifetime of junction critical current
electrical destruction of junctions and shunts

Despite the fact that the dc SQUID is by far the most sensitive low frequency amplifier ever built, these problems are sufficiently daunting that the SQUID remains a relatively obscure and little used device. The fact that these problems remain to this day, can largely be explained by the need to operate present day SQUIDs at cryogenic temperatures, whereas conventional semiconductor electronics operates at room temperature. It is unlikely however that the need for low temperatures is the only reason for the SQUID's slow rate of development. It should be recognized that semiconductor electronics is more than adequate for most applications. Furthermore, the inclusion of room temperature elements in a circuit may make the SQUID's contribution to the total noise completely negligible, and one would do just as well with a noisier amplifier. The discovery of $Y_1Ba_2Cu_3O_7$ type superconductors [13] may yet lead to useful devices which operate at 77 K and higher

(14), which would put the above ideas to the test. These remarkable discoveries will undoubtedly lead to much greater study of the dc SQUID. I hope that this work will thus achieve a much greater relevance and appreciation than I had previously expected.

Admittedly however, this thesis will deal only with the behavior of the dc SQUID at temperatures below 4.2 K; and much of the discussion will be on the behavior below 1 K. With much of the popular press focused on higher temperatures, it often seems strange to be working to achieve lower temperature operation. The reasons for these apparently contradictory research priorities should be borne clearly in mind. By working at higher temperatures, say room temperature ideally, one can dispense with expensive and bulky refrigeration equipment and cryogenic liquids. Thus, high temperature operation saves money. On the otherhand, the sensitivity of the dc SQUID is directly proportional to its temperature (this simple rule fails at high temperatures where the devce is normal and at very low temperatures where the sensitvity is limited by the Heisenberg uncertainty principle). Thus, low temperature operation yields higher sensitivity.

There are several factors which will ensure the continued vitality of cryogenic SQUID based measuring systems. First of all, there are very few cryogenic amplifiers. It is difficult to even operate semiconductor devices at low temperatures, let alone build anything as sensitive as the dc SQUID. Thus, if an experiment is to be cooled to cryogenic temperatures to begin with, it may well be easiest to use a SQUID, and one then gets the added benefit of a high sensitivity. This situation occurs most notably in the gravity wave experiments discussed in the next section. Secondly, the SQUID is extremely sensitive to magnetic

fields - a physical quantity which is not so easily measured by conventional electronics. Thirdly, although the SQUID has excess low frequency noise, or "1/f noise", so do conventional amplifiers, and the SQUIDs have generally shown much lower levels. In addition, the experimental situation strongly indicates that the 1/f noise is not intrinsic to the operation of the SQUID, and is a function of the processing or construction. Thus, we can expect future SQUIDs to be the most sensitive amplifiers for very low frequencies as well. Finally, it is interesting to note that the SQUID is essentially a current sensing element, whereas a Field Effect Transistor (FET), for example, is a voltage sensing device. Roughly speaking, the SQUID is best matched to a low impedance, while an FET is best matched to a high impedance. We can thus see that SQUIDs and semiconductor based devices tend to be complementary in several ways and that one should therefore expect continued applications for both.

0.2 A Useable Quantum Limited Linear Amplifier at Low Frequencies

The main reason for continued interest in the dc SQUID is that it excels at performing very low noise measurements. In most of the experiments in which a SQUID is currently being used, the SQUID acts as a linear, phase preserving amplifier. In the final analysis, such an amplifier cannot be made arbitrarily sensitive. Caves has shown that because of quantum-mechanics, such an amplifier can never exceed an energy sensitivity per unit bandwidth of $\hbar/2$.[15] This result is essentially a consequence of the Heisenberg amplitude-phase uncertainty relation, and is very general. The result can also be interpreted as

saying that such an amplifier will add at least $\hbar/2$ of noise. This extra noise can be thought of as arising from electrical zero point-motion in the resistive shunts of the SQUID. Thus at zero temperature, all of the ordinary thermal noise in the SQUID, as given by Eq. (0.1), will disappear, and one will be left with just the quantum zero point motion. Koch et al. [16] have analyzed numerically the case of quantum + thermal noise, and found agreement with the predictions of Caves.[15]

Unfortunately, as will be discussed in Chapters 4 and 12, the intrinsic energy sensitivity ε_v is not the true energy sensitivity of the SQUID [16,17] (this is similar to the case for a conventional amplifier, where the output noise arises from a voltage noise term, e_n, and a current noise term, i_n, and the specification of just e_n, for example, does not completely characterize the sensitivity of the amplifier). Rather one finds that a more complicated expression is involved, which I will denote simply as ε. In particular, ε_v does not in general approach $\hbar/2$, only ε does. This is unfortunate because ε_v is easy to measure whereas ε is quite difficult to measure. In fact ε has not yet been measured for a low noise dc SQUID, and following this rule, I will here only report measurements of ε_v.

For typical SQUIDs ε is expected to be of the order of ε_v, and thus one might hope to get a reliable estimate of ε by measuring ε_v and using simulations of the SQUID behavior to predict the ratio $\varepsilon/\varepsilon_v$. This is the technique I will pursue. The work of Tesche and Clarke [10,11] implies that in the classical thermal limit $\varepsilon \propto \varepsilon_v/2.83$, and thus ε_v underestimates the true energy sensitivity of the SQUID. In the classical thermal limit, we thus expect:

$$\varepsilon \propto 9k_BTL/(2.83R) = 3.19k_BTL/R \qquad (0.3)$$

for β=1 and $\beta_C << 1$, while for $\beta \approx 1$ and for $\beta_C \approx 1$:

$$\varepsilon \approx 4.94 k_B T (LC)^{1/2} \qquad (0.4)$$

Unfortunately, in the quantum limit, the relationship between ε and ε_v is not known in general. It is also not, in general, known how the relationship between ε and ε_v varies as one makes the transition from the classical to the quantum regime, so that one can only use the classical results as a rough guide. The calculations of Koch et al. [16] were done only for a few selected SQUID parameters, and they found that $\varepsilon/\varepsilon_v$ depended upon the SQUID parameters. Similarly, the calculations were done at only a few temperatures, which did not reveal the nature of the transition from the classical to the quantum regime. An alternative analytical calculation of ε and ε_v vs temperature has been provided by Danilov et al.[17], but it does not appear to be correct because of the neglect of noise rounding of the SQUID characteristics, and it is in disagreement with the predictions of Koch et al. in the low temperature limit.

The calculation of the ratio $\varepsilon/\varepsilon_v$ in the quantum regime is an important unsolved problem. From the experimental point of view, we will use the classical results of Tesche and Clarke[10,11] as a guide, and stop our extrapolation when ε approaches $\hbar$.

Virtually all attempts to produce a quantum limited SQUID have been based upon Eqs. (0.1) or (0.2). The original approach to low noise SQUID design was to decrease L and C as much as possible, while keeping $\beta \approx 1$ and $\beta_C \approx 1$ by appropriately adjusting R and I_o. Indeed this approach has produced SQUIDs which which were apparently dominated by quantum noise.[18-20] Unfortunately, these SQUIDs were virtually useless as amplifiers because the inductance had been made so small that it was

impossible to efficiently couple an input signal to them. The important point here is that a SQUID by itself is not an amplifier, one must attach some kind of input circuit, so Eq. 0.1 must be used with some caution in choosing which parameters to reduce and by how much.

The main goal of the work described in this thesis was to develop a useable quantum-limited SQUID, and this thesis mainly records the problems encountered therein. We had a very specific goal in mind - the device was to achieve the quantum limit at a frequency of 1 kHz and at a temperature of 20 mK with an inductance sufficiently large that it could be tightly coupled to a 1 μH input coil. These rather detailed specifications were tailored so that the device could be used in existing and soon to be built Weber bar type gravity wave detectors, as will be discussed below. However, such a device could be easily used in the laboratory as a general purpose quantum limited amplifier, and would be useful for a much wider class of problems.

Rather than attempting to reduce L and C, we reduced the final parameter, the temperature T. Our original technique consisted of taking a more or less standard dc SQUID and cooling it to 20 mK in a dilution refrigerator. Since the noise would be very small at this low temperature, we used a second dc SQUID to amplify the noise in the first. This bootstrap approach is described in detail in Chapter 2.

At first we simply did not realize how difficult such a project would be. The reason was that no one had published any results on dc SQUIDs operated below 1K. In fact, we are still the only group that has published such data. The temperature range below 1 K is new and totally unexplored territory for the dc SQUID. I remember that my main worries were: that the SQUID might not cool below 0.5 K, that structure on the

I-V would make the SQUID unuseable, that the shunts would go superconducting, and that the many electrical connections would not survive repeated thermal cyclings. We soon found that most of the original fears were groundless or easily circumvented. However, one large and unexpected problem soon became apparent.

0.3 SQUIDs at Low Temperatures : 1/f Noise Considerations

At low temperatures, the SQUIDs displayed large amounts of excess low frequency noise. In many amplifiers, at low frequencies, one commonly finds the noise per unit frequency bandwidth increasing as 1/f, see Fig. 0.2. Such noise is found in many different physical systems, and commonly goes under the name "1/f noise".[21-23] Experimental investigations of different systems have shown that there is no common physical mechanism behind all of this 1/f noise. Rather, 1/f noise can arise from many distinct processes, and the source must be sought out anew in each case. This makes the area very eclectic and difficult. The investigation of the low temperature excess noise revealed many peculiarities, even by 1/f noise standards. In particular, the 1/f noise was actually closer to $1/f^{2/3}$ in most of our devices, whereas slopes very close to unity are the rule in most systems. This noise was particularly bad for three reasons: as the temperature was lowered the excess noise actually increased, the power spectrum of the noise scaled like $1/f^{2/3}$ and persisted out to high frequencies where it rapidly came to dominate the total noise at low temperatures, and finally we soon found that the noise was flux-like and hence not removable by any modulation scheme. Because this noise was the dominant source in our

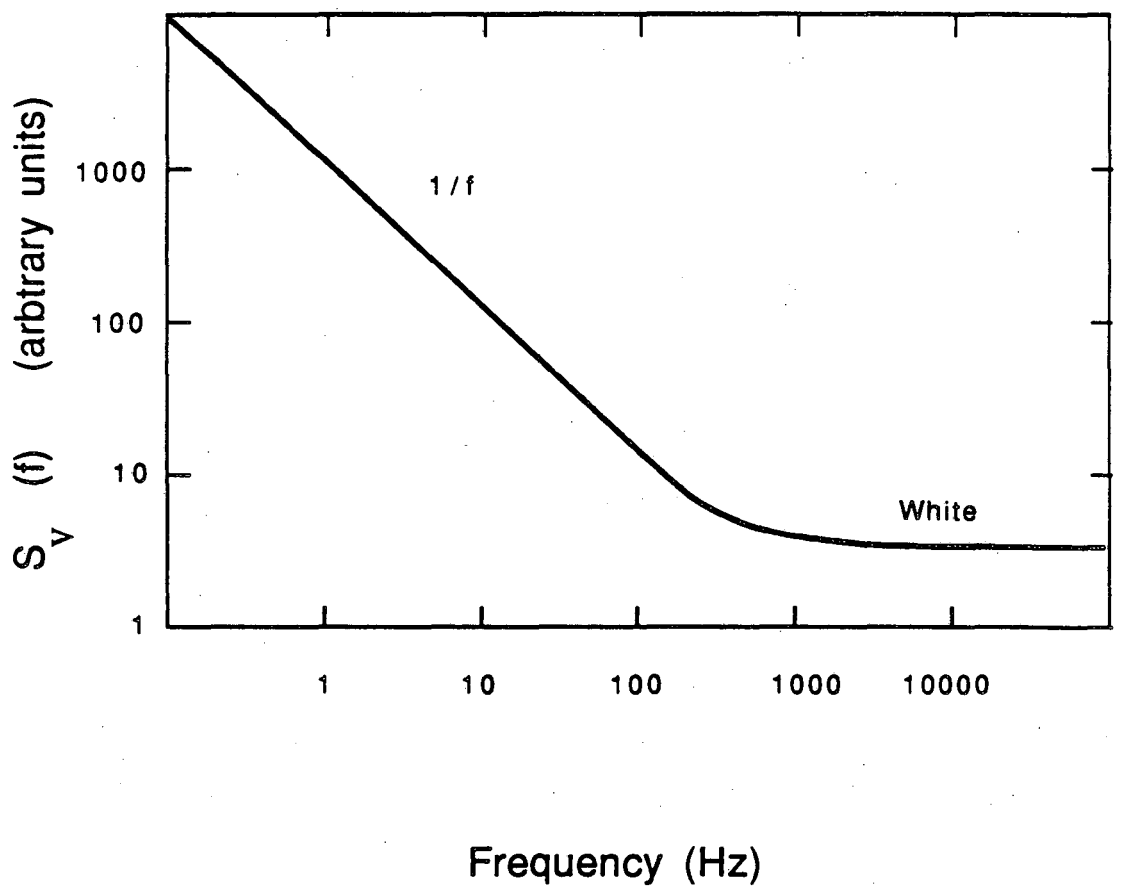

Fig. 0.2 Noise spectrum generated by the combination of a a 1/f noise source and a white noise source.

SQUIDs at low temperatures, a great deal of effort was expended in trying to understand its properties and its ultimate cause.

The experimental investigation followed Occam's razor: The simplest and most obvious causes were explored first. Unfortunately, there are a great many possible sources one can be suspicious of, and I can say conclusively that all of these attempts to locate the source have failed miserably (see Chapter 8). Nevertheless a great deal has been learned about the properties of the source, and in the meantime I have managed to eliminate a second source of 1/f noise which occurs at higher temperatures (see Chapter 7).

Although understanding of the low temperature excess noise has eluded me, I have been able to find devices which consistently show significantly lower excess noise at 1 kHz. These devices have an unusual shape, but there is no obvious reason for the slope of the noise to be different. With the present level of understanding of the low temperature excess noise and SQUID behavior at low temperature, I can summarize the requirements for successful low frequency and low temperature SQUID design:

(1) $\beta = 1$

(2) $\beta_c \ll 1$, and preferably $\beta_c < 0.25$

(3) "split SQUID" design with L large (see Chapter 8).

The first condition is well-known and true for most SQUID optimizations. The second condition reduces the effects of self resonant structure and is particularly important at low temperature, as is discussed in Chapter 4. The third requirement is entirely empirical and merely records the only way I presently know how to minimize the effect of the low temperature excess noise.

0.4 SQUIDs at Low Temperatures: Hot Electron Effects

A secondary problem with our early SQUID experiments was that the cell which held the SQUIDs was not cooling below about 100 mK. This was due to a poor thermal connection between the dilution refrigerator and the cell. This was eventually eliminated by changing the original stainless steel cell to a copper cell. After the cooling problem was fixed, the cell was able to run as low as 20 mK. At this lower temperature it soon became apparent that the SQUIDs inside were not cooling below about 140 mK. Now, a SQUID is operated in the resistive state, and its reistive shunts dissipate this power, so it is not surprising that the shunts might heat up. But the physical mechanism which determined the size of this heating turned out to be more subtle than expected.

After some thought, we realized that the electrons in the shunt were being driven out of thermal equilibrium with the phonons in the shunts. A simple theory for this "hot electron effect" is presented in Chapter 9. The basis for this calculation was a particularly clear paper by Gantmakher on the electron-phonon scattering rate.[24] These ideas were tested by performing heating measurements on thin metal film resitors, as is discussed in Chapter 10. With the effect confirmed, I then went back and redesigned the SQUID shunts in order to minimize the heating from the hot electron effect. The modification consisted of the addition of large volume "cooling fins" to the shunts, and allowed us to lower the SQUID shunt temperature to about 50 mK. This temperature is close to the quantum-classical crossover regime for the SQUIDs, and any

additional improvement in the device should push it firmly into the quantum regime.

0.5 The Detection of Gravitational Radiation

From the above discussion, one might conclude that my work was simply directed at building a high performance SQUID. Certainly, this was the task, but the motivation for pursuing this research came from quite a different direction. The detection of gravitational radiation remains one of the great unsolved experimental problems of this century.[25] The most sensitive scheme operating yet is the cryogenic Weber bar antenna [26] as used by research groups at Stanford[27], Rome[28], and elsewhere. In the Stanford system, a 5 ton bar of Al is suspended in a vacuum chamber and cooled to roughly 2 K, see (Fig. 0.3). The bar is cooled to reduce the random thermal vibration and thereby to improve the sensitivity. The bar is carefully isolated vibrationally from the outside world to prevent extraneous noise, and its motion is monitored with sensitive transducers. The idea is that a passing gravity wave will compress the bar and leave it ringing at its fundamental frequency. This vibration is converted into an electrical signal by a motion transducer. The signal is then amplified by a low noise amplifier, generally a dc SQUID, at which point it can be analyzed with conventional electronics.

Unfortunately, several factors conspire to make this scenario very difficult to achieve. Firstly, the interaction of a gravity wave with the bar is exceedingly weak and will decrease with the square of the distance of the source from the bar. Secondly, it is not possible to

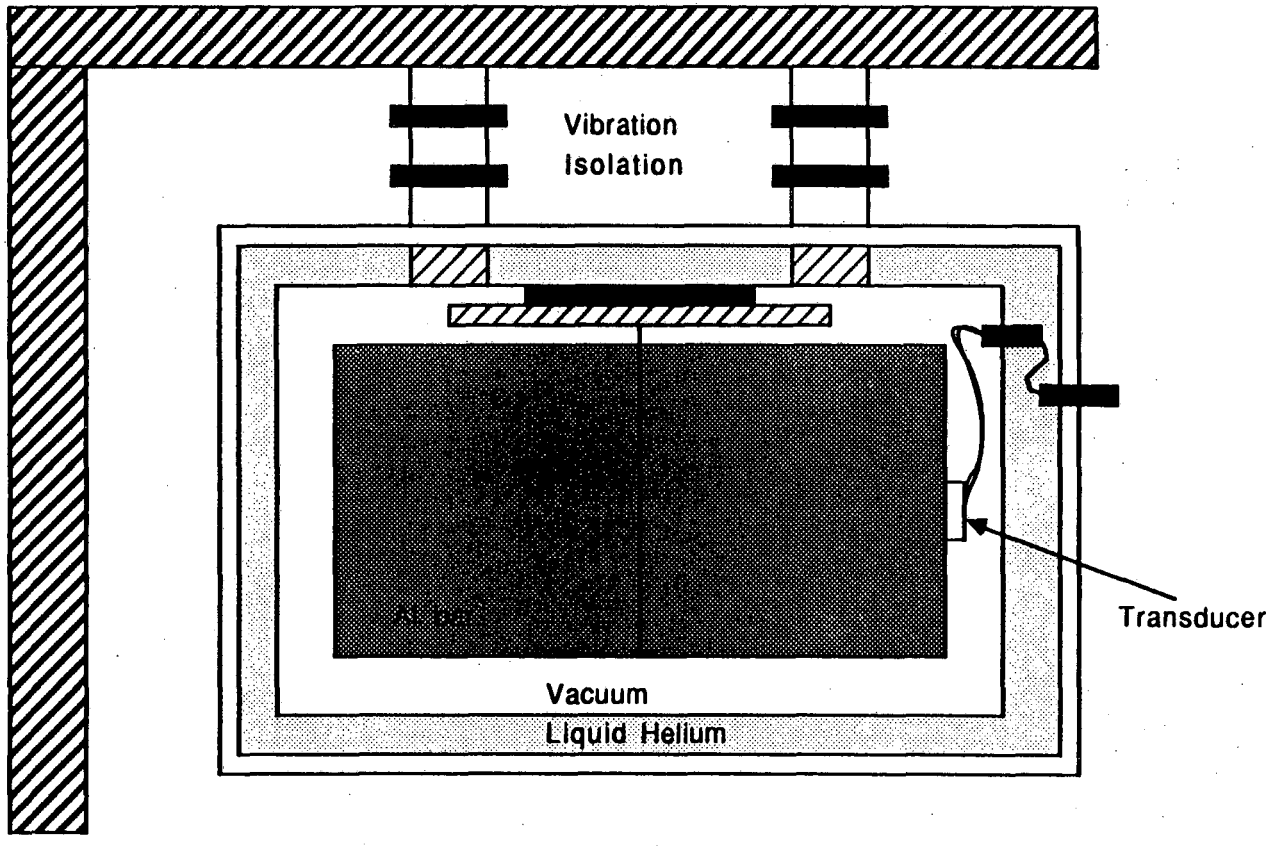

Fig. 0.3 Schematic of Weber bar type gravity wave antenna.

make a detectable laboratory source of gravity waves and there are very few large natural sources.[29] The most likely source is the core collapse of a massive star to a black hole, following a supernova explosion. Such an event could radiate a significant fraction of a stellar mass as gravitational radiation if the star has a large quadropole moment.[29] With the present detectors, such an event would have to occur within our own local group of galaxies, if not within the Milky Way, in order to be detected. It has been estimated that a supernova explosion occurs on the average every 200 to 300 years in our galaxy, although arguments for considerable higher rates have been advanced.[30] It is unlikely that most of these explosions would actually have a large quadropole moment. With such a time scale, at best, one can just hope to be very lucky. The goal of the next generation of Weber bars is to improve the sensitivity so that supernovas within the Virgo cluster can be detected. This large group contains about 2500 galaxies and is about 30 million lightyears distant. One might optimistically expect about one event a month, which is an entirely acceptable rate. Of course the great distance means that the signal will be very small.

The improvement in the bars' sensitivities since Weber's first bar has been phenomenal. The sensitivity can be described by the smallest strain that the bar can detect. The strain is defined as $\Delta\ell/\ell$, where ℓ is the length of the bar, and $\Delta\ell$ is the change in length arising from, for example, the effect of a gravity wave. Whereas Webers' room temperature antennas[26] could measure strains of a few times 10^{-16}, the cryogenic bar at Stanford[27] can presently measure to about 10^{-18}. For a bar length of ℓ = 1 meter, this means that the bar can detect a change

in its length of just 10^{-18} m, or about one thousandths of the diameter of a proton. The next generation of bars is aimed at producing a sensitivity of 10^{-20}. This work is directed at four seperate areas: Cooling the bar to 20 mK, improving the vibration isolation, improving the transducer, and obtaining a quantum limited SQUID sensor. The sensitivity of the system is directly affected by the performance of the SQUID, and this is the main concern of this thesis.

0.6 Optimization for the Detection of Pulses

While the experimental investigation of the SQUID noise was proceeding I had also been trying to understand what kind of SQUID would be needed for use in a gravity wave detector. In particular, I wanted to know what kind of input coil inductance and coupling coefficient α^2 were required, where $M^2 = \alpha^2 L_i L$, L is the SQUID inductance, L_i is the input coil inductance, and M is the mutual inductance between the SQUID and the input coil. This knowledge was of fundamental importance because we did not want to waste our effort on devices which would not work in the detectors. Of course, the requirements had already been worked out at some level by several groups, and the original SQUID specifications noted above were given to us by the Stanford Gravity Wave Group. According to our existing models of SQUID optimization, however, these specifications did not make much sense. In particular, they required a tight coupling between the SQUID and the input coil, i.e. $\alpha^2 \rightarrow 1$. The chief result of our optimization was embodied in the "golden rule" $Q\alpha^2 = 1$; that is, the best performance was attained when the input circuit Q and coupling coefficient α were chosen such that $Q\alpha^2 = 1$ [31-32]. Now

cryogenic Weber bars have $Q = 10^6$ so that $\alpha^2 = 10^{-6}$ should have been optimum, and hence the requirement of strong coupling did not appear to be correct.

It was not clear what was wrong. Our optimization models looked correct, but a closer examination showed that they were derived for somewhat specialized conditions which the bars did not satisfy. On the otherhand, the Stanford scheme for optimizing the gravity wave antenna initially appeared quite mysterious to me, and it was obvious only that it used completely different ideas of signal optimization.[33] In addition, they had failed to include correlation effects and the system was so complicated that the optimization had to be carried out with the aid of a computer. As if this were not confusing enough, recent theoretical refinements of the behavior of a SQUID when it is coupled to an input circuit cast considerable doubt on the validity of both optimization procedures. John Martinis and John Clarke had built on some original work of Claudia Tesche and Roger Koch to develop a consistent SQUID noise theory which would work for strong coupling. The strong coupling region, α^2 near 1, was precisely where the gravity wave detectors were to run according to the detector groups. It was clear that both of the earlier models were incorrect for this region.

The resolution of these difficulties took more than a year. I found a paper by P.F. Michelson and R.C. Taber[33] to be especially illuminating, and used it as the basis for a more general approach. In Chapter 12, I work out the optimimum conditions for a model tuned circuit. The big surprises were twofold. First of all, the gravity wave optimization results were essentially correct. The inclusion of correlation effects and the strong coupling theory produced only

qualitative changes in the optimization conditions. These changes lead to substantial improvements at higher α^2 and are interesting because they predict that it will be possible to attain quantum limited performance with a SQUID which would not be considered quantum limited in the conventional treatment. The biggest surprise was that the old $Q\alpha^2 = 1$ rule and much of the corresponding optimization theory were incorrect for the problem at hand.

The more general purpose of the optimization calculations is to learn how to use the enormous sensitivity of the SQUID. There is little point to building low noise SQUIDs if they cannot be used at the quoted sensitivity. Most measuring systems squander their low noise, for example, by poorly coupling a low Q input circuit to the SQUID, and by not using signal processing techniques to maximize the signal to noise ratio. In order to perform low frequency quantum limited measurements, the input circuit and optimal filtering will have to be very carefully executed.

The optimization theory presented in Chapter 12 may ultimately have great relevance to the use of "high Tc" SQUIDs at 77 K or higher temperatures. It is generally understood that by choosing the SQUID parameters appropriately, one can achieve good energy sensitivity even at 77 K. What has not received much attention is that for many common applications the noise from the SQUID will be negligible compared to the noise from the resistive 77 K portions of the input circuit. It therefore seems irrelevant that the "high Tc" SQUIDs possess good energy sensitivities. The results of Chapter 12 show that, in fact, this is not the case. That is to say, despite the high temperature of any source resistance in the input circuit and the large amount of Nyquist noise it

generates, for certain signals it is still possible to obtain the full energy sensitivity of the SQUID if one employs the proper optimization strategy.

One of the most exciting things about working with SQUIDs is that the most interesting things are yet to be done, and they are just now becoming possible. In the near future, one should expect to see low frequency quantum-limited amplifiers and measurements being made. In the longer term, it appears quite possible to perform so-called "quantum non-demolition" measurements.[15,34] In such a measuring system the amplifier and input circuit are designed to be sensitive to only one of the quantum mechanical variables describing the input circuit Hamiltonian. Such an arrangement allows one to decrease the quantum mechanical uncertainty in the measured variable at the expense of the uncertainty in the unmeasured conjugate variable. Such input circuits do not conform to the assumptions used in discussing the so-called "quantum-limit" to the SQUID sensitivity. In this sense the "quantum-limit" does not exist if the experimentalist is clever enough to measure only the proper variables.

0.7 Appendix A: Introduction to SQUIDs

It is the purpose of this appendix to provide the interested and unfamiliar reader with a brief introduction to the dc SQUID. More complete and detailed treatments can be found in Refs. (5-8).

Configuration of the SQUID

The dc SQUID is constructed from a loop of superconducting material which is broken in two places by superconducting tunnel junctions, see Fig. 0.1. For the SQUIDs discussed in this thesis, the superconductors are Nb, and Pb or PbIn. Each junction is in the form of a thin-film superconductor-insulator-superconductor sandwich. The insulating layer is very thin, typically 1 to 2 nm, and the junction area is typically 2 μm on a side. The purpose of the junctions is to electrically weakly couple together the two pieces of the superconducting loop. Ordinarily, a thin-film resistor is connected across each junction, and electrical leads are attached to each side of the loop. In normal operation, bias current is supplied to the SQUID through these leads, and the voltage across the SQUID is monitored. A SQUID which is to be used as an amplifier will also have a thin film coil deposited on top of the superconducting loop. This coil is used to inductively couple magnetic flux to the SQUID loop, and is the signal input for the SQUID.

It should be noted that there is a related superconducting electrical device which has only a single superconducting junction in its loop, this is the rf SQUID. Its method of operation, electrical behavior, and experimental development are all quite distinct from those

of the dc SQUID. All of the measurements which are reported in this thesis were made on dc SQUIDs, and I will not consider the rf SQUID any further (see Refs. 5-8 for a discussion of the rf SQUID).

Flux Quantization, ac Josephson Effect, and dc Josephson Effect

It is the superconducting properties of the loop and the tunnel junctions which determine the behavior of the dc SQUID. There are three superconducting effects which, together, produce the SQUID's sensitivity to magnetic field: flux quantization, the ac Josephson effect and the dc Josephson effect.

Superconductivity is a manifestation of quantum behavior on a macroscopic scale. The electrons in a superconductor have condensed into a state which is distinctly different from the state of the electrons in a normal metal. In particular, for a superconductor, there exists a complex order parameter $\psi = n^{1/2} e^{i\theta}$ which specifies the state of the system, where $n^{1/2}$ and θ are the magnitude and phase, respectively. When a magnetic field is applied, the order parameter undergoes a gauge transformation:

$$\psi \longrightarrow \psi \cdot \exp\left[\frac{2ei}{\hbar}\int \bar{A}.d\bar{s}\right] \qquad (0.5)$$

where $\bar{A}$ is the magnetic vector potential, and the line integral is taken on a path through the superconductor. Different paths may possess different amplitudes, and will constructively or destructively interfere with each other. The order parameter must be single-valued at every point in space in order to be well-defined. If one takes a path integral all the way around the SQUID loop, one finds that this requires

that:

$$\delta_2-\delta_1 + \frac{2e}{\hbar}\int\bar{A}\cdot d\bar{s} = 2n\pi \qquad (0.6a)$$

where δ_2 is the phase difference across one junction, and δ_1 is the phase difference across the other. If the superconductor is large compared to the London penetration depth, then the integral is simply equal to the magnetic flux passing through the SQUID loop, and one can write:

$$\delta_2 - \delta_1 = -2\pi\Phi/\Phi_0 + 2n\pi \qquad (0.6b)$$

where $\Phi_0 = 2e/h = 2.07X10^{-15}\ Tm^2$ is the flux quantum. If there were no tunnel junctions, but rather a continuous superconducting loop, one would have $\delta_2 = \delta_1 = 0$, and Eq. (0.6b) would become:

$$\Phi = n\Phi_0 \qquad (0.7)$$

That is, the flux in a superconducting loop is quantized in units of the flux quantum. Because of the presence of the Josephson junctions, the flux is not quantized in a dc SQUID, rather, the phase differences across the two junctions becomes related to the magnetic flux, as in Eq. (0.6b).

The phase difference across a tunnel junction has physical significance. Josephson [2] discovered that if two superconductors are coupled together by a tunnel junction, a current:

$$I = I_0\sin(\delta) \qquad (0.8)$$

will flow from one superconductor to the other, where δ is the superconducting phase difference between the two sides of the tunnel junction. Current will flow when there is no voltage difference between the superconductors, and this behavior is called the dc Josephson effect. I_0 is the critical current of the junction, and is the maximum

supercurrent that the junction can sustain. The magnitude of I_o is determined by the height, thickness, and area of the junction barrier, and by the superconducting properties of the electrodes (see Chapter 6).

When there is a dc voltage, V, across a superconducting tunnel junction, Josephson[2] found that an alternating current is generated. This current is generated at a frequency:

$$f = 2eV/h = V/\Phi_o \qquad (0.9a)$$

and the phase difference across the tunnel junction increases with time at a rate:

$$d\delta/dt = 2\pi f \qquad (0.9b)$$

These two simple relations describe the ac Josephson effect.

SQUID Behavior

From Eqs. (0.6), (0.8), and (0.9), and elementary circuit theory, one can construct a mathematical model for the behavior of the dc SQUID. The full system of equations is presented in Chapter 4 (Eqs. 4.3). The solution of these equations is complicated because they are non-linear in the junction phase differences, and in general one must solve the equations numerically. However, in the limit of vanishingly small voltages, V, and when the loop inductance is small, the equations can be solved analytically. When V = 0, one can neglect any affects arising from the ac Josephson effect, and one need only consider Eqs. (0.6) and the dc Josephson effect. Now, the current which flows through one arm of the SQUID, I_1, can be written as the sum of the current which flows through the capacitor, the resistor and the junction in that arm:

$$I_1 = V/i\omega C + V/R + I_o\sin(\delta_1) \qquad (0.10a)$$

similarly, for the other arm of the SQUID:

$$I_2 = V/i\omega C + V/R + I_0\sin(\delta_2) \qquad (0.10b)$$

At zero voltage, the total current, I, which flows through both arms of the SQUID is just:

$$I = I_1 + I_2 = I_0[\sin(\delta_1) + \sin(\delta_2)] \qquad (0.11)$$

From Equation (0.6b) one can write:

$$\delta_2 = \delta_1 - 2\pi\Phi/\Phi_0 + 2n\pi \qquad (0.12)$$

and thus Eq. (0.11) becomes:

$$I = I_0[\sin(\delta_1) + \sin(\delta_1 - 2\pi\Phi/\Phi_0)] = 2I_0\sin(\delta_1 - \pi\Phi/\Phi_0)\cos(\pi\Phi/\Phi_0) \qquad (0.13)$$

The meaning of Eq. (0.13) is as follows. At zero voltage, a supercurrent will flow through the SQUID which depends on both the phase differences across the junctions, and the magnetic flux in the SQUID loop. For any given flux, the maximum amount of supercurrent that can flow is:

$$I = 2I_0\left|\cos(\pi\Phi/\Phi_0)\right| \qquad (0.14)$$

Thus, the SQUID's response is periodic in the magnetic flux, with the fundametal period Φ_0. When $\Phi = n\Phi_0$, where n is an integer, the supercurrent attains its maximum value, $2I_0$. When $\Phi = (n+1/2)\Phi_0$ the supercurrent vanishes. Equation (0.14) is identical to that of a two slit diffraction pattern, as encountered in optical interference experiments, and it occurs for fundamentally similar reasons. The application of a magnetic field causes the phases of the order parameters in the two arms to shift relative to each other. As the flux is increased, this produces alternatively constructive and destructive interference. This simple behavior is the reason for the devices name Superconducting QUantum Interference Device, or SQUID.

It should be recognized that real SQUIDs are generally not operated in the zero voltage state, but rather are biased with a fixed current

which is in excess of I_0. In this case, the voltage across the SQUID is periodic in Φ. Also, the SQUID is ordinarily biased near $(n+1/4)\Phi_0$ or $(n+3/4)\Phi_0$. A small change in the flux in the SQUID will then produce a change in the voltage across the SQUID, which can be detected with conventional room temperature electronics. Also, a real SQUID will have a non-negligible inductance, the critical currents for the two junctions will usually differ, and there will be thermal noise from the resistive shunts. The inclusion of these effects is beyond the scope of this Appendix, and a detailed discussion can be found in Ref. (10).

References

(1) R.C. Jacklevic, J. Lambe, J.E. Mercereau, and A.H. Silver, "Macroscopic Quantum Interference in Superconductors", Phys. Rev. 140, A1628, (1965). Phys Rev. Lett. 12, 159, (1964). Phys. Rev. Lett. 14, 887, (1965).

(2) B.D. Josephson, "Possible New Effects in Superconductive Tunneling", Phys Lett., 1, 251, (1962).

(3) P. W. Anderson and J.M. Rowell, "Probable Observation of Josephson Superconducting Tunneling Effect", Phys Rev. Lett. 10, 230, (1963).

(4) J. Clarke, W.E. Tennant, and D. Woody, J. Appl Phys, 42, 3859, (1971).

(5) T. Van Duzer and C.W. Turner, "Principles of Superconductive Devices and Circuits", Elevier, (1981).

(6) L. Solymar, "Superconductive Tunneling and Applications", Chapman and Hall, London, (1972).

(7) Recent work on superconducting devices can be found in I.E.E.E.

Trans. Magn., and in particular in the most recent Proceedings of the Applied Superconductivity Conference, published in I.E.E.E. Trans. Magn..

(8) J. Clarke, "Fundamental Limits on SQUID Technology", Advances in Superconductivity, eds. B. Deaver and J. Ruvalds, p 13-50, (1983).

(9) Commercial SQUID measuring systems are available from a number of companies, including B.T.I., San Diego, Calif..

(10) C.D. Tesche and J. Clarke, "dc SQUID: Noise and Optimization", J.Low Temp. Phys., 29, 301,(1977).

(11) J.J.P. Bruines, V.J. de Waal, and J.E. Mooij, "Comments on: " dc SQUID: Noise and Optimization", J.L.T.P., 46, 383, (1982).

(12) V.J. de Waal, P. Schrijner and R. LLurba, "Simulation and Optimization of a dc SQUID with Finite Capacitance", J. Low Temp. Phys. 54, 215 (1984).

(13) For the original work on the Lanthanum compounds for which they received the Nobel Prize, see: J.G. Bednorz and K.A. Muller, Z. Phys. B 64, 189 (1986); For the original work on the YBCO compounds see: M.K. Wu et al., Phys. Rev. Lett., 58, 908 (1987).

(14) R.H. Koch, C.P. Umbach, G.J. Clark, P. Chaudhari, and R.B. Laibowitz, "Quantum Interference Devices Made from Superconducting Oxide Thin Films", Appl. Phys. Lett., 51, 22 (1987).

(15) C.M. Caves, K.S. Thorne, R.W.P. Drever, V.D. Sandberg, and M. Zimmermann, "On the Measurement of a Weak Classical Force Coulped to a Quantum-Mechanical Oscillator.1. Issues of Principle", Revs. of Modern Phys. 52, 341 (1980).

(16) R.H. Koch, D.J. Van Harlingen, and J. Clarke, "Quantum Noise Theory for the dc SQUID", Appl. Phys. Lett., 38, 380 (1981).

(17) V.V. Danilov, K.K. Likharev, A.B. Zorin, "Quantum Noise in SQUIDs", IEEE Trans. Magn., MAG-19, 572 (1983).

(18) M.W. Cromar and P. Carelli, Appl. Phys. Lett., 38, 723 (1981)

(19) R.F. Voss, R.B. Laibowitz, A.I. Broers, S.I. Raider, C.M. Knoedler, and J.M. Viggiano, IEEE Trans. Magn., MAG-17, 395 (1981).

(20) D.J. Van Harlingen, R.H. Koch, and J. Clarke, Appl. Phys. Lett., 41, 197 (1982).

(21) A. van der Ziel, "Noise", Prentice-Hall Inc., Englewood Cliffs, N.J. (1954).

(22) P. Dutta and P.M. Horn, Rev. Mod. Phys. 53, 497 (1981).

(23) "Noise in Physical Systems and 1/f Noise - 1985", eds. A. D'Amico and P. Mazzetti, North-Holland, (1986).

(24) V.F. Gantmakher, "The Experimental Study of Electron-Phonon Scattering in Metals", Rep. Prog. Phys. 37, 317 (1974).

(25) For an entertaining and refreshingly opinionated version of important problems in Physics, the interested reader can consult: V.L. Ginzburg, "Key Problems of Physics and Astrophysics", Mir Publishers, Moscow, (1978).

(26) J. Weber, "Detection and Generation of Gravity Waves", Phys. Rev. 117, 307 (1960); "General Relativity and Gravitational Waves", Wiley-Interscience, New York (1961); "Gravitational Radiation Experiments", Phys. Rev. Lett. 24, 276 (1970); "Evidence for the Detection of Gravitational Radiation", Phys. Rev. Lett. 22, 321 (1969).

(27) R.P. Giffard, S.P. Boughn, W.M. Fairbank, M.S. McAshan, H.J. Paik, and R.C. Taber, in "Physics and Astrophysics of Neutron Stars and Black Holes", Society Italiana di Fisica, Bologna, (1978).

(28) C. Cosmelli, P. Carelli, M.G. Castellano, and V. Foglietti, "Long Term Operation of Low Noise dc-SQUID Coulped to a Very High Q Gravitational Radiation Detector", IEEE Trans. Magn., Mag-23, 454 (1987).

(29) C.W. Misner, K.S. Thorne, and J.A. Wheeler, "Gravitation", W.H. Freeman and Co., San Francisco (1973).

(30) K S. Thorne, Theoretical Principles in Astrophysics and Relativity, ed. N. Lebovitz, Univ. of Chicago, Chicago (1978).

(31) C. Hilbert and J. Clarke, "dc SQUID as a Tuned Radiofrequency Amplifier", IEEE Trans. Magn. Mag-21, 1029 (1985).

(32) C. Hilbert and J. Clarke, "DC SQUIDs as Radiofrequency Amplifiers", J. Low Temp. Phys., 61, 263 (1985).

(33) P.F. Michelson and R.C. Taber, " Sensitivity Analysis of a Resonant Mass Gravitational Wave Antenna with Resonant Transducer", J. Appl. Phys., 52, 4313 (1981).

(34) V.B. Braginsky, Y.I. Voronstov, and K.S. Thorne, "Quantum Nondemolition Measurements", Science 209, 547 (1980).

CHAPTER 1: SQUID Fabrication and Design Types

1.1 Introduction

In this Chapter, I will describe the fabrication procedure which was used to build the SQUIDs. I will discuss it in some detail because of its possible connection with the source of the low temperature excess noise, as will be discussed in Chapter 8. Insofar as it was possible, the procedure uses conventional photolithographic and thin-film deposition techniques. The fabrication of dc SQUIDs may be broken into three stages: the design and construction of the projection masks, the processing of the wafer, and the oxidation and completion of the Josephson junction tunnel barriers.

The patterning of the SQUIDs is done photolithographically. Ultraviolet light is projected through an emulsion slide or mask onto a photosensitive resist which covers a wafer substrate. The mask contains opague and transparent areas, corresponding to parts of the SQUID. The original masks for our planar thin-film dc SQUIDs were made by John Martinis.[1] In addition, Claude Hilbert made a number of input coil masks[2] and assisted me greatly in making the mask for the magnetometer pick-up loop described in Chapter 3.[3] All of these early masks were made using Rubylith paper and standard photographic reduction techniques, and resulted in 2.5 X 2.5 inch emulsion glass slide masks. During 1985, I began to make numerous new SQUID masks. These were all made using the U.C. Berkeley computer assisted design (CAD) mask designing program KIC. The resulting computer patterns can be transferred from the computer to magnetic tape, which is read by a

pattern generator to produce the 2.5 X 2.5 inch emulsion on glass, slide masks.

I carried out the processing of the wafers in the Electrical Engineering and Computer Sciences Microfabrication Laboratory at Berkeley (the Microlab) and in Professor Clarke's laboratory in 137 Leconte. The materials depositions, ion milling, and junction oxidations were carried out in Leconte. The remainder of the steps were completed in the considerably cleaner environment of the Microlab.

The procedure for fabricating the SQUIDs was developed by Dale Van Harlingen, Roger Koch, John Martinis, and Claude Hilbert. I have made numerous small modifications to this procedure for several different reasons. First of all, in order to search for the cause of the low temperature excess noise (see Chapter 8), I made numerous small variations in the procedure, as well as a few materials changes. Secondly, I had extreme difficulty getting part of the old procedure to work reliably: the IBM "mushroom technology".[4] The technique involves developing the photoresist so as to leave two small 2 μm dots of resist on the wafer, see Fig. 1.1. These would ultimately form the windows for the Josephson Tunnel junctions, so their size was of considerable importance. There are two problems with the mushroom technology. First of all a slight overdevelopment will completely develop away the windows, whereas a slight underdevelopment leaves too large of a window or undeveloped resist elsewhere on the SQUID. In other words, the technique is inherently unstable. Secondly, even if the windows can be developed to the proper size, because of their small size they may not open during the liftoff, thereby destroying the junctions. Accordingly, in all of the masks I made, I abandoned this approach and adopted a

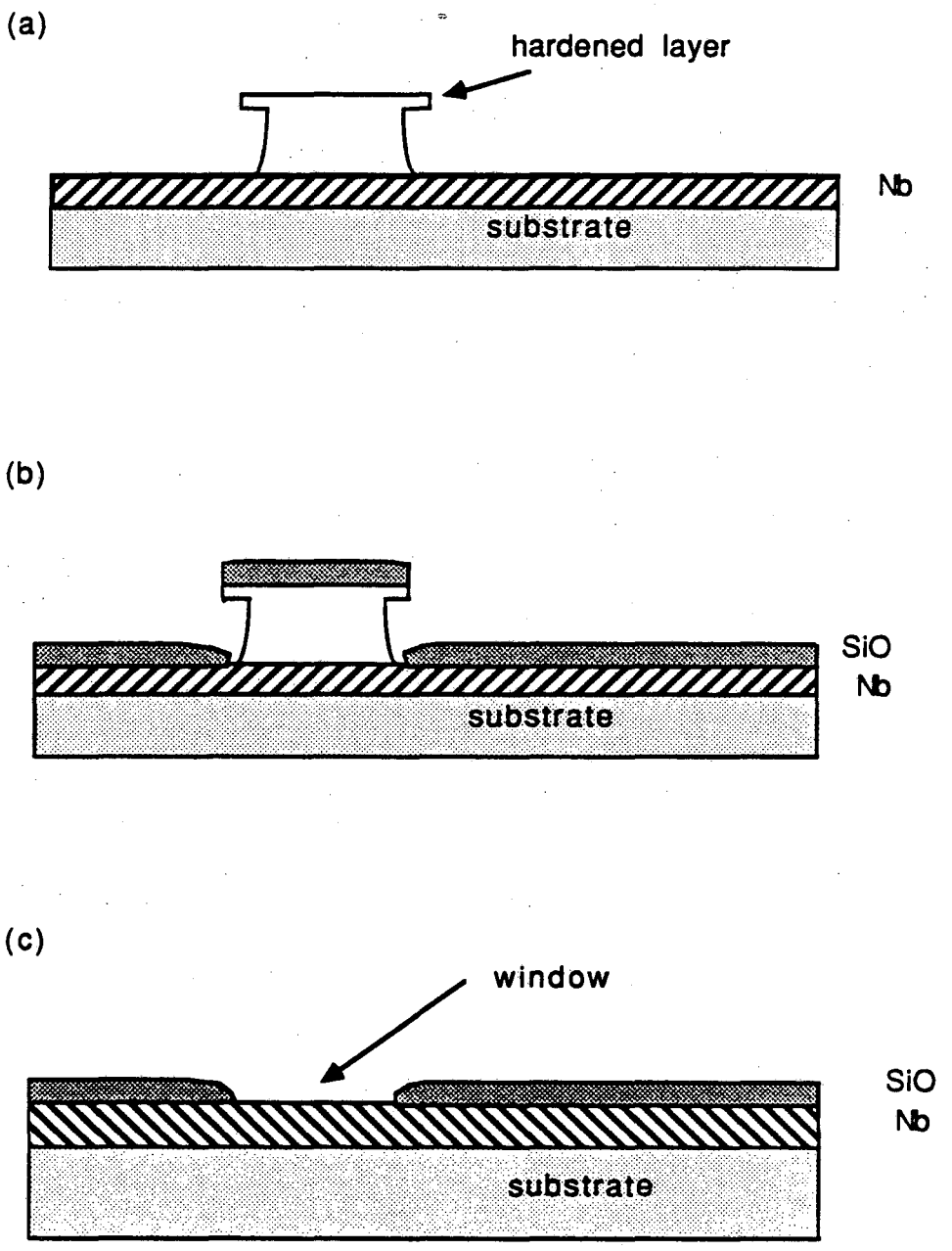

Fig. 1.1 Liftoff technique for construction of a window in SiO. (a) Photoresist mushroom, (b)deposition of SiO, (c) Liftoff in acetone removes photoresist and leaves window.

cross strip window technique. Instead of forming a window from a single small dot, I used the overlap between two long lines which crossed perpendicular to each other. Since it is much easier to produce two thin lines than a single small dot, this was a much better technique. It is interesting to note that many other groups made the same decision independently at about this time, and that cross strip windows are now very common in SQUIDs. The reason is not hard to understand; this single change took out about half of the work and frustration involved in making the SQUIDs. Thirdly, I had occasional, but recurring, problems with the old procedure for the Cr adhesion layer. The Cr was used to make an overlying thin-film layer stick better to the underlying layer, ie. it acted as a kind of glue. However the Cr was very difficult to evaporate to a controlled thickness and I often got electrical shorts from a thicker than average layer. These shorts would occur between the SQUID and the input coil and were electrically undesirable. Following suggestions from Professor Clarke, I tried the IBM technique of using a very thin layer (less than 1nm) of Ti as an adhesion promoter.[4] I can confirm that this works very well and I have not encountered shorting or peeloff with the Ti. Fourthly, in order to save time and to generate many different types of test SQUIDs, from the start I put 36 SQUIDs on a wafer instead of the old 9 to a wafer. This was an essentially trivial way to pick up a factor of four in the effective processing speed. In practice, I made four different SQUID types on each wafer, for 9 of each type. As a result, the SQUIDs were 5 X 5 mm on a side and mechanically tougher then the old 5 X 12 mm chips. Besides being very efficient, this technique had the advantage of creating different types of SQUIDs which had undergone identical processing, and thus enabled me to eliminate the

possibilty of wafer to wafer variations between different SQUID types. Fifthly, the discovery of the hot electron effect in the low temperature SQUIDs lead to a subtantial modification to the size of the shunt, and in the largest shunts to an additional processing step which added a thick AuCu film (see Chapter 11) . Finally, I would like to note the development of our Nb-AlOx-Nb junction by Bonaventura Savo.[5] Although I did not incorporate this into my low temperature SQUIDs, I report on critical current noise in these junctions in Chapter 6, and describe Savo's procedure.

1.2 Fabrication Procedure

The processing of the wafers for the construction of the SQUIDs is built up from the repeated application of a small number of steps. I will label these steps as follows: CLEAN, HMDS, SPIN, BAKE, CHLOROBENZENE, EXPOSE, DEVELOP, EVAPORATE, SPUTTER, LIFTOFF, PLASMA ETCH, ION MILL, DICE. In detail, these steps consist of the following procedures:

CLEAN: In order to remove grease and dirt from the wafer, the wafer is soaked in detergent solution[6]. The wafer is periodically sprayed with DeIonized water (DI), until the DI wets the surface without beading. The wafer is then sprayed with DI water for about 1 minute in order to remove the detergent, and is blown dry with compressed nitrogen. If the wafer has photresist on it from a previous step, the wafer is first cleaned in 1/2 water 1/2 Microposit 1112A remover[7] for 2 minutes. This chemically strips off all of the resist. The wafer is then washed with DI for 1 minute, and the above detergent cleaning is

done.

HMDS: Immediately after cleaning, the wafer is immersed in hexamethyldisilizane vapor (HMDS) for 5 minutes. This step improves adhesion of the photoresist to metal layers on the wafer, and is generally done on all steps, whether or not any metal is present.

SPIN: Following HMDS treatment, the wafer is placed on a wafer spinner and photoresist applied. For Liftoff steps, Microposit 1450J (7) was spun at 6000 RPM for 30 seconds. For Plasma etching, Microposit 1350B was spun at 5000 RPM for 30 seconds. These resists became obsolete at the microlab in 1987, and we now use 1400-17 instead of 1350B, and 1400-31 instead of 1450J.(7)

BAKE: Following the SPIN, the photoresist is hardened by baking. Before 1986, the resist was baked for 20 minutes using temperature controlled ovens. The 1450J was baked at 70 ^{o}C, and the 1350B was baked at 90 ^{o}C. From 1986 on, the resist was baked on temperature controlled hotplates for 5 minutes, at the same temperatures as was used previously.

CHLOROBENZENE: The 1450J resist is used for liftoffs. The liftoff works better when the baked resist is treated with chlorobenzene. Following the bake, the resist is soaked in liquid chlorobenzene at 18 ^{o}C for 10 minutes. The chlorobenzene is then removed from the wafer by blowing it off with compressed nitrogen. The wafer is then at 90^{o}C. This is now done for 3 minutes on the hotplate, and used to be done for 10 minutes in the ovens. This procedure leaves a hardened surface layer of chemically altered photoresist. During later development of the photoresist, the uderlying resist is eaten away more rapidly, leaving an overhanging upper layer, see Fig. 1.2. During deposition of a film, the

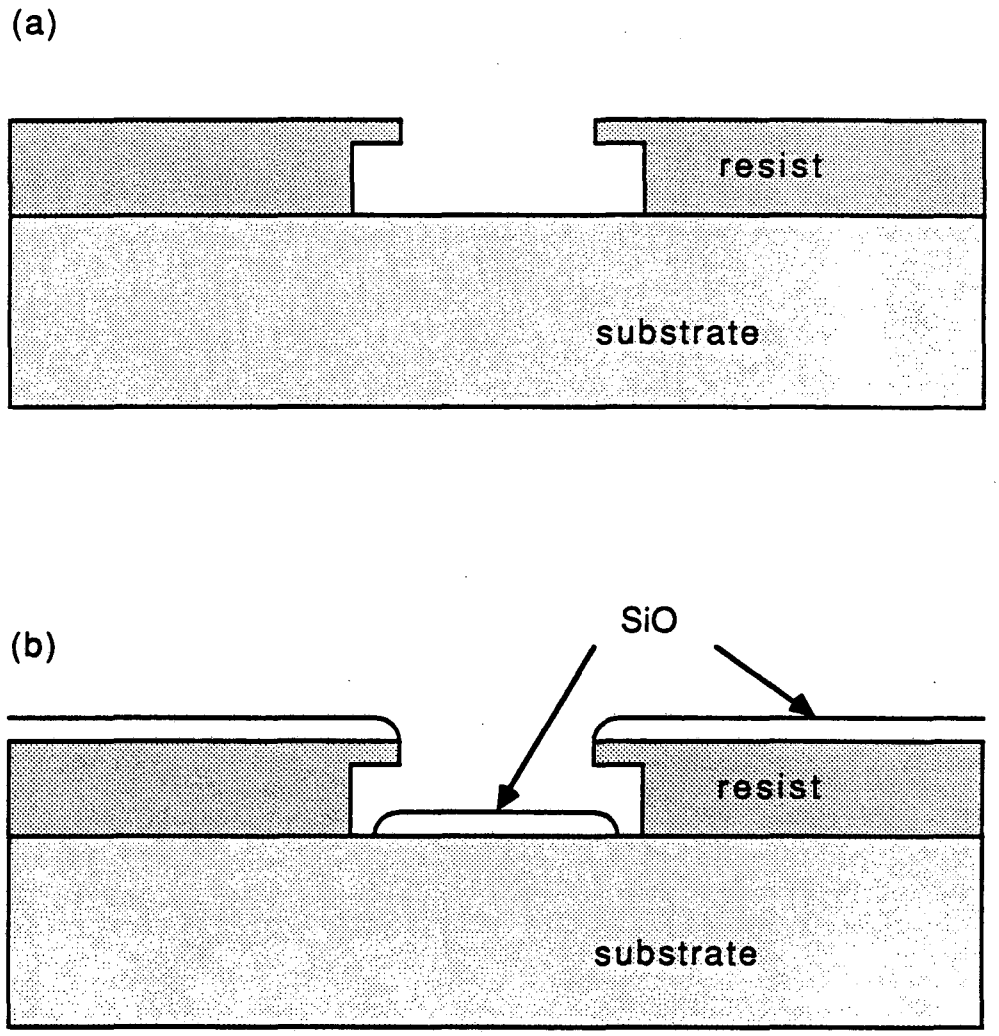

Fig. 1.2 (a) Photoresist layer has an overhanging hardened surface after treatment with chlorobenzene and development, (b) this produces a cleaner edge for the deposited film, as it is not connected to the overlying film.

overhang shades the edges of the film and prevents the connection of the film on top of the resist with that lying in the developed region, thus leading to a cleaner liftoff.

EXPOSE: After the photoresist has been baked (and chlorobenzened if it is 1450J) the wafer is placed on a Canon 4X Projection Mask Aligner and exposed under the mask pattern.

DEVELOP: After exposure, the wafer is placed in Concentrated Microposit Developer.(7) For the 1450J, full strength developer is used for about 30 seconds. The exact time is gauged by watching the resist develop away and by previous experience with the given exposed layer. For the 1350B, the developer is half diluted with DI water, and typical development times are about the same. Following development, the wafer is rinsed in DI for 1 minute, and blown dry with compressed nitrogen.

EVAPORATE: After the resist has been developed, a layer of material may be deposited by evaporation or sputtering. The wafer is attached to an Al holder by using silicone high vacuum grease. The holder is suspended upside down over the evaporation source. The chamber is then evacuated to a pressure of typically 1 X 10^{-6} Torr using an oil based diffusion pump with a nitrogen cooled cryotrap. The materials that are evaporated are: Cr or Ti for an adhesion promoter, AuCu for the resistive shunts, and SiO for the insulating layers. The thickness of the layer and the deposition rate is monitored with a quartz crystal microbalance.(8) Cr was used under all AuCu layers except when using sapphire substrates, in which case no adhesion promoter was used. Cr was also used under the SiO layers until 1985, after which time I began to use Ti for the reasons discussed above. The Cr was 0.99 pure powder which was evaporated at a rate of about 0.5nm per sec, for 10 seconds.

sec. The Cu was 0.9999 pure, in the form of 1 mm diameter pellets. The Au was drawn wire of unknown purity. The Au and Cu were combined in a single W boat, (occasionally Ta was used, but this does not work very well as the AuCu tends to alloy with the boat) in the ratio of 25% by weight of Cu. The boat is heated in vacuum and the AuCu is deposited onto the wafer at the rate of about 1 nm/sec. The SiO, of unknown purity, was in the form of large chunks which were placed into a chambered SiO evaporation boat. During an evaporation, the SiO is slowly heated up to white heat over about five minutes, and is then deposited onto the wafer at the rate of about 1 nm/sec by opening a shutter.

SPUTTER: The Nb for the SQUID body, contacts, and input coil was deposited by sputtering in an Argon atmosphere. Most of the SQUIDs were formed with Nb from a Sloan S-300 sputtergun.[9] A few of the SQUIDs, as discussed in Chapter 7, were formed in a different sputtering system; this system will be described in Chapter 6. The Sloan sputtergun is a dc system which has a cylindrical Nb ring as the sputtering target. Its operation is as follows. The wafers are affixed to an Al holder using silicone vacuum grease, which also provides a thermal ground to prevent severe heating of the wafer and the photoresist. The chamber is pumped to about 2 X 10^{-6} Torr, and bottled Ar bled through at about 5 μm. An Argon plasma is ignited by applying about 600 V between the cathode and the anode, and increasing the Ar pressure in the chamber to about 10 mTorr. Once the plasma has started, the Ar pressure is decreased to about 7 mTorr, and the plasma is run at a voltage of 400 V and a current of 4 A. The deposition rate is roughly 10 nm/sec, and typical film thicknesses are from 200 to 400 nm. Residual resistivity ratios, (R_{300K}/R_{10K}), of about 4 to 5 are typically obtained, and

superconducting transition temperatures are generally greater than 9.0 K.

LIFTOFF: After an evaporation or sputtering, a cotton swab, which has been dipped in acetone, is used to remove the vacuum grease which was placed on the backside of the wafer. For a liftoff, the entire wafer is then soaked in a beaker of acetone, and occasionally agitated. The acetone works its way under the deposited film and dissolves any photoresist. The film will then slowly peel away from areas of the wafer which had photoresist on them, but remain affixed to areas where the photoresist was developed away. The process can take as much as an hour for a 300 nm SiO film, or as little as 5 min for a 30 nm AuCu film. After most of the film has lifted off, the progress can be checked on a light microscope. Fresh acetone baths are used at intervals of about 15 minutes until the liftoff is complete.

PLASMA ETCH: All of our Nb etching is done with a reactive ion, barrel plasma etcher that was built by the Microlab Staff. The etching gas is 0.6 Torr of SF_6O_2. Before etching the wafer, the empty barrel vacuum chamber is preheated to about 100 ^{o}C and cleaned by an initial SF_6O_2 plasma discharge. The system is then bled back up to atmospheric pressure, the wafer is placed in the bottom of the chamber, the system is pumped to 0.1 Torr, and then SF_6O_2 bled at 0.6 Torr for several minutes. The plasma is ignited by applying Radio Frequency (RF) power, and typically runs at about 175 W. The progress of the etch can be watched through a viewport, and generally takes about 2 min for a 200 nm thick Nb film.

ION MILL: We use an Iontech VS 2.5 Argon ion beam [10] to remove oxides from the surface of Nb films. This technique is used before

completing Nb superconducting contacts between different Nb layers, and for cleaning the Nb electrode of a tunnel junction prior to barrier formation. The beam voltage is 400 V, and the beam density at the wafer is about 0.5 mA cm^{-2}. An exposure of 40 seconds results in the removal of about 20 nm from the surface.

DICE: After the last photoresist layer has been developed, the front surface of the wafer is scribed, between the devices, with a diamond point using a wafer scribing machine. The wafer is then sectioned into individual 5 X 5 mm^2 chips by carefully applying force so as to break the wafer along successive scribe marks.

With these processing steps defined, I can represent the SQUID fabrication as the following sequence:

Resistive shunts: CLEAN, HMDS, SPIN 1450J, BAKE, CHLOROBENZENE, EXPOSE, DEVELOP, EVAPORATE Cr and 35 nm of AuCu, LIFTOFF.

Nb body and contacts: CLEAN, SPUTTER 200 nm of Nb, CLEAN, SPIN 1350B, BAKE, EXPOSE, DEVELOP, BAKE, PLASMA ETCH, CLEAN.

First SiO layer: HMDS, SPIN, BAKE, CHLOROBENZENE, EXPOSE, DEVELOP, EVAPORATE 200 nm of SiO, LIFTOFF.

Second SiO layer: CLEAN, HMDS, SPIN, BAKE, CHLOROBENZENE, EXPOSE, DEVELOP, EVAPORATE 300 nm of SiO, LIFTOFF.

Input coil (optional - only used on some type A SQUIDs): CLEAN, HMDS, SPIN, BAKE, CHLOROBENZENE, EXPOSE, DEVELOP, SPUTTER 400 nm of Nb, LIFTOFF, CLEAN, HMDS, SPIN, BAKE, EXPOSE, DEVELOP, PLASMA ETCH.

Counterelectrode: CLEAN, SPIN, BAKE, CHLOROBENZENE, EXPOSE, DEVELOP, DICE

In words, the procedure is as follows. The SQUIDs are made 36 at a time on five centimeter diameter Si wafers which have a 1.2 μm layer of thermally grown oxide. I process the wafers one at a time, and I generally will complete all of the processing on a single wafer, before beginning another wafer. The wafer is first degreased in a detergent solution. Photoresist is then spun on and photolithographically patterned for the shunts. A 10 nm layer of Cr is evaporated as an adhesion promoter and a 30 nm layer of AuCu is evaporated on top. We have also used sapphire wafers, and then the Cr is not needed. The photoresist is then lifted off leaving the resistive shunts. The wafer is then cleaned of all remaining photoresist in a commercial resist stripper and again cleaned in detergent. A 200 nm layer of Nb is then sputtered down from a dc sputtering gun in a 7 mTorr Argon atmosphere at 400 V and 4 A with a rate of approximately 10 nm/sec. The wafer is again cleaned in detergent and photolithographically patterned. The Nb is then reactive ion etched in an SF_6O_2 plasma at 0.5 Torr and 175 W. This etching defines the contacts and the Nb portions of the SQUID body. The wafer is then stripped of photoresist and cleaned in detergent. A new layer of photoresist is then spun on and patterned. A 1.5 nm layer of Ti is then evaporated to improve adhesion and a 200 nm layer of SiO is evaporated on top. The photoresist is then lifted off leaving an insulating layer of SiO over the SQUID body except for two 2 μm strips which will form one cross in a cross strip window configuration. The wafer is again cleaned and patterned for a second Ti underlayer and 200 nm SiO layer. The second layer is then lifted off leaving SiO over the SQUID body except for the second pair of lines in the cross strip window. The intersection of the two crossed windows defines the 2X2 μm^2

Josephson junction windows. The wafer is again cleaned and new photoresist spun on and patterned for the counterelectrode. At this stage the SQUIDs are complete except for the formation of the Josephson junctions. The wafer is then diced into 36 chips of 5 mm on a side and the individual SQUIDs are processed seperately.

1.3 Junction Oxidation and Completion

The chips are ordinarily stored at room temperature in air until a SQUID is needed. An individual SQUID chip is then selected for the oxidation procedure. The junction windows are inspected optically for size and cleanliness. The chip is sprayed with DI to remove bits of Si from the dicing and blown dry with N_2. The chip is then secured to a glass slide by using a small amount of silicone vacuum grease on the backside of the chip. The slide is placed on the Argon ion mill, and the system pumped down to 1 μTorr. The Nb electrode is first cleaned in an Argon ion mill at 300 V and 0.5 mA/cm^2 for 40 sec. The system is then bled up to atmospheric pressure with N_2 gas, and the chip is transferred to the RF oxidation head. As this transfer takes place in air, it is done as quickly as possible, in order to minimize the oxidation of the freshly cleaned Nb surface.

The Nb is then oxidized in an Ar-O(5%) RF plasma. RF power for the plasma is provided at 7 MHz by a Hartley oscillator, see Fig. 1.3. The plasma is ignited using a Tesla coil, and typically runs at 9 mTorr of pressure and 45 W of RF power. Oxidation times are typically 60 sec. After oxidation, the Argon-Oxygen mixture is pumped out of the chamber, and a 200 nm thick layer of Pb-In(5 Wt%) is evaporated. A liftoff is

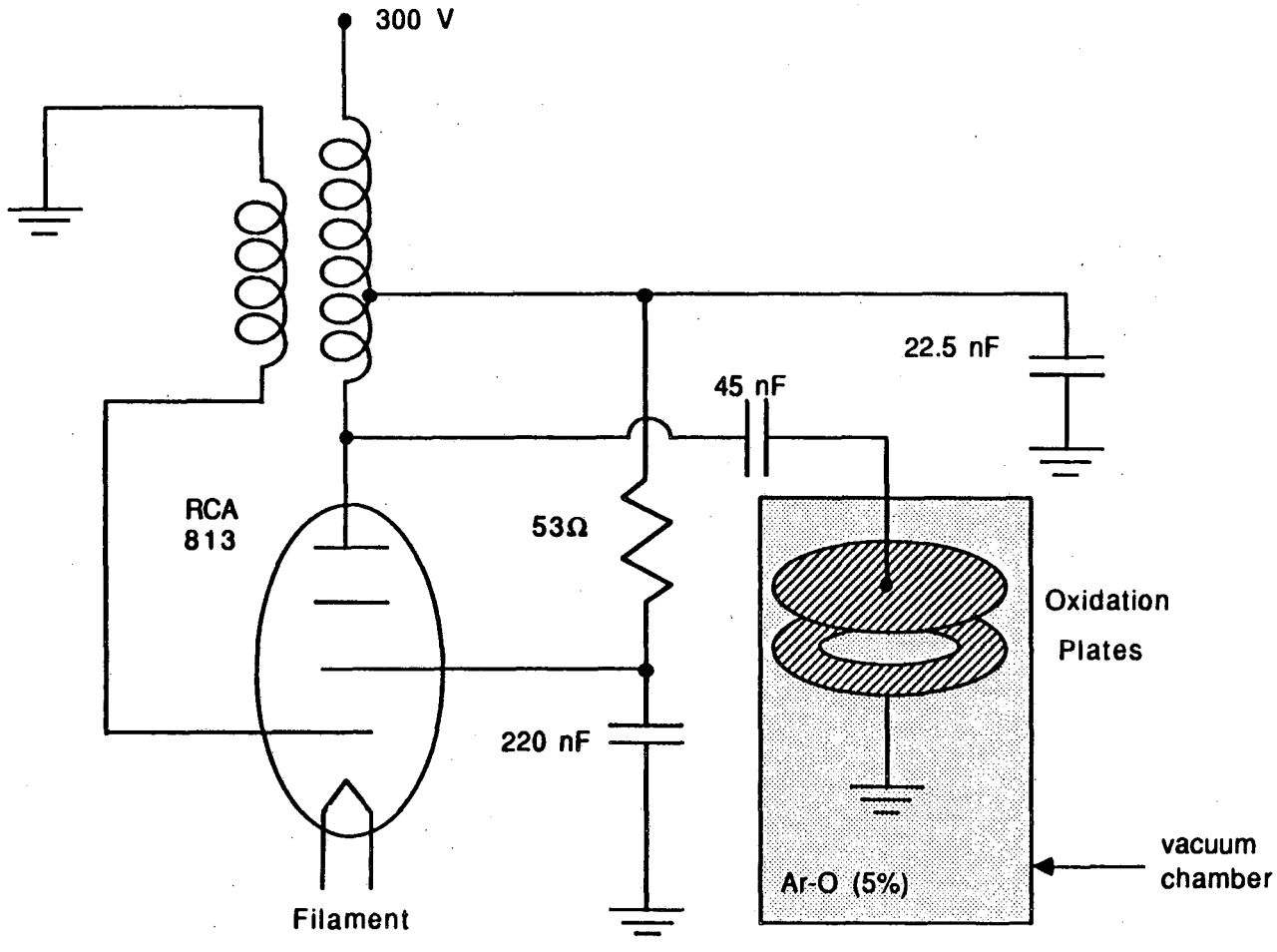

Fig 1.3 The Hartley oscillator provides RF power to the Ar-O(5%) plasma. The arrangement is used for the oxidation of the Josephson junction tunnel barriers.

then used to define the counterelectrode. The process typically yields critical current densities of order 50 A/cm^2.

At this stage the chip may be covered or "passivated" with a 200 nm layer of SiO. Generally, I only passivated SQUIDs which I intended to keep for extended use, such as devices with coils. Accordingly, most of the SQUIDs were left unpassivated.

1.4 The Different SQUID Types

Figures 1.4 through 1.19 show the geometrical configurations of the different SQUIDs on which I will report results. The figures do not show the SiO insulating layers, except insofar as they reveal the position of the junctions, and generally do not show the resistive shunts.

All of the dc SQUIDs tested were planar thin-film devices made as descibed above (with the exception of two outside devices discussed in Chapter 8). Although the processing varied only slightly from one wafer to the next, the size construction, and shape of the SQUIDs varied enormously. The parameters of the different SQUID types which were tested are discussed in Chapter 4, and are summarized in Table 4.1. The SQUIDs may be divided into three classes based upon their size and construction:

Old Style or Nb SQUIDs: Types: A, F. This class consists of SQUIDs which have their bodies made out of Nb. It includes the large SQUIDs which have been made for many years by our group. The basic shape is a Nb washer about 900 μm on a side with a 200 μm inside hole, and was designed following the pioneering work of Ketchen and Jaycox[11]. The type A devices have been used for many years by the Clarke group, and

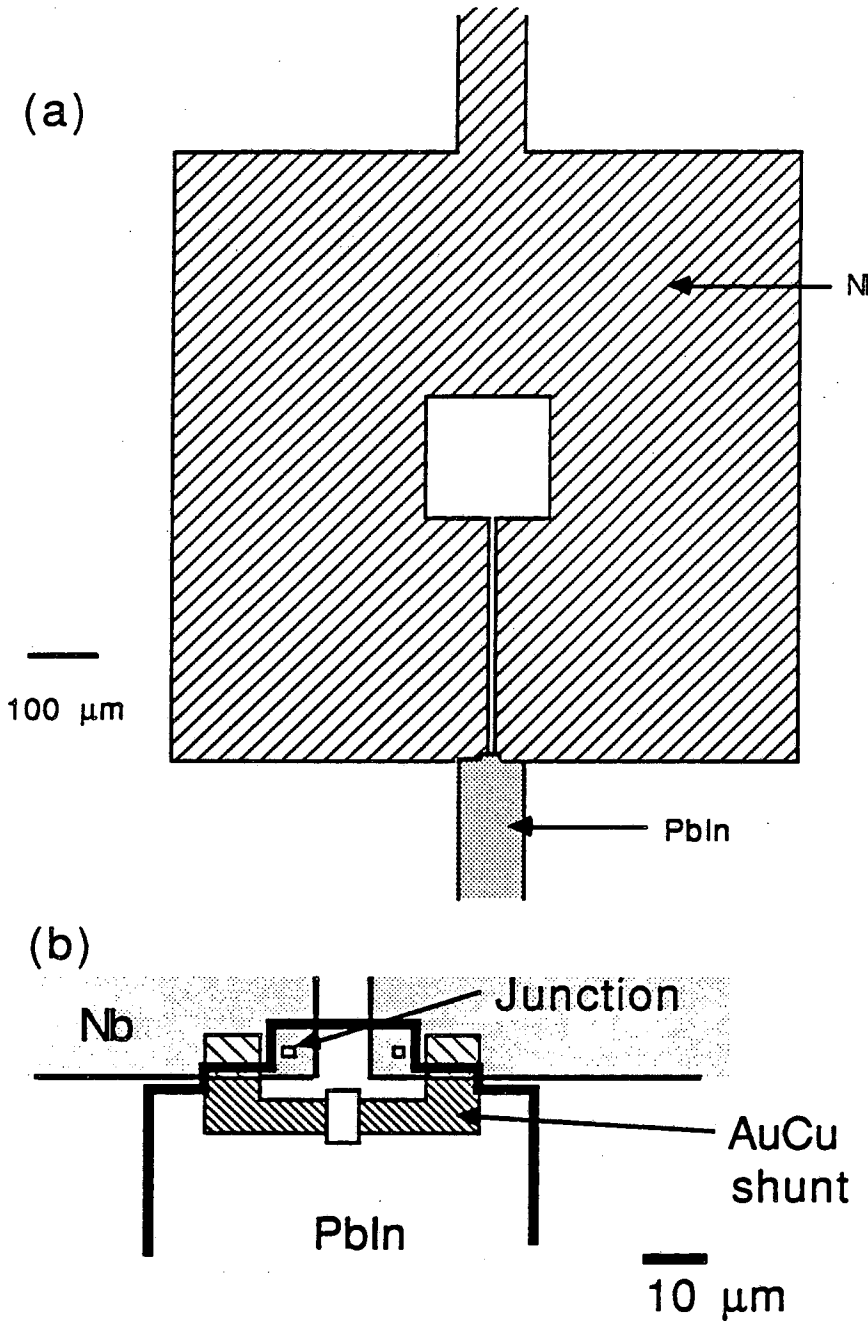

Fig. 1.4 (a) Schematic of a Type A dc SQUID, see also Fig. 3.1. (b) shows details of junctions.

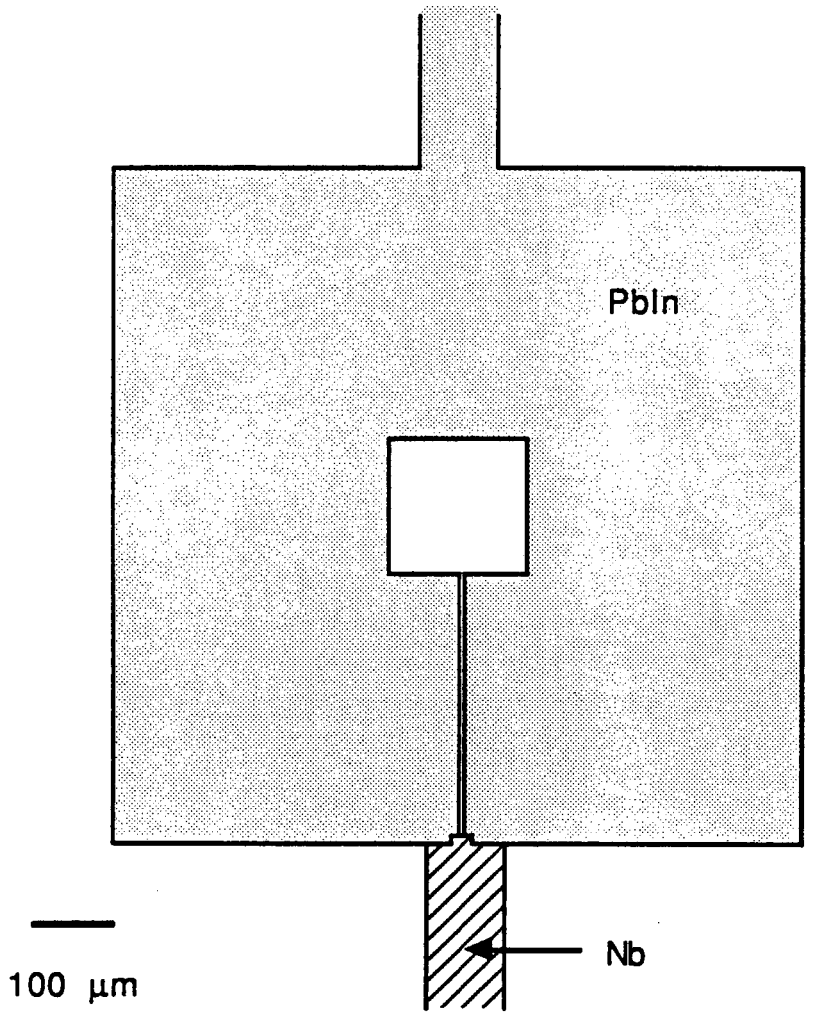

Fig. 1.5 Schematic of a type A' dc SQUID.

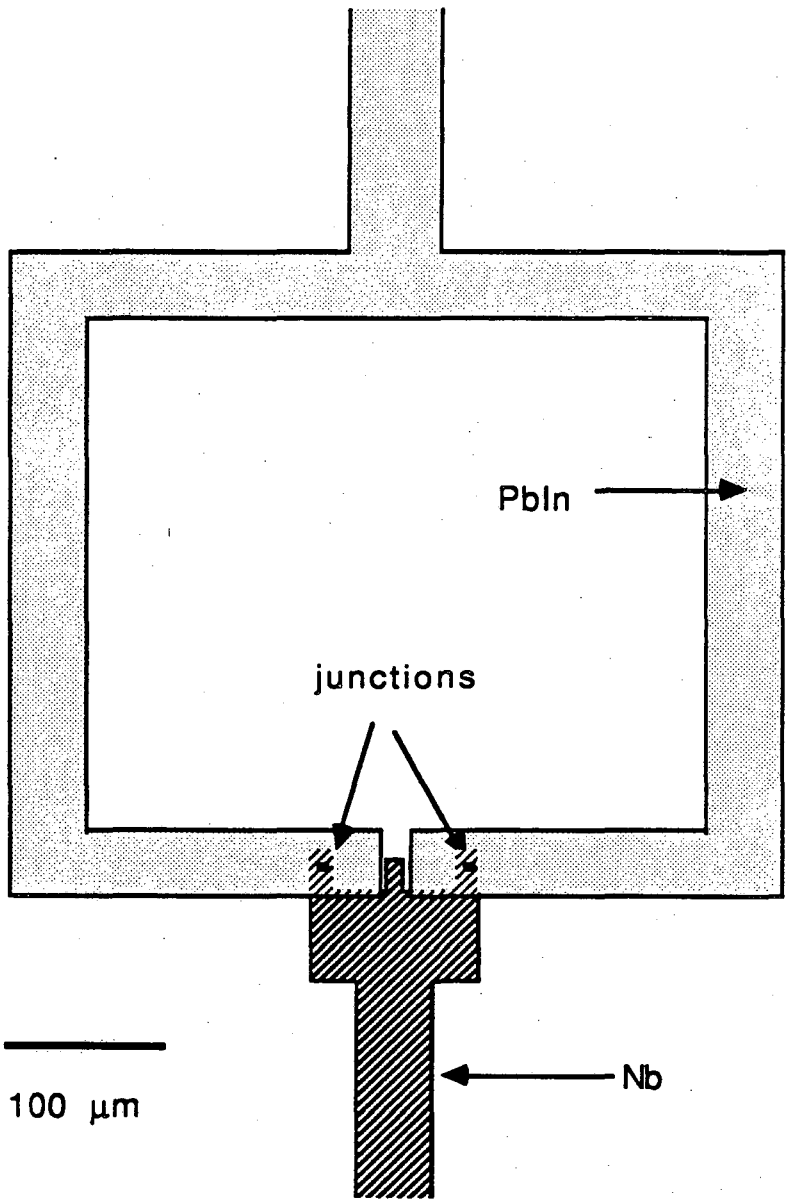

Fig. 1.6 Schematic of a Type B dc SQUID.

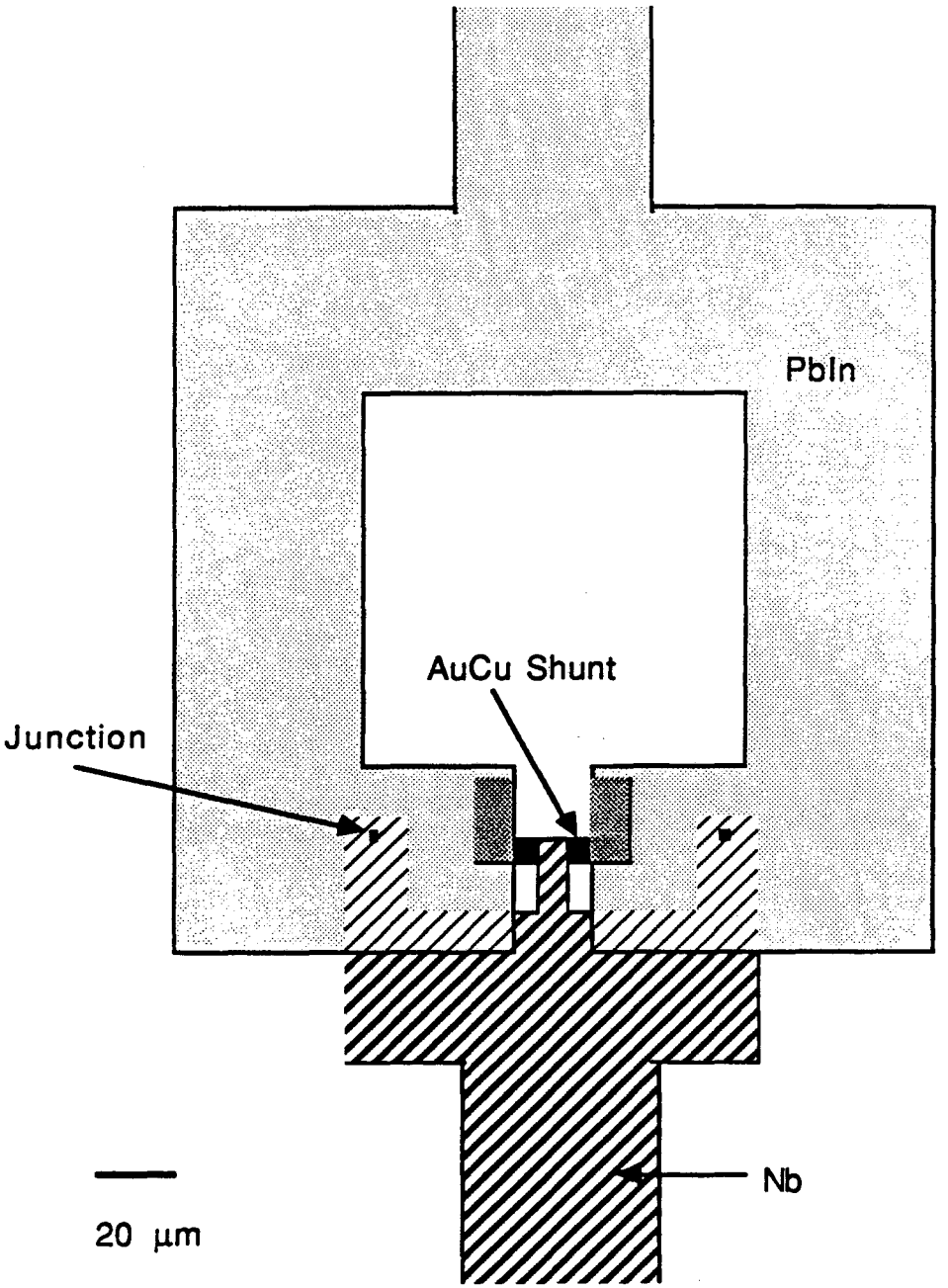

Fig. 1.7 Schematic of a Type C dc SQUID.

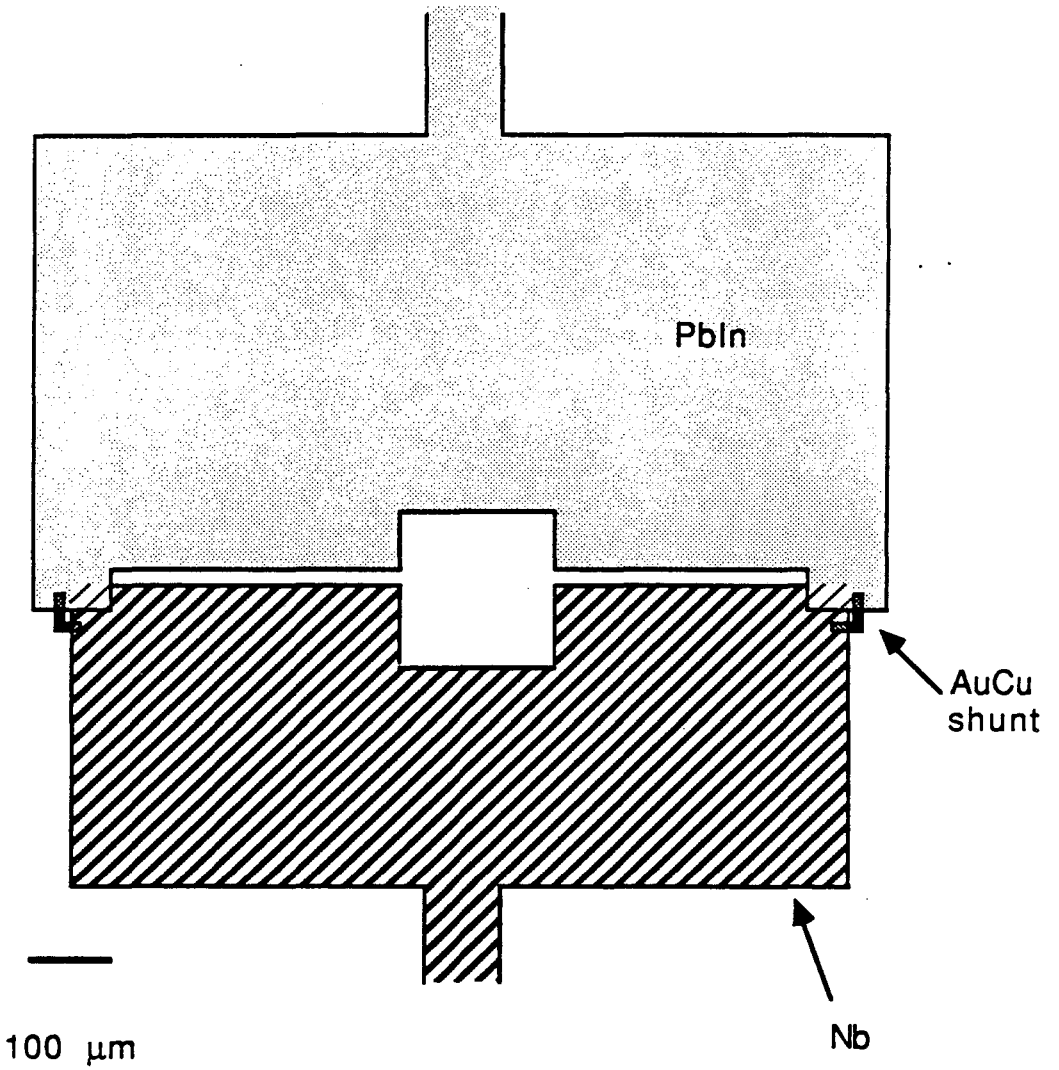

Fig. 1.8 Schematic of a Type D dc SQUID.

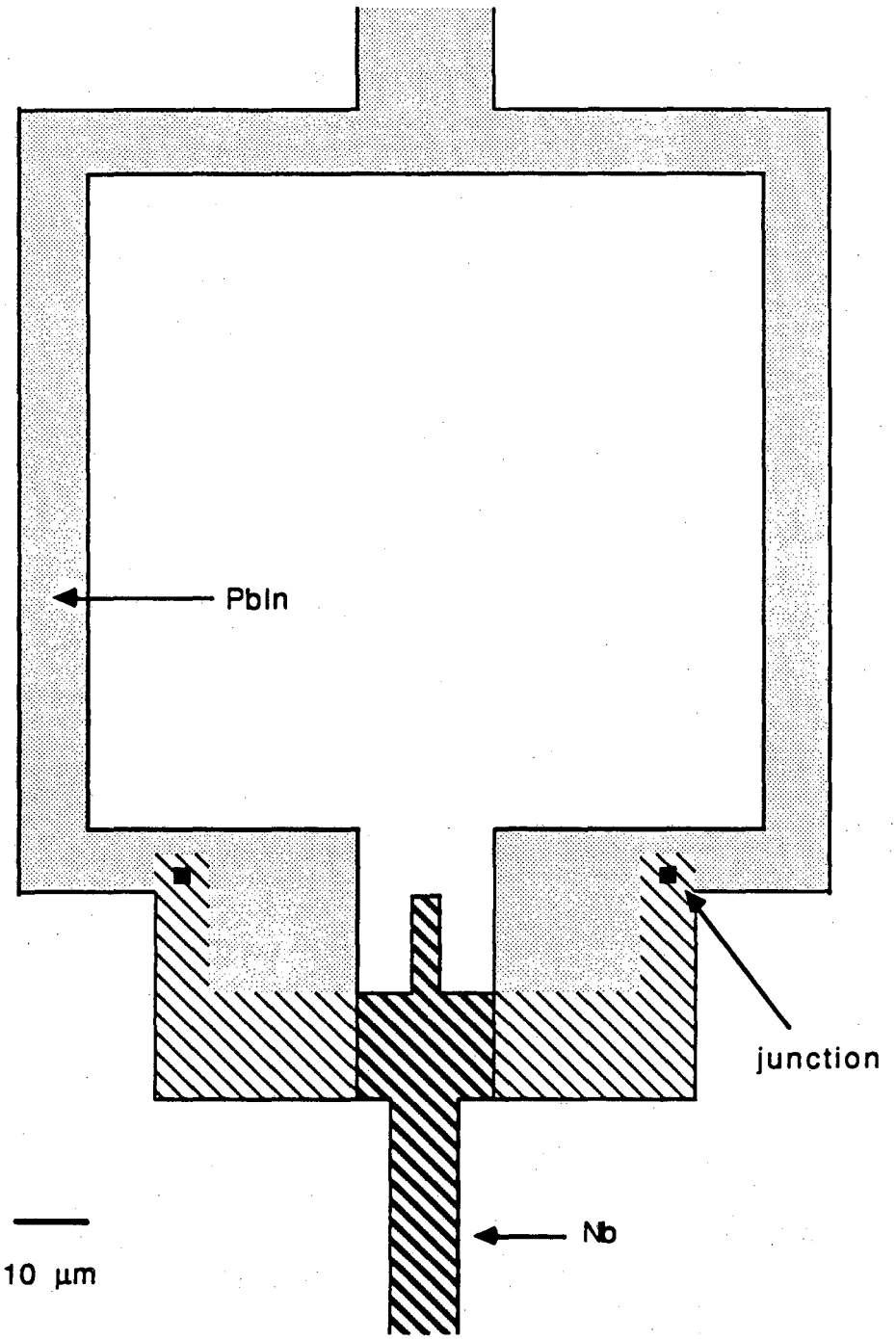

Fig. 1.9 Schematic of a Type E dc SQUID.

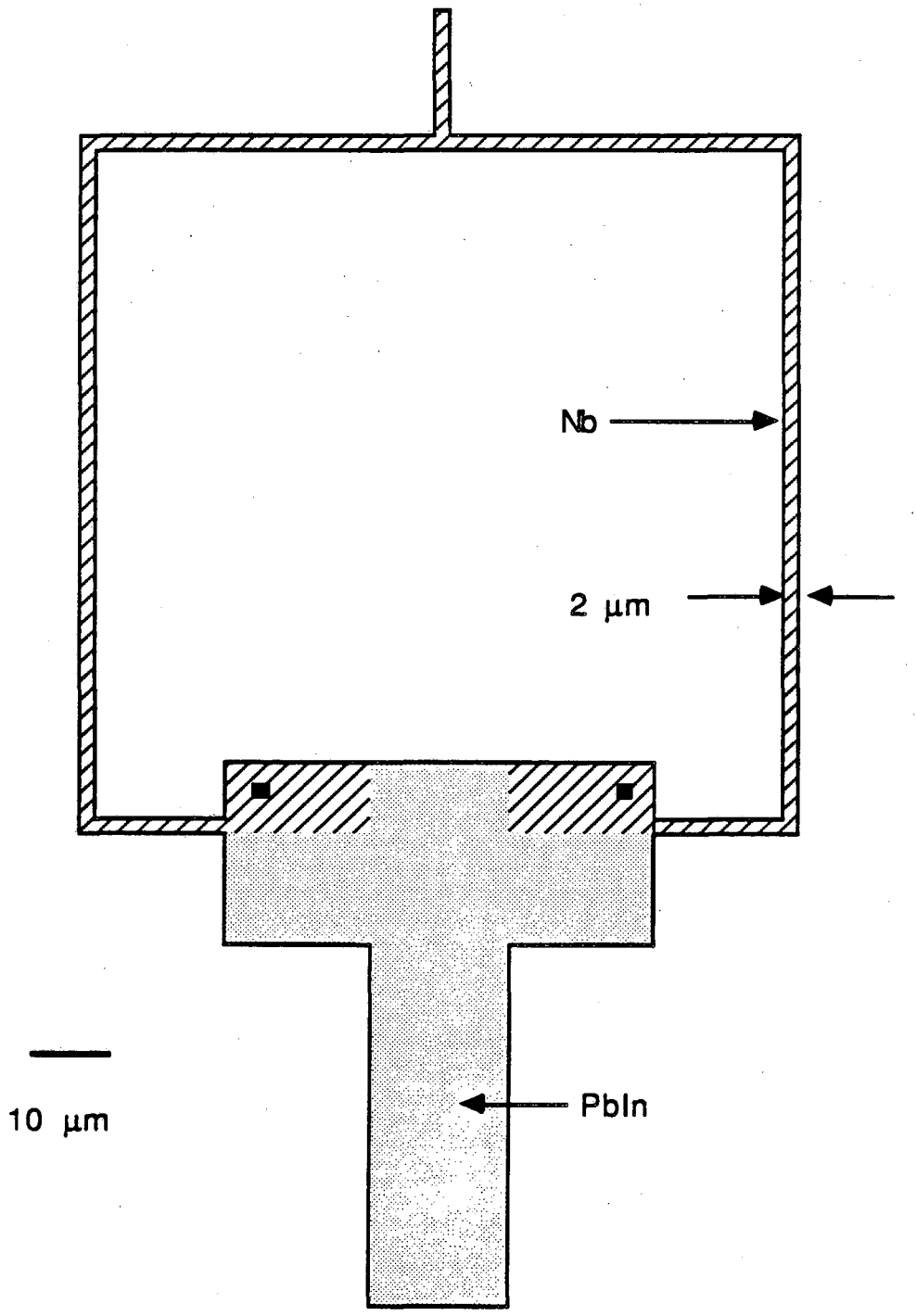

Fig. 1.10 Schematic of a Type F dc SQUID.

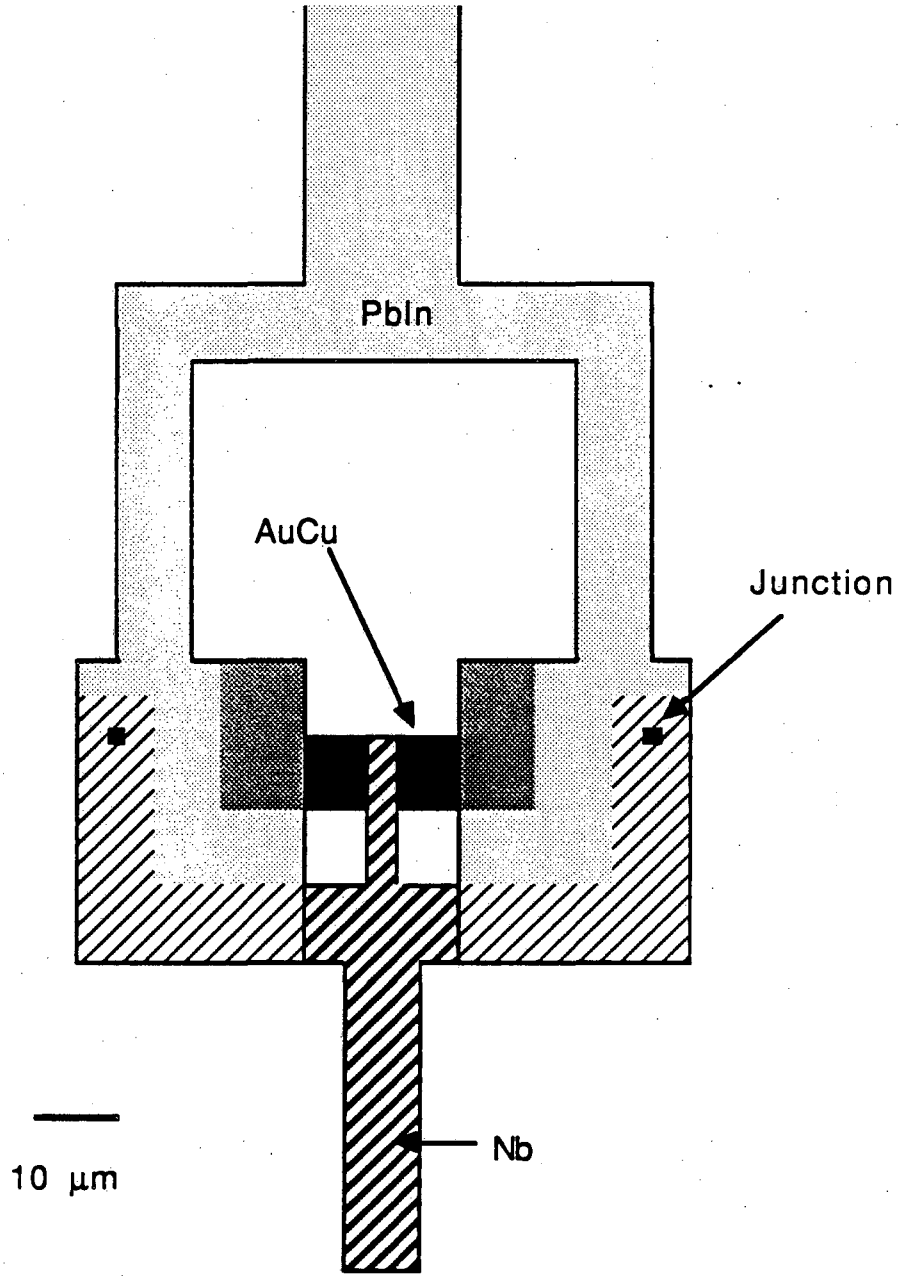

Fig. 1.11 Schematic of a Type G dc SQUID.

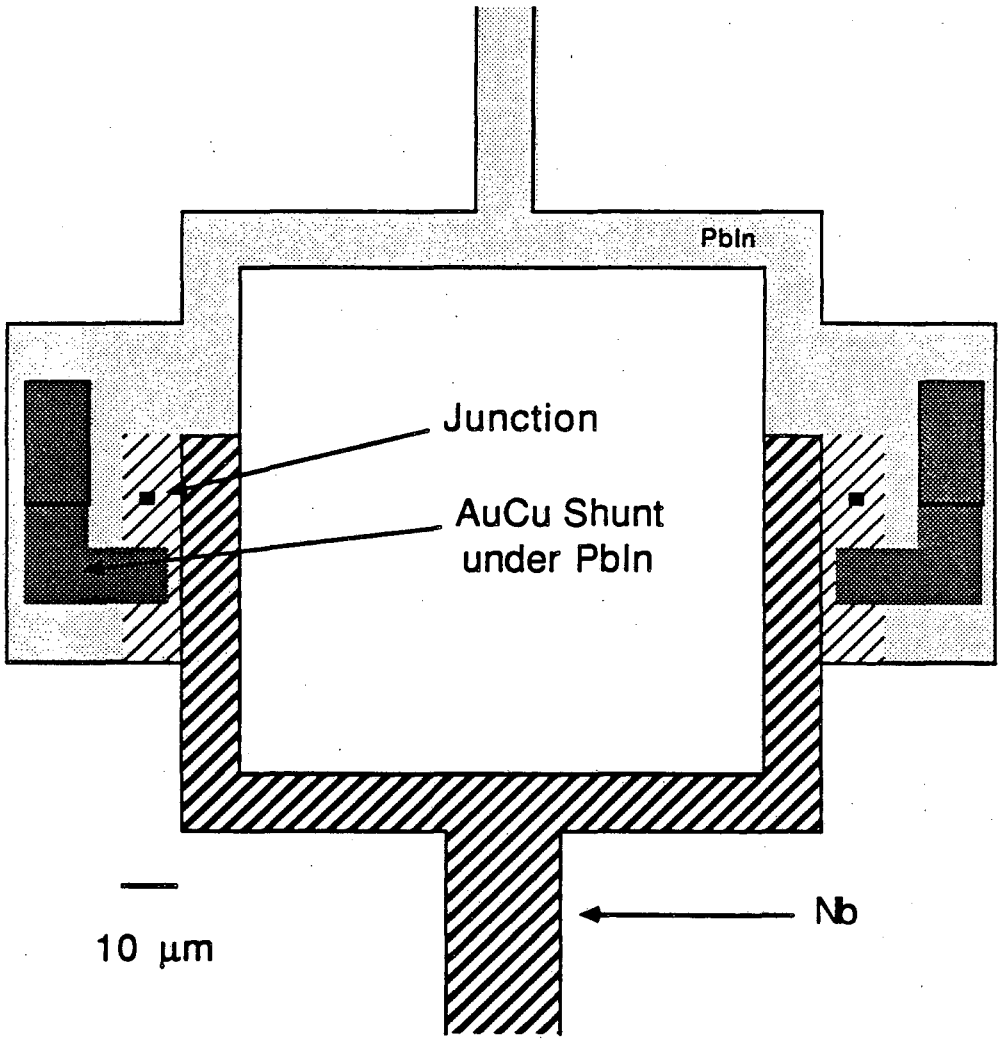

Fig. 1.12 Schematic of a Type I dc SQUID.

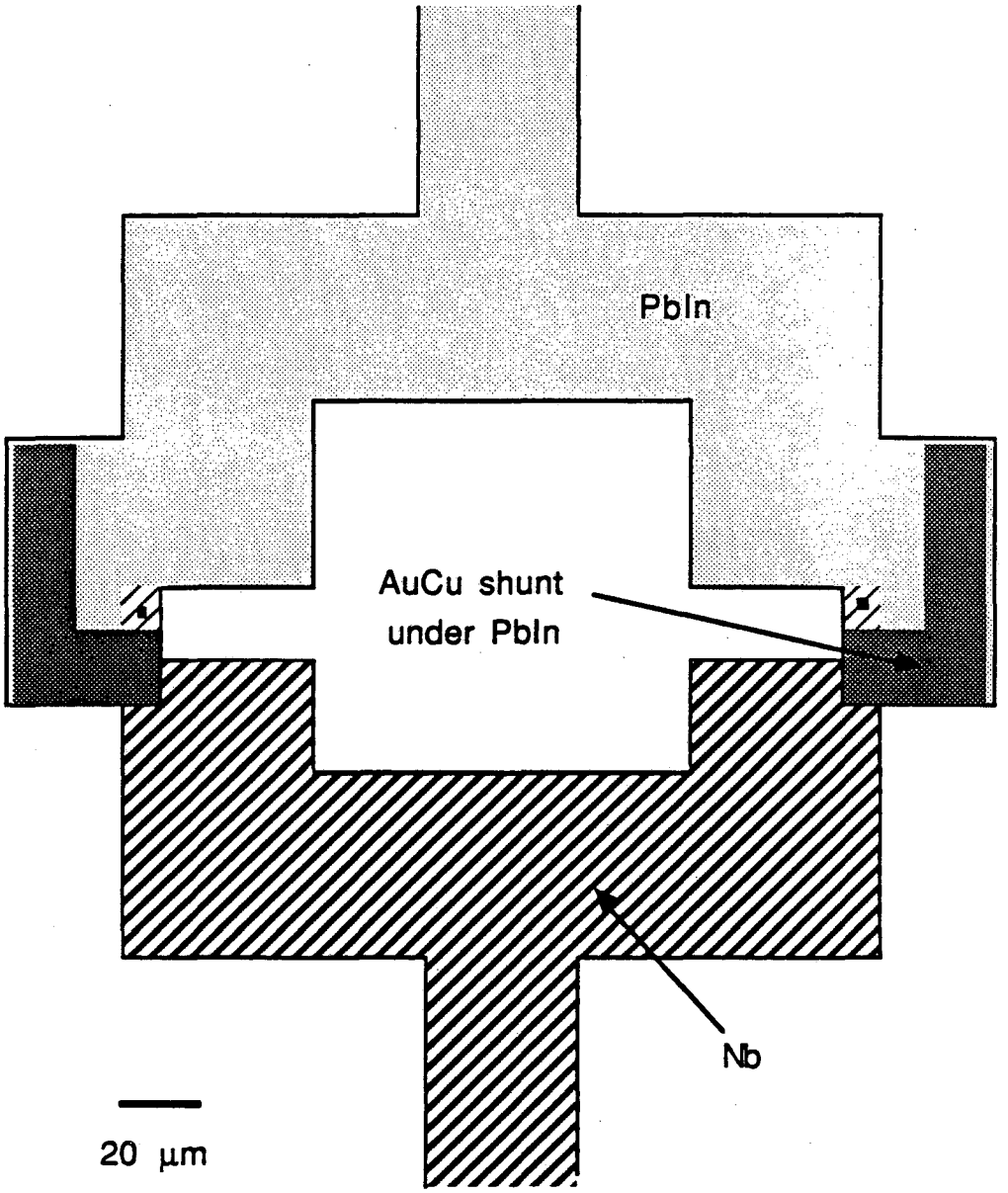

Fig. 1.13 Schematic of a Type J dc SQUID.

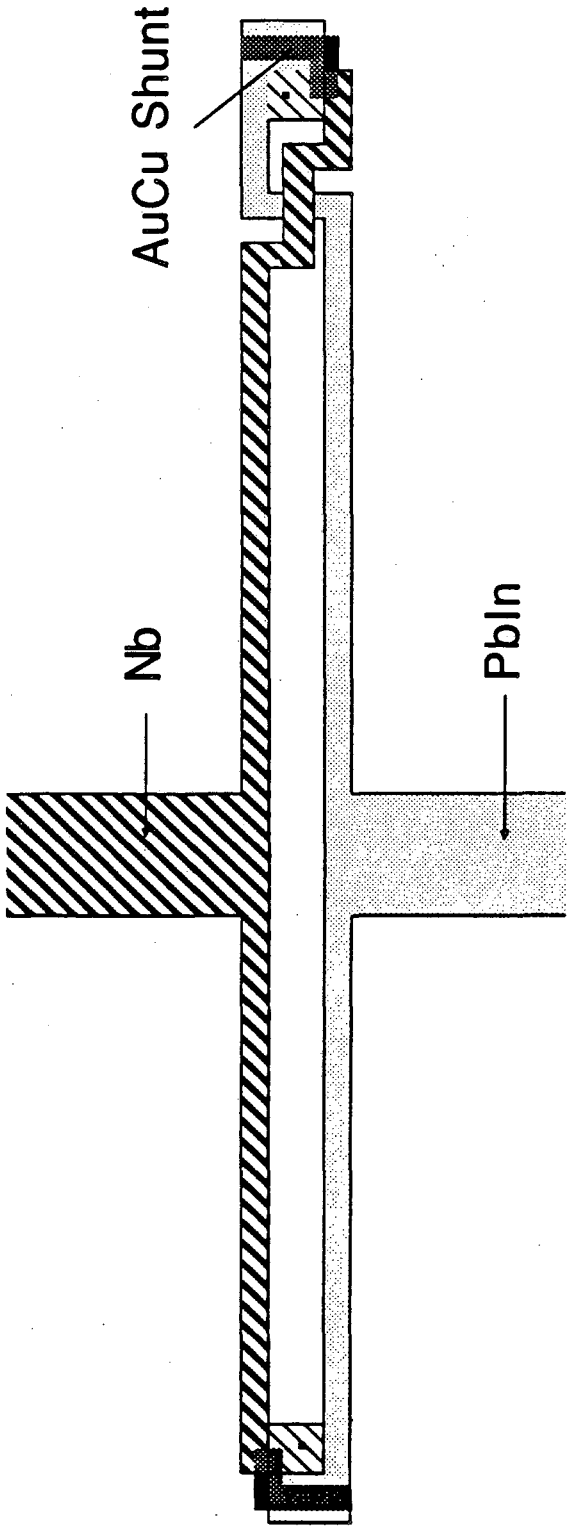

Fig. 1.14 Schematic of a Type K dc SQUID.

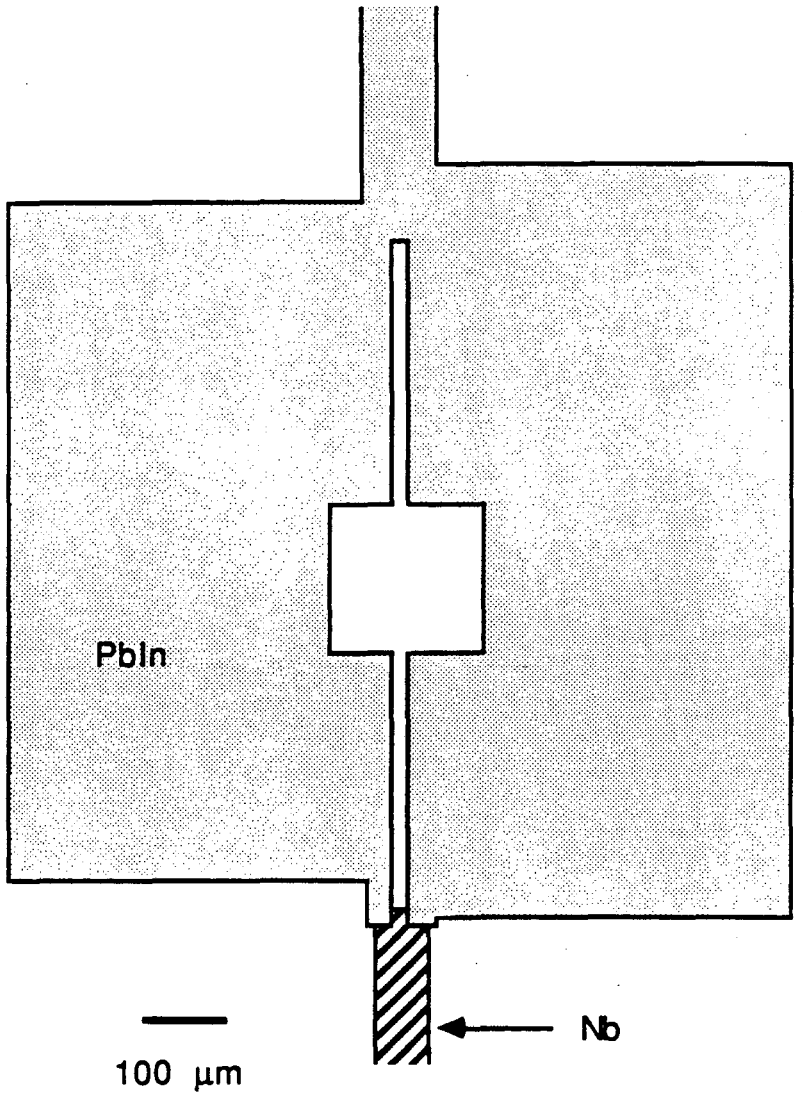

Fig. 1.15 Schematic of a Type L dc SQUID.

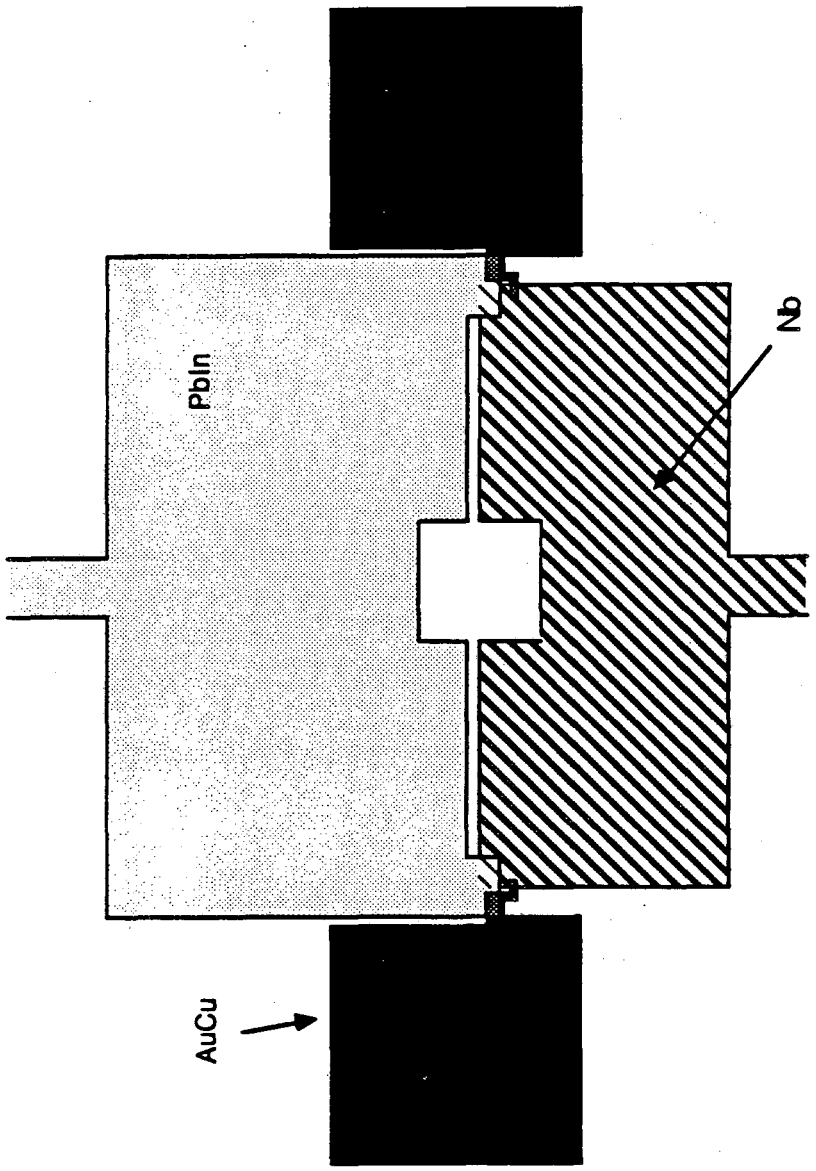

Fig. 1.16 Schematic of a Type M dc SQUID.

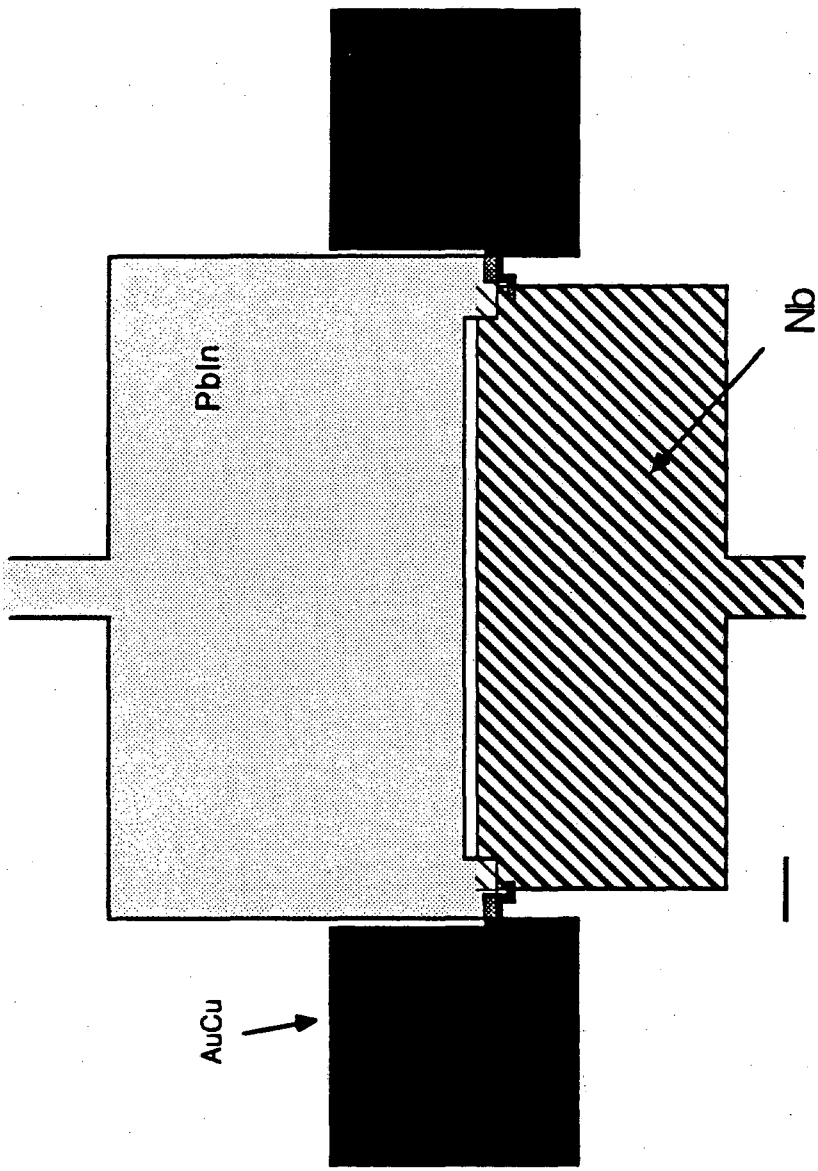

Fig. 1.17 Schematic of a Type N dc SQUID.

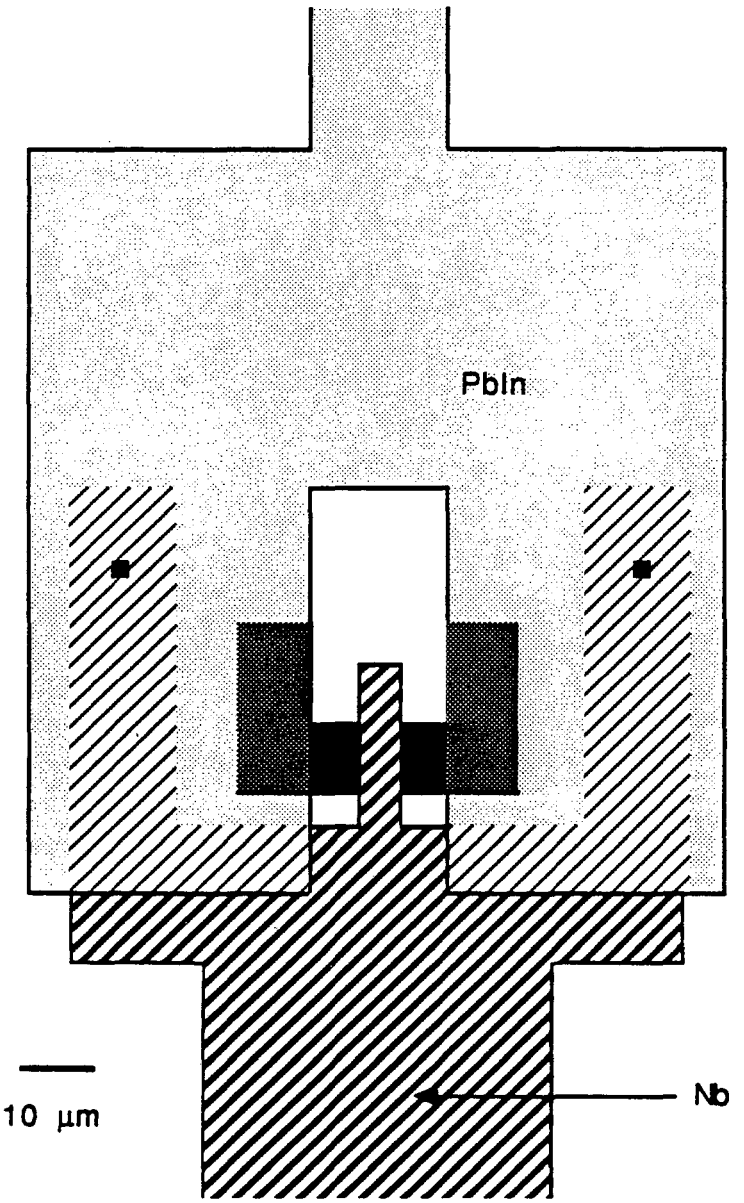

Fig. 1.18 Schematic of a Type O dc SQUID.

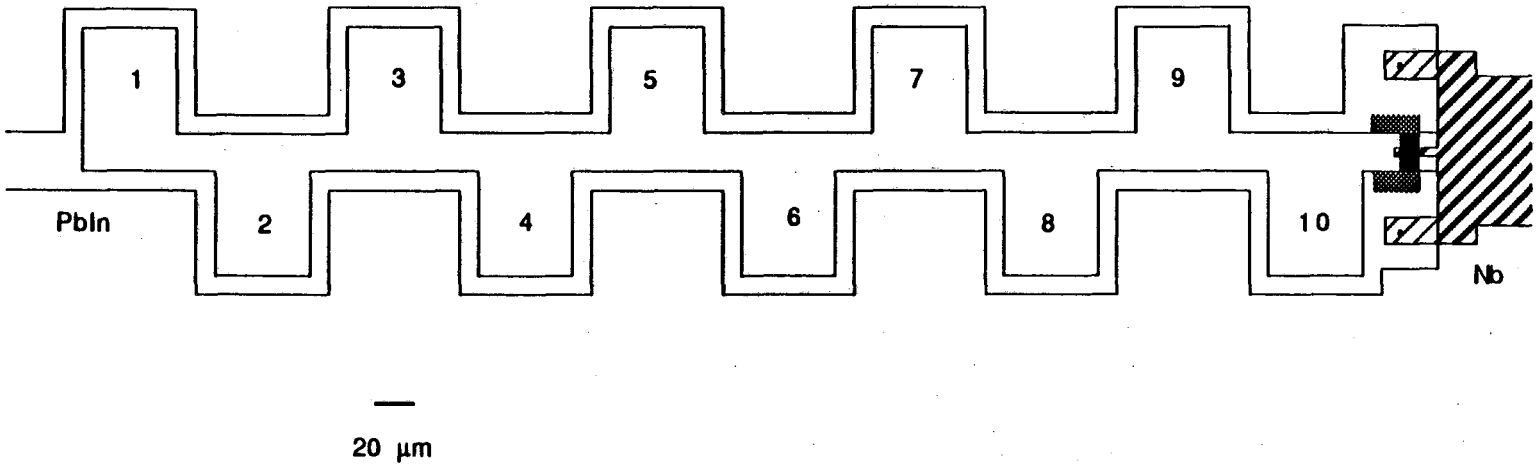

Fig. 1.19 Schematic of a Type P dc SQUID. Numbers label the 10 small loops which make up the single SQUID loop.

were designed so that they could be efficiently coupled to a many turn, thin-film, spiral input coil.

Reverse or Pb SQUIDs: Types: B, C, E, G, H, I, P. These SQUIDs have the SQUID body made out of Pb or PbIn instead of Nb. The materials have thus been interchanged or reversed, compared to the old style SQUIDs. These devices come in a large range of shapes and sizes.

Split SQUIDs: Types: D, M, N, J, K. These devices have bodies which are made from roughly equal amounts of Nb and PbIn, and have their junctions and shunts separated by the body diameter of the SQUID.

References

(1) J. M. Martinis and J. Clarke, "Measurements of Current Noise in the dc SQUID", IEEE Trans. Magn. Mag-19, 446 (1983).

(2) C. Hilbert and J. Clarke, "Input Impedance of an Amplifier Based on a dc Superconducting QUantum Interference Device", Appl. Phys. Lett. 45, 799 (1984).

(3) F.C. Wellstood, C. Heiden, and J. Clarke, "Integrated dc SQUID Magnetometer with a High Slew Rate", Rev. Sci. Instrum. 55, 952, (1984).

(4) The term "mushroom technology" is an unofficial, but highly descripitive, name which comes from the resembalance of the small photoresist dots to mushrooms when viewed under an SEM. See for example: J.H. Greiner, C.J. Kercher, S.P. Klepner, S.K. Lahiri, A.J. Warnecke, S. Basavaich, E.T. Yen, J.M. Baker, P.R. Brosious, H.-C.W. Huang, M. Murakami, I. Ames, "Fabrication Processes for Josephson Integrated Circuits", IBM J. Res. Devlp., 24, 195 (1980).

(5) B. Savo, F.C. Wellstood, J. Clarke, "Low Frequency Excess Noise in

Nb-Al_2O_3-Nb Josephson Tunnel Junctions", Appl. Phys. Lett., 50, 1757 (1987).

(6) Peirces RBS-35 Detergent Concentrate, Peirce Chemical Co., Rockford, Ill..

(7) Shipley Chemical Co., Inc., Newton, Mass..

(8) Discussions of microbalances and other thin-film techniques and properties can be found in: L.I. Maissel and R. Glang, "Handbook of Thin-film Technology", McGraw-Hill, New York (1983 reissue).

(9) Sloan Technology Corporation, Santa Barbara, California.

(10) Ion Tech, Inc., Fort Collins, Colorado.

(11) M.B. Ketchen and J.M. Jaycox, "Ultra-low-noise Tunnel Junction SQUID with a Tightly Coupled Planar Input Coil", Appl. Phys. Lett. 40, 736 (1982).

Chapter 2: Experimental Arrangements and Measurement Procedures

2.1 Introduction

The design of cryogenic equipment[1-3] is most strongly influenced by the unique and difficult environment in which the cold part of the equipment resides. The production of temperatures below 1 Kelvin is in itself a major undertaking. For continuous operation below 300 mK, one must use a dilution refrigerator.[4-5] Presently, this necessitates an elaborate system of pumps, pipes, valves, gauges, filters, thermometers, and a fair amount of patience on the part of the operator.

The use of low noise dc SQUIDs necessitates additional measures. Magnetic and RF shielding must be used to prevent interference from the outside world. The SQUIDs require electrical wiring for bias currents and outputs. This wiring must be low-pass filtered to prevent room temperature and external noise from reaching the SQUID. Because normal portions of the circuit will dissipate heat and insulators have very poor thermal conductivity at 20 mK,[3] one must use low powers, and thermally ground all heated elements. In these low temperature experiments, the thermal grounding is broadly accomplished by bathing the elements in superfluid ^{4}He.

At low temperatures, the noise in a dc SQUID becomes very small. In order to measure this noise, one needs a very sensitive amplifier. This is most simply accomplished by using a second dc SQUID to amplify the noise in the first. In fact this is not an ideal arrangement. The measured SQUID has a relatively high output impedance, which increases as T decreases, whereas the measuring SQUID is best matched to a low

impedance. In addition the measuring SQUID's gain and output impedance will vary with the temperature. By placing the measuring SQUID in a flux-locked feedback loop, the measuring system becomes largely independent of the properties of the measuring SQUID. The difficulty is then to achieve low noise operation over a useful bandwidth. Details of the measuring feedback electronics and its performance are covered in Chapter 3. In the following sections, I will discuss in turn the various components in the measuring system and the measurement techniques used to take the low temperature data.

2.2 The Refrigerator

The dilution refrigerator was an Oxford Instruments Limited, Model 75 Dilution Unit.[6] The base temperature of the refrigerator is about 18 mK, and the effective cooling power is about 1 μW at 30 mK with a circulation rate of about 60 μmoles/sec. The refrigerator is mounted on a 1 K Cu pot and insert which were designed by Steve Diamond, Michel Devoret, and John Martinis (see Fig. 2.1). Both the 1 K pot and the insert were constructed by the Physics Department Machine Shop. The heat exchanger, mixing chamber, and cell are surrounded by a Cu and brass thermal radiation shield which is clamped to the refrigerator still. The space available for the cell is approximately cylindrical, with a height of 13 cm, and a diameter of about 7.5 cm, and is limited by the size of the radiation shield. The temperatures of the pot, still, heat exchanger, and mixing chamber are measured by means of carbon resistors. The temperature of the pot, still, and mixing chamber can be changed by applying power to resistive heaters. The temperature of the pot can also

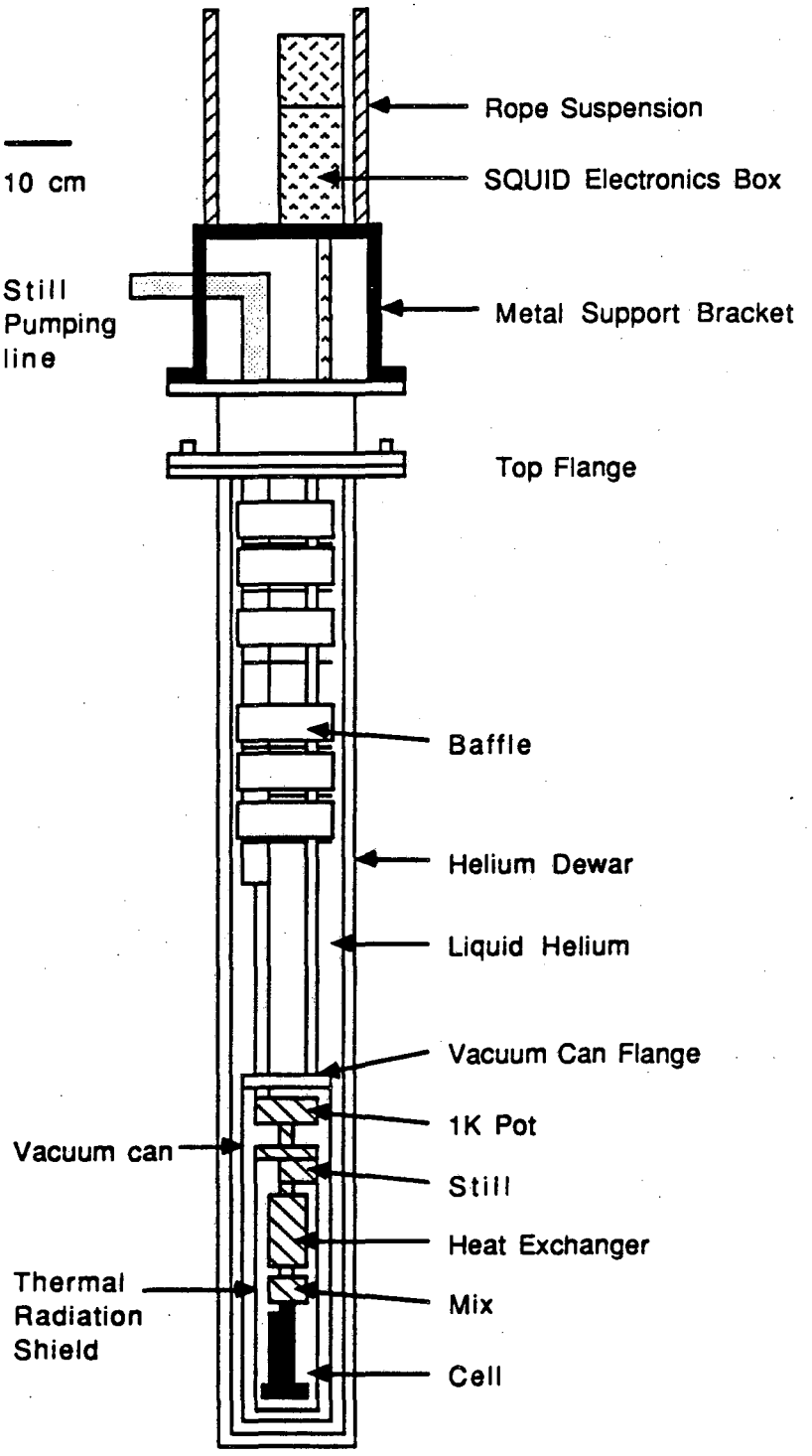

Fig. 2.1 Configuration of the dewar, refrigerator, and cell.

be regulated by changing the pumping speed or ^{4}He intake from the bath. The temperature of the refrigerator can also be changed by altering the circulation rate. For stable operation at temperatures above the mixing chamber's base temperature, the mixing chamber heating is provided by an analog feedback system which monitors the temperature and adjusts the power accordingly.

2.3 The Cell

As far as this thesis work is concerned, the most important piece of the low temperature apparatus is the experimental chamber which holds the SQUID. The configuration of this "cell" is shown in Fig. 2.2. The main purpose of the cell is to hold the measured SQUID, SQUID(1), in good thermal contact with the refrigerator and shield it from external noise, while simultaneously allowing the measuring SQUID, SQUID(2), to measure its noise and gain.

SQUID(2) is also placed in the cell, and is cooled along with SQUID(1). This was done for two reasons. First of all, it greatly simplifies the wiring of the system and the checking of its operation. Secondly, it greatly reduces problems of shielding, interference, and thermal drift to have both SQUIDs together and at the same temperature inside of a single shield. In principle, the cooling of the measuring SQUID(2) would also allow for more sensitive measurements to be made. In fact though, the present measuring system is limited mainly by the room temperature preamplifier, and additional cooling below 4.2 K results in only modest improvements in the sensitivity.

The cell is constructed of three main pieces, an inner mount and

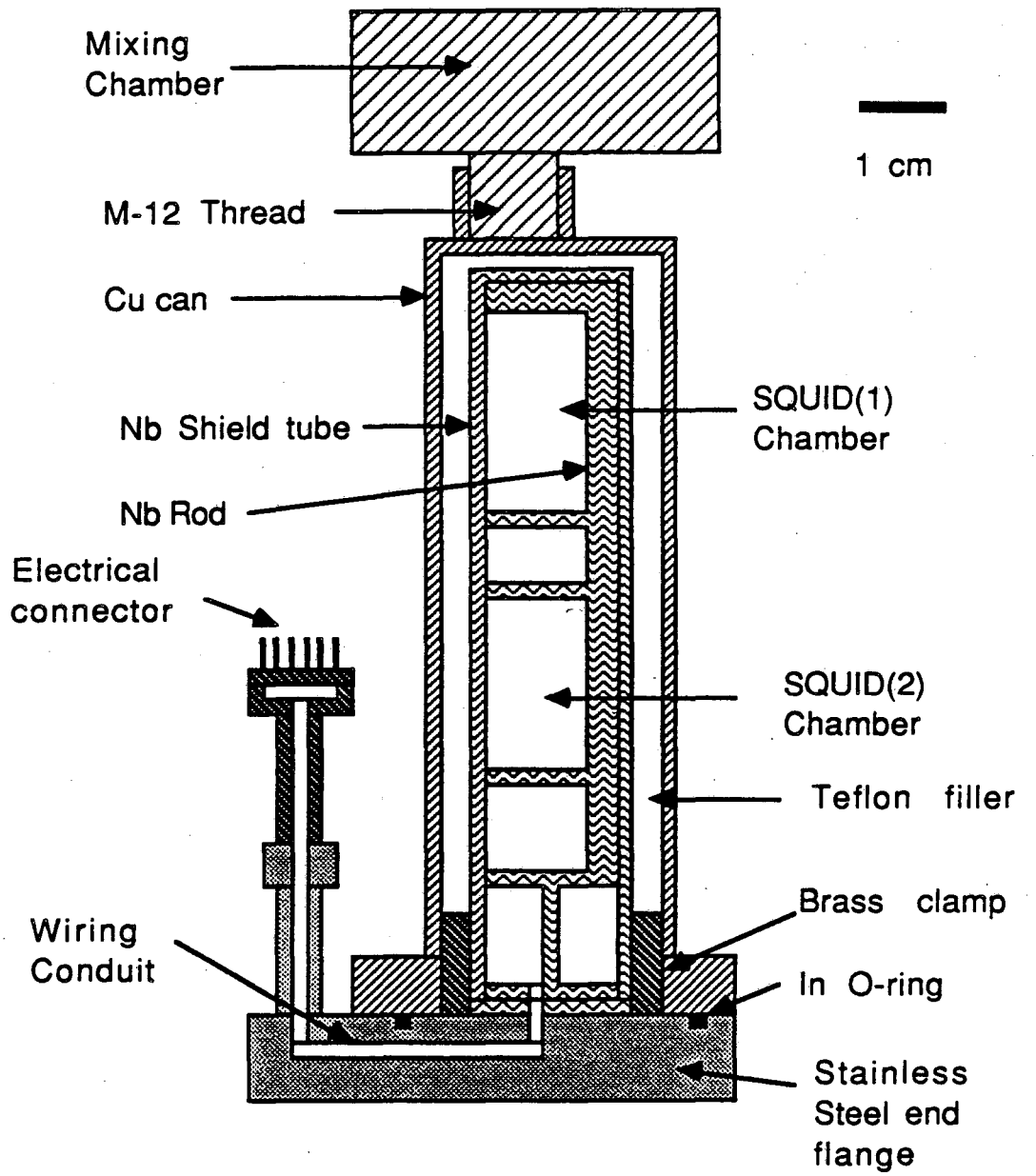

Fig. 2.2 Configuration of the experimetal cell, showing the two SQUID chambers and electrical feedthroughs.

shield, an outer steel base flange, and an outer cell vacuum can. The shield consists of a superconducting Nb tube which is open at one end. The inner mount supports the two SQUIDs and their wiring. The mount consists of a Nb support rod which has had slots cut in it (see Fig. 2.3). The slots accept fiberglass or phenolic canvas blocks which serve as the mounting stages for the SQUIDs and wiring. The Nb support rod also serves to magnetically isolate the two SQUIDs from each other and from the magnetic flux generated by each others bias currents. The end of the Nb rod is bolted to the base flange, and serves as a superconducting endcap for the shield tube. A simple brass clamp is used to grasp the shield tube and hold it firmly against the base flange and endcap.

The cell vacuum can serves three purposes. First of all, the can seals in the liquid ^{4}He that is used as the cooling fluid in the cell. The base flange and can are bolted together and the interface sealed with an In O-ring to make a superfluid leaktight joint. Secondly, the can is made of OFHC Cu to provide a good thermal connection between the mixing chamber and the ^{4}He in the cell. This connection is formed by a Cu M-12 screw on the mixing chamber, and a matching M-12 threaded hole in the Cu of the vacuum can. This connection also serves to mechanically hold the cell in place. Finally, the vacuum can serves as a normal metal electrical and magnetic shield. The relatively thick (2.5 mm) walls have a high electrical conductance, and produce good magnetic shielding down to frequencies of order a few Hz. At high frequencies, the can and flange form a closed RF shield which is broken only by the connectors for the wiring (which are not RF shielded).

The base flange serves several purposes. The wiring for the two

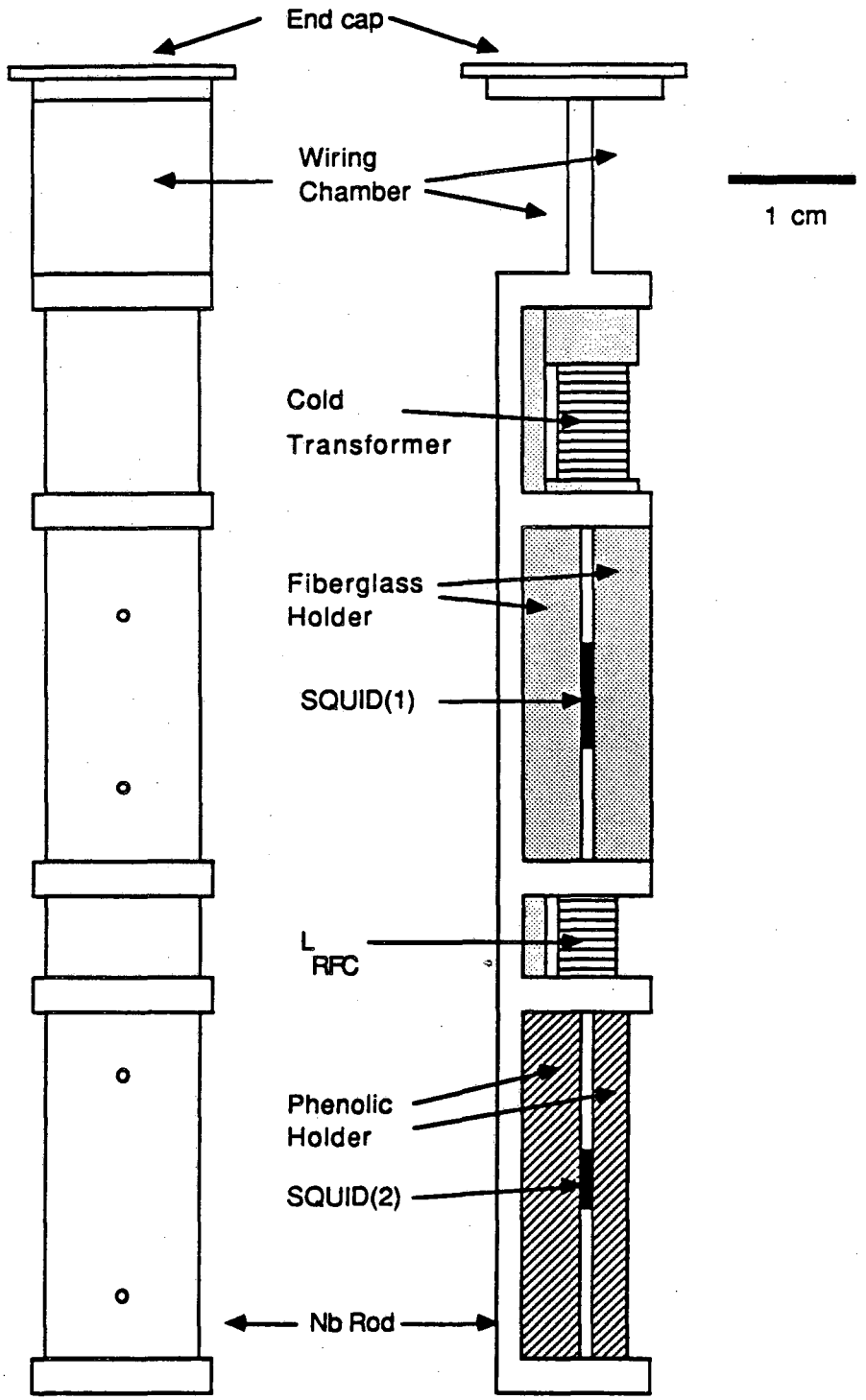

Fig. 2.3 Configuration of the SQUID holder and SQUID mounts.

SQUIDs is brought out through the base flange. Upon leaving the mount, the wires enter a protective teflon sleeve and pass through a tube in the flange which reemerges on the upper side of the flange some distance from the vacuum can. The connection from the flange to the outside world is made via two superfluid leaktight connectors.[7] The connectors are mounted on thin brass sleaves which are hard-soldered to small stainless steel tubes (see Fig. 2.2). The tubes are welded to the flange at the point where the wiring emerges from the top side. The entire arrangement is superfluid leaktight. This procedure was used to allow easy soft soldering of the connectors to the brass peices. The brass peices were made to be thin so that they would flex in response to a strain, thus enabling the joint to survive repeated cooling and warming.

An important secondary feature of the cell is that it can be readily removed from the refrigerator. This allows the cell to be tested in a separate system. A special insert and a second set of feedback electronics was built especially for this purpose. The insert fits into a standard 4 inch inside diameter glass ^{4}He dewar, which can be pumped on to get to about 1.2 K. Before every run on the refrigerator, the cell is ordinarily tested at 4.2 K. The time and expense for a refrigerator run are sufficiently great that such a check is very worthwhile, as many simple SQUID and wiring problems can be quickly found and corrected. The 4.2 K insert also allows us to perfect or try different measuring schemes and test the SQUID operation in a well-known regime. This was extremely useful in the initial phases of the experiment, and also provides us with an important cross-check on the behavior of the system in the refrigerator.

2.4 The Helium Fill Line

During normal operation of the refrigerator, the cell is filled with superfluid ^{4}He. This is done to provide thermal contact to all of the cell contents. Solid to ^{4}He thermal contact is notoriously poor,[3] but for the small power levels we will use (typically several pW to the SQUIDs, up to several tens of nW in some of the normal metal wiring) it is more than adequate.

When the cell is warm, the ^{4}He is stored in a keg which is connected to the cell gas handling system. This system is completely separate from the refrigerator's own gas handling system. ^{4}He can enter and exit the cell via the ^{4}He fill line. For safety's sake, it is important that the fill line does not become plugged while the cell is full of liquid ^{4}He. Such plugging could easily occur if air or some other impurity froze in the cold portion of the fill line. We have adopted several measures to prevent such an occurrence. First of all, the cell gas handling system, cell, and fill line are all evacuated by means of a diffusion pump which has a liquid nitrogen cooled cold trap before admitting ^{4}He. Secondly, before the gas can enter the fill line, it must pass through a liquid nitrogen cooled charcoal cold trap in the cell gas handling sytem. This trap should remove all impurity gases except H_2. Thirdly, the fill line includes a relatively large diameter Cu-Ni tubing wound in a spiral in the 4.2 K bath surrounding the refrigerator. This section acts as a filter and safely freezes out any small amount of impurity before it enters into the smaller diameter fill line below. Fourthly, the ^{4}He is maintained at an over-atmospheric pressure, typically 25 to 16 psi absolute. Should a small leak open to air, the ^{4}He will leak out of the

line rather than air into the line. Finally, if all else fails, a thin Cu diaphragm has been soft soldered to an opening in the cell flange. Should the fill line plug, and the cell warm up, the diaphragm would burst at an overpressure of about 10 atmoshperes, thereby preventing more serious damage to the cell and refrigerator.

Superfluid ^{4}He is a very good thermal conductor from about 0.7 K to the λ-point, 2.14 K.[3] Because the refrigerator has a very small cooling power, it is also important that the fill line be very well thermally grounded before reaching the cell. The thermal conductance of the fill line can be reduced by making the fill line long and thin. We have used Cu-Ni capillary with a 100μm inside diameter and a 375 μm outside diameter. It is divided into 5 sections: 4.2 K flange to the pot (15 cm), pot to the still (18 cm), still to the heat exchanger (71 cm), heat exchanger to the mix (61 cm). From the mix to the cell a large diameter capillary about 20 cm long is used; there is no harm because the ^{4}He is already as cold as it will get. The lengths from the 4.2 K flange to the pot and from the pot to the still are rather short, but the pot and still have a large cooling power, so the additional load is not of great consequence. It is important that the ^{4}He be cooled as it progresses to the cell, as this will lessen the heat load on the mix. At the end of each capillary section (at the pot, the still, the heat exchangers, and the mix), the fill line is joined to a heat exchanger. The exchangers are made from sintered Cu powder which has been compressed inside a Cu block. The sinter presents a large surface area to the ^{4}He fluid and allows the fluid to cool to the temperature of the cold point. The blocks are bolted to the various cold points, and the fill line capillary is soldered to it, forming a superfluid leaktight

seal.

The small diameter and long length of the capillary means that it takes a long time to evacuate the cell at room temperature. There is also a relatively slow recovery of ^4He upon warming the system. Consequently, it is important to keep the dead volume in the cell as small as possible. Unused portions of the cell interior have accordingly been filled with fiberglass or teflon where possible. The total dead volume of the cell is of order 10 cm^3.

2.5 Thermometry

Carbon resistors are used to monitor the temperatures of the 1 K pot, the plate, the still, and the mixing chamber.[8] These are only roughly calibrated, and are used only for diagnostics on the operation of the refrigerator. The main thermometers for the experiment are bolted to a Cu sleeve, which is clamped to the outside of the cell. During a typical run, a carbon resistor thermometer and a doped Ge thermometer are used. The carbon resistors are subject to drift arising from thermal strain, and must be periodically calibrated. The Ge thermometers are stable, but are subject to breakage. Both types of thermometers depend upon thermally activated variable range hopping, and the conductance versus temperature dependence is nontrivial.[9] The original thermometers were calibrated by Professor N.E. Phillips' group. The original carbon resistor was manufactured by Speer[8] and had a room temperature resistance of about 200 Ω. It failed after about 2 years (presumably from stress during thermal cycling) and was replaced by an uncalibrated Matsushita carbon resistor[10], which also had a room

temperature resistance of about 200 Ω. The resistor was prepared by A. Cleland in the form of a thin section of the original resistor which was then clamped between two Cu blocks to ensure good thermal contact.[8] The Ge thermometer was labeled 8185, and was the C-50 type manufactured by Cryo Cal [11]. The Matsushita was calibrated against the Ge 8185 resistor.

As a check on the calibration of the above thermometers, and an additional Ge thermometer, I have used the noise thermometry technique, which is described in Chapter 10. Essentially, there is always a third thermometer in the cell. This is the small bias resistor R_X, which is shown in Fig. 2.4. When SQUID(1) is not biased, this resistor puts Nyquist current noise into the input circuit. This is readily measured by SQUID(2), and its value scales directly with the temperature of the ^{4}He in the cell. This thermometer also provides a test of whether the inside of the cell is as cold as the outside.

During some of the experiments, an additional Neutron Transmutaion Doped (NTD) Ge thermistor was attached to the sleave. This thermometer was part of Professor Sadoulet's project on NTD bolometric particle detectors, and was operated by Ning Wang.[12] It provided a sensitive check on the thermal stability of the refrigerator, as well as another temperature reading on the outside of the cell.

2.6 Cooling the Cell

Before beginning a refrigerator run, the operation of the SQUIDs is tested at 4.2 K on the test insert. The cell is ordinarily run with a broken O-ring in the test insert, in order to bring the SQUIDs into

contact with the ^{4}He bath. Once the devices are found to be working correctly, the cell is warmed up to room temperature. The In O-ring on the cell is replaced to ensure that no ^{4}He will leak out of the cell when it is on the refrigerator. The carbon and Ge thermometers are then attached to the cell. They are bolted onto a 1 mm thick Cu sleave which is clamped to the cylindrical outside surface of the cell vacuum can.

After the cell thermometers are attached, the cell is screwed to the mixing chamber of the refrigerator, and the ^{4}He fill line is soft soldered to the cell. The cell is then evacuated through the fill line. Because the fill line is long and narrow and is constricted by four sintered heat exchangers, removing air from the cell is a very slow process. The pumping begins with a mechanical pump, and, after an hour, proceeds with a liquid nitrogen trapped oil diffusion pump. The total pumpdown time is ordinarily greater than 4 hours, after which time the cell pressure has probably been reduced to less than 3 mm. For pumping times shorter than about three hours, the cell fill line frequently becomes plugged after subsequent cooling to 4.2 K.

While the cell is being evacuated at room temperature, the refrigerator wiring and thermometry are tested for continuity and shorts. The wiring is then plugged into the cell. Wiring which goes to the cell is fastened against the outside of the cell using nylon thread or insulated Cu wire. The radiation shield is then attached, and the system inspected visually for mechanical contacts between the cell or wiring and the radiation shield. The refrigerator vacuum can is then bolted to the vacuum flange, and the vacuum space surrounding the cell and refigerator is pumped out to 0.8 mTorr or less. Once the cell and refrigerator vacuum can have been evacuated, a helium leak detector is

attached to the refrigerator vacuum can pumping system. The cell is then pressurized to about 25 psi with He and the vacuum can is checked for room temperature He leaks. The sensitivity is typically about $\pm$ 1 X 10^{-9} cc/sec STP.

Assuming that no leaks are found, the vacuum space is filled with about 500 mTorr of H_2 which will serve as a thermal exchange gas for the cooling to 4.2 K. (H_2 solidifies at 14 K). The dewar for the refrigerator is filled with liquid nitrogen, and raised into position around the refrigerator insert. The refrigerator is then allowed to cool overnight to 77 K.

The following morning, the thermometers are checked to verify that the refrigerator is at 77 K. The nitrogen is then removed and two concentric μ-metal shields are placed around the dewar, centered on the refrigerator. ^{4}He gas is bled through the dewar for 15 to 20 minutes to remove traces of nitrogen remaining in the dewar. This lessens the chance of plugging the He liquid input to the 1 K pot, and should reduce the amount of frozen nitrogen in the ^{4}He bath. ^{4}He liquid and cold gas is then very slowly transferred into the dewar. The temperature of the refrigerator and the pressure of the hydrogen exchange gas are monitored carefully as the slow transfer proceeds. If the transfer is too fast, the exchange gas will freeze out and leave the refrigerator uncooled. On the otherhand, if the transfer is done carefully, after about two hours the refigerator can be brought to 14 K before the exchange gas freezes out. Once the exchange gas is frozen out, the transfer resumes at normal speed, and the dewar is rapidly filled. The needle valve for the liquid ^{4}He input to the 1 K pot is then opened and the 1 K pot is pumped to about 2 mm of pressure. This brings the pot to a temperature of about

1.5 K. Circulation of the ^3He-^4He mixture for the refrigerator then begins, and after about 1 hour, the entire refrigerator and cell have cooled to about 1.5 K. Once the cell has cooled below 4 K, it starts to fill with liquid ^4He through the cell fill line, and this generally takes about 1/2 hour. Subsequent operation of the refrigerator is standard, with the mixture condensing in the refrigerator in about 2 hours, the mixture undergoing phase seperation in another hour. The refrigerator typically stabilizes at 25 mK after an additional 8 hours. After four or five days the refigerator will reach the base temperature of about 18 mK. The long time constant appears to be associated with the cooling of the plastics, teflon, or epoxy in the SQUID cell.

2.7 Magnetic and RF Shielding

The high sensitivity of the dc SQUID to magnetic fields means that the device must be carefully isolated from magnetic noise from the outside world. The shielding adopted here was built from several layers. The first layer of shielding is due to the laboratory (B231 Birge) being located approximately 8 meters below ground in the second basement of a steel and reinforced concrete building. This provides considerable attenuation of radio and other large manmade RF signals, and an ordinary battery powered radio will not detect any stations.

Unfortunately, a radio which is operated in the lab is not completely quiet. One can easily hear bursts of RF from the numerous experiments being operated in the vicinity. Most of this noise seems to be associated with the operation of pulsed laser systems. In addition, the laboratory is permeated with audio frequency magnetic fields. The

biggest audio culprits are: the ubiquitous 60 Hz powerline noise and its harmonics, cathode ray tubes, and computers or other digital devices which are placed in non-shielding cases. All of these sources can be readily detected with a small handheld magnetic pickup and amplifier.

The attenuation of the numerous laboratory sources is accomplished mainly by enclosing the refrigerator dewar and SQUID electronics in a copper mesh screened room. The room is roughly 2.5m X 2.5m X 2.5m with #20 gauge Cu mesh formed from three foot wide panels which are soldered together at the edges. During data taking, the entrance to the room is sealed by a Cu mesh door which is held closed against the mesh of the screen room wall by means of four clamps. The screening action becomes ineffective below several hundred Hz, and above frequencies of about 100 MHz, where one starts to find resonant cavity modes. The operation of the screened room can be tested qualitatively by merely opening the door, and more quantitatively by placing a magnetic pickup inside of the screened room, and watching the output on an oscilloscope.

The next layer of shielding is accomplished by two concentric μ-metal shields. The shields rest on a stand centered on the cell, and surround the refrigerator dewar. They are in the form of cylinders with both ends open. The larger of the μ-metal shields is 76.5 cm in height, and 38 cm in diameter, with a wall thickness of 1.58 mm. The smaller inner shield is 50 cm in height, 25 cm in diameter, and 1.2 mm in thickness. Together, the two shields should provide an attenuation of about 10^{-4} in applied low frequency magnetic fields. The two shields should also provide a similar attenuation of the static field of the Earth [14]. Direct measurements show that the static field is less than 20 mG.

The next layer of shielding is accomplished by the metal dewar, which surrounds the refrigerator, and its mating metal top flange. This shield is broken by the rubber O-ring used to seal the top flange to the dewar, and by the numerous wires entering the top. It is therefore probably not very effective at high frequencies.

The next layer of shielding includes the closed stainless steel vacuum chamber for the refigerator, and the Cu thermal radiation shield which surrounds the cell and mix. The next layer of shielding is formed by the Cu cell walls, as noted above, and the last layer of shielding is formed by the superconducting Nb shield tube. SQUID(1) is placed at the far, closed end of the tube where the attenuation of all external fluctuating fields is a maximum. SQUID(2) is located about 1/3 of the way from the open end of the shield tube.

Wiring going into the screened room can also carry external noise (generally RF) into the room. This is handled by only using grounded BNC for SQUID wiring, and, where possible, using low pass RF filters at the screened room. During a measurement, all 60 Hz powerlines are disconnected from the inside of the screened room. The thermometry wiring for the refrigerator is all passed through low pass (100 kHz knee) filters at the wall of the screened room. The measuring feedback electronics box for SQUID(2) is located in a RF shielded box at the top of the refrigerator insert. It draws its power from a box of automobile batteries also located in the screened room. Its only output, the feedback voltage, exits the screened room on an unfiltered line, but is buffered in the feedback box. The flux bias for SQUID(1) is low pass filtered (100 kHz knee) at the wall of the screened room, and is also passed through RC filters in the dewar and the cell. The filtering of

the SQUID(1) current bias is done at 4.2 K, using a combination of RC and μ-wave filters, and in the cell, using a simple RL network as will be discussed below. The operation of the shielding for the SQUID(1) lines can be tested simply by moving their small battery supplies into the screened room, so that they do not make connection to the outside.

2.8 The SQUID Measuring Circuit - Construction

The dc SQUID circuit used to measure the noise in a second dc SQUID is shown in Fig. 2.4. SQUID(1) is the measured SQUID, while SQUID(2) is the measuring SQUID. The current source I_{b1} is constructed from mercury cell batteries and RC filters, as is shown in Fig. 2.5. The construction of the current source $I_{\phi 1}$ is similar. The feedback coil for SQUID(2), labelled M_f in Fig. 2.4, is hand wound from 10 turns of 4 mil Nb wire and placed into a 0.125 inch hole 50 mil below the SQUID. The inductor L_{RFC} is 20 turns of 3 mil Nb wire wound on a 0.5 cm fiberglass form. The small resistor R_x is formed from a 25 μm diameter piece of manganin wire roughly 0.5 cm long. The wire is spot welded to the Nb wire which forms the rest of the input circuit, and its ends are soldered to the Cu wires which supply the bias current.

2.9 Circuit Operation

The operation of the SQUID measuring system is somewhat unusual because one SQUID is used to measure another, and because of the use of a voltage bias on the measured SQUID. The arrangement is shown in Fig.

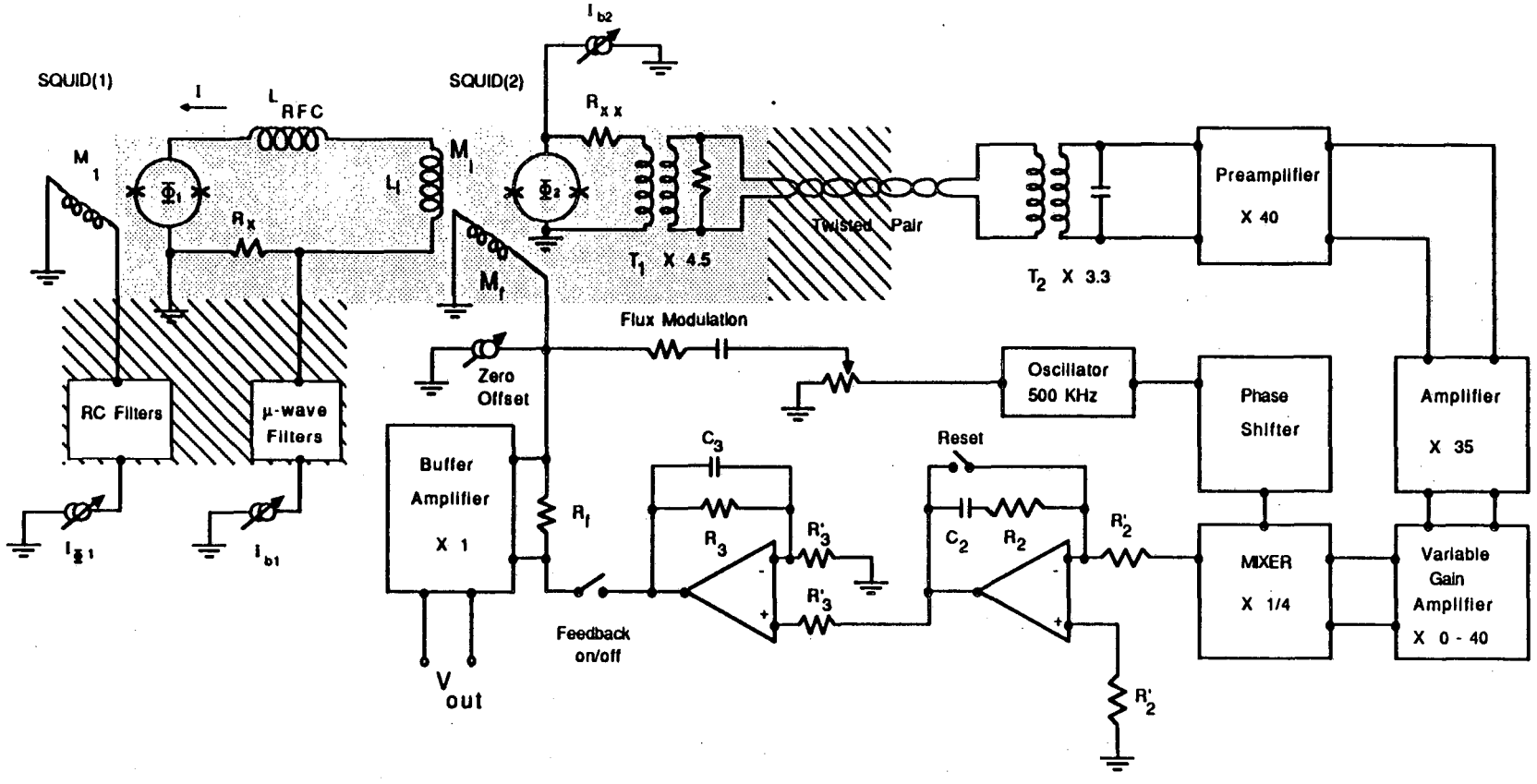

Fig. 2.4 Electrical arrangements for the SQUID measuring system and feedback electronics.

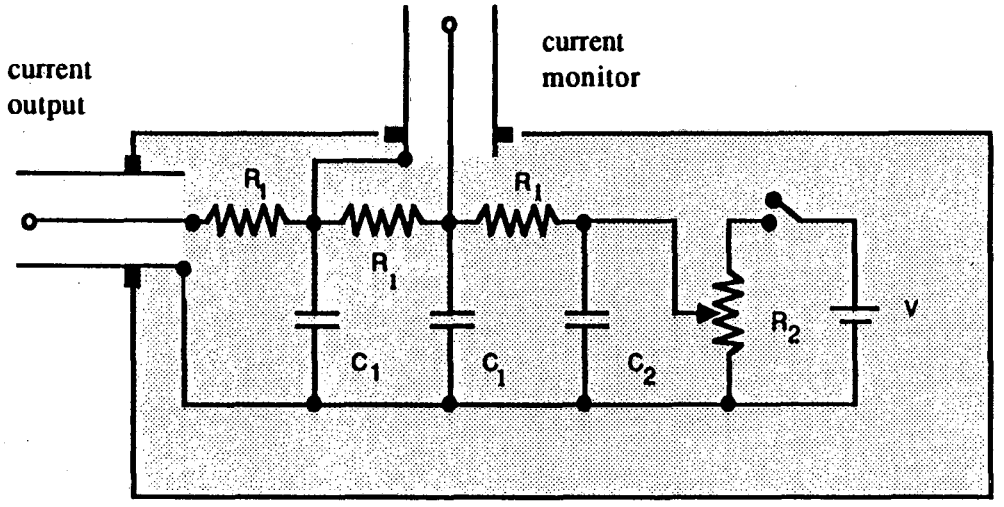

Fig. 2.5 Construction of the SQUID(1) current and flux bias sources. R_1 =10kΩ , V=16.4 Volts, C_1=20μF, C_2=100μF, R_2= 0 to 50KΩ potentiometer.

2.4. Both SQUIDs were held at approximately constant voltage (at low frequencies) by means of resistors R_x and R_{xx} (which had resistances which were much less than the SQUID shunt resistance R). Because the voltage is fixed, a change in the flux in SQUID(1) will produce a change in the current I passing through SQUID(1). This change in current will produce a change in the flux in SQUID(2) via the spiral input coil L_i. SQUID(2) is maintained in a flux locked loop by room temperature feedback electronics, the operation of which is described in detail in Chapter 3. The feedback electronics produces an output voltage V_o which is directly proportional to the flux applied to SQUID(2). Since this flux is linearly related to the current I in SQUID(1), it can be seen that the output of the feedback loop is directly proportional to the current passing through SQUID(1).

The input circuit also acts to filter out high frequency noise coming down the I_{b1} leads. When SQUID(1) is biased at a non-zero voltage, it gives its arm of the input circuit a much higher resistance than R_x. Noise which may be present on I_{b1} is thus shunted through R_x rather than through SQUID(1). The 12 μH inductor L_{RFC} aids in this filtration at high frequencies. Similarly, high frequency noise from SQUID(1) is prevented from reaching the SQUID(2) input coil by L_{RFC}. With a typical SQUID(1) impedance of 8 Ω, all frequencies below about 250 KHz are passed, which leaves a wide measurement bandwidth.

2.10 Data Taking

The purpose of the data taking is to characterize the noise, gain and operating characteristics of the measured SQUID as a function of the

operating point and temperature. The above arrangement permits the taking of such data on a single SQUID per refrigerator cooldown. As the data taking time is rather long (typically 1-2 weeks) there is little advantage in measuring more than one SQUID at a time. Data are generally taken at a sequence of temperatures between 4.2 K and 20 mK. In addition to noise measurements, there are several quantities which are measured to provide information about SQUID(1), to find the system calibration, and to check the system operation. I now discuss the technique used for each type of measurement in turn.

2.10a Calibration of the Feedback Loop

The voltage output, V_o, from the feedback electronics is proportional to the flux, Φ, applied to SQUID(2). This proportionality constant, $\partial V_o/\partial \Phi$, is just M_f/R_f, where M_f is the feedback coil mutual inductance with the SQUID, and R_f is the feedback resistance (see Fig. 2.4). It can be measured using one of two techniques. One technique is to break the feedback loop and feed a known amount of current down the feedback coil. By watching the output of the preamplifer, one can see the gain of SQUID(2) get larger and smaller as the flux goes from, say, 0 to $\Phi_o/2$. One can thereby judge the amount of current it takes to put one flux quantum into the SQUID. The loop can then be relocked. If an identical amount of current is now fed to the feedback coil, the output voltage of the loop will change by an amount corresponding to one flux quantum. This procedure is tedious to perform in practice, and does not allow for very accurate measurement because of drift and the difficulty of ascertaining when exactly one flux quantum has passed.

I have, however, developed another way to find the calibration. It is very quick and accurate, and I now use it almost exclusively. The technique is somewhat interesting in its own right as it is makes use of the behavior of feedback and the periodicity of the SQUID characteristics in Φ_0. Suppose that SQUID(2) is in feedback, and no external current is being sent to the feedback coil. The output voltage of the feedback loop will be some voltage, say V_A, which we can suppose is zero volts without any loss of generality. I now supply some external current, $-\Delta I_f$, to the feedback coil. This would ordinarily put some flux into SQUID(2), but since the system is in a flux-locked loop, the feedback electronics will send down exactly the same amount of current, but of opposite sign, to cancel out the applied flux. The voltage output of the electronics will then be $V_B = V_A + \Delta I_f R_f$, corresponding to the current supplied by the feedback, see Fig. 2.6. If the feedback loop is now broken and reset one finds that the voltage output of the SQUID(2) can change. If ΔI_f is small, so that there is less than 1/2 a flux quantum introduced into SQUID(2), then upon reset, the device returns to the original Voltage V_B. If however, more than 1/2 a flux quantum is applied, the voltage will not be the same, but rather will jump to some new value V_B', with a voltage difference $\Delta V_0 = V_B - V_B'$. If a large flux Φ is applied to SQUID(2), when the feedback loop is reset, the electronics will send down only enough current to bring the flux in SQUID(2) to $N\Phi_0$, where N is the integer closest to Φ/Φ_0. Thus in Fig. 2.6, increasing the flux from point A to D increases the voltage from V_A to V_D, and upon reset, the voltage jumps by $2\Delta V_0$ to V_D'. The voltage jumps are thus quantized, with the step difference, ΔV_0, corresponding to the number of volts it takes to generate one flux quantum. By putting down different

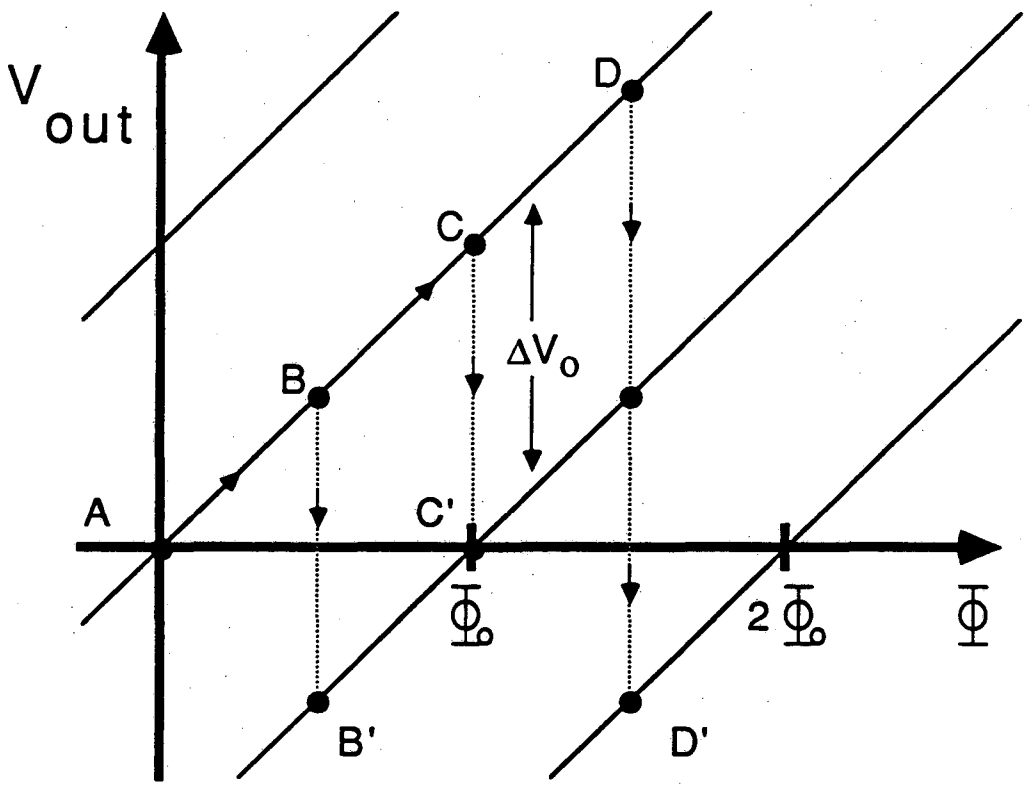

Fig. 2.6 Output voltage vs. applied flux for the feedback electronics, the function is multivalued.

amounts of flux, one can readily gauge the step size. In practice, I generally put down a current corresponding to something in the neighborhood of one flux quantum. I then record the voltage, reset the feedback loop, and again record the voltage. The voltage difference then corresponds to one flux quantum, with an accuracy limited by the accuracy of the voltmeter, and one has the flux to output voltage conversion.

2.10b Calibration of the Current Passing Through the SQUID

The output of the feedback electronics is a voltage. From the above section we can calculate how much flux this corresponds to in SQUID(2). Sending a current I through the SQUID input coil will induce a flux $I \cdot M_i$ in the SQUID(2), conversely, if we know M_i we can calulate the current I from the output voltage. The determination of M_i can be done in two ways. First of all, M_i is determined by the fixed geometry of the measuring SQUID and its input coil, and is a constant for all SQUIDs of its type. It can be measured directly in a bare SQUID by watching the I-V characteristic of the SQUID as a known amount of current is fed to the input coil. Modulation through one or more flux quantum can be readily measured, and the total flux is thus known and can be divided by the applied current to find the mutual inductance. When SQUID(1) is hooked into the circuit of Figure 2.5, the measurement can be made in the following manner. When the SQUID(1) is biased with less than the critical current, the SQUID(1) and input coil arm of the input circuit is superconducting. All of the current (provided that it is less than the critical current of SQUID(1)) then will go through the input coil.

In practice then, one feeds down a small known amount of current, I_{b1}, and measures the change in the feedback output voltage. From the feedback calibration, this corresponds to a known amount of flux, and so the mutual inductance can be calculated. The presence of resistance in the SQUID(1) arm of the circuit would cause some of the current to pass through R_X, and one would underestimate the mutual inductance. Since the mutual inductance is fixed, and is generally well-known from independent measurements, this is a good check for excess resistance in the SQUID(1) arm of the circuit.

2.10c Calibration of R_x

In order to know the bias voltage across SQUID(1), it is necessary to know the value or R_X. This can be measured in two ways. The first technique is to turn SQUID(1) off, the resistor R_X generates a Nyquist noise current in the input circuit:

$$S_I = 4k_BTR_X[R_X^2 + \omega^2(L_{RFC} + L_i)]^{-1}$$

This generates a noise flux in the input coil which is readily measured by SQUID(2). With an R_X of about 0.1 Ω, and an L of 12 μH, this produces a Lorentzian noise spectrum with a roll-off of about 1 kHz. To find R_X then, the temperature of the refrigerator is fixed at some known level T. One then measures the spectrum of the noise at the feedback output, and extracts the level of the Lorentzian noise from R_X. This is then converted into an equivalent current noise in the input circuit. The resistance R_X can then be calculated directly from Nyquist's formula.

The second technique is performed with SQUID(1) on. A Microwave generator is attached capacitively to the I_{b1} line, and μ-wave power

sent down at some frequncy f. The microwaves will generate a Josephson current step on the current-vs-voltage (I-V) characteristic at a voltage V = hf/2e, where e is the charge of an electron, and h is Planck's constant. An I-V is then taken (see below) and the step's location is found in terms of the current I_{b1} and the feedback output voltage V_{out}. The microwave frequency is then changed by a small amount Δf, and the voltage at which the step appears will change by an amount $\Delta V = h\Delta f/2e$. A second I-V is then taken, and the position of the new step is found, say $I_{b1} + \Delta I_{b1}$, and $V_{out} + \Delta V_{out}$. The resistance R_x can then be shown to be:

$$R_x = \frac{\Delta V}{\left[\Delta I_{b1} - \frac{M_f \Delta V_o}{M_i R_f} \right]}$$

2.10d The Current vs. Voltage Characteristics

One important and informative characteristic of a SQUID is its current vs voltage trace (I-V) for fixed applied magnetic flux. This can be readily obtained to a high resolution by using the above circuit. The experimental arrangement is shown in Fig. 2.7. The flux in SQUID(1) is first fixed by fixing current $I_{\phi 1}$. The bias current I_{b1} is then swept from zero to some maximum while the ouput voltage of the feedback loop is monitored. The level of current I_{b1} is monitored by measuring the voltage across a series 10 kΩ resistor in the bias box. This output is used to drive the x-axis of an x-y recorder, while the voltage from the feedback electronics is used to drive the y-axis. Once the SQUID comes out of the zero voltage state, to a good approximation, the voltage

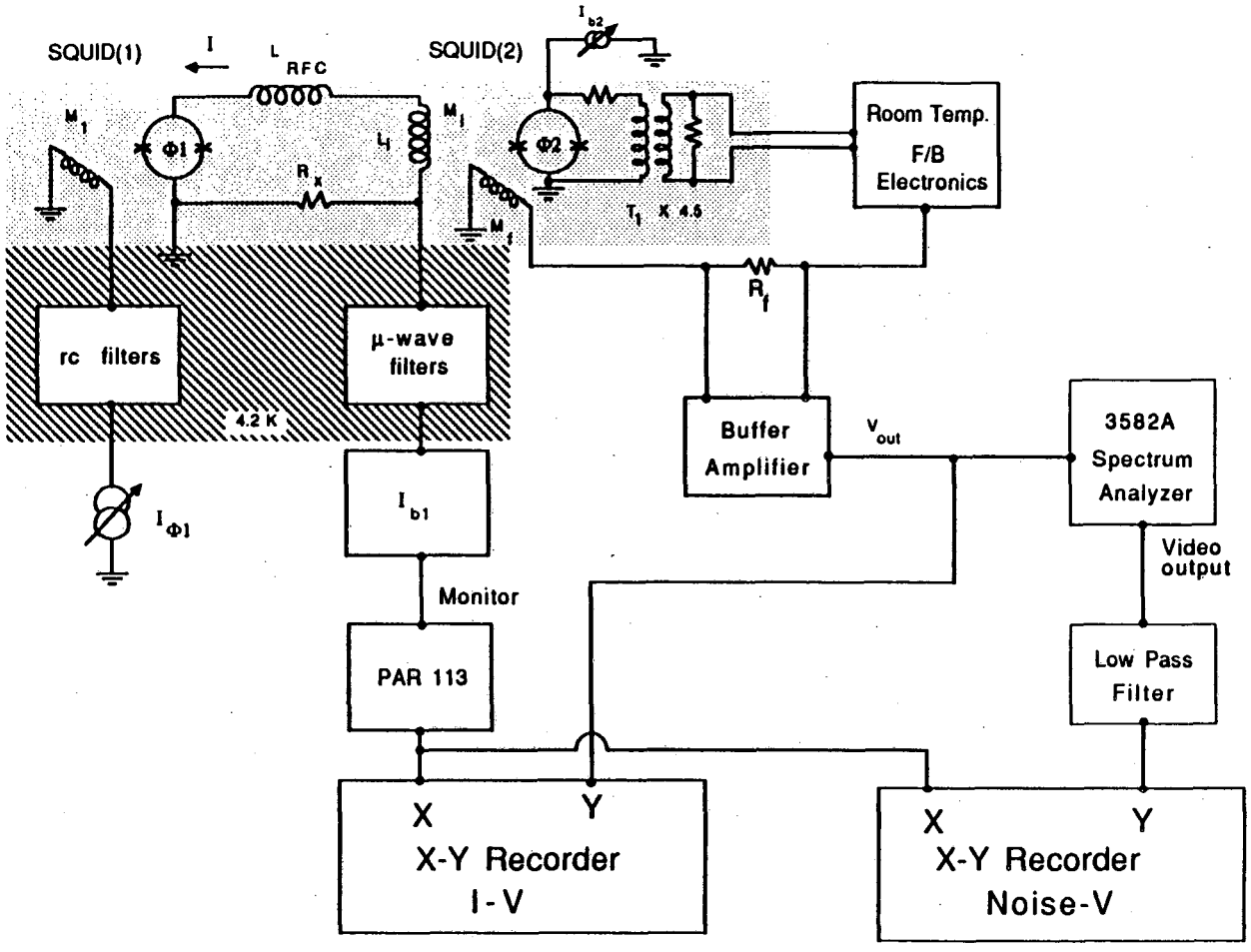

Fig. 2.7 Schematic of the experimental arrangement for measuring I-V and Noise-V maps. The light gray area is cooled by the dilution refrigerator. The darker shaded area is in the 4.2 K He bath. All other components are at room temperature.

across the SQUID is linearly related to I_{b1}. Similarly, the output of the feedback electronics is linearly related to the current passing through the SQUID. Together then, the trace forms the current-voltage characteristic. I generally measure curves for Φ = 0, $\Phi_0/4$, $\Phi_0/2$, and $3\Phi_0/4$, and for V from zero to 20 μV.

I wanted to remark briefly on an important, and occasionally confusing, convention that I will frequently use. I will generally call the flux at which a SQUID passes the maximum amount of current zero applied flux, or possibly Φ_0. Of course since the SQUID characteristic is periodic in the flux, there is no way to know whether this is really zero flux, it could be any $N\Phi_0$, where N is an integer. When the operating flux of a SQUID is given, it should thus be understood in the sense of modulo Φ_0. For asymmetrical SQUIDs (see Chapter 4), there is a second complication, the maximum current through the SQUID will not occur at $\Phi = N\Phi_0$, but rather at some non-integral Φ/Φ_0. Similarly, the minimum current will not occur at $\Phi_0/2$. In such cases, I will still adhere to the convention of calling the flux of maximum current Φ_0, and the flux of minimum current $\Phi_0/2$.

2.10e The Current vs Flux Characteristics

Another important characteristic of the SQUID is a plot of the current through the SQUID versus the applied flux (I-Φ), for fixed bias voltage. This is obtained in a manner very similar to that for the I-V. The bias voltage across SQUID(1) is first fixed by fixing I_{b1} (in fact, the voltage across the SQUID will vary slightly, as the flux is changed, because the voltage bias is not held perfectly fixed by R_x, but this is

a small effect, of order $R_X/R_D \lesssim 1\%$). The flux in SQUID(1) is swept by varying $I_{\Phi 1}$, and the amount of current is measured by monitoring the voltage across a series 10 kΩ resistor in the current supply. The voltage across the resistor is used to drive the x-axis of an x-y recorder and the output voltage of the feedback loop is used to drive the y-axis.

The resulting plot forms the I-Φ characteristic. The calibration of the flux axis is trivial and self-checking. The SQUID characteristics are periodic in the flux quantum, one need only find the distance between successive current maxima or minima to determine the amount of current $I_{\Phi 1}$ needed to generate one flux quantum in SQUID(1). The slope of the curve at a given flux is then the flux gain $\partial I/\partial \Phi$ at the point for SQUID(1).

2.10f Noise vs. Voltage Maps

It is also possible to measure the noise from SQUID(1) as a function of the bias voltage (N-V). This is generally done simultaneously with the I-V plot, see Fig. 2.7. The resulting noise plot is used to find the noisy and quiet portions of the I-V for later study, and together with the I-V, forms a kind of map of the SQUID. To take the noise map, the bias flux is first fixed, and the bias current is swept by hand. The bias current is monitored in the usual way, and drives the x-axis of an x-y recorder. The output from the feedback electronics is then sent to a Hewlett-Packard 3585A spectrum analyzer. The analyzer is operated as a narrow band (typically about 300 Hz) rms noise detector about a single frequency (typically in the range of 10 to 20 kHz). An analog output of

the noise level is sent through a 0.15 Hz low pass filter, the ouput of which is then used to drive the y-axis of the x-y recorder. The resulting plot is proportional to the current noise, S_I, flowing through SQUID(1) as a function of the voltage.

2.10g Noise vs. Flux Maps

It is also possible to obtain the noise as a function of the bias flux (N-Φ). This is ordinarily done simultaneously with the I-Φ map, using the same technique to measure the noise as was done for the noise versus voltage plot. Examples of I-V, I-Φ, N-V, and N-Φ maps are presented in Chapter 4.

2.10h Flux Noise Spectra

The I-V, I-Φ, N-V, and N-Φ maps are used to locate quiet areas for further study. Most of the remaining data which are taken are in the form of noise spectra. The measurement system is shown schematically in Fig. 2.8. We first fix $I_{\Phi 1}$, which sets the flux in SQUID(1), and I_{b1} which fixes the voltage across SQUID(1). The output from the feedback electronics is then sent through a Princeton Applied Research (PAR) 113 amplifier (low frequency roll-off set at 0.03 Hz), which is generally followed by a low pass Krohn-Hite filter. The output of the filter is sent to a Hewlett-Packard 3582A spectrum analyzer, which fourier transforms the voltage as a function of time and power averages to produce the noise power spectral density. For each bias point, four overlapping spectra are taken from 0.1 to 25.5 Hz, 1 to 255 Hz, 10 to

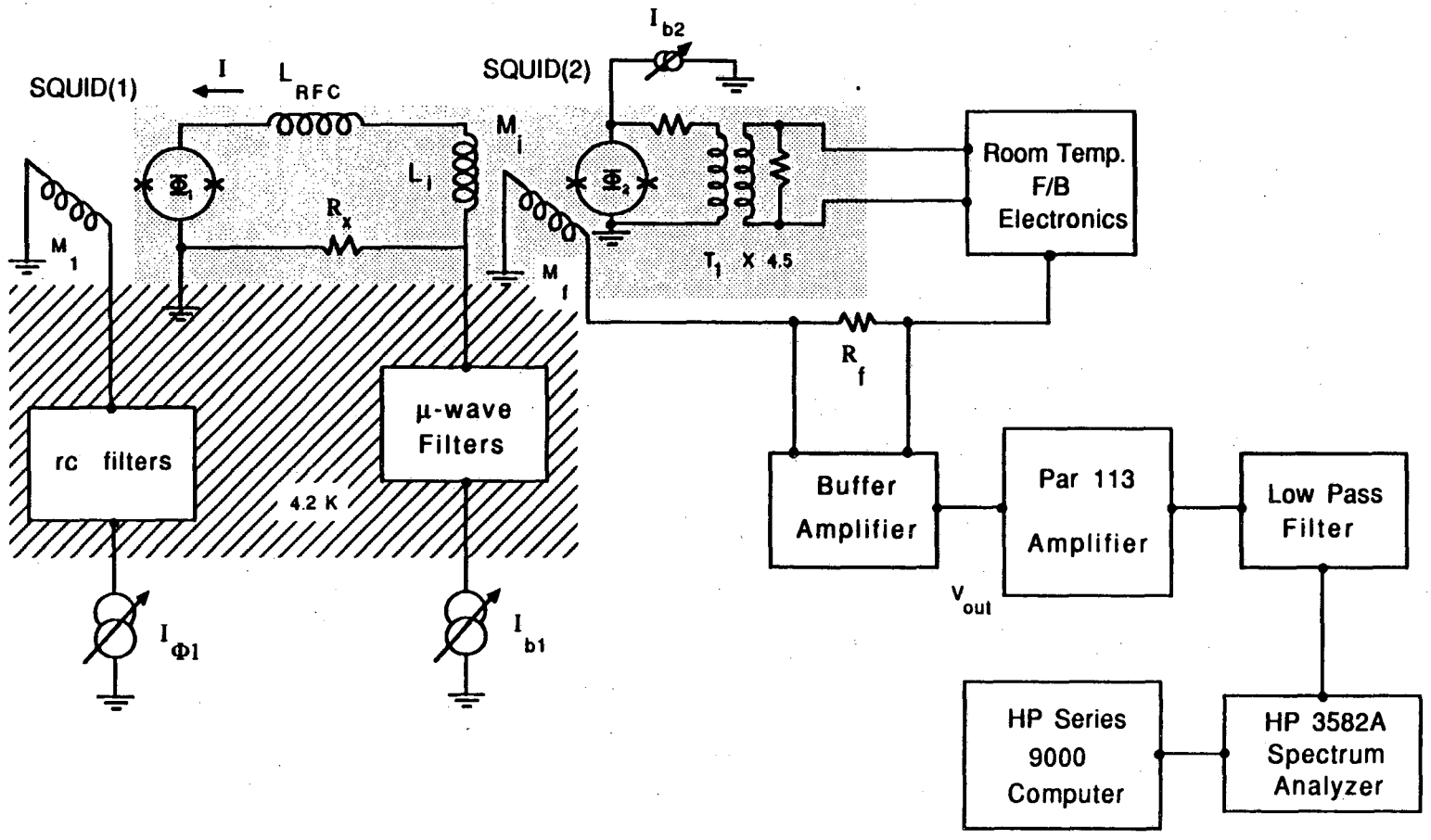

Fig. 2.8 Schematic of the experimental arrangement for measuring noise spectra.

2550 Hz, and 100 to 25500 Hz. Each spectra contains the rms voltage noise spectral density at 256 uniformly spaced frequencies. The spectra are generally averaged for 256 scans, the slowest scan is the 0.1 to 25.5 Hz which takes about 40 min to complete. I have occasionally taken scans from 0.04 to 10 Hz, and from 0.01 to 2.5 Hz, but do so only infrequently because of the large averaging time required. From the calibration of the flux gain, $\partial I/\partial \Phi$, the noise spectrum can be converted into an equivalent flux noise spectrum in SQUID(1). The spectra are transferred to an HP series 9000 microcomputer and are stored on discs, along with the temperature and other measurement details, for later analysis. Noise spectra are generally taken at voltages where the noise properties look good from the maps. Spectra are then usually taken at flux of 0, $\Phi_0/4$, $\Phi_0/2$, and $3\Phi_0/4$. In addition, at each temperature a spectrum is generally taken with SQUID(1) off. This serves as a background check and is also used to do noise thermometry on R_X (see Chapter 10). Examples of noise spectra can be found in Chapter 8.

References

(1) For general information about cryogenic design, the interested reader can consult this and the following two references. G.K. White, "Experimental Techniques in Low Temperature Physics", Clarendon Press, Oxford, (1979).

(2) A.C. Rose-Innes, "Low Temperature Techniques", English Univ. Press, London (1964).

(3) O.V. Lounassma, "Experimental Principles and Techniques Below 1K", Academic Press Inc., New York (1974).

(4) D.S. Betts, "Helium Isotope Refrigeration", Contemp. Phys. 9, 97 (1968).

(5) J.C. Wheatly, O.E. Vilches, and W.R. Abel, "Principles and Methods of Dilution Refrigeration", Physics 4, 1 (1968).

(6) Oxford Instruments North America, Inc., Bedford, Mass.

(7) BTI, San Diego, California.

(8) The resistors on the pot, still, heat exchangers, and mix, were provided by Oxford, and were manufactured by Speer Electronic Components, Bedford, Penn. 16701. The company has since gone out of buisness. The carbon thermometer on the experimental cell was obtained directly from Speer.

(9) B.I. Shklovskii, A.L. Efros, "Electronic Properties of Doped Semiconductors", Springer-Verlag, New York (1984).

(10) Matsushita Electronics Components Co., Osaka, Japan.

(11) Cryo Cal, Inc., St. Paul, Mn.

(12) N. Wang, B. Sadoulet, T. Shutt, J. Beeman, E.E. Haller, A. Lange, I. Park, R. Ross, C. Stanton, and H. Steiner, "A 20 mK Temperature Sensor", presented at IEEE Nuclear Symposium, San Francisco, 1987, to be publ. in IEEE.

(13) A simple system can be purchased from Radio Shack for about $10. Radio Shack is a Division of Tandy Corp., Fort Worth, Texas.

(14) S.M. Freake, and T.L. Thorp, "Shielding of Low Magnetic Fields with Multiple Cylindrical Shells", Rev. Sci. Instrum., 42, 1411 (1971).

CHAPTER 3: The Feedback Electronics, and the Operation of an Integrated dc SQUID Magnetometer[1]

3.1 INTRODUCTION

For a number of years Professor Clarke's group was involved with using cylindrical[2] dc SQUIDs as magnetometers for geophysical measurements.[3] The SQUID was flux modulated at 100 kHz and was operated in a flux-locked loop, the output of which was proportional to the applied magnetic field. These devices were highly reliable,[3] and their sensitivity, typically 10 fT $Hz^{-0.5}$, at frequencies above about 10^{-2} Hz, was more than adequate. However, the slew rate of these SQUID measurement systems was limited by the associated room temperature electronics to about 10^5 Φ_0/sec. Since the area of the SQUID is about 7 mm^2 , a magnetic field of about 0.3 nT is required to generate one flux quantum and the corresponding maximum slew rate of the applied magnetic field is about 30 $\mu T\ s^{-1}$.

This slew rate is adequate for many applications. However, when the system is operated in the field occasional atmospheric electrical actitvity can cause the feedback loop to unlock. These electrical events, called "sferics" or "atmospherics", are usually the result of distant lightning storm activity which is propagated around the Earth through multiple reflections off of the ionosphere and the ground.[4] In addition there is always the possibilty of manmade noise from radio stations, electrical machines, and automobiles. Fortunately, geophysical magnetic measurements have generally been made in quite remote locations where the dominant activity appears to be of natural origin. The

fluctuations are typically 1 nT in magnitude and extend up to frequencies of 10 kHz, typically producing a rate of field change of 100 μT s^{-1}. The occurrence of these large events can vary from once a day to once every few minutes, depending on the level of atmospheric electrical activity. Since geophysical measurements may be required at frequencies as low as 1 mHz,[3] the system may not be useful if unlocking occurs more often than once every hour. One simple way to overcome this difficulty is to attenuate the high frequency components of the sferics by placing a copper cylinder around the SQUID to act as a low pass filter. However, as discussed in Ref. 2, Nyquist noise in the shield limited the sensitvity above 1 Hz to about 100 fT $Hz^{-1/2}$. This loss of sensitvity has undesirable consequences in certain types of measurements.[5]

To overcome these limitations, we have developed a new magnetometer. Its magnetic field sensitivity is comparable with that of the earlier cylindrical dc SQUIDs, and its maximum slew rate with respect to magnetic field has been increased by about a factor of 200. The magnetometer was designed around an existing planar[6,7] dc SQUID with a planar spiral input coil,[8] and incorporates a thin-film pick-up loop that is deposited on the same chip as the SQUID. The increase in slew rate was achieved both by improving the electronics and by increasing the sensitivity of the SQUID. First, the flux modulation was increased to 500 kHz, and a two-pole integration circuit was used in the electronics.[9] Secondly, because the flux sensitivity is an order of magnitude greater than that of the cylindrical SQUID, one is required to couple in an order of magnitude less flux in order to achieve a given magnetic field sensitivity.

Although the precise details of the superconducting input circuit are particular to our specific SQUID design, the design could be readily adapted to any thin-film dc SQUID that has sufficiently high coupling to the input coil. Similarly, the electronics has been tailored for magnetotelluric work, but the high slew rate and broadband operation achieved would be useful in many other SQUID based systems.[8,10-15] In fact, the electronics was used with only very minor modifications for the low temperature measurements discussed in the rest of this thesis, and this is the major reason I discuss it now in some detail.

3.2 The SQUID and Input Circuit

The configuration of the SQUID magnetometer chip is shown in Fig. 3.1, and its parameters are summarized for convenience in Table 3.1. The design was chosen to attain a sensitivty of at least 10 fT $Hz^{-1/2}$ at frequencies where the noise from the SQUID is white. The SQUID is a type A from the original J. M. Martinis masks (see Chapter 1). It is tightly coupled to a 20 turn input coil which was designed by C. Hilbert, and has an inductance of 120 nH. The input coil is connected to a single-turn, thin-film, pick-up loop. The pick-up loop has an area A_p= 47 mm^2 and is formed from a 25 μm wide line of Nb which is 400 nm thick. The estimated inductance of the loop is $L_p \approx$ 40 nH, based on the loop geometry. The dimensions of the loop were limited by the available area on the chip and by the 1.1 cm field of view of the projection mask aligner. For optimum sensitivity, the loop inductance should be equal to the input coil inductance of 120 nH. The inductance is thus somewhat below the value for optimum sensitivity [15], but, near optimum, the

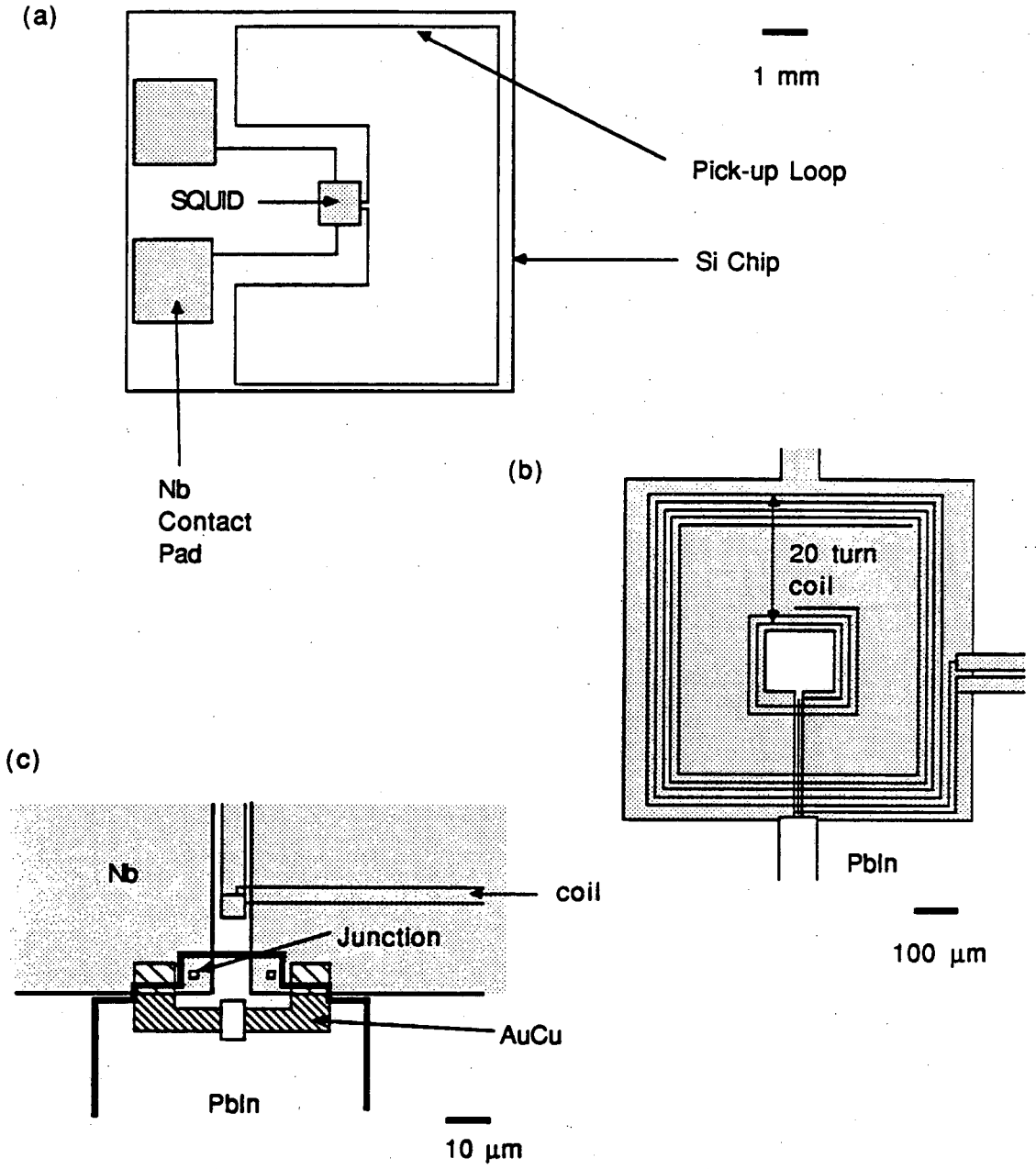

Fig. 3.1 Construction of the SQUID magnetometer; (a) Chip and pick-up coil, (b) SQUID and input coil, (c) details showing junctions and shunts.

Table 3.1 Typical parameters of the SQUID Magnetometer

SQUID inductance	L	400 pH
Critical current per junction	I_o	10 μA
Shunt resistance per junction	R	8 Ω
Number of turns on input coil	N	20
Inductance of input coil	L_i	120 nH
Mutual inductance between input coil and SQUID	M_i	6 nH
Inductance of pick-up loop	L_p	40 nH
Area of pick-up loop	A_p	47 mm^2
Effective pick-up area of SQUID	A_s	0.16 mm^2
Effective pick-up area of the magnetometer	A_m	1.48 mm^2

sensitivity depends quite weakly on L_p, so there is little loss in sensitivity due to this mismatch. To estimate the sensitivity of the magnetometer I assume that the magnetic field to be detected, δB, is applied to only the pick-up loop. The resulting flux change in the SQUID, $\delta\Phi$, is related to δB by:

$$\delta\Phi = A_p M_i \delta B/(L_i+L_p) \qquad (3.1)$$

where $M_i = \alpha(LL_i)^{1/2}$ is the mutual inductance between the input coil and the SQUID.

In practice Eq. 3.1 will be modified because the applied magnetic field also threads the spiral coil and the SQUID. I can estimate these corrections as follows. In the absence of the input coil, a flux $\delta\Phi_s = \delta B \cdot A_{eff}$ would thread the SQUID loop, where A_{eff} is the effective pick-up area of the SQUID. From the construction of the SQUID, the flux $\delta\Phi_s$ is of opposite sign to that enclosed by the pick-up coil, and thus the direct SQUID pick-up tends to decrease the field sensitivity. The estimated effective pick-up area of a SQUID is:

$$A_s \simeq l_{in} l_{out} \qquad (3.2)$$

where l_{in} is the inside diameter of the SQUID loop, and l_{out} is the outside diameter of the SQUID loop. For the type A SQUID used in the experiment l_{in} = 180 μm. and l_{out} = 900 μm, yielding an effective area of $A_s \approx 0.16$ mm^2. The second correction involves the amount of flux threading the 20 turn coil. Suppose the pick-up loop was not present, and an external flux $\delta\Phi_s$ was being applied to the SQUID, since the input coil is tightly coupled to the SQUID, the total amount of flux threading the input coil will just be $N\delta\Phi_s$ where N is the number of turns on the input coil. When incorporated into the input circuit, this will couple a total amount of flux $\delta\Phi'$ into the SQUID where:

$$\delta\Phi' = N\delta\Phi_s M_i/(L_i+L_p) \tag{3.3}$$

The total flux produced in the SQUID is thus:

$$\delta\Phi = \delta B \{-A_s - NA_s M_i/(L_i+L_p) + A_p M_i/(L_i+L_p)\} \tag{3.4}$$

where for the SQUID used here:

$$-A_s \approx -0.16 \text{ mm}^2 \tag{3.5}$$

$$-NA_s M_i/(L_i+L_p) \approx -0.12 \text{ mm}^2$$

$$A_p M_i/(L_i+L_p)\} = 1.76 \text{ mm}^2$$

The effective area of the magnetometer can the be defined as:

$$A_M = -A_s - NA_s M_i/(L_i+L_p) + A_p M_i/(L_i+L_p) \approx 1.48 \text{ mm}^2$$

The two corrections produce a 16% reduction in the magnetic field sensitivity. Notice that A_M is much smaller than the pick-up area A_p. Thus, when adding a pickup coil, one does not take full advantage of the coil area. The main loss factor is from the ratio $M_i/(L_i+L_p) \approx 0.04$.

Substituting Eqs. 3.5 into Eq. 3.4, one finds that 1.4 nT is required to produce one flux quantum in the SQUID. The estimated effective pickup area of the bare SQUID is 0.16 mm^2, which means that

roughly 13 nT are required to produce 1 Φ_0 in the bare SQUID. The addition of the pick-up coil has thus increased the magnetic field sensitivity by about a factor of 9.

The rms value of the equivalent magnetic field noise, $S_B^{1/2}$, in the pick-up loop is found by replacing $\delta\Phi$ with $S_\Phi^{1/2}$, where S_Φ is the spectral density of the equivalent flux noise in the SQUID. Using a typical value of $S_\Phi^{1/2} = 4 \times 10^{-6}\ \Phi_0\ Hz^{-1/2}$ we obtain $S_B^{1/2} \approx 5 \times 10^{-15}\ THz^{-1/2}$ in the white noise region, about a factor of 2 better than required.

The fabrication procedure for the SQUID and the pick-up coil has been described in Chapter 1. The SQUID was mounted in a fiberglass holder just above a 2.5 mm diameter 10-turn coil of hand-wound Nb wire that provides feedback flux, ac modulation flux, and dc offset. Two pieces of Nb foil were pressed against the Nb pads of the SQUID to provide electrical contact. To measure the intrinsic noise of the SQUID, the fiberglass mount was inserted into a Pb shield tube. For use as a magnetometer, the SQUID was unshielded. In either case the device was immersed directly into a 4.2 K liquid helium bath.

3.3 The Feedback Electronics

The feedback electronics is based on an earlier design,[2] and has been upgraded to improve the frequency response and the slew rate. It is shown schematically in Fig. 3.2. The major improvements are the use of wideband transformers to couple the SQUID to the preamplifier, an increase in the flux modulation frequency from 100 to 500 kHz, and the use of a two-pole integration circuit. The operation of the electronics

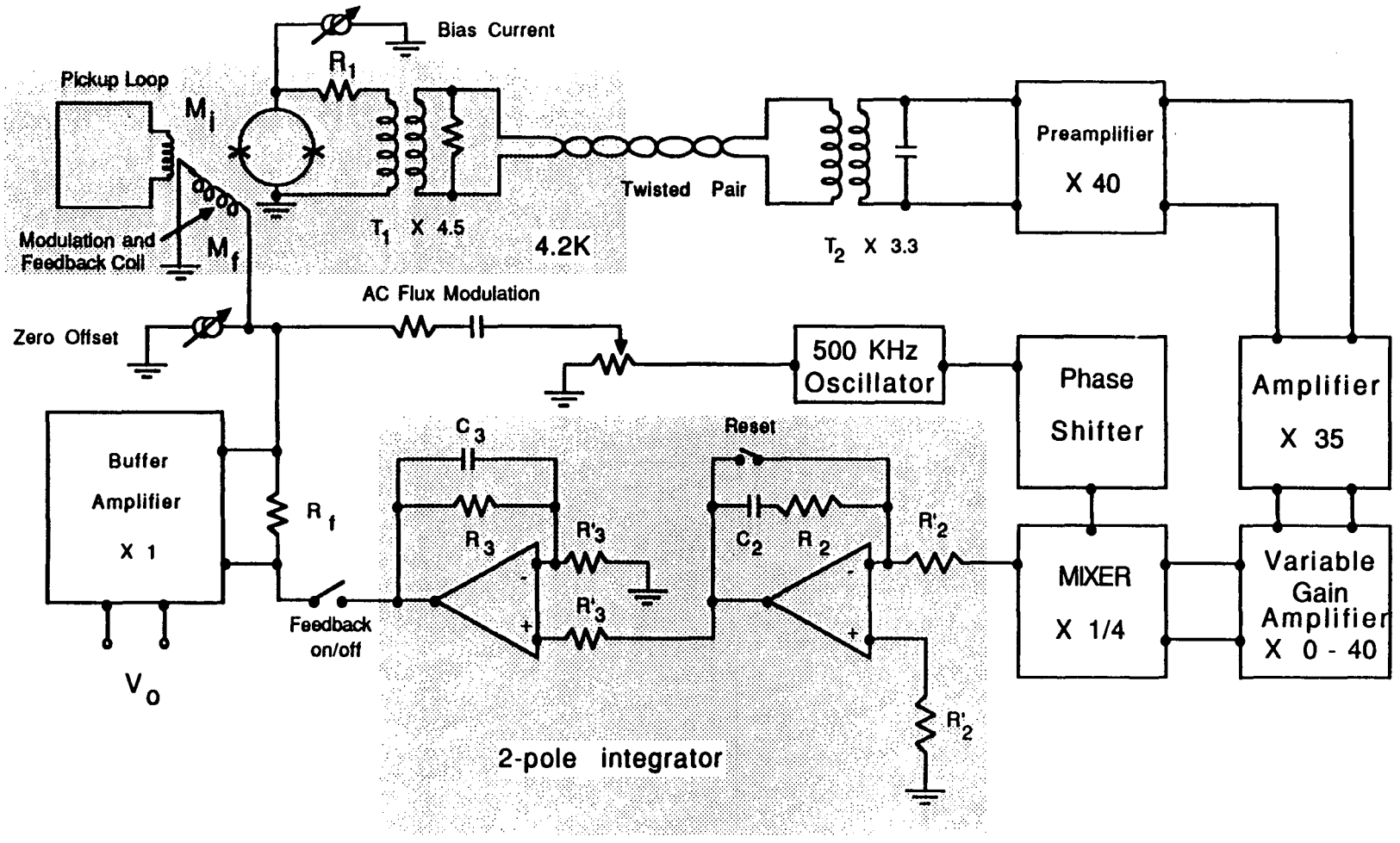

Fig. 3.2 Electrical schematic of the magnetometer and feedback electronics. The following component values were used: M_f = 80pH, R_f = 5kΩ, R_{xx} = 0.7Ω, R_2 = 100Ω, C_2 = 2nF, R'_2 =20kΩ, R_3 = 1.1 MΩ, C_3 = 180 pF, R_3' = 11 kΩ.

is conventional.[2] A 500 kHz square-wave modulation flux with a peak-to-peak amplitude of $\Phi_0/2$ is applied to the SQUID. When the quasistatic flux applied to the SQUID is exactly $n\Phi_0$ or $(n+1/2)\Phi_0$, where n is an integer, the resulting voltage across the SQUID consists of a square wave at 1 MHz. When this signal is lock-in detected at 500 kHz, the mean output voltage will be zero. If one now applies a small additional flux $\delta\Phi$ ($<< \Phi_0$) to the SQUID, there will be a component at 500 kHz across the SQUID, with magnitude and phase depending on the magnitude and sign of $\delta\Phi$. When this signal is lock-in detected, there will be a non-zero average output which is proportional to $\delta\Phi$. The signal from the integrator is amplified, passed through an integrator, and fed back to flux lock the SQUID.

The input stage of the preamplifier is a type 2n5434 room temperature JFET, which was chosen because of its exceptionally low 1/f and white noise. In order to achieve a low system noise, it is necessary to present an optimum impedance to the preamplifier. To determine this optimum source impedance, Christoph Heiden connected a parallel LCR tuned circuit, resonant at 485kHz and cooled to 4.2 K, across the input. The noise was measured at the output of the preamp as a function of the impedance of this circuit, which was varied by changing the value of the parallel resistance. The optimum source resistance, R^{opt}, was between 1.5 and 2 kΩ. The amplifier noise voltage was $e_n \approx 1$ nV $Hz^{-1/2}$. This yields an amplifier noise current $i_n = e_n/R^{opt} \approx 0.5$ pA $Hz^{-1/2}$ at 500 kHz. The noise temperature of the preamplifier is then $T_n = e_n i_n/2k_b \approx$ 18 K. Although this value seems fairly high compared to the 4.2 K bath temperature, it should be realized that the SQUID produces an output voltage noise of order:

$$S_V(f) = 4k_bT\gamma_VR/2 \qquad (3.6)$$

where $\gamma_V \simeq 8$ for our SQUIDs at T = 4.2 K. At the normal bias point of our SQUIDs at 4.2 K, the dynamic resistance is about the same as the SQUID shunt resistance R. And thus the output of the SQUID appears to be about four times hotter than an equivalent passive resistor at the same bath temperature. Thus the SQUID appears to be at about 17 K, which is comparable to the noise from the preamp. The preamp will thus make a non-negligible contribution to the system noise, and further improvement would be desirable.

Since the dynamic resistance of our SQUIDs at 4.2 K at the optimum bias point is about 8 Ω, one requires an impedance transformation of about 200 to match the SQUID to R^{opt}. In addition, the bandwidth should be as large as possible in order to achieve a high slew rate. The requirement of a large bandwidth precludes the use of a cooled resonant LC circuit. Similarly, we have found that the bandwidth of a single, cooled transformer is too small because of the presence of stray capacitance between the leads coupling the secondary of the transformer to the preamplifier. To overcome these difficulties we have used two different arrangements, both of which have performed satisfactorily.

The first arrangement involved a single room temperature transformer. The primary was wound from 5 turns of #16 copper wire and the secondary from 110 turns of #24 copper wire, on a Ferroxcube 4C4-A100 core. The inductance of the primary was about 2.5 μH. It was necessay to use low resistance leads between the SQUID and the primary coil to avoid significant degradation of the sensitivity because of additional resistance and Nyquist noise in these wires. The rather thick leads required (15 strands of #34 Cu wire) would yield an undesirably

high level of liquid helium boil-off in a system designed for field use.

To overcome this heat leak problem, we developed a second coupling system with two transformers, one cooled and one at room temperature, see Fig. 3.2. The cooled, superconducting transformer consisted of 62 and 280 turns of 50 μm diameter niobium wire for the primary and secondary, respectively, wound on a 6 mm diameter bakelite form. The primary inductance was about 10 μH. With a turns ratio of about 4.5, this transformer reflected a SQUID impedance of about 160 Ω into the secondary circuit, a value substantially lower than the shunting impedance of the cable due to stray capacitance, roughly 5 kΩ at 500 kHz. The primary and the secondary coils of the room temperature transformer consisted of 39-1/2 and 125 turns respectively of #26 copper wire wound on a 4C4-A60 core. The primary inductance was about 96 μH. In the absence of losses, the combined impedance transformation of the two transformers was about 200. To prevent the primary of the cold transformer from shorting out the SQUID at low frequencies, we inserted a 0.7 Ω resistance in series with the primary (see Fig. 3.2). Without this resistor, it would not be possible to send dc bias current through the SQUID.

3.4 Why Use a Two-Pole Integrator ?

By using a two-pole integrator in the feedback loop, one can significantly increase the system slew rate at low frequencies. The open loop gain of the system can be written in the form:

$$G(\omega) = (V_\Phi G_A M_f / R_f) G_I(\omega) \qquad (3.7)$$

where: V_Φ is the flux-to-voltage transfer coefficient of the SQUID,

$G_A(\omega)$ is the gain of the transformers, $G_I(\omega)$ is the gain of the integrator, amplifiers and mixers, M_f is the mutual inductance between the SQUID and the feedback coil,and R_f is the feedback resistance. When the feedback switch is closed, a flux $\Phi_a(\omega)$ applied to the SQUID gives rise to a feedback flux:

$$\Phi_f(\omega) = \Phi_a(\omega)G(\omega)/(1+G(\omega)). \qquad (3.8)$$

Thus, the small signal frequency response of the system is given by:

$$\Phi_f(\omega)/\Phi_a(\omega) = G(\omega)/(1+G(\omega)) \qquad (3.9)$$

When the loop is locked, the flux in the SQUID, Φ_s, is just the difference between the applied flux Φ_a and the feedback flux Φ_f. This is ordinarily called the error signal, or, in this case, the error flux Φ_e:

$$\Phi_s = \Phi_e = \Phi_a - \Phi_f . \qquad (3.10)$$

But the error flux is related to the feedback flux by G, thus:

$$\Phi_f = \Phi_e G(\omega). \qquad (3.11)$$

Because the loop will unlock if the error flux exceeds $\Phi_o/4$, the value at which the output from the SQUID is a maximum, one finds a maximum slew rate of:

$$d\Phi_e/dt \propto \omega\Phi_o/4 \qquad (3.12)$$

This result is valid provided that the feedback amplifier does not saturate. This corresponds to a maximum rate of change in the applied flux of:

$$(d\Phi_a/dt)_{max} = (1+G(\omega))\omega\Phi_o/4 \qquad (3.13a)$$

and in the feedback flux:

$$(d\Phi_f/dt)_{max} = G(\omega)\omega\Phi_o/4 \qquad (3.13b)$$

For an unlocked SQUID, $(d\Phi_a/dt)_{max} \propto \omega\Phi_o/4$, so that the feedback has increased the maximum allowed slew rate of the applied field by a factor

of (1+G). A more rigorous discussion of this formula is presented in the following two sections.

Clearly, to achieve the highest possible slew rate one must use the largest possible gain $G(\omega)$. On the otherhand, if the gain is too large, the feedback loop becomes unstable. At a sufficiently high frequency, the phase shifts introduced by the integrator and other circuit elements causes the feedback to become positive. If the gain is greater than unity when the phase shift goes to 180 degrees, the system will break into sustained oscillation. This results in an upper limit to the useable gain. As has been demonstrated by Giffard, a substantial improvement in slew rate at low frequencies can be achieved by introducing a second pole into the integrator.[10] The gain of the integrator is then of the form:

$$G(\omega) = \frac{-iA\omega_1}{\omega}\left[\frac{1 + i\omega/\omega_2}{1 + i\omega/\omega_3}\right] \qquad (3.14)$$

where:

$$A = \frac{M_f R_3 \epsilon}{R_f R_2' R_3' C_2 \omega_1} \approx \omega_1/\omega_3 \quad \text{(provided } \omega_1^2 << \omega_2^2 \text{)}$$

ω_1 is the frequency where $|G|$ falls to unity

$\omega_2 = 1/R_2C_2$

$\omega_3 = 1/R_3C_3$

$\epsilon = V_d(\Phi_s)/\Phi_s$

$V_d(\Phi_s)$ is the voltage at the output of the mixer when there is a

flux Φ_s in the SQUID.

For stable operation we should have $\omega_2 \approx \omega_1/4$ as will be shown below. Also, for the circuit at hand, $\omega_3 << \omega_2$.

The second pole at ω_3 allows one to obtain higher gain at lower frequencies and hence to achieve a higher slew rate than is possible

with a single pole. In practice, as we shall see, the frequency dependence of the gain introduced by the other components ultimately limits the slew rate by imposing an upper bound on ω_1.

3.5 Loop Stability Considerations

The condition for the maximum stable gain can be understood quite simply by considering the differential equation describing the time dependent behavior of the feedback loop. A 1-pole system can be idealized as in Fig. 3.3. For the 1-pole circuit, the feedback flux is just:

$$\Phi_f = -\frac{M_f}{R_f C_{int} R_{int}} \int_{-\infty}^{t} V_d(\Phi_s(t'))\, dt' \quad . \tag{3.15}$$

For the two-pole system, the situation is more complicated. The two-pole integrator used in the electronics (see Fig. 3.2) replaces the 1-pole integrator in Fig. 3.3. When the loop is locked, the flux in the SQUID is again:

$$\Phi_s = \Phi_e = \Phi_a - \Phi_f \quad . \tag{3.16}$$

The feedback flux is now given by:

$$\Phi_f = \frac{iA\omega_1}{\omega}\left[\frac{1 + i\omega/\omega_2}{1 + i\omega/\omega_3}\right]\Phi_s \tag{3.17}$$

where I am working in the frequency domain. When Eq. 3.17 is substituted into Eq. 3.16, the resulting expression may be transformed into a second order differential equation in the time domain:

$$\left[\omega_3\frac{d\Phi_a}{dt} + \frac{d^2\Phi_a}{dt^2}\right] = \frac{d^2\Phi_s}{dt^2} + \frac{d}{dt}\left[\frac{A\omega_1\omega_3}{\omega_2} + \omega_3\right]\Phi_s + A\omega_1\omega_3\Phi_s \tag{3.18}$$

The terms in the first brackets with ω_3 may be neglected anywhere $\omega >> \omega_3$.

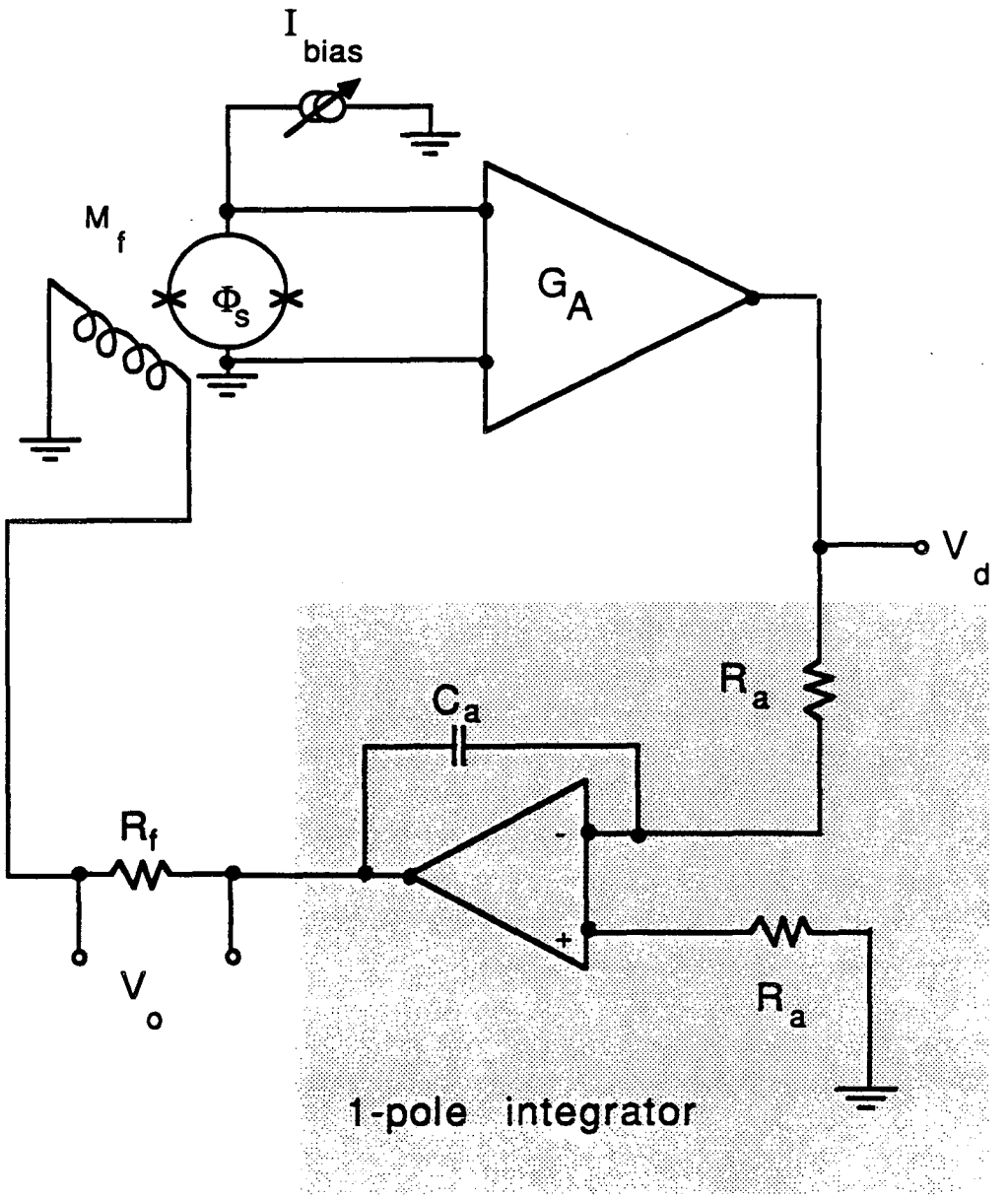

Fig. 3.3 Idealized one-pole integrator circuit.

The term with ω_3 by itself in the second brackets may be neglected as it is negligible for typical $A\omega_1\omega_3$ and ω_2. The differential equation thus reduces to the form:

$$\frac{d^2\Phi_a}{dt^2} = \frac{d^2\Phi_s}{dt^2} + \left[\frac{\omega_1\omega_3}{\omega_2}\right]\frac{d(A\Phi_s)}{dt} + A\omega_1\omega_3\Phi_s \qquad (3.19a)$$

This is the equation for a driven anharmonic oscillator. The driving term is proportional to the second derivative of the applied flux. The anharmonicity is due to the non-linear response of the SQUID as included in the term A which contains the term $V_d(\Phi_s)$.

In order to analyze the situation further, it is necessary to model the SQUID-to-mixer response function $V_d(\Phi_s)$. For small Φ_s the response will be linear, while for large Φ_s the response is bounded and periodic. The simplest model is to take a triangular response with period Φ_o, see Fig. 3.4. For small Φ_a, Eq. 3.19a then reduces to a driven linear harmonic oscillator.

For small perturbations the situation can be analyzed exactly, and is well-known in feedback or automatic control theory.[16] There are two seperate issues that need to be addressed: is the loop stable, and is the transient response well-behaved? The loop is defined to be stable if after a small perturbation the loop eventually returns to its inital state. For the linear approximation to the above second order equation, all of the solutions to the equation have time dependences of the form $\exp(i\omega_x t)$, where the ω_x are the solutions to the associated second order equation (the associated equation is generated by Fourier transforming the corresponding homogenous differential equation). In order for the loop to be stable, all of the ω_x must possess a positive real imaginary part. Only in this case will the solutions die down after a long period

of time. For the above differential equation in the linear approximation, the associated equation is:

$$0 = \omega^2 - i\omega A\omega_1\omega_3/\omega_2 - A\omega_1\omega_3 \qquad (3.19b)$$

The solutions are $\omega_x = iA\omega_1\omega_3/(2\omega_2) \pm \{A^2\omega_1{}^2\omega_3{}^2/(4\omega_2{}^2) + A\omega_1\omega_3\}^{1/2}$. Since both roots have a positive imaginary part, the feedback loop will be stable. The real part of the solution is the frequency at which the loop rings. For small ω_1/ω_2 this is just ω_1.

The loop transient response is controlled by the Q of the oscillator. If the Q is too high, the loop rings for long periods of time after being driven. If the Q is too low, the loop response is slow (which is to say the loop bandwidth is low). The dividing line between these two extremes is the case of critical damping. The condition corresponding to critical damping is $1/2Q = 1$ where for small ω_1/ω_2 one finds $Q \propto (\omega_2/\omega_1)^{1/2}$. The condition for good transient response thus becomes:

$$\omega_1 \propto 4\omega_2 \ , \qquad (3.20)$$

which is one of the results to be shown. This condition was stated by Giffard [10] (and is well-known for other systems), although it clearly holds only for a linear SQUID response. It should also be realized that the loop can be run for higher Q, corresponding to the underdamped case. In this case however, the closed loop gain becomes much larger than unity when $|G| \rightarrow 1$, because of the decreased damping. Near ω_1, One typically sees an increase in the closed loop gain, and the noise, which grows progressively as the Q is increased until the system breaks into continuous oscillation. Although the solutions to 3.11b are always stable, in a real system there are always parasitic components which produce additional phase shifts at high frequencies. Thus 3.11b must be

regarded as an approximation, and the real equation will possess oscillating solutions if ω_1 is made too large.

3.6 Maximum Slew Rate Considerations

The concept of maximum slew rate is not very well defined. The ability of a loop to track a given signal depends not only on the properties of the loop but also on the nature of the applied signal. In section 3.4 I briefly considered the case where the signal was of sinusoidal form. In general, a signal with a different time dependence will yield a different maximum slew rate.

To illustrate this, consider an input flux of the form:

$$\Phi_a = bt^2/2 + at + c \qquad (3.21)$$

where b, a, c are constants. Then $d^2\Phi_a/dt^2 = b$. Substituting this into differential equation 3.18, one finds:

$$d^2\Phi_s/dt^2 = b - \omega_1\xi^{-1}\, dv_d(\Phi_s)/dt - \omega_1\omega_2\xi^{-1}\, V_d(\Phi_s). \qquad (3.22)$$

Now the system will not unlock iff the error flux Φ_s never exceeds $\Phi_0/4$. In particular this means that the $d^2\Phi_s/dt^2 = 0$ as $t \to \infty$, and $d\Phi_s/dt = 0$ as $t \to \infty$, otherwise the error flux will grow without bound, (there is a third possibility; that the derivatives of Φ_s oscillate positive and negative with time for all time; this would imply that the system is unstable and is in free and self-sustained oscillation; a case we are not interested in.).

Substituting this into the differential equation 3.22, one finds:

$$b = \omega_1\omega_2\xi^{-1}\, v_d(\Phi_s) \qquad (3.23)$$

Thus we can see that the only parameter of the input signal which matters is the second derivative or curvature. What this means is that

the two-pole loop will track a constant flux or a constantly changing flux with no error. This implies that the loop cannot be unlocked by signals which have no dervitaves beyond the first. When subjected to a constant curvature signal, on the otherhand, the error flux in the loop settles down to Φ_s such that the above relation is satisfied. There will be a maximum b for which the equation still has a solution because the voltage out of the SQUID attains a maximum when $\Phi_s = \Phi_o/4$ and begins to decrease thereafter. This maximum b is thus:

$$b_{max} = \omega_1\omega_2\xi^{-1}\, v_d(\Phi_o/4) \qquad (3.24)$$

The term $\xi^{-1}v_d(\Phi_o/4)$ is typically of order $\Phi_o/4$, and thus the maximum slew rate becomes:

$$(d^2\Phi_a/dt^2) = b_{max} \approx \omega_1\omega_2\Phi_o/4 \qquad (3.25)$$

3.7 Performance

The open loop gain and parameters of the two-pole loop were varied empirically to obtain the maximum possible slew rate. At this maximum rate, however, we observed excess white noise, indicating that the system was about to go unstable. Thus for all subsequent measurements the gain was reduced somewhat until no excess noise was observed. To enable us to compare the measured frequency response and slew rate with the values expected from the open loop gain, we determined $G(\omega)$. Fig. 3.4 shows our estimation of $G(\omega)$ from the measured low frequency gains and the calculated response of the integrators. In addition we have plotted the measured effect of the transformer resonace which produces a deviation from the $1/\omega^2$ dependence near 100 kHz and a small peak near 400 kHz. Note that these contributions have been mixed down from

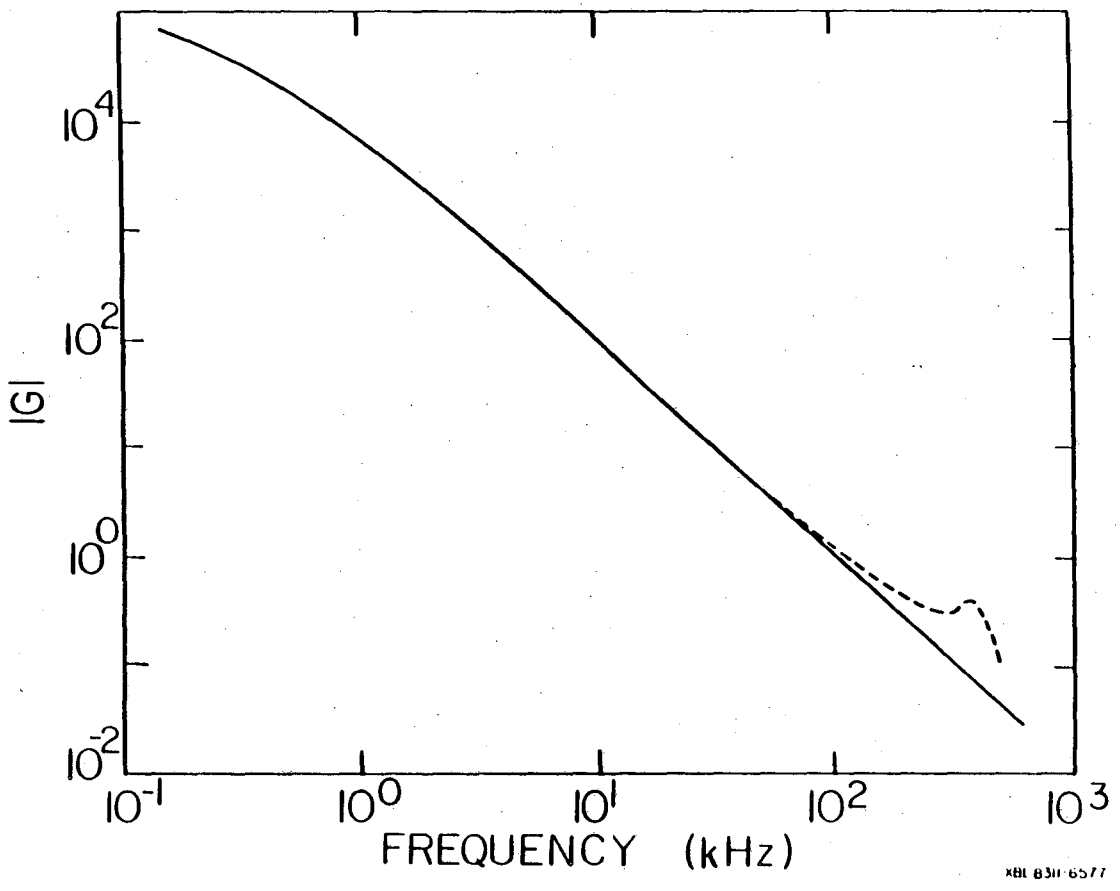

Fig. 3.4. Open loop gain $|G(\omega)|$ determined from the measured low-frequency gain and the calculated response of the two-pole integrator (solid line). The measured effect of the transformer resonance is also shown (dashed line).

frequencies 500 kHz higher; the actual resonance frequency of the transformer is at about 900 kHz. The value of $\omega_2/2\pi$, about 800 kHz, plays no significant role in the response of the amplifier. The noise, dynamic range, frequency response and slew rate were determined with these circuit parameters. The performance is summarized in Table 3.2

To calibrate the magnetometer, we measured its response to a known external magnetic field in the absence of a superconducting shield. The field required to produce one flux quantum in the SQUID was 1.32 nT, a value within 6% of the value predicted by Eq 3.4.

Fig. 3.5 shows the spectral density of the flux noise of the SQUID in a superconducting shield. The noise is white at frequencies above 10 Hz, and corresponds to a flux noise of about 3.8 $\mu\phi_0$ $Hz^{1/2}$. This value is somewhat higher than the predicted value:[17]

$$S_\phi(f)^{1/2} = (18k_bTL^2/R)^{1/2} \approx 2\ \mu\phi_0 Hz^{-1/2} \qquad (3.31)$$

for the parameters listed in Table 3.1. I believe that this discrepancy

Table 3.2 Measured performance of the SQUID magnetometer

Magnetic Field to generate ϕ_0	1.32 nT
flux noise of SQUID, $S_\phi^{1/2}(f)$	$4 \times 10^{-6}\ \phi_0 Hz^{-1/2}$ (f>10Hz) $1.4 \times 10^{-5}/(f/1Hz)^{1/2}\phi_0 Hz^{-1/2}$ (f<10Hz)
field sensitivity, $S_B^{1/2}(f)$	$5 \times 10^{-15}\ THz^{-1/2}$ (f>10Hz) $2 \times 10^{-14}/(f/1Hz)^{1/2}\ THz^{-1/2}$ (f<10Hz)
Dynamic range (f<6kHz)	$\pm 2 \times 10^7\ Hz^{1/2}$
Frequency response (± 3 dB)	70 kHz
Maximum slew rate (6 kHz)	$3 \times 10^6\ \phi_0 s^{-1}$ $4 \times 10^{-3}\ Ts^{-1}$

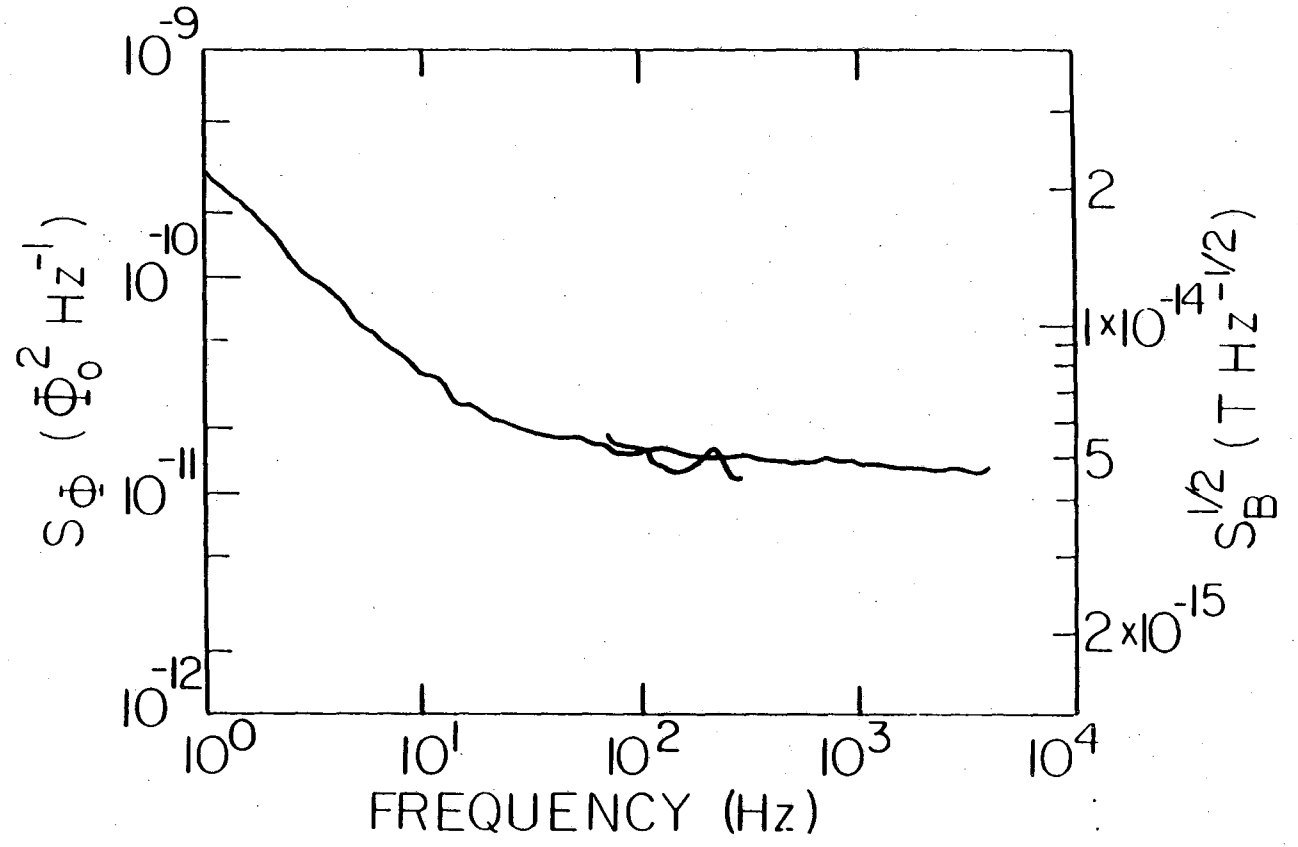

Fig. 3.5. Spectral density of the flux noise (left-hand ordinate) in the flux-locked SQUID when it is in a superconducting shield at 4.2 K. Right-hand ordinate shows corresponding rms value of the effective magnetic field noise in the magnetometer.

arises largely from the preamplifier noise. At frequencies less than 10 Hz, the spectral density of the noise varies approximately as 1/f, where f is the frequency. This excess noise spectral density is very typical for this type A SQUID geometry (see Chapter 7 for more discussion of the implications of this simple fact). The corresponding magnetometer sensitivity is shown on the right hand axis of Fig. 3.5, and is about 5 fT $Hz^{-1/2}$ in the white noise region. We note that the 1/f noise of the magnetometer is actually higher than that of the cylindrical SQUID when referred to an equivalent magnetic field noise.

The maximum low frequency flux that could be applied without causing the electronics to saturate was $\pm$ 78 ϕ_0. This value is set by the maximum output voltage of the integrator, and the feedback resistance R_f, and could easily be increased by an order of magnitude. The dynamic range was thus 2 X 10^7 $Hz^{1/2}$ in the white noise region.

We determined the frequency response of the shielded flux-locked SQUID by applying a small alternating flux and measuring the signal at the output of the electronics as a function of frequency. The measured response (Fig. 3.6) is approximately flat to 80 kHz, peaks at about 150 kHz, and falls rapidly above 600 kHz. The frequency response predicted from $G(\omega)$, including only the frequency response of the two-pole integrator, becomes very large near 100 kHz. This is because $\omega_2 >> \omega_1$, and we have neglected the response of the transformer. To approximate the frequency response of the transformer, we introduce a frequency $\omega_2'/2\pi$ = 120 kHz (see Fig. 3.4) above which the gain is assumed to roll off as $1/\omega$. This ω_2' plays the role that ω_2 would have, and a more exact treatment would need to take into acount more accurately the transformer response. The frequency response predicted from this $G(\omega)$ is also shown

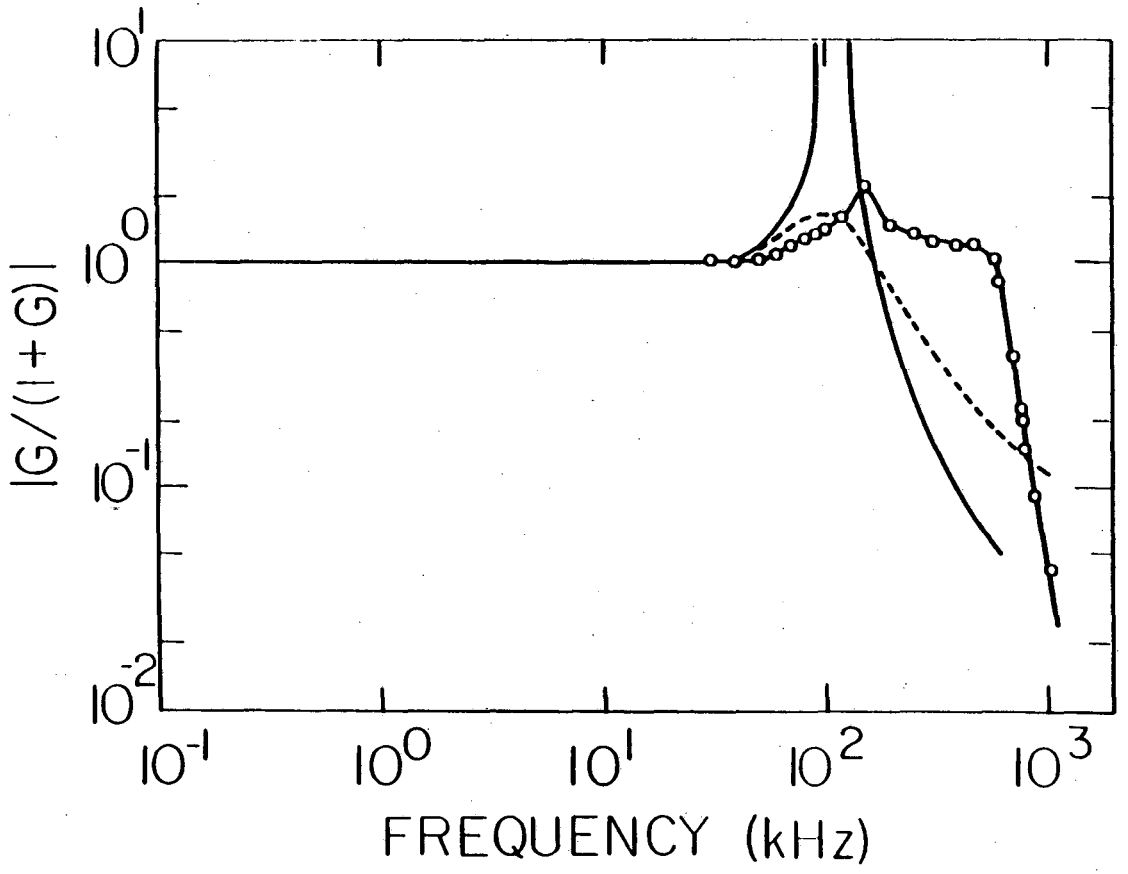

Fig. 3.6. Measured frequency response (solid line through circles) of shielded flux-locked SQUID. Solid curve shows response predicted from G(ω) without transformer resonance. Dashed line is predicted from G(ω) with transformer resonance, modeled by replacing ω_2 with ω_2'.

in Fig. 3.6. Although the divergence has been removed, the measured closed loop gain still differs significantly from the prediction above 100 kHz. We believe that this extended frequency response arises predominantly from the transformer resonance, and from additional closed loop gain produced by the mixer near the 500 kHz modulation frequency. Moreover, the rapid roll off above 600 kHz indicates a large additional phase shift, and suggests that the system will become unstable for a small increase in the closed loop gain. Thus we see that the system gain can be increased only to the point where parasitic effects begin to dominate the response.

The slew rate was determined from the maximum sinusoidal flux, $\Phi_f \sin\omega t$, that could be fed back without causing the system to unlock. Figures 3.7 and 3.8 show the maximum Φ_f and $\omega\Phi_f$ vs. frequency. The maximum slew rate, $\omega\Phi_f$, occurs at a frequency of about 6 kHz and is approximately 3 X 10^6 $\Phi_0 s^{-1}$. At frequencies below 6 kHz, the slew rate is limited by the dynamic range of the system. At higher frequencies, Φ_f falls off as $1/\omega^2$, as expected, flattening out as the transformer resonance and mixer response begin to contribute. The slew rate predicted from Eq. 3.6b and $G(\omega)$ with and without the transformer contribution are also shown; as with the frequency response, the prediction deviates markedly from the measured curve above about 100 kHz.

As a practical test of the magnetometer, we operated it without a superconducting shield both in our laboratory and in the open, in the center of campus about 50 m away from the nearest building. In order to screen out interference from radio and television stations, we enclosed the cryostat in #40, 250 μm thick, copper mesh. The ambient magnetic

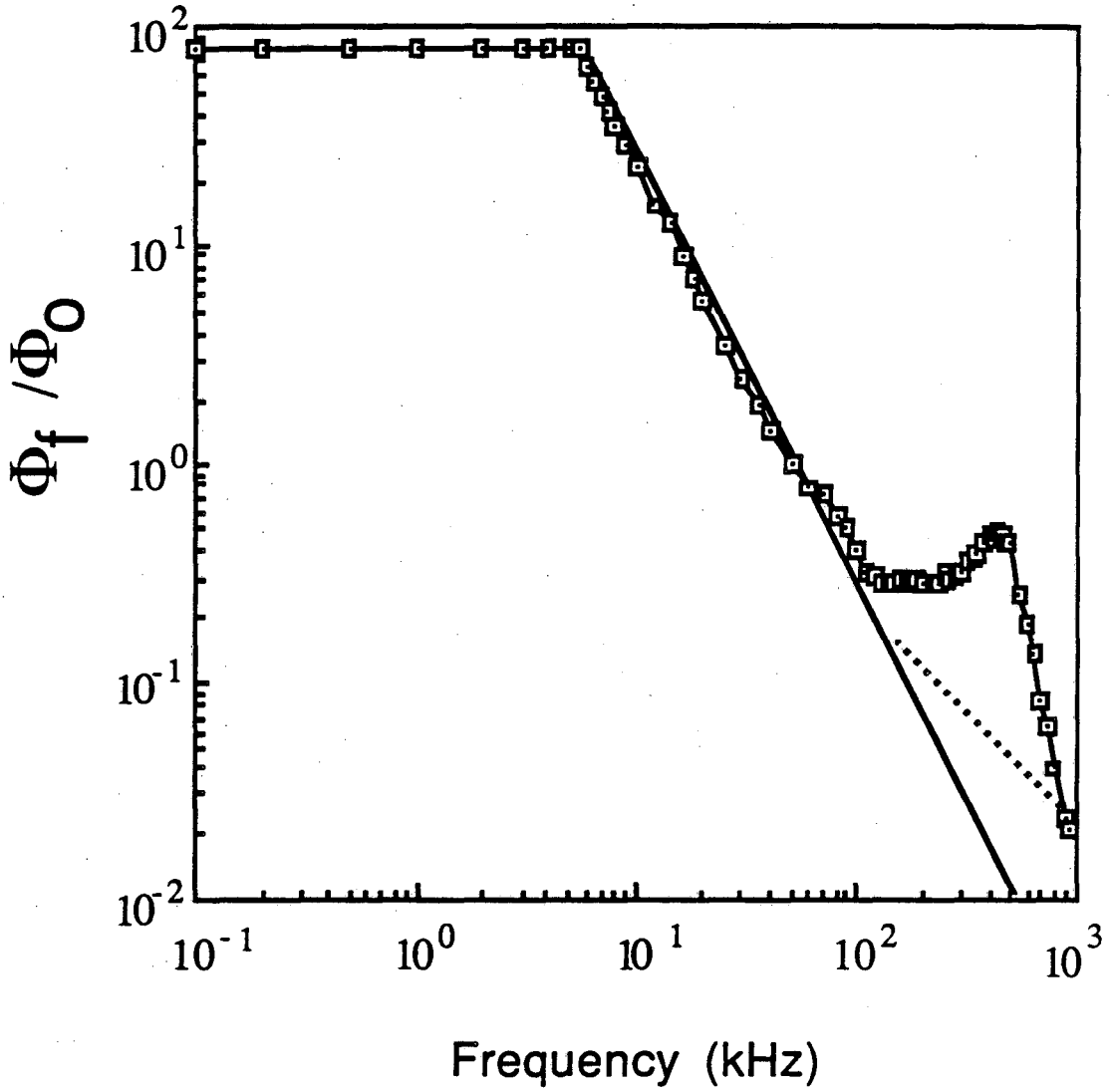

Fig. 3.7 Maximum amplitude of sinusoidal flux that can be fed back without causing the system to saturate or break lock (solid line through the open circles). Solid and dashed lines. are prefictions from $G(\omega)$ as in Fig. 3.4.

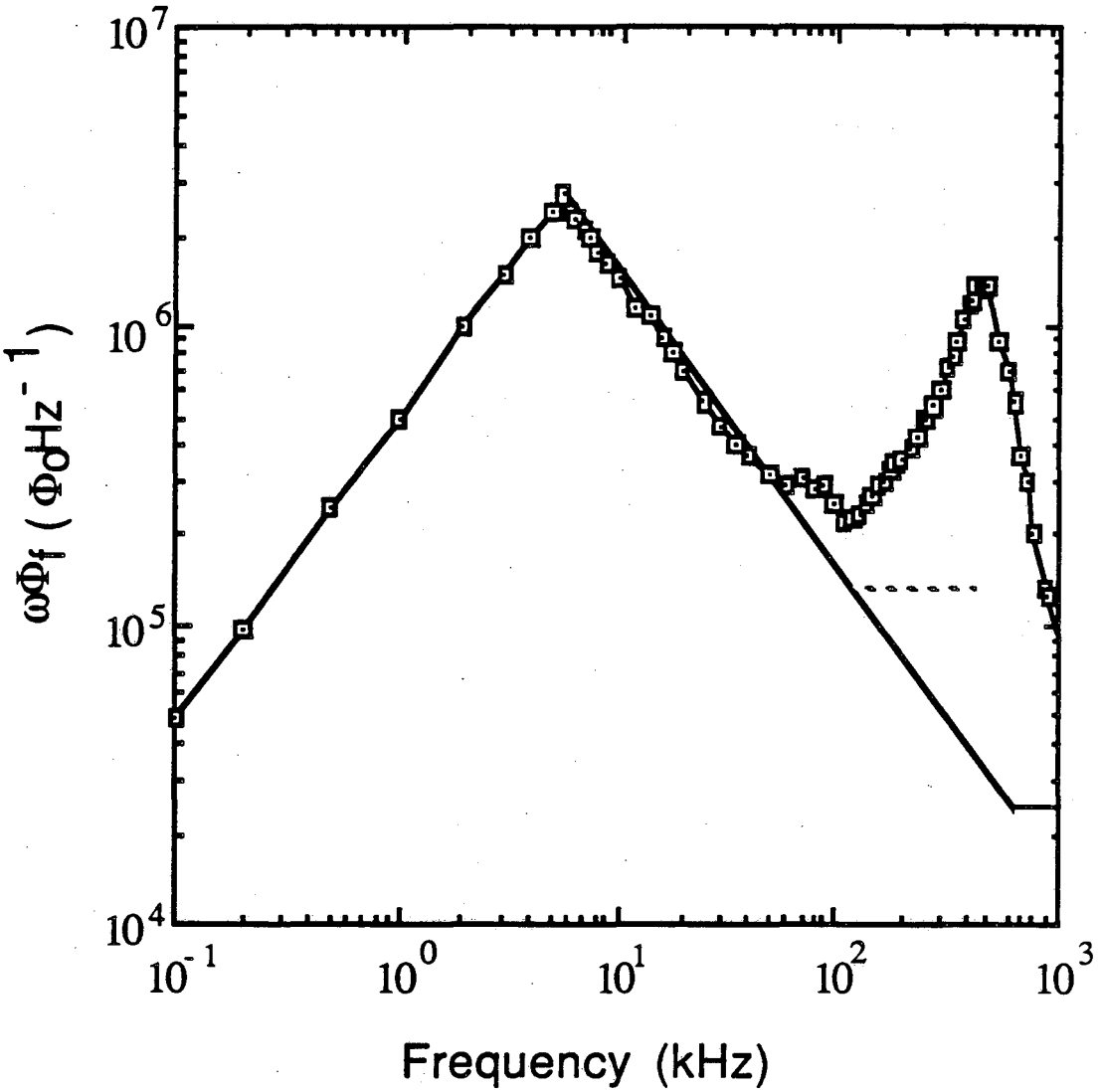

Fig. 3.8 . Slew rate vs frequency (solid line through open circles). Solid and dashed lines are predictions from $G(\omega)$ as in Fig. 3.4.

field fluctuations in the laboratory tests were dominated by 60-Hz oscillations from powerlines, typically 10^{-7} T peak-to-peak, with odd harmonics readily visible out to 5 kHz. During daytime operation in the laboratory, we found that the system lost lock several times per day. We believe that this unlocking was mostly due to large switching transients from the departmental machine shop, which is situated directly below our laboratory, although it could have arisen from other equipment in the building. However, for the few days that we tested the magnetometer, it would stay locked in overnight when the shop was closed. During one of the overnight tests, we experienced a local thunderstorm (which, incidentally, is a rare occurrence in the San Francisco Bay Area) in which I observed nearby cloud-to-cloud lightning. I did not observe any strokes to ground. I estimated the cloud height at about 2 km by noting that the cloud base was relatively low but well above the tops of the Berkeley hills (maximum height about 500 m). "Dim" flashes produced an output spike from the magnetometer, which did not unlock, but "bright" flashes always caused the magnetometer to unlock. During daytime operation outside the building over a period of 4 hours the only unlocking event occured when a walky-talky was operated within a few tens of meters of the SQUID. Thus, we feel that during field operation under normal conditions, the magnetometer is likely to remain locked in for an entire day. However, local thunderstorms are almost certain to cause the magnetometer to unlock.

3.8 Conclusions

One interesting aspect of the operation in the field is that the

SQUID works in the unshielded magnetic field of the Earth. Although the Earth's field (40 μT) is much smaller than H_{c1} for Nb (200 mT), the thin film geometry has a large demagnetizing factor, and consequently a large demagnetizing field, H_D, is developed. We can estimate this field as $H_D \propto H_E\, d/\ell$ where H_E is the Earth's field, d is the SQUID diameter, and ℓ is the Nb film thickness. For a 200 nm film thickness and a 1 mm SQUID diameter this becomes $H_D \propto 200$ mT, which is the critical field of Nb. This means that the SQUID is probably in an intermediate or mixed normal-superconducting state, and it is fortuitous that the SQUID functions.

The above electronics has proven itself to be very useful and durable. At this time (1988) the electronics shop has made roughly 10 to 20 of the high frequency feedback boxes, including the two boxes that I operate, and on the whole, different researchers have successfully applied them to a number of SQUID based projects. However, various shortcomings have been noted, and I will remark on three of them.

First of all, the sensitivity is less than one would hope. In the above work, the lowest noise observed was about 4 $\mu\phi_0 Hz^{-1/2}$, whereas the SQUID should have been generating only about 2 $\mu\phi_0 Hz^{-1/2}$. The additional noise was undoubtedly from the electronics. Of course ideally, one would like the preamp to contribute a negligible amount of noise compared to the SQUID. This has been difficult to achieve because the input FET is not sensitive enough, and is probably somewhat mismatched to the SQUID. In addition, the two transformer coupling scheme ensures that there will be some losses in the voltage gain between the SQUID and the preamp because of leakage of field from the air core cold transformer. The performance could be improved through a

more careful study of the optimal matching impedance, or by using a lower noise FET.

There is a related problem that can also give rise to lower sensitivity. The feedback loop is designed so that low frequency flux in the SQUID gets converted to higher frequencies at the SQUID output by mixing with the 500 kHz square wave modulation. On the otherhand, it is unavoidable that higher frequency noise will get mixed down to lower frequencies. Thus a 0 Hz and a 1 MHz signal will both be converted to a 500 kHz SQUID output. For the 1 MHz to 500 KHz conversion, there will be some non-unity transfer coefficient, which can readily be estimated as:

$$2\cos(\alpha)/\pi, \qquad (3.32)$$

where α is the phase difference between the 500 kHz modulation and the 1 MHz signal. Further along in the loop, both of these 500 kHz signals will be mixed down to dc. Thus any flux noise in the SQUID at 1 MHz will appear as a low frequency noise at the feedback output. This kind of behavior is common to many clocked systems and is referred to as aliasing. In order for the low frequency output of the feedback loop to be an accurate representation of the low frequency signal in the input circuit, it is thus important that any signal from the input circuit not contain 1Mhz components. This is one of the reasons for the 12 μH coil inserted into the input circuit of the measuring SQUID system discussed in Chapter 1.

In any case, it is difficult to envisage a room temperature preamp which is substantially (say a factor of 5) better than the existing one coming along any time soon. In fact we have not been able to locate anything better than the 2N5434 FET. The ultimate solution to the sensitivity problem, in my view, is simply to abandon the FET and use a

second SQUID as a low noise preamp to read out the front end SQUID. As was discussed in Chapter 2, this is the course I have pursued in this thesis to perform very low noise measurements on the refrigerator.

The second point is that even higher slew rates are desirable. If the slew rate is needed at high frequencies, the reader can consult the next paragraph. At low frequencies, the slew rate is not limited by the loop gain, but rather by the dynamic range of the feedback output. Thus the loop tracks the signal until it gets so large that the amplifier driving the feedback current is saturating (about $\pm$ 10 volts for the present setup). By simply extending the supply voltage or choosing high voltage op-amps at the output, it should be possible to significantly increase the low frequency slew rate. For example, by going from 10 volts to 100 volts, the peak slew rate should go to about 3×10^7 at 2 kHz, with no other modifications. The slew rate at lower frequencies will be proportionally increased, whereas there will be no improvement at higher frequencies. A second possibility is to decrease the feedback resistor R_f. In practice though, making R_f too small degrades the system sensitivity.

The third shortcoming is that higher frequency operation is desired. With the present setup, I believe it will be difficult to get another factor of 5 in the bandwidth. This will also almost certainly result in an additional loss of sensitivity. The present setup can effectively be used out to 1/4 MHz, if one is willing to live with relatively higher noise at higher frequencies, and if considerable tweeking of the loop components is done. The central problem is that it is difficult to control the stray phase shifts over such extended circuits at these frequencies. The only way out of the dilemma is to substantially reduce

the size of the feedback circuit. The ultimate solution here may well be a cryogenic feedback electronics, or a SQUID based op-amp. Such a configuration could potentially operate up to a GHz. Such a device would be a very useful alternative to a bare SQUID. A significant step in this direction has been already been reported by Jutzi et al., who have used an on-chip superconducting analog to digital converter to read out the SQUID, which is then flux-locked with conventional electronics.[18]

Finally, I note that the 1/f noise in the present system, which is generated by the SQUID, could be greatly reduced by using one of the Pb based SQUIDs or new Nb SQUIDs which will be discussed in Chapter 7.

References

(1) Major parts of this Chapter were published in: F.C. Wellstood, C. Heiden, and J. Clarke, "Integrated dc SQUID Magnetometer with a High Slew Rate", Rev. Sci. Instrum. 55, 952, (1984).

(2) J. Clarke, W.M. Goubau, and M.B. Ketchen, J. Low Temp Phys. 25,99 (1976).

(3) J. Clarke, T.D. Gamble, W.M. Goubau, R.H. Koch, and R.F. Miracky, Geophys. Prospect. 31, 149 (1983).

(4) A readable account of sferics, whistlers, and other atmospheric electrical and magnetic activity is presented in: Introduction to Space Sciences, ed. Hess and Mead, article by M. Suigiura and J.P. Heppner, Gordon and Breach, (1968).

(5) W.M. Goubau, P.M. Maxton, R.H. Koch, and J. Clarke, Geophysics, 49, 433 (1984).

(6) J.M. Martinis and J. Clarke, IEEE Trans. Magn. MAG-19, 446 (1983).

(7) C. Hilbert and J. Clarke, Appl. Phys. Lett. 43, 694 (1983)

(8) M.B. Ketchen and J.M. Jaycox, Appl. Phys. Lett. 40, 736, (1982).

(9) A dc SQUID with a two-pole integrator circuit is commercially available from B.T.I.. Giffard (Ref. 10) has descibed a SQUID with a two-pole integrator in the feedback loop.

(10) R.P. Giffard, in "Superconducting Quantum Interference Devices and Their Applications", edited by H.D. Hablom and H. Lubbig, Walter de Gruyter, Berlin, p 445 (1980).

(11) M.W. Cromar and P. Carelli, Appl. Phys. Lett., 38, 723 (1981).

(12) P. Carelli and V. Fogglietti, J. Appl. Phys. 53, 7592 (1982); IEEE Trans. Magn. MAG-19, 299 (1983).

(13) B. Muhlfelder, W. Johnson, and M.W. Cromar, IEEE Trans. Magn. MAG-19, 303 (1983).

(14) J.F. Garnier, J.C. Villegier, D. Duret, and A. Regent, IEEE Trans. Magn. MAG-19, 591 (1983).

(15) V. J. de Waal, T.M. Klapwijk, and P. van den Hamer, J. Low Temp. Phys. 53, 287 (1983).

(16) See for example, F.E. Nixon, "Principles of Automatic Controls", Prentice-Hall Inc., New York (1954).

(17) J. Clarke, C.D. Tesche, R.P. Giffard, J. Low Temp. Phys. 37, 405 (1979).

(18) W. Jutzi, D. Drung, E. Crocoll, R. Herwig, M. Neuhaus, "Measured Performance Parameters of Gradiometer with Digital Output", Applied Superconductivity Conference, San Francisco, Calif., Aug. 21-25 (1988), to be published in IEEE Trans. Magnetics and Magnetic Materials.

Chapter 4: Estimation of the SQUID Parameters α, β, and L

4.1 Why is Accurate Parameter Estimation Important?

The dc SQUID is an interesting scientific device because it has an extremely high sensitivity. Paradoxically, because the sensitivity is so high, it can be difficult to measure. It should be recognized that, in general, the sensitivity of a SQUID based circuit will depend not only on the properties of the SQUID, but also on the configuration of the input circuit and the form of the signal. Nevertheless, for a wide class of problems, one can provide a number which characterizes the SQUID sensitivity and is independent of the rest of the circuit. This "figure of merit" is the energy sensitivity.

I know of only two ways to estimate the energy sensitivity of the dc SQUID. One can in principle build a circuit and measure how small of an energy can be detected. This is quite difficult because the minimum detectable energy is extremely small, and, in general, one must employ the technique of optimal filtering as will be discussed in Chapter 12. This is generally not done. Instead, the energy sensitivity is estimated based on measurements of the SQUID noise, and model estimates of SQUID behavior when it is connected to an input circuit. These models require knowledge of a few SQUID parameters, some of which are themselves not easily estimated. Thus, the accurate estimation of a SQUID's parameters is important for the determination of the SQUID's sensitvity.

I should note that it can be misleading to say "the energy sensitivity". There are two distinct quantities that are commonly called the energy sensitivity, (although in fact, as will be shown in Chapter

12, neither in general represents the true energy sensitivity of a SQUID measuring system). The most commonly measured energy sensitivity is what I will call the intrinsic[1] or flux noise energy sensitvity per unit bandwidth, which I will denote as ε_V throughout this thesis. It is defined as:

$$\varepsilon_V = S_V(f)|V_\Phi|^{-2}/2L = S_\Phi(f)/2L \qquad (4.1)$$

where: $S_V(f)$ is the voltage noise power per Hertz at the output of the bare dc SQUID, L is the SQUID inductance, V_Φ is the SQUID flux-to-voltage transfer function, f is the frequency, and $S_\Phi(f)$ is the spectral density of the equivalent magnetic flux noise in the SQUID. In fact, the quantity ε_V is not a good measure of the energy sensitivity of the dc SQUID, which is to say that a SQUID may be able to detect more or less than ε_V in a unit bandwidth. A better measure is what I will call the total energy sensitivty ε. This quantity is defined by the relation:[1,2]

$$\varepsilon = (\varepsilon_V\varepsilon_J - \varepsilon_{VJ}^2)^{-1/2} \qquad (4.2)$$

where: ε_V is defined above

$\varepsilon_J = S_J(f)L/2$, and $S_J(f)$ is the power spectral density of the circulating current in the SQUID loop

$\varepsilon_{VJ} = S_{VJ}(f)/2$, and $S_{VJ}(f)$ is the cross correlation power spectral density between the SQUID's circulating current and voltage.

The significance of ε is that at a frequency ω_0, the smallest energy that can be detected by a SQUID with a linear input circuit is $\varepsilon\omega_0$ (see Chapter 12).

The quantity ε_V is the only one of the sensitivities that was measured for this thesis. It is important to mention explicitly why this

is the case. Now ideally, one would like to measure ε. For a good SQUID, the energy $\varepsilon\omega_o$ is an extremely small quantity, and at low frequencies, it is generally much smaller than k_bT, where T is the temperature of the SQUID. The technique that one could use to measure ε directly is covered in Chapter 12. It involves a significantly more sophisticated approach than the simple noise measurement schemes used here. On the otherhand, one might try to measure the three quantities ε_v, ε_j, and ε_{vj}, and then use Eq. 4.2 to get ε. This suffers from two problems. First of all, it is difficult to measure ε_j and ε_{vj}. This requires a second SQUID measuring system which is coupled to the first.[3] The only measurement of these quantities I am aware of was performed by Martinis and Clarke,[3] and could only be done on very low resistance, non-optimal, SQUIDs. Secondly, it is quite difficult to measure the ε_v, ε_j, and ε_{vj} accurately enough to get a useful estimate of ε from the above formula. Theoretical models[4] of the behavior of the SQUID suggest that $\varepsilon_v\varepsilon_j$ is not much bigger than ε_{vj}^2, and so the expression amounts to the difference of two large numbers.

From the above discussion we can see that it will be necessary to measure $S_\Phi(f)$ and L in order to estimate ε_v. The measurement of $S_\Phi(f)$ forms the bulk of the experimental work because of its smallness. The experimental approach to measuring this quantity was presented in Chapters 2. This leaves just the inductance L as the only relatively inaccessible parameter. The estimation of the inductance L, and two related quantities α and β, is somewhat complicated and is the main subject of this Chapter.

Now, in all of this discussion of the estimation of the energy sensitivity, there is a very important point that seems to be

universally understood and yet also universally ignored. It should be pointed out that the above estimates of the energy sensitivity and the inductance rest on the validity of the equations of motion for the SQUID. Which is to say, the measured SQUID must act like an ideal SQUID in order for us to reliably apply the above results. Much data has been reported elsewhere on devices with very non-ideal characteristics. In such cases, one still sees the authors blindly plugging into formulas for the senstivity, with little regard for the fact that the equations of motion that produced their observed I-V's cannot possibly be the same as those used in the theoretical estimates of the sensitivity. Such an approach is clearly unjustified and highly suspect. In order to apply the results of this section, and to get accurate estimates of the energy senstivity of the SQUID it is important that the device show characteristics which are in substantial agreement with those produced by the model equations of motion. This point cannot be overemphasized.

It is interesting to note that the issue is somewhat subtle because of the effects of noise rounding. At high temperatures, the I-V can appear very smooth due to noise rounding. When the device is cooled however, the noise rounding disappears, and it is common to see large amounts of structure. Clearly, such a device also cannot be described by just the bare SQUID RSJ model, although this is not evident until the device is cooled sufficiently to remove noise rounding.

4.2 Techniques for Estimating L

The SQUID inductance L can be estimated by studying the geometry of the SQUID loop. Jaycox and Ketchen in particular have provided simple

formulas for the inductance of washer shaped SQUID loops.[5] However, it is difficult to obtain reliable numbers from the geometry of the SQUID loop because most SQUIDs have complicated shapes and are often coupled to nearby circuits which can cause screening of the geometrical inductance. The formulas thus provide only a rough, although very useful, estimate of the inductance of most SQUIDs.

An alternative technique which is frequently used is to carefully measure the current-vs-voltage (I-V) characteristic of the SQUID, and note the modulation depth. The modulation depth is defined as the maximum change in current that occurs when the SQUID is biased at a fixed voltage (near 0) and the flux is swept over one Φ_0. For a symmetrical SQUID, the maximum current occurs at $\Phi = 0$, and the minimum occurs at $\Phi = \Phi_0/2$ (see Fig. 4.1). The modulation parameter of the SQUID, $\beta \equiv 2LI_0/\Phi_0$ is then estimated using calculated curves of the modulation depth vs β, as for example in ref. 5, or see Fig. 4.2. For a symmetric SQUID with $\beta<<1$, it can be shown that the modulation depth approaches the value $A = 1 - \pi\beta/4$, as is shown by the dashed line at low β in Fig. 4.2. Similarly, in the high β limit, it can be shown that $A \propto 1/\beta$, as is shown by the dashed line at high β in Fig. 4.2. A reasonable approximation to the shape in the intermediate regime is given by $A=1/(1+\beta)$. Measurement of the SQUID critical current I_0 then allows an estimation of L through the relation $L = \beta\Phi_0/2I_0$.

4.3 Problems with the Modulation Depth Estimate of L

The modulation depth procedure for estimating L has three serious deficiencies. First of all, the I-V characteristics and the modulation

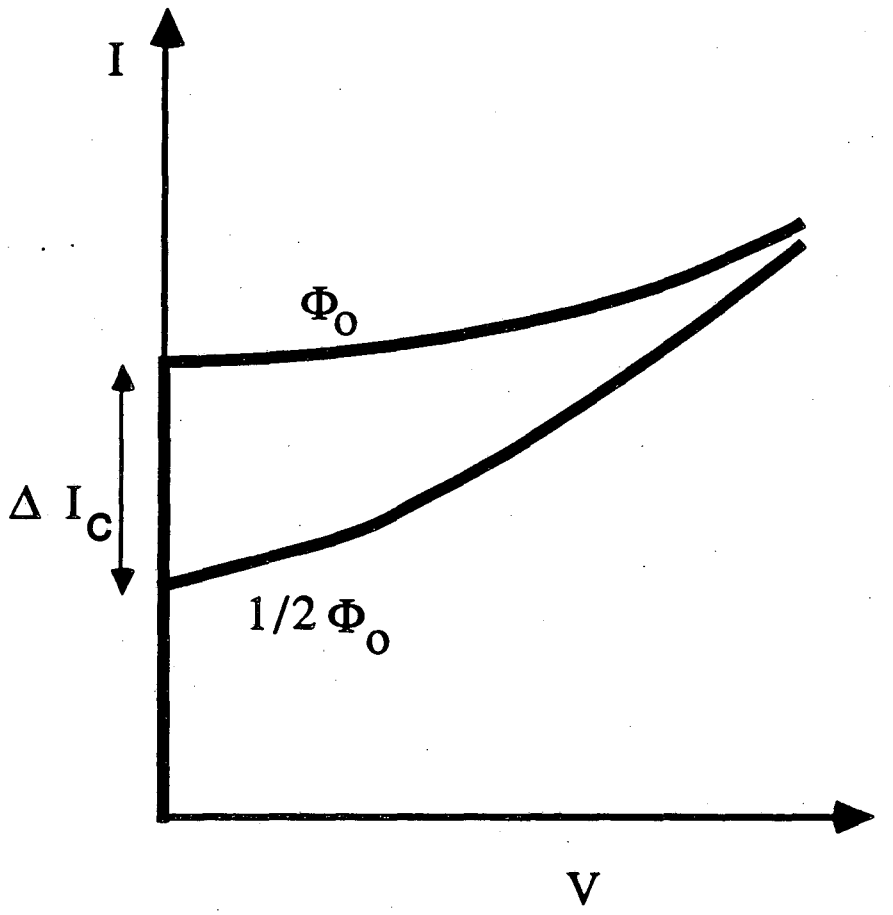

Fig. 4.1 Schematic of current vs voltage characteristic of a SQUID at zero and one half of a flux quantum.

depth are temperature dependent due to the effects of noise rounding, i.e. the shape of the I-V changes with temperature, especially as V-->0. The calculated modulation curves on the other hand are generally reported only for T=0. It is difficult to accurately gauge the T=0 I-V characteristics from the I-V of a typical SQUID at 4.2 K.

Secondly, modulation depth depends not only on the total critical current of the SQUID, but also on the asymmetry in critical current between the two junctions. This can be quantified by a parameter $\alpha = (I_{02}-I_{01})/(I_{01}+I_{02})$. Fig. 4.2 was calculated on the assumption that the asymmetry α was zero. The critical current of the junctions is one of the most difficult parameters to control, and substantial variations are common in our own SQUIDs, as we will show. Thus unless one measures the asymmetry α, as well as the total critical current, one can not be certain of the inductance.

Finally I note a somewhat deeper problem. Fig. 4.1 is based on the bare SQUID Resistively Shunted Junction model[4] (RSJ). The RSJ model will of course predict the shape of the entire I-V, and not just the zero-voltage characteristics. A proper fit would then involve fitting the I-V curve rather than just a small piece of it. This would not be a problem if the measured I-V closely resembled the calculated I-V, for then both fits would yield the same estimate. On the otherhand, it is quite common to see I-V's which have large amounts of structure on them. Such devices cannot possibly be adequately described by just the bare RSJ model, and there must be some additional circuit elements. In this case the assumptions used in deriving Fig. 4.2 cannot be satisfied, and its use in estimating the inductance cannot be readily justified. Experimentally then, one can only use the technique with any confidence

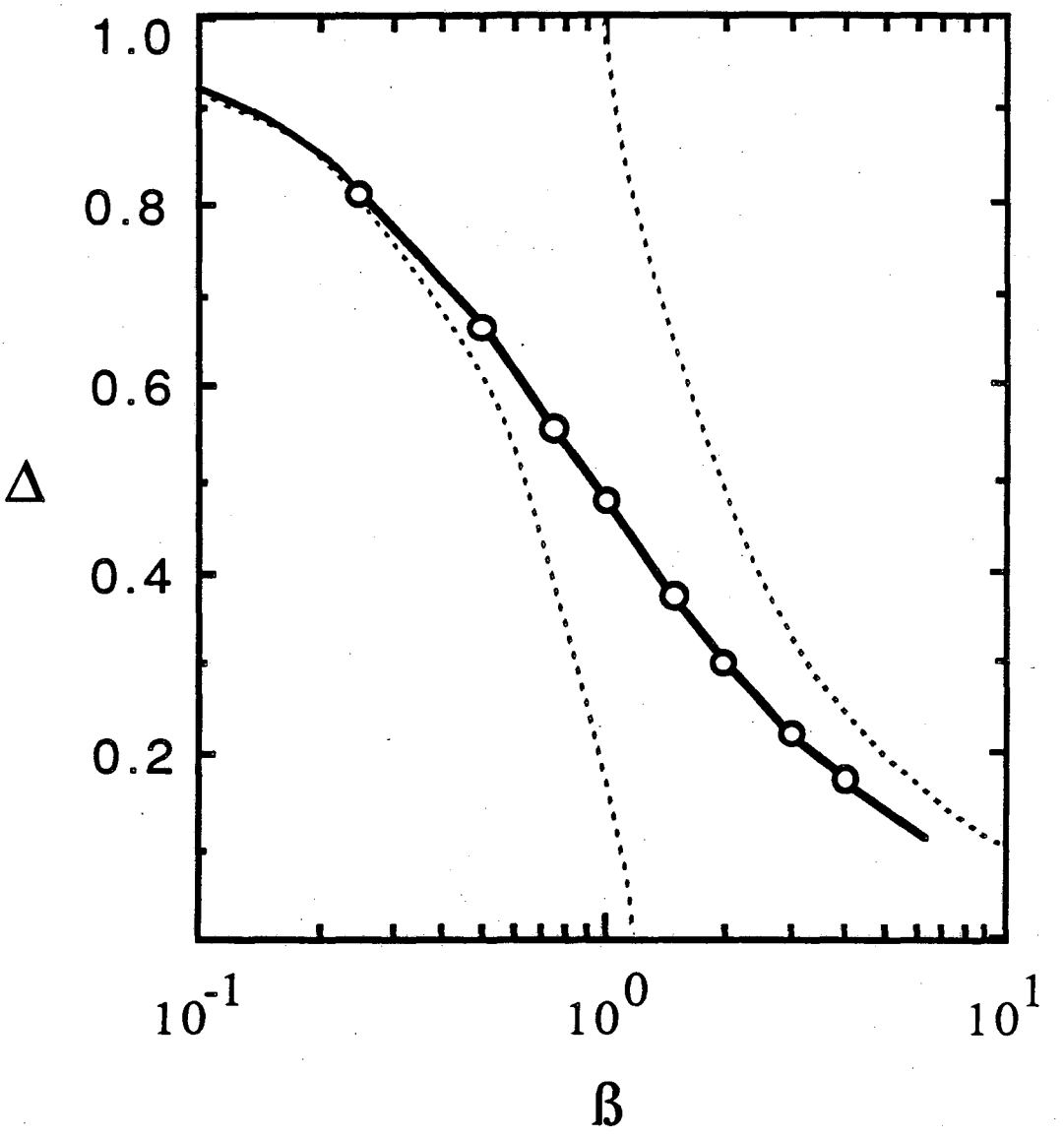

Fig. 4.2. Modulation depth $\Delta = \Delta I_C / 2 I_O$ vs ß for zero critical current asymmetry. Dashed lines show small ß approximation at small ß and large ß approximation at large ß.

on devices which have well-behaved current-vs-voltage characteristics.

It should be recognized that the problem of estimating L when the SQUID has non-ideal behavior is considerably easier than the problem of estimating the energy sensitivity of a SQUID with non-ideal behavior. This is because the 0-voltage I-Φ is considerably less dependent on details of the SQUID-circuit because all the time derivatives drop out. On the otherhand, knowing L for a non-ideal device may be completely useless if the energy sensitivity is no langer simply related to $S_{\Phi}(f)/2L$.

The way out of these difficulties is threefold. First of all, it is necessary to accurately estimate the asymmetry α. Essentially, I can then calculate new curves of modulation depth vs β for this α, and hence obtain β. In practice, one must use a somewhat more complicated procedure to find both β and α, but the principle is the same. Secondly, in these experiments, I can obtain the I-V at very low temperatures where noise rounding effects are negligible. And finally, I attempt to produce devices which have essentially ideal I-V characteristics at low temperatures, and assume that in this case the device can be adequately descibed by a bare SQUID RSJ model.

4.4 Calculation of T=0, V=0 Modulation Depth Curves

The calculation of the zero temperature, modulation depth vs. asymmetry curves is based upon the ideal equations of motion of the dc SQUID. These can be written as[6]:

Current equations:

$$I = I_1 + I_2 \ , \tag{4.3}$$

$$J = (I_1 - I_2)/2 \ ,$$

$$I_1 = I_{o1} \sin(\delta_1) + (V_1 - V_{n1})/R_1 + C_1 dV_1/dt \ ,$$

$$I_2 = I_{o2} \sin(\delta_2) + (V_2 - V_{n2})/R_2 + C_2 dV_2/dt \ .$$

Voltage equations:

$$V = (V_1 + V_2 + L_1 dI_1/dt + L_2 dI_2/dt)/2 \ ,$$

$$V_1 = d\delta_1/dt \ \Phi_o/2\pi \ ,$$

$$V_2 = d\delta_2/dt \ \Phi_o/2\pi \ .$$

Phase equation:

$$\delta_2 = \delta_1 - 2\pi\Phi/\Phi_o - 2\pi LJ/\Phi_o - 2\pi\eta LI/2\Phi_o \ ,$$

where the various parameters have been defined in Appendix A. The Eqs. can be put into a dimensionless form by introducing the variables:

$$i = I/I_o \tag{4.4}$$

$$v = V/I_o R \qquad \phi = \Phi/\Phi_o$$

$$\theta = t 2\pi I_o R/\Phi_o$$

When the voltage is zero, the SQUID can sustain a maximum supercurrent $i_c(\phi)$, which depends upon the applied flux Φ. This is the curve we wish to generate. Setting v = 0 in the above equations, and taking T = 0 to remove the noise terms, one finds:

$$i = (1-\alpha) \sin\delta_1 + (1+\alpha) \sin\delta_2 \tag{4.5a}$$

$$2j = -(1-\alpha) \sin\delta_1 + (1+\alpha) \sin\delta_2 \tag{4.5b}$$

$$\delta_2 = \delta_1 - 2\pi\phi - \pi\beta j - \pi\beta\eta i/2 \tag{4.5c}$$

The Eqs. 4.5 can be simplified to just two equations by using Eq. 4.5b to replace j in Eq. 4.5c. We thus are left with:

$$i = (1-\alpha)\sin\delta_1 + (1+\alpha)\sin\delta_2 \tag{4.6a}$$

$$\delta_2 = \delta_1 - 2\pi\phi - (\pi\beta/2)[-(1-\alpha)\sin\delta_1 + (1+\alpha)\sin\delta_2] - \pi\beta\eta i/2. \tag{4.6b}$$

This set of coupled nonlinear equations can be solved for the current i as a function of the applied flux. In general, the equations have several solutions i for a given value of the flux. This is particularly true at large β. The solution which we are interested in is the largest permissible i that occurs at a given ϕ; this will be taken as $i_c(\phi)$. One interesting aspect of these equations is that they are independent of the junction capacitance. Thus the zero voltage $I(\phi)$ will be the same for devices with different β_c, and we are spared having to ascertain another difficult SQUID parameter.

The Eqs. 4.6 have been solved by numerous authors, using a variety of techniques.[6-11] The major thrust of their works has been in exploring the behavior of SQUIDs or double junction interferometers, and in developing novel devices. The purpose here is somewhat different: I wish to construct a technique for estimating L and α from experimental data. The equations will need to be solved yet again to achieve this. I have adopted the technique used by Tesche and Clarke,[6] which works as follows. First introduce two functions F and F':

$$F(i,\delta_1) = i - (1-\alpha)\sin\delta_1 - (1+\alpha)\sin\delta_2 \qquad (4.7a)$$

$$F'(i,\delta_1) = \partial F/\partial\delta_1 = -(1-\alpha)\cos\delta_1 - (1+\alpha)[1+\pi\beta(1-\alpha)\cos\delta_1]\cos\delta_2 \qquad (4.7b)$$

Now setting F=0 gives us Eq. 4.6a, and setting F'=0 in Eq. 4.7b allows us to select the largest i. To proceed, choose a δ_1 and insert it into Eq. 4.7b with F'=0 to obtain $\cos\delta_2$, and hence $\sin\delta_2 = (1-(\cos\delta_2)^2)^{1/2}$. Next substitute these values of δ_1 and δ_2 into Eq. 4.6a to obtain i. Next use the values of i and δ_1 to calculate δ_2 from Eq. 4.6b. Thus, starting from a δ_1, I have chosen an i and a δ_2 such that Eq. 4.6b is satisfied. I then calculate F and F' from Eqs. 4.7 and test whether they are simultaneously zero. If not the process, which is a 1-D search, is

repeated until a zero is located. In general there will still be several local maxima, so one must sweep δ_1 from 0 to 2π. One now chooses the zero which produces the largest current, and this is $I_c(\Phi)$ for V=0.

The calculation was implemented on a Tektronix 6130 computer using a simple Fortran program. The region δ_1 from 0 to 2π is first searched for zero crossings using a straightforward 2 X 10^4 point grid search. The interval with the largest current is then examined with a bisection search routine to determine the δ_1 crossing accurately. The current at this δ_1 is then found, and corresponds to the maximum current that can flow in the zero voltage state at the given Φ, α, β. The routine is susceptible to certain errors, in particular, missing a zero interval or choosing the wrong maxima. This arises because of the rapidly varying nature of the functions F and F'. These difficulties are alleviated in a direct fashion by the initial fine grid search at the expense of computing time.

Curves are constructed for a range of α and β. I fix α and β, and then find $i_c(\phi)$ for ϕ from 0 to 1 in steps of 1/50. The result is then a curve of i as a function of ϕ for the given α and β. From this curve, I then extract the minimum current, i_{min}, and the maximum current, i_{max}. The modulation depth is then just $(i_{max}-i_{min})/i_{max}$ I have also found it useful to extract a second parameter from the $i_c(\phi)$ curve. The maximum slope $r_1 = (\partial i/\partial \phi)_{max}$ and the minimum slope r_2 are strongly dependent upon the asymmetry α. I have found the ratio of these two slopes $r \equiv |r_2/r_1|$ to be very useful. I then sweep the α and β and generate a corresponding family of curves of modulation versus r.

These curves of modulation depth versus slope ratio can be parameterized by either α or β. Fig. 4.3 shows curves parameterized for

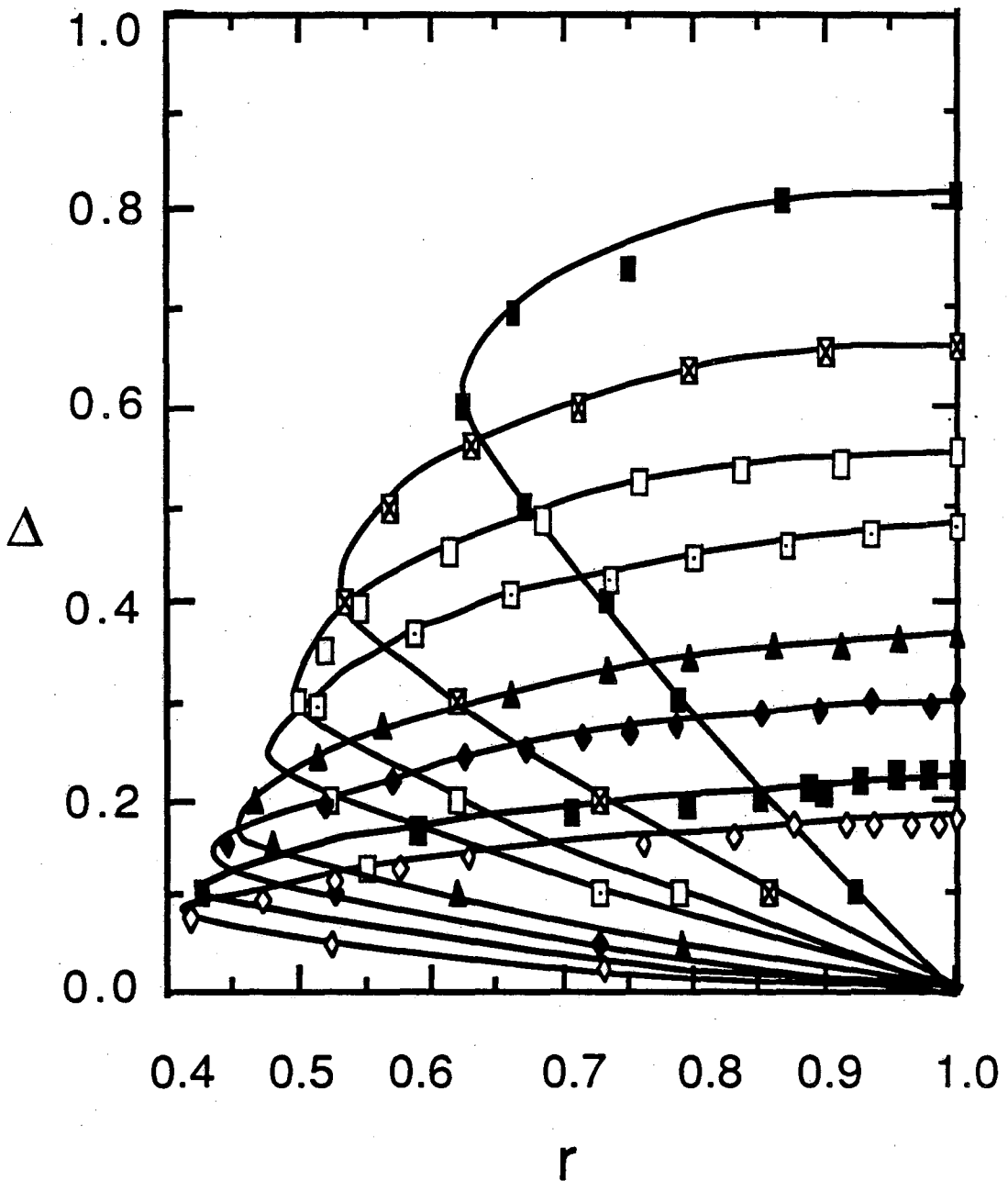

Fig. 4.3 Modulation depth vs slope asymmetry r. From top to bottom the curves are for fixed β, with β : 0.25, 0.5, 0.75, 1.0, 1.5, 2, 3, and 4 respectively.

β, with the low α portions of the curves occurring at larger Δ, and the high α portions of the curve occurring at small Δ. At large α, all the different curves approach the same modulation depth $(1-\alpha)$, a well-known result. At small α, the modulation depth is relatively insensitive to α. This is especially true for large β SQUIDs. Notice also that the ratio of the slopes, r, approaches a minimum for any given β, and, the larger β, the smaller is this minimum r.

4.5 Estimation of L and α

In order to estimate the SQUID inductance, one will need to know the SQUID's critical current I_0, the measured modulation depth, and the measured ratio of the slopes r. These can all be found from the I-V or the I-Φ. One now uses Fig. 4.3 directly to obtain α and β, interpolating between the points where necessary. From I_0 and β, one can now find $L = \beta\Phi_0/(2I_0)$.

The above analysis admits of errors in several stages. First of all, the actual SQUID need not have the ideal equations of motion. Secondly, the presence of a sizeable inductive asymmetry would invalidate the approach. For the SQUIDs of this thesis, however, the inductive asymmetry η should be quite small because of the generally symmetric geometrical construction of the SQUIDs. Thirdly, at certain values of r and modulation depth, the technique does not allow for the accurate estimate of α and β. This happens at the small r portion of each fixed β curve, where curves of different β cross. It should be remarked that the surface is in fact everywhere double valued, which is to say that there are always two different α's and β's which can produce the same

modulation and r. This usually does not cause any problem because one of the solutions will generate an L which is very far from the expected geometrical inductance, and may be safely discarded. Near the high r part of every curve, however, the different L's approach each other, and the technique becomes inaccurate. Fourthly, the measured I_o and r can be in error.

Table 4.1 shows the results of just such an analysis for the SQUIDs of this thesis. One should not view this as merely a large collection of numbers, for there is much revealed about the fabrication procedure, the validity of the RSJ model, and the range of SQUIDs studied in this thesis.

Large asymmetries in the critical current are rather common. For all of the SQUIDs of Table 4.1, one finds an average $|\alpha|$ of about 0.28. This means that on the average, the two critical currents differ by about 30%. This is an indication of the difficulty of making reproducible critical current densities in the Nb-NbOx-PbIn junctions. This is all the more disconcerting when one realizes that the junctions in each SQUID were made simultaneously in exactly the same RF oxidation plasma, and went through all of the same processing steps simultaneously. This is the most favorable case one could hope for. It also indicates that it is necessary to ascertain the assymetry in order to get an accurate estimate of the inductance from the modulation depth.

The results have been grouped according to device type. Devices with the same letter in their name have the same geometry (this is true for all of the devices except the type A's which can have slightly different geometries, although all are very similar, see Chapter 1). Devices with the same geometry should yield the same inductance L if the

Table 4.1: Parameters of Measured SQUIDs

Device	Date	T (mK)	$2I_0$ (μA)	A	r	α	β	L (nH)
A1	7- 2-85	150	3.66	0.484	0.632	0.45	0.7	0.396
A2 (*)	7-21-85	130	10.8	0.328	0.61	0.6	1.35	0.26
A3 (**)	5-25-85	160	5.78	0.635	0.779	0.22	0.495	0.18
A4	8-10-85	120	0.71	0.89	0.99	0.0	0.16	0.47
A'5	9-16-85	170	6.23	0.392	0.754	0.39	1.2	0.399
A6 (***)	2-19-87	1390	2.04	0.6	0.83	0.18	0.58	0.59
A7 (***)	2-16-87	4200	17.2	0.176	0.953	0.25	4.0	0.48
A8 (***)	2-12-87	4200	3.84	0.53	0.905	0.11	0.79	0.43
B1	10-27-87	160	3.00	0.304	0.709	0.55	1.7	1.17
C1	9-21-85	120	6.15	0.32	0.60	0.68	0.52	0.18
C2	11-15-85	150	5.32	0.618	0.826	0.18	0.55	0.214
C3	1-31-86	1400	21.2	0.292	1.0	0.0	2.1	0.205
C4	2- 6-86	1400	7.1	0.55	0.954	0.06	0.75	0.219
C5	2- 8-86	1400	3.07	0.379	0.766	0.62	0.24	0.16
D1	5-30-86	110	6.34	0.313	0.597	0.64	1.35	0.44
D2	8-29-86	50	4.55	0.414	0.772	0.35	1.1	0.50
E1	2-19-86	95	5.51	0.563	0.96	0.05	0.725	0.27
E2	5-21-86	510	15.1	0.291	0.96	0.13	2.1	0.29
F1	2-27-86	140	5.73	0.32	0.945	0.15	1.93	0.70
G1	3-12-86	110	4.15	0.39	0.76	0.61	0.24	0.12
I1	6-27-87	105	4.13	0.668	0.905	0.09	0.45	0.225
J1	8- 5-86	50	21.6	0.283	0.919	0.25	2.1	0.20
K1	8-14-86	35	11.42	0.23	0.939	0.23	2.9	0.53
M1	10-31-87	25	5.64	0.39	0.99	0.02	1.4	0.514
M2	5- 6-88	20	6.2	0.35	0.71	0.55	1.4	0.47
N2	12-11-87	20	17.7	0.196	0.886	0.5	3.4	0.398
O1	5-19-87	30	1.36	0.97	0.964	0.05	0.03	0.046
P1	6- 5-87	23	1.77	0.352	0.665	0.55	1.25	1.46
NBS1	7-21-87	20		(see Chapter 8)				0.08
FIN1	4-10-88	43		(see Chapter 8)				0.04

(*) 20 turn input coil, left open for measurement of β.
(**) Magnetometer configuration, (geometry described in Chapter 3)
(***) These were variants of the type A, discussed in Chapter 7.

analysis is correct. Not surprisingly, one can see a roughly constant L for the devices in each group, at about the 10 or 20% level. However, there is a notable exception. In the type A devices, differences as large as 50% occur. This is undoubtedly because some of the type A devices were of slightly different construction, and some were made with coils (as noted) while others were made without coils. The presence of a coil apparently produces an inductive screening, and can cause a considerable reduction in the inductance of the SQUID. Without exception, the devices with coils also showed large amounts of structure on their I-V characteristics at low temperatures. For this reason, I stopped putting coils on the measured SQUIDs, and only the early type A's were ever tested with coils in place. A second discrepancy occurs in devices with larger α. One sees that the inductance of the higher α devices is generally underestimated, this is equivalent to saying that we observe more modulation than we should. I do not know the source of this discrepancy. Although such behavior is consistent with an inductive asymmetry, η, a η asymmetry is not consistent with the construction of the SQUIDs.

The results of Table 4.1 demonstrate the range of SQUID parameters that have been investigated. This is summarized in Table 4.2. One can see that I have made two orders of magnitude variations in α, β, and L, while $2I_0$ has been varied by about a factor of 30. The reason for these large variations was to test the behavior of the excess noise in the SQUID as a function of the SQUID parameters, as will be discussed in considerable length in Chapters 5, 6, 7, and 8. For completeness, in Table 4.3 I have also listed the origin of the different devices according to the wafer substrate upon which they were fabricated.

Table 4.2: Parameter Range of tested SQUIDs

Quantity		Device	Value	
largest	β	A7	4.0	
smallest	β	O1	0.03	
largest	α	C1	0.68	
smallest	α	C3, A4	< 0.01	
largest	$2I_o$	FIN1	43.0	μA
smallest	$2I_o$	A4	0.71	μA
largest	L	P1	1.46	nH
smallest	L	O1	0.046	nH

Table 4.3: Devices Made on the Same Wafer

Wafer	wafer material	devices
b	Si, 100, .05 Ωcm, 12 kA thermal oxide	A3
f	Si, 100, .05 Ωcm, 12 kA thermal oxide	A1
h	Si, 100, .05 Ωcm, 12 kA thermal oxide	A2 A4
i	Si, 100, .05 Ωcm, 12 kA thermal oxide	A5 B1 C's D's
k	Si, 100, .05 Ωcm, 12 kA thermal oxide	E1 F1 G1
l	Si, 100, 20 Ωcm, no thermal oxide	E2
m	Al_2O_3	I1 J1 K1
n	Si, 100, .05 Ωcm, 12 kA thermal oxide	A6 A7 A8
o	Si, 100, .05 Ωcm, 12 kA thermal oxide	O1 P1
p	Si, 100, .05 Ωcm, 12 kA thermal oxide	M1 N1
q	Si, 111, 20 Ωcm, 12 kA thermal oxide	M2

4.6 Some Measured SQUID Characteristics

Ideal SQUID I-V characteristics have been calculated by many authors.[6-11] Measured I-V curves are often very poor, which is to say they often possess kinks, steps, or negative resistance regions which are not generated by the ideal models. In itself, this would not necessarily be a bad thing, except that the structure is generally associated with large amounts of white noise, and we do not know theoretically how to estimate the true energy sensitivity in such regimes.

The structure is undoubtedly due to high frequency effects in the SQUID which change the SQUID equations of motion from the ideal RSJ model. This seems mostly to be due to two effects:

(1) Large β_c introduces hysteresis into the SQUID characteristics.

(2) The incorporation of an input coil or input circuit causes screening of the SQUID, and generally introduces large amounts of resonant structure.

Working at small β_c and without an input coil eliminates most of the structure. In practice, $\beta_c<0.2$ produces nearly ideal characteristics in a device without an input circuit. It should also be noted that high temperature causes a considerable reduction in the apparent structure due to the effects of noise rounding. This structure becomes increasingly apparent as the temperature is lowered.

To illustrate some of these effects, I now present data from two SQUIDs. While almost all of the SQUIDs tested in this thesis produced

very nice looking characteristics at 4.2 K, only a minority had very nice I-V's at low temperatures. The following two devices are representative of this minority, and should be taken as a demonstration that SQUID's with nearly ideal characteristics can be produced even at low temperatures. It should be clearly understood that SQUID's with larger β_c, or an input coil, showed much more structure.

There are two important points about the SQUID I-V characteristics taken with the SQUID readout system discussed in Chapter 2. First of all, the voltage across the device is not directly measured. Rather, I record the quantity $I_{b1}R_X = V_X$, while the voltage across the SQUID is given by: $V = V_X - IR_X$ (see Chapter 2), where I is the current passing through the SQUID, and R_X is the value of the bias resistor (see Fig. 2.7). This technique produces the tilted I-V characteristics shown below. At zero voltage, the I-V characteristic appears to have a finite resistance, this is merely a result of plotting $I_{b1}R_X$ instead of V. Secondly, it should be realized that the current axis suffers from no such skewed coordinate system, but is directly measured by SQUID(2).

The first SQUID is device E1, which has an estimated β_c of 0.1, (see Table 4.1 for more data). I-V characteristics at the temperatures 4.2, 1.6, 0.54, 0.30 and 0.095 K are shown in Figs. 4.4 a, e, i, m, and q respectively. For this same SQUID, I also present the I-Φ characteristics in Figs. 4.4c, g, k, o, and s; the noise vs. V in Figs. 4.4 b, f, j, n, and r; and the noise vs. Φ in Figs. 4.4d, h, l, p, and t. The I-V and I-Φ characteristics are all very smooth, with no discernible structure at even the lowest temperature. At low voltages, one can clearly see the noise rounding of the I-V increase as the temperature is increased. The noise vs. V does begin to show a slight

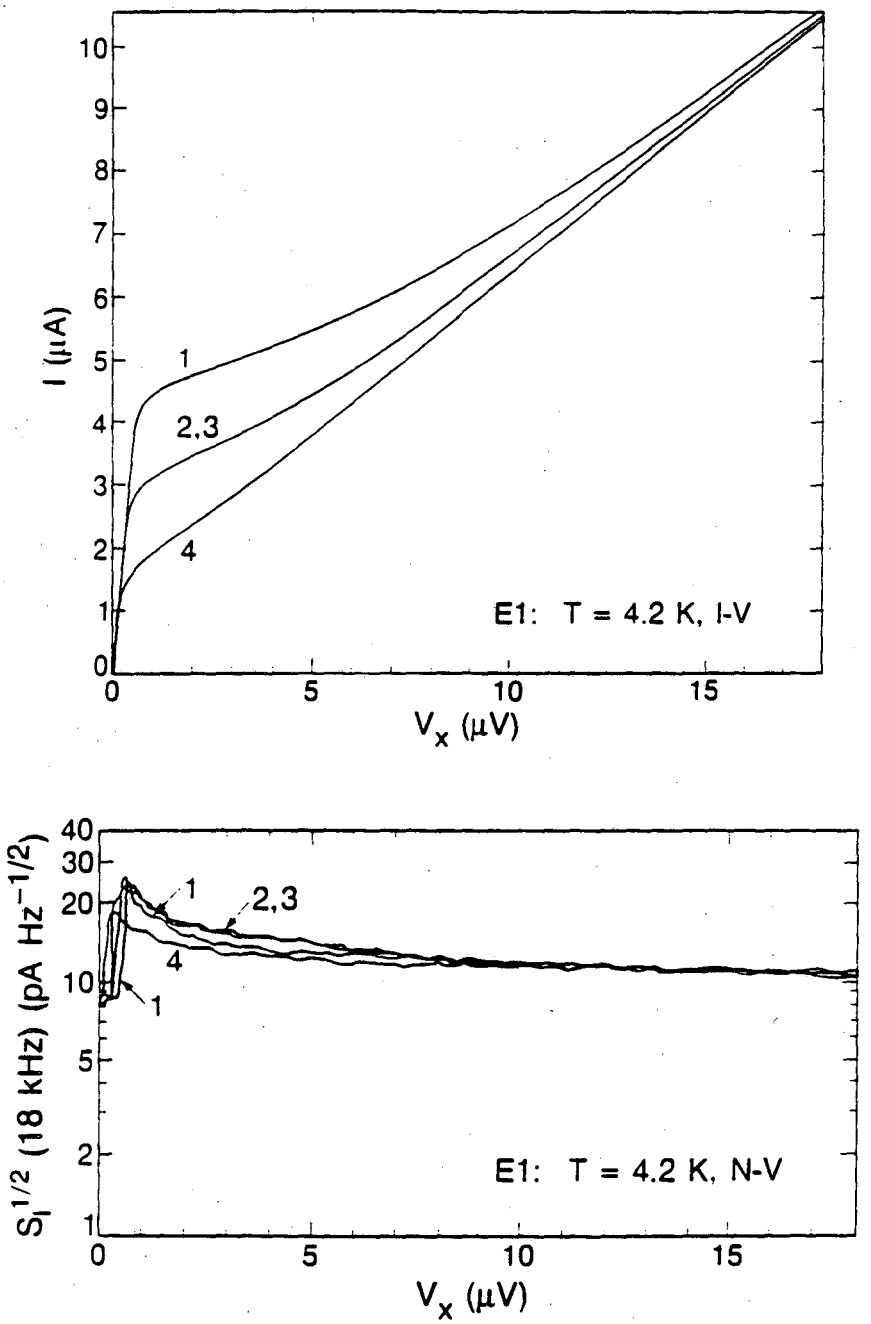

Fig. 4.4 (a) I-V of SQUID E1 at 4.2K, the curves 1 to 4 curves are for fixed flux bias current: 78.8, 0, 110.8, and 23 μA, respectively. (b) Noise vs V for the same flux bias currents as in (a).

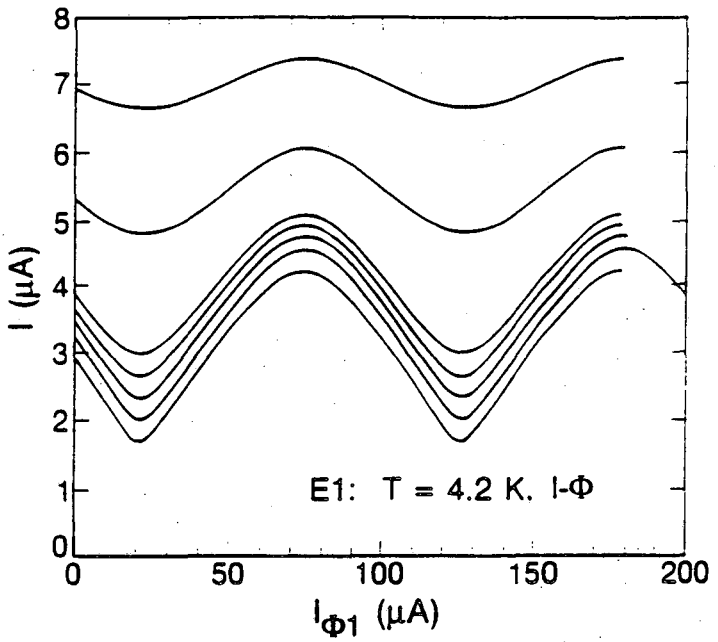

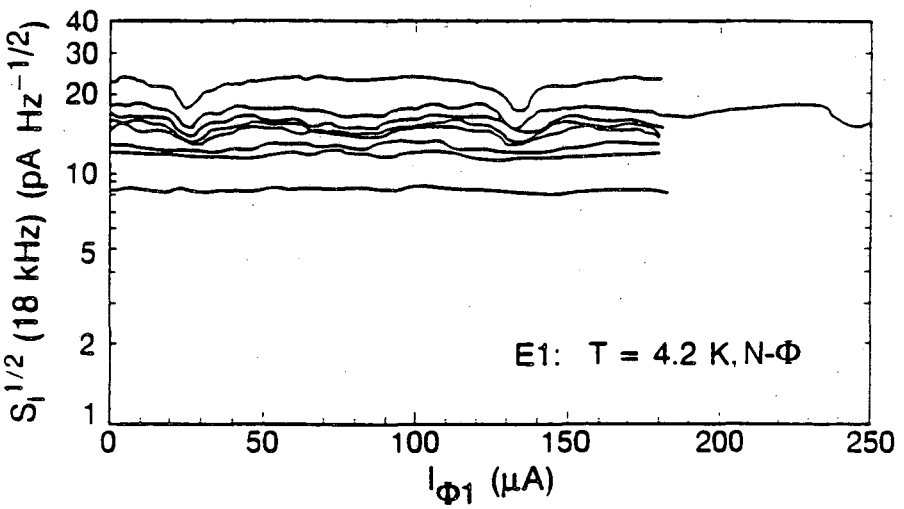

Fig. 4.4 (c) I-Φ for SQUID E1 at 4.2K, from top to bottom, the curves are for voltages V_X of: 10.8, 7.2, 3.6, 2.88, 2.16, 1.44, and 0.72 μV respectively. (d) Noise vs flux bias current, from bottom to top, the curves are for V_X : 0, 10.8, 7.2, 3.6, 2.88, 2.16, 1.44, and 0.72 μV respectively.

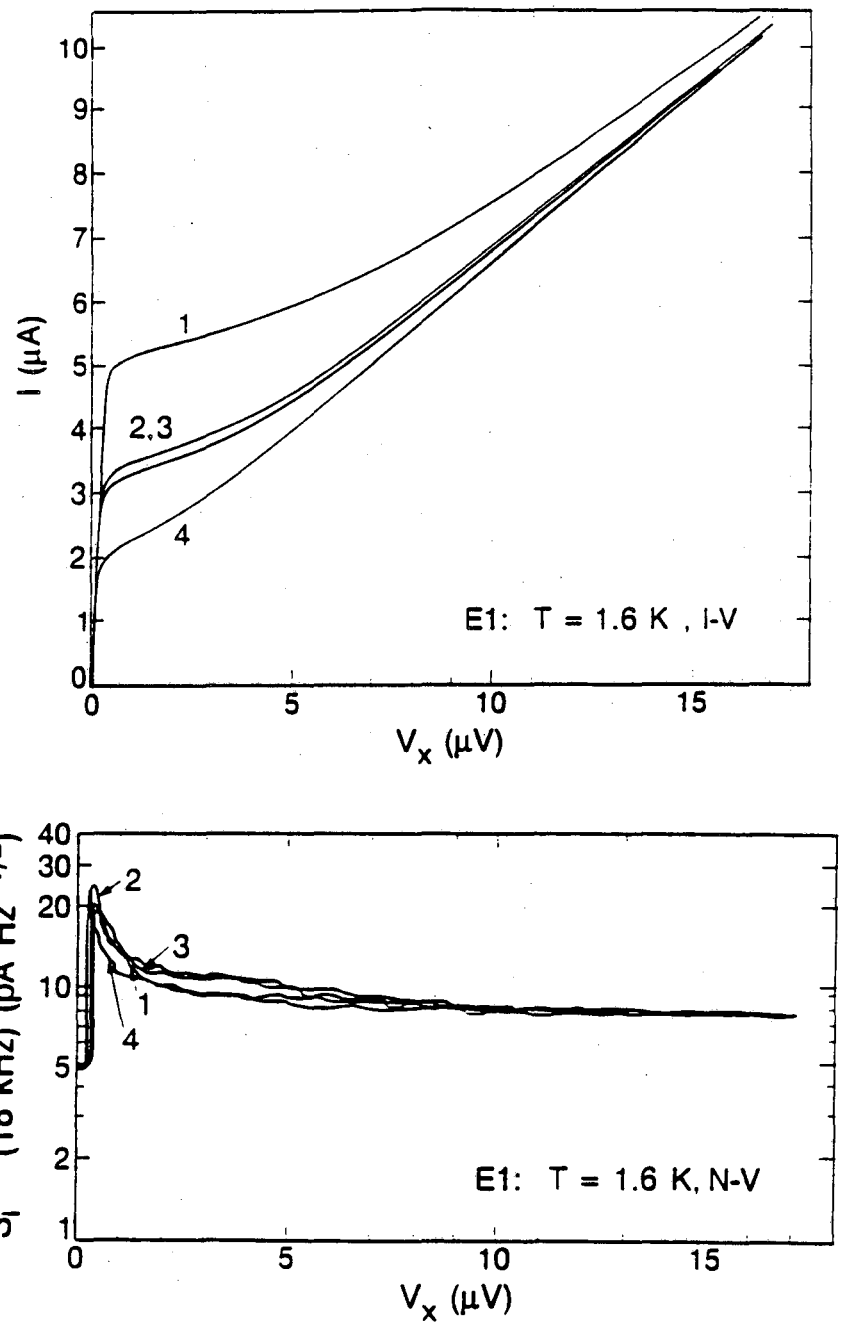

Fig. 4.4 (e) I-V of SQUID E1 at 1.6K, the curves 1 to 4 curves are for fixed flux bias current: 38.5, 74.2, 0, and 93.9 μA, respectively. (f) Noise vs V for the same flux bias currents as in (e).

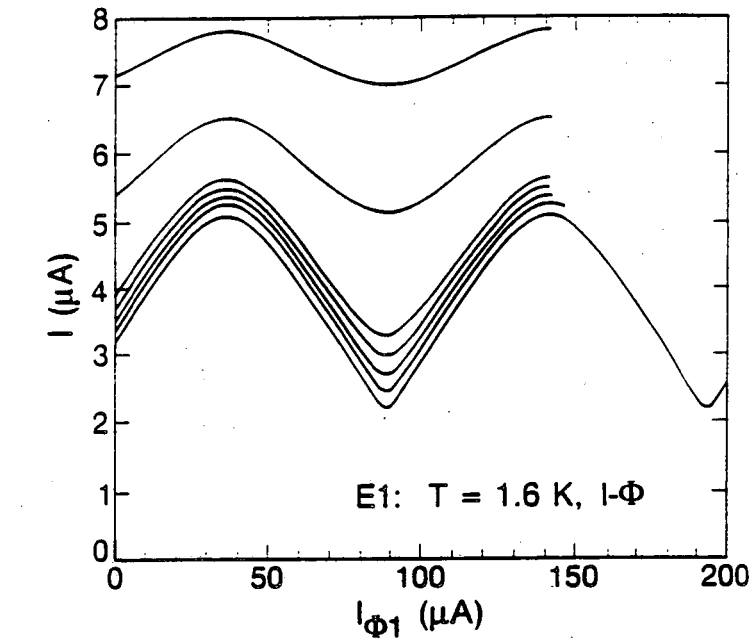

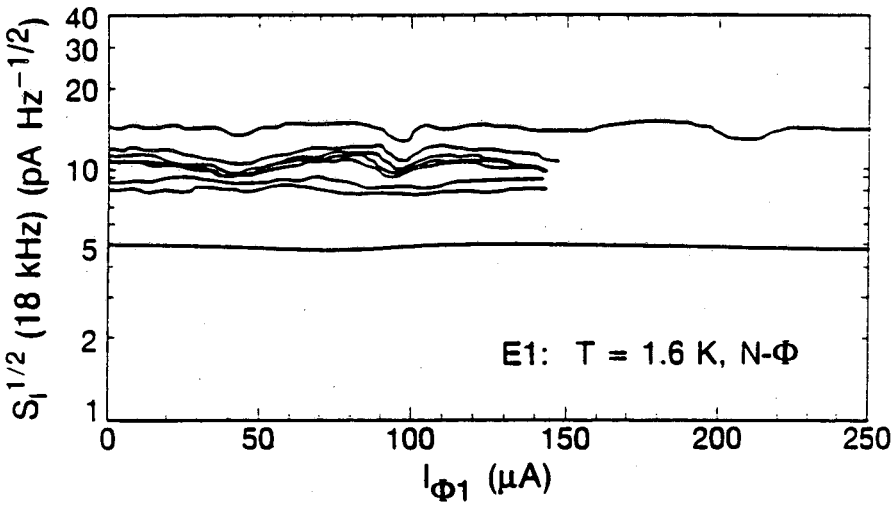

Fig. 4.4 (g) I-Φ for SQUID E1 at 1.6K, from top to bottom, the curves are for voltages V_X of: 10.8, 7.2, 3.6, 2.88, 2.16, 1.44, and 0.72 μV respectively. (h) Noise vs flux bias current, from bottom to top, the curves are for V_X : 0, 10.8, 7.2, 3.6, 2.88, 2.16, 1.44, and 0.72 μV respectively.

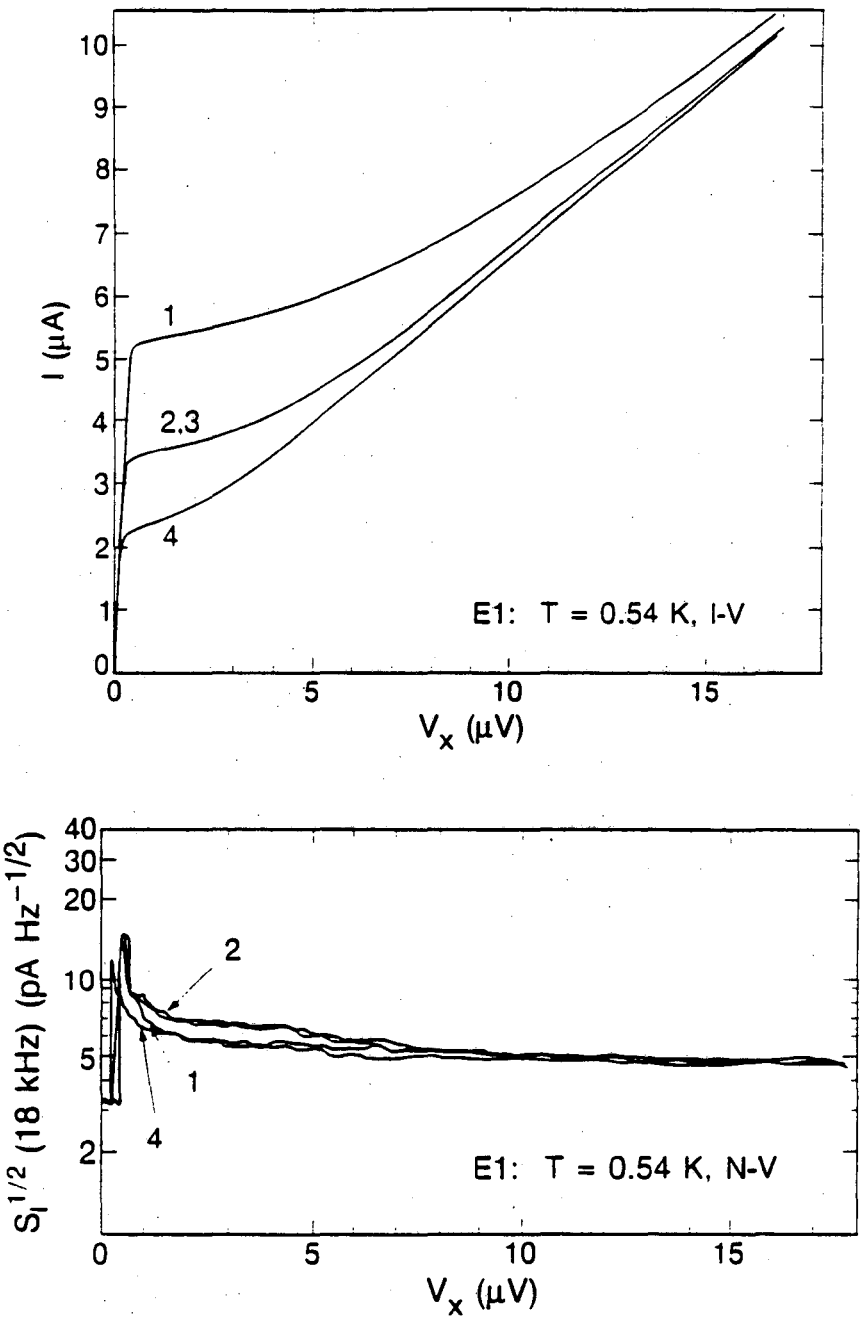

Fig. 4.4 (i) I-V of SQUID E1 at 0.54K, the curves 1 to 4 curves are for fixed flux bias current: 37.8, 0, 75.6, and 93.2μA, respectively. (j) Noise vs V for the same flux bias currents as in (i).

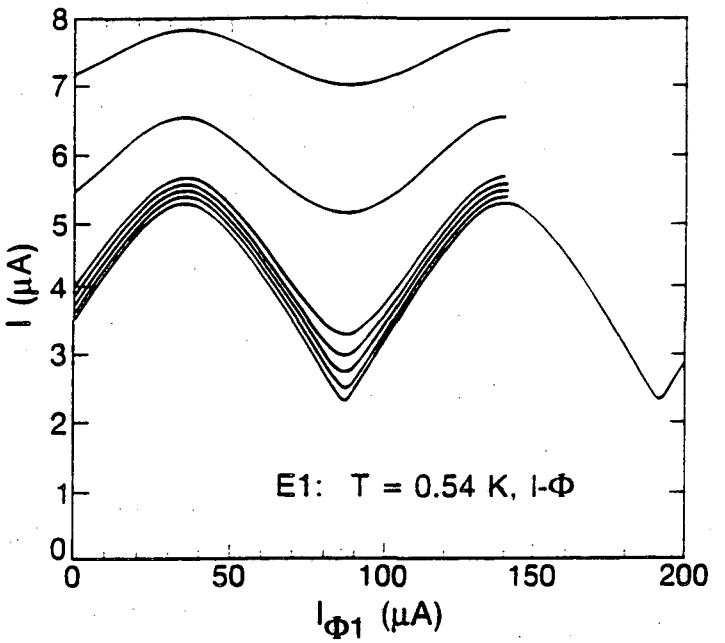

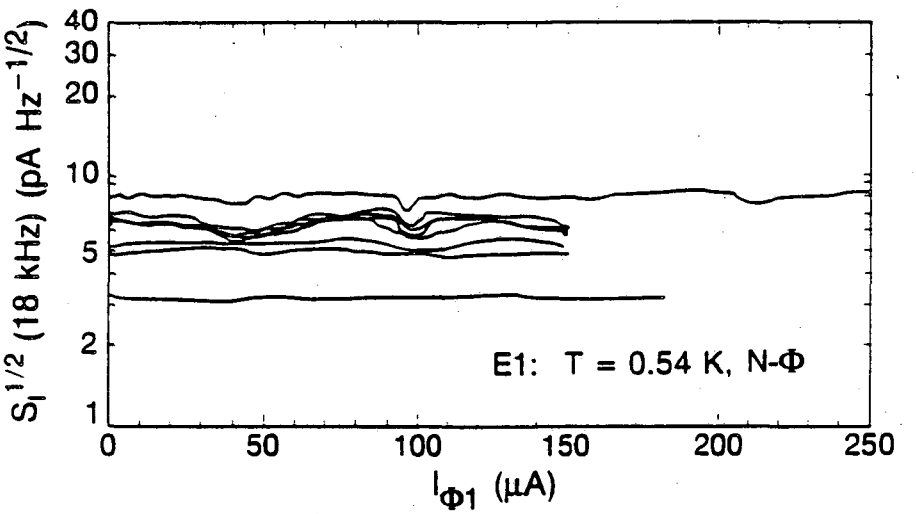

Fig. 4.4 (k) I- Φ for SQUID E1 at 0.54K, from top to bottom, the curves are for voltages V_X of: 10.8, 7.2, 3.6, 2.88, 2.16, 1.44, and 0.72 μV respectively. (l) Noise vs flux bias current, from bottom to top, the curves are for V_X : 0, 10.8, 7.2, 3.6, 2.88, 2.16, 1.44, and 0.72 μV respectively.

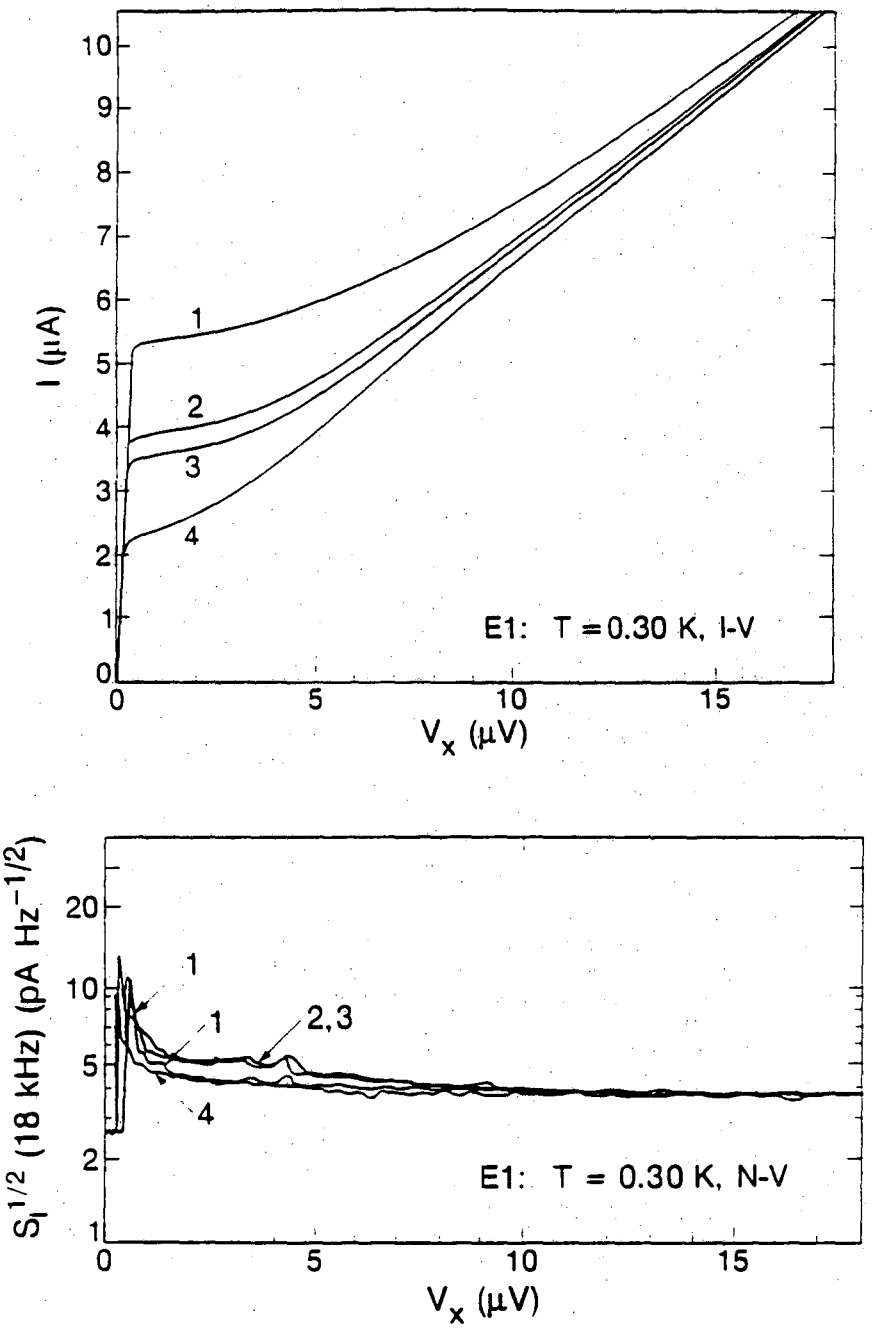

Fig. 4.4 (m) I-V of SQUID E1 at 0.3K, the curves1 to 4 curves are for fixed flux bias current: 38.5, 69.9, 0, and 92.9μA, respectively. (n) Noise vs V for the same flux bias currents as in (m).

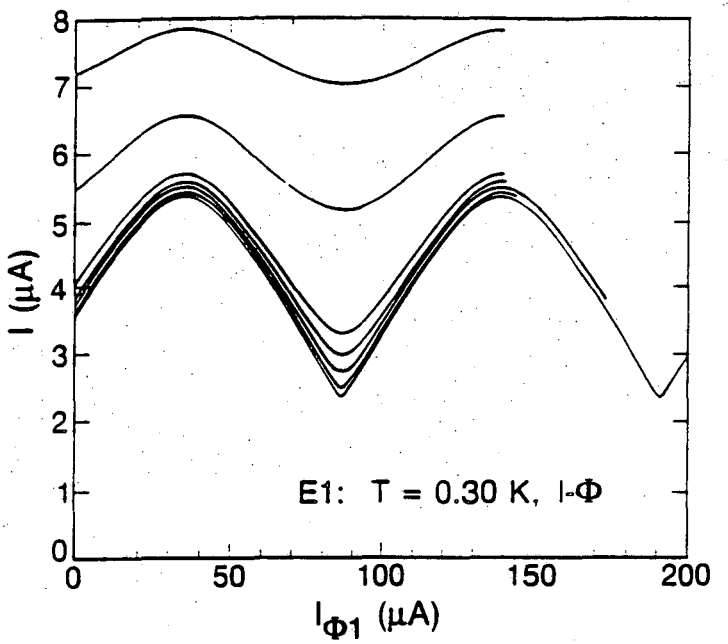

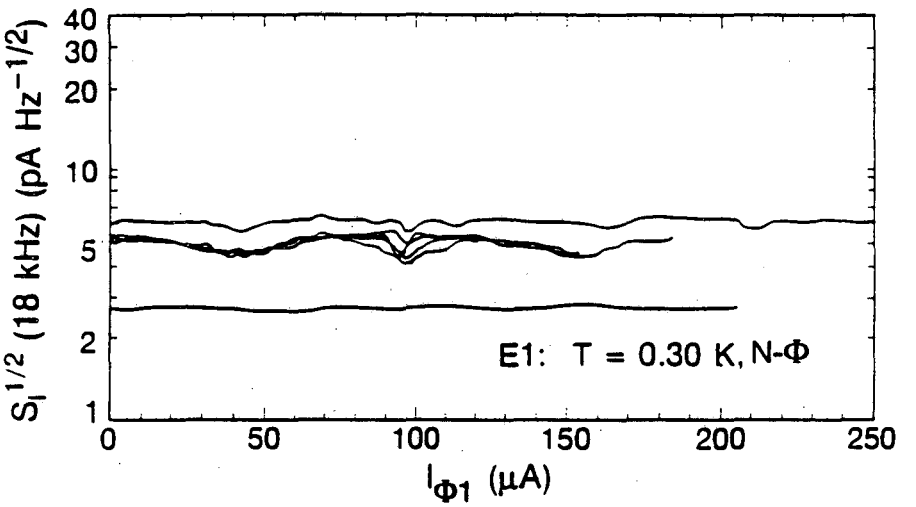

Fig. 4.4 (o) I- Φ for SQUID E1 at 0.30K, from top to bottom, the curves are for voltages V_X of: 10.8, 7.2, 3.6, 2.88, 2.16, 1.44, and 0.72 μV respectively. (p) Noise vs flux bias current, from bottom to top, the curves are for V_X : 0, 3.6, 2.88, 2.16, 1.44, and 0.72 μV respectively.

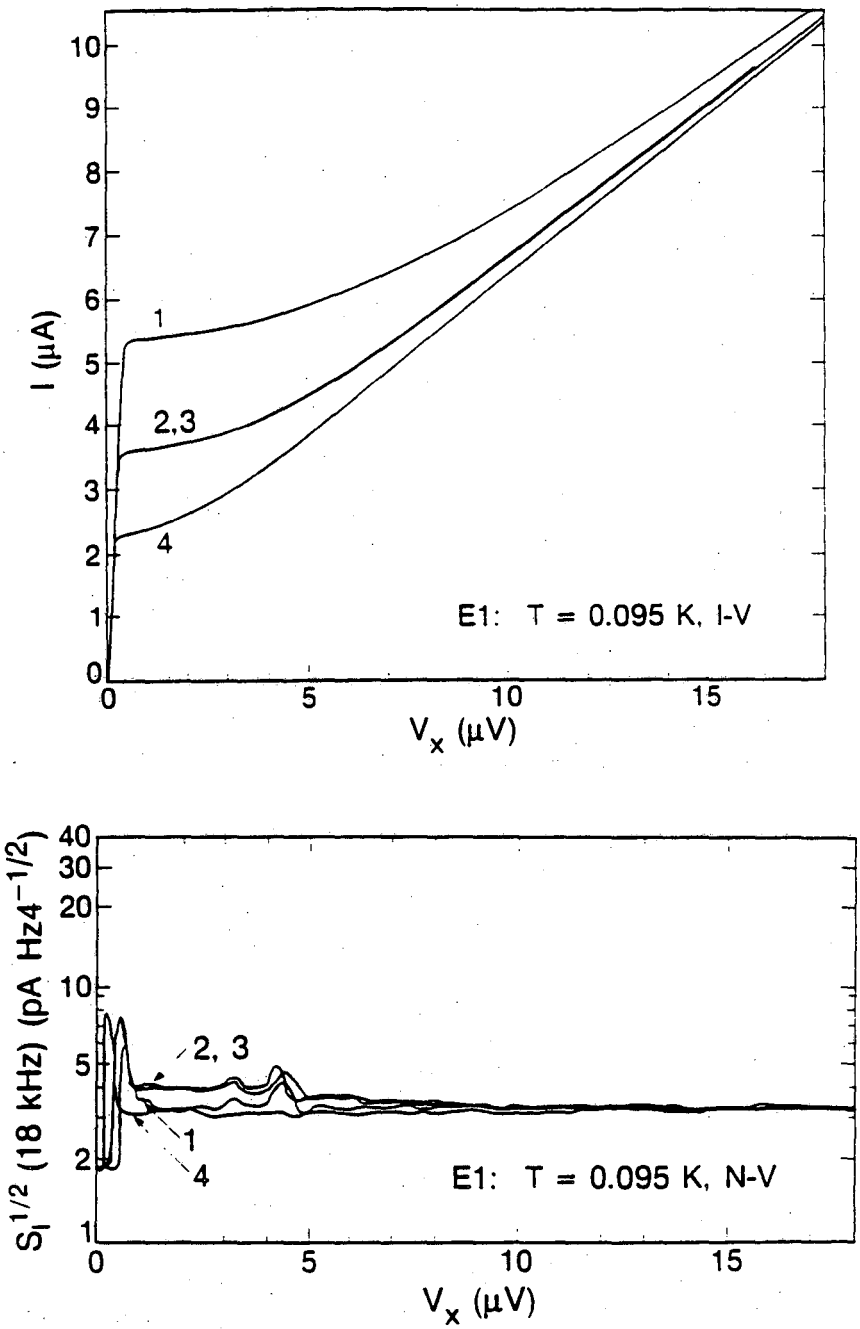

Fig. 4.4 (q) I-V of SQUID E1 at 0.095K, the curves 1 to 4 curves are for fixed flux bias current: 37.1, 0, 72.8, and 91.1 μA, respectively. (r) Noise vs V for the same flux bias currents as in (q).

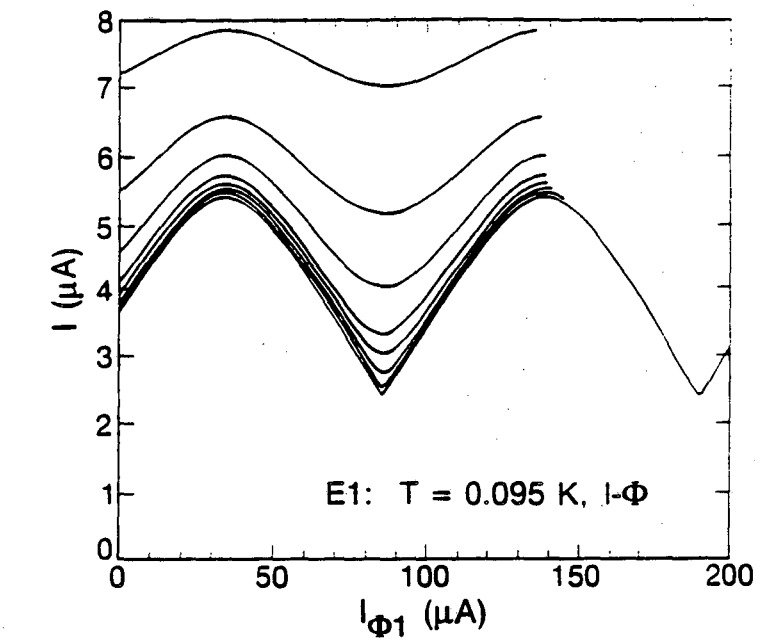

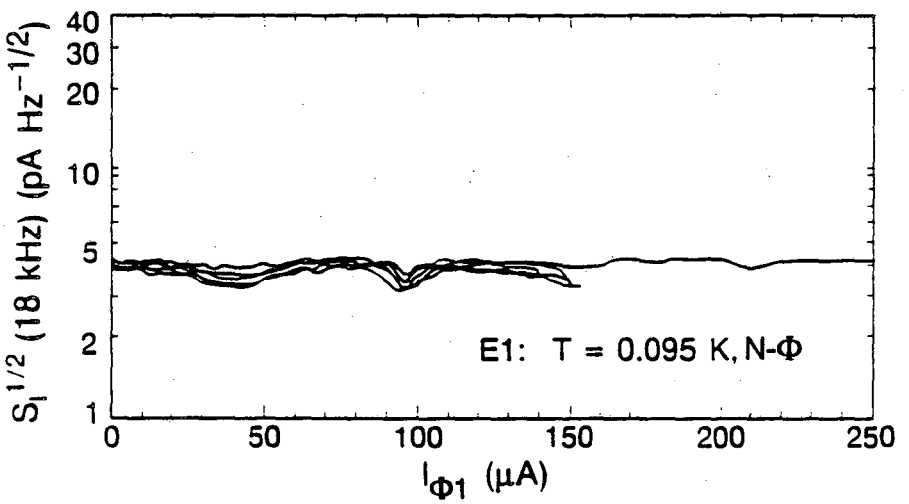

Fig. 4.4 (s) I-Φ for SQUID E1 at 0.095K, from top to bottom, the curves are for voltages V_x of: 10.8, 7.2, 5.04, 3.6, 2.88, 2.16, 1.44, and 0.72 μV respectively. (t) Noise vs flux bias current, from bottom to top, the curves are for V_x: 3.6, 2.88, 2.16, 1.44, and 0.72 μV respectively.

increase in the noise at around 3.5 μV as the temperature is lowered below 0.5 K. One can also clearly see that the low voltage portions of the I-V, where the noise rounding is prominent, is associated with a large amount of noise. As the temperature is lowered, this low voltage region of high noise gets smaller in extent, and one can obtain good performance quite close to the 0-voltage portion of the I-V. Other than the small feature in the noise at low temperatures, the characteristics are essentially ideal, and could easily be fitted to an ideal SQUID model.

The second SQUID is device D2. The I-V characteristics for this device are shown in Figs. 4.5 a, e, i, and k, at temperatures of 4.0, 0.95, 0.51, and 0.024 K respectively. The noise vs. V are shown in Fig. 4.5 b, f, j,and l. The I-Φ are shown in Figs. 4.5 c and g, and the noise vs. Φ are shown in Figs. 4.5 d and h only for the temperatures 4.0 and 0.95 K. The I-V at 4 K is smooth, with no discernible structure. As the temperature is lowered to 0.95 K, a small current step becomes visible at around 10 μV. By 0.51 K, the step has grown quite sharp, and a second small feature is visible at $\Phi_0/2$ at about 5 μV. At the lowest temperature, both steps are clearly visible. The appearance of the I-V as the temperature is lowered is reflected in the behavior of the noise vs. V plots. One sees a small rise in the noise at voltages that correspond to a step. As the temperature is lowered and the step becomes sharper, the noise typically becomes larger in the imediate vicinity of the step voltage. At voltages far from a step, there appears to be little affect upon either the noise or the I-V characteristics. The I-Φ and noise vs. Φ are all fairly smooth. This is undoubtedly because they did not happen to pass through the region of a step.

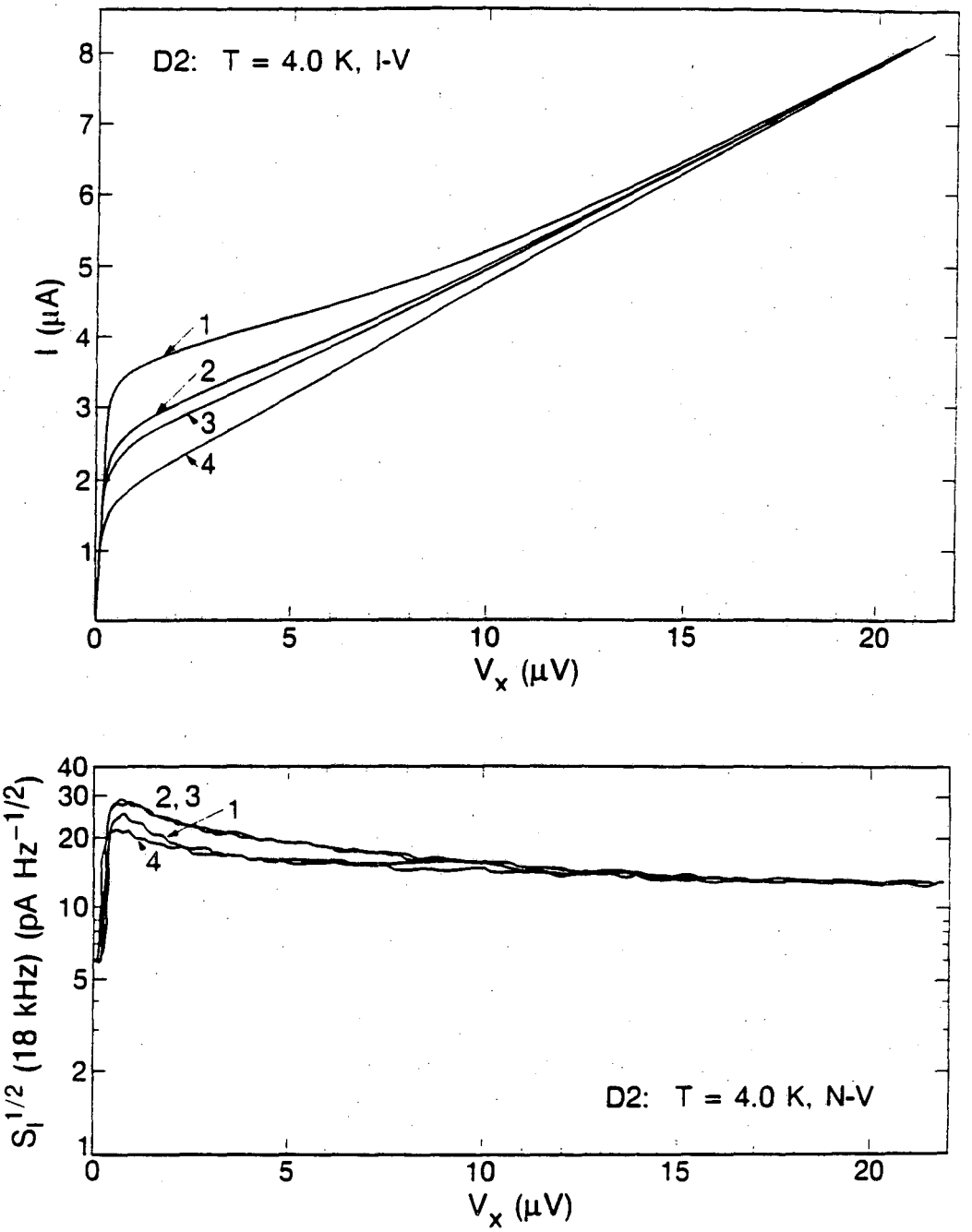

Fig. 4.5 (a) I-V of SQUID D2 at 4.0K, the curves 1 to 4 curves are for fixed flux bias current: 6.83, 0, 8.78, and 1.88 μA, respectively. (b) Noise vs V for the same flux bias currents as in (a).(9-2-86).

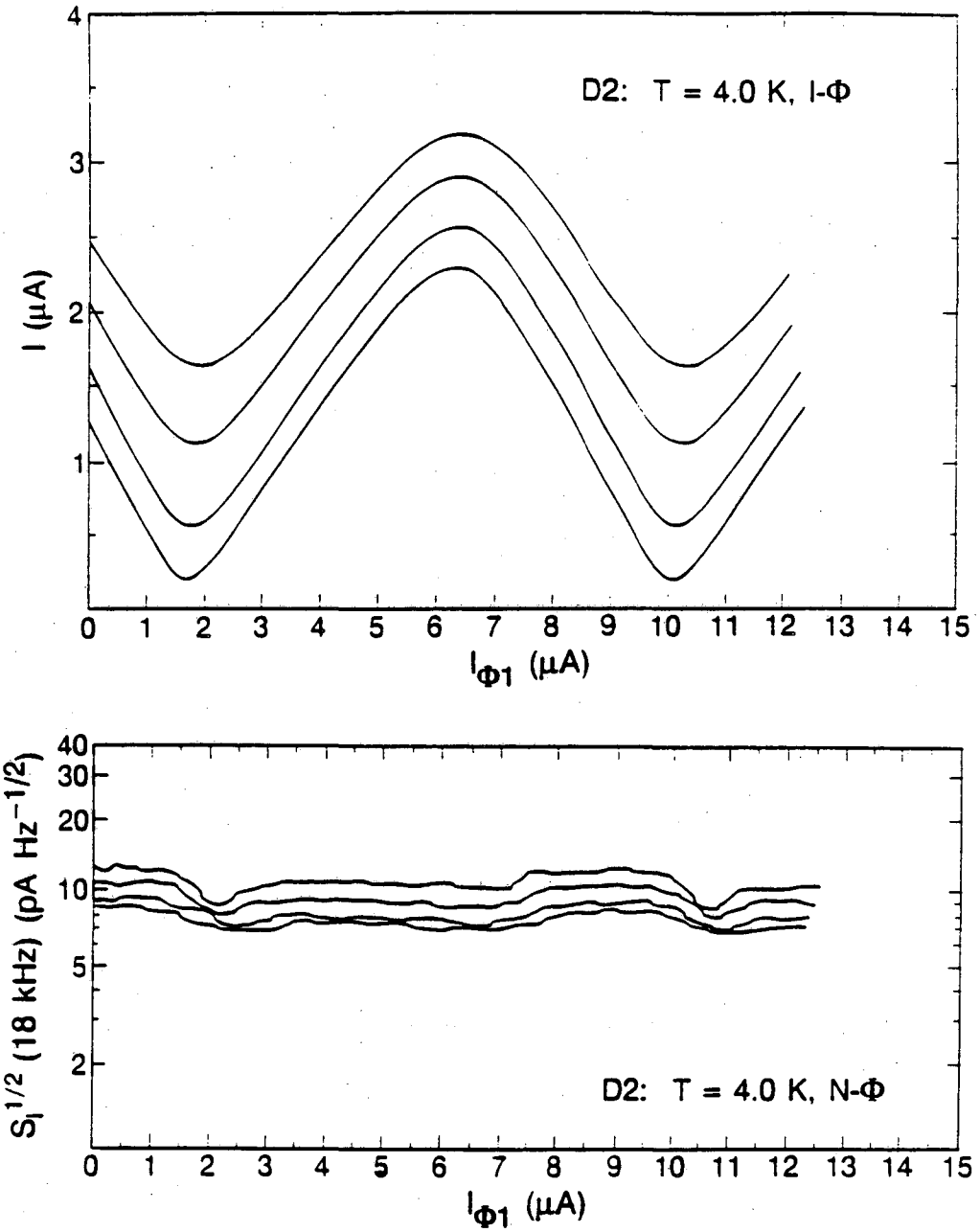

Fig. 4.5 (c) I-Φ for SQUID D2 at 4.0K, from top to botttom, the curves are for voltages V_x of: 4.32, 2.88, 1.44, and 0.72 μV respectively. (d) Noise vs flux bias current, from top to bottom, the curves are for voltages V_x : 0.72, 1.44, 2.88, 4.32 μV respectively.

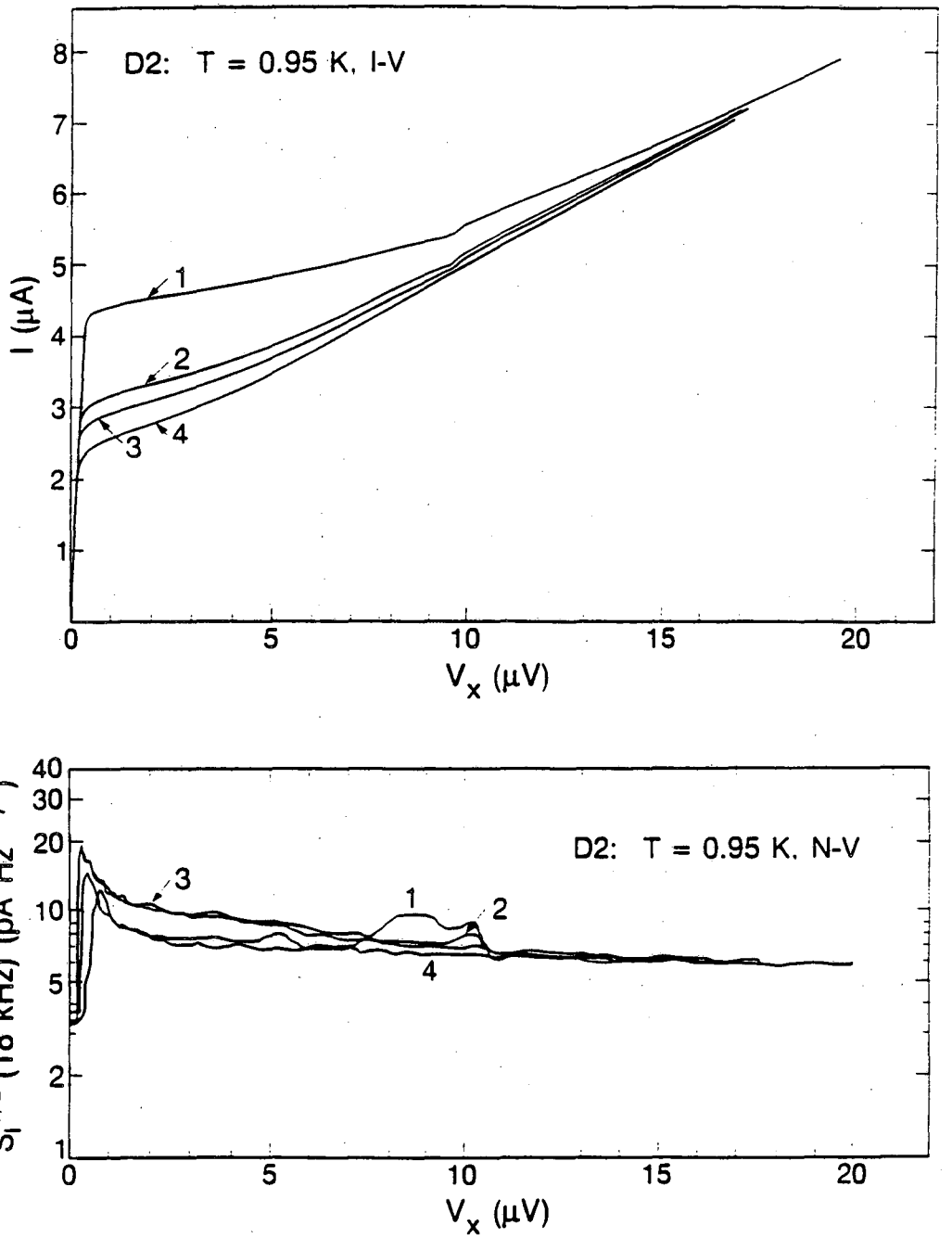

Fig. 4.5 (e) I-V of SQUID D2 at 0.95K, the curves 1 to 4 curves are for fixed flux bias current: 5.33, 7.98, 0, and 0.7 μA, respectively. (f) Noise vs V for the same flux bias currents as in (e).(9-1-86).

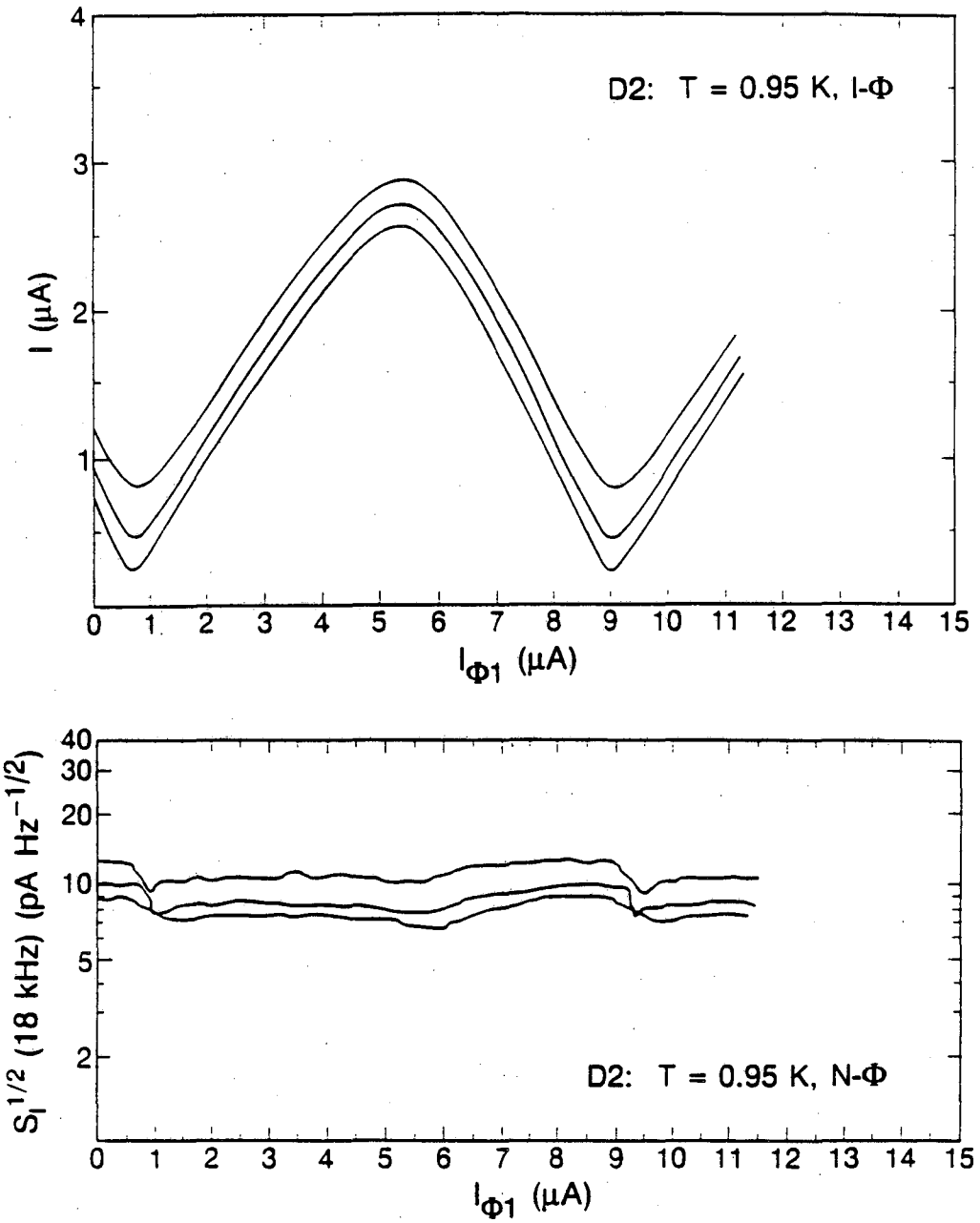

Fig. 4.5 (g) I-Φ for SQUID D2 at 0.95K, from top to botttom, the curves are for voltages V_x of: 2.88, 1.44, and 0.72 μV respectively. (h) Noise vs flux bias current, from top to bottom, the curves are for voltages V_x : 0.72, 1.44, 2.88 μV respectively.

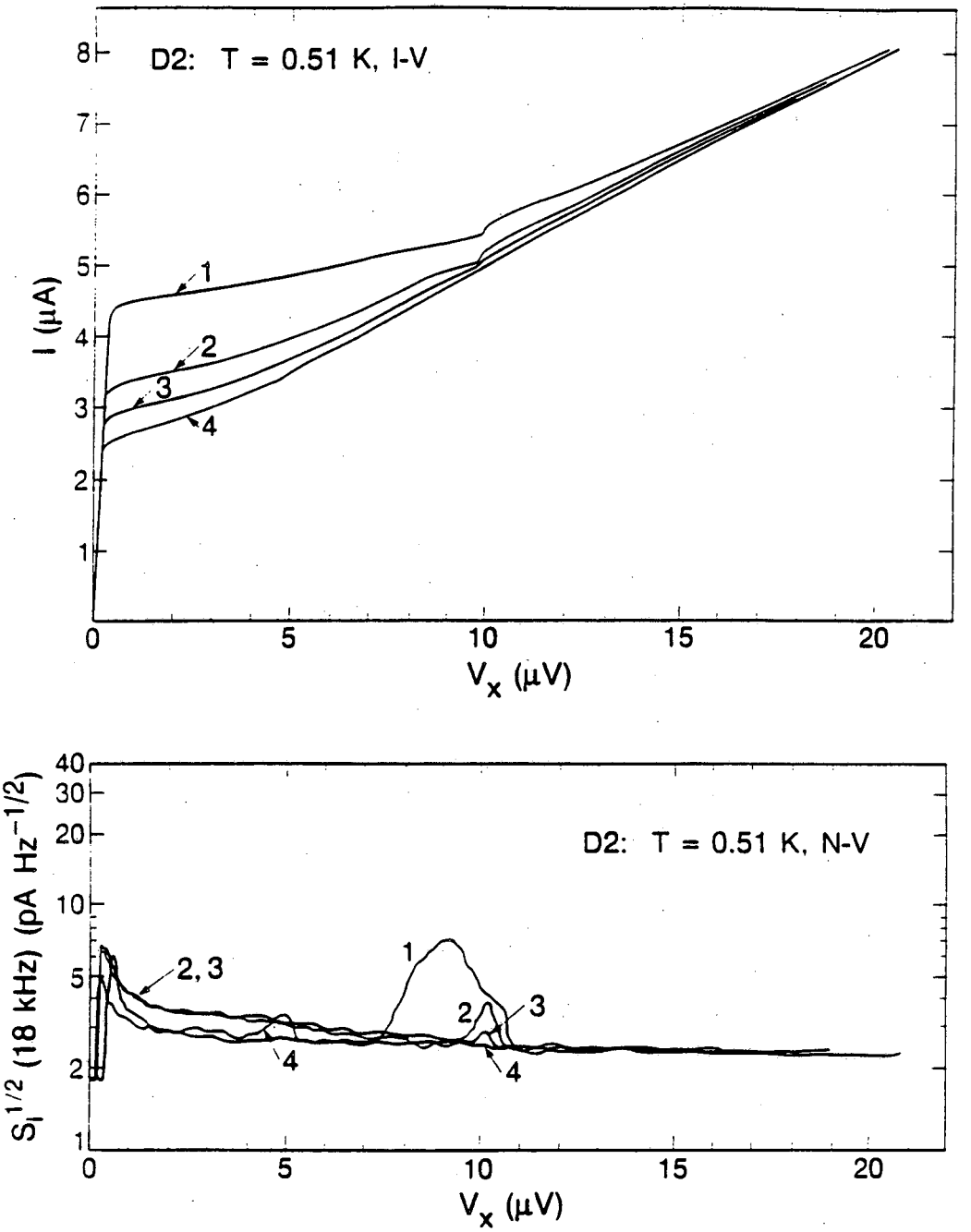

Fig. 4.5 (i) I-V of SQUID D2 at 0.51K, the curves 1 to 4 curves are for fixed flux bias current: 5.44, 7.76, 0, and 0.57 μA, respectively. (j) Noise vs V for the same flux bias currents as in (i).(8-31-86).

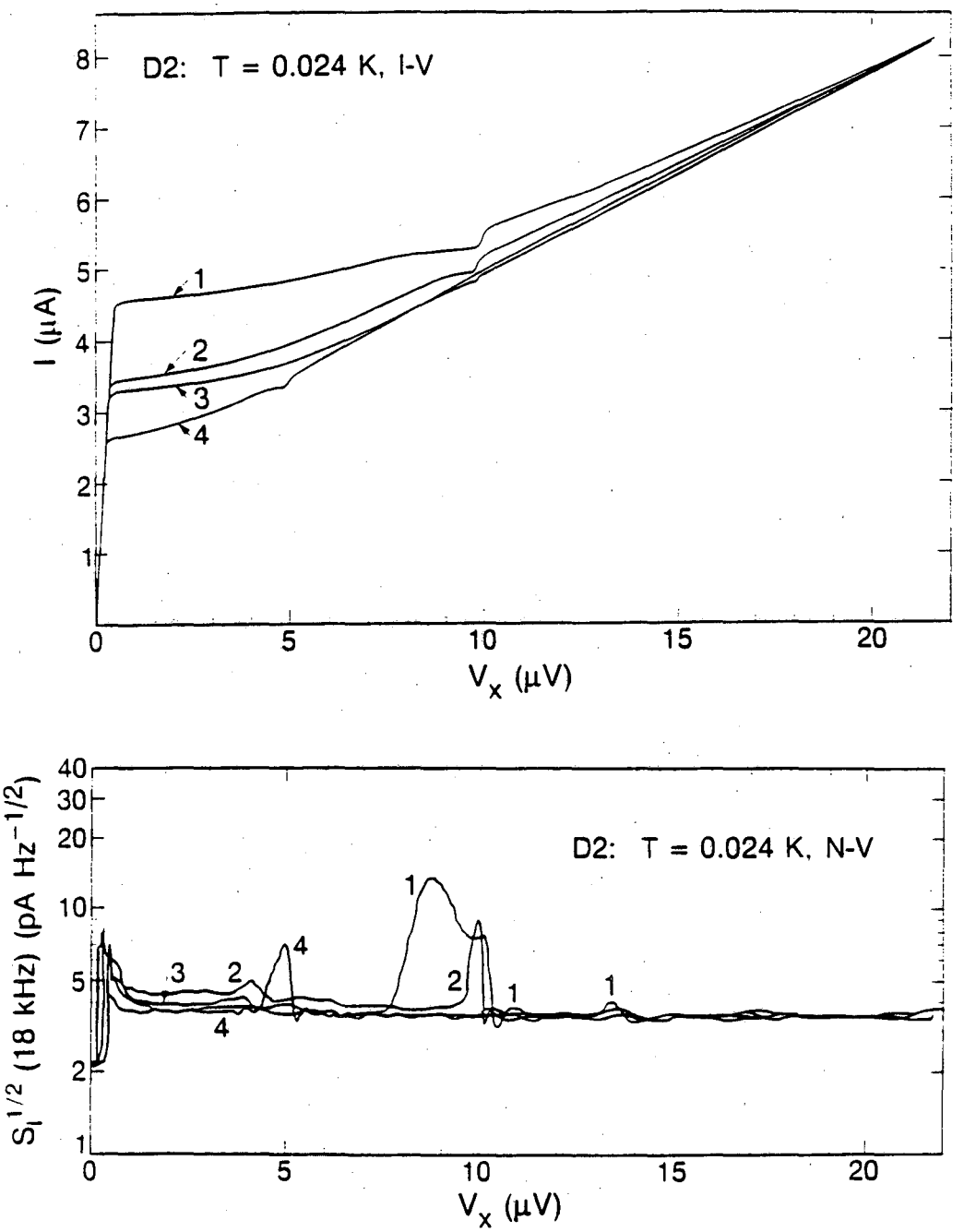

Fig. 4.5 (k) I-V of SQUID D2 at 0.024K, the curves 1 to 4 curves are for fixed flux bias current: -2.53, 0, -5.72, and -7-08 μA, respectively. (l) Noise vs V for the same flux bias currents as in (k).(8-28-86).

4.7 Appendix A: The SQUID Parameters

I record here the definitions of the various SQUID parameters as used in this thesis (see Fig 4.6):

I_{oj} is the critical current of juction number j, where j=1,2

$I_o = (I_{o1} + I_{o2})/2$

R_j is the resistance of shunt j,

L_1 (L_2) is the inductance of the left (right) arm of the SQUID,

M is the mutual inductance between the two SQUID arms,

L is the SQUID ring inductance and equals L_1+L_2-2M,[6]

C_j is the capacitance of junction j,

V_j is the voltage across juction j,

Φ is the applied flux,

$\Phi_o \equiv 2.07 \times 10^{-15}$ Tm^2 is the flux quantum,

I_j is the current flowing through the j-th SQUID arm

$I = I_1 + I_2$ is the bias current,

$J = (I_2-I_1)/2$ is the circulating current in the SQUID loop

V is the voltage across the SQUID,

V_{nj} is the random Nyquist voltage due to R_j, and is proportional to T

T is the SQUID temperature

t is the time.

The dimensionless variables are:

$i = I/I_o$

$v = V/I_oR$

$\tau = t2\pi I_oR/\Phi_o$, $\phi = \Phi/\Phi_o$

$j = J/I_o$

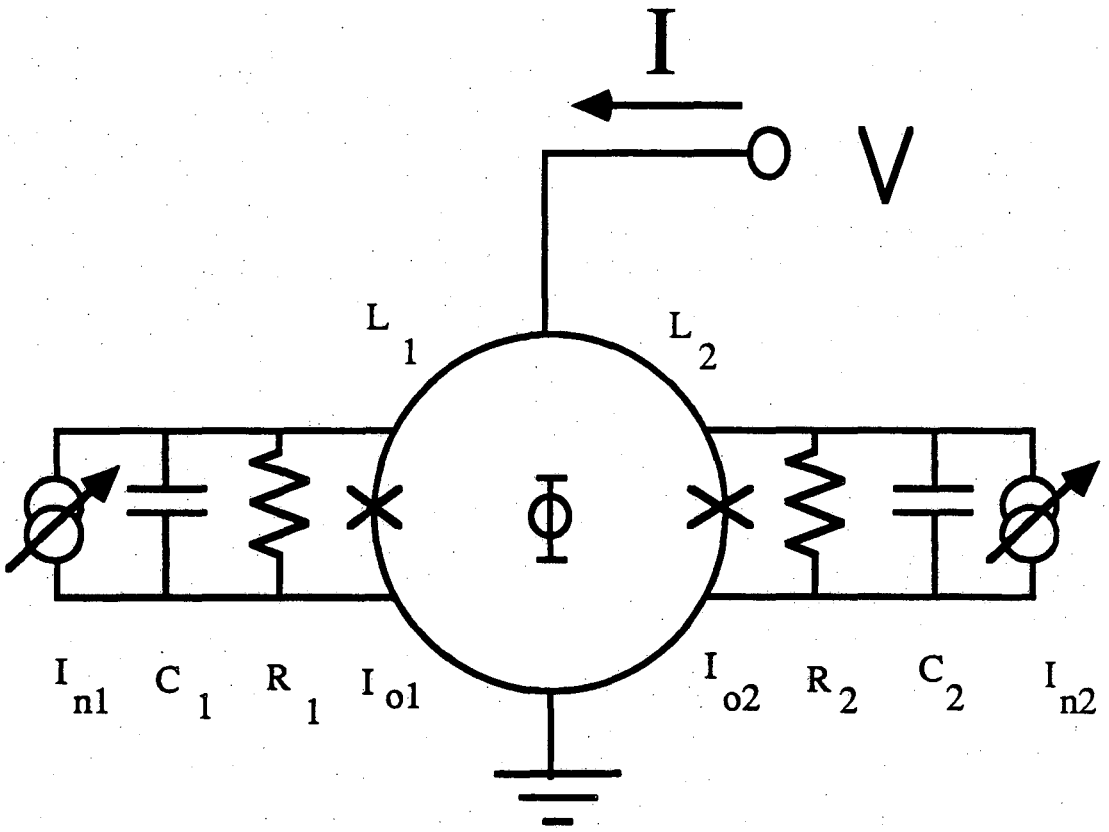

Fig 4.6. Lumped circuit model schematic of the dc SQUID, with labelled SQUID parameters.

$$\beta = 2LI_o/\Phi_o, \qquad \beta_c = 2\pi I_o R^2 C/\Phi_o, \qquad \alpha = (I_{o2}-I_{o1})/(I_{o2}+I_{o1})$$

$$\eta = (L_2-L_1)/L, \qquad \rho = (R_1+R_2)/(R_2-R_1), \qquad \xi = (C_2-C_1)/(C_2+C_1)$$

$$\Gamma = 2\pi k_b T/I_o\Phi_o$$

References

(1) V.V. Danilov, K.K. Likharev, A.B. Zorin "Quantum Noise in SQUIDs", IEEE Trans. Magn., MAG-19, 572 (1983).

(2) R.H. Koch, D.J. Van Harlingen, and J. Clarke,"Quantum Noise Theory for the dc SQUID", Appl. Phys. Lett. 38, 380 (1981).

(3) J.M. Martinis and J. Clarke, "Current Noise Measured in the dc SQUID", J. Low Temp. Phys., 65, 459 (1986).

(4) C.D. Tesche and J. Clarke, J. Low Temp. Phys. 37, 397 (1979).

(5) J.M. Jaycox and M.B. Ketchen, "Planar Coupling Scheme for Ultra Low Noise dc SQUIDs", IEEE Trans. Magn. MAG-17, 400 (1981).

(6) C.D. Tesche and J. Clarke, "dc SQUID: Noise and Optimization" J. Low Temp. Phys. 29, 301 (1977).

(7) A.Th.A. De Waele and R. DeBruyn Ouboter, Physica 41, 225 (1969).

(8) J. Clarke and J.L. Paterson, Appl. Phys. Lett. 19, 469 (1971).

(9) T.A. Fulton, L.N. Dunkleburger, R.C. Dynes, Phys. Rev. B6, 855 (1972).

(10) W. -T. Tsang and T. Van Duzer, J. Appl. Phys. 46, 4573 (1975).

(11) V. J. de Waal, P. Schrijner, R. Llurba, "Simulation and Optimization of a dc SQUID with a Finite Capacitance", J. Low Temp. Phys., 54, 215 (1984).

Chapter 5: Parameter Fluctuations and Excess Noise

5.1 Introduction

The main subject of this thesis is excess noise in the dc SQUID. Accordingly, it is important to explain what is meant by excess noise and how it can arise. This Chapter is devoted to a theoretical investigation of a broad class of hypothetical noise sources; what I call "parameter fluctuations". I say hypothetical because in fact most of these have never been observed experimentally. Nevertheless, it is our purpose here to understand how these sources would behave if they were present. In this way we can attempt to find the source of the excess noise in our SQUIDs by comparing the observed properties of the noise with the expected behavior of the hypothetical sources.

5.2 Parameter Fluctuations as Sources of 1/f Noise

The behavior of the dc SQUID can be treated theoretically by numerically solving the classical equations of motion as given by Eqs. (4.3). These equations describe the evolution of the phases δ_1 and δ_2 with time. In solving these equations, one can include the effects of thermal noise V_{n1} and V_{n2} arising from the Nyquist noise in the resistive shunts of the SQUID. The resulting voltage, V, across the SQUID will undergo random fluctuations in time, and this is the ideal or thermal noise at the SQUID output. For frequencies much smaller than the Josephson frequency, it is known that the equations predict that this noise will be independent of frequency or "white".[1,2]

The calculations are non-trivial because of the non-linear equations and also because the noise is generally required at frequencies which are small compared to the Josephson frequency. Numerical simulations are thus quite slow because the calculation must thus span very different time scales. The simulations show that one should expect a certain level of white noise at frequencies much less than the Josephson frequency. In addition, this noise should scale in a certain way with the parameters and depend linearly on the temperature (forgetting about quantum mechanical zero point motion).

I can then define excess noise in the SQUID as any noise which cannot be explained as arising from the Nyquist noise in the shunt resistors as found in the above simulations. Experimentally, the excess noise is often readily identifiable from the ideal noise because it has a 1/f type spectrum rather than the expected white noise. Thus at low frequency one sees more and more noise. There is nothing that says that all excess noise in the SQUID must be of this form, it is just that this form has a very clear signature and is thus readily identified as <u>not</u> arising from the shunts' Nyquist noise.

The presence of 1/f noise or excess low frequency noise in a real device cannot be explained through the Eqs. (4.3). At the very least, some modification is necessary. The possible modifications are of two types. <u>Firstly</u>, it is possible to alter the equations of motion or to introduce additional equations into the set. Such equations could in principle produce low frequency noise due to the complicated non-linear dynamics. We do not follow such an approach here, although it has been attempted elsewhere for similar systems.[3] The reasons are outlined below. <u>Secondly</u>, it is possible to generate 1/f noise by assuming that

one of the parameters in the equations is varying in time so as to produce a 1/f spectrum. In the Eqs. (4.3) it is generally assumed that the physical parameters:

$$\Phi\ ,\ I,\ I_{o1},\ I_{o2},\ R_1,\ R_2,\ C_1,\ C_2,\ L_1,\ L_2,\ M,$$

are constants in time, where I have treated the voltage V across the SQUID as the output parameter (ie. the dependent parameter) of the SQUID. If instead, one of the parameters varied in time so as to produce a 1/f power spectrum, the result might be a 1/f spectrum at the output of the SQUID. Such a hypothetical source I describe as being due to a parameter fluctuation.

In treating this problem I will make three simplifying assumptions:

(1) The equations of motion are correctly described by Eqs. (4.3).

(2) The fluctuations are very slow compared to the Josephson frequency, so that the equations of motion may be solved quasi-statically.

(3) The fluctuations are very small, so that a linear approximation may be made.

The second and third assumptions are generally very well satisfied for 1/f noise. The first assumption is the weakest because in a real SQUID, the equations of motion are not directly accessible, and hence their exact form is not known. What evidence do we have that the equations of motion are are a reasonable basis for descibing the SQUID? Experimentally, it is observed that the static I-V, I-Φ, the white noise N-V, and white noise N-Φ characteristics are adequately described by the unmodified equations, provided β_c is not too large, and the device does not possess an input circuit. These experimental observations put some constraints on any modified equations, and suggest that the unmodified

equations are a reasonable basis for analyzing the bare SQUID's behavior.

For the remainder of this Chapter, I will make an additional assumption. I will suppose that the current I is the output variable, and that V is the independent variable. I will do this in order to present the results in a form which will be useful for interpreting my experimental data. It should be recognized that this does not require any changes in the SQUID equations. Experimentally, this situation corresponds to fixing the voltage at low frequencies (generally less than about 500kHz) across the SQUID, while allowing the current I through the SQUID to vary. Because only the low frequency portion of V is fixed, the high frequency dynamics of the SQUID are unaffected, and one gets the same I-V as when the SQUID is run with a current bias.

5.3 The Quasi-Static Solution

The above assumptions allow one to use a linear quasi-static approximation. The procedure is as follows. First fix all of the parameters. Then solve the Eqs. (4.3), obtaining I as a function of V for a given $\Phi,\alpha,\beta,\ldots$; this can be written $I(V,\Phi,\alpha,\beta,\ldots)$. Now pick a parameter, say α and vary it by $\Delta\alpha$. Again solve Eqs. (4.3), and obtain $I(V+\Delta V,\Phi,\alpha+\Delta\alpha,\beta,\ldots) = I(V,\Phi,\alpha,\beta,\ldots) + \Delta I$. One can then write, to first order:

$$\Delta I = (\partial I/\partial\alpha)\Delta\alpha \ . \qquad (5.1)$$

For a spectral density S_α, the corresponding power spectrum in I is:

$$S_I = (\partial I/\partial\alpha)^2 S_\alpha \qquad (5.2)$$

If S_α has a 1/f spectrum, then S_I will too, provided only that $\partial i/\partial\alpha \neq$

0. The two power spectra are connected by a transfer function $(\partial I/\partial\alpha)^2$. In general, the transfer functions connecting variations in a given parameter to variations in the output current I are non-trivial. That is to say, they need to be calculated numerically, and they are dependent upon the flux bias, voltage, and other SQUID parameters. It is this non-trivial dependence which enables us to experimentally distinguish one source from another.

5.4 Parameters and the General Treatment

The equations of motion are not generally solved in the form of Eqs. (4.3). Rather they are first put into a more convenient form by transforming to dimensionless variables. These dimensionless parameters are generally formed from combinations of the various physical parameters. This variable change makes the equations neater, but it makes the effect of a parameter fluctuation less transparent because the fluctuations should occur in the original physical parameter rather than the mathematically convenient dimensionless parameter. Thus, I will need to consider both parameter sets to describe the noise. The original "physical parameters" are:

$$\Phi\ ,\ V,\ I_{o1},\ I_{o2},\ R_1,\ R_2,\ C_1,\ C_2,\ L_1,\ L_2,\ M.$$

Where I have taken the output as the current I flowing through the SQUID. In principle, any of the parameters can be thought of as being the input parameter, and this is the view I will take below when I will assume that one of the remaining parameters is fluctuating.

I can think of the above set of physical parameters as a vector $\bar{x}$ in an 11-dimensional space. Thus by giving the coordinates of $\bar{x}$ one

specifies the parameters of the SQUID and its operating point. The output current I then becomes a non-linear scalar function of $\bar{x}$.

Following Tesche and Clarke[1], I now introduce what I will call the "associated physical parameters":

$$\Phi\ ,\ V,\ I_o,\ R,\ C,\ L,\ \alpha,\ \rho,\ \eta.$$

These parameters are defined in Appendix A of Chapter 4, and form yet a third parameter set, as not all are dimensionless parameters. One can think of this set as specifying a vector $\bar{y}$ in a 9-dimensional space.

Again following Tesche and Clarke,[1] one can introduce the eight "dimensionless parameters":

$$\beta,\ \beta_C,\ \Phi,\ v,\ \alpha,\ \eta,\ \rho,\ \xi$$

Where again, the definitions can be found in Appendix A of Chapter 4. One can think of this set as specifying a vector $\bar{z}$ in an 8-dimensional space. The dimensionless parameters can be generally grouped into symmetric and antisymmetric sets [4]:

symmetric: $\beta,\ \beta_C,\ v,\ \Phi$

antisymmetric: $\alpha,\ \rho,\ \eta,\ \xi$

The classification depends upon whether the parameters involve the sum or the difference of the physical parameters. The antisymmetric parameters involve the difference of two of the physical parameters, and the symmetric are the remaining parameters.

One important difference between the symmetric and antisymmetric groups is that they behave differently under scale changes in the physical parameters. For example, suppose that $I_{o1} \rightarrow \kappa I_o$ and $I_2 \rightarrow \kappa I_{o2}$ where κ is a number. Then one finds that some or all of the symmetric parameters will scale:

$$\beta \rightarrow \kappa\beta\ ,\quad \beta_C \rightarrow \kappa\beta_C\ ,\quad v \rightarrow v/\kappa\ ,\ \Phi \rightarrow \Phi\ .$$

On the otherhand, the antisymmetric parameters do not change, thus:

$$\alpha \dashrightarrow \alpha \ , \quad \eta \dashrightarrow \eta \ , \ \rho \dashrightarrow \rho \ , \ \xi \dashrightarrow \xi .$$

Scale changes in any of the physical parameters will produce similar behavior, although in general only some of the symmetric parameters will scale. The point is that the antisymmetric parameters are scale invariant.

With the dimensionless variables, the equations of motion become:[1]

$$\frac{d\delta_1}{d\theta} = \frac{i/2 - j - (1-\alpha)\sin\delta_1}{(1-\rho)} + v_{n1} - \frac{\beta_c(1-\xi)}{(1-\rho)} \frac{d^2\delta_1}{d\theta^2}$$

$$\frac{d\delta_2}{d\theta} = \frac{i/2 + j - (1+\alpha)\sin\delta_2}{(1+\rho)} + v_{n2} - \frac{\beta_c(1+\xi)}{(1+\rho)} \frac{d^2\delta_2}{d\theta^2}$$

$$v = \frac{(1+\eta)}{2} \frac{d\delta_1}{d\theta} + \frac{(1-\eta)}{2} \frac{d\delta_2}{d\theta}$$

$$j = \frac{\delta_1 - \delta_2 - 2\pi\phi}{\pi\beta} - \frac{\eta i}{2} \qquad (5.3)$$

Te output current can then be computed from:

$$I(\bar{x}) = I_o \cdot i(\beta,\alpha,\phi,\ldots) = I_o \cdot i(\bar{z}) \qquad (5.4)$$

where i is a function only of the dimensionless variables. It should be noted that R, L, I_o, and C do not occur explicitly in the dimensionless equations of motion. In the vector notation a fluctuation $\Delta\bar{x}$ in the vector $\bar{x}$ will produce a change in the output Δi given by:

$$\Delta i = \bar{\nabla}_z i \cdot \Delta\bar{z} = \bar{\nabla}_z i \cdot \bar{\bar{A}} \cdot \Delta\bar{x} \qquad (5.5)$$

where:

$$\Delta\bar{z} = \bar{\bar{A}} \cdot \Delta\bar{x}$$

and A is a matrix which connects the physical parameter vector $\bar{x}$ to the dimensionless parameter vector $\bar{z}$:

$$\left[\bar{\bar{A}} \right]_{jk} = \frac{\partial z_j}{\partial x_k}$$

As is customary, the partial derivative is taken with all of the other parameters held fixed. The power spectrum produced in i by a fluctuation in the physical parameter vector $\bar{x}$ can then be written as:

$$S_i = \sum_{j,k} \left[\bar{\nabla}_z i \cdot \bar{\bar{A}} \right]_j \left[\bar{\nabla}_z i \cdot \bar{\bar{A}} \right]_k S_{jk} \qquad (5.6)$$

where: S_{jk} is the correlation power spectrum between the j-th and k-th component of the vector parameter $\bar{x}$.

The above formulation allows for the possible existence of correlations between the fluctuations in different SQUID parameters. Because of the large number of such possible correlations (S_{jk} has 61 independent components), and the physical implausibility of most of them, I will treat only a select subset. In particular, I will only consider the effects of correlations between "like" physical parameters. Thus, for example, I_{o1} and I_{o2} are both currents, and sufficently alike that one could readily construct physical mechanisms which produce correlated fluctuations in both.

5.5 The Components of $\bar{\nabla}_z i$

The components of $\bar{\nabla}_z i$ connect variations in the dimensionless parameters to variations in the dimensionless output current i. Explicitly, the components are:

$$\bar{\nabla}_z i = \left(\frac{\partial i}{\partial \beta}, \frac{\partial i}{\partial \beta_C}, \frac{\partial i}{\partial v}, \frac{\partial i}{\partial \phi}, \frac{\partial i}{\partial \alpha}, \frac{\partial i}{\partial \rho}, \frac{\partial i}{\partial \eta}, \frac{\partial i}{\partial \xi} \right)$$

Of the eight components, only $\partial i/\partial \phi$ and $\partial i/\partial v$ can be readily obtained experimentally. $\partial i/\partial \phi$ is just the flux gain, or flux to current transfer function, and can be obtained from the I-ϕ curves as discussed in Chapter 2. $\partial i/\partial v$ is just R/R_D, where R_D is the dynamic resistance of the

SQUID at the bias point, and can be found from the SQUID I-V.

The partial $\partial i/\partial \eta$ can be evaluated for small β_c and v, once it is realized that:

$$i(v,\phi,\eta) = i(v,\phi - i\eta\beta/4, 0)$$

as has been shown by Tesche and Clarke.[1] Thus the SQUID characteristics for non-zero η can be generated from the zero η characteristics. The change in i produced by a change in η can thus be written as:

$$\Delta i = \frac{\partial i}{\partial \phi}\left[\frac{-i\beta\Delta\eta}{4} - \frac{\eta\beta\Delta i}{4}\right]$$

solving for Δi one finds:

$$\frac{\partial i}{\partial \eta} = -\left[\frac{i\beta}{4}\right]\left[1 + \frac{\eta\beta}{4}\frac{\partial i}{\partial \phi}\right]$$

For a typical SQUID, $\eta\beta$ is small, and the partial reduces to:

$$\partial i/\partial \eta = -(i\beta/4)\partial i/\partial \phi$$

The remaining 5 partials must be calculated numerically, as they are not simple functions of the SQUID parameters or bias point, and are not easily obtained experimentally. I will make qualitative comments below.

The partial $\partial i/\partial \beta_c$ can generally be neglected for the SQUIDs in this thesis because of the small size of β_c and the low voltage at which the SQUIDs are operated. I will similarly neglect $\partial i/\partial \xi$. For a more complete discussion of these terms, see section 5.10 on capacitance fluctuations.

The partials $\partial i/\partial \beta$, and $\partial i/\partial \alpha$ can be obtained from curves of I-ϕ, as calculated in Chapter 4, in the limit v << 1. Since the SQUIDs in this thesis are generally operated in this limit, the I-ϕ should prove satisfactory. Fig. 5.1 shows i as a function of β for fixed ϕ and α = 0. Such curves have been published elsewhere.[1,4] Fig. 5.2 shows a rough

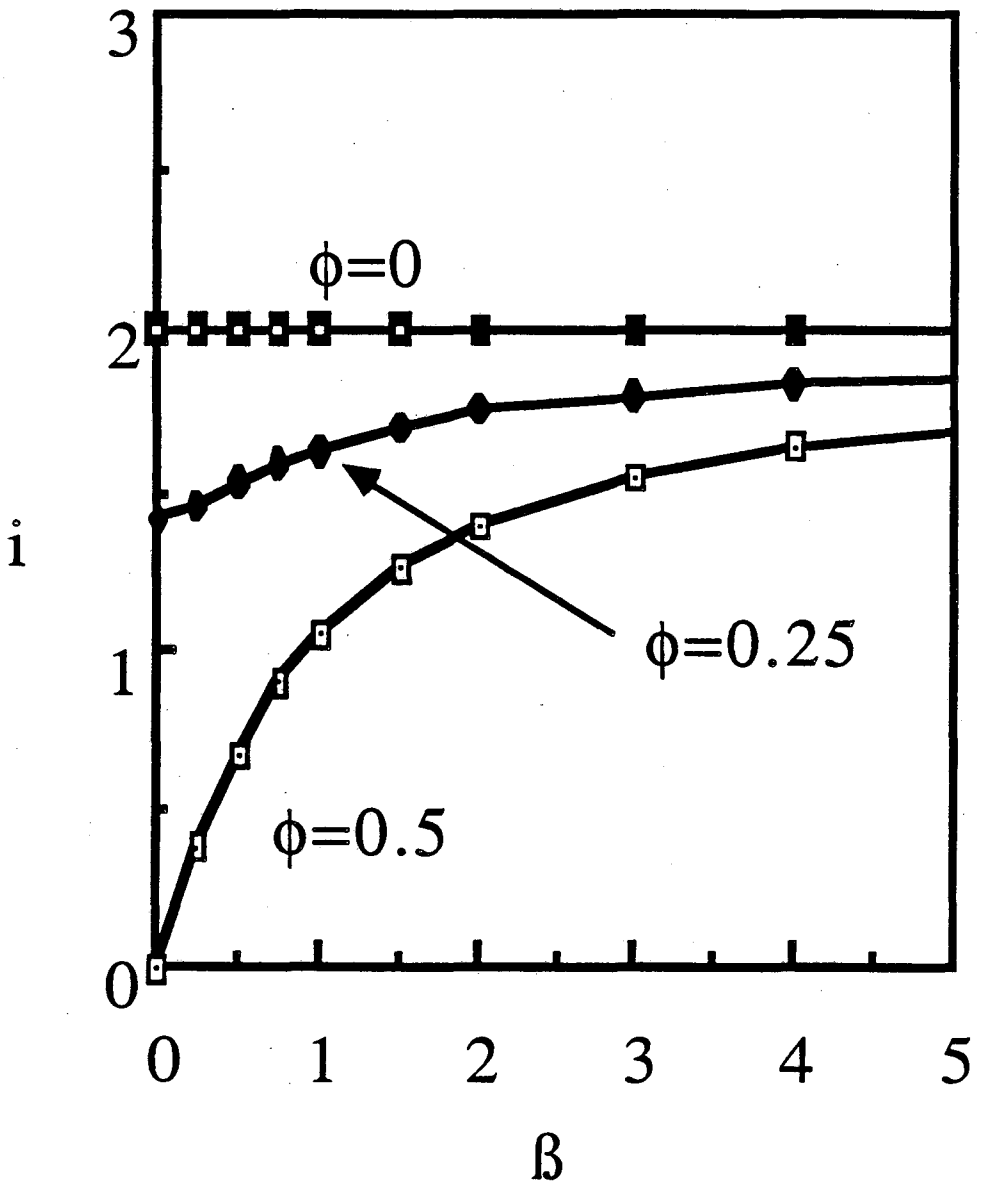

Fig. 5.1. Reduced current i vs β for a symmetrical SQUID.

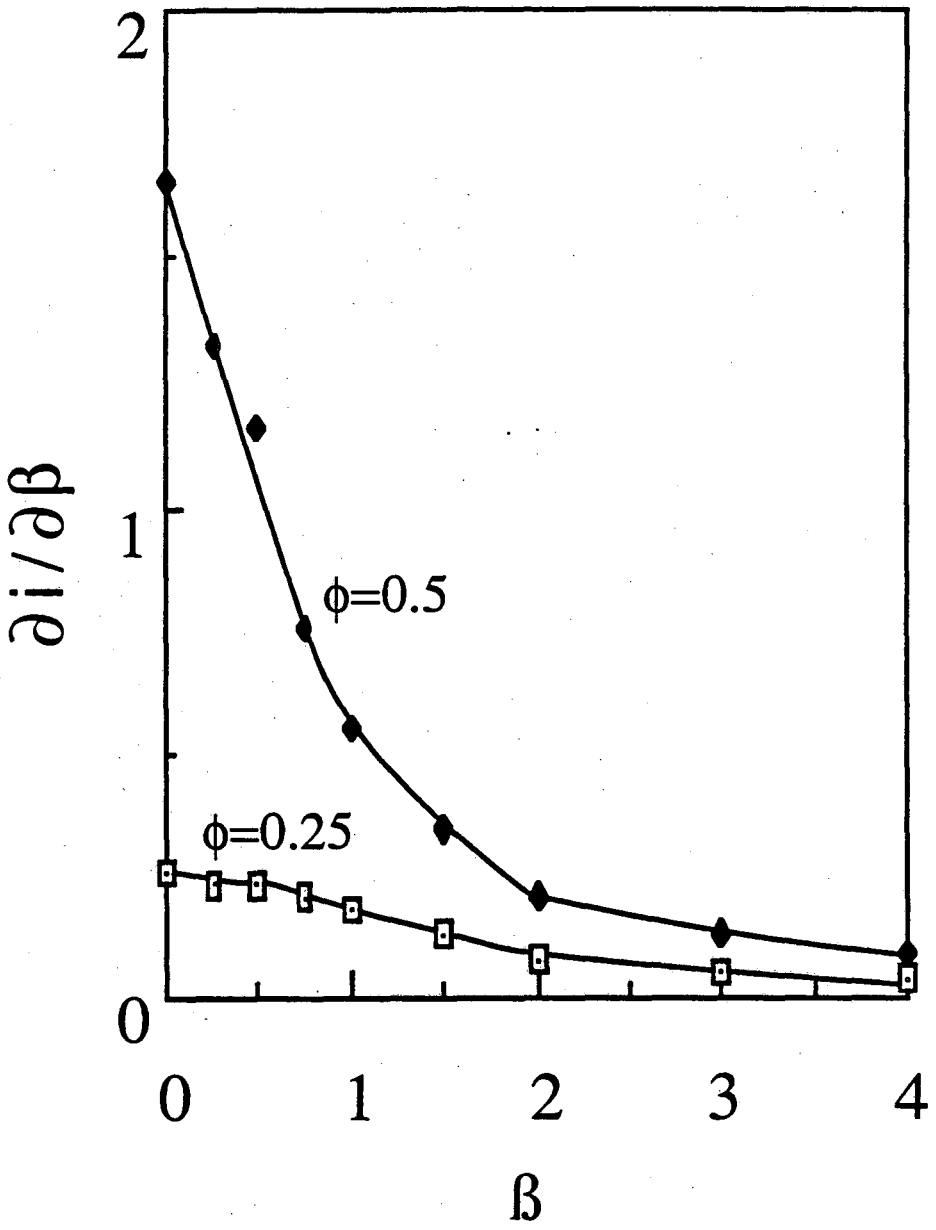

Fig. 5.2. $\partial i / \partial \beta$ vs β for a symmetrical dc SQUID. $\partial i / \partial \beta = 0$ for $\phi = 0$.

calculation of $\partial i/\partial\beta$ for fixed Φ and $\alpha=\eta=0$. The behavior of $\partial i/\partial\beta$ is qualitatively as follows. For a symmetric SQUID $\partial i/\partial\beta$ vanishes at Φ_0 and attains a maximum at $\Phi_0/2$. Similarly, $\partial i/\partial\beta$ vanishes for v>>1.

The behavior of $\partial i/\partial\alpha$ is qualitatively as follows. In the low voltage limit, there are two effects. First of all, the entire I-Φ shifts along the Φ axis, by an amount which depends upon α. Secondly, as was noted in Chapter 4, the modulation depth also changes if α changes. This effect not only depends upon α, but also upon β.

The only remaining partial is $\partial i/\partial\rho$. for v<<1, i is independent of ρ as was remarked in Chapter 4. Similarly, for v >> 1, the I-V follows the resistive line, and is again independent of ρ. Thus $\partial i/\partial\rho$ --> 0 for v << 1 and for v >>1. There is a qualitative argument which descibes ρ fluctuations elsewhere. At zero voltage, no current flows through the resistive shunts, and the I-Φ are accordingly independent of both R and ρ. For a finite fixed voltage, a current V/R_1 flows in shunt one, and V/R_2 flows in shunt two. If ρ fluctuates, there must be a correlated antisymmetrical fluctuation in the two R's. Since the voltage is fixed, the currents through the two arms will change. This has two effects. First of all, Teshe and Clarke[1] showed that to first order, the effect of finite ρ is to produce a circulating current $i\rho/2$. This produces a flux in the SQUID because the circulating current flows through the inductive arms of the SQUID. Thus there will be more flux noise at larger i. At Φ_0 and $\Phi_0/2$, the I-V is independent of Φ, so this term will not contribute to the noise, rather, the noise will behave as a voltage dependent flux noise. Secondly, if ρ is not zero, there will generally be a net change in in the current flowing through the two resistors. This is simply due to the fact that a decrease in resistance

in a small resistor will draw more current than the increase in resistance a large resistance will stop drawing. In both cases, the larger is V, the more current flows through the shunts, and the greater will be the noise at the SQUID output.

5.6 The Flux Φ

This is a trivial case. Fluctuations in the magnetic flux, Φ, produce an output spectrum:

$$S_I = (\partial I/\partial \Phi)^2 S_\Phi \quad . \qquad (5.7)$$

The quantity $\partial I/\partial \Phi$ is readily measured experimentally, and its characteristics are well-known. In particular, for symmetric SQUIDs, it goes to zero when Φ is an integral or half integral multiple of Φ_0. For any SQUID, there will always be two points per Φ_0 where this transfer function disappears owing to the periodicity and the boundedness of the I-Φ characteristic. An experimental test for flux noise thus consists of measuring the observed noise as a function of the flux gain and seeing if the required scaling is observed.

5.7 The Voltage V

The voltage is ordinarily considered fixed in this thesis. If we suppose however that it can fluctuate, then the current through the SQUID will also fluctuate. The resulting noise spectrum is again trivial:

$$S_I = (\partial I/\partial V)^2 \, S_V \quad . \qquad (5.8)$$

There is no need to change to dimensionless variables to understand this

expression. The quantity $\partial I/\partial V$ is just $1/R_D$, where R_D is the dynamic resistance of the SQUID at the bias point. Since R_D is easily measured experimentally when one takes an I-V characteristic, it is a simple matter to test for excess noise due to fluctuations in the dc voltage.

5.8 The Critical Currents I_{o1} and I_{o2}

Fluctuations in the critical current are of particular importance because they are frequently observed to produce 1/f noise in real junctions and SQUIDs. The mechanism which produces these fluctuations is discussed in Chapter 6. The analysis of the effect of critical current noise on the SQUID is complicated because the critical currents I_{01} and I_{02} enter into four of the dimensionless SQUID parameters: β, β_c, α, and v as well as the scaling factor I_o.

We consider a SQUID biased at a fixed voltage (at low frequencies) and suppose that the junctions undergo a critical current change:

$$I_{o1} \dashrightarrow I_{o1} + \Delta I_{o1} \quad \text{and} \quad I_{o2} \dashrightarrow I_{o2} + \Delta I_{o2} .$$

The current I which flows through the SQUID will thus change. The dimensionless current through the SQUID will go from $i(v,\phi,\beta,\alpha,\beta_c,\ldots)$ to $i(v+\Delta v,\phi,\beta+\Delta\beta,\alpha+\Delta\alpha,\beta_c+\Delta\beta_c,\ldots)$. To first order, the change in i is just:

$\Delta i = \Delta v\ \partial i/\partial v + \Delta\phi\ \partial i/\partial\phi + \Delta\beta\ \partial i/\partial\beta + \Delta\beta_c\ \partial i/\partial\beta_c + \Delta\alpha\ \partial i/\partial\alpha$. The variations in the dimensionless parameters can be reexpressed as variations in the physical parameters I_{o1} and I_{o2} by using the chain rule:

$$\Delta i = \left[\frac{\partial v}{\partial I_{o1}} \frac{\partial i}{\partial v} + \frac{\partial \beta}{\partial I_{o1}} \frac{\partial i}{\partial \beta} + \frac{\partial \beta_c}{\partial I_{o1}} \frac{\partial i}{\partial \beta_c} + \frac{\partial \alpha}{\partial I_{o1}} \frac{\partial i}{\partial \alpha} \right] \Delta I_{o1} +$$

$$+\left[\frac{\partial v}{\partial I_{o2}}\frac{\partial i}{\partial v}+\frac{\partial \beta}{\partial I_{o2}}\frac{\partial i}{\partial \beta}+\frac{\partial \beta_c}{\partial I_{o2}}\frac{\partial i}{\partial \beta_c}+\frac{\partial \alpha}{\partial I_{o2}}\frac{\partial i}{\partial \alpha}\right]\Delta I_{o2} \qquad (5.9)$$

$$\Delta i = a_o\,\Delta I_{o1} + b_o\,\Delta I_{o2} \qquad (5.10)$$

Where, for convenience, I define a_o and b_o such that the above relation holds.

Now fluctuations in I_{o1} and I_{o2} will produce a change in the current I. Since $I = I_o \cdot i$, the fluctuation in I will just be:

$$\Delta I = \Delta I_o \cdot i + I_o \cdot \Delta i = i \cdot (\Delta I_{o1} + \Delta I_{o2})/2 + I_o \cdot (a_o \Delta I_{o1} + b_o \Delta I_{o2}) \qquad (5.11)$$

The resulting power spectrum is then:

$$S_I = (i/2 + I_o a_o)^2 \cdot S_{Io1} + (i/2 + I_o b_o)^2 \cdot S_{Io2} + 2(i/2 + I_o a_o)(i/2 + I_o b_o) \cdot S_{I12} \qquad (5.12)$$

where: S_{Io1} is the power spectrum of the critical current fluctuations in junction 1, S_{Io2} is the power spectrum of the critical current fluctuations in junction 2, S_{I12} is the correlation power spectrum between the critical current fluctuations in the two junctions.

Eq. 5.12 is complicated to evaluate because of the many partials that occur in the a_o and b_o terms. But most of the partials can be evaluated exactly by using the definitions in Appendix A of Chapter 4:

$$\frac{\partial v}{\partial I_{o1}} = \frac{-v}{2I_o} \qquad \frac{\partial v}{\partial I_{o2}} = \frac{-v}{2I_o} \qquad \frac{\partial i}{\partial v} = \frac{R}{R_D}$$

$$\frac{\partial \beta}{\partial I_{o1}} = \frac{\beta}{2I_o} \qquad \frac{\partial \beta}{\partial I_{o2}} = \frac{\beta}{2I_o}$$

$$\frac{\partial \beta_c}{\partial I_{o1}} = \frac{\beta_c}{2I_o} \qquad \frac{\partial \beta_c}{\partial I_{o2}} = \frac{\beta_c}{2I_o}$$

$$\frac{\partial \alpha}{\partial I_{o1}} = \frac{-\alpha}{2I_o} - \frac{1}{2I_o} \qquad \frac{\partial \alpha}{\partial I_{o2}} = \frac{-\alpha}{2I_o} + \frac{1}{2I_o} \qquad (5.13)$$

Equation 5.12 is too general to be of much use. Accordingly, I now consider three cases: (a) only one junction fluctuates, (b) both junctions fluctuate symmetrically, and (c) both junctions fluctuate independently.

(a) For the case where only one of the junction fluctuates, I will suppose without loss of generality that it is junction 1. In this case:

$$S_{Io2} = S_{I12} = 0 \tag{5.14}$$

Equation 5.8 then reduces to:

$$S_I = S_{Io1} \cdot (i/2 + I_o a_o)^2 \tag{5.15}$$

Substituting for A by using the partials in 5.13, and neglecting $\partial i/\partial \beta_c$, one finds:

$$S_I = \frac{1}{4}\left[i + \frac{-R}{R_D} v + \beta \frac{\partial i}{\partial \beta} - (1+\alpha) \frac{\partial i}{\partial \alpha} \right]^2 \cdot S_{Io1} \tag{5.16}$$

In the limit $\alpha = 0$ and $v = 0$, Eq. 5.15 reduces to:

$$S_I = \frac{1}{4}\left[i + \beta \frac{\partial i}{\partial \beta} - \frac{\partial i}{\partial \alpha} \right]^2 \cdot S_{Io1} \tag{5.17}$$

Since $\partial i/\partial \alpha$ changes sign as a function of ϕ, the magnitude of the noise will depend upon ϕ. At certain ϕ, the three terms in brackets will add together to produce a large effect, while at other points they will tend to cancel. When i is a maximum both $\partial i/\partial \alpha$ and $\partial i/\partial \beta$ vanish, and the noise is simply:

$$S_I = i^2 S_{I01}/4 \propto S_{Io1}$$

in the low voltage limit.

This case is of some interest because one occasionally finds junctions that are much noisier than usual. The presence of an unusually

noisy junction in a SQUID would reveal itself by the difference in the noise at $\pm \Phi_0/4$, and 5.8 could serve more generally as a starting point for determining the noise due to each junction individually. In addition, some junctions display Lorentzians. These are peculiar to the individual junction, and thus one should expect to see the shape of the noise spectrum change as one varies the flux between $\pm \Phi_0/4$ in SQUIDs which are dominated by critical current noise.

(b) For the case when both junctions fluctuate symmetrically, it is simplest to start from Eq. 5.11 and take a scale change:

$$I_{o1} \dashrightarrow \kappa I_{01} \qquad I_{02} \dashrightarrow \kappa I_{02} \tag{5.18}$$

now let $\kappa = 1 + \Delta\kappa$, and the resulting changes in the I_{oj} are:

$$\Delta I_{o1} = I_{o1}\Delta\kappa \qquad \Delta I_{02} = I_{02}\Delta\kappa \tag{5.19}$$

Substituting into 5.11, and neglecting β_c terms one finds after some rearrangement:

$$\Delta I = I_o\left[\, i + \frac{-R}{R_D} v + \beta \frac{\partial i}{\partial \beta} \,\right]\Delta\kappa$$

$$S_I = \left[\, i + \frac{-R}{R_D} v + \beta \frac{\partial i}{\partial \beta} \,\right]^2 S_{Io} \tag{5.20}$$

Where $S_{Io} = I_o^2\, S_\kappa$ is the fluctuation produced in I_o by the fluctuation in κ. This expression yields noise at Φ_0, $\Phi_0/2$, and equal amounts of noise at $\pm \Phi_0/4$ for a symmetrical SQUID.

This case is of interest for two reasons. First of all, one would expect this type of fluctuation to easily arise. The most common case would be if the bath temperature underwent a fluctuation. Secondly, if a SQUID is biased in a flux locked loop, as was discussed in Chapter 3, symmetrical current fluctuations do not produce noise at the output of

the feedback loop.[5] Thus, this type of noise is removed by the standard electronic modulation technique which was described in Chapter 3.

(c) For the case of independent fluctuations in the two junctions, I set $S_{I12} = 0$ in Eq. 5.12. If I suppose that the two junctions are equally noisy, then one finds:

$$S_I = S_{Io}\{[i + \beta(\partial i/\partial\beta) - v(\partial i/\partial v)]^2 + (\partial i/\partial\alpha)^2\}, \qquad (5.21)$$

where: $S_{Io} = (S_{Io1} + S_{Io2})/4$ and I have assumed that $S_{Io1} = S_{Io2}$ and $\alpha = 0$. This expression yields equal amounts of noise at $\pm \Phi_o/4$ for a symmetrical SQUID. Also, the noise does not scale with the flux gain $\partial i/\partial\Phi$. For $i(\Phi)$ a maximum, $\partial i/\partial\alpha$ and $\partial i/\partial\beta$ vanish. If in addition $v << 1$, then $S_I = i^2 \cdot S_{Io} \propto S_{Io1} + S_{Io2}$.

5.9 The Shunt Resistances R_1 and R_2

Fluctuations in resistance are not generally known to contribute to the 1/f noise in SQUIDs.[6] The resistances R_1 and R_2 enter into the equations of motion only through the dimensionless parameters ρ, ν and β_c. These are defined as follows:

$$R_1 = R/(1+\rho), \qquad R_2 = R/(1-\rho), \qquad (5.22)$$

or: $R = 2R_1R_2/(R_1+R_2), \qquad \rho = (R_1+R_2)/(R_2-R_1).$

A change in R_1 or R_2 will thus produce a change Δi in the dimensionless current i according to:

$$\Delta i = \frac{\partial i}{\partial R_1}\Delta R_1 + \frac{\partial i}{\partial R_2}\Delta R_2 \qquad (5.23)$$

I now apply the chain rule to calculate the partial derivatives:

$$\frac{\partial i}{\partial R_1} = \frac{\partial i}{\partial \nu}\frac{\partial \nu}{\partial R_1} + \frac{\partial i}{\partial \rho}\frac{\partial \rho}{\partial R_1} + \frac{\partial i}{\partial \beta_c}\frac{\partial \beta_c}{\partial R_1}$$

$$\frac{\partial i}{\partial R_2} = \frac{\partial i}{\partial \nu}\frac{\partial \nu}{\partial R_2} + \frac{\partial i}{\partial \rho}\frac{\partial \rho}{\partial R_2} + \frac{\partial i}{\partial \beta_c}\frac{\partial \beta_c}{\partial R_2} \qquad (5.24)$$

Most of these partials can be readily evaluated:

$$\frac{\partial i}{\partial \nu} = \frac{R}{R_D}$$

$$\frac{\partial \nu}{\partial R_1} = \frac{-\nu R}{2R_1^2} \qquad \frac{\partial \nu}{\partial R_2} = \frac{-\nu R}{2R_2^2}$$

$$\frac{\partial \rho}{\partial R_1} = \frac{\rho R}{R_1(R_2-R_1)} \qquad \frac{\partial \rho}{\partial R_2} = \frac{-\rho R}{R_2(R_2-R_1)}$$

$$\frac{\partial \beta_c}{\partial R_1} = \frac{\beta_c R}{R_1^2} \qquad \frac{\partial \beta_c}{\partial R_2} = \frac{\beta_c R}{R_2^2} \qquad (5.25)$$

Substituting for the evaluated partials, we can thus write the fluctuation in i as:

$$\Delta i = \left[\frac{\nu(1+\rho)^2}{2R_D} + \frac{\partial i}{\partial \rho}\frac{(1+\rho)^2(1-\rho)}{2R} + \frac{\partial i}{\partial \beta_c}\frac{\beta_c(1+\rho)}{R}\right]\Delta R_1 +$$

$$+ \left[\frac{\nu(1-\rho)^2}{2R_D} - \frac{\partial i}{\partial \rho}\frac{(1-\rho)^2(1+\rho)}{2R} + \frac{\partial i}{\partial \beta_c}\frac{\beta_c(1-\rho)}{R}\right]\Delta R_2$$

$$= c\Delta R_1 + d\Delta R_2 \qquad (5.26)$$

Where c and d are defined such that the equality holds. The resulting noise in I is:

$$S_I = I_o^2 \left(c^2 \cdot S_{R1} + d^2 \cdot S_{R2} + 2cdS_{R12}\right) \qquad (5.27)$$

where S_{Rj} is the spectral density of resistance fluctuations in R_j, and S_{R12} is the correlated power spectral density of the resistance fluctuations between R_1 and R_2.

I now consider two simple cases: (a) just R_1 is fluctuating and (b) when both resistances fluctuate symmetrically.

(a) When just R_1 fluctuates, $S_{R2} = S_{R12} = 0$ in Eq. 5.27, and one finds:

$$S_I = I_o^2 c^2 \cdot S_{R1} \tag{5.28}$$

In the limit where $\rho = 0$, and neglecting β_c terms, this becomes:

$$S_I = I_o^2 \left[\frac{v}{2R_D} - \frac{\partial i}{\partial \rho} \frac{1}{2R} \right]^2 S_{R1} \tag{5.29}$$

The term $\partial i/\partial \rho$ scales roughly as v, so that the overall noise in I scales as v^2. The term $\partial i/\partial \rho$ also contributes a flux dependence to the noise, so that the noise at $\Phi_o/4$ is different from that at $-\Phi_o/4$ even for a symmetrical SQUID. Thus, this case will not produce a flux-like noise.

(b) Secondly I consider the case where R_1 and R_2 are fluctuating symmetrically. This could arise from say a change in the bath temperature. Such a fluctuation represents a scale change in resistance, and thus we expect the antisymmetric parameters will remain unchanged. It is easiest to start from Eq. 5.26 and take:

$$R_1 \dashrightarrow \kappa R_1 \qquad R_2 \dashrightarrow \kappa R_2 \tag{5.30}$$

where $\kappa = 1 + \Delta\kappa$ is a number. The resulting changes in the R_j are:

$$\Delta R_1 = R_1 \Delta\kappa \qquad R_2 = R_2 \Delta\kappa \tag{5.31}$$

Substituting into Eq. 5.26 one finds:

$$\Delta I = I_o(cR_1 + dR_2)\Delta\kappa$$

$$S_I = I_o^2 \left[\frac{v}{2R_D} \right]^2 (R_1(1-\rho)^2 + R_2(1+\rho)^2)\, S_\kappa \tag{5.32}$$

The most important properties of this expression are that it scales like v^2 and is not proportional to the flux gain $\partial i/\partial \Phi$.

5.10 The Parameters L_1, L_2 and M

The inductances L_1, L_2, and M only enter into the equations of motion through the parameters β and η. The inductance L of the SQUID loop is just:(1)

$$L = L_1 + L_2 - 2M. \tag{5.33}$$

A fluctuation in L_1, L_2, and M will thus produce a fluctuation Δi in the current i given by:

$$\Delta i = \frac{\partial i}{\partial \beta}\frac{\partial \beta}{\partial L}\left[\Delta L_1 + \Delta L_2 - 2\Delta M\right] + \frac{\partial i}{\partial \eta}\left[\frac{\partial \eta}{\partial L_1}\Delta L_1 + \frac{\partial \eta}{\partial L_2}\Delta L_2 + \frac{\partial \eta}{\partial M}\Delta M\right] \tag{5.34}$$

All of the partials except $\partial i/\partial \beta$ can be evaluated exactly. The easy ones are:

$$\frac{\partial \beta}{\partial L} = \frac{\beta}{L}$$

$$\frac{\partial \eta}{\partial L_1} = -\frac{1}{L} - \frac{\eta}{L} \qquad \frac{\partial \eta}{\partial L_2} = -\frac{1}{L} + \frac{\eta}{L} \qquad \frac{\partial \eta}{\partial M} = \frac{2\eta}{L} \tag{5.35}$$

and in the small η limit where most SQUIDs operate (see section 5.5):

$$\frac{\partial i}{\partial \eta} = -\frac{i\beta}{4}\frac{\partial i}{\partial \phi} \tag{5.36}$$

I now will consider three cases: (a) where just M fluctuates, (b) where L_1, L_2, and M fluctuate symmetrically, and (c) I will also remark on an associated problem; when fluctuations occur in L, they may also

cause fluctuations in Φ.

(a) Fluctuations in M are not known to contribute to the excess noise in SQUIDs. The reason is undoubtedly because M is set by the geometry of the SQUID and by the permeability of the surrounding medium. At low temperatures, for typical materials, both should be highly constant.

It is easiest to start from Eq. 5.34, and set $\Delta L_1 = \Delta L_2 = 0$:

$$\Delta i = \left[- \frac{\partial i}{\partial \beta} \frac{2\beta}{L} - \frac{\partial i}{\partial \eta} \frac{2\eta}{L} \right] \Delta M \qquad (5.37)$$

$$S_I = I_o^2 \left[\frac{\partial i}{\partial \beta} \frac{2\beta}{L} + \frac{\partial i}{\partial \eta} \frac{2\eta}{L} \right]^2 S_M \qquad (5.38)$$

Where S_M is the spectral density of fluctuations in M. For the small η limit, where most SQUIDs are operated, the expression reduces to:

$$S_I = I_o^2 \left[\frac{\partial i}{\partial \beta} \frac{2\beta}{L} \right]^2 S_M \qquad (5.39)$$

For fixed Φ, when i is a maximum, $\partial i/\partial \beta$ is zero, while when i is a minimum, $\partial i/\partial \beta$ is a maximum. Thus the noise does not scale with the flux gain, and hence will not appear as a flux-like noise.

(b) For the case of symmetric fluctuations in L_1, L_2, and M, let:

$$\Delta L_1 = L_1 \Delta \kappa \qquad \Delta L_2 = L_2 \Delta \kappa \qquad \Delta M = M \Delta \kappa \qquad (5.40)$$

where $\Delta \kappa$ is a small number. Upon substitution into Eq. 5.31 one finds:

$$\Delta i = \left[\frac{\partial i}{\partial \beta} \frac{\beta}{L} \right] L \Delta \kappa \qquad (5.41)$$

and thus:

$$S_I = \left[\frac{\partial i}{\partial \beta} \beta I_o \right]^2 S_\kappa \qquad (5.42)$$

The most important properties of this noise are that it does not scale with flux gain $\partial i/\partial \Phi$, and it depends upon the β of the device.

(c) Now there is an important complication that must be considered in a real SQUID. Changes in the inductance may be accomplished by changing the size of the SQUID. Experimentally, we expect that a change in the size of the SQUID will cause a change in the flux. This is because flux is ordinarily generated by applying a magnetic field B to the SQUID, and the flux is given by the dot product of this field with the the SQUID area. The noise at the SQUID output is then simply:

$$S_I = I_o^2(\partial i/\partial \phi)^2 \cdot B^2 \cdot S_A/\phi_o^2 \qquad (5.43)$$

where S_A is the spectrum of the area fluctuations. The inductance L scales roughly with the square root of the area of the SQUID. I can write this as $L = \gamma A^{1/2}$, where γ is a proportionality factor. The noise in I thus becomes:

$$S_I = (\partial i/\partial \phi)^2 \cdot B^2 \cdot (\beta/\gamma^2)^2 \cdot S_L \qquad (5.44)$$

The resulting contribution to the noise from inductance fluctuations scales as a flux noise, and depends upon the field at the SQUID, as well as the SQUID inductance. For a symmetric β=1 SQUID at ϕ=0.25, it can be shown that the noise produced by this indirect inductance effect will be a factor of about $4\phi^2$ larger than the noise produced by the direct inductance effects calculated in the previous section. Thus, unless the SQUID is very small or is cooled in an ultralow magnetic field, the indirect effect should dominate.

5.11 The Parameters C_1 and C_2

Fluctuations in the capacitance are not generally known to produce excess noise in the dc SQUID. This is undoubtedly because the capacitance of most SQUIDs is dominated by the parasitic capacitance

arising from the thin oxide layer of the Josephson junction. The capacitance of each junction is simply:

$$C = \varepsilon A/d \tag{5.45}$$

where: ε is the dielectric constant of the oxide barrier, A is the juction area, and d is the junction thickness. For the SQUIDs in this thesis, the capacitance is estimated to be about 0.5 pF, based upon $\varepsilon = 27\varepsilon_0$, $A = 4\ (\mu m)^2$, and d = 2 nm. One can generally expect the junction area, thickness, and dielectric constant to be constant to a very good approximation. However, it is conceivable that the motion of a dislocation in the barrier could affect the effective area or distance, or could lead to polarizabilty changes. On the otherhand, such fluctuations would also produce fluctuations in the critical current of the junction, which would generally be expected to mask any associated effects produced by the capacitance.

The junction capacitances C_1 and C_2 only enter into the equations of motion via the dimensionless parameters β_C and ξ. The situation for non-zero ξ does not seem to have been analyzed in the literature, and I have no comments on the effects one would expect.

I will now consider the case of symmetric fluctuations in C_1 and C_2. The antisymmetric parameters will be unaffected by such a fluctuation. The only remaining parameter which includes the capacitance is β_C. The effect of a fluctuation in capacitance is simply:

$$\Delta i = \frac{\partial i}{\partial \beta_C}\frac{\partial \beta_C}{\partial C}\Delta C = \frac{\partial i}{\partial \beta_C}\frac{2\pi I_0 R^2}{\Phi_0}\Delta C \tag{5.47a}$$

$$\Delta I = I_0 \cdot \Delta i = \frac{\partial i}{\partial \beta_C}\frac{2\pi I_0^2 R^2}{\Phi_0}\Delta C \tag{5.47b}$$

Neglecting $\partial i/\partial \beta_c$, the current fluctuations will be scaled by $I_o^2R^2$. Thus devices with the same C and S_c will show different levels of noise S_I depending upon their value of I_oR.

I have not attempted a detailed evaluation of the quantity $\partial i/\partial \beta_c$, but I note a few of its properties. First of all, the low temperature zero voltage I-ϕ curves are independent of β_c, as was discussed in Chapter 4 (provided of course that the device is not hysteretic). In addition, for $\nu >> 1$, i is independent of β_c. One can thus conclude that $\partial i/\partial \beta_c$ --> 0 both as v --> 0 and as ν --> ∞, at least in the low temperature small β_c limit.

Unfortunately, $\partial i/\partial \beta_c$ does not vanish in the region $0 < \nu < 1$ where real SQUIDs operate. Near $\beta_c = 1$, the effect of a small change in β_c becomes large as the device can change from non-hysteretic to hysteretic. V.J. de Waal et al.[2] have calculated the effect of finite capacitance on the properties of the dc SQUID. They have published a calculated I-V characteristic for the case $\beta = 1$, $\beta_c = 1.6$, and $\Gamma = 0.05$. The effect of large β_c on the I-V are not simple. At $\phi = \phi_o$, the primary effect is an increase in the dynamic resistance for $\nu < 0.5$. The curve thereby arrives at the high voltage resistive line at a lower current and voltage than it would if the device had $\beta_c = 0$. At $\phi = \phi_o/2$, and $\phi = \phi_o/4$, the I-V develops what appears to be a large, rounded current step near $\nu = 0.5$, with the current on these branches actually exceeding that on the $\phi = 0$ branch. In addition Tesche has published an analysis of the complicated effects produced by a stray capacitance shunting across the SQUID inductor.[7] Experimentally, it is also observed that the effect on the I-V for large β_c is particularly pronounced near steps or resonances in the characteristics, and the

effect of changes in β_C should be correspondingly large near such features.

To summarize, one expects that capacitance fluctuations should produce noise at the output of the SQUID which will depend upon both the flux and the voltage bias. The effects should be largest in devices with large β_C, should be most prominent around ν = 0.5 and in devices with structure.

References

(1) C. D. Tesche and J. Clarke, "dc SQUID: Noise and Optimization", J. Low Temp. Phys., 29, 301 (1977).

(2) V.J. de Waal, P. Schrijner, R. Llurba, "Simulation and Optimization of a dc SQUID with a Finite Capacitance", J. Low Temp. Phys. 54, 215 (1984).

(3) See for example: H. Seppa, T. Ryhanen, "Influence of the Signal Coil on dc SQUID Dynamics", IEEE MAG-23, 1083 (1987).

(4) L. Solymar, "Superconductive Tunneling and Applications", Chapman and Hall, London (1972).

(5) R.H. Koch, J. Clarke, W.M. Goubau, J.M. Martinis, C.M. Pegrum, and D.J. Van Harlingen, "Flicker (1/f) Noise in Tunnel Junction dc SQUIDs", J. Low Temp. Phys. 51, 207 (1983).

(6) SQUID NBS1 displayed excess low frequency noise for T<0.5 K, which was probably due to portions of the AuIn resistors going superconducting, (see Chapter 8 for further discussion of this device).

(7) C. D. Tesche "Analysis of a Double-Loop dc SQUID", J. Low Temp. Phys. 47, 385 (1982).

Chapter 6: Critical Current Noise in Nb-Al_2O_3-Nb Junctions[1]

6.1 Introduction

This Chapter is concerned with excess noise which arises from fluctuations in the critical current of a Josephson junction. Such noise has been known for at least the last 10 years, and the cause has been debated for most of this time. Although understanding has come slowly, the basic underlying mechanism which produces this excess noise is now generally agreed upon. The detailed microphysics, however, has still not been entirely resolved, and much remains to be understood both theoretically and experimentally.

As will be discussed in the next section, the fluctuations in critical current are the result of microscopic physical processes within the junction barrier. One should thus expect that barriers which are prepared differently or are made of different materials should generally show different amounts of noise. From the experimental point of view, perhaps the most important question that has not been answered is: what junction materials or preparation techniques will yield the lowest 1/f noise? This work was part of an attempt to address this question from the practical end. We wished to determine the noise level in a very promising system, Nb-Al_2O_3-Nb junctions, and compare them with our conventional Nb-NbOx-PbIn junctions.

6.2 The Basic Picture: Trapped Charge

The basic physical mechanism which produces critical current

fluctuations has been known for some time, and has similarities to the model proposed by McWhorter in 1959 to explain 1/f noise in semiconductors.[2] Although there are many differences, both mechanisms concern the random trapping and release of charges from defect states or "traps". While experimental support for McWhorter's model came in quickly, this has not been the case for the noise in tunnel junctions. Only in the last few years has it received extensive experimental support. This experimental work has largely been pursued by C.T. Rogers and R. Buhrman at Cornell University.[3-5]

The scenario for a critcal current fluctuation is as follows. Consider two metals seperated by a thin insulating layer, see Fig. 6.1. Since the insulating layer is an insulator, there will be present a potential energy barrier which will prevent electrons from freely passing from one metal to the other. Electrons can pass from one side of the barrier to the other if they have enough energy or, if the barrier is thin and low, by quantum mechanical tunnelling. The height of the barrier and its thickness will control the current flowing through the barrier.

For the junctions we will be discussing, the barrier height is of order 1 volt, the thickness is of order 1 nm, and the temperature is typically 4.2 K or less. In this case, the dominant pathway is quantum mechanical tunnelling. In addition, for the case we will be considering, both metals are superconducting. In this case, the junction can support a maximum supercurrent, the critical current I_o, of:[6]

$$I_o = \frac{\pi}{2qR_n} \Delta(T) \tanh\left[\frac{\Delta(T)}{k_B T}\right] \qquad (6.1)$$

where: $\Delta(T)$ is the superconducting energy gap at temperature T, q is the electronic charge, and R_n is the normal state resistance of the tunnel

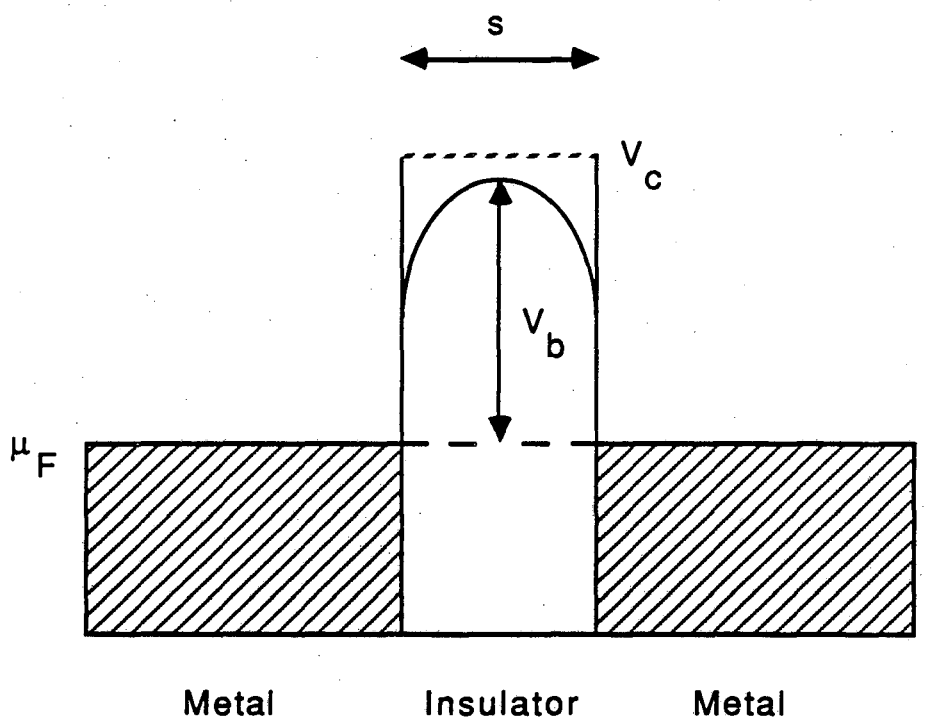

Fig. 6.1. Schematic of the insulating tunnel barrier between two metal electrodes. Rounding of the barrier edge is caused by image charge effects. The height of the barrier is V_b , the barrier thickness is s, the conduction band in the insulator is an energy V_c above the fermi level μ_F. The shaded area represents occupied electron states in the metal.

barrier.

R_n can be calculated explicitly from the normal state properties of the metals and from the barrier height and thickness, provided one makes simplifying assumptions. Many treatments have been published of this problem.[7-12] Stratton has provided a general expression for the current density, j, through a normal junction when one applies a voltage V:[11]

$$j = j_o\, e^{-b_1}(1-e^{-qc_1V}) \qquad (6.2)$$

where:

$$j_o = \frac{4\pi m_z q}{h^3 c_1^2}\left[\frac{\pi c_1 k_b T}{\sin(\pi c_1 k_b T)}\right]$$

$$b_1 = \alpha s\int_{x_1}^{x_2}(qV_b(x))^{1/2}dx$$

$$c_1 = \frac{\alpha s}{2}\int_{x_1}^{x_2}(qV_b(x))^{-1/2}dx$$

$$\alpha = \frac{2(2m_x)^{1/2}}{\hbar}$$

h is Planck's constant, and $\hbar = h/2\pi$,

x_1 and x_2 are the positions of the classical turning points (in units of the barrier thickness s),

the barrier lies in the y-z plane, m_x denotes the mass of the electrons in the direction perpendicular to the y-z plane, and m_z the mass along the parallel direction; we will take these to be equal to the free electron mass m.

We will be concerned only with the low temperature and low voltage limit, in which case Eq. 6.2 reduces to:

$$j = \frac{4\pi m q^2 V}{h^3 c_1}\, e^{-b_1} \qquad (6.3)$$

For a uniform junction, the total current through the junction is I =

jA, where A is the junction area. I can accordingly define the junctions normal state resistance as $R_n \equiv V/I$. From Eq. 6.3 I then find:

$$R_n = \frac{h^3 c_1}{4\pi m_z q^2 A} e^{b_1} \qquad (6.4)$$

A fluctuation in the height V_b, or thickness s of the barrier will thus cause an exponential change in the critical current of the device. From Eqs. 6.4 and 6.1, it is clear that other physical parameters enter into the critical current. A fluctuation in the temperature, for example, could also lead to a change in the critical current, because of the temperature dependence of $\Delta(T)$. This mechanism was originally proposed as an explanation for 1/f noise in Josephson juctions and SQUIDs,[13] but it has since been found not to be the dominant source.[14]

The present understanding is rather that it is the barrier height, V_b, which is fluctuating. The microphysical mechanism which produces this barrier change is the trapping or release of charges from defect states in the insulating barrier. For example, the presence of an additional negative charge in the insulator raises the barrier height because of coulomb repulsion between the trapped charge and the tunnelling electrons. This fluctuation in barrier height is produced locally in a small region of the barrier, while over most of the junction the height is unchanged. The exact shape of the barrier is complicated by image charge effects from the two neighboring metal surfaces. Schmidlin[12] has calculated the resulting potential energy barrier due to point charges, and generalized Eq. 6.3 to take into account nonuniformity of the resulting barrier. Interpreting his results in the present context, he found that a positive charge in the barrier would produce a change in the critical current, ΔI, given by:[12]

$$\Delta I = \frac{I_o}{A} 4\pi\beta_t a s^2 g(a) \qquad (6.5)$$

where a is the position of the charge within the barrier in units of the barrier thickness s, and where:

$$\beta_t = \frac{\alpha q^2 Z}{8\pi\varepsilon[eV_b(a)]^{1/2}} \qquad (6.6)$$

Z is the strength of the point charge in the barrier

g(a) is a complicated function,[12] which is nevertheless close to unity for our conditions

Eq. 6.5 is valid provided $\beta_t << 1$. For larger β_t the problem must be solved numerically. For a Z of 1, and typical parameters for Al_2O_3, Schmidlin[12] has calculated $\beta_t \simeq 0.7$. Thus, one cannot use this expression for a multiply charged trap in Al_2O_3. We must not rule out the possibility that a trap may be multiply charged, and in fact this seems to be common experimentally. Schmidlin has calculated the case of a doubly charged positive trap in Al_2O_3 and finds a maximum change in the critical current about 9 times larger than that of the singly charged trap.[12] It should also be noted that Schmidlin's analysis has left out the effect of electric field penetration into the Al metal electrodes, and that a number of other simplifying approximations have been made in the analysis.

Although the idea is physically incorrect, it is sometimes useful to treat the change in critical current as if it were due to a change in the area of the junction, caused say by the local raising of the barrier height (see Fig. 6.2). The equivalent area fluctuation is then:

$$\Delta A = A\Delta I_o/I_o = 4\pi\beta_t a s^2 g(a) \qquad (6.7)$$

Supposing that this area is a small circular region, one finds an

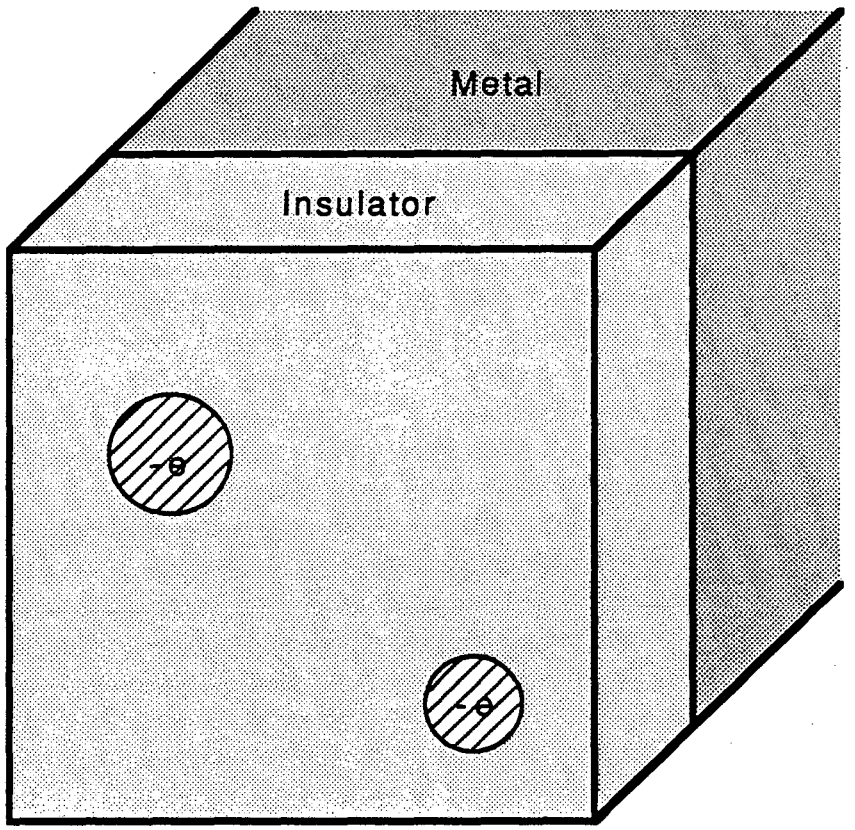

Fig. 6.2. Point charges in an insulating barrier produce regions where the tunnelling current density is reduced to zero because of coulomb repulsion.

effective trap radius r_t given by:

$$r_t = 2s(\beta_t ag(a))^{1/2} \qquad (6.8)$$

in the small β_t limit.

Now, if the charge were always present in the barrier, the change in critical current would be permanent, and no noise would be seen. If, however, the charge randomly enters and leaves the barrier because of thermal excitation, then the critical current of the junction will randomly fluctuate. This will be possible if the free energy barrier for charge transfer is not too much larger than k_BT, then thermal processes can empty or fill the trap. The charge trapping state, or trap, will then have a characteristic occupation and emptying time according to the free energy barrier and the temperature.

The exact cause of the free energy barrier, and the microphysical processes that set the time scale for trapping are still subjects of study. Rogers and Burhman have argued that the charges are due to ionic polarization of the medium arising from ionic reconfiguration in the barrier, rather than the occupation of defect states by electrons.(4) They have furthermore argued that the trapping times at low temperatures are determined by quantum mechanical tunnelling of the *atoms* between two ionic configuration. A different interpretaion is that the charges are due to the presence of electrons in the barrier. The distinction between these two scenarios is not essential for understanding our experimental results, and we do not have any convincing arguments either for or against Rogers and Buhrman's proposal. However, we do not observe levelling off of the noise at low temperatures, and hence have found no support for atomic tunnelling (see section 8.4d for similar results in the Nb-NbOx-PbIn system).

A single trap with a well-defined trapping time will yield a Lorentzian in the power spectrum of the fluctuations in I_o, as has been shown generally by Machlup.[15] The presence of just one trap would lead to a two state system, and one would see the critical current fluctuate between just two values, corresponding to the presence and absence of the trapped charge. Just such behavior has been observed in small area junctions, and is the strongest support for the model.[3-5] In order to get 1/f noise from such a mechanism, one must invoke the presence of several trap states with different time constants. The states then produce Lorentzians which add up to produce a 1/f spectrum if the distribution of trapping times is correct.

One important question not addressed by this model is how many traps one would expect in a given barrier. Little detailed information is known about this. This is undoubtedly because the subject is very complicated. First of all, the barriers, as they are commonly grown, should be filled with defects. The oxide layer on many Josephson devices is grown by RF plasma oxidation (see Chapter 1). Such a process should leave many dangling bonds because of the occurrence of relatively high energy ions in the plasma. In addition, the thin insulating layer must meet with two metal surfaces at an interface which most likely also posseses many unfilled bonds. The nature of the defects will thus depend upon the method of preparation of the barrier and the materials used, as well as on the presence of barrier contaminants.

Nonetheless, I can make a few qualtitative comments about what materials might form good barriers. First of all, all other things being considered equal, one would expect that a low energy oxidation technique, such as thermal oxidation at room temperature, should produce

fewer defects than a high energy process, such as RF oxidation. Secondly, from Schmidlin's formula, one can see that the presence of a trap will produce a current change which scales with $I_o\beta_t s^2 g(a)/A$. Thus for two barriers with the same number of traps, the same critical current, and the same area, one would expect that the barrier with lower $K = \beta_t s^2 g(a)$ should have the lower noise. Supposing that $g(a) \simeq 1$ for both, and substituting for β_t we can see that:

$$K = \frac{7.39\ Zs^2}{\varepsilon} \left[\frac{m_x}{meV_b(a)} \right]^{1/2} \qquad (6.9)$$

Thus a high thin barrier with a large dieletric constant should produce less noise per trap. Now for NbOx:

$$\varepsilon \simeq 27,\ V_b \simeq 0.2\ V,\ \text{and}\ s \simeq 2.0\ nm$$

while for Al_2O_3:

$$\varepsilon \simeq 9,\ V_b \simeq 1.4\ V,\ \text{and}\ s \simeq 1.0\ nm.$$

One thus finds $K_{Al}/K_{Nb} \simeq 0.3$, and thus the Al_2O_3 barrier should be quieter for the same number of traps.

Beyond these two simple observations, one would have to address the detailed chemistry of the insulator-metal system, in order to determine how many traps are produced. Such an analysis is beyond the scope of this Chapter, although clearly of relevance.

I might mention that there is an alternative way of thinking about 1/f noise in junctions. Kleinpenning[16] has formulated an approach in which the barrier fluctuations are related to a complex dielectric function in the insulator. The complex ε produces dissipation in the juction and a resistive component to the capacitive impedance. Because of Nyquist's relation, this leads to a fluctuation in the barrier

height. The model appears to be equivalent to the above point charge model at large length scales where one can ignore the presence of individual traps and consider only the average trapped charge distribution. What makes the model so interesting, assuming it is correct, is that the resistive losses in many dielectric materials have been measured, and one could presumably use such information to select good candidate materials for junction barriers. In addtion, the model makes specific predictions about how the 1/f noise should vary with temperature, which may turn out to be of relevance for future high Tc SQUIDs.

6.3 The All Nb Junctions: Preparation

Rowell and co-workers[17-20] have demonstrated that Nb-Al_2O_3-Nb Josephson tunnel junctions combine high qualtity electrical characteristics with excellent long-term durability. Furthermore, *in situ* thermal oxidation of the thin Al film produces tunnel barriers with predictable tunnelling resistances. A number of other workers,[21-28] have confirmed these results. Thus these "all Nb" junctions are attractive candidates for a number of applications, including computer elements, single electron tunnelling mixers, and SQUIDs. However, if these junctions are to be used for SQUIDs in low frequency applications, it is highly desirable that their critical currents exhibit low levels of excess noise at low frequencies.

B. Savo fabricated both shunted and unshunted junctions for measurements of noise and subgap leakage, respectively. The junctions were in nine groups of 5 on a 50 mm diameter oxidized Si wafer, with

nominal areas of 3X3, 6X6, and 11X11 μm^2. The configuration of the junctions is shown in Fig. 6.3. The fabrication procedure was as follows. First a Au (25 wt% Cu) layer was evaporated and lifted off to form the resistive shunts. A 240 nm layer of Nb was then sputtered on at 8 nm/s, and dry etched in a SF_6O_2 to form the base electrode. After a 1 nm Cr layer was deposited to improve adhesion, two successive 200 nm thick SiO layers were evaporated to form windows for junctions and the resistive shunts. Up to this point, the procedure was exactly the same as the one we use to produce Nb-NbOx-PbIn junctions; after this it differed. Next, a Nb film was sputtered down to make contact with the shunt through a window in the SiO, and lifted off. Then a final photoresist layer was patterned for the counterelectrode. The wafer was then diced into nine chips, each of which could be processed individually to form the Al_2O_3 barrier and Nb counterelectrode.

The deposition and oxidation of the Al and the deposition of the Nb counterelectrode were carried out without breaking vacuum in an oil diffusion pumped system with a base pressure of about 0.7 μTorr. The chamber contained two dc magnetron sputterguns[29] with 76 mm diameter planar targets of Al and Nb respectively, and a 25 mm diameter ion mill. The chip was rotated in turn to a position 60 mm below each source. We cleaned the Nb base electrode using the ion mill in 1.9 mTorr of argon at 400 V and at a current density of 50 $\mu A\ cm^{-2}$. The milling rate (determined in seperate experiments) was about 2.5 nm min^{-1} and the time was about 1.3 min. We then sputtered a film of Al approximately 5 nm thick at 33 nm min^{-1}, and oxidized it for a period of 80 minutes in an atmosphere of 60% Ar - 40% O_2 at pressures ranging from 1 to 300 Torr. This process yielded critical current densities ranging from 30 to 470 A

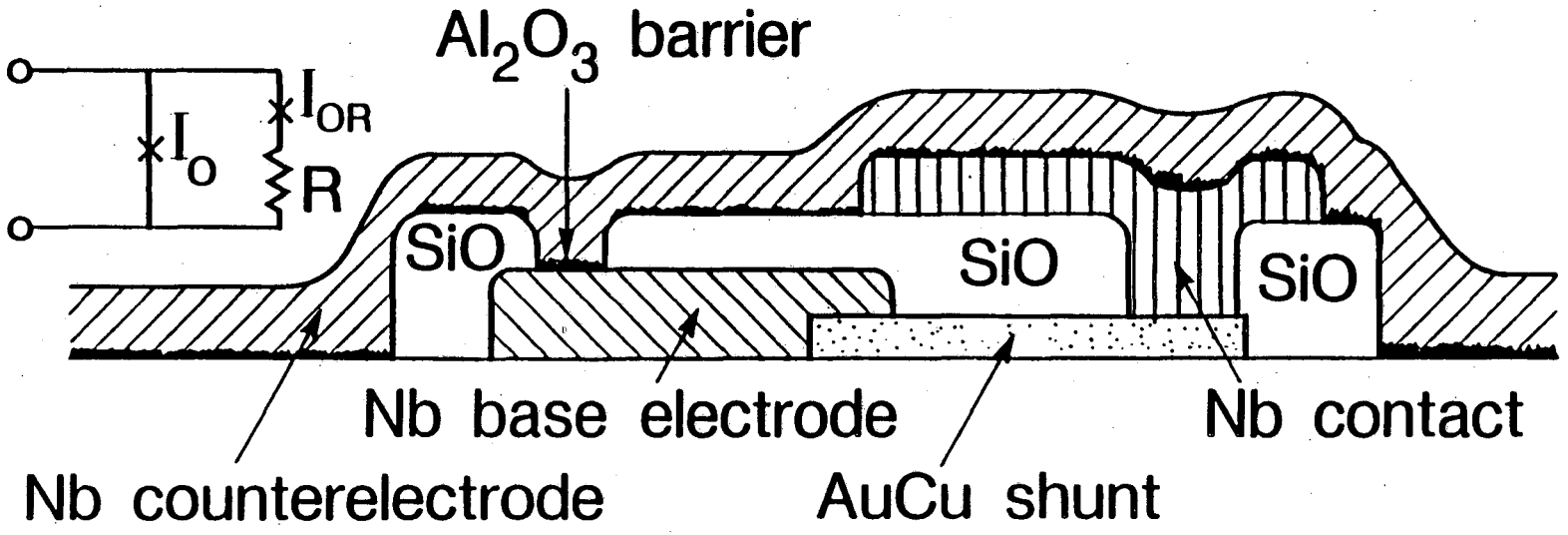

Fig. 6.3. Cross-sectional configuration of junction with shunt. Inset shows junction with critical current I_{oR} in series with shunt resistor.

cm^{-2} at 4.2 K. As reported by others,[20,22] the critical current density varied as approximately the inverse of the pressure. Finally we sputtered a 200 nm Nb counterelectrode at 60 nm min^{-1} with a voltage of 300 V and a power of 165 W in 8 mTorr of Ar.

In the case of unshunted junctions, this procedure yielded junctions with V_m (2 mV) of up to 18 mV at 4.2 K for the largest junctions.[30] The smallest junctions exhibited lower values of V_m, as has been reported by other authors.[24] Significantly higher ion mill current and/or higher deposition rates for the counterelectrode gave rise to markedly lower values of V_m.

6.4 Noise Measurements

We measured the low frequency noise from four shunted tunnel junctions which were made from two chips which were completed seperately. We connected each junction in series with a small resistance R_x (much less than the shunt resistance R), a large inductance, and the superconducting input coil of a flux locked dc SQUID. The configuration is the same as that described in Chapter 2, except that SQUID(1) has been replaced by a single resistively shunted junction (see Fig. 2.8). At the low frequencies of our measurements, the junction was biased at a constant voltage, V, which was determined by the current source connected across R_x. For $v << I_oR$, the signal at the output of the SQUID electronics was proportional to fluctuations in the critical current I_o. The equivalent 1/f noise produced by the SQUID itself was subtracted from the total noise at the SQUID output. When refered to the input circuit, this noise was 3.5 pA $Hz^{-1/2}$ at 4.2 K and 1 Hz, and was

generally a small contribution to the total noise.

Table 6.1 lists the measured parameters of the four junctions, including their measured areas. Figure 6.4 shows the spectral density of the critical current noise, $S_{I_O}^{1/2}(f)$, versus frequency for two of the junctions. The noise of junction 1 (9 μm^2) at 4.2 K, shown in Fig. 6.4(a), is white at frequencies down to about 20 Hz, with a feature that is approximately Lorentzian extending from this frequency down to about 0.8 Hz; at lower frequencies S_{I_O} scales approximately as 1/f. The Lorentzian arises from a switching process associated with two states in the barrier;[3-5] this switching process is clearly visible in the time trace shown in the inset. Fig. 6.4(b) shows the noise in the same

Table 6.1. Properties of four junctions: A is the junction area, T is the temperature, S_{I_O} is the spectral density of the critical current noise at 1 Hz and a_o is the logarithmic slope of the spectral density.

No.	A (μm^2)	T K	I_o (μA)	$S_{I_O}^{1/2}$ ($pAHz^{-1/2}$)	$S_{I_O}^{1/2}/I_o$ ($pA\mu A^{-1}Hz^{-1/2}$)	a_o
1	9.0	4.2	9.6	36	11.1	(*)
		1.5	11.4	17	4.5	1
2	7.8	4.2	2.6	6	6.6	≈1
3	115.	4.2	48.	34.5	7.7	0.8
		1.4	55.	50.2	9.8	0.8
4	34.	4.2	11.9	40.8	19.8	≈1

(*) Lorentzian below 10 Hz.

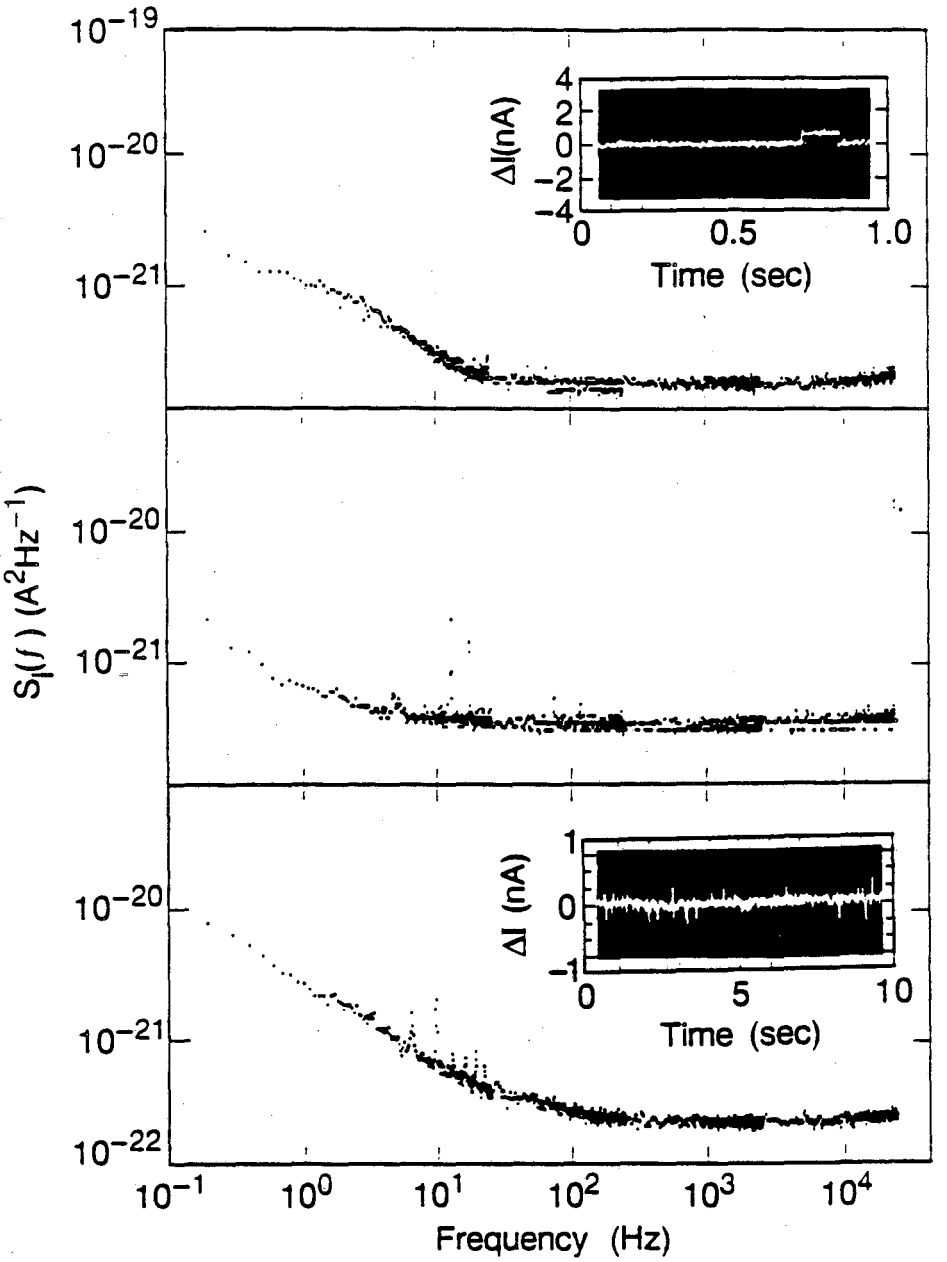

Fig. 6.4. S_{I_0} vs frequency for (a) junction 1 at 4.2 K, (b) junction 1 at 1.5 K, and (c) junction 3 at 1.4 K. The insets in (a) and (c) show critical current fluctuations vs time.

junction at 1.5 K. The Lorentzian component has disappeared, and S_{I_O} is white down to approximately 1 Hz, below which it scales as 1/f. Fig. 6.4(c) shows the measured noise for junction 3 (115 μm^2) at 1.4 K. There is no observable Lorentzian structure associated with a single switching process, and the spectral density scales as $1/f^{0.8}$. The time trace (inset) reveals several possible switching events associated with at least two traps.

Table 6.1 also lists $S_I^{1/2}$ (1 Hz). It should be emphasized that this value is not a good estimator of the noise at other frequencies, if, for example, there is a Lorentzian in the vicinity of 1 Hz. Since for a given density of independent identical traps per unit area one expects S_{I_O} to scale as I_o^2/A, we have also listed $S_{I_O}^{1/2}$ (1 Hz) $A^{1/2}/I_o$, where A is the area of the junction. At 4.2 K, this quantity varies by a factor of about 3. This variation is hardly surprising given the apparently small number of traps in each junction. Note that $S_{I_O}^{1/2}$ (1 Hz) $A^{1/2}/I_o$ ranges from a value comparable to that typical of our Nb-NbOx-PbIn junctions at 4.2 K, 20 pAμm/μA $Hz^{1/2}$, to a value substantially lower.

It is possible to make a number of deductions about the switching processes in these junctions. If we assume that the process locally reduces the critical current to zero, we can estimate the effective area of the trap from the height of the critical current pulse. The effective radius of the traps are 13 nm, and 15 nm for juctions 1 and 3 respectively. This radius is larger than that expected for singly charged traps. From Eq. 5.24, the expected effective trap radius is 1.1 nm for a singly charged trap, and 3.6 nm for a doubly charged trap. Thus the observed trap radius is larger than expected for even a doubly

charged trap, although only by about a factor of 3 to 4. As the critical current change grows rapidly with the charge of the trap,[12] a triply charged trap would probably have about this radius. In the case of junction 1, the critical current mostly remained in the "low" state with brief intervals in the high state. The resulting time trace appeared as a sequence of widely spaced pulses. The average pulse interval τ was 13, 63, and 1024 sec at temperatures of 4.2, 3.2, 2.1 K. Since the bias voltage V, typically 1.5 μV, is small compared to k_BT/e, one can try to fit these trapping times to an Arrhenius expression of the form:

$$\tau = \tau_0 \exp(E_a/k_BT), \qquad (6.10)$$

where: $1/\tau_0$ is an attempt frequency and E_a is an activation energy. The temperature dependence of τ yields $E_a \approx (1.8 \pm 0.1)$ mV and $1/\tau_0 \approx (10 \pm 3)$ sec^{-1}. Both E_a and $1/\tau_0$ are much smaller than the values found by other workers in NbOx and InOx barriers.[3-5,31-32] The duration of a given pulse, that is the time in the high current state, was found to be exponentially distributed with a temperature independent mean of 110 ms.

It is interesting to note that E_a is only slightly larger than the energy gap Δ in the Nb films. If we interpret this in terms of trapped electrons in the barrier, then there is a natural explanation. We believe that the data shown here can be explained as arising from one of several possible processes applicable to the case $V << \Delta/e$. The simplest scenario is as follows (it does not fit the details of what we observe, but is the easiest to explain and could obviously be recast to fit the data). Suppose that an electron with an energy within k_BT of the gap edge tunnels into a trap state which also lies at an energy about Δ above the fermi level. This single electron must be drawn from the superconducting quasiparticle population. Since the number of

quasiparticles scales as approximately $\exp(-\Delta/k_bT)$, the rate at which the trap fills will have the same temperature dependence. The trap empties when the electron tunnels out into an available quasiparticle state near the gap edge: For $k_BT << \Delta$, the density of available final states is nearly temperature independent, giving rise to a temperature independent emptying rate. Thus the temperature dependence of τ arises from the availability of quasiparticles. This is quite a different picture than that appropriate for $V >> \Delta/e$, where there is a temperature independent supply of quaiparticles created by pair breaking.

Two other observations on junction 1 are worthy of note. First the height of the critical current pulse increased proportionately more than the total critical current as the temperature was lowered. We have no explanation for this phenomenon. Secondly, after the junction was stored at room temperature for two weeks, we found that the Lorentzian in Fig. 6.4a was shifted slightly lower in frequency, by about 30%, but there was no other discernible change in its behavior. Thus the traps in Al_2O_3 appear to be much more stable than those observed for example in InO_x barriers.[32]

6.5 Conclusions

In summary, we have fabricated Nb-Al_2O_3-Nb Josephson tunnel junctions using a process that involves ion milling of the Nb base electrode prior to deposition of the Al film. The critical currents of the junctions exhibit low levels of excess low-frequency noise, and it is possible to observe switching processes associated with individual traps in junctions as large as 11X11 μm^2. The traps appear to be

multiply charged, and are characterized by very low activation energies, about 1.8 meV, and very low attempt frequencies, about 10 sec^{-1}. The combination of high durability and low levels of 1/f noise makes these junctions eminently suitable for use in SQUIDs. It should be emphasized however, that the noise properties reported here may depend critically upon the details of fabrication; other technologies may yield significantly higher or lower noise levels.

References

(1) Major portions of this Chapter have appeared in : B. Savo, F.C. Wellstood, and J. Clarke, "Low-Frequency Excess Noise in Nb-Al_2O_3-Nb Tunnel Junctions", Appl. Phys. Lett. 50, 1757 (1987).

(2) For an account of McWhorter's work see: A. Van der Zeil, "Noise", Prentice Hall, Chapter 5; or A.L. McWhorter "1/f Noise and Related Surface Effects in Germanium", M.I.T. Lincoln Lab. Report, No. 80 (1955).

(3) "Discrete Lorentzian Structure in Low Frequency Voltage Noise Spectra of Very Small Area Josephson Tunnel Junctions", C.T. Rogers and R.A. Buhrman,IEEE Trans. Magn., MAG-21, no.2, 126(1985).

(4) C.T. Rogers and R.A. Buhrman,IEEE Trans. Magn., Mag.19, 453(1983).

(5) C.T. Rogers, R.A. Buhrman, H. Kroger, and L.N. Smith, Appl. Phys. Lett. 49, 1107 (1986).

(6) V. Ambegaokar, A. Baratoff, "Tunneling Between Superconductors", Phys. Rev. Lett., 10, 486 (1963).

(7) A. Sommerfeld and H. Bethe, Handbuch der Physik, ed. H. Geiger and K. Scheel, vol. 24/2, 450, Springer-Verlag, Berlin (1933).

(8) R. Holm, J. Appl. Phys. 22, 509 (1951).

(9) J.G. Simmons, J. Appl. Phys. 34, 1793 (1963).

(10) J.G. Simmons, J. Appl. Phys. 35, 2655 (1964).

(11) R. Stratton, J. Phys. Chem. Solids 23, 1177 (1962).

(12) F.W. Schmidlin, "Enhanced Tunneling Through Dielectric Films Due to Ionic Defects", J. Appl. Phys. 37, 2823, (1966).

(13) R.F. Voss and J. Clarke, Phys. Rev. B 13, 556 (1976).

(14) For a discussion of some of the shortcomings of the temperature fluctuation model, consult: P. Dutta and P.M. Horn, "Low-frequency Fluctuations in Solids: 1/f Noise", Rev. Mod. Phys., 53, 497 (1981).

(15) S. Machlup, "Noise in Semiconductors: Spectrum of a Two-Parameter Random Signal", JAP 25, 341 (1954).

(16) T.G.M. Kleinpenning, "on Low Frequency Noise in Tunnel Junctions", Solid State Electronics, 25, 78 (1982).

(17) J.M. Rowell, M. Gurvitch, and J. Geerk, Phys. Rev. B 24, 2278 (1981).

(18) M. Gurvitch, M.A. Washington, and H.A. Huggins, Appl. Phys. Lett. 42, 472 (1983).

(19) J.V. Gates, M.A. Washington, and M. Gurvitch, J. Appl. Phys. 55, 1419 (1984).

(20) H.A. Huggins and M. Gurvitch, J. Appl. Phys. 57, 2103 (1985).

(21) J.M. Lumley, R.E. Somekh, J.E. Evetts, and J.H. James, IEEE Trans. Magn. MAG-21, 539 (1985).

(22) S. Morohashi, F. Shinoki, A. Shoji, M. Aoyagi, and H. Hayakawa, Appl. Phys. Lett. 46,1179 (1985).

(23) S. Morohashi, S. Hasuo, and T. Yamaoka, Appl. Phys. Lett. 48, 254 (1986).

(24) N. Nakagawa, K. Nakaya, I. Kurosawa, S. Takada, and H. Hayakawa, Jon. J. Appl. Phys. 25, L343 (1986).

(25) J. Niemeyer, Y. Sakamoto, E. Vollmer, J.H. Hinken, A. Shoji, H. Nakagawa, S. Takada, and S. Kosaka, Jpn. J. Appl. Phys. 25, 183 (1986).

(26) K. Tanabe, H. Asano, and O. Michikami, Jpn. J. Appl. Phys. 25, 183 (1986).

(27) A. Braginski, J. Talvacchio, M.A. Janocko, and J.R. Gavaler, J. Appl. Phys. 60, 2058 (1986).

(28) IEEE MAG-23 (1987) contains several papers on Nb-AlOx-Nb junctions.

(29) Ion Tech, Inc., Fort Collins, Colorado.

(30) V_m(2mV) is defined as I_0*(resistance at 2 mV) = 2 mV$\cdot(I_0/I_x)$, where I_x is the excess current that flows when the junction is biased at 2 mV.

(31) C.D. Tesche, "SQUID 85 Superconducting Quantum Interference Devices and Their Applications (de Gruyter, Berlin, 1985), p 797.

(32) R.T. Wakai and D.J. Van Harlingen, Appl. Phys. Lett. 49, 593 (1986).

Chapter 7: High Temperature Flux Noise and Critical Current Noise in SQUIDs[1]

7.1 Introduction

The existence of 1/f noise in SQUIDs causes serious limitations to certain types of low-frequency measurements.[2-3] Virtually all of these SQUID measurements are currently being made in the ^{4}He temperature range. If one attempts to increase the SQUID's sensitivity by reducing L and/or C, one typically finds that the 1/f noise energy is increased, and the 1/f noise extends to progressively higher frequencies. Thus, the development of low noise SQUIDs at low frequencies is largely a study of the sources of 1/f noise.

This Chapter concerns the "high temperature flux noise", which occurs in many of our dc SQUIDs, and how it can be distinguished from critical current fluctuations. By high temperature, I mean here the temperature range from 1.2 to 4.2 K. This noise is distinctly different from that produced by critical current fluctuations (which was discussed in Chapter 6), and is also distinguishable from the low temperature excess noise which will be discussed in Chapter 8. The situation has not been completely resolved. We still do not know the underlying micro-physical process which produces the high temperature flux noise. Nevertheless, the results I present below have enabled us to identify the material responsible for the noise and have provided two empirical techniques for eliminating or greatly reducing the noise.

Professor Clarke's group has built and operated many different types of dc SQUIDs over the years.[4-6] When tested at 4.2 K, these devices

have all shown 1/f noise at low frequencies. The origin and nature of this noise seems to have been debated continuously since Voss and Clarke proposed that the noise arose from critical current fluctuations in the Josephson junctions driven by equilibrium temperature fluctuations.[7] This turned out generally not to be the case. It was only with the publication of results by Koch et al.[8] that the subject was put on a firm foundation. They found that in several different thin-film devices the 1/f noise was an "apparent flux noise", exhibiting properties that were consistent with fluctuations in an external magnetic flux. Furthermore, the excess flux noise at 1 Hz, $S_\Phi(1\ \text{Hz})$, was generally of the order of $10^{-10}\ \Phi_0^2\ \text{Hz}^{-1}$. The expected 1/f noise in the critical current was too small to account for the 1/f noise observed in these SQUIDs. I will reexamine this conclusion below using the results of Chapter 5.

In their study, the authors[8] built a clever flux and current modulation biasing system which allowed them to distinguish between noise which arose from critical current fluctuations and noise which arose from magnetic flux changes. They then tested one of John Martinis's type A SQUIDs and found conclusively that the noise was caused by a fluctuating flux rather than a fluctuating critical current. The level of 1/f noise was known in the groups earlier SQUIDs, but its nature was not. They noticed, however, that the level of 1/f noise in the type A SQUID was very comparable to the level seen in all the other SQUIDs tested until then. They further noted that the level of 1/f noise in these SQUIDs was generally higher than might be expected from critical current noise. They then concluded that the excess 1/f noise in these dc SQUIDs was due to a unknown source of flux noise.

The developments I will report here show this conclusion to be generally incorrect for other SQUIDs. Although the type A SQUIDs do show 1/f flux noise, this is not true for many other SQUIDs. It should be noted that several other groups had earlier found that their devices were dominated by critical current noise, or had substantially smaller levels of 1/f noise.[9-10] On the whole, from the work of Rogers and Burhman,[11] and Celasco et al.,[12] critical current noise was to be expected and the flux noise stood out as a very strange and unexplained anomaly.

One factor which made the flux noise especially puzzling was that it did not seem to depend upon the type of SQUID or the materials used, and yet the noise was produced by the SQUID. This turned out to be an illusion. The production by other groups of SQUIDs which did not show appreciable flux noise, clearly demonstrated that the flux noise did depend upon the details of construction.

My investigation of the high temperature flux noise proceeded as a parasitic or secondary experiment. I was mostly interested in understanding the puzzling behavior of the low temperature excess noise (Chapter 8), and on the side I collected data on the excess noise at high temperatures. This necessarily makes the results on the high temperature flux noise somewhat scattered and incomplete. The results occurred in three stages: the magnetometer, the Pb based SQUIDs, and the new Nb based SQUIDs.

One reason for my continuing interest in the high temperature flux noise is that, in many ways, it is similar to the low temperature excess noise. As will be discussed in Chapter 8, the low temperature excess noise is also a flux noise which displays an independence of device type

and construction that is very hard to understand. It is possible that the underlying mechanisms, both of which are unknown, may be similar. This gives the high temperature flux noise the status of a model test system which is better known and more open to investigation. In addition, it has recently been found that the "high T_c" material $YBa_2Cu_3O_7$ can display large amounts of 1/f flux noise.[13] The potential importance of this material will undoubtedly spur more research into the cause of excess flux noise in SQUIDs.

7.2 The Magnetometer

As was noted briefly in Chapter 3, the magnetometer showed the same level of 1/f noise as a bare type A SQUID. Fig. 3.5 shows a clear 1/f spectrum with $S_\Phi^{1/2}(f)(1Hz) \simeq 14\ \mu\Phi_0 Hz^{-1/2}$. This level is identical to that which we commonly find in our Nb type A SQUIDs without a pickup coil.[6] This demonstrated unequivocally that the noise was not due to a fluctuating external magnetic field.

To see this more clearly, consider the flux change, $\delta\Phi$, produced in a SQUID with a pick-up coil, when the SQUID is placed in a fluctuating magnetic field. From Eq. 3.1, we can write:

$$\delta\Phi \simeq A_p M_i \delta B/(L_i+L_p) \qquad (3.1)$$

where: δB is the applied magnetic field,

A_p is the area of the pickup loop

L_p is the inductance of the pick-up loop

L_i is the inductance of the input coil

M_i is the mutual inductance between the SQUID and the input coil.

On the otherhand, for a SQUID without an input coil, the flux produced

in the SQUID is just:

$$\delta\Phi = \delta B \cdot A_S \qquad (7.1)$$

where A_S is the effective pickup area of the SQUID (see Chapter 3). The ratio between the flux produced in a SQUID with a pickup coil to that produced in a bare SQUID is approximately:

$$M_i A_p / ((L_i + L_p) A_S) \qquad (7.2)$$

For the magnetometer of Chapter 3, this ratio was found to be about 9. Thus for a given external field change δB, the magnetometer should produce a response which is nine times larger than that from a bare SQUID. The fact that the noise is unchanged by the addition of a pick-up loop (to within about 10%) means that the noise cannot be due to a uniform magnetic field change.

This null result does not exclude the possibility of local sources of magnetic field. If a source were so close to the SQUID that its field were not uniform over the area of the magnetometer loop, then the signal in the SQUID would not scale with the loop area, A_p.

In addition it does not rule out a source which generates a fixed amount of flux noise per superconducting loop. Koch et al.[8] found that the noise in the SQUID did not seem to depend upon on the size of the SQUID. One might then speculate that for any loop, one gets a certain amount of flux noise. In fact this would be very difficult to observe with the magnetometer. Suppose that there occured a small flux change, $\delta\Phi$, in the pick-up loop. This would induce a flux change in the SQUID $\delta\Phi_S = \delta\Phi M_i/(L_i+L_p) \approx \delta\Phi/25$, for the magnetometer of Chapter 3. This is much smaller than the flux change $\delta\Phi$ that one would expect from the superconducting SQUID loop itsef, and hence would be difficult to detect.

There was one additional fact to note about the magnetometer. The closed superconducting pickup loop was tightly coupled to the SQUID, and thus caused a corresponding reduction of the SQUID's inductance. We can estimate the screened inductance L' of the SQUID as follows:[14]

$$L' = L(1-\alpha_e^2) \qquad (7.3)$$

where α_e is the equivalent coupling constant:

$$\alpha_e^2 = \alpha^2 L_i/(L_i + L_p) \simeq 0.64 \qquad (7.4)$$

For the magnetometer: $\alpha^2 \simeq 0.75$, $L_i = 120$ nH, and $L_p \simeq 40$ nH. One thus expects:

$$L' \simeq 0.44\ L. \qquad (7.5)$$

The SQUID should have shown a substantial reduction in its inductance. Unfortunately, we did not check for this experimentally. Nevertheless, the existance of such effects is well-known [15]. We can conclude then that the level of the 1/f noise also does not depend on the inductance of the SQUID. This fact puts a constraint on any models of the 1/f noise which attempt to explain it as either critical current noise or as some kind of dynamical effect arising from the SQUID equations of motion.

7.3 The Pb and PbIn SQUIDs

In the investigation of the low temperature excess noise (see Chapter 8), I first tested for material and size dependence. This circumstance allowed me to also test the material and size dependence of the high temperature 1/f noise. Almost immediately, I found a SQUID type with substantially less high temperature 1/f noise. The device was a type C with a PbIn SQUID loop (see Chapter 1 for a discussion of the different SQUID types). It showed the then remarkably low flux noise

level of about 4 $\mu\Phi_0 Hz^{-1/2}$ at 1 Hz and 4.2 K, as compared with 14 $\mu\Phi_0 Hz^{-1/2}$ ± 10% for virtually all of the type A SQUIDs. Measurements on other type C SQUIDs revealed essentially the same low noise behavior. Thus, regardless of the nature or origin of the excess noise, these devices were inconsistent with the idea of a constant level of 1/f flux noise in all SQUIDs. Results for several C SQUIDs are shown in Fig. 7.1.

More importantly, further investigation of the C SQUIDs revealed that their noise was not a flux noise but rather was dominated by critical current fluctuations. This conclusion was based on the results of Chapter 5, and three distinct experimental facts:

1. The observed level of the 1/f noise was in reasonable agreement with that expected from typical critical current noise in Nb-NbOx-PbIn tunnel junctions.
2. The level of the 1/f noise was not the same for all the C SQUIDs, but rather it tended to scale with the critical current of the different SQUIDs. This can be seen directly in Fig. 7.1 where the devices with the highest critical currents display the largest 1/f noise. This is what one would expect for critical current noise, if there is a reproducible average number density of fluctuating charges in the tunnel barrier.
3. Finally, and most importantly, the noise was measured at different flux bias points and compared with the expected noise for a critical current or flux noise. There was nearly the same level of noise, S_I, at Φ_0 where there is no flux gain, as at $\Phi_0/4$ where the flux gain is a maximum. Therefore, the observed excess noise cannot be a flux noise.

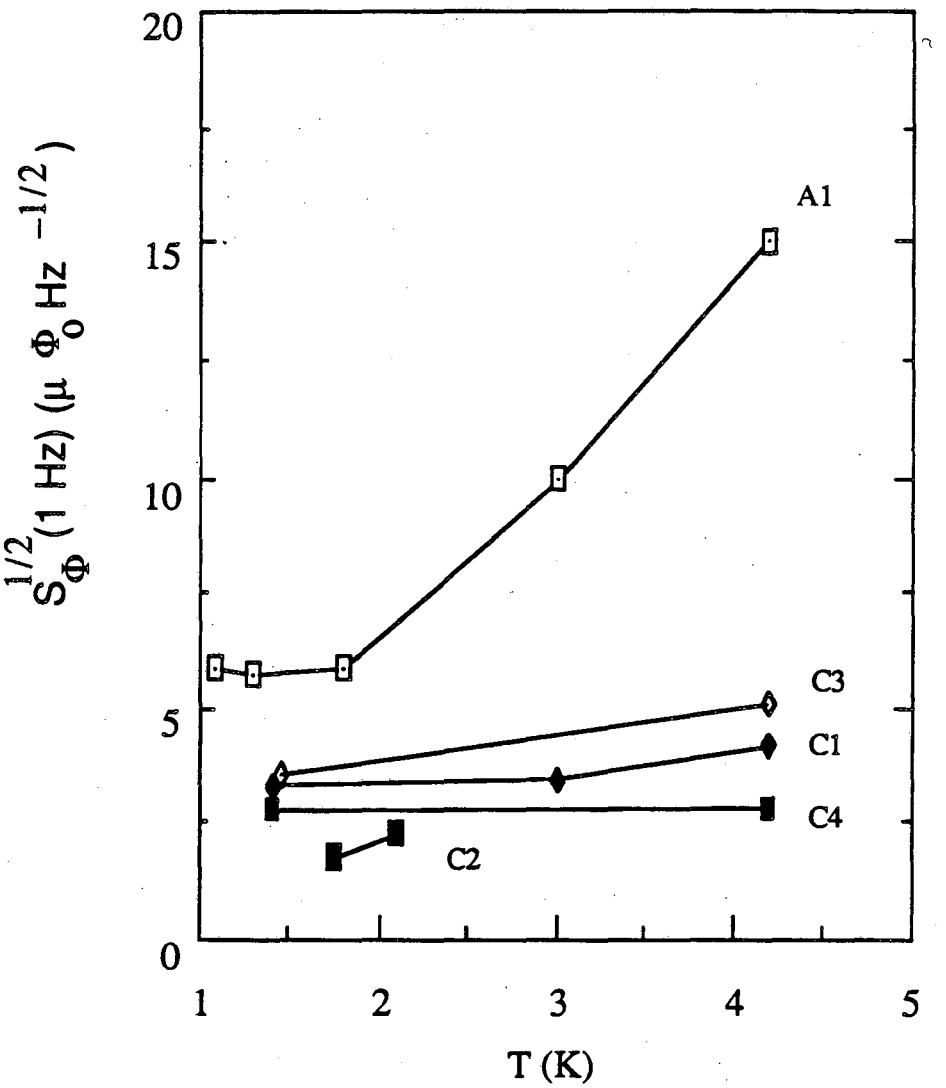

Fig. 7.1 Excess flux noise at 1 Hz vs temperature in four Pb based SQUIDs and in a type A SQUID. All SQUIDs were biased near $\Phi_0/4$. The type C SQUIDs show a much lower level of noise then the typical type A SQUID shown.

In order to analyze the 1/f noise at different flux bias points, Φ, including places where $\partial I/\partial\Phi$ vanishes, it is best to convert the equivalent flux noise to an output current noise S_I. Fig. 7.2 shows the result of such an analysis for the excess noise in four type C SQUIDs.

The experimental data can then be directly compared with the results of Chapter 5, to see if they are consistent with critical current noise. From the results of Chapter 5, assuming that the junctions are equally noisy and the SQUID is symmetric, the noise produced by the critical current fluctuations is:

$$S_I = S_{Io}\{[i + \beta(\partial i/\partial\beta) - v(\partial i/\partial v)]^2 + (\partial i/\partial\alpha)^2\} \qquad (5.21)$$

where: $S_{Io} = (S_{Io1} + S_{Io2})/4 = S_{Io1}/2$, and S_{Io1} is the critical current noise in each junction. The 1/f noise at the SQUID output should vary with the flux because the different partials vary with flux. I can use the simulations of Chapter 5 to estimate the partials $\partial i/\partial\alpha$, and $\partial i/\partial\beta$. In order to compare this expression with the data, I will need the factor S_{Io}. The approximate value is known from independent noise measurments at Φ_o taken on my other SQUIDs. This empirically determined noise level is about:

$$S_{Io1}(1Hz) = (84\ KpA\mu mHz^{-1/2}\mu A^{-1})^2\ I_o^2/(AT) \qquad (7.6)$$

where A is the area of one of the junctions, and T is the temperature. The linear temperature dependence is usually seen only roughly, and the observed critical current noise magnitude tends to vary substantially about this level, due to junction to junction variations. Nonetheless, the relation provides a useful estimate for our Nb-NbOx-PbIn junctions, and will allow me to compare results at different temperatures.

Figure 7.3 shows the results of such an analysis. While the agreement is qualitatively correct, it is not spectacular. This is

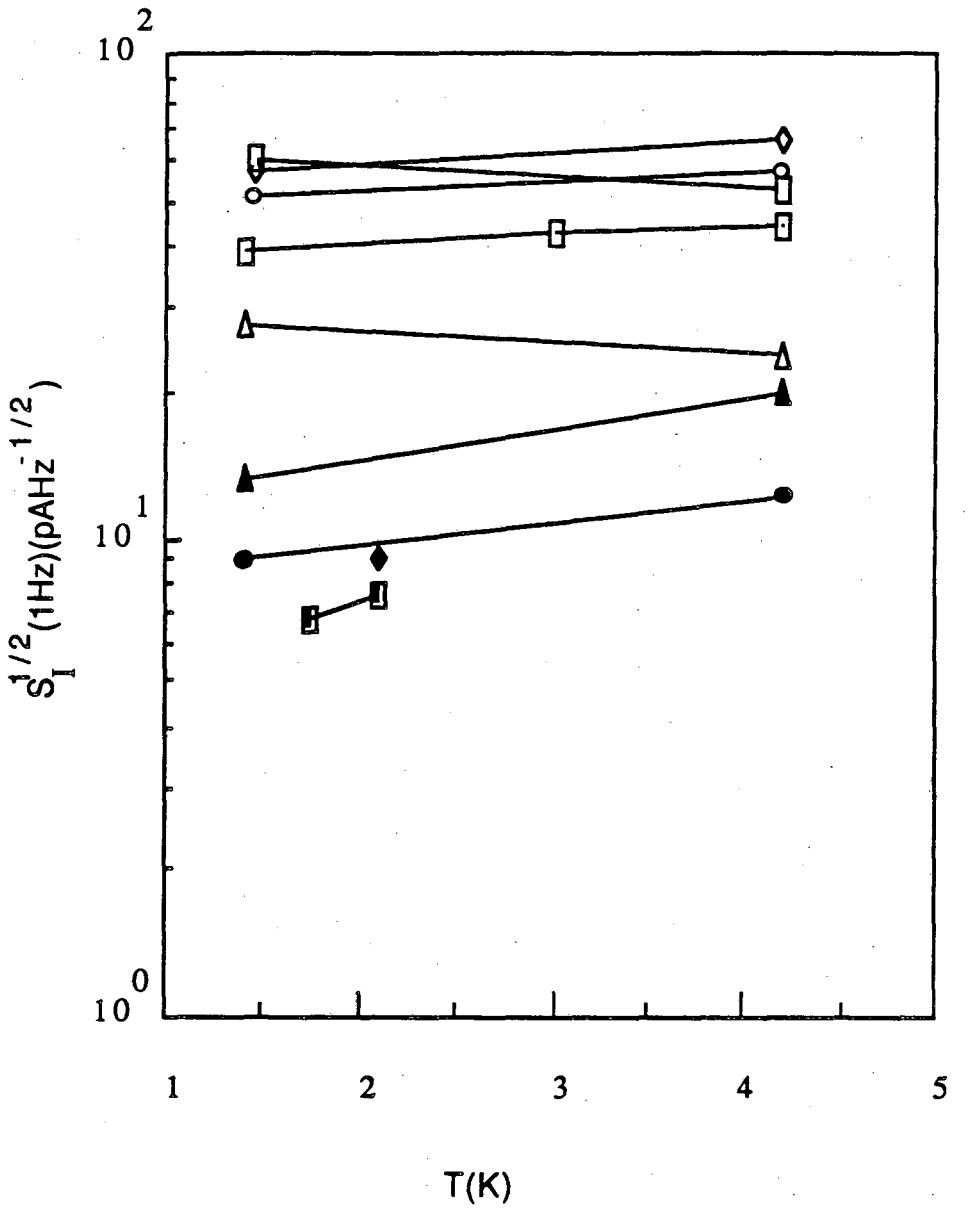

Fig. 7.2 Excess output current noise at 1 Hz vs temperature for four SQUIDs: ▯C1 at $\Phi_0/4$, ♦C2 at Φ_0, ▮ C2 at $\Phi_0/4$, o C3 at $\Phi_0/4$, ◊C3 at Φ_0, ▯ C3 at $\Phi_0/2$, ΔC4 at $\Phi_0/4$, ▲C4 at Φ_0, ● C4 at $\Phi_0/2$.

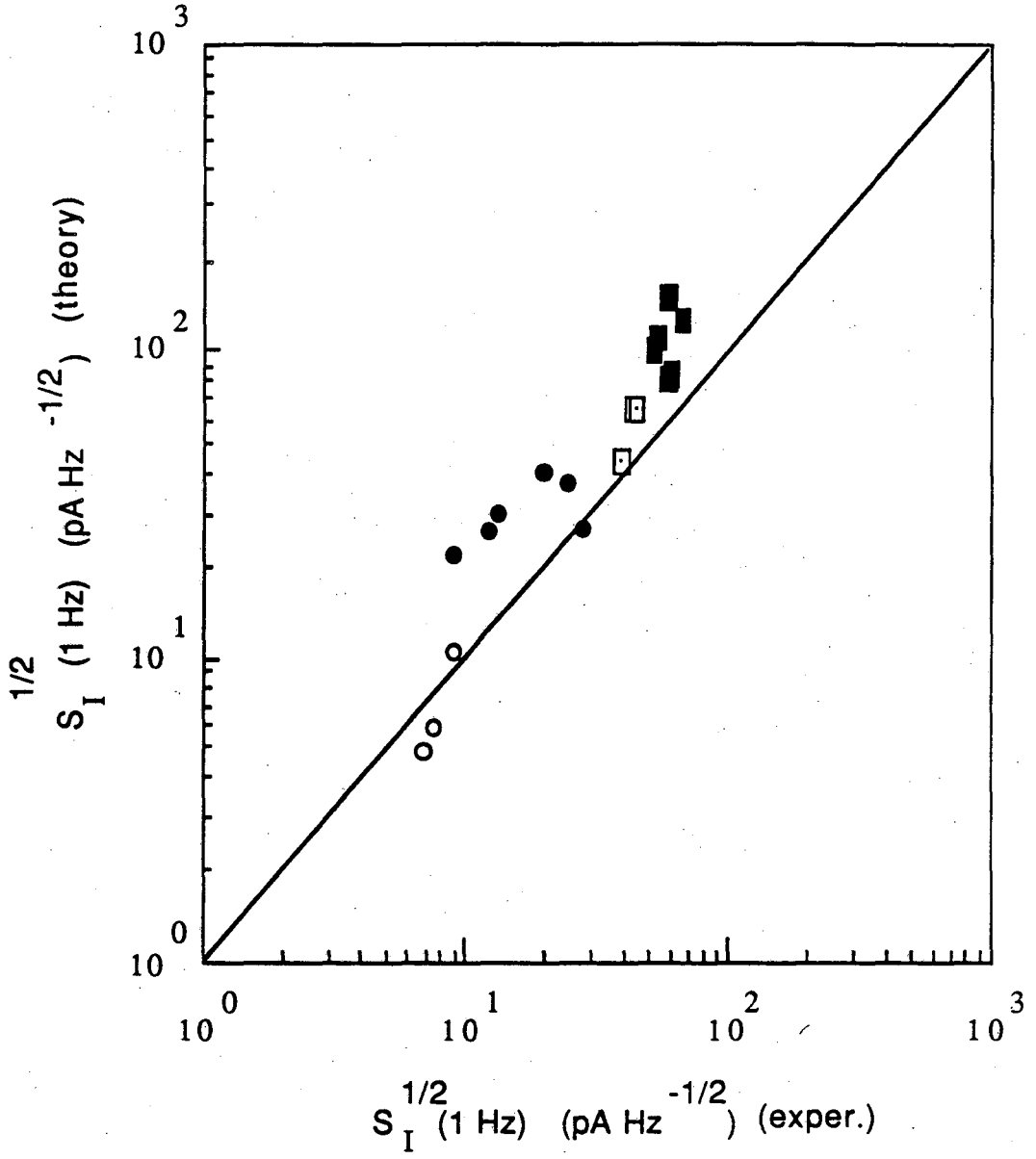

Fig. 7.3 Noise expected from critical current fluctuations vs observed excess noise level for SQUIDs: ⊡ C1, o C2, ■ C3, ● C4.

undoubtedly due to several factors. First of all, the critical current noise undoubtedly varies from one device to the next, and from one junction to the next. In fact, this is easily seen to be the major cause for the discrepancies. Since the noise at Φ_0 is simply the critical current noise, the data at Φ_0 can be compared directly with the empirical relation Eq. 7.6. One finds that C3 and C4 are about twice as quiet at Φ_0 as would be expected from Eq. 7.6, and this lifts all of the points above the line. Secondly, the parameters and partials are only approximately known, and variations in the noise between the two junctions in any one SQUID make Eq. 5.21 inaccurate. Finally, the noise at $\Phi_0/4$ may not be entirely due to critical current noise. There may still exist a small amount of 1/f flux noise in these devices. This is especially true at the lower temperature points, as will be seen in considerable detail in Chapter 8.

Unfortunately, the noise-vs-flux technique does not let us accurately estimate the residual level of 1/f flux noise in the device because of the lack of accurate knowledge about the many parameters involved. A better test would have been to use the flux and current modulation scheme of Koch et al.[8]

Following these revelations, I looked at the noise in several other Pb SQUIDs, as well as in Nb and half Pb half Nb SQUIDs. Most of these measurements were not careful noise-vs-flux evaluations, but rather just noting the noise at $\Phi_0/4$ and possibly Φ_0. As such they did not allow for a check on the noise mechanism in any detail. Nevertheless, the magnitude of the noise showed a remarkable and easily understood behavior. Devices with Pb or PbIn based loops generally showed low levels of 1/f noise which were consistent with typical critical current

fluctuations. On the otherhand, devices with Nb loops showed 1/f noise which was too large for expected critical current noise, and was always close to 14 $\mu\Phi_0 Hz^{-1/2}$, the typical number that occurs in the earlier Nb devices, (it should be noted that although the loops were of different materials, as discussed in Chapter 1, the junctions were of identical Nb-NbOx-PbIn construction). This consistent and remarkable behavior allowed us to make the conclusion that the high temperature flux noise was being produced in the Nb loop of the SQUID, and not in the PbIn or Pb loops.

7.4 Critique of Koch et al.

The above results on PbIn loop SQUIDs would not have been so surprising if it had not been for Koch et al.[8] In particular they reported results on three Pb based SQUIDs and found typical levels of 1/f noise. A careful look revealed that this was not quite the case. In particular, it should be noted that neither the flux-vs-noise nor the electronic modulation scheme was used to determine the nature of the noise in any of their Pb based SQUIDs.

The first "Pb based" device (which was called a type C in Koch et al., but is quite different from the type C devices in this thesis) had been mislableled as having a Pb loop when in fact the loop was Nb.[16] Thus, the level of 1/f noise was consistent with that known to exist in our other Nb SQUIDs, and there is no contradiction with my results on the Pb bodied SQUIDs.

The remaining two Pb based devices (which the authors labeled E1 and E2), in fact, presented the least convincing case for flux noise of any

of their devices.[17] These two devices were the low inductance "quantum limited SQUIDs",[18] and were made with PbIn-PbOx-Pb junctions. The observed level of 1/f noise was 17 $\mu\Phi_0 Hz^{-1/2}$ for the first device, and 6.5 $\mu\Phi_0 Hz^{-1/2}$ for the second. There were two remarkable things here, first of all, the two devices were displaying noise which differed from each other by a factor of 7 in the power. Secondly, although the first SQUID showed a nearly typical level of 1/f noise, the second was considerably quieter than normal. Such behavior is inconsistent with a constant flux noise source, and quite unlike that seen in the Nb based SQUIDs.

Is it possible that the 1/f noise in these two devices was due to critical current fluctuations? Unfortunately, I do not have independent data on critical current noise in PbIn-PbOx-Pb junctions. Ref. 8 does present data on the critical current noise in a few junctions of this type, although it is not clear how representative the data is. Using this, I can construct a possible scenario. The highest level of 1/f critical current noise for the four junctions reported was, at 4.2 K:

$$S_{I_0}/I_0^2(1Hz) = 4 \times 10^{-11}\ Hz^{-1} \qquad (7.7)$$

for a 6 μm^2 junction. From Chapter 6, we expect that $S_{I_0}A/I_0^2$ is constant for a given junction type (although it should be noted that no such scaling is evident for the junctions of ref. 8, nonetheless, we will need to scale the data in some way for the junction at hand, and the assumption is reasonable). For this junction one finds:

$$S_{I_0}^{1/2}A^{1/2}/I_0 \propto 16\ pA\ \mu m\ \mu A^{-1}\ Hz^{-1/2} \qquad (7.8)$$

The junctions in SQUIDs "E1" and "E2" of ref. 8 had an area of π mm^2. The expected critical current noise from each of the junctions should then be:

$$S_{Io1}^{1/2} \simeq I_o \cdot 9 \text{ pA } \mu A^{-1} \text{ Hz}^{-1/2} \qquad (7.9)$$

From the results of Chapter 5, assuming that the junctions are equally noisy, the noise produced by the critical current fluctuations is:

$$S_I = S_{Io}\{[i + \beta(\partial i/\partial\beta) - v(\partial i/\partial v)]^2 + (\partial i/\partial\alpha)^2\} \qquad (5.21)$$

Eq. 5.21 gives the output current noise from the SQUID if it were voltage biased. The SQUIDs of ref. 8, however, were biased with a constant current, and we wish to refer the noise back to the SQUID as a flux noise. For the constant current case, the output voltage noise is just:

$$S_V = R_D^2 \cdot S_I \qquad (7.10)$$

where S_I is given above, and R_D is the dynamic resistance of the SQUID at the bias point. The flux noise is then just:

$$S_\Phi = R_D^2 S_I/(\partial V/\partial\Phi)^2 \qquad (7.11)$$

Combining Eqs. 5.21 and 7.11, one arrives at a final expression for the flux noise:

$$S_\Phi = R_D^2 \cdot S_{Io}\{[i + \beta(\partial i/\partial\beta) - v(\partial i/\partial v)]^2 + (\partial i/\partial\alpha)^2\}/(\partial V/\partial\Phi)^2, \qquad (7.12)$$

The known device parameters for device "E1" were: T=4.2 K, I_o=550μA, L=1.9pH, C=0.3pF, $A_{junction}=\pi\mu m^2$, $\partial V/\partial\Phi$=6.8 mV/Φ_o, R_D=4.7Ω, R=1.3Ω, β=1, and β_c = 0.9. The bias current and voltage were not recorded, but a reasonable assumption would be: v=0.25 and i=1.5. The values of $\partial i/\partial\beta$ and $\partial i/\partial\alpha$ can be estimated from the numerical simulations of Chapter 4. Assuming that the device had α = 0, and η = 0, one finds:

$$\partial i/\partial\beta \simeq 0.18, \qquad \partial i/\partial\alpha \simeq 1.25$$

Substituting these values into Eq. 7.11 one finds:

$$S_\Phi^{1/2}(1\text{Hz}) \simeq 10\ \mu\Phi_o\text{Hz}^{-1/2}$$

This is to be compared with the 17 $\mu\Phi_o\text{Hz}^{-1/2}$ found experimentally. For

the case of ref. 8 device "E2", the known device parameters were: T=4.2K, I_o=380μA, L=2.5pH, C=0.3pF, $A_{junction}=\pi\mu m^2$, $\partial V/\partial\Phi$=6.5mV/Φ_o, R_D=3.2Ω, R=1.6Ω, β=0.9, and β_c = 0.9. The bias current and voltage were not recorded, but a reasonable assumption would again be: v = 0.25 and i=1.5. The values of $\partial i/\partial\beta$ and $\partial i/\partial\alpha$ can be estimated from the numerical simulations of Chapter 4. Assuming that the device had α = 0, and η = 0, one again finds:

$$\partial i/\partial\beta \simeq 0.18, \qquad \partial i/\partial\alpha \simeq 1.25$$

Substituting these values into Eq. 7.11 one finds:

$$S_\Phi^{1/2}(1Hz) \simeq 4.7\ \mu\Phi_o Hz^{-1/2}$$

This is to be compared with the 6.5 $\mu\Phi_o Hz^{-1/2}$ found experimentally. In both cases, the estimated flux noise produced by the estimated critical current noise is less than a factor of three smaller in the power than the observed noise. Therefore, a plausible case can be made that critical current noise was in fact the cause of the observed noise. The fact that the estimate correctly predicts that the 1/f noise in "E2" should be larger than that in "E1" is also encouraging.

Although it will never be known for sure what the cause of the excess noise was in these particular devices, the preceding criticism demonstrates that the results are not inconsistent with critical current noise. More generally, the conclusions of Koch et al.[8] are unwarranted for Pb based devices and there is no real disagreement with the results on my type C SQUIDs.

7.5 The New Nb SQUIDs

Dr. Bonaventura Savo's (see Chapter 6) work on Nb-AlOx-Nb junctions

had an unexpected fringe benefit. The fabrication system he constructed included a new planar dc sputtergun for performing the Nb depositions (material from this newer sputtergun I will call "new Nb"). This provided me with an opportunity to test SQUIDs which had Nb loops deposited from an entirely different system. Previously, all of the SQUIDs made in the group were made with Nb deposited from the exact same cylindrical dc sputtergun (material deposited from this original sputtergun, I will call "old Nb"). This includes all of the SQUIDs tested by Koch et al.,[8] as well as all of the SQUIDs mentioned so far in this thesis.

For this set of tests, I adopted a special SQUID configuration. The body of the loop was made of the new Nb while the junctions were fabricated with a base layer from the old Nb. The junctions were made in the form of the old Nb-NbOx-PbIn, rather than with new Nb or with Savo's all Nb procedure. In this way, I could use junctions with known critical current noise behavior, and change only the loop material. The configuration employed is shown in Fig. 7.4. The SQUID were simple variants of the type A configuration (see Chapter 2). The main difference was that a small region where the junctions reside has been cut away, and an additional processing step introduced to allow for filling in this small region with a second layer of Nb. The main body of the loop was deposited first using Savo's sputtergun. The pressure of the Argon sputtering gas was deliberately held to about 1 μm (as compared with about 7 μm in the old system). The Nb was then etched in an SF_6O_2 plasma. Next, the AuCu shunts were deposited and lifted off. Photoresist was then spun on and patterned for the additional step. The pattern left two small holes through the resist which defined where the

old Nb would be deposited (see Fig. 7.4). The new Nb surface in this small region was then cleaned using an ion mill, and the old Nb sputtered down. The milling was necessary to ensure good contact between the two Nb layers, and between the old Nb and the resistive shunt. The final pattern for the old Nb was then defined by lift-off, and the remainder of the steps proceeded as in Chapter 2.

I built three modified type A SQUIDs using the new Nb: A6, A7, and A8. The results for the excess noise magnitude at 1 Hz are summarized in Table 7.1. It is to be admitted that the noise is not as low as in the case of the Pb based loops, and is at best only about a factor of 2 smaller in the rms than the old Nb SQUIDs. However, this seems to be almost entirely due to a larger than usual level of critical current noise, as can be seen by the higher than expected level of excess noise when there is no flux gain (Φ_0 or $\Phi_0/2$). The flux dependence of the excess noise has one interesting characteristic. There is generally a large difference in the noise at $\Phi_0/4$ and $3\Phi_0/4$. This difference is noticeable whether the noise is expressed as a flux or a current noise. Such a situation could not arise for a constant flux noise source. On the otherhand, if one of the junctions has more critical current noise than the other, than as was discussed in Chapter 5, one should expect to see different levels of excess noise at $\pm \Phi_0/4$. This difference then is probably just a consequence of the variation in critical current noise from one junction to the next. A second interesting aspect of this is that in device A8, a Lorentzian was visible in the noise spectrum. The knee frequency was around 10 Hz. The Lorentzian was most visible when the device was biased at $\Phi_0/4$, and was clearly visible at Φ_0 and $\Phi_0/2$. On the otherhand, it was not visible at $3\Phi o/4$, and this fact accounts

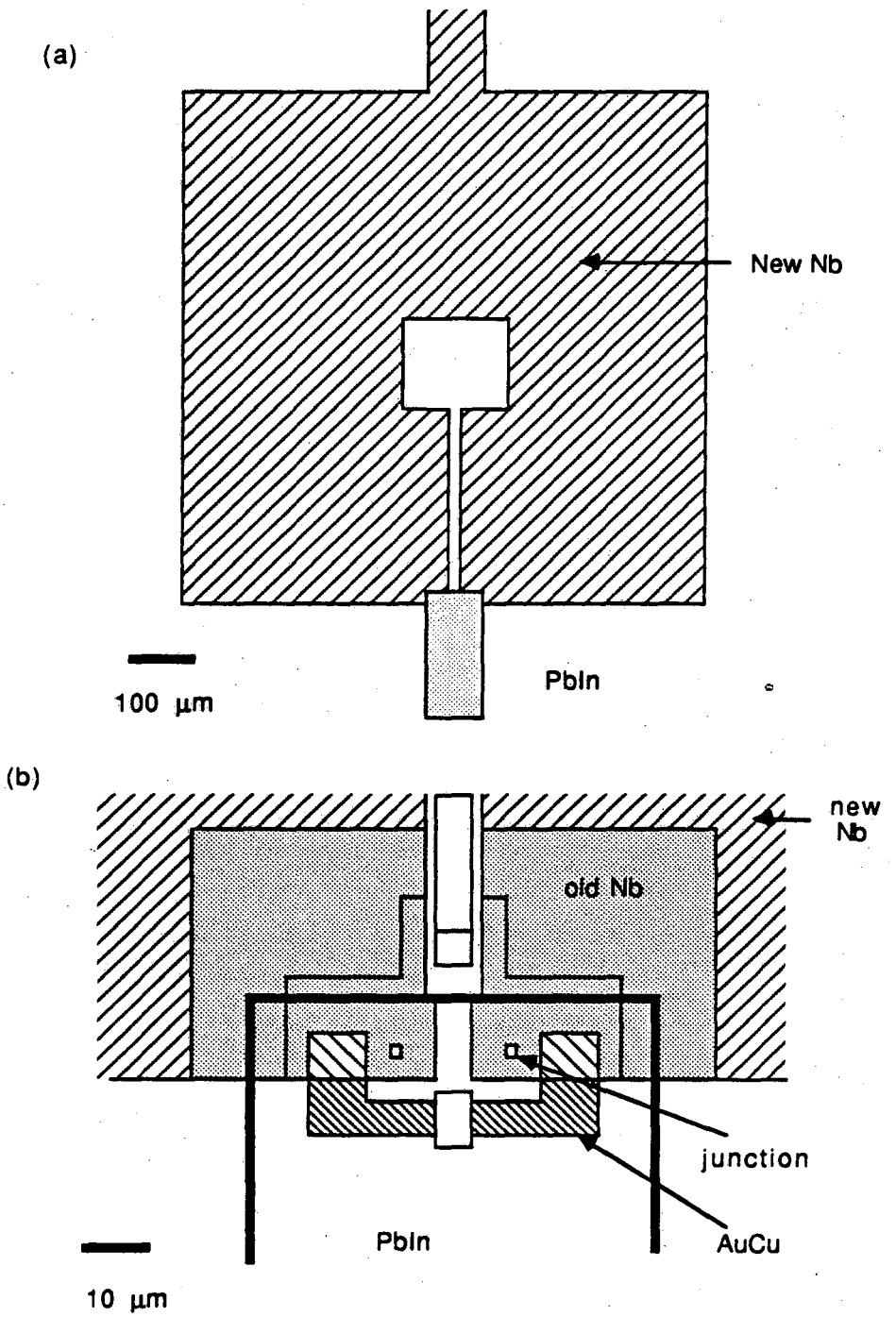

Fig. 7.4 Configuration of modified Type A SQUIDs A6, A7, and A8

for the lower level of excess noise at $3\Phi_0/4$. This is the pattern one would expect to see if one of the junctions is noisier than the other (see Chapter 5), and is strong evidence that the Lorentzian is being

Table 7.1 Excess noise at 1Hz and 4.2K, in three new Nb type A SQUIDs. $S_I^{1/2}$ is the excess output current noise at 1Hz for the data (exp) and theory (thr) in units of $pAHz^{-1/2}$, and $S_\Phi^{1/2}$ is the excess equivalent flux noise at 1Hz in units of $\mu\Phi_0 Hz^{-1/2}$.

SQUID	β	α	i	v	R/R_D	$\partial i/\partial\alpha$	$\partial i/\partial\beta$	Φ	$S_\Phi^{1/2}$	$S_I^{1/2}$ exp	$S_I^{1/2}$ thr
A6	0.31	-0.18	2.42	0.34	1.4	0	0	0	--	24	10
			1.68	0.38	1.45	0.63	0.23	0.25	7.2	16	6.6
			1.8	0.38	1.45	-0.51	0.23	0.75	5.7	22	6.9
			1.16	0.4	2	0	1.3	0.5	--	6.5	3.9
A7	3.66	-0.25	2.03	0.07	0.68	0	0	0	--	95.	120.
			1.9	0.07	0.92	1.5	0.02	0.29	9.6	66.	148.
			1.9	0.07	0.92	-1.6	0.02	0.72	22.	160.	150.
			1.72	0.07	1.55	0	0.1	0.5	--	88.	120.
A8	0.80	0.11	2.24	0.27	0.97	0	0	0	--	48.	27.
			1.55	0.28	1.46	-1.2	0.2	0.25	14.6	66.	26.
			1.65	0.28	1.46	0.97	0.2	0.75	7.33	37.	23.
			2.12	0.59	1.62	0.97	0.2	0.75	7.7	31.	22.
			1.34	0.29	2	0	0.63	0.75	--	39.	17.

produced by critical current fluctuations in just one of the junctions.

From this data, one can place a limit on the amount of excess flux noise that may still be present in the SQUIDs. The most favorable case is A6, for which one finds that the residual 1/f flux noise can be no more than 5 $\mu\Phi_0 Hz^{-1/2}$. This is nearly an order of magnitude lower in the power than SQUIDs made with the old Nb.

It is natural to wonder what in the sputtering is responsible for producing the excess noise and what is the key difference between the two systems. I have not done a systematic study of this, and so I do not know the answer. There seem to be two distinct possibilities. First of all, the two sputtering systems may be generating different purity Nb films, and this somehow affects the source of the 1/f noise. However, the residual resistivity ratios were about the same for the two systems: R(300K)/R(10K) $\approx$ 4 to 5, so it would have to be a secondary contaminant. Secondly, the microcrystalline structure of the Nb films may be different because of the different sputtering conditions. In particular, I operated Savo's sputtering system at the relatively low pressure of 1 μm, while the old system operated at about 7 μm. It is interesting to note that the microcrystalline structure of many sputtered thin-films is a sensitive function of the pressure in this range, the substrate temperature, and of the details of the sputtering configuration.[19] Different micro- rystalline structure could affect the 1/f noise if it is being produced by the motion of flux vortices in the film, for this would lead to different flux pinning properties.

7.6 Conclusions

In conclusion, the high temperature flux noise, which has been seen in the Berkeley SQUIDs for many years, is directly associated with the sputtered Nb body. SQUIDs constructed from a second Nb sputter system show less 1/f noise. SQUIDs constructed with Pb or PbIn bodies do not show detectable levels of 1/f flux noise, and are dominated by critical current noise in the junctions. Despite knowing the source's location and noise spectra, the exact microphysical mechanism which produces this noise is still not understood.

As a final remark, I note that it is generally possible to minimize the effects of critical current noise. First of all, the electronic modulation technique of Koch et al.[8] largely eliminates this noise. Unfortunately, the scheme is a considerable complication. For very low frequency applications, however, this is undoubtedly the best approach. Secondly, by a proper choice of SQUID parameters, one can minimize the equivalent flux noise produced by critical current noise. It is easy to see from Eq. 5.21 that a large β SQUID will show more equivalent flux noise than a small β SQUID. Thus it is desirable to make β small for low 1/f noise. In the limit β --> 0 the equivalent flux noise produced by critical current noise approaches a limit. In this limit, one finds for $\alpha = 0$, $\eta = 0$, $v = 0$, and $\Phi = \Phi_0/4$:

$$i = 1.414, \quad \partial I/\partial \Phi = 2\pi I_0(.707)/\Phi_0, \quad \beta \cdot \partial i/\partial \beta = 0, \quad \partial i/\partial \alpha = 0$$

The noise at the SQUID output is then, assuming equally noisy junctions:

$$S_I = S_{Io1} i^2/2 = S_{Io1}$$

I can now substitute $S_{Io1} = aI_o^2/A$, where A is the area of the junction, and $a \approx 20$ pA μm μA^{-1} $Hz^{-1/2}$ @ 1Hz is the typical 1/f noise in our

junctions. If the noise is reexpressed as an equivalent flux noise in the SQUID, one finds:

$$S_\Phi = S_I/(\partial I/\partial \Phi)^2 = a\Phi_o^2/(A2\pi^2) \qquad (7.13)$$

For a 4 μm^2 Nb-NbOx-PbIn junction at 4.2 K one finds that this small β limit corresponds to: $S_\Phi \propto 2.2\ \mu\Phi_o Hz^{-1/2}$. Finally, from this formula it is clear that one can also decrease the effect of the critical current noise by going to larger area junctions. It should be noted that one generally attempts to make A is small as possible to decrease the junction capacitance, and thereby improve the SQUID sensitivity. Because of the critical current noise's inverse dependence upon the junction area A, however, we can see that it is undesirable to go to small area junctions for low frequency applications. Of course, if the junction is made so small that it contains no trapped charge sites, then it will be quiet.

References

(1) A brief account of some of this work appeared in: F.C. Wellstood, C. Urbina, J. Clarke, " Excess noise in the dc SQUID from 4.2 K to 20 mK", IEEE Trans. Magn. Mag-23, 1662 (1987).

(2) One application where low frequency senssitivity is required are experiments on the non-invasive detection of neuromagnetic acitivity in the human brain. For a large collection of work on biophysical measurements using SQUIDs, the interested reader can consult: "Biomagnetism", Proc. of the third Int. Workshop on Biomagnetism, West Berlin, 1980, eds. S.N. Erne, H.D. Hahlbohm, H. Lubbig, W De Gruyter,

New York (1981).

(3) Perhaps the most demanding low frequency applications of the SQUID are in the relativity gyroscope experiments, and in proposed superconducting gyroscope navigation systems; See for example: H.A. Chan, H.J. Paik, M.V. Moody, J.W. Parke, "Superconducting Techniques for Gravity Survey and Inertial Navigation", IEEE Trans. Magn., MAG-21, 411 (1985).

(4) M.B. Ketchen, W.M. Goubau, J. Clarke, G.B. Donaldson, "Superconducting Thin-Film Gradiometer", J. Appl. Phys. 49, 4111 (1978).

(5) John Clarke, W.M. Goubau, and M.B. Ketchen "Tunnel Junction dc SQUID: Fabrication and Performance", J. Low Temp. Phys. 25, 99 (1976).

(6) J.M. Martinis and J. Clarke, "Current Noise Measured in the dc SQUID", J. Low Temp. Phys. 65, 459 (1986).

(7) R.F. Voss and J. Clarke, Phys. Rev. B13, 556 (1974).

(8) "Flicker (1/f) Noise in Tunnel Junction dc SQUIDs", R.H. Koch, J. Clarke, W.M. Goubau, J.M. Martinis, C.M. Pegrum, and D.J. Van Harlingen, JLTP, vol. 51, nos.1/2, 207, (1983).

(9) C.D. Tesche, K.H. Brown, A.C. Callegari, M.M. Chen, J.H. Greiner, H.C. Jones, M.B. Ketchen, K.K. Kim, A.W. Kleinsasser, H.A. Notarys, G. Proto, R.H. Wang, and T. Yogi, "Well-coupled dc SQUID with Extremely Low 1/f Noise", Proc. LT-17, 263-264, V. Eckern, A. Schmid, W. Weber, H. Wuhl, Eds., Elsevier Science Publishers, Amsterdam, 1984.

(10) V. Foglietti, W.J. Gallagher, M.B. Ketchen, A.W. Kleinsasser, R.H. Koch, F.I. Raider, and R.L. Sandstroms, "Low Frequency Noise in Low 1/f Noise dc SQUIDs", unpublished.

(11) See chapter 6 ref. 3-5.

(12) M. Celasco, A. Masoreo, P. Mazzetti, A. Stepanescu, "Electrical

conduction and current noise mechanisms in discontinous metal films. I. Theoretical.", Phys. Rev. B, Vol 17, no. 6, pp 2553, (1978).

(13) M.J. Ferrari, M. Johnson, F.C. Wellstood, J. Clarke, P.A. Rosenthal, R.H. Hammond, M.R. Beasley "Magnetic Flux Noise In Thin-Film Rings of $YBa_2Cu_3O_{7-\delta}$", Appl. Phys. Lett. (1988), to be published.

(14) J.M. Martinis and J. Clarke, "Signal and Noise Theory for a dc SQUID Amplifier", J. Low Temp. Phys. 61, 230 (1985).

(15) C. Hilbert and J. Clarke, "Measurements of the Dynamic Input Impedance of a dc SQUID",J. Low temp. Phys. 61, 237 (1985).

(16) J.M. Martinis, Private Communication.

(17) Prof. Clarke had made me aware of this fact early on, and as a result I repeatedly wondered about the case of the Pb SQUIDs and 1/f noise, and for a long time had in the back of my mind taking a second look at the noise.

(18) D.J. Van Harlingen, R.H. Koch, and J. Clarke, "Superconducting Quantum Interference Device with a very Low Magnetic Flux Noise", Appl. Phys. Lett. 41, 197 (1982).

(19) J. A. Thorton, "Influence of Substrate Temperature and Deposition Rate on Structure of Thick Cu Coatings", J. Vac. Sci. Techn. 12, 830 (1975); and D.W. Hoffman and J. A. Thorton, "Internal Stresses in Cr, Mo, Ta, and Pt Films Deposited by Sputtering From a Planar Magnetron Suorce", J. Vac. Sci. Techn. 20, 355 (1982).

Chapter 8: Low Temperature Excess Noise in the dc SQUID (1),(2)

8.1 Introduction

In certain applications one requires amplifiers with very low noise at low frequencies. An outstanding example is the cryogenic Weber bar antenna[3] for detecting gravity waves, for which one would like to have quantum limited behavior at 1 kHz. These requirements have prompted us to study the effects of reducing the temperature of the SQUID as a means of improving its sensitivity. Unfortunately, when the SQUIDs are cooled below 1 K, we often find a large increase in the amount of excess noise. The properties of this noise, which I will call the low temperature excess noise, and the investigation of its cause is the subject of this chapter. This noise remains as the most important source of noise in our SQUIDs at temperatures below 100 mK and frequencies below 3 kHz. As such, an understanding of its cause is of importance for future gravity wave detectors. I have accordingly gone into considerable detail about possible sources which I have investigated so far.

Using the thin-film technology described in Chapter 1, I have fabricated a variety of planar dc SQUIDs configurations, and tested 22 individual SQUIDs on the refrigerator. The junctions were nominally 2x2 μm^2 Nb-NbOx-PbIn or Nb-NbOx-Pb tunnel junctions, with sizes ranging from 1X1 to 2X3. The resistive shunts were 30-35 nm thick AuCu films. This alloy was chosen because it remains normal down to at least 18 mK, because it does not oxidize under atmospheric conditions, and because of our previous experience in the ^{4}He temperature range. We measured the characteristics and noise of each SQUID(1) using a second dc SQUID(2) in

a flux-locked loop as shown in Fig. 2.8, and as was described in detail in Chapter 2.

As an example, Fig. 8.1 shows the flux noise spectrum in SQUID F1 at 140 mK with $\Phi \simeq \Phi_0/4$. Along the x-axis I have plotted the frequency in Hz, and along the y-axis I have plotted the root mean square of the equivalent flux noise spectral density in SQUID(1). The spectrum is smooth except for a few sharp lines. These lines are not of interest; those at multiples of 60 Hz are due to powerline interference, while the band near 2500 Hz appears to be due to vibrations. Accordingly, I will exclude these sharp lines from further consideration. On the otherhand, the smooth background is not so easily understood. The spectrum is manifestly non-white; at low frequencies there is much more noise than at high frequencies. At frequencies f>10 kHz the spectrum begins to flatten and eventually begins to increase again. This increase in the noise at high frequencies is spurious and is due to a rapid increase in the noise and closed loop gain of the SQUID(2) measuring system as the |G|=1 freqency is approached (see Chapter 3). As a result, I will generally exclude frequencies above 10 kHz from further consideration.

The remaining smooth noise power spectrum can be fit to a function of the form:

$$S_\Phi(f) = (a_0^2 + b_0^2/f^\alpha)$$

where f is the frequency, and a_0, b_0 and α are determined by the fit. This functional form represents the uncorrelated sum of white noise and an excess $1/f^\alpha$ type noise power spectrum. For the data of Fig. 8.1, a fit for frequencies between 10 Hz and 10kHz yields: $a_0 = 0.55\ \mu\Phi_0 Hz^{-1/2}$, $b_0 = 7.4\mu\Phi_0 Hz^{-1/2} Hz^{\alpha/2}$, and $\alpha = 0.65$.

The important point about this plot is that there is excess $1/f^\alpha$

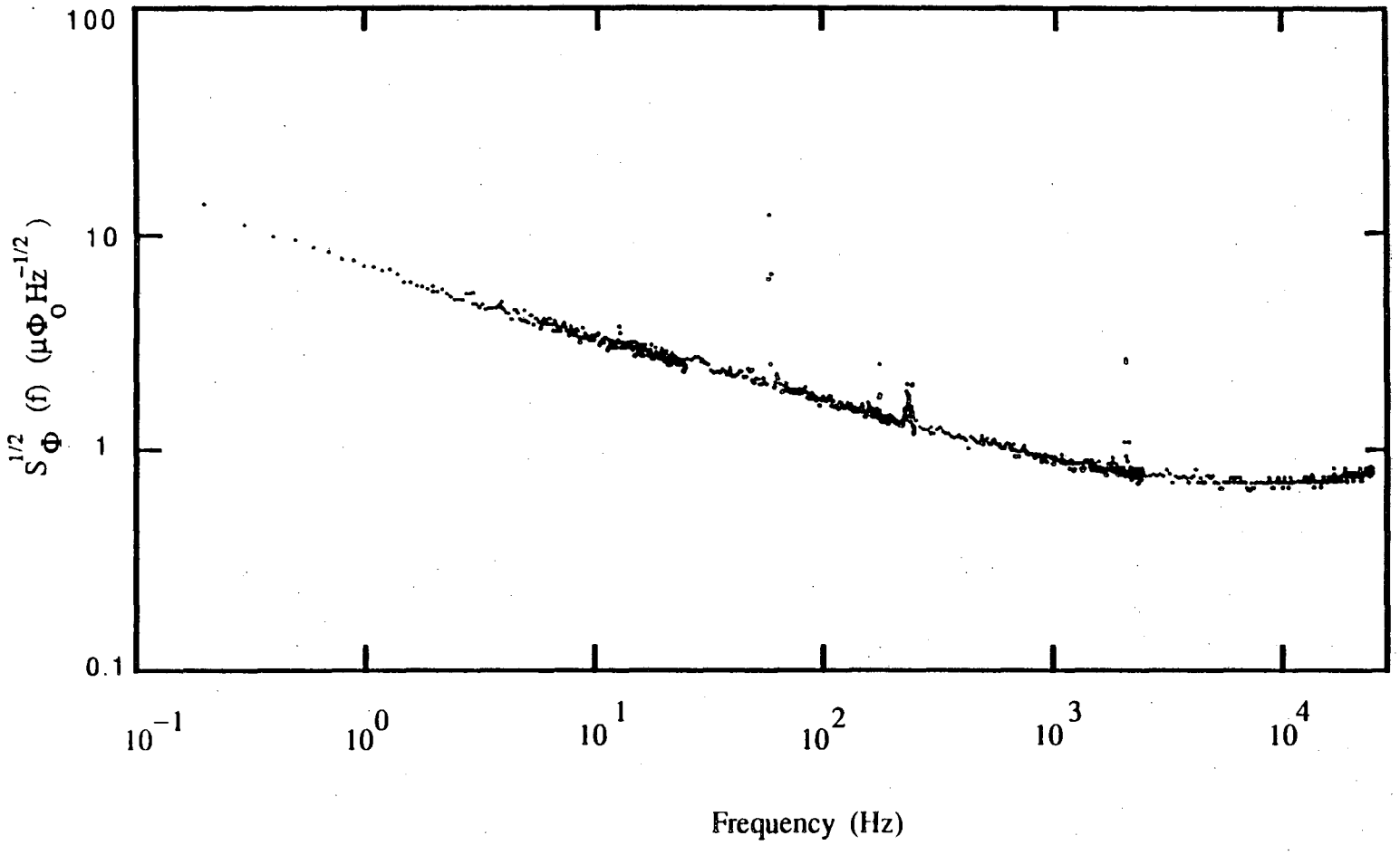

Fig. 8.1 Equivalent Flux noise spectrum from SQUID F1 (2-27-86): at T =140 mK, V = 2 μV, Φ= 0.25.

noise and it is large compared to the white noise even at a frequency of 1 kHz. I will call this noise the "low temperature excess noise". This plot is very typical, plots for all of the other SQUIDs would show only qualitatively small differences in slope and magnitude of the excess noise. Figs. 8.2 through 8.5, show additional flux noise spectra from 4 other SQUIDs, with the temperatures and the operating points listed in the figure captions. Table 8.1 lists the parameters of the fit for these five SQUID. The excess noise in each case scales as $1/f^{\alpha}$, and at 1 kHz it exceeds the white noise level.

It should be emphasized to begin with that we do not have any theoretical model which describes where this low temperature excess noise is coming from. Our experimental efforts have accordingly been directed along three distinct paths. Firstly, we would like to learn the properties of the noise, for example, how it depends upon temperature.

Table 8.1. Low temperature noise parameters in five SQUIDs which were biased near $\Phi=\Phi_0/4$.

SQUID	T (mK)	a_0 $\mu\Phi_0 Hz^{-1/2}$	b_0 $\mu\Phi_0 Hz^{-1/2+\alpha/2}$	α
F1	140	0.55	7.4	0.65
E2	130	0.37	5.7	0.58
K1	35	0.67	11.0	0.78
M1	23	0.52	17.5	0.95
M2	25	0.44	14.9	0.94

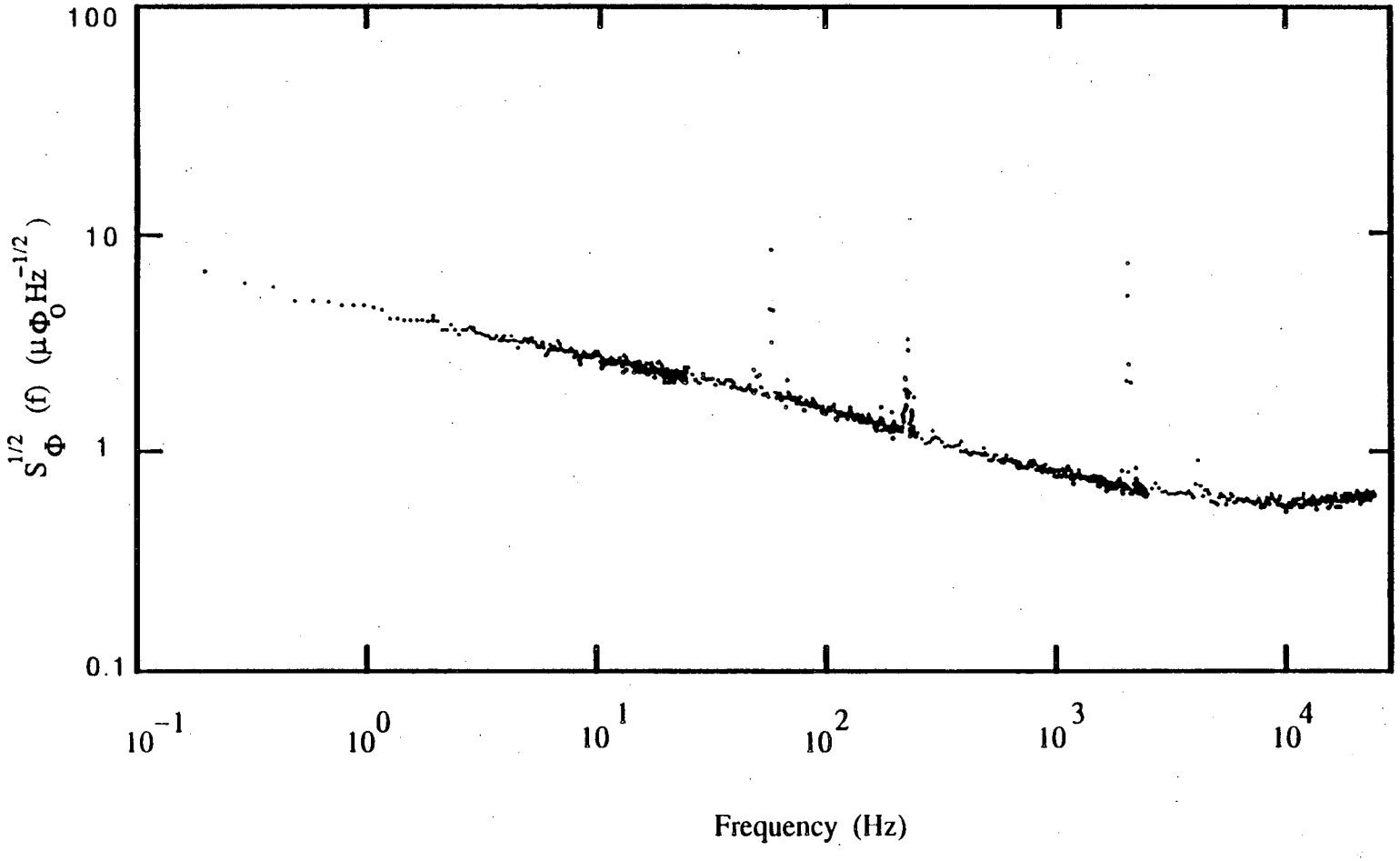

Fig. 8.2 Equivalent Flux noise spectrum from SQUID E2 (5-18-86): at T =130 mK, V = 10 μV, Φ= 0.25.

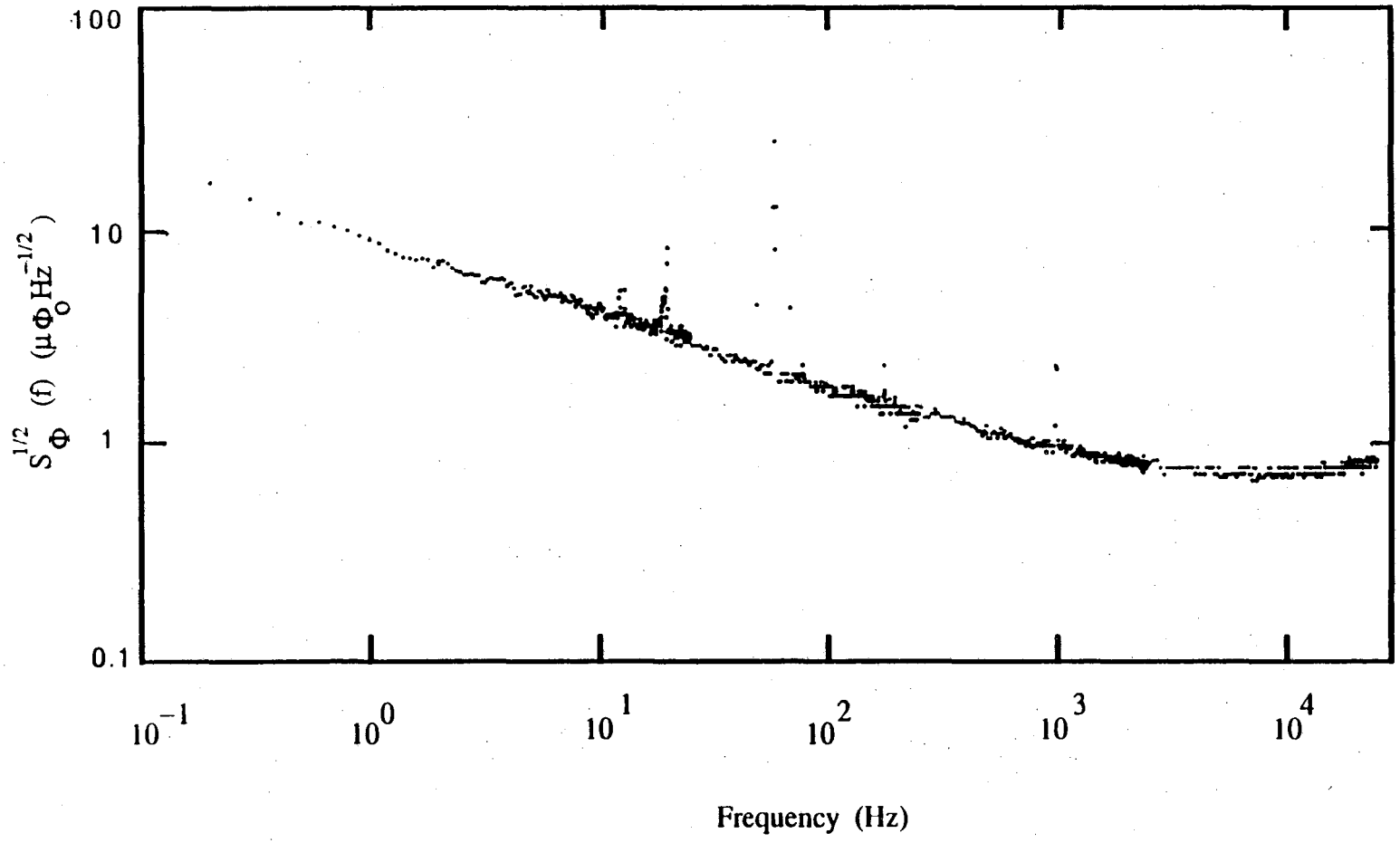

Fig. 8.3 Equivalent Flux noise spectrum from SQUID K1 (8-14-86): at T = 35 mK, V = 0.9 μV, $\Phi = 0.25$.

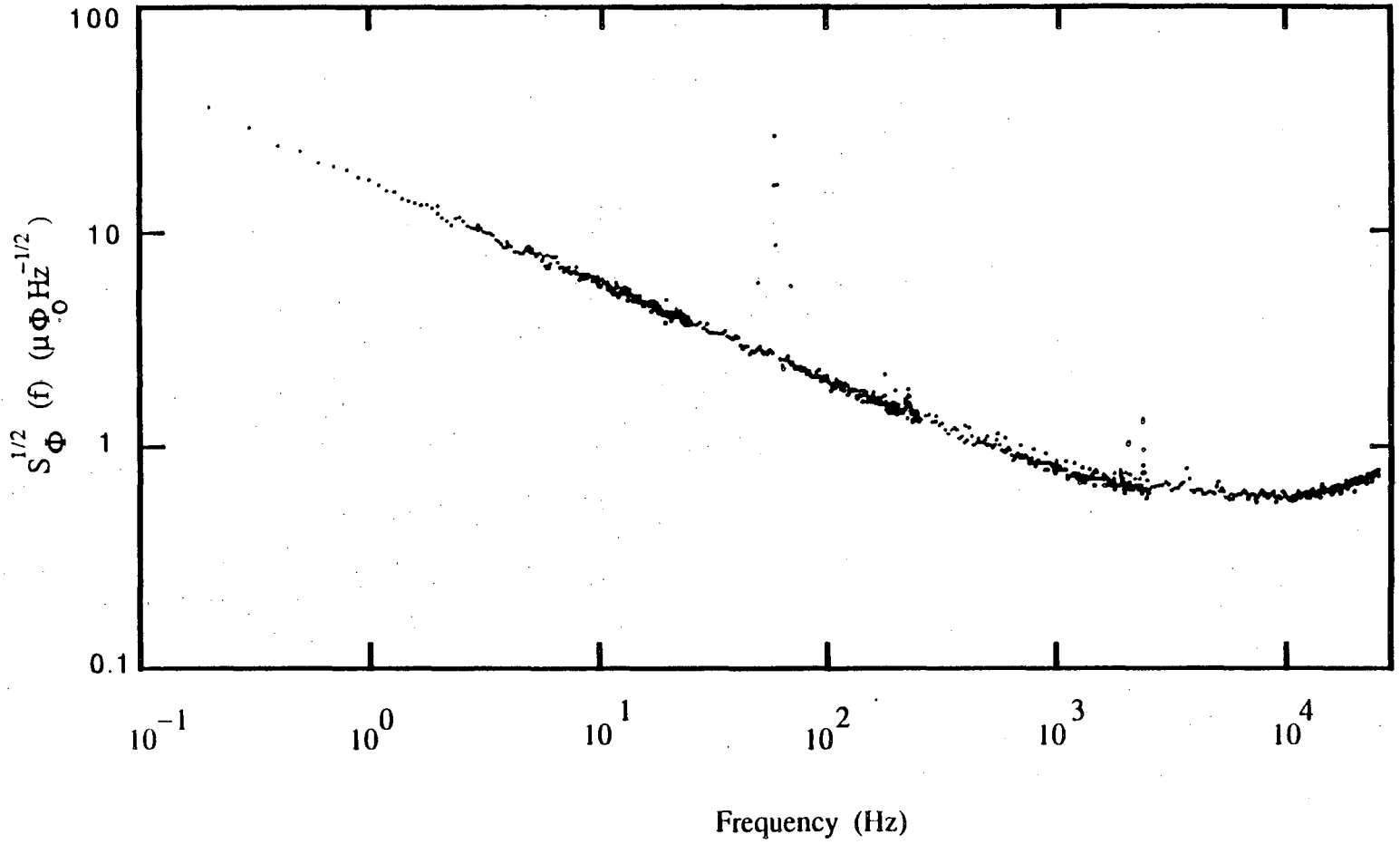

Fig. 8.4 Equivalent Flux noise spectrum from SQUID M1 (11-3-87): at T = 23 mK, V = 0.9 μV, Φ = 0.25.

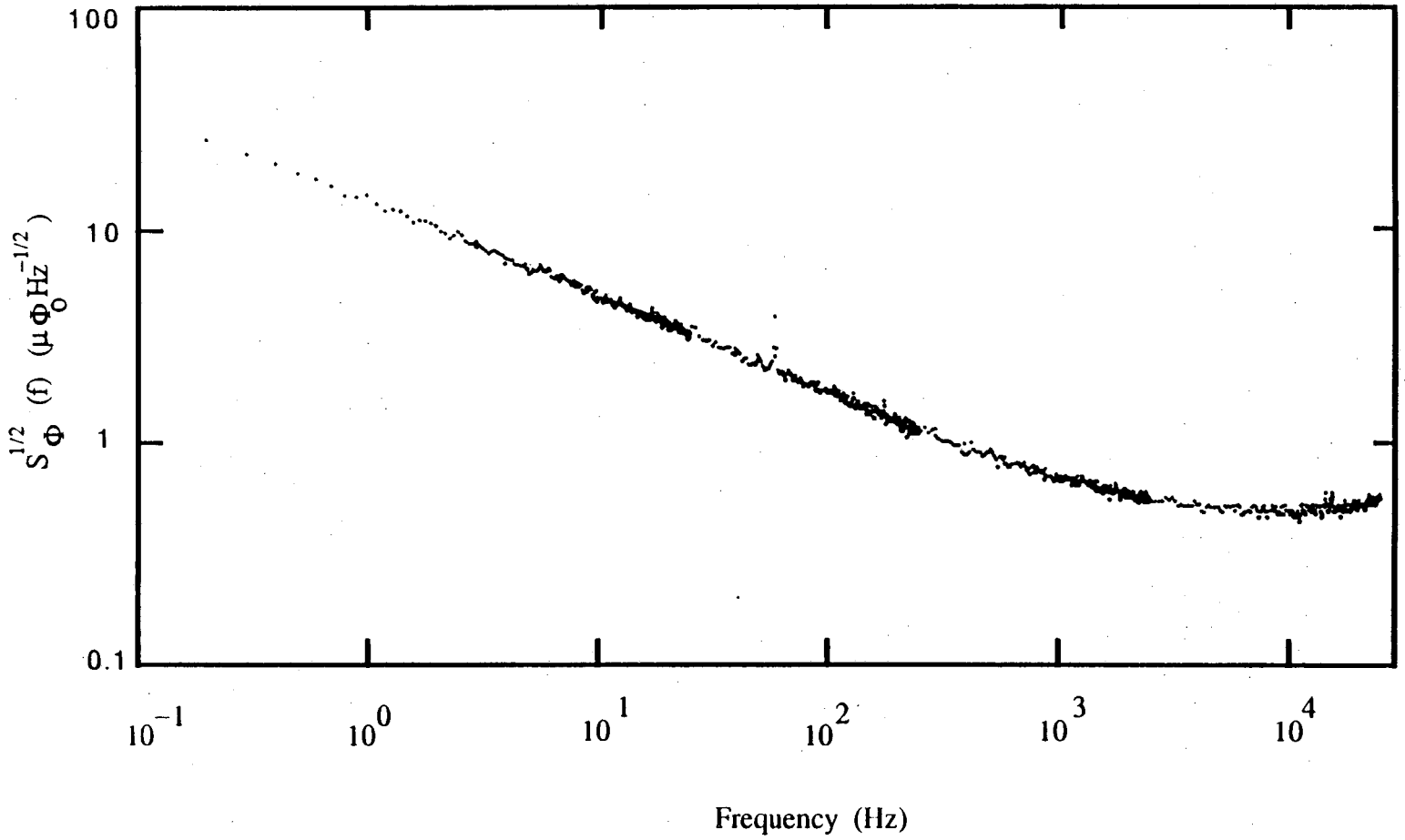

Fig. 8.5 Equivalent Flux noise spectrum from SQUID M2 (5-8-88): at T = 25 mK, V = 2 μV, Φ= 0.25.

We would also like to know whether the noise depends upon any particular SQUID parameter, such as the SQUID inductance, or bias. The point is that not all noise sources produce the same output noise as the SQUID parameters are varied. In this investigation, I will make heavy use of the results of Chapter 5 concerning parameter fluctuations. Secondly, we would like to know how common the noise is; in particular, does it occur in all of our SQUIDs and does it occur in SQUIDs built elsewhere? This is important becuse it does not require any understanding and does not depend upon any model. One simply tests someone else's SQUID and sees if it is any better. This step also serves as a strong test on our fabrication procedure, and gives us an indication of how general the phenomena is. Finally, we would like to be able to find the source of the noise and eliminate it. At the least, we would like to eliminate the possibility that the noise is being caused by particular sources. There are a host of general questions we would like to answer if the source cannot be pinned down exactly. For example: we would like to know whether the source is something which is intrinsic or extrinsic to the SQUID; is it a real physical source or does it arise from the equations of motion of the SQUID? If the source is a physical one, is it in the body of the SQUID or somewhere off the chip?

A point of continuing frustration is that there is no way to know if the noise is being produced by one or more mechanisms. However I can argue that there is probably just one mechanism which is producing this low temperature excess noise. First of all, all known 1/f noise in SQUIDs at higher temperature seems to be adequately described by just two distinct 1/f sources (critical current noise and high temperature flux noise),[4] one of which usually greatly dominates the other in any

particular device. It seems quite remarkable in fact that one should ever see two independent sources which produce 1/f noise of comparable magnitude. For if there is no physical law connecting the two, it is just a matter of blind chance that the effects would be comparable. At low temperatures it would be even more surprising because each of the sources would have to satisfy additional constraints, the peculiarity of which will become evident below, and in addition none of these sources would reveal themselves at higher temperatures. This seems a priori very unlikely. In fact, as will be seen, the properties of the low temperature excess noise are so puzzling that it scarcely seems possible to construct a single physical system which could produce this kind of noise, let alone two distinct systems. The possible fallacy here is that the observed complexity may arise from the sum of two processes.

In summary, we want to know what the low temperature excess noise depends upon and what it is caused by. Even if we cannot eliminate the source, perhaps we can minimize its effect. Whether or not such a program can be completed in a reasonable amount of time, it is the only way to proceed. The experimental tests have generally progressed from the easiest tests to the hardest, and from the sources I would most suspect to those I would least suspect. Such suspicions are poorly founded in fact, and one accordingly cannot expect much initial chance of success.

It should be emphasized that the main strategy for finding the source of the excess noise was to vary as many of the SQUID parameters as possible over as large a range as was possible. The hope was that one of the variations would produce a corresponding variation in the excess noise. As a result, not all of the properties of the excess noise have

been systematically investigated, rather, I have made use of the large base of existing data to draw conclusions.

I begin now with a discussion of the observed properties of the low temperature excess noise. I then discuss the investigation of specific hypothetical noise sources, and end with suggestions for future work.

8.2 Properties of the Low Temperature Excess Noise

8.2a Flux Noise

One very important property of the low temperature excess noise is its dependence on Φ. I observe that the output excess noise from the SQUID scales directly with the flux gain or flux to current transfer function $\partial I/\partial \Phi$. I will make extensive use of this behavior, for it puts strong constraints on the possible sources of the noise and eliminates many of them.

Figure 8.6a shows an example of the output current excess noise at 1 Hz, $S_I^{1/2}(1\ Hz)$, versus $|\partial I/\partial \Phi|$. When $|\partial I/\partial \Phi| = 0$, the noise does not go to zero, but to a value which is small compared to that found when the flux gain is large. This residual level of excess noise at zero flux gain is merely the critical current noise remaining in the device at low temperatures. As $|\partial I/\partial \Phi|$ increases from zero, the excess noise increases, eventually becoming linear in $|\partial I/\partial \Phi|$. This indicates the presence of a flux-like noise term. In Fig. 8.6b, I have plotted this same data as S_I vs the square of the flux gain. The solid line is a straight line fit to the data and corresponds to:

$$S_I = a_1 + b_1 \cdot (\partial I/\partial \Phi)^2 \qquad (8.1)$$

(a)

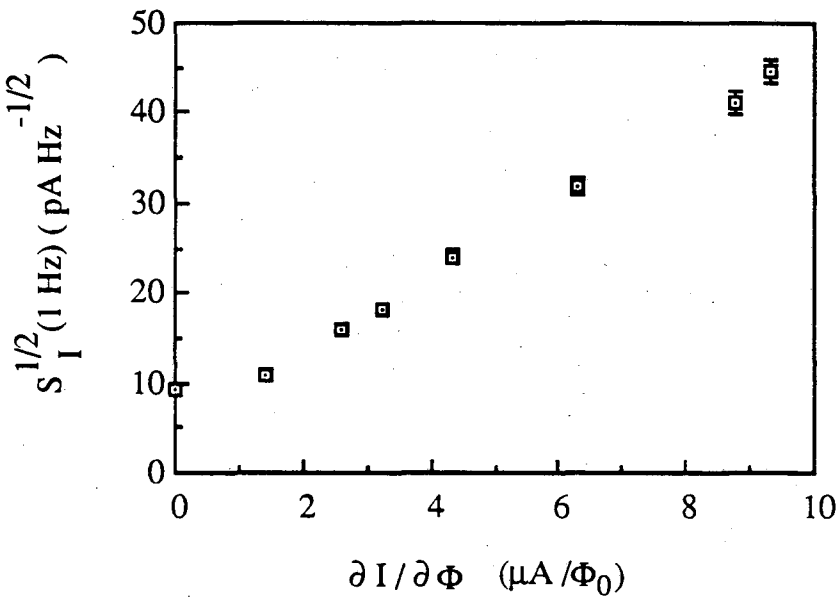

(b)

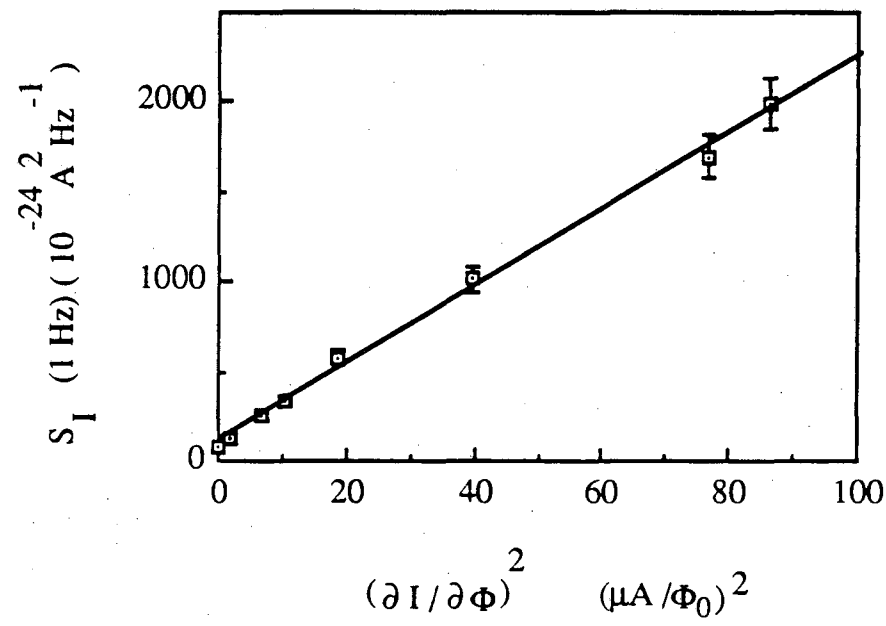

Fig .8.6 (a) Output rms excess current noise at 1 Hz vs. flux gain for SQUID E2 at 110 mK. (b) Output excess noise power at 1 Hz vs. square of flux gain. Solid line is linear plus constant fit.

where: a_1 is the output current noise when the gain is zero, and $b_1 = S_\Phi$ is a constant level of flux noise. The good fit to this functional form shows that the excess noise is behaving as the *uncorrelated* sum of two noise sources, a constant flux-like term, b_1, and a critical current term, a_1. From the results of Chapters 5 and 7, we know that the critical current term a_1 should only be appoximately constant. It is a fair approximation here because this term is important only near Φ_0 and $\Phi_0/2$, where the flux gain vanishes. Elsewhere, the b_1 term greatly dominates, and it makes little difference whether a_1 varies slightly.

Cruder measurements on our other SQUIDs reveal exactly the same behavior; there is a constant term b_1 which produces an output current noise directly proportional to the flux gain. As is discussed below, the magnitude of b_1 does depend upon the temperature and the SQUID type.

The most natural explanation for this behavior is that there is a fluctuating magnetic flux in the SQUID loop. That is, there appears to be a physical source of flux noise in the SQUID. However, these observations do not prove this conclusively. There are other SQUID parameters which can produce flux-like noise, and we will have to study each in turn. In fact, I have no direct proof that the magnetic flux is actually fluctuating in the SQUID. Such a measurement would require a separate flux sensor, and we have not made such a measurement as the signal would be very small and at least require a second SQUID measuring system. I discuss a second possible approach to this problem in section 8.5.

8.2b Operating Point Independence

The second major property of the low temperature excess noise is its lack of dependence on the operating point of the SQUID; this is an extension of the results of the previous section. *This independence is seen only if the excess noise is expressed as an equivalent flux noise.* That is, if we extract the flux term $b_1 = S_\Phi$ from Eq. 8.1, then it is a constant not only for all bias flux, but also for all bias voltages. The operating point independence can be easily seen from casual observation of the noise spectra as the SQUID bias voltage is changed, or from the noise vs voltage plots, if the noise is measured at a low frequency where the excess noise dominates (in pracice 1 kHz is generally adequate). This behavior is most clearly seen in detail by taking flux noise spectra at different voltages (see section 8.4e for two particular examples).

The level of the flux noise is also independent of the way in which the SQUID is biased. By removing SQUID(1), and leaving the input circuit for SQUID(2) disconected, it is possible to measure the excess noise in SQUID(2). As described in Chapter 3, in feedback operation, the flux in SQUID(2) is switched back and forth between positive and negative $\Phi_0/4$ at 500 kHz. In this situation, the symmetrical noise modes discussed in Chapter 5 do not contribute to the noise at the feedback output.[4] The observed level of the excess noise in SQUID(2) was within 10% of that found when the same SQUID was tested as SQUID(1).

This independence of operation makes a great deal of sense if there is actually a physical source independently producing flux noise in the SQUID.

8.2c Repeatability

The third major property of the low temperature excess noise is that it is very stable and reproducible, or repeatable. If one takes the same SQUID and measures its noise from one day to the next, or one week to the next, the level does not change measurably. This suggests that the noise is stationary, and in particular shows that there are apparently no thermal remnant magnetization effects.[5] If the SQUID is warmed up and left at room temperature (or more often in a refrigerator freezer to prevent decay of the junctions) for weeks or months the noise is also unaffected. This behavior suggests that once the SQUID is built, the source is fixed, and is relatively immune to the environment.

This repeatability exists not only for the noise level in a particular device, but also between devices of the same type. It does not matter whether the devices are made on the same or different wafers, or whether their critical currents differ. So long as they are of the same type, their noise will have about the same level (I mean here of course only when it is expressed as a flux noise). Also, if one takes a chip from an old wafer which was made many years ago and completes the junctions the noise level is comparable to that from a similar device made within a few days.

There is also an approximate noise invariance even between different types of devices. Fig. 8.7 shows $S_\Phi^{1/2}(1Hz)$, the rms excess equivalent flux noise at 1 Hz, for 11 SQUIDs. In this figure, I have not tried to fit the spectra to a function of the form (white + $1/f^\alpha$), but rather, I have merely recorded the excess noise level at 1 Hz. Remarkably, the spread in $S_\Phi^{1/2}(1\ Hz)$ at low temperatures is only about

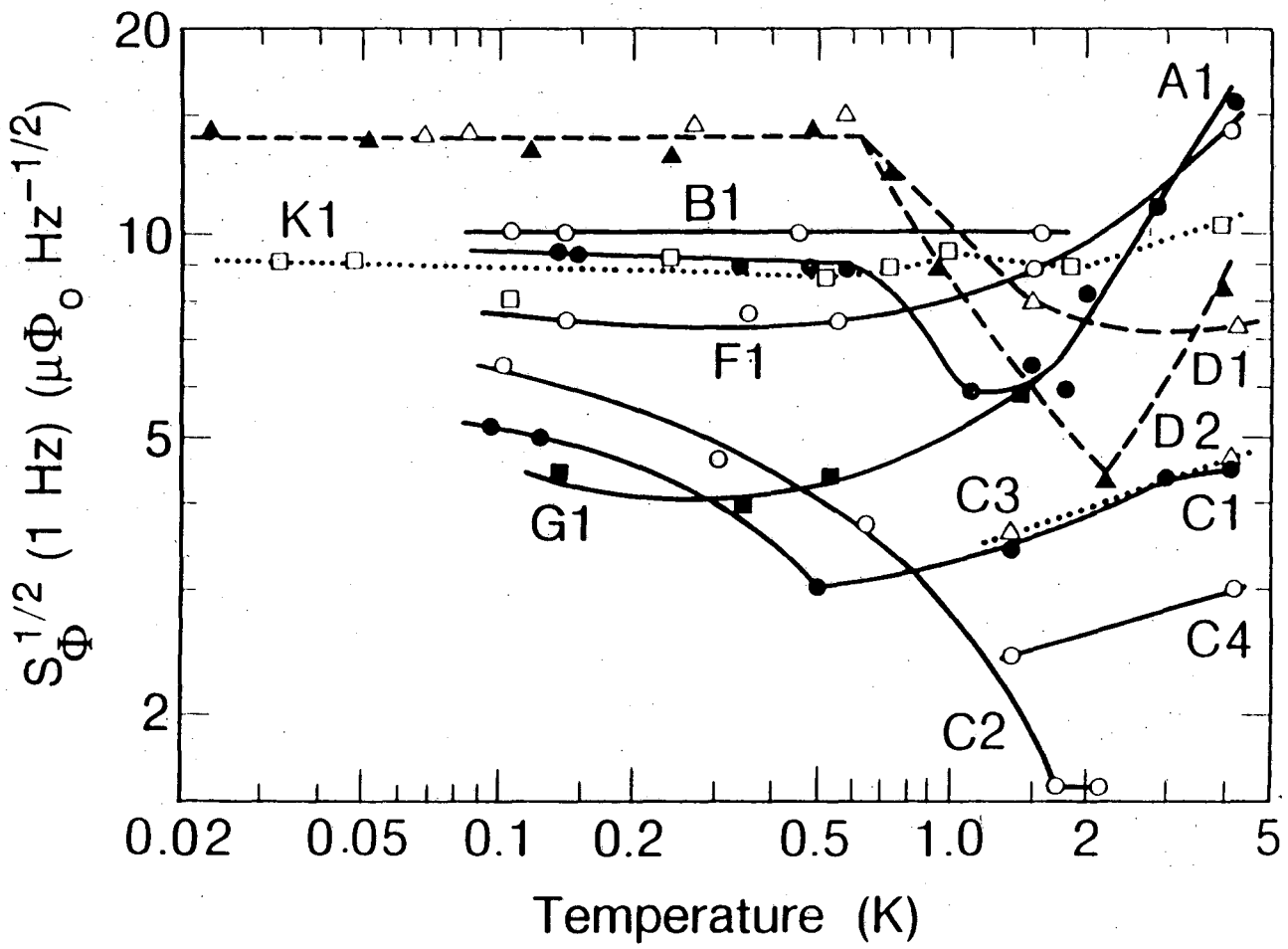

Fig. 8.7 Excess equivalent rms flux noise at 1 Hz vs. temperature for 11 SQUIDs. All devices are biased near 0.25 or 0.75 Φ_0.

a factor of 3 despite enormous differences in the size of the SQUIDs, the linewidth of the SQUID loop and composition (see Fig. 1.5 to 1.19). To first order then, the level of the noise does not depend upon the device type.

This brings up a very important point. A priori, there is no justification for presenting the noise as an equivalent flux noise. One could just as well have plotted the noise at the output of the SQUID, S_I or S_V. Such a replot of our data would be very scattered however, and would show no obvious relations from one device to the next. The fact that when the noise is expressed as an equivalent flux noise, it is almost independent of the SQUID, is evidence that the noise is being generated by a physical source of flux noise, and that this source is independent of the operation of the SQUID. Thus, the SQUID appears to behave as a passive sensor, merely detecting changes in the flux from an independent source.

This repeatability allows me to test for smaller differences between devices, as is discussed in the next two sections. In a certain sense though, the repeatabilty is unfortunate, because it is only from seeing a variation in the noise level that we will know we have altered the source of the noise. Also, if the noise varied greatly from one device to the next, we would at least have some hope of finding a quiet device by testing enough of them.

8.2d Geometry Dependence

The fourth major property of the excess noise is its dependence on the geometrical shape of the SQUID. As was noted above, to first order,

the excess noise does not depend on the device type. Since the shape or geometrical configuration of the SQUID is different for the different SQUID types, I can express this by saying that the observed level of the low temperature excess noise is independent of the SQUID geometry. This independence is, again, seen only if one plots the excess noise as an equivalent flux noise.

However, the geometry independence is only a rough approximation, for there is a weak dependence which remains, and this seems to be very reproducible. Different device types will behave similarly with respect to the level, slope and temperature dependence of the noise. These variations do not seem to be associated with any materials changes, for SQUIDs with the same shape but different material composition show about the same level of noise, as for example in the type A and A' devices. The variation in the noise between different SQUID types is generally much larger than the variations between devices of the same type. Thus in Fig. 8.7, the spread in rms noise at 1 Hz is only about a factor of $\pm$ 2. The variation between the excess noise in devices of the same type is generally no larger than about 20 % in either the slope or the magnitude at 1 Hz.

I now consider the noise behavior seen in different geometries.

Large SQUIDs (those which are more than about 400 μm in diameter) show a rapid increase in the magnitude of the excess noise as the temperature is decreased below 1 K. Often there is a small broad peak in the magnitude of the noise at around 0.5 K. At lower temperatures, the noise stays flat or increases slowly as the temperature is lowered to 20 mK, see Fig. 8.8a.

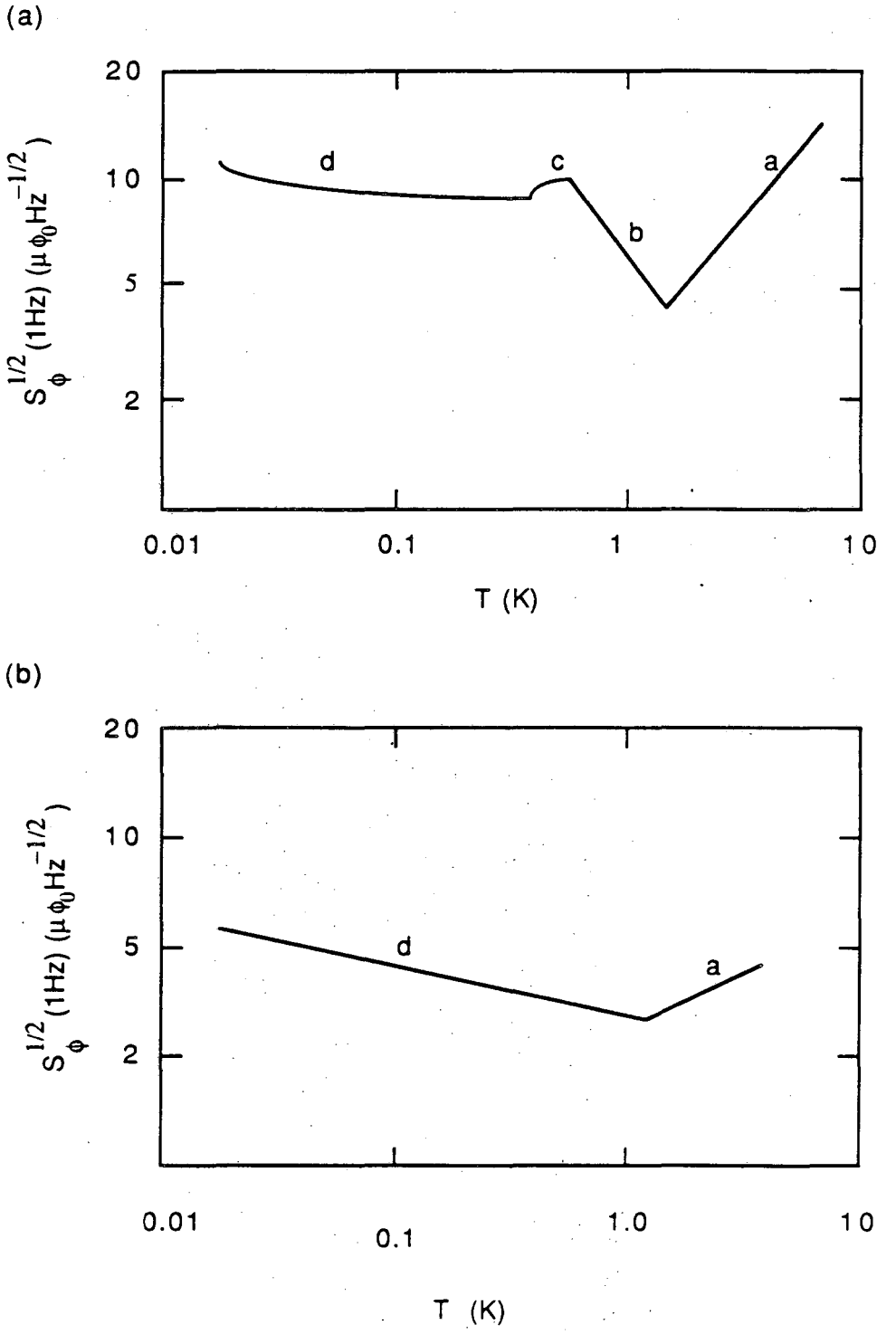

Fig. 8.8 (a) Behavior of flux noise in large SQUIDs, (b) small SQUIDs.

Small SQUIDs: (those which are less than about 400 μm in diameter) show a slow and steady rise in the noise as the temperature is lowered below about 0.5 K. There is no evidence of peaks or bumps (see Fig. 8.8b). Generally, the smaller the SQUID, the smaller is the excess flux noise, although the scaling is not linear and also depends on other factors. The smallest device tested was SQUID O1, which showed $1/f^{2/3}$ noise with a magnitude that scaled as approximately $1/T^{1/2}$ and attained 6.8 $\mu\Phi_0 Hz^{-1/2}$ at 1 Hz and 25 mK.

Large Split SQUIDs: (SQUIDs with half Nb and half PbIn loops of diameter 900 μm or greater) show noise which is roughly the same as that of the Large SQUIDs. However, the slope of the noise is generally close to 1, rather than close to 2/3. Because of their higher slope, these SQUIDs showed the lowest excess noise at frequencies above 1 kHz.

Small, Thick and Narrow Linewidth SQUIDs: As the linewidth of the body loop of a small SQUIDs is varied, the noise continues to behave like that of a small SQUID. However, the devices with narrow linewidths tend to display more noise than those with larger linewidths and the same body diameter. There does not appear to be any rigorous scaling with the linewidth or ratio of the linewidth to the diameter, however, as can be seen from Table 8.2.

The Multiloop SQUID P1: The SQUID P1 was configured as 10 small 50 μm diameter loops, connected closely in series (see Fig. 1.19). At low temperatures, the device showed excess noise with a slope (close to 2/3) and a temperature dependence (flux noise magnitude scaled as roughly $T^{-1/2}$) which were similar to those of SQUID G1, which was made with a single 50 μm loop (see Table 8.2). However, the magnitude of the noise was about 6 times larger in P1. This result suggests that, to first

order, the low temperature flux noise scales roughly as the number of loops in the SQUID, and that each loop contributes incoherently to the sum.

The geometry dependence is weak, but consistent. Small diameter devices have less noise than large devices. But there is no observed proportionality to the area. The linewidth also seems to enter, with narrower lines giving higher noise. This is suggestive of a local source, ie. a noise source composed of randomly placed incoherent flux sources on the loop itself or on the substrate. For such a source, it

Table 8.2. Linewidth dependence of the magnitude of the low temperature excess noise in 7 SQUIDs at temperatures near 140 mK. ℓ is the linewidth of the SQUID body, d is the outside diameter of the SQUID body, $S_\Phi^{1/2}(1Hz)$ is the magnitude of the excess flux noise at 1 Hz.

Device	ℓ (μm)	d (μm)	d/ℓ	$S_\Phi^{1/2}(1Hz)$ ($\mu\Phi_0 Hz^{-1/2}$)
O1	25	70	2.8	4.2
G1	10	70	7	4.5
B1	50	500	10	10.
E1	10	120	12	5.1
E2	10	120	12	4.8
F1	2	100	50	7.5
P1*	10	70	7	11.

(*)Device P1 was composed of 10 loops of the given diameter which were connected in series (see Fig. 1.19).

can be shown that the narrower linewidths should yield higher noise, and also that for a fixed ratio of linewidth to diameter, the expected noise is independent of the loop diameter.

8.2e Temperature Dependence

The fifth major property of the low temperature excess noise is its temperature dependence. The behavior of the magnitude of the excess noise at 1 Hz vs. temperature is shown in Fig. 8.7, and was discussed briefly above. Here I will emphasize how unusual this temperature dependence is.

Above 1 K, excess noise in the SQUID is produced by a combination of high temperature flux noise and critical current noise. As our SQUIDs are cooled below 1 K, the excess noise magnitude eventually begins to increase. The nature of this increase depends repeatably on the device type. Large devices tend to show noise which increases rapidly between 0.7 and 0.5 K, with a nearly temperature independent level below about 0.5 K. The large devices also tend to show a small broad peak in the noise at around 0.5 K. For example, in the case of SQUID A1, as one lowers the temperature below 4.2 K the excess noise drops rapidly, reaches a minimum at about 1 K and increases to a plateau below about 0.5 K (see Fig. 8.7). The small devices do not show any rapid rise in the noise, and they do not display any peaks in the noise magnitude. Rather, the small devices tend to gradually get noisier as the temperature is lowered. This temperature dependence may often be described adequately by a $T^{-1/2}$ or a $T^{-1/3}$ law, as for example in device C2 in Fig 8.7.

It is important to recognize further that the level of the noise is dependent upon the bath temperature of the SQUID, and not on the temperature of the SQUID shunts. In Chapter 9, 10, and 11, I will discuss the temperature of the electrons in the shunts, which is considerably hotter than the bath temperature in many of the devices. Typically, the SQUID shunts remain at about 140 mK, for most of our SQUIDs, as the bath temperature decreases below this. On the otherhand, one continues to see small changes in the magnitude and slope of the noise as the temperature of the bath is lowered from 140 mK to 20 mK. This strongly suggests that it is the bath temperature, or temperature of the SQUID body, which is controlling the low temperature excess noise, rather than the shunt temperature. This is interesting because it is the shunt temperature which sets the white noise level of the SQUID.

The temperature dependence is quite unusual for an excess noise source. Many noise sources are thermally driven and have linear equations of motion. As a result, the excess noise scales as T. It is possible to get a thermal 1/T dependence, but it requires that some part of the system response changes faster than 1/T so as to offset the decreasing thermal driving term. This dependence rules out many simple physical mechanisms, but would be considered normal, for example, for a magnetic system obeying a modified Curie-Weiss law.

8.2f Slope of the Noise

The sixth major property of the low temperature excess noise is that most of the power spectra have a very unusual slope. It should be noted that there are many theories of 1/f noise.[6] Some of these

attempt (and I might add unsuccessfully) to find general explanations for all 1/f noise. Other models are concerned only with very specific systems, as for example the trap model of 1/f noise in Josephson junctions. Most of these models will generate noise which is close to $1/f^1$. It is often difficult to get a model to yield noise which is $1/f^\alpha$ where α is as small as 0.67 over an appreciable frequency and temperature range (without making very ad hoc assumptions). The Dutta-Horn model is an example.[7] In this theory, thermal activation is assumed, and the frequency dependence of the slope is found to depend upon the temperature dependence of the magnitude of the noise. One finds that for a slope of 2/3, say at 1 Hz, and a temperature independent noise magnitude, the spectrum will only scale like $1/f^{2/3}$ over about two decades. On the otherhand, the observed noise frequently extends over four or more decades with only the slightest evidence of any curvature, see for example Fig. 8.1 to 8.5. The point is that the slope is quite low compared to what is commonly seen for low frequency noise in other systems. The relatively small slope thus stands as a difficult anomaly to explain with conventional 1/f noise theories.

It should be remarked, that most of the SQUIDs showed low temperature excess noise level which scaled as $1/f^{2/3}$. There was one geometry which showed an unusually high slope of 1 to 0.9. This was the large split configuration of the type D and M SQUIDs (see Fig. 8.9). The only difference between the two types is the shunt size (see Chapter 11).

This geometry dependence of the slope is one of the most puzzling aspects of the low temperature excess noise. One would really expect the magnitude of the noise to change from one body type to another. It is

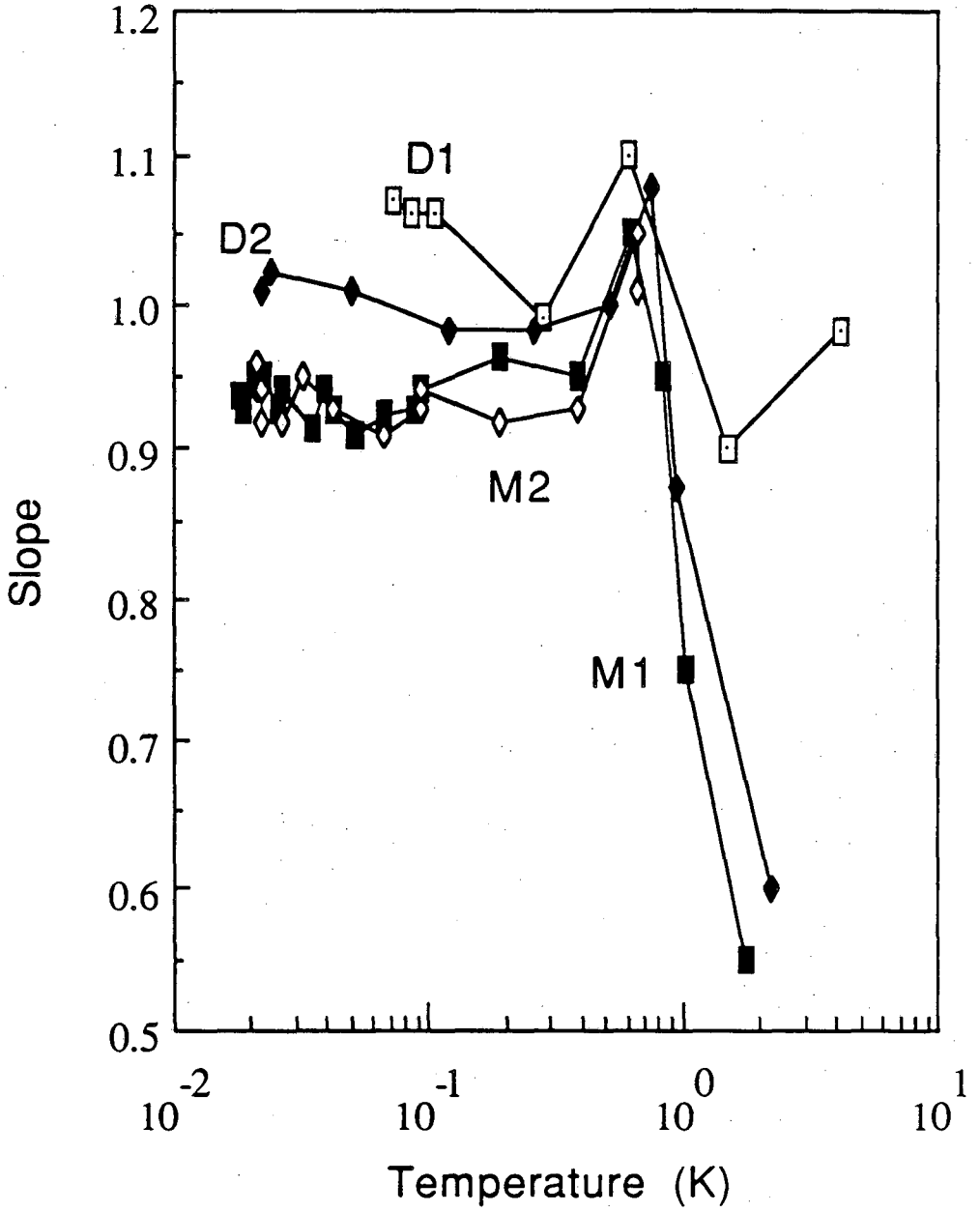

Fig. 8.9 Slope of excess noise in four SQUIDs which were baised near $\pm\Phi_0$ /4. Spectra were fit to white + $1/f^{\alpha}$, for 10Hz<f<10kHz.

very difficult to conceive of a mechanism which could change the slope of the noise and be associated with a global property such as the shape of the entire SQUID. The observed behavior tends to rule out shortrange effects, because a shortrange effect would not care about the shape of the entire SQUID. But it is difficult to make any rigorous statements, because of course a great many things differ between the Type D or M SQUIDs and other SQUIDs and it is difficult to know what is the factor which causes the change in the slope. For instance, it is not just that the SQUIDs were in a split configuration, for tests on other split SQUIDs with different body shapes still yield noise spectra which are close to $1/f^{2/3}$. It is also interesting to note that the type D SQUIDs were made on a wafer along with 3 other types of SQUIDs, and that the other three types showed noise much closer to $1/f^{2/3}$. The type D and M SQUIDs were also made on entirely different wafers. So it is not simply a matter of some variation in the processing.

It should be noted, also, that the spectra are often not good fits to $1/f^{\alpha}$ (even taking white noise into account), see for example Fig 8.2. One usually sees small deviations of about 10% in the rms. These are not noise but reproducible, small, and broad (they generally extend over about a factor of 10 in the frequency) bumps or dips in the noise. One also frequently sees the noise flatten slightly below 1 Hz, and apparently steepen above 10 kHz, as in Fig. 8.2. The higher frequency portion is difficult to judge, however, because of the presence of white noise from the SQUID and the measuring electronics.

It is interesting to note that, if two spectra show different slopes, then the noise will differ in magnitude by an arbitrarily large amount at some frequency. A priori, it is thus quite surprising that the

magnitudes should show so little variation at 1 Hz. This simple result provides valuable insight into the nature of the low frequency noise. I believe that the most natural interpretation is as follows. Suppose that the noise spectrum is built up of a large number of independent Lorentzians. Then at any single frequency, one can obtain different values for the slope, depending upon how the roll-off frequencies for the different Lorentzians are distributed. If however, the process which produces the noise always generates roughly the same number of Lorentzians and the same distribution with frequency, then in general, the magnitude at any frequency will tend to be about the same. The slope would thus not be a fundamental parameter of the noise, because the observed $1/f^{\alpha}$ behavior is really only approximate. It is thus probably more appropriate to compare two devices by giving the noise at some standard frequency, say 1 Hz, then to obtain a magnitude at 1 Hz by trying to fit to a $1/f^{\alpha}$ law.

In addition the slope has an unusual temperature dependence. At low temperatures, the slope is nearly constant. As one approaches 0.5 to 0.7 K however, the slope often begins to decrease. For large devices, an examination of the spectra often reveals that the noise begins to flatten at low frequencies in this temperature regime. The higher the temperature, the greater the frequency to which the flattening extends; and thus the spectra are not describable by a $1/f^{\alpha}$ law in this temperature region.

In the case of the large split devices, which show a peak in the noise at around 0.6 K, one also sees a peak in the slope. Fig. 8.9a shows the slope at 1 Hz as a function of T for three devices. All three devices are of the large split configuration, and show a prominent noise

bump around 0.5 K. This bump is found in both the slope and the magnitude. The noise in all three devices are similar, although the slopes and magnitudes are slightly different.

8.2g Amplitude Distribution of the Noise

A noise source is not completely charaterized by its power spectrum. In particular, one may ask the additional question: how are the noise amplitudes distributed?[8] If a process is the sum of many independent sources, or if, equivalently, the system can occupy a great many different states, then one would expect a gaussian distribution for the amplitudes. If, on the otherhand, only a few processes are involved, then one might expect to see well-defined levels corresponding to the system being in one or another of a few states.

The open points in Fig. 8.10 show the amplitude distribution of the noise from SQUID M2 at 22 mK, $\Phi = 0.75\ \Phi_0$, and V = 1.2 μV. The noise was passed through a low pass filter (35 Hz) and digitized on an HP 3582A spectrum analyzer. The time traces were extracted from the analyzer and the amplitudes were binned and summed on a computer. The solid line and solid points are a rough fit to a gaussian distribution. The quality of even this poor fit is sufficient to demonstrate that the noise is highly gaussian, with no evidence of any favored levels in this frequency range. This essentially suggests that the noise is being produced by transitions between a great many states in the system.

This result is consistent with direct observations of the noise amplitude vs time when it is displayed on an oscilloscope trace. The noise appears to be random, and is scarcely distinguishable from white

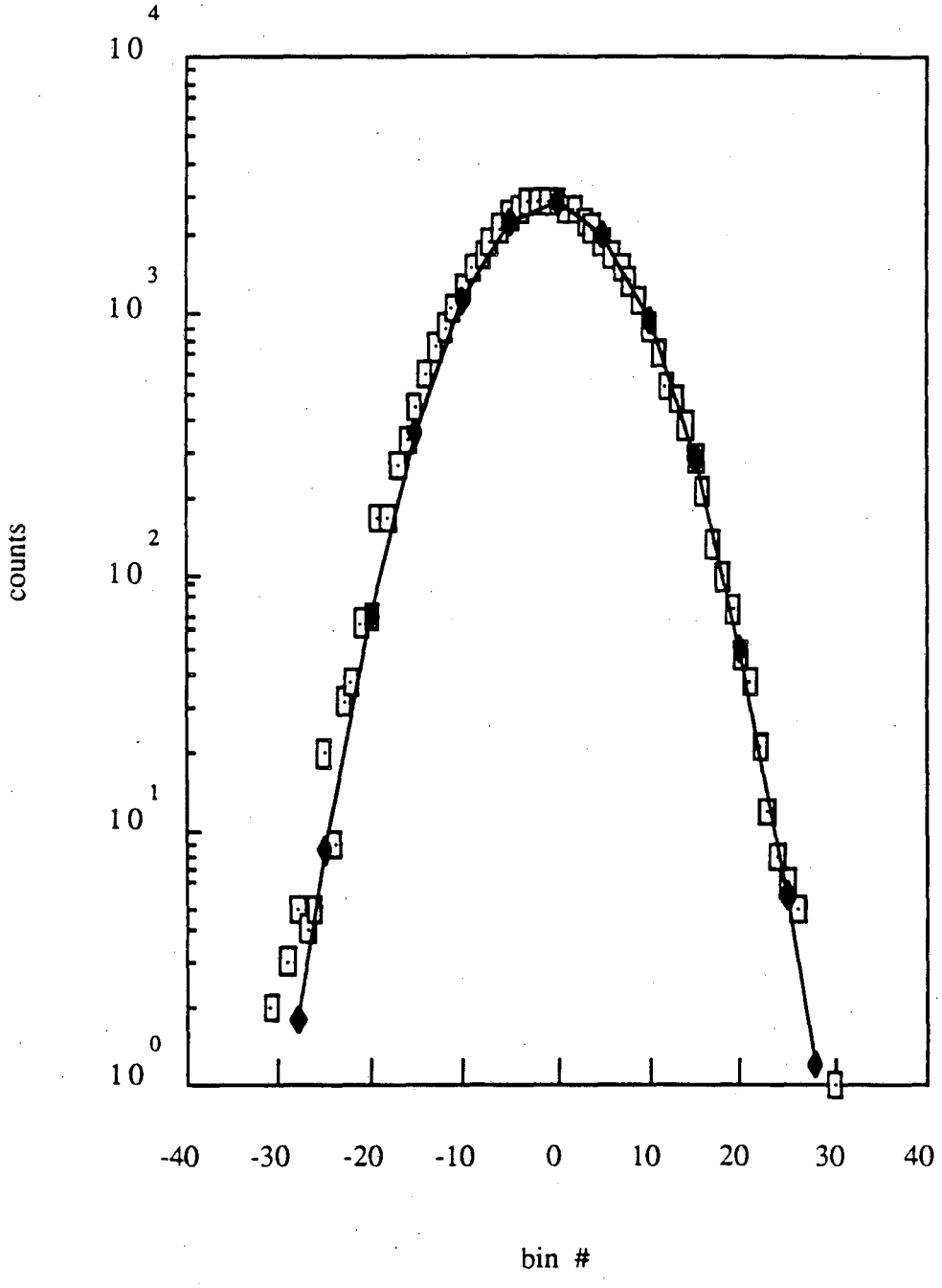

Fig. 8.10 Noise amplitude distribution from SQUID M1.: number of times the output acheived a certain amplitude vs. the amplitude. Solid line is gaussian fit to data.

noise. There is no evidence for individual states at either high or low sweep rates. I have also tried searching for more subtle noise vs time behavior by sending the output from the SQUID to a loudspeaker. Again, the noise was scarcely distinguishable from white noise, and I could not discern any pattern.

8.3 Occurrence of Low Temperature Excess Noise in SQUIDs

The preceeding section has discussed the properties of the low temperature excess noise that we have found in our SQUIDs. All of these have been fabricated in Berkeley. It is remarkable, and also very unfortunate, that all of these devices displayed comparable, and large, levels of excess noise. We have accordingly tried to obtain measurements of the noise in SQUIDs which were not made in Berkeley, in the hope that such SQUIDs would not have the excess noise.

This is of necessity a short section. As of this writing we have obtained results on just two SQUIDs which were not fabricated in Berkeley. No other group has published noise data on SQUIDs operated below 1 K (as this section was being finished, I recieved a preprint on some very encouraging low noise measurements down to 300mK by an IBM Yorktown group). In short, we have very little data, and any conclusions we can draw will be of the most tentative nature.

8.3a SQUID NBS1

We were very fortunate to obtain a dc SQUID, which I will call NBS1, from Michael Cromar of the National Bureau of Standards (NBS), Boulder

Colorado. The device is geometrically similar to the Berkeley type A design described in Chapter 1. It is a Nb/NbOx/PbIn based dc SQUID which was fabricated at NBS, using a fabrication procedure which is generally similar to the Berkeley procedure, and has been described elsewhere.[9] One important difference from the Berkeley SQUIDs is that AuIn is used for the resistive shunts rather than AuCu. Since AuIn is superconducting below 0.4 K, the SQUID will only function above this temperature. The parameters of the device are listed in Table 8.3. The device possesses a 50 turn input coil which was left open for the noise measurements. The coil introduced parasitic resonances which generated a considerable amount of structure in the I-V. This structure was associated with high levels of white noise. As a result, we could only measure the noise at fluxes between Φ_0 and $\Phi_0/4$ due to large amounts of noise unlocking the measuring SQUID(2) system everywhere else.

Using the measurement techniques described in Chapter 2, I obtained the excess noise as a function of temperature. Fig. 8.11 shows the magnitude of the excess noise at 1 Hz, expressed as an equivalent rms

Table 8.3 Parameters of the SQUIDs NBS1 and FIN1.

	NBS1	FIN1
$I_{o(\mu A)}$	10	21
L (pH)	80	80 (*)
R (Ω)	8	1.5
β_c	0.5	0.25

(*) This is the bare SQUID inductance, screening from the gradiometer reduces the measured SQUID inductance to roughly 40 pH.

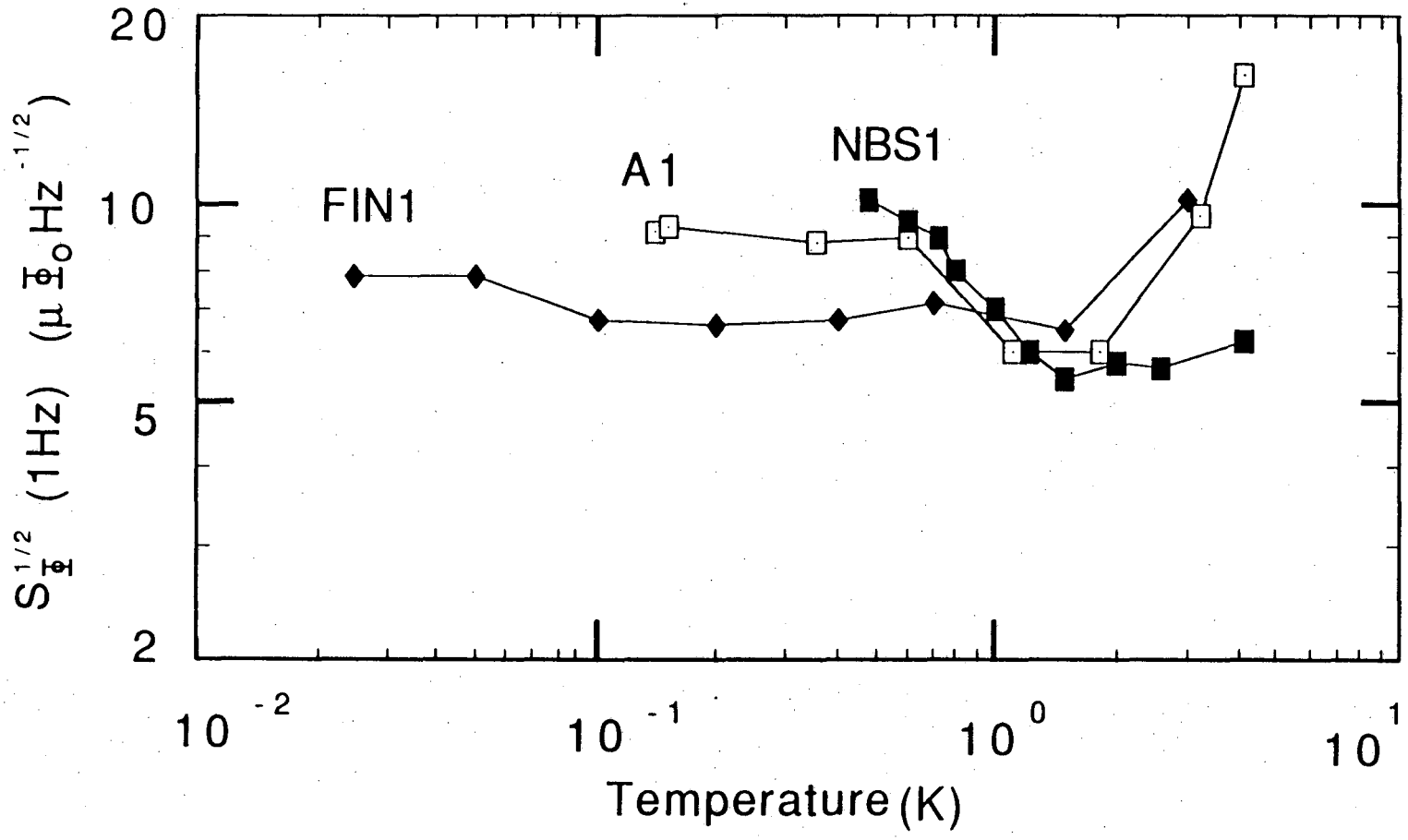

Fig. 8.11 Excess noise in A1 and the outside SQUIDs NBS1 and HUT1, at $\Phi = \Phi_0/4$.

flux noise spectral density in the SQUID, versus temperature. NBS1 was biased at a voltage of 4.0 μV and a flux of 0.1 Φ_0. Above 1K, the coils excess noise was dominated by critical current fluctuations, while at lower temperatures the noise appears to be dominated by a fluctuating magnetic flux. Because only a portion of the I-Φ was measurable, this conclusion could not be drawn with complete confidence. Nevertheless, the observed noise at Φ_0 decreased steadily with temperature, while that at $\Phi_0/4$ showed a rapid increase below 1 K. At 4.2 K, the noise levels at Φ_0 and at $\Phi_0/4$ were comparable, being consistent with critical current noise. On the otherhand, by 0.5 K, the noise at Φ_0 was substantially smaller than at $\Phi_0/4$, indicating the existance of a flux noise term. Below 1 K, the SQUID showed an excess noise level and temperature dependence at $\Phi_0/4$ which was very comparable to that seen in the type A SQUIDs. At the lowest temperatures, the excess noise power spectral density scales as $1/f^{\alpha}$, where α is close to 2/3 for NBS1.

The excess noise magnitude in NBS1 shows a rapid increase below 1 K which is very similar to that seen in the similarly shaped SQUIDs (type A) of Ref. 1. Examination of the noise spectra from NBS1 in the 0.6 to 1.48 K region show that the spectrum does not scale as $1/f^{\alpha}$, but rather levels off at low frequencies, as shown in Fig. 8.12. This behavior is reminiscent of that seen in certain spinglass systems, as is discussed in the concluding remarks.

8.3b The Helsinki SQUID

We were very fortunate to also obtain a dc SQUID from Finland. The dc SQUID, which I will call FIN1, was provided by Matti Kajola and

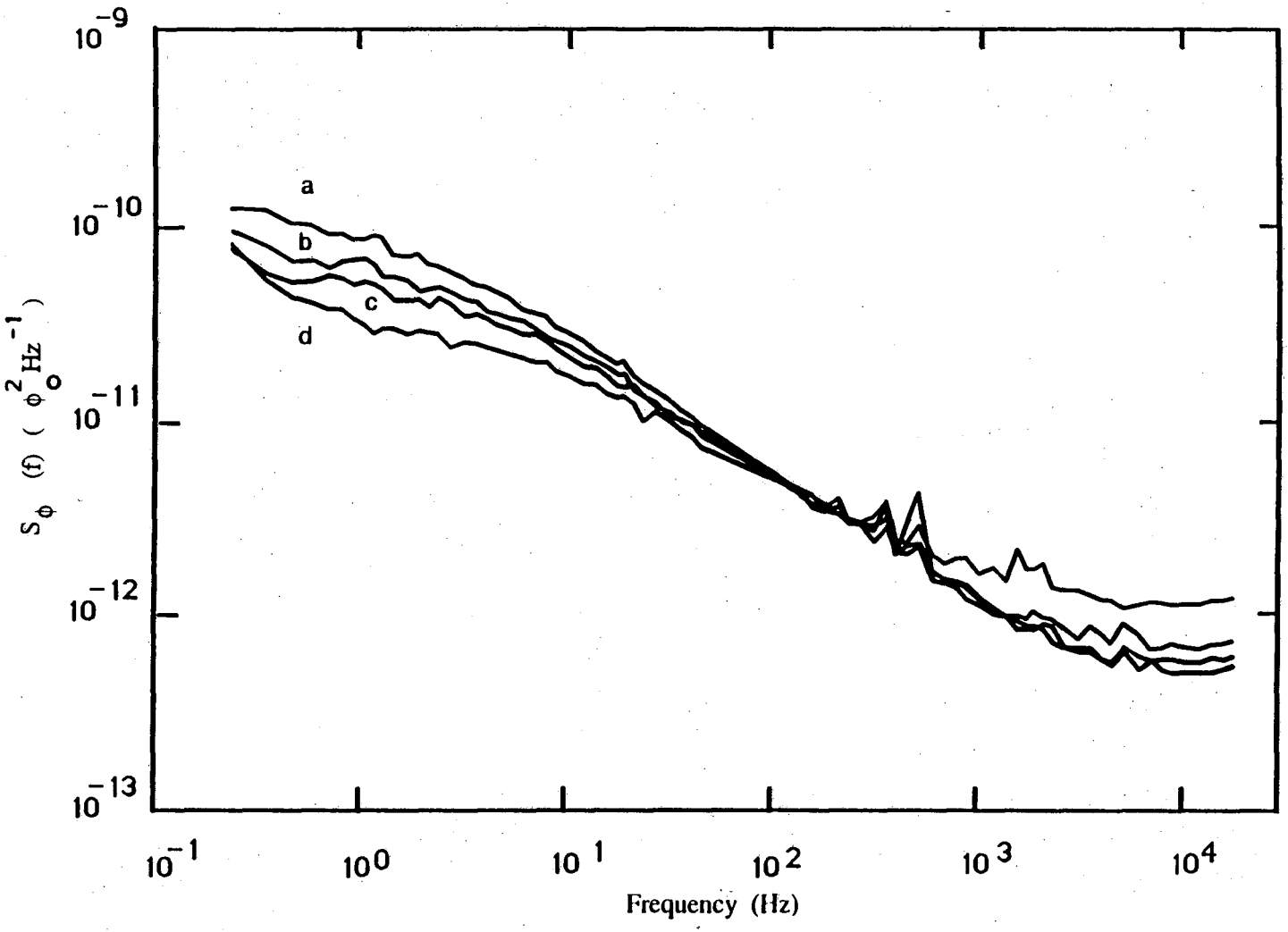

Fig. 8.12 Flux noise spectral density for SQUID NBS1 at temperatures of: (a) 0.6, (b) 0.8, (c) 1.0, (d) 1.48 K. The SQUID is biased near $\Phi_0/4$.

co-workers at the Technical Research Center (VTT) and the Helsinki University of Technology. The 10 layer fabrication procedure is roughly similar to that used at Berkeley, although considerably more complicated, and has been descibed in detail elsewhere.[10] There are several differences: The shunts are made of 200 nm of Ti followed by 20 nm of Au, the devices are passivated with 750 nm of SiO, the SQUID is formed from two parallel loops and is connected to a gradiomter via a double transformer, coplanar leads are used to bias the SQUID so as to prevent magnetic flux generated by the bias current from coupling to the SQUID, and the SiO insulating layers and PbIn counterelectrode are deposited by electron beam evaporation rather than from a resistively heated source.

Since Ti is superconducting below 0.39 K, one would expect FIN1 to only work at higher temperatures. In fact the SQUID works down to 20 mK. This may be because of contamination in the shunt material or because of alloying of the Ti and the Au. The parameters of the device are listed in Table 8.3.

The SQUID was operated at 5.2 μV and 0.2 Φ_0. The excess noise magnitude in HUT1 is nearly temperature independent below 1K, with only a small upturn below 100 mK (see Fig. 8.11), and the slope α is nearly constant over the entire range. This behavior is similar to that reported in Ref. 1 for similar small SQUIDs, although the slope, about 0.86, is steeper than the typical 2/3.

The presence of the gradiometer coil on the SQUID caused a considerable amount of structure on the I-V characteristic. As a result, I was again only able to measure the noise between $\Phi = 0$ and $\Phi_0/4$. This made it difficult to seperate the contributions of the critical current

noise from any flux-like noise. Nevertheless, the noise at $\Phi = 0$ showed a steady decrease as the temperature was lowered so that at low temperatures, the critical current noise was much smaller than the output current noise S_I at $\Phi_0/4$. The device did show measurable critical current fluctuations even at 20 mK, where they contributed an estimated 10 % to the total excess noise seen in the device when it is biased at $\Phi_0/4$. This is somewhat unusual, and may be due to the significantly higher current density in the junctions. At 25 mK I measured $S_I^{1/2}/2I_o \simeq$ 2 $pA\mu A^{-1}Hz^{-1/2}$ for the two 6.2 μm^2 Nb/NbOx/PbIn junctions.

In summary, I have measured the excess noise in two dc SQUIDs made at two different outside facilities and found that both SQUIDs possessed low temperature excess noise which is qualitatively similar to that seen in our own SQUIDs. This suggests that the noise is either fairly common in SQUIDs, or that some feature of the measuring arrangement or technique is producing the noise.

8.4 Elimination of Likely Sources

In this section I would like to examine the possibility that the low temperature excess noise is being generated by a few hypothetical sources. These hypothetical sources may be broadly classified into three groups: SQUID parameter fluctuations, physical sources, and dynamical effects. I will make extensive use of the results of Chapter 5 to discuss hypothetical noise sources arising from fluctuations in the SQUID parameters. By physical sources I mean a physical system which produces a real magnetic fluctuation in the SQUID, not just a noise which looks like an equivalent amount of flux noise. An example of such

a hypothetical physical source would be a moving flux bundle in the body of the SQUID. By dynamical effects, I will mean noise which is in some manner generated by the non-linear equations of motion of the SQUID. It should be recognized that such affects will only arise if there are additional terms in the SQUID equations. It is accordingly quite difficult to arrive at general conclusions on such mechanisms, nonetheless I will have something to say.

In discussing all of the hypothetical sources, I will make extensive use of the observed properties of the noise. From the behavior of the excess noise it is possible to eliminate most possible sources, as summarized in Table 8.4, and as will be discussed in the following sections.

Table 8.4 Hyptothetical sources of low temperature excess noise that we have been able to rule out.

Possible noise source	Properties of source
Fluctuations in electronics, I_0, R, L, or I_{b1}	not a flux noise
Fluctuations in $I_{\phi 1}$	depends upon M_1
Fluctuations in $(I_{01}-I_{02})/2$	not a flux noise at large α
Fluctuations in $(L_1-L_2)/2L$	flux noise scales as I^2
Fluctuations in $(R_1-R_2)/2R$	flux noise depends upon I_{b1}
External magnetic field	flux noise scales as $(\text{area})^2$ of SQUID
Flux vortices in the SQUID	material and field dependent
SQUID substrate	material dependent
SQUID mount	material dependent
Normal metal near SQUID	depends upon presence of normal metal
Helium in cell	depends upon presence of helium
Heating effects	depends upon power suppplied to SQUID
Fluctuations in ϕ_o	depends upon $(\text{area})^2$ of SQUID
Fluctuations in T	secondary parameter fluctuation

8.4a Noise from SQUID(2) or the Feedback Measuring Electronics.

There are several independent reasons why the measuring SQUID or electronics cannot be the cause of the noise. First of all if SQUID(2) or the feedback electronics did generate an excess noise, it would not appear to be a flux noise with respect to SQUID(1). Rather, it would be independent of the operation of SQUID(1), producing the same noise S_I at Φ_o as at $\Phi_o/4$. In particular one would expect the magnitude to be unchanged when SQUID(1) was off, or had no flux gain. This is not at all what is observed experimentally.

An excess noise from the feedback electronics would also not depend upon the temperature of SQUID(1). In addition, I have used two different electronics configurations without any effect on the behavior of the low temperature excess noise. The first configuration used was a 100 kHz modulation feedback box. In June 1985, this was replaced with a completely different feedback electronics, the 500 kHz modulation electronics which was described in Chapter 3. All subsequent measurements were made using this electronics box. I have also used three different measuring SQUIDs, two of them with 20 turn input coils and a third with a more sensitive 50 turn input coil. I have also varied the operating point for the measuring SQUID. None of these changes has ever produced any effect on the level of the excess noise in SQUID(1).

I have also measured the excess noise in SQUID(2) without any input circuit, and found that it possessed excess noise which was the same (within 10%) as when the device was itself measured in the SQUID(1) position. Thus the excess noise cannot be produced by any kind of interaction between the measuring SQUID and the measured SQUID. Finally,

if a simple resistor is placed in the loop instead of a SQUID, one does not see any excess noise (just that from the measuring SQUID). For these reasons, I have concluded that the low temperature excess noise is not being generated by the electrical measuring system.

8.4b Fluctuations in the Bias Current I_{b1} of SQUID(1).

As in the preceding case, fluctuations in I_{b1} would not appear to be a flux noise. In particular, when SQUID(1) is off the fluctuating current I_{b1} would flow entirely through the SQUID(2) input coil because that arm of the input circuit is superconducting, see Fig. 2.5. On the otherhand, when SQUID(1) is biased, the coil side of the circuit becomes very resistive, and the current through the coil would change very little from a fluctuation in I_{b1}. Thus, excess noise in I_{b1} would produce a large signal when SQUID(1) is off and a small signal when SQUID(1) is on. In fact just the opposite is seen, when SQUID(1) is off there is no detectable excess noise (other than from SQUID(2)), while when SQUID(1) is on, there is a large amount of excess noise (if the SQUID is biased with some flux gain). In addition, fluctuations in I_{b1} would not depend upon the temperature of the measuring SQUID. Furthermore, the experiments on resistive samples discussed in Chapter 10 did not reveal any excess 2/3 noise, although the bias current source was the same as that used in the SQUID measurements.

8.4c Fluctuations in the Flux Bias Current for SQUID(1), $I_{\phi 1}$.

A current $I_{\phi 1}$ applied to the modulation coil of SQUID(1) will

produce a flux $I_{\phi 1}M_1$ in SQUID(1), where M_1 is the mutual inductance between the modulation coil and SQUID(1), see Fig. 2.5. Noise in this current will thus produce a real flux noise in SQUID(1). There are several tests which I have applied to rule out this hypothetical source. First of all, the mutual inductance between the flux coil and the SQUIDs represented in Fig. 8.7 varied by about a factor of 50. If the current $I_{\phi 1}$ were independent of the SQUID, one would accordingly expect the noise to scale with this mutual inductance. The measured rms flux noise however, ranged over a much smaller factor. In particular, no such scaling with M_1 was observed. I have also measured the noise in the same SQUID for two values of the mutual inductance which differed by about one order of magnitude. No observable difference was seen in the low temperature excess noise. I have also placed the current source $I_{\phi 1}$ at the current bias source and tested for any excess noise, in a similar fashion as discussed for the source I_{b1}, and seen no measurable noise.

There is one additional effect which I will descibe which has also let us rule out this hypothetical source. It frequently happens that when SQUID(1) is operated, the device has flux gain even when no current $I_{\phi 1}$ is sent down, which is to say that the device naively appears to be at some flux, say $\phi_o/4$, rather than at the expected zero flux. This can happen for two reasons. First of all, it may indicate the presence of trapped magnetic flux in the SQUID, the In pads, or the superconducting shields. We have some evidence that this is in fact the case, because one occasionally warms up through the In transition at 3.2 K and then upon recooling finds that the SQUID is at some different flux value when no current is applied. The second possibility is that in asymmetric devices, zero applied flux can correspond to a point of finite flux

gain. In either case, one can measure the noise when the $I_{\Phi 1}$ current source is completely detached and the line is left open or closed, and one sees no affect on the level of the noise in the SQUID.

This offset behavior has allowed us a careful check on noise from $I_{\Phi 1}$, but at another level, it is quite disturbing. For it suggests that there is a flux-like source in the SQUID or that sizeable magnetic fields are present. If this source were to vary slighly, then it could easily produce the observed excess noise. The possibility of such a source will be discussed in section 8.4i.

8.4d Critical Current Noise

The occurrence of fluctuations in the critical currents of individual Josephson junctions means that excess noise will be produced in the SQUID, as discussed in Chapter 5. Whether or not such noise can be observed depends upon the magnitude of the effect compared to the other sources of excess noise in the SQUID. For many years, the Berkeley SQUIDs were dominated by high temperature flux noise, as discussed in Chapter 7. In such SQUIDs, the critical current noise was generally not observable at 4.2 K. By using a clever current and flux modualtion scheme, Koch et al.[4] were able to show that there was critical current noise in the SQUIDs, and that its level was close to that expected from the results on individual junctions (see Chapter 7).

As discussed in Chapter 7, this situation changed when it was discovered that the high temperature flux noise could be greatly reduced, if not eliminated, by replacing the usual Nb SQUID body with a PbIn body. In these devices, the noise at high temperatures was clearly

dominated by critical current noise. The study of critical current noise in the devices thus became comparitively more important, as this was now the limiting source of excess noise at low frequencies and high temperatures.

This study made use results of Chapter 5. In particular, when the SQUID is biased at $\Phi = 0$ and $v<<1$, the total noise in I produced by the critical current fluctuations is just $S_I = (S_{Io1} + S_{Io2})/4$. Since at $\Phi = 0$, the SQUID is insensitive to flux noise, one could easily obtain the critical current noise in the two junctions. In this way, I was able to obtain results on the critical current noise in SQUID junctions down to temperatures as low as 20 mK, in the same devices that I was measuring large amounts of low temperature flux noise. Thus one does not have to use clever modulation schemes to find the amount of critical current noise in a SQUID, one merely needs a low noise measuring system.

As discussed in Chapter 5, there are two modes of fluctuation of the SQUID parameters: Symmetric, for example fluctuations in $I_0=(I_{01}+I_{02})/2$, and antisymmetric, for example, fluctuations in $\alpha=(I_{01}-I_{02})/(I_{01}+I_{02})$. The antisymmetric modes produce flux-like noise, whereas the symmetric modes do not. Since the observed low temperature excess noise is flux-like, I can immediately rule out symmetric critical current fluctuations as the source.

Fig. 8.13 shows the excess noise $S_I^{1/2}(f)/2I_o$ at 1 Hz vs. temperature for five different SQUIDs which were biased at $\Phi = 0$. This then represents a plot of the critical current noise in the junctions. A line of slope unity has been drawn through the data. $S_I(f)$ scales approximately as $I_o^2T^2$ over the temperature range from 0.1 to 4.2 K. This behavior is in marked contrast to that observed by Rogers and

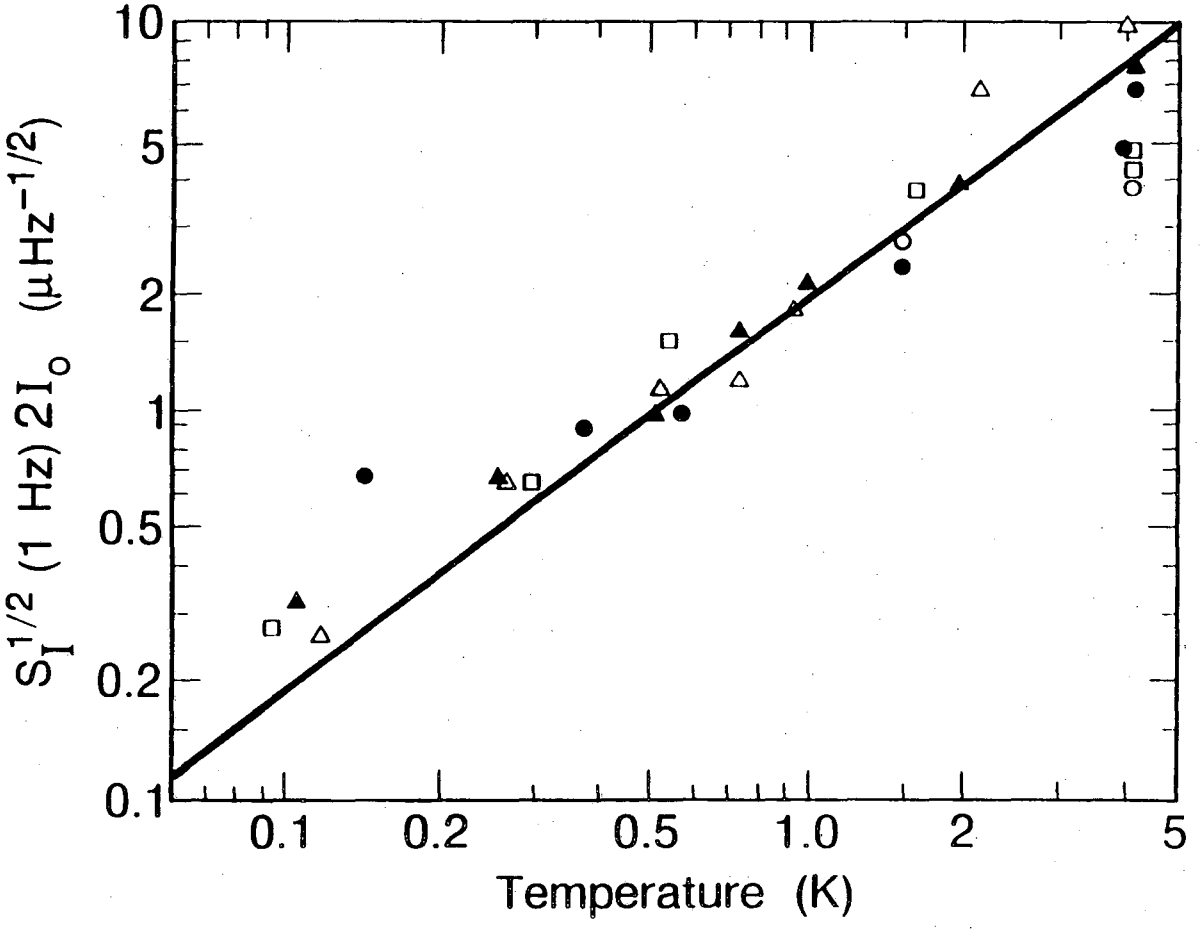

Fig. 8.13 $S_I^{1/2}$ (1 Hz)/2 I_o at Φ = 0 vs temperature for 5 devices: ○ C3, △ D2, □ E1, ● F1, ▲ K1.

Buhrman[11] and Wakai and Van Harlingen[12] on very small single junctions. In the former cases the noise flattened off at temperatures below about 15 K, while in the latter case the noise was nearly independent of temperature in the liquid ^{4}He range. This difference is most likely because of the much smaller bias voltages used here, and the smaller current density in our SQUID junctions.

The scaling with T^2 implies that critical current fluctuations are a negligible source of excess noise at low temperatures, while the scaling with I_0^2 implies that one can lower the critical current fluctuations by reducing the critical current. This temperature behavior is completely *inconsistent* with the measured properties of the low temperature excess noise. Furthermore, the measured critical current fluctuations were too small to account for the measured flux noise at any temperature below 1K. In addition, there is no evident scaling of the low temperature excess noise with the critical current of the device, despite critical currents ranging from 0.75 μA to 20 μA.

I note here that the magnitude of the critical current noise at higher temperatures is dependent upon the particular junction, and one sees considerable variations from one junction to the next. This is not at all what is observed for the low temperature excess noise, which is very repeatable from one device to the next. The nature of the critical current noise at lower temperatures would thus have to be very different from that at higher temperatures in order to explain the data.

I also remark here that I do not know any plausible model which would produce pure asymmetric critical current fluctuations, without also producing a symmetric component. In addition I have built "split " SQUIDs where the junctions are seperated by differences as large as 1

mm. As discussed above, these devices can show different slopes to the noise, although this does not seem to be directly associated with the split configuration. It is difficult to conceive of an affect which could anti-correlate the critical current fluctuations in the junctions over such distances.

For the above reasons, I conclude that the low temperature excess noise is not caused by critical current fluctuations.

8.4e Symmetric Fluctuations in the Shunt Resistances

There are several independent reasons why the low temperature excess noise cannot be due to fluctutions in the shunt resistance. First of all, the Au(Cu 25 Wt%) shunt material was chosen specifically because its small electron mean free path produces a temperature independent resistivity. The resistance at low temperatures is dominated by elastic collisions with impurities, so that one would not expect to see any resistance fluctuations. Secondly, in Chapter 10 I will present independent measurements on individual AuCu thin film resistors which were constructed in the same way as the SQUID resistive shunts. By biasing the resistors with current, one can detect fluctuations in resistance directly. No excess noise was observed (other than from the measuring SQUID), so we have some direct evidence that there is nothing peculiar happening in the shunts.

In addition from Chapter 5 section 3, symmetric fluctuations in the shunt resistances, R_1 and R_2, will not produce flux-like noise. In particular there will be comparable output noise S_I generated at Φ_0 and at $\Phi_0/4$. This is not what is seen experimentally.

Furthermore, in Chapter 5 it is shown that symmetric fluctuations in R_1 and R_2 will produce equivalent flux noise which will scale with the bias voltage of the SQUID. I tested for this scaling in several SQUIDs. For example in device A5 (9-18-85), at a temperature of 95 mK, and $\Phi = \Phi_0/4$, the excess rms equivalent flux noise spectra agreed to better than 5 % at bias voltages of 0.43 μV and 1.15 μV. The ratio of the two voltages was about 2.7, and should have produced a corresponding change in the excess noise if it were due to resistance fluctuations. Similarly, in device E1 (2-19-86) at T = 95 mK, and $\Phi = \Phi_0/4$, the excess equivalent rms flux noise spectra agreed to better than 5% at bias voltages of 1.8 μV and 6.8 μV.

For the above reasons, I conclude that the low temperature excess noise is not caused by symmetric fluctuations in the SQUID shunting resistance.

8.4f Symmetric Fluctuations in the SQUID Inductance

As discussed in Chapter 5.10, symmetric fluctuations in the SQUID inductances L_1 and L_2, do not produce flux-like noise. In this case, the noise will typically be as largest at $\Phi_0/2$ and vanish at Φ_0. This is not at all what is observed experimentally.

However, there is a real complications to this scenario. First of all, if there is a fixed magnetic field at the SQUID, then a change in the inductance can generally be expected to also produce a change in the flux applied to the SQUID (see eq. 5.44). If the magnetic field is sufficiently large, then the change in the flux will produce effects much larger than the direct effects of the changing inductance. In this

case, the inductance fluctuations will produce noise which will appear to be a flux noise. From Eq. 5.44, however, we would expect that this noise would scale like $L^2 S_L$. A reasonable assumptions about S_L would be $S_L \propto L^2$, as would arise from a susceptibility change or a length change. One would then expect to see the noise scale as L^4. Although it is possible that the data would be consistent with an L^1 dependence, an L^4 dependence is much too large. In addition, I have tried varying the field at the SQUID by cooling down in the presence of the Earth's magnetic field, and then replacing the μ-metal shields below T_c. This should produce a larger trapped field at the SQUID. No affect on the low temperature excess noise has been observed.

For the above reasons, I conclude that the low temperature excess noise is not due to symmetric fluctuations in the inductance.

8.4g Asymmetric Fluctuations in the SQUID Inductance

From the discussion in section 5.10, it can be seen that asymmetric fluctuations in L_1 and L_2 would produce a flux noise spectral density which is roughly proportional to I^2. The current I can be varied by changing the flux bias point or the bias voltage. As discussed above, the measured flux noise is independent of the operating point, and one can safely conclude that the low temperature excess noise is not due to asymmetric inductance fluctuations.

8.4h Asymmetric Fluctuations in the Shunt Resistors

As discussed in 5.9, asymmetric fluctuations in R_1 and R_2 would

produce a flux noise spectral density proportional to V^2, while the measured flux noise is independent of V. In addition, measurements on individual resistors do not show any excess noise.

I have also built "split" SQUIDs, such as the type D SQUIDs, where the resistors are seperated by nearly 1 mm. The type D devices , and similar ones, do in fact show different slope, but other split devices do not. It is quite difficult to understand what mechanism could give rise to an antisymmetic fluctuation in the resistance over such large distances, without depending upon the seperation of the shunts or also inducing some symmetric fluctuation.

8.4i Fluctuations in the External Magnetic Field

Fluctuations in an external magnetic field would lead to a flux noise, $S_\Phi^{1/2}(f)$, which scaled as the effective pick-up area of the SQUID (see section 3.2). The SQUIDs I tested had effective pick-up areas which ranged over a factor of about 1500 (one of the devices, A3, was a magnetometer with a pick-up loop deposited on the chip). On the otherhand, the measured rms flux noise was nearly independent of the size of the SQUID. There is a residual size dependent variation of about a factor of three in $S_\Phi^{1/2}(1Hz)$ for all of the SQUIDs. I can thus conclude that the low temperature excess noise cannot be due to a uniform field threading the SQUID. This is not the end of the matter however.

I note quite generally that, because of the more rapid decrease with distance of any multipole terms, any distant fluctuating source will generate a nearly uniform magnetic field at the SQUID. On the other

hand, sources within a distance comparable with the transverse dimension of the SQUID will generate a nonuniform field. The noise that a local source produces will thus not scale with the area of the SQUID. The fact that the flux noise is nearly independent of area cannot be used to eliminate local sources. This then remains as an important possible source of noise which I have not been able to eliminate from consideration. It should be recognized that the smallest SQUIDs tested had an outside diameter of only about 50 μm, and that, therefore, the local source would have to be not more than a few times this distance away. This does not leave a very large volume for the source. For example, the chip itself is about 380 μm thick, so that a source on the backside of the chip would not appear to be a local source for many of the SQUIDs tested. In the next five sections, I consider various possible local sources which are within range of the largest SQUIDs.

8.4j Noise from the Substrate

The possibility that the low temperature excess noise was being generated in the substrate was tested for by building SQUIDs on different substrates. The great majority of the SQUIDs built in the group have been made on heavily p-doped Si wafers which were between 15 and 20 mils thick, and which had a 1.2 μm layer of thermally grown oxide on the surface. The resistivity of these wafers was typically 0.01 to 0.05 Ωcm at room temperature. This is a very high level of doping, about 10^{19} carriers per cm^3 ,and is very close to degenerate doping.[13] The reasons for this choice of substrate doping is historicaly obscure. Nevertheless, it has persisted over the years, so that virtually all of

the group's SQUIDs have been made on such wafers.

I tested two alternative substrates. The first was a 380 μm thick wafer of Si which did not have any thermal oxide, and which had a resistivity of about 40 Ωcm at room temperature. This resistivity repsresents about 10^{17} carriers per cm^3, about two orders of magnitude smaller than in the heavily doped wafers. Device E2 was tested on this substrate, and showed levels of noise completely comparable with that found in device E1 which was made on the heavily doped wafers. The second alternative substrate was a 500 μm thick sapphire wafer. This wafer was donated by the Microlab, and initially came with a 1-2 μm layer of epitaxial Si. I stripped off this layer by using an SF_6O_2 plasma etch, before beginning the SQUID fabrication. SQUIDs K1 and J1, were fabricated on this wafer. Both devices showed low frequency excess noise levels and behavior which were comparable to that found on the Si wafers. I have accordingly concluded that the low temperature excess noise does not arise in the substrate.

8.4k Noise from the SQUID Mount

After the substrate, the solid object closest to the SQUID is the SQUID holder or mount. For most of the experiments, the holder consisted of a phenolic canvas stage, and a phenolic canvas cover plate, see Fig. 8.14a. The choice of phenolic canvas was made because it reportedly[14] has a lower permitivity than the G-10 fiberglass which our group ordinarily uses. Plastic screws clamped the cover plate firmly to the stage, with the SQUID sandwiched in between. The SQUID was held about 400 μm away from the surface of the stage by In pads which formed the

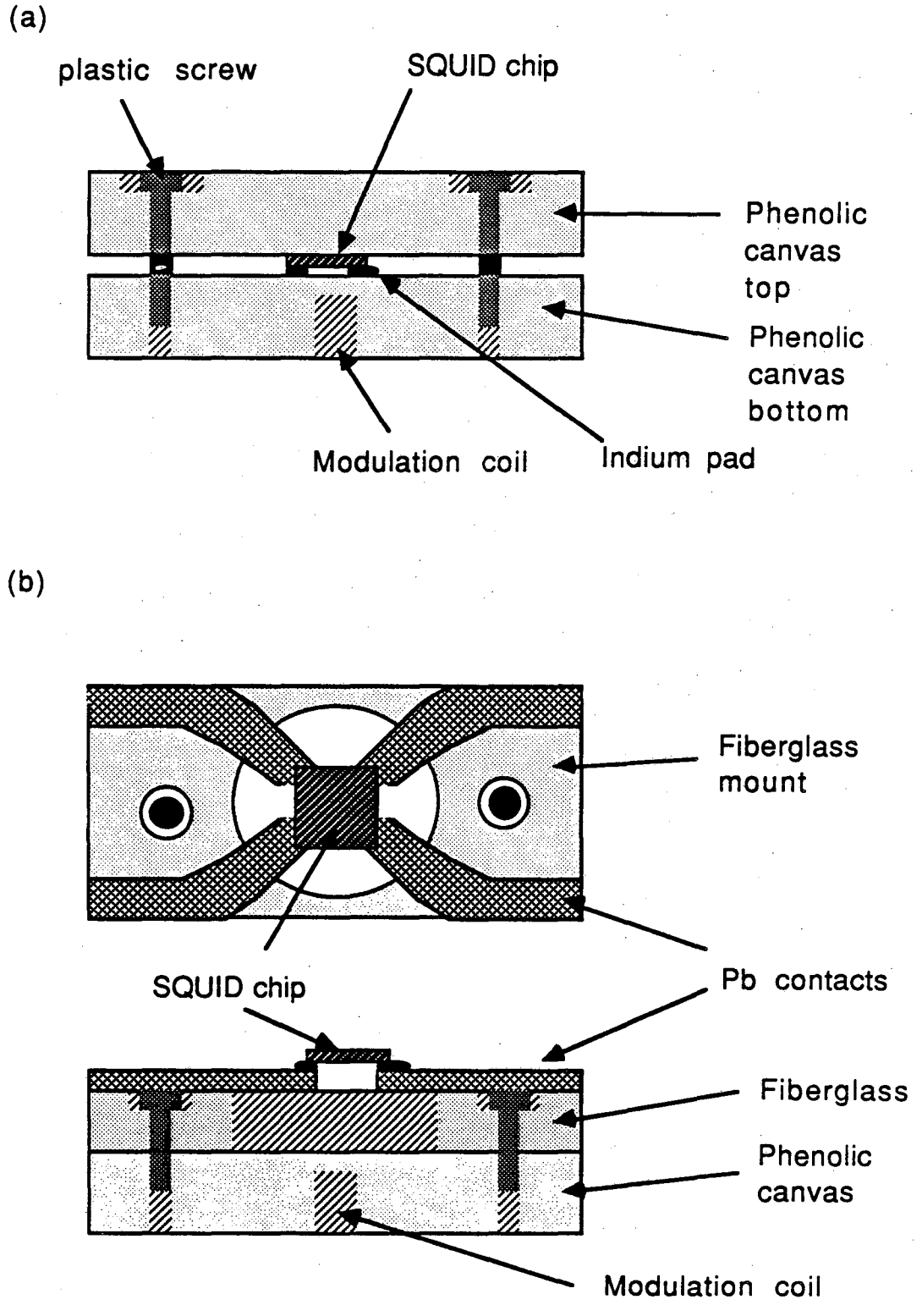

Figure 8.14 (a) Construction of the phenolic canvas SQUID holder. (b) Construction of the superconducing SQUID holder.

electrical contact between the SQUID's thin-film connection pads and Nb foil pads on the surface of the stage.

Replacement of the stage and cover with similar ones made of G-10 fiberglass did not result in any change in the level or behavior of the low temperature excess noise. In addition, replacement of the plastic screws with brass screws or replacement of the superconducting modulation coil with a Cu one did not produce any change in the excess noise.

I have also tested a mount which supported the SQUID on superconducting Pb arms, see Fig 8.14b. The Pb arms were epoxied to a fiberglass support which was never closer than 5 mm to the SQUID. The SQUID was affixed to the Pb arms solely by the In pads, and no coverplate was used. The SQUID was located about 4 mm from the modulation coil and about 2mm from the inside surface of the Nb shield tube, much closer than usual. This alters the spacing between the SQUID and the modulation coil and the placement of the SQUID in the cell. Tests on SQUID P1 showed no measurable difference in the noise after replacing the phenolic mount with the superconducting mount. I have also varied the amount of In used to form the contacts for the pads, and have altered the proximity of the In to the SQUID. This was done on both the fiberglass and phenolic canvas mounts without any measurable effect on the excess noise.

From the above negative results, I have concluded that the low temperature excess noise is not associated with the SQUID holder.

8.41 Helium in the Cell

The cell is ordinarily filled with superfluid ^{4}He. As described in Chapter 2, the ^{4}He serves as a working fluid to maintain thermal contact within the cell. When the cell is operated without any ^{4}He in it, the SQUIDs will not cool below a temperature of about 1 K, as judged by the level of the white noise. This is too warm to reveal much about the presence or absence of the low temperature excess noise.

As an alternative test, device D1 (6-4-86) was tested with different ratios of ^{3}He and ^{4}He in the cell. The cell was first tested with ^{4}He in the cell. The cell was then warmed above 14 K, and the ^{4}He removed with a liquid He cooled charcoal pump. The cell was then re-cooled and approximately 500 cc STP ^{3}He was condensed in the cell, allowing the contents of the cell to cool to about 70 mK (this experiment was done with the stainless steel cell can, and this was the minimum temperature the can could attain due to poor thermal contact to the mixing chamber). The noise was then measured with SQUID(1) biased near $\Phi_0/4$. Next an equal amount of ^{4}He was introduced into the cell, and the noise again measured. Finally, the ^{3}He was diluted further (to about 5%) by filling the cell with ^{4}He, and the noise was again measured. There was no measurable difference in the excess noise for the four ^{3}He concentrations.

However, it should be recognized that what is of importance would be the ratio of ^{3}He to ^{4}He at SQUID(1). At 70 mK, the two isotopes will not exist as a single mixture, but rather they will be seperated into two phases. A ^{3}He rich phase, containing almost entirely ^{3}He, floats on top of a denser superfluid ^{4}He phase which also contains at most a few

percent ^{3}He. Since SQUID(1) is fairly high in the cell, the initial small volume of ^{3}He would not be expected to cover the SQUID. Rather, the cooling was probably provided by a small residual amount of the dilute superfluid ^{4}He phase, which was left in the cell from the earlier run. This dilute phase would be saturated with 5 to 6% of ^{3}He. The subsequent fillings of the cell with ^{4}He should thus have little affect, as in this case the added volumes of ^{4}He were sufficient only to convert part, or all, of the ^{3}He rich phase into the 5 to 6% dilute phase. The real test was thus between the initial pure ^{4}He noise data, and any one of the subsequent ^{3}He tests.

From the fact that the excess noise does not depend upon the concentration of ^{3}He, I have concluded the noise is not associated with the helium in the cell. However, a better test would have been to entirely fill the cell with ^{3}He.

8.4m Materials From Which the SQUID is Built

A broad class of hypothetical sources are those which arise from some physical process in the metal or insulators from which the SQUID is constructed. These materials are few in number, and their occurrence in the SQUID fabrication has been discussed in Chapter 1. I will here consider each material.

AuCu shunts. All of the SQUIDs which were made in Berkeley had AuCu alloy shunts (see Chapter 1). The material compostion was never varied. On the otherhand, the amount of material, and its proximity to the SQUID were varied enormously. The area varied from 600 μm^2 for many of the devices, to 16 X 10^4 μm^2 for the large area cooling fins on the type M

devices (see chapter 11). There does not appear to be any correlation of the noise with the shunt size. Also, small area SQUIDs generally have less low temperature excess noise, but they have the same size shunts as the large area SQUIDs.

The second major test of the shunt material concerns the SQUIDs not made in Berkeley. These had Ti or AuIn as the shunt material instead of AuCu, as was discussed in section 8.3. Low temperature excess noise was observed, and its behavior was quite comparable to that in Berkeley SQUIDs of comparable dimensions. Thus the noise cannot be directly associated with the shunt material.

SiO. The insulating layers that define the Josephson junctions and electrically isolate the SQUID from an input coil (if one is included on the device) are made of SiO, which is deposited as described in Chapter 1. SiO is used in all of the SQUIDs, including those not made in Berkeley. We tested for noise generated by SiO by varying the amount of SiO on the SQUID. The addition of an extra 200 nm thick layer of SiO on top of the SQUID, as we commonly use for passivating the SQUIDs, has no measurable effect on the low temperature excess noise. Also, the type A SQUIDs are completely covered with the two SiO layers that define the junctions. These layers cover all of the Nb and also fill in the center hole of the SQUID loop. Most of the other SQUIDs have relatively small patches of SiO which do not cover the center hole, but rather are concentrated only near the junctions. The noise in all of these devices is comparable however, and there does not seem to be any correlation between the SiO and the low temperature excess noise.

Nb and PbIn. As noted above, all of the SQUIDs had some combination of Nb and Pb or PbIn forming the body of the SQUID. We tested for noise

from these materials by varying the total and the relative amount of each material, as can be seen from Figs. 1.4 to 1.19. No dependence on these materials has been seen. This is in marked contrast to the case for the high temperature flux noise, as discussed in Chapter 7, where a strong material dependence was found.

The type A and A' devices are a particularly sensitive test for material dependences (see Figs. 1.4 and 1.5). The two device types are nearly identical except for the exchange of Nb for PbIn in the body and electrode. The low temperature excess noise level, slope, and temperature dependence are virtually identical for the two cases. I can thus conclude that the low temperature excess noise is independent of the SQUID body or loop material.

Adhesion promoters Ti and Cr. As was described in Chapter 2, we generally use adhesion promoters under the AuCu and SiO in order to make them stick better to the underlying layers. My early wafers all used Cr under the SiO insulating layers and the AuCu resistors. I later switched to Ti under the SiO, with no measurable effect on the behavior and level of the low temperature excess noise. On the devices constructed on sapphire, there was no adhesion promoter under the AuCu, and only Ti was used under the SiO. The saphire devices thus had no Cr. As was discussed above, the devices built on sapphire showed comparable levels of low temperature excess noise.

Because the adhesion promoters for SiO were used only directly under the SiO, the devices varied enormously in the amount of their area which was covered by the promoter. As was the case for the SiO, the observed level of the low temperature excess noise showed no correlation with this area. I can thus conclude that the excess noise was not affected by

the presence of the adhesion promoters.

Contaminants. There is the possibility that a layer of contaminant or surface oxide is present on the SQUIDs. This is a very difficult hypothetical source to rule out. If the contaminant is introduced by the processing, the crudest test would be to try devices which were built elsewhere using different techniques. These tests were descibed in in section 8.3, and the two outside devices both showed typical levels of low temperature excess noise. Thus either all three techniques produce the same contaminant, or something in the common measuring environment is introducing the contaminant. One contaminant I have tried to test for qualitaively is the amount of condensed gas which must freeze on the SQUID in the course of its cooling on the refigerator. The cell has been evacuated, as described in Chapter 2, for times as long as 10 hours to as short as 3 hours, with no measurable affect on the noise. Unfortunately, the amount of gas remaining in the cell is not known, and it is not clear what gas could be responsible for the observed effects.

Contaminants are, almost by definition, those materials which are unexpected and not completely under control. This makes it impossible to rule out this hyptothetical source at this time. In my opinion, it remains the most likely source of the low temperature excess noise.

8.4n Motion of Flux Lines in the Body of the SQUID.

The most obvious way to rule out this mechanism would be to test for the presence of flux lines in the SQUID, and also to see if they are moving. The possibility of doing a direct test is discussed in section 8.5 on future work, and has not been done yet.

However, various indirect arguments are possible. First of all, smaller area SQUIDs should tend to have fewer flux bundles in them, simply because the density of flux bundles should be more or less fixed by the static magnetic field at the SQUID. If the bundles moved about independently, then we would expect the noise to scale as the total number of bundles, or equivalently, as the area of the superconducting metal in the device. The effect is somewhat more subtle however as can be seen from the following argument.

Consider a vortex, containing 1 Φ_0 of flux in its core, which is in the body of a SQUID loop as shown in Fig. 8.15. If the vortex starts at point P near the center of the loop and moves to point Q near the outside edge of the loop, the flux coupled into the SQUID will change by an amount of order Φ_0. This change is produced by moving the vortex the distance of the linewidth, ℓ. The transfer function from vortex position to flux in the SQUID is then of order:

$$\partial\Phi/\partial x \propto \Phi_0/\ell$$

Thus, devices with smaller linewidths are more sensitive to the motion of flux trapped in their loop. However, a smaller linewidth also means that there will be less superconduting material. One would therefore expect narrow linewidth devices to have fewer flux bundles present. For a SQUID with outside diameter d, and linewidth ℓ, the total area of the superconducting thin film will be:

$$A_{TF} \propto d^2 - (d-2\ell)^2 = 4d\ell - 4\ell^2$$

If one assumes a constant density of flux vortices, η_f, per unit of superconductor area, then the total number of vortices in the SQUID body is:

$$N_f = 4\eta_f(d\ell - \ell^2)$$

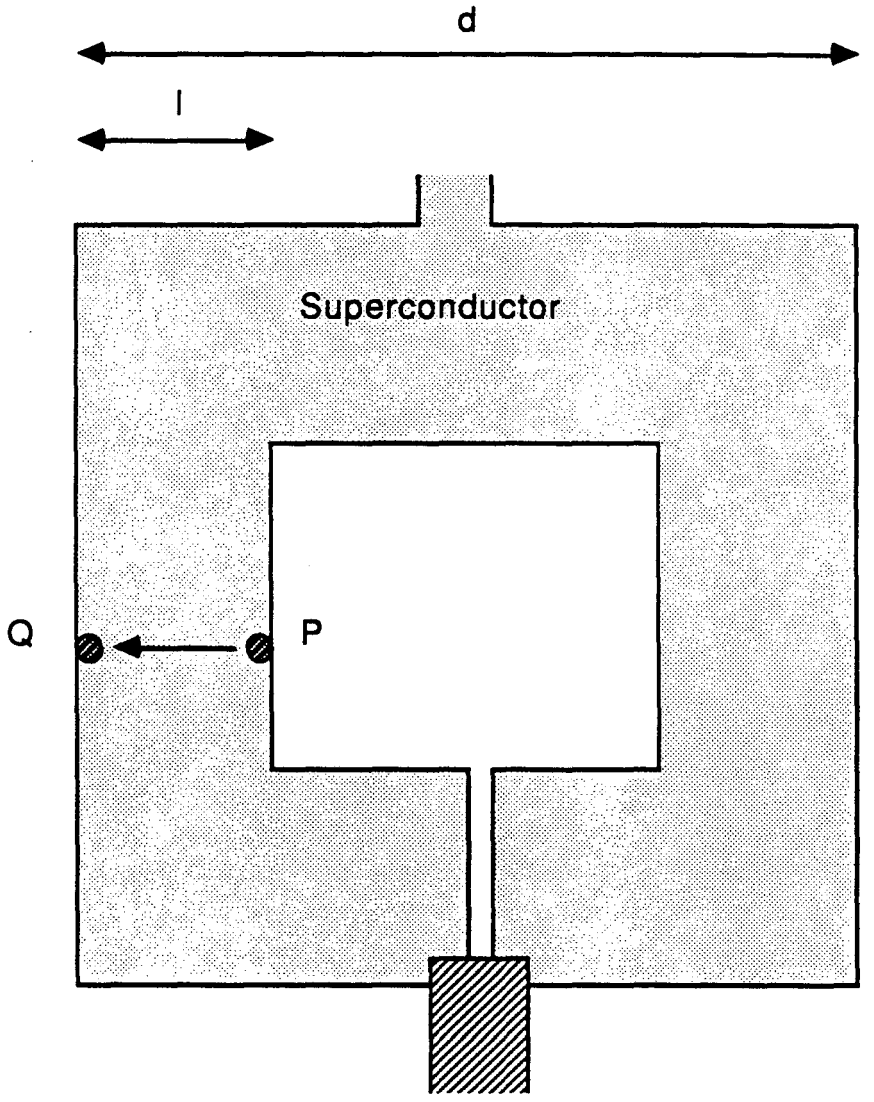

Fig. 8.15 A votex moves from P to Q, causing a change in flux in the SQUID loop.

I will now assume that each vortex undergoes motion such that the spectral density of its position, $S_x(f)$, obeys a 1/f law. Each vortex will then contribute a flux noise of order:

$$S_{\Phi 1}(f) = (\partial\Phi/\partial x)^2 S_x(f) \simeq \Phi_0^2 \, S_x(f)/\ell^2$$

If the vortex motion is independent and incoherent, then the total flux noise produced in the SQUID from the motion of all N_f of the vortices will be just:

$$S_\Phi(f) \simeq N_f \Phi_0^2 S_x(f)/\ell^2 \simeq 4\eta_f(-1 + d/\ell)\Phi_0^2 S_x(f)$$

For devices with small linewidth ℓ, the flux noise should thus increase like d/ℓ. It is interesting to note that this formula is scale invariant (stretching the SQUID by some factor does not alter the expected noise level). Thus, this model naturally explains the approximate device size independence of the low temperature excess noise. Also, experimentally, I find that devices with smaller linewidth do show increased noise. By contrast, if the vortices move coherently, then the total flux noise produced in the SQUID will be just:

$$S_\Phi(f) \simeq N_f^2 \Phi_0^2 S_x(f)/\ell^2 \simeq 16\eta_f^2(d-\ell)^2 \Phi_0^2 S_x(f)$$

This expression does depend upon the size of the SQUID, and accordingly does not fit the observed properties of the excess noise.

While the above incoherent model is encouraging, it should be recognized that it is physically quite implausible. The motion $S_x(f)$ of vortices should also be affected by the presence of pinning sites in the superconductor, the normal metal resistance of the superconductor, the temperature, and the presence of driving currents. The temperature dependence should be thermally activated, which is not consistent with the properties of the low temperature excess noise. Pb, PbIn, and Nb should differ markedly in their pinning properties. In addition, the

pinning force should be so large as to make flux motion impossible at these low temperatures and small driving currents. The Pb and PbIn surfaces in particular are microscopically very rough and should produce deep pinning centers.

The motion of flux bundles is an example of a hyptothetical noise source which can explain scale invariance of the noise, but which does not appear capable of explaining the observed temperature and material dependence. This source cannot be unequivocably ruled out, as we do not have a detailed picture of possible mechanisms. However, in my opinion, it is not the cause of the low temperature excess noise for the reasons stated above.

It is interesting to note that the scale invariance essentially comes from the geometry of the SQUID body and the assumption of a uniform spatial distribution of independent sources on the SQUID body. In fact it matters little whether the sources are flux bundles or some arbitrary source of local magnetic field. Thus the independence of material may reflect the possibilty that the noise is not being generated by flux bundles, but rather by some other source which is not so directly associated with the SQUID body material.

8.4o High Temperature Flux Noise Source.

The occurrence of high temperature flux noise in some of our SQUIDs was discussed in Chapter 7. Because the low temperature excess noise is also a flux noise, it is natural to wonder whether the two are associated. However, it should be recalled that the presence of high temperature flux noise was connected with the Nb in the SQUID loop, and

that replacing the Nb with Pb or PbIn removes the high temperature flux noise. On the otherhand, the low temperature excess noise is present in SQUIDs made with Nb, Pb, and PbIn, and is thus quite independent of the occurrence of the high temperature flux noise.

In addition, some of the properties of the high temperature flux noise are quite different. The high temperature flux noise has a slope which is ordinarily very close to unity, and a 2/3 slope would be very anomalous. Furthermore, the high temperature flux noise seems to decrease at least as fast as T^2 when the temperature is lowered, at least between 4.2 K and 1 K, whereas the low temperature excess noise shows an inverse temperature dependence below 1K. In conclusion, the high temperature flux noise and the low temperature excess noise appear to be completely independent sources of excess flux noise, and although the detailed physical processes are unknown in each case, they are probably distinct.

8.4p Equations of Motion.

Is it possible that the low temperature excess noise is being generated by some dynamical effect arising from the non-linear equations of motion? There are two approaches to this issue. First of all, the observed characteristics of the SQUID are an indication of the equations of motion. Deviations in the I-V are representative of additional terms in the equations of motion. These deviations can commonly arise from the high frequency properties of the circuit to which the SQUID is attached, and would not commonly be expected to generate excess 1/f noise. In fact we have measured excess noise in devices with very large amounts of

structure, and very non-ideal behavior. This noise is of essentially the same nature and magnitude as that which we have measured in devices which were nearly ideal. In fact there does not appear to be any correlation between the level of the excess noise and the amount of structure on the I-V. This mitigates against most dynamical processes, as they usually depend critically on the equations of motion.

Secondly, the characteristic frequency of the SQUID is set by the Josephson frequency. It is generally difficult to produce universal low frequency noise in a system with a vastly shorter time scale. In particular, most dynamical 1/f models are very sensitive to the bias point, due to the fact that the noise arises from mixing terms in the non-linear equations of motion. In addition, by sweeping the Josephson frequency over a large range one would expect the frequency dependent inpedances of the circuit to change, and produce a corresponding effect in any noise mechanism. Experimentally however, we have observed excess noise from Josephson frequencies of 350 MHz to about 10 GHz, and its magnitude is apparently independent of the bias.

Thirdly, it is difficult to understand why the temperature dependence and slope of the noise would be affected by changing the shape of the device, but not the device parameters. The shape after all does not enter directly into the equations of motion.

In conclusion, the low temperature excess noise does not have any symptoms which would indicate it is generated by a dynamical SQUID mechanisms. In addition, it has some behavior which appears to be difficult to explain in a dynamical context. However, I can not make any more rigorous statement, owing to the number of model circuits which may be considered.

8.4q Secondary Parameter Fluctuations.

There are various secondary parameters which may also be thought of as hypothetical sources, for example the dynamic resistance or the flux gain.[15] Such parameters are determined by the SQUID equations, and as such their fluctuation can always be ascribed to changes in the equations of motion or fluctuations in the primary SQUID parameters. In this sense I have already considered their effects above. However, such fluctuations would generally be the result of correlated fluctuations in several parameters, and this makes the analysis more complicated. I will consider only two such cases explicitly.

Bias Power. By varying the bias voltage of the SQUID, I can vary the power being dissipated in the SQUID. As such, the fact that the noise has been found to be independent of the bias voltage means that it is also independent of the power being dissipated in the SQUID. For example, as was discussed in section 8.4e, device E1 at T = 95 mK, had its bias voltage varied from 1.8 μV to 6.8 μV, with no measurable change in the excess noise level. Since the dynamic resistance is large at these low biases and temperatures, the current is practically unchanged, and the ratio of the voltages will then be almost the same as the ratio of the power dissipated. In this case, then, the power dissipation in the SQUID was altered by a factor of about 3.8, and there was no measurable effect on the level of the excess noise.

Temperature: The temperature enters directly into the SQUID equations of motion through the Nyquist noise terms V_{n1} and V_{n2}. In the dimensionless equations, this introduces a term of the form $\Gamma = I_o T/e\Phi_o$ and thus the effects would scale with I_o. No such scaling with I_o is

observed.

However, the temperature also enters indirectly into the equations of motion, and can lead to correlated changes in several SQUID parameters. It is useful to have a bound on the magnitude of the cell's temperature fluctuations. N. Wang[16] has taken temperature fluctuation spectra on a neutron transmutation doped Ge thermistor (NTD #12, 7-24-88) at 25 mK. The resistor was glued with conducting epoxy to a Cu holder which was bolted to the outside of the Cu cell. The Ge resistors are doped almost to the degeneracy level, and have a temperature dependent resistivity which behaves as:[17]

$$R = R_0 \, e^{[\Delta^{1/2} \cdot T^{-1/2}]} \qquad (8.1)$$

where for the given thermistor, N. Wang has measured:

$$\Delta = 6.25 \text{ K} \qquad \text{and } R_0 = 0.5 \text{ M}\Omega$$

The current vs. voltage characteristic of the resistors are quite non-linear, and the above relation is for the low voltage portion of the curve. The resistor was operated slightly into the non-linear regime at a constant current bias of I = 0.5 nA and V_{dc} = 1.13 mV. The voltage across the Ge resistor was buffered by a X1 differential opamp pair, amplified X100 by a PAR 113, and then fed into an HP 3582A spectrum analyzer. The voltage noise spectrum was flat above about 10 Hz (with the exception of a 2 μV rms 60 Hz peak and a few harmonics), with an amplitude:

$$S_V^{1/2}(f) = 37 \text{ nV Hz}^{-1/2}$$

Below 10 Hz, the spectrum scaled as $1/f^2$, corressponding to a slow drift in the mixing chamber's temperature. The noise above 10 Hz is produced almost entirely by the buffer amplifier and PAR 113, and so the above

noise merely places an upper limit on the temperature fluctuations of the cell. From Eq. 8.1 one can convert the measured voltage fluctuations into equivalent temperature fluctuations. One finds:

$$S_T^{1/2}(f>10Hz) \leq 0.11\ \mu K\ Hz^{-1/2}$$

By measuring the SQUID I-V characteristics at different T, one can find $\partial I/\partial T$ for fixed flux bias current $I_{\phi 1}$, and fixed bias voltage V. The temperature fluctuations can then be converted into an equivalent flux noise in the SQUID by using:

$$S_\phi^{1/2}(f) = S_T^{1/2}(f)\cdot \partial I/\partial T\cdot \partial \phi/\partial I$$

Now $\partial I/\partial T\cdot \partial \phi/\partial I$ is generally quite small below 1 K, being typically much less than $10^{-2}\ \phi_0/K$. If I take a very conservative estimate of $10^{-1}\ \phi_0/K$, then the limit on the thermally generated excess noise in the SQUID is:

$$S_\phi^{1/2}(f) = 1.1 \times 10^{-8}\ \phi_0\ Hz^{-1/2}$$

This is a very low level, and is much too small to account for the observed magnitude of the low temperature excess noise.

8.4r Fluctuations in the Fundamental Constant ϕ_0

It is interesting to note that the fundamental parameter ϕ_0 also occurs in the equations of motion. Leaving aside the very serious experimental and theoretical objections one could raise to a variation in this parameter, let me naively examine whether such a hypothetical variation could produce the low temperature excess noise.

First of all, the parameter ϕ_0 enters into the SQUID equations in the parameters β, β_c and ϕ. Fluctuations in β and β_c would not produce flux-like noise. On the otherhand, fluctuations in ϕ are flux noise. The

magnitude of the fluctuating reduced flux will scale directly with the flux that is passing through the SQUID. Thus a device which had 10Φ of flux in it would be 100 times noisier in the power than a device with just Φ in it. If we assume that the typical trapped magnetic field in our configuration is more or less the same from one cool down to the next, then our large area SQUIDs will typically have something like 600 times (the ratio of the largest area to the smallest area) more flux in them than the smallest SQUIDs. One would accordingly expect to see 600 times more rms noise in the larger SQUIDs. No such rapid dependence is seen, and I conclude that variations in Φ_0 are not the source of the low temperature excess noise.

8.4s Applied Magnetic Field During Cooling

In a typical run, the SQUID is surrounded by two μ-metal shields (see Chapter 2). These reduce the static field at the SQUID to less than 2 μT. The SQUIDs are cooled through the superconducting transition in this reduced field to prevent large amounts of trapped flux permeating the SQUID and the superconducting shields. It is unlikely that the Meissner effect is complete in the Nb shield tube and, as a result, a substantial fraction of the reduced field is probably trapped in the Nb. We have also occasionally cooled SQUIDs through the superconducting transition without using the μ-metal shielding, as for example, in a test run with device A1 (7-6-85). In such a situation the field trapped in the Nb shield must probably be of order the Earth's magnetic field, about 40μT. After cooling below T_c, the shields were replaced, so as to reduce external noise. No affect on the level of the excess noise was

observed compared with the excess noise seen on earlier runs where the μ-metal shields were kept in place during cooling.

In connection with the flux vortices discussed above, it is interesting to note that a type A SQUID cooled in a 2 μT field would enclose about 800 Φ_0. The smallest SQUID, a Type O, would enclose less than 2.5 Φ_0. It is unlikely that 2 or 3 flux vortices could produce a good $1/f^{2/3}$ spectrum, as 1/f type spectra are ordinarily built out of a large number of Lorentzians. Also, 2 μT is a conservative estimate for the trapped field, in which case it is likely that there are no trapped vortices in the smallest SQUIDs.

8.5 Suggestions for Future Work

Since there is still much to be learned about the low temperature excess noise, it is of interest to mention some experiments that would yield important new information.

Probably the most important work to be done is to test more SQUIDs from other laboratories. The best test would be for other groups to measure the noise in their own SQUIDs in the range below 1K. This would also supply an excellent check on the measuring system and cell.

In fact, the region down to 0.3 K is readily acessible with a Helium 3 system, and already much could be revealed about the presence or absence of low temperature excess noise from such measurements. It is somewhat puzzling that such a modest effort has not been undertaken by others. It should be recognized however, that many SQUIDs do not work well below 1 K. The most common commercial SQUIDs will usually not even work over the range from 1 to 4.2 K. These devices are made with

self-shunting junctions which have a very large temperature dependence. Most SQUIDs also seem to be made with "resistive" shunts which go superconducting at around 0.4 K (shunts of AuIn, Ti), or 1 K (shunts of Mo), thus rendering the SQUIDs inoperable at a fairly high temperature.

Another experiment would be to cool down two SQUIDs and test for correlations in their noise. This would prove definitively that the noise was local in character, and was not being driven by some external disturbance.

A careful study of the noise in the presence of large and known magnetic fields, would also be very interesting. This would be a good test for spin glasses (see section 8.6 below), because it is expected that the noise spectra should show large effects in even fairly low fields of a few tenths of mT.

Another interesting (but difficult) experiment would be to heat the SQUID body only in small regions and see if the excess noise level was affected. As I noted above, the excess noise is not dependent on the resistor temperature, but rather on the temperature of the body. If one could heat up the body to say 1 K, while keeping the shunts cold, one would expect the excess noise to be as small as it is at 1 K, and the device should have small noise. With sufficient care, one could localize the source of the noise by heating small regions and seeing where the excess noise is affected.

Another experiment that would be very interesting is to construct what I call a scanning SQUID or flux microscope. This would be a small SQUID which is mounted so as to face a moveable platform. The platform would support a sample in close proximity to the SQUID loop. By moving the platform with respect to the SQUID, one could scan the local

magnetic field near the sample, obtaining a spatial picture of the magnetic field. With careful alignment and a small measuring SQUID, one should be able to obtain 10 μm resolution fairly easily. With such a device, one could search for the presence of trapped flux, map out the distribution of current flowing in the SQUID body, do local susceptometry tests on the Nb and substrate, and measure the local magnetic noise as a function of position. In this way, one could directly test for flux bundles, and locate the position of the source of the low temperature excess noise. The device is interesting in its own right, and I think it will be a useful invention. One can easily conceive of other applications, such as local NMR, local thermometry, or local conductivity measurements. I have made preliminary tests on a crude 4.2 K model, and the idea seems to be sound. The platform was a fiberglass block which held a sample about 0.5 mm from the SQUID, and which was moved on a slide-rod by a fiberglass pushrod. The pushrod went to the top of the dewar where it was connected to a micrometer, allowing me to control the motion of the platform in one direction. The SQUID was run in a locked-in configuration using the 4.2 K test insert 500 kHz electronics (see Chapter 2). During tests on a Nb thin-film sample, I was able to maintain lock over a few mm of travel while the feedback output varied up and down by about Φ_0.

Another interesting experiment would be to test for the excess noise in an rf SQUID. This would be a good test because the equations of motion are very different for an rf SQUID, and one could thereby hope to rule out dynamical models. The problem here is that the white noise in the rf SQUID is so much higher that one would have a difficult time detecting the presence of the expected level of excess noise. However,

the noise in the rf SQUID is largely determined by the tank circuit and preamplifier. One could adopt the highly unusual expedient of using a low noise dc SQUID as the preamplifier to measure the noise in the rf SQUID.

It would be of considerable interest to construct a SQUID with several loops connected in series. As was discussed above, data on SQUID P1, which had 10 loops connected in series, suggested that the noise scaled as roughly the number of loops. By connecting loops in parallel, one can essentially produce a fractional number of loops. The incoherent sum of the noise from 10 loops in parallel should be 10 times smaller than the noise in a single loop. The inductance will also be 10 times smaller, so that the noise energy due to the excess noise should be unchanged. SQUIDs with lower L have lower white noise, so that there is some advantage to pursuing such a construction

There are a great many other tests that could be done, and the area is wide open for experimental work.

8.6 Concluding Remarks

The origin of the low temperature excess noise remains unknown. Investigation of the known materials in the SQUID has not yielded the source. Investigations of the SQUID parameters has ruled out virtually all of them. Many of these investigations have involved at least two independent tests for the effects. Fig. 8.16 summarizes our unsuccessful search for the source. There is nonetheless one (difficult to understand but reproducible) way to alter the level of the noise, by changing the geometry of the SQUID loop. This connection is one path which may lead

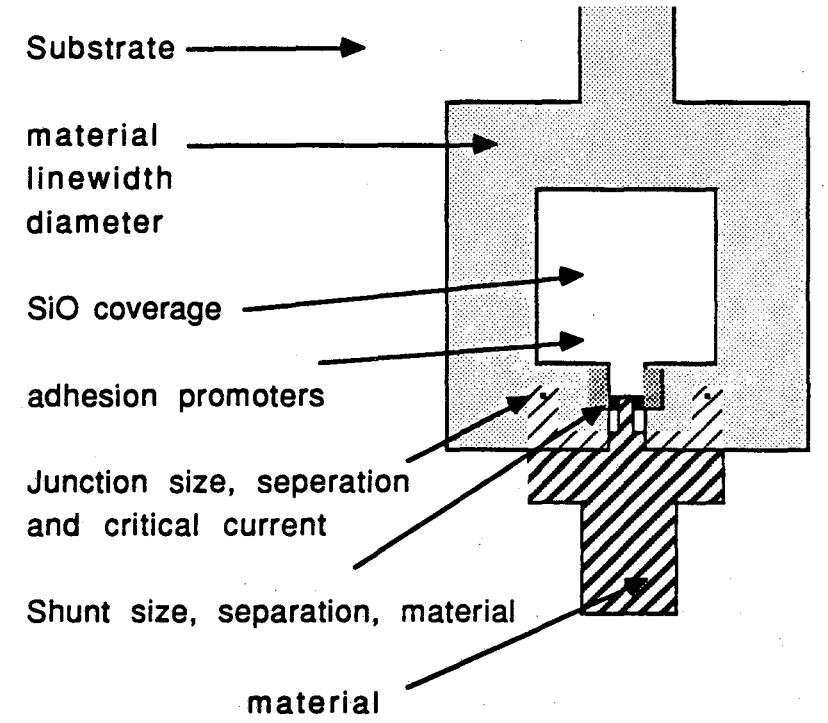

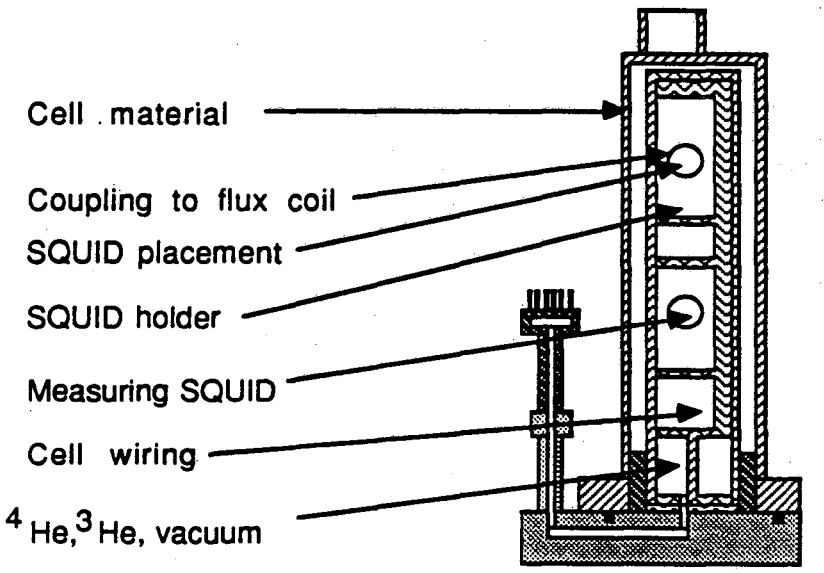

Fig. 8.16 Parts tested for sources of low temperature excess noise.

to the identification and removal of the low temperature excess noise.

One broad class of sources we have been able to examine in general are possible external sources of magnetic noise. If the source is far from the SQUID, then it will of necessity produce a field which is uniform across the SQUID at the low frequencies we are concerned with here. The resulting flux noise power in the SQUID would then scale with the square of the SQUID area. Since no such dependence is seen, we can categorically rule out the possibility that the noise is being generated by a distant source. Distant, in this case, means on the length scale of the SQUID diameter. If the source is closer than the SQUID diameter, then the above argument will fail because the magnetic field may vary over the SQUID diameter.

A strong candidate for a local source would be the presence of a spin-glass[18] contaminant on the surface of the SQUID or chip. Spin-glass systems have recently been shown to exhibit $1/f^m$ noise (with $0.6 < m < 1.0$) [5,19] that increases in magnitude as the temperature is lowered through the transition temperature.[19] Noise in a spin-glass system can also exhibit changes in slope which are very similar to those seen in Fig. 8.12 or Fig 8.9. The slope changes occur on passing through the glass transition.[19] I note that the increase in the noise as the temperature is lowered over a certain range mitigates against many phenomena, for example, thermally activated flux motion. However, spin-glass systems can show a similar anomalous inverse temperature dependence to the noise. If a spin-glass is indeed the source of the noise, the fact that the noise does not depend on the area of the SQUID implies that the material must be very close to the SQUID.

One important conclusion that can be drawn from the above discussion

is that none of the hypothetical parameter sources generates any appreciable excess noise at low temperatures. This is encouraging because it suggests that once the source of the low temperature excess noise is found and eliminated, there will be no other comparable source of excess noise left in the dc SQUID. With the source of the low temperature excess noise still unknown, this is the most optimistic conclusion that can be drawn.

It should be recognized that many of the tests were done simultaneously. This occasionally complicates the interpretation, for if the noise were to dissappear we would not know which parameter had produced the effect. This is the chief difficulty with finding why the smaller devices have lower noise, or why the split devices can generate different slopes. By necessity, when one alters the geometry of a device, a great many things are changed simultaneously, and it is difficult to isolate one effect from the other. This fact, in part, accounts for the multiple tests that were applied to the devices.

References

(1) Portions of the work presented in this chapter have been published in ref. 2 and: F.C. Wellstood, C. Urbina, and J. Clarke "Low Frequency Noise in Superconducting Quantum Interference Devices Below 1 K", Appl. Phys. Lett. 50, 772 (1987).

(2) F.C. Wellstood, C. Urbina, and J. Clarke, " Excess Noise in dc SQUIDs, From 4.2 K to 0.022 K", IEEE Trans. Magn., Vol. Mag-23, 1662 (1987).

(3) For example: M. Bassan, W. M. Fairbank, E. Mapoles, M. S. McAshen,

P. F. Michelson, P. Moscowicz, K. Rall, R. C. Taber, Proc. of the Third Grossamer Meeting on General Relativity, North Holland 1983.

(4) R. H. Koch, J. Clarke, W. M. Goubau, J. M. Martinis, C. M. Pegrum, and D. J. Van Harlingen, "Flicker (1/f) Noise in Tunnel Junction dc SQUIDs", J. Low Temp. Phys. 51, 207-224, 1983.

(5) M. Occio, H. Bouchiat, and P. Monod, "Observations of 1/f Magnetic Fluctuations in Spin Glasses", J. of Magnetic Materials 54-57, 11 (1986).

(6) For a collection of 1/f results, models and theories see: "Noise in Physical Systems, and 1/f Noise", A. Damico and P. Mazzetti eds., North-Holland Physics Publishing, New York (1986).

(7) P. Dutta and P.M. Horn, "Low Frequency Fluctuations in Solids: 1/f Noise", Rev. Mod. Phys. 53, 497 (1981).

(8) I thank M. Wiessmann for reminding me of the importance of this section, private communication.

(9) See references in: B. Muhlfelder, J.A. Beall, M.W. Cromar, R.H. Ono, and W.W. Johnson, "Well Coupled, Low Noise dc SQUIDs", IEEE Trans. Magn., Mag-21, 427 (1985).

(10) J. Knuutila, M. Kajola, R. Mutikainen, J. Salmi, Extended abstracts of the 1987 Int. Superconducting Electronics Conf., Tokyo, 261 (1987).

(11) C. T. Rogers and R. A. Buhrman, "Nature of Single-Localized-Electron States Derived from Tunneling Measurements", Phys. Rev. Lett. 51, 859-862, 1985.

(12) R. T. Wakai and D. J. Van Harlingen, "Low-frequency Noise and Discrete Charge Trapping in Small Area Tunnel Junction dc SQUIDs", Appl. Phys. Lett. 49, 593 1986.

(13) S. M. Sze, "Physics of Semiconductor Devices", John Wiley and Sons,

New York (1981).

(14) M.B. Simmonds "Magnetic Properties of Construction Materials: Observations Made While Developing a Susceptometer", Proc. SQUID Magnetometer Workshop, Coolfont, 89 (1984).

(15) Tesche seems to have been the first to consider this case explicitly: C. D. Tesche, "Parameter Fluctuations and Low Frequency Noise in Josephson Junction Devices", Appl. Phys. Lett. 41, 99-100, 1982.

(16) N. Wang, B. Sadoulet, T. Shutt, J. Beeman, E.E. Haller, A. Lange, I. Park, R. Ross, C. Stanton. and H. Steiner, "A 20 mK Temperature Sensor". Presented at IEEE Nuclear Symposium, San Francisco, 1987, to be publ. in IEEE.

(17) This law is of the form found for modified variable range hopping. The interested reader can consult: B.I.Shklovskii and A.L. Efros, "Electronic Properties of Doped Semiconductors", Springer Series in Solid State Physics Vol. 45, Springer-Verlag, New York (1984).

(18) For more information on spin glasses, the interested reader can consult: D. Chowdhury, "Spin Glasses and Other Frustrated Systems", Princeton University Press, (1986).

(19) W. Reim, R. H. Koch, A. P. Malozemoff, M. B. Ketchen, and H. Maletta, "Magnetic Equilibrium Noise in Spin-Glasses: $Eu_{0.4}Sr_{0.6}S$", Phys. Rev. Lett. 57, 905-908, 1986.

Chapter 9: Hot Electron Effect in Normal Metals: Theory

9.1 Introduction

There has been considerable experimental effort directed toward obtaining dc SQUIDs with sensitivities limited only by the Heisenberg uncertainty principle. The equation governing all of these attempts is the classical thermal result of Tesche and Clarke:[1,2]

$$\varepsilon_V \propto 16k_BT(LC)^{1/2} \qquad (9.1)$$

where : $\varepsilon_V = S_\Phi/2L$ is the intrinsic SQUID energy sensitivity [3]

L = SQUID loop inductance

C = SQUID junction capacitance

T = temperature

S_Φ = flux noise spectral density in the SQUID

Although ε_V is known to be an inadequate figure of merit, it is easily measured and can be used to estimate the true energy sensitivty ε (see Chapter 0).[3,4]

The original approach to low noise SQUID design was to decrease C by making the tunnel junctions as small as was photolithographically possible and also to simultaneously reduce L. This approach has been recently extended to the use of submicron edge tunnel junctions by Wakai and Van Harlingen.[5] Unfortunately, all of these devices presently suffer from two problems: (1) the small inductance makes these devices difficult to actually use as amplifiers, and (2) there is a high level of 1/f noise which has meant that the SQUIDs approached the quantum limit only for $f \gtrsim 1$ Mhz. By using double transformer input circuits,[6] or multiloop SQUIDs[7] different research groups have begun to use dc

SQUIDs with inductances as low as 15 to 30 pH in sensitive applications. The second difficulty remains in these devices however, and in addition, because of the complicated input circuits, the devices display considerable resonant structure.

For the past four years we have undertaken a different technique which has yielded large inductance SQUIDs with substantially superior performance above 10 kHz. Our procedure is to:

(1) retain a large SQUID inductance so that the device may be easily coupled to,

(2) retain 4 μm^2 junction windows which can be produced photolithographically,

(3) reduce the final variable, the temperature T, to 20 mK using a dilution refrigerator.

This approach is not without its difficulties. In the previous Chapter I described the puzzling and highly unusual behavior of the low temperature excess noise which is present below 1 K. We still do not know the cause of this excess noise, and it is admittedly still the largest source of noise in our SQUIDs at 1 kHz and at low temperature. However, by testing a large number of SQUIDs with different shapes, sizes, and materials I have been able to find a particular geometry which gives consistently lower 1/f noise for f > 1 kHz. These are the Type D and M SQUIDs. I soon discovered that these devices had a second problem: although at relatively high temperatures the white noise decreased like T as the temperature was lowered (as expected from the classical thermal result), cooling below 150 mK did not produce any additional decrease in the white noise. Evidently this problem also occurred in the SQUIDs with higher levels of low temperature excess

noise, but it was hidden in the large amount of excess noise. It is only in SQUIDs with a low level of excess noise that we can hope to see that the white noise levels off.

I have attributed this levelling off of the white noise as due to the shunts heating above the bath temperature, as will be discussed in detail in Chapter 11. The heating is caused by the applied bias voltage across the SQUID. The power that this voltage generates is very small. It is so small that it does not seem possible to explain the heating as being due to a conventional Kapitza thermal boundary resistance.[8] Rather, it appears that the heating is due to the electrons being driven out of equilibrium with the phonons. This effect is virtually unknown in normal metals at higher temperatures because the electrons and phonons are effectively well-coupled. At low temperatures however, the effective coupling is much weaker and the effect becomes very prominent in small samples.

In this Chapter, I discuss the mechanism for electron cooling at low temperatures. In the following two chapters, I will present experimental evidence for the presence of these "Hot Electron Effects", and I will compare the theory with experimental data.

9.2 Simple Theory of Hot Electrons in Normal Metals: Assumptions

Consider two thermodynamic systems coupled together by an interaction, see Fig. 9.1. If power P is applied to one of the systems then it will heat up until it is transferring power P into the second system. If the coupling is weak the two systems will be driven out of equilibrium and there will be well defined, but different, temperatures

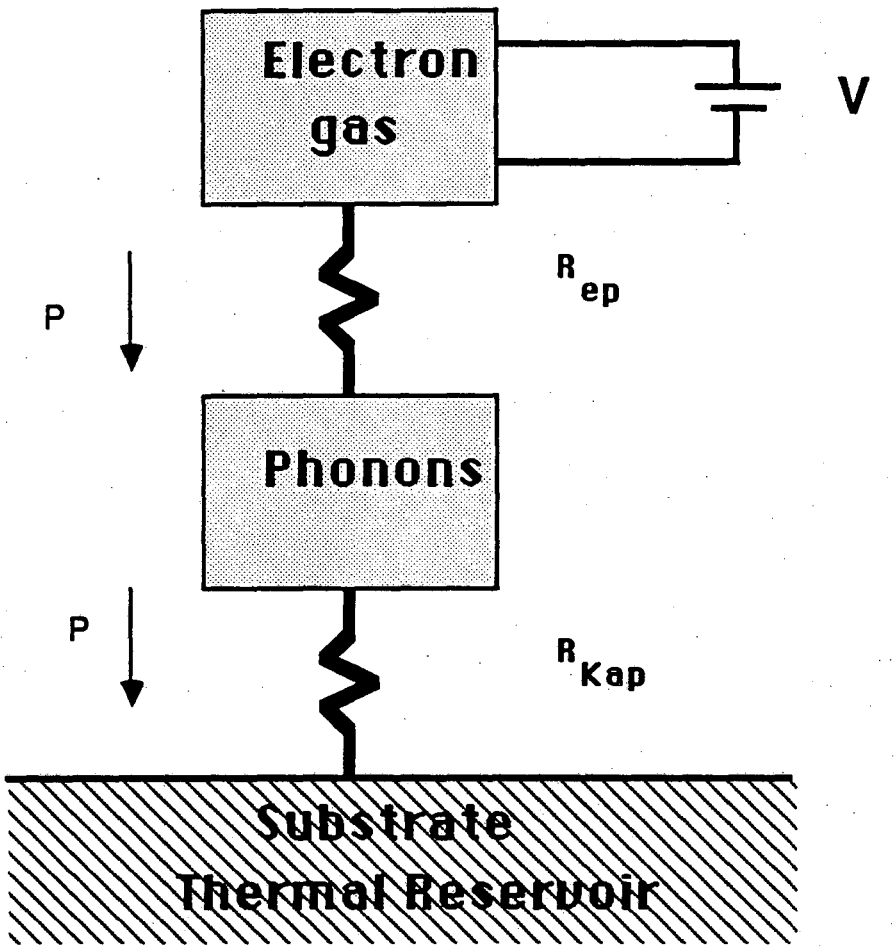

Fig. 9.1 Schematic of thermal system in a metal. Power P is applied to the electrons by means of battery voltage V, causing the electrons to heat. Power flows from the electrons to the phonons through the thermal resistance R_{ep} which is mediated by the electron-phonon interaction. Phonons then transport the heat to the electrically insulating substrate through the Kapitza thermal resistance R_{Kap}.

for each system. The electrons and phonons in a normal metal can be thought of as two such systems which are coupled together by the electron-phonon interaction. Application of a voltage to the metal transfers energy to the charged electrons, but not directly to the phonons. It is only by emitting or scattering phonons that the electrons can release this energy to the phonons. The phonon system itself is generally thermally coupled to some other large thermal reservoir. We will take this reservoir to be a second phonon system, the substrate or bath phonons, and the coupling is then described by a Kapitza thermal boundary resistance, R_{Kap}. We can similarly formally define a thermal resistance between the electrons and the phonons, R_{ep}.

Standard low temperature heating occurs when the phonons in the metal become much hotter than the phonons in the reservoir. This will be the case when $R_{Kap} >> R_{ep}$ and sufficient power is applied. On the otherhand, when $R_{ep} >> R_{Kap}$ and power is applied, the temperature difference will be greatest between the electrons and the phonons. Hot electron, or non-equilibrium, effects are well-known in semiconductors.[9] The small carrier concentration means that each electron recieves proportionately more energy, and R_{ep} is correspondingly large. W.A. Little appears to have been the first to estimate the size of the hot electron effect in normal metal.[8] The effect was apparently first seen experimentally as a "hot phonon" effect,[10-12] by researchers who were studying the behavior of heat exchangers for use in dilution refrigerators. More recently Roukes et al.[13] have observed a "hot electron" effect in a thin Cu film using a SQUID readout similar to the configuration we describe below. Roukes et al. have also provided a simple heating model of the effect based on an

argument by P.W. Anderson et al..[14]

The theory presented below yields a simple and tranparent expression which is exact for the assumptions made and clearly shows the dependence of the effect on the parameters of the normal metal. There exist more complicated models which do not assume that the baths have well-defined temperatures.[15] It turns out that a well-defined electron temperature is a good approximation however,[15] and so I will take this as given. I make the following assumptions:

(1) The electron gas is at some well-defined temperature T_e which is much less than the Fermi temperature T_F.

(2) The phonons are at some well-defined temperature T_p which is much smaller than the Debye temperature θ_D.

(3) The Fermi surface is spherical and the electrons have a parabolic energy band.

(4) The electron-phonon interaction is a scalar deformation potential,[16] and I can neglect Umklapp processes.

(5) The dimensions of the metal are much larger than the average thermal phonon wavelength.

Assumptions (1-4) are actually most reasonable in the low temperature regime, the regime we are interested in. Assumption (1) is well-satisfied for any ordinary normal metal. Assumption (2) implies that we need only consider the acoustic phonons. These phonons have a simple linear dispersion relation; phonons with wavevector $\bar{q}$ have an energy $\varepsilon_q = \hbar sq$, where s is the speed of sound. Similarly, assumption (3) means that I will take a quadratic dispersion relation for the electrons, electrons of wavevector $\bar{k}$ and effective mass m^* will have energy $E_k = \hbar k^2/2m^*$. Assumption (4) means that only the longitudinal

acoustic phonons will be important, as the transverse modes do not couple via the deformation potential. A brief discussion of the deformation potential and its matrix elements has been included in Appendix A.

A few comments are in order about the applicability of these assumptions to the noble metals. First of all, the quadratic dispersion relation implies a spherical Fermi surface, a constant Fermi velocity on the surface, and a uniform density of states at the Fermi level. On the otherhand, the Fermi surface of the noble metals is distinctly nonspherical, with prominent necks connecting spheres in a multiply connected surface.[17] These details are not too serious for the problem considered here, as one can take the experimentally determined parameters for the surface averaged density of states and Fermi velocity.

A more serious problem is that a scalar deformation potential is not always a good approximation to the electron-phonon interaction.[18] In particular, in the noble metals the transverse modes can couple to the electrons at the necks of the Fermi sphere. This leads to a substantial increase in the scattering rate at the necks. It should be possible to extend the approach to the case of a nonscalar interaction potential. Nonetheless, I will take the scalar deformation potential because it is the simplest realistic model interaction. The matrix for this interaction can be written as:

$$|M|^2 = |M_0|^2 q/\Omega \qquad (9.2)$$

where: $\bar{q}$ is the phonon wavevector, and M_0 is independent of $\bar{q}$ and may be approximated by:

$$M_0^2 = \frac{\hbar}{2\mu s} \left[\frac{2\varepsilon_F}{3} \right]^2 \qquad (9.3)$$

where: μ is the mass density per unit volume of the metal, ε_F is the Fermi energy, Ω is the volume of the sample, and s is the speed of sound (see Appendix A).

An additional simplifying assumption I will make is that I can ignore Umklapp processes. In the case of the noble metals this assumption is not entirely reasonable. At the necks on the Fermi surface, electrons can scatter out of the first Brillouin zone by making arbitrarily small changes in wavevector. Such a scattering event corresponds to an Umklapp process. Although Umklapps are very important for momentum transfer, due to the large resulting wavevector change when the scattered electron is translated back into the first Brillouin zone, no such enhancement occurs in the energy transfer. As a result, the effect of the Umklapp processes should be minor for the problem at hand.

9.3 Calculation of Energy Loss Rate

The basic microphysical processes which transfer heat between the electrons and the phonons are shown in Fig. 9.2. In Fig. 9.2a an electron with wavevector $\bar{k}$ and energy E_k emits a phonon of wavevector $\bar{q}$ and energy ε_q, and the electron leaves with energy $E_{k'}$ and wavevector $\bar{k}' = \bar{k} - \bar{q}$. In Fig. 9.2b, an electron with energy E_k absorbs a phonon of wavevector $-\bar{q}$ and energy ε_q, and leaves with an energy $E_{k'}$ and wavevector $\bar{k}' = \bar{k} - \bar{q}$. Again, I have entirely ignored umklapp transitions, so that the wavevectors are strictly conserved.

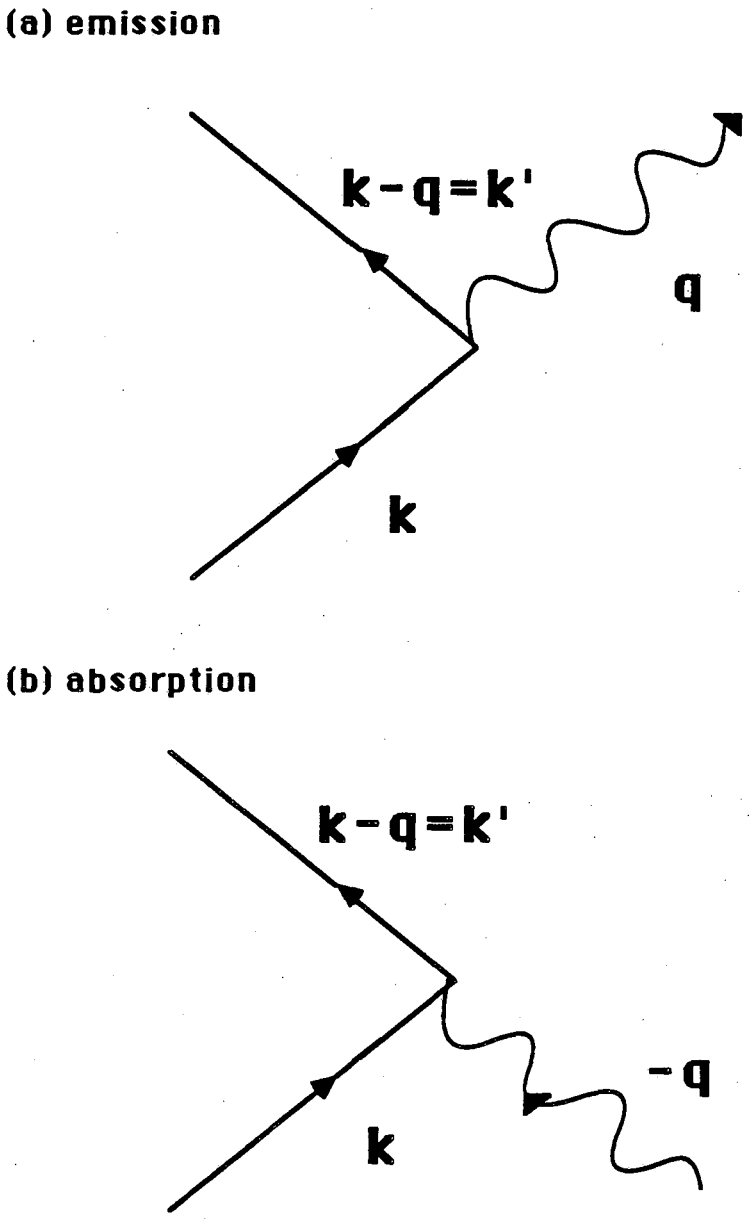

Fig. 9.2 (a) Emission , and (b) absorption of phonons by an electron of wavevector $\bar{k}$.

Consider the rate at which an electron with wavevector $\bar{k}$, is scattered to wavevector $\bar{k}' = \bar{k} - \bar{q}$ with the emission of a phonon of wavevector $\bar{q}$. With the assumptions (1) through (4), and an application of Fermi's golden rule, this rate can be written as:[19]

$$\tau^{-1}_{kk'} = \frac{2\pi}{\hbar} M^2 \delta(E_k - E_{k'} - \varepsilon_q)(1-f(E_{k'}))(n(q)+1) \qquad (9.4)$$

where: $\varepsilon_q = \hbar sq$ is the phonon energy, f(E) is the Fermi-Dirac distribution, n(q) is the Bose-Einstein distribution, (1-f) is the probability that the final state $\bar{k}'$ is empty, and (n+1) is the stimulated plus spontaneous emission rate factor. The rate at which an electron loses energy in this transition is therefore:

$$dU_{kk'}/dt = -\varepsilon_q \tau^{-1}_{kk'} \qquad (9.5)$$

Summing over all allowed phonon $\bar{q}$, one obtains the total energy loss rate for an electron of wavevector $\bar{k}$:

$$dU_k/dt = \Sigma_{q'} dU_{kk'}/dt \qquad (9.6)$$

Now summing over all of the initial electron states, one obtains the total rate at which the electron gas emits energy:

$$P_{emitted} = -\Sigma_k f(E_k)\, dU_k/dt \qquad (9.7)$$

I now express the summations as integrals over the appropriate density of states and write:

$$P_{emitted} = \int_{-\infty}^{\infty} f(E_k) D_e(E_k) dE_k \int D_p(\bar{q}) \varepsilon_q \frac{2\pi}{\hbar} |M|^2 \delta(E_k - E_{k'} - \varepsilon_q) X$$
$$X(1-f(E_{k'}))(n(q)+1) d^3\bar{q} \qquad (9.8)$$

where $D_e(E_k)$ is the electron density of states at energy E_k, and $D_p(\bar{q})$ is the phonon density of momentum states.

Similarly, the rate at which the electron gas will absorb power from

the phonons is:

$$P_{absorbed}=\int_{-\infty}^{\infty} f(E_k)D_e(E_k)dE_k \int D_p(\bar{q})\varepsilon_q \frac{2\pi}{\hbar} |M|^2 \delta(E_k - E_{k'} + \varepsilon_q)(1-f(E_{k'}))n(q)d\bar{q}^3 \tag{9.9}$$

The net rate at which power is emitted by the electrons is thus:

$$P = P_{emitted} - P_{absorbed} \tag{9.10}$$

$$P = \int_{-\infty}^{\infty} f(E_k)D_e(E_k)dE_k \int D_p(q)\varepsilon_q \frac{2\pi}{\hbar} |M|^2 (1-f(E_{k'})) \cdot \left[(n(q)+1)\delta(E_k - E_{k'} - \varepsilon_q) - n(q)\delta(E_k - E_{k'} + \varepsilon_q) \right] d\bar{q}^3$$

This expression can be put in the form:

$$P = P_o(T_e) - P_1(T_p, T_e) \tag{9.11}$$

where:

$$P_o(T_e) = \int_{-\infty}^{\infty} f(E_k)D_e(E_k)dE_k \int D_p(\bar{q})\varepsilon_q \frac{2\pi}{\hbar} |M|^2 \delta(E_k - E_{k'} - \varepsilon_q)(1-f(E_{k'}))d\bar{q}^3 \tag{9.12}$$

$$P_1(T_e, T_p) = \int_{-\infty}^{\infty} f(E_k)D_e(E_k)dE_k \int_{-\infty}^{\infty} D_p(\bar{q})\varepsilon_q \frac{2\pi}{\hbar} |M|^2 n(\varepsilon_q)(1-f(E_{k'})) \cdot \left[\delta(E_k - E_{k'} - \varepsilon_q) - \delta(E_k - E_{k'} + \varepsilon_q) \right] d\bar{q}^3 \tag{9.13}$$

The first term describes the rate at which the electron gas emits energy when the phonon gas is at zero temperature. The second term includes all of the effects of a finite phonon temperature. The integrands in both terms are highly peaked about $E = \varepsilon_F$, the Fermi energy. This leads to

considerable simplification, and the integrals can be calculated exactly for the assumptions made.

As is shown in Appendix B, one finds for P_o:

$$P_o(T_e) = \Sigma \, \Omega \, T_e^5 \tag{9.14}$$

where:

$$\Sigma = \frac{M_o^2 \, D(\varepsilon_F) k_B^5 \Gamma(5) \xi(5)}{2\pi\hbar^5 s^3 v_F \Omega} \tag{9.15}$$

$\Gamma(n) = (n-1)(n-2)\cdots(1)$ is the gamma function

$\xi(n)$ = Riemann zeta function, $\xi(5) \approx 1.037$

Ω is the volume of the normal metal

The expresssion for Σ can be simplified considerably by noting that the electronic heat capacity per unit volume is just $c_{el} = \gamma T_e$ where γ is given by:

$$\gamma = \frac{\pi^2}{3\Omega} \, D_e(\varepsilon_F) k_B^2 \tag{9.16}$$

where $D_e(\varepsilon_F)$ is the density of electron states at the Fermi level (not per unit volume, but per unit energy). V.F. Gantmakher[19] has defined the thermal average electron-phonon scattering rate as $\tau^{*-1} \equiv \alpha^* T^3$, where α^* is a thermally averaged electron-phonon scattering constant. Ghantmakher and Gasparov[20] have studied the scattering rate in pure samples of the noble metals Cu and Ag using the radio frequency size effect (RFSE). This technique allows the determination of the scattering rate as a function of position on the Fermi surface for temperatures from about 1K to 4.2 K. They have found very strong scattering anisotopy for the reasons stated above, and a clear T^3 dependence. Gantmakher[19] has calculated this rate theoretically for the assumptions I have used above and found (I have rewritten things slightly for my notation):

$$\alpha^* = \frac{6\xi(3)M_o^2 k_B^3}{\pi\hbar^5 s^3 v_F} \qquad (9.17)$$

where $\xi(3) \simeq 1.202$ is the Riemann zeta function evaluated at n=3. We can thus write Σ as:

$$\Sigma = 6\xi(5)\alpha^*\gamma/\pi^2\xi(3) \simeq 0.524\ \alpha^*\gamma \qquad (9.18)$$

An analysis of the $P_1(T_p,T_e)$ expression shows that in fact P_1 does not depend upon the electron temperature. The calculation of P_1 is considerably messier than that of P_o, but in the end it reduces to a simple form. Readers who find this interesting can consult Appendix C. This is a result of detailed balance. One finds:

$$P_1(T_e,T_p) = \Sigma\Omega T_p^5 \qquad (9.19)$$

The net emitted power can thus be written quite simply as:

$$P = \Sigma\Omega(T_e^5 - T_p^5) \qquad (9.20)$$

The expression is quite reasonable. Its appearance is similar to the Stefan-Boltzmann law for the exchange of thermal radiation between two surfaces at different temperatures. There are of course two important differences. The power scales as the volume of the sample and the fifth power of its temperature, rather than the area of the sample and the fourth power of its temperature, as would be found for the photons treated in the Stefan-Boltzmann law. When $T_e = T_p$ the net emitted power vanishes as it must when the electrons and phonons are at the same temperature. For this to occur for all temperatures T_e, the phonon temperature dependence and the electron temperature dependence must be the same, or else the cancellation would fail and there would be a net power transmission when the two systems are in thermal equilibrium. The volume dependence arises from the fact that the total number of electrons is proportional to the volume, and we are calculating the rate

for the entire gas. A very simple back of the envelope calculation of this law is given in Appendix D; this derivation is essentially in the spirit of refs. 8, 11 and 12.

I can now adress more precisely the observability of the hot electron effect. In order to see the effect convincingly, two conditions must be satisfied:

(i) The electrons must heat up compared to the bath temperature T_o, for the sake of argument, then, we require something like $T_e \geq 2T_o$.

(ii) The difference in temperature between the electrons and phonons should be greater than the difference in temperature between the phonons and the bath, thus $(T_e-T_p) \geq (T_p-T_o)$.

Combining these two conditions one finds that they require at minimum $T_e = 2T_o$ and $T_p = 1.5T_o$. Now in dynamic equilibrium, the electrons will transmit power to the phonons at the same rate that the phonons transmit power to the bath. I now suppose, as in Fig. 9.1, that the phonons are coupled to the bath by a Kapitza resistance. The condition thus becomes:

$$P = \Sigma\Omega(T_e^5 - T_p^5) = \sigma A(T_p^4 - T_o^4)$$

where $\sigma = 1/(R_K T_0^3 A)$, is the Kapitza thermal conductivity per unit area. Now substituting the observability conditions for T_e and T_p, one finds:

$$T_o = \frac{\sigma A(1.5^4 - 1)}{\Sigma\Omega(2^5 - 1.5^5)} = 0.166\,\frac{\sigma A}{\Sigma\Omega}$$

Reinserting the inequalities, and supposing a thin film geometry one finds that the hot electron effect will be observable only for:

$$T_o \leq 0.166\sigma/(\Sigma\ell)$$

where ℓ is the film thickness. We thus see that the effect is most easily seen for a thin-film system, and that the film thickness is the only extensive parameter that enters into the observability condition. For representative values of σ and Σ (to be discussed in the next chapter), and our typical SQUID resistor film thickness of 30 nm, this condition becomes: $T_o \leq 0.74$ K. At this small thin film thickness, we thus expect the effect to be readily observable below 1K.

There is a confusing point about the T^5 law and the Stefan-Boltzmann T^4 law, which describes the transport of heat out of the sample by electromagnetic radiation. At low temperatures, T^5 becomes much smaller than T^4. We thus might expect that at low temperatures the electrons will radiate more energy by emitting photons than phonons. Let us suppose the electron gas is at temperature T_e and the phonon system is at 0 K. The power emission from phonons will equal that from photons when $\sigma_B A T_e^4 = \Sigma\Omega T_e^5$, where σ_B is the Stefan-Boltzmann constant, and A is the area of the sample. This will happen when $T_e = \sigma_B A/\Sigma\Omega$. For thin films this becomes $T_e = \sigma/\Sigma\ell$, where again ℓ is the film thickness. Evaluation of the constants for the case of a 30 nm thick Cu film gives the temperature as roughly 1 nK, which is well below the acessible temperature range investigated in this thesis.

The simple heating law has one very important consequence. In the steady state the emitted power P will equal the power, P_a, applied by, for example, a voltage source. One can thus write the electron temperature in terms of the power and the phonon temperature:

$$T_e = \left[\frac{P}{\Sigma\Omega} - T_p^5 \right]^{1/5} \qquad (9.21)$$

For a 0 K phonon bath, the electrons will only cool to $T_{min} = [P/\Sigma\Omega]^{1/5}$.

Thus, there is a minimum temperature to which the elctrons in a normal metal can be cooled when power is applied. This minimum temperature scales as the fifth root of the dissipated power per unit volume. For example, in order to reduce the electron temperature by a factor of 2, we must decrease the power per unit volume by a factor of 32.

9.4 Implications for SQUID Design

This simple law has important implications for designing SQUIDs for operation below 1 K. Typical thin-film SQUIDs have normal metal resistive shunts with relatively small volumes. At best, the sensitivity of a SQUID is limited by the Nyquist noise from these resistors. This Nyquist noise scales with the temperature of the electrons in the shunts. Unfortunately however, these same shunts dissipate most of the bias power applied to the SQUID (a small amount of power is undoubtedly lost by μ-wave radiation and by driving external loads).

From the above discussion, we can see that, because of the hot electron effect, the electrons in the shunts will never be able to cool below $T_{min}=(P/\Sigma\Omega)^{1/5}$. Now, it is not possible to operate a SQUID with arbitrarily low power and obtain a high sensitivity, as at low voltages the noise in the SQUID is very high (see Figs. 4.4 to 4.5). For all practical purposes the applied power can be considered fixed at some value. For a SQUID then, it will be necessary to increase the volume of the shunts or the Σ factor in order to lessen the electron heating. Σ is determined by the shunt material, and among the noble metals there is not much variation. In Appendix E, I have calculated Σ for a number of different materials from experimentally measured parameters. One should

realize that the choice of materials is limited because of the need for the metal to be normal, perferably non-magnetic, and suitably durable to survive fabrication. The simplest parameter to vary is thus the volume of the normal metal shunt.

In general, the phonon system will heat above the bath temperature as well. At sufficiently high temperatures, the temperature drop between the phonons in the metal and the substrate phonons will be greater than between the electrons and the phonons in the metal. Also if the metal is very poorly coupled to the substrate, then the thermal resistance between the phonon systems will be relatively more important. From the above discussion, we saw that the hot electron effect will be important for $T_o < 0.17(\sigma/\sum\ell)^{1/5}$. For a real thin-film system, as will be discussed in section 9.7, the above remarks will be modified due to finite size effects.

The remarks above clearly apply only to devices which are constructed with normal metal shunts. Devices which are built with self-shunted junctions or weak links should produce qualitatively different (and probably much worse) heating effects.

9.5 Spatial Effects and Diffusion Lengths

In the above analysis, I have implicitly assumed that the electron gas is heated uniformly throughout the volume, so that the electron gas is everywhere at the same temperature. In a real sample, this would correspond to, for example, heating a sample by sending a uniform density of current through it. I wish now to consider effects associated with non-uniform heating of the electron gas.

I want to consider this regime for quite practical reasons. One way to make the volume of the SQUID shunt larger is to simply increase its size. However, the SQUID must be operated with a particular value of resistance, and simply enlarging the resistor would make the resistance too small. Thus one is also required to change the shape of the resistor in order to both increase the volume and keep the resistance fixed, in particular the resistor must be made longer as it is made thicker and wider. Long resistive shunts will however cause a second problem. As the shunt length rises, so does the inductance associated with the shunt, and the behavior of the SQUID is altered from the model schematic of Chapter 5. In addition, the shape of the SQUID body will need to be altered in order for the shunts to fit. These changes are generally undesirable.

A different approach, which does not alter the SQUID parameters, is to attach a large volume of metal to the shunt as shown in Fig. 9.3. The current from the SQUID flows mainly through the small connecting strip, which then determines the SQUID resistance. The large volume carries only a very small portion of the SQUID bias current I. The heating of the electron gas is thus very non-uniform, and is greatest in the small connecting strip. I am mainly interested in determining how effective the large volume is in cooling the small heated region.

The key concept to recognize is that at low temperatures the electrons will travel a relatively large distance, on the average, before they emit a phonon. If the rate of phonon emission is τ^{-1}, then an electron will travel a distance $\ell_{in} = v_F\tau^{-1}$ before emitting a phonon. The emission rate can be readily calculated from the results of the previous section. The thermal average rate is from Gantmakher[19] just:

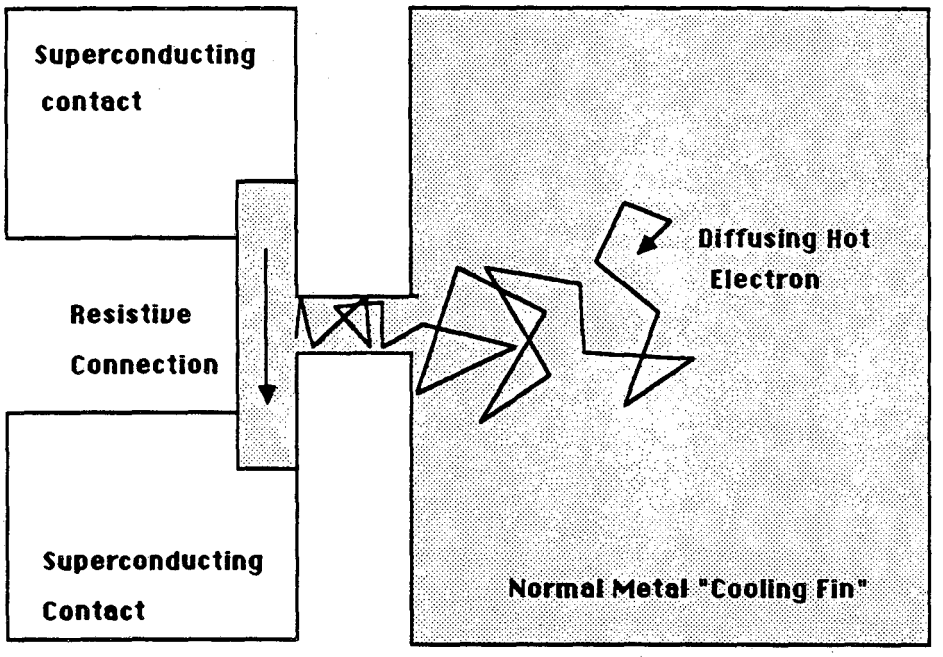

Fig. 9.3 Low T operation of a resistor which is attached to a large cooling fin. Most of the applied current flows through the resistive connection, causing the electrons there to heat up. Hot electrons are generated in the connection and diffuse into the cooling fin where they can lose energy by phonon emission.

$$\tau^{-1} = \alpha^* T^3$$

In the next chapter, we will see that α^* is of order 10^7/sec in our films, and at 20 mK, τ^{-1} = 80/sec. With a Fermi velocity of 1.5 X 10^6 m/sec, the electrons will travel a path length of about 10^6 m before emitting a phonon. The AuCu alloy film has a short electron elastic mean free path. This length can be estimated from the low temperature resistivity of the film, and one finds $\ell_e \simeq 20$ nm. The electron will thus diffuse through the film, making many elastic collisions before finally emitting a phonon. The diffusion length, or net average distance that the electron moves before emitting a phonon, is then $\ell_d = (\ell_e \ell_{in})^{1/2} \simeq 2$ mm at a temperature of 20 mK.

Consider a thin film in which the electrons are heated locally at a spot, with the remainder of the film being unheated, (see Fig. 9.4). The hot electrons will diffuse out into the unheated portions of the film, where they will then cool by emitting phonons. Similarly, cold electrons from the remainder of the film will diffuse into the hot region. Approximately then, we can see that all of the electrons within a diffusion length of the heated region will share the applied power and be involved in phonon emission. The electrons will thus radiate power from an effective area of about $A_{eff} = \pi \ell_d^2$. If we assume that all of these electrons are at some temperature T_e, then from the preceding section, the total power they will radiate is:

$$P = \Sigma A_{eff} \ell T_e^5 \qquad (9.22)$$

where I have also assumed that the phonon temperature can be neglected, and that the film thickness is ℓ. Substituting for A_{eff} and ℓ_d, we can write this as:

$$P = \Sigma \pi \ell \ell_e v_F \alpha^* T_e^2 \qquad (9.23)$$

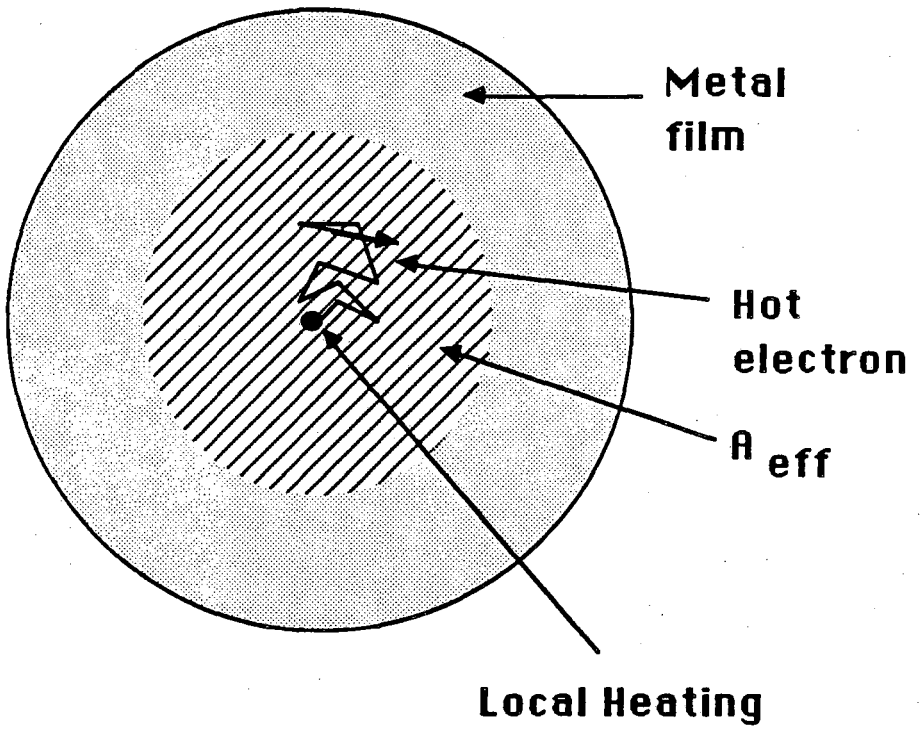

Fig. 9.4 Spatial hot electron effects: Local heating of the electrons in a 2-D metal film produces a region of area A_{eff} where the hot electrons can diffuse before emitting a phonon.

In dynamic equilibrium, the power P lost to phonons will exactly equal the power applied to the electrons P_a. This expression can be inverted to yield the electron temperature as a function of the applied power:

$$T_e = [P/\Sigma\pi h \ell_e V_f \alpha^*]^{1/2} \qquad (9.24)$$

This expression is interesting because we no longer see the fifth root dependence. This is because as the electron temperature or power increases, the electrons do not diffuse as far, and thus the effective volume of the sample decreases. The power law one finds in the non-local heating regime thus depends upon the shape or dimensionality of the sample.

The calculations in the first section correspond essentially to the zero dimensional case, where all sample dimensions are small compared to the electron diffusion length. The one dimensional limit would correspond to a narrow line of material which is heated at one end, or to a two dimensional plane of material which is heated along a line. The two dimensional case was considered above, and corresponds to a thin-film which is heated locally at one point, or to a three dimensional sample which is heated along a line. The three dimensional case would correspond to a solid volume of material which is heated at a point. It is quite simple to work out the rough power dependences for each case using the ideas of the two dimensional case illustrated above, and one finds:

$$\begin{aligned} &\text{0-D} \quad P \propto T^5 \qquad (9.25)\\ &\text{1-D} \quad P \propto T^{7/2}\\ &\text{2-D} \quad P \propto T^2\\ &\text{3-D} \quad P \propto T^{1/2} \end{aligned}$$

The effective volume idea is only an approximation. In particular, colder electrons tend to travel larger distances, and the electrons towards the edges of the effective volume are certainly less energetic on the average. Thus we expect that we may have underestimated the volume of material that is actively emitting energy. On the otherhand, the power emission rate is a strong function of the temperature of the gas, so that the edges of the volume should emit relatively little power even if they are only slightly colder. In order to resolve these issues, and obtain a more accurate estimate of the spatial effects, it would be necessary to construct a Boltzmann transport model. I will not present such a model here. Instead, I will consider a very approximate analysis of the effects of non-thermal phonons which shows up a second weakness in the model.

9.6 The Kapitza Resistance and Phonon Heating

The emission of phonons from the hot electron gas is non-thermal, as we will see below. On the otherhand, I have assumed in calculating the electron heating properties that the phonon states are occupied according to a thermal distribution. In this section, I will relax the assumption that the phonons are thermally distributed, while retaining the assumption that the electrons still have a well-defined temperature. This will involve a self-consistent calculation of the phonon spectrum and the electron gas heating for a very simple, model, thin-film system.

From section 9.2, it is simple to calculate the number of phonons of energy ε_q that the the electron gas will emit per unit of time. The electron gas can be treated as a phonon source which produces a

non-thermal spectral distribution. In addition, the phonons can be transmitted to the substrate, and one can think of the substrate-metal interface as a phonon sink. The substrate will be at some temperature, it will have a thermal distribution of phonons, and so the interface will also act as a source of thermal phonons. We would like to calculate the resulting phonon distribution in the metal.

I will here take a very simple-minded approach and neglect any size effects. This is <u>not</u> a good approximation for the thin films studied because the thermal wavelength is much longer than the film thickness, as is discussed in the next section. It is nevertheless the simplest assumption one could make, and it underlies Kapitza resistance calculations and measurements, where it is generally taken for granted. I will also neglect phonon-phonon interaction, which is a good assumption at low temperatures and small length scales.

Consider Fig. 9.5, a normal metal film with volume Ω and thickness ℓ makes contact with a substrate through an interface area A. If the metal contains an isotropic distribution of phonons with an energy density per unit volume u, then they will produce an energy flux J on the interface of:

$$J = us/3 \tag{9.26}$$

where s is the speed of sound in the sample. In general, not all of the phonons incident upon the interface will be transmitted through to the substrate. I will define the number p as the fraction of incident phonons which escapes upon each attempt. The total power P emitted will in this case be:

$$P = pJ_0A = uspA/3 \tag{9.27}$$

In addition, thermal phonons from the substrate will be transmitted into

the metal volume. The net rate of energy loss will be:

$$P = uspA/3 - u_0 s_0 p_0 A/3 \qquad (9.28)$$

where u_0, s_0, and p_0 are the phonon energy density, speed of sound, and transmission probability for the substrate. For the purposes of this section, I will take the substrate temperature as zero, so that $u_0 = 0$. This simplifies the problem somewhat.

Now, if the phonons are thermal, Eq. 9.28 reduces to the Kapitza heating law, and we can estimate the effective escape probability p by comparison with experimental Kapitza resistance data. Alternatively, W.A. Little has calculated theoretical estimates for the transmission probability using his acoustic mismatch theory of the Kapitza resistance.[8] He finds that the transmission probability is independent of the phonon energy (in the acoustic regime at least), and depends only upon properties of the two materials and upon the phonon's angle of incidence to the interface.

Equations 9.28 and 9.27 can be interpreted in term of the loss rate of phonons, ie. the rate at which phonons are escaping from the metal into the substrate. Let $n(\varepsilon_q)$ represent the number of phonons with wavevector $\bar{q}$, where I now no longer assume that this is a Bose-Einstein distribution. The average rate at which phonons are lost from the volume is:

$$\left[\frac{dn(\varepsilon_q)}{dt} \right]_{loss} = n(\varepsilon_q) sp/3\ell \qquad (9.29)$$

In dynamic equilibrium, the loss rate of phonons will equal the rate at which phonons are being generated by electron-phonon emission and absorption, thus:

$$\left[\frac{dn(\varepsilon_q)}{dt}\right]_{gen} = \left[\frac{dn(\varepsilon_q)}{dt}\right]_{loss} \qquad (9.30)$$

The rate at which phonons are generated by the electron gas will of course depend upon the distribution of phonons because of absorption and stimulated emission effects. I can thus write generally:

$$\left[\frac{dn(\varepsilon_q)}{dt}\right]_{gen} = \left[\frac{dn(\varepsilon_q)}{dt}\right]_{emission} - \left[\frac{dn(\varepsilon_q)}{dt}\right]_{absorption} \qquad (9.31)$$

Now the emission rate will scale with $n(\varepsilon_q)+1$ and the absorption rate will scale as $n(\varepsilon_q)$. I can thus write:

$$\left[\frac{dn(\varepsilon_q)}{dt}\right]_{gen} = \Gamma_e(n(\varepsilon_q) + 1) - \Gamma_a n(\varepsilon_q) \qquad (9.32)$$

where Γ_e and Γ_a are emission and absorption factors which will be derived below, and which do depend upon the phonon energy but not upon the phonon distribution. From Eq. 9.30 and 9.32 one finds:

$$n(\varepsilon_q) = \frac{\frac{3\ell\Gamma_e}{sp}}{1 + \frac{3\ell}{sp}(\Gamma_e - \Gamma_a)} \qquad (9.33)$$

the Γ's can be readily calculated by suitably integating over Gantmakher's [19] formula for the electron-phonon scattering rate. One finds:

$$\Gamma_e = \Gamma_o F_e(y) \qquad (9.34)$$

$$\Gamma_a = \Gamma_o \exp(y) F_e(y)$$

where: $\Gamma_o = m^2 k_B T_e M_o^2/\pi\hbar^5$

$$F_e(y) = \frac{y}{e^y - 1}$$

$$y = \varepsilon_q/k_B T_e$$

I can thus write the phonon occupancy as:

$$n(\varepsilon_q) = \frac{\frac{3\ell\Gamma_o F_e(y)}{sp}}{1 + \frac{3\ell}{sp}\,\Gamma_o(\,e^y - 1)F_e(y)} \tag{9.35}$$

Now a phonon gas at temperature T_e has a thermal equilibrium number density given by the Bose-Einstein distribution:

$$n_o(\varepsilon_q, T_e) \equiv \frac{1}{e^y - 1} \tag{9.36}$$

I can thus write the above formula for for the phonon occupancy in the metal in the remarkable form:

$$n(\varepsilon_q) = \left[\frac{1}{\left[\frac{1}{\frac{3\ell\Gamma_o\varepsilon_q}{spk_BT_e}}\right] + 1} \right] n_o(\varepsilon_q, T_e) \tag{9.37}$$

I can write this in a simpler form by defining the parameter:

$$E' = \frac{spk_BT_e}{3\ell\Gamma_o} = \frac{\pi p\hbar^5 s}{3\ell m^2 M_o^2} \tag{9.38}$$

Thus I can write:

$$n(\varepsilon_q) = \frac{\varepsilon_q}{E' + \varepsilon_q}\, n_o(\varepsilon_q, T_e) \tag{9.39}$$

This is clearly a non-thermal ditribution.

I now examine this expression in various limits. Notice that if p = 0, then E' = 0, and $n(\varepsilon_q) = n_o(\varepsilon_q, T_e)$. This is exactly what one would expect. If none of the phonons can escape, and the electrons are held at some temperature T_e, then the phonons will come into equilibrium with a Bose-Einstein distribution of temperature T_e. Similarly, for phonon energies much greater than E', one finds a thermal equilibrium phonon spectrum of temperature T_e, while for phonon energies much less than E',

one finds a suppression of the number of phonons in the sample from the Bose-Einstein distribution. The important parameter is clearly the energy-like term E'.

For a representative AuCu thin film sample with the following characteristics:

$s = 5000\ ms^{-1}$ $\quad p = 0.05$ $\quad \ell = 30\ nm$

$\varepsilon_F = 6\ eV$ $\quad \mu = 9 \times 10^3\ kg/m^3$ $\quad m^* = 9.11 \times 10^{-31}\ kg$,

I find E' = 1.35 mev, which corresponds to an equivalent temperature of 15.6 K. This is much larger than any of the phonon energies we will be concerned with; I will be interested in hot electron temperatures from about 20 mK to 200 mK. Thus the phonon occupancy will be greatly suppressed compared to a Bose-Einstein distribution, and will appear very non-thermal.

Since ε_q/E' is a very small parameter in the region of interest, I can approximate the form of the phonon spectrum to first order as:

$$n(\varepsilon_q) = \frac{\varepsilon_q}{E'}\, n_o(\varepsilon_q, T_e) - \frac{\varepsilon_q^2}{E'^2} n_o(\varepsilon_q, T_e) \qquad (9.40)$$

It is now a simple matter to calculate the rate at which the electron gas emits power. Since all of the power that the electrons lose is transferred to the phonons, and the phonons are in a steady state, it is only necessary to calculate the rate at which the phonons transfer energy out of the metal volume. This is just :

$$P = \int \varepsilon_q\, n(\varepsilon_q) D_p(\bar{q}) d\bar{q}^3 = \int \frac{\varepsilon_q^2}{E'} n_o(\varepsilon_q) D_p(\bar{q}) d\bar{q}^3 + \int \frac{\varepsilon_q^3}{E'^2} n_o(\varepsilon_q) D_p(\bar{q}) d\bar{q}^3 \qquad (9.41)$$

The integrals are very similar to those worked out in the preceding sections; one finds to first order in ε/E':

$$P = \sum \Omega T^5 - \sum \Omega \beta' T^6 \qquad (9.42)$$

Where the correction term, β', is ordinarily very small for our films, and the T^5 term dominates. Although simplifying assumptions were used in this section, it is difficult to see how they could significantly affect the smallness of the correction term.

9.7 Criticism of the Simple Heating Model

The above simple heating model is what one might classically construct for heat transfer by phonons in a bulk system. However, it is quite inadequate for the system at hand. The central difficulty is that the thin-film resistors are much thinner than the average phonon wavelength at the low temperatures we are concerned with. Fig. 9.5 shows a plot of the thermal phonon wavelength:

$$\lambda = hs/k_B T$$

where h is Planck's constant, and s = 4000 ms^{-1} is a representative speed of sound in a solid. At a temperature of 20 mK, the thermal wavelength is about 10 μm. This is much larger than any of the film thicknesses used in the thin-film resistors.

This simple fact has important implications. At low temperatures and low energies, there are no available phonon modes to which an electron can transfer energy. Thus, not only is there no well-defined phonon temperature in the resistor, there is not even a resistor phonon system with which the electrons can interact. This argument is somewhat misleading, however, because I have so far neglected the role of the substrate on the phonon spectrum of the resistor. The thin-film resistor and the substrate are mechanically well-coupled together. If the lattice

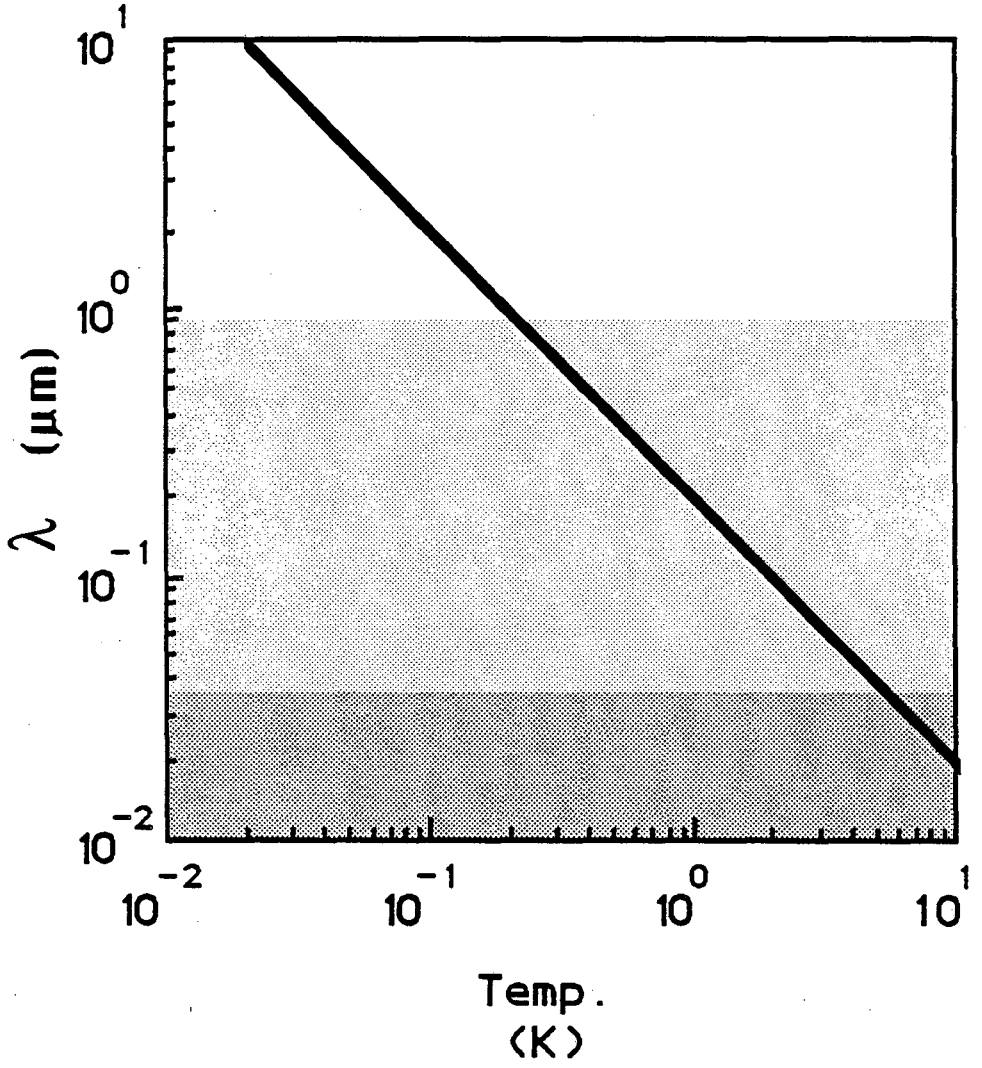

Fig. 9.5 Thermal phonon wavelength versus temperature for 4000 m/s speed of sound. Shaded region below 1 μm represents thickness of thickest resistor film tested in Chapter 10, shaded region below 40 nm represents thickness of typical shunt resistor film.

oscillations of the entire system (resistor + substrate) are quantized, one obtains a single phonon system. Because of the large size of the substrate system, this system will possess much lower frequency phonon modes than the resistor will by itself. These low frequency modes will cause lattice motion, not just in the substrate, but also in the resistor, because the two are coupled together. It is these low frequency motions which produce the deformations with which the electron gas can interact. Thus the substrate is all important for generating the phonon states into which the hot electrons can release energy at low temperatures.

The central problem of a more accurate treatment is to contruct the phonon spectrum, density of states, and electron-phonon interaction Hamiltonian for the combined resistor + substrate system. This is a complicated problem because of the complicated behavior of phonons at interfaces and boundaries. Scattering of a longitudinal acoustic wave off of a boundary produces a reflected longitudinal wave and a reflected transverse wave.[21] The amplitude of the two waves depends upon the angle of incidence and the mechanical properties of the medium. Similarly, passage of an transvers acoustic wave through an interface can cause the generation of a longitudinal reflected wave, a transverse reflected wave, a longitudinal transmitted wave, and a transverse transmitted wave.

This behavior is called mode conversion in the literature, and means that the acoustic longitudinal and transverse modes are coupled together at interfaces and boundaries. This in turn means that the electrons in the thin film resistor will be coupled to both the longitudinal and transverse modes in the resistor + substrate system.

I have not yet completed the analysis of this problem because of the apparent difficulties involved, and I do not know the final answer. The role of the substrate is however one possible explanation for discrepancies between the RFSE experiments for the electron-phonon scattering rate and those found in the thin-film experiments, which will be discussed in the following chapter. At the least, one can see that the effect of the substrate has not been properly included in the theory.

9.8 Appendices

Appendix A: The Deformation Potential

Ziman has provided a semiquantitative discussion of the origin of the deformation potential.[16] The discussion below follows Ziman's treatment, and has been included here for the sake of completeness.

Let us assume that a metal sample of volume Ω is at T = 0. Suppose that the ions in a small volume V in the metal are suddenly compressed. This compression can be described by a strain field $\bar{u}(\bar{r})$: a lattice point initially at $\bar{r}$ is displaced to $\bar{r} + \bar{u}(\bar{r})$. If the strain field is uniform across the volume, the fractional change in volume resulting is just:

$$\Delta V/V = \bar{\nabla}\cdot\bar{u}(\bar{r}) \qquad (9.43)$$

This fractional change in volume is called the dilatation or the deformation, and is frequently written as just Δ. The electrons will respond to this ionic motion by moving towards regions of higher positive charge density. As a result, the local Fermi level will change.

In the limit of very small deformation, the Fermi level becomes:

$$\varepsilon_F = \varepsilon_{Fo} - \frac{2}{3}\,\varepsilon_{Fo}\,\frac{\Delta V}{V} \tag{9.44}$$

Now, the electrons can move much faster than the ions, and an increase in the Fermi level in any region will cause electrons to flow out of the region. This occurs because the electrochemical potential μ_F is constant throughout the metal and is equal to its initial value ε_{Fo}. The compressed region will thus build up a positive charge and this charge sets up an electrical potential $\phi(\bar{r})$ which exactly compensates for the above calculated change in the Fermi level. One can write:

$$\mu_F = \varepsilon_{Fo} - \frac{2}{3}\,\varepsilon_{Fo}\,\frac{\Delta V}{V} + e\phi(\bar{r}) = \varepsilon_{Fo} \tag{9.45}$$

And thus the potential energy change ΔW that the compression has induced in the metal is just:

$$e\phi(r) = \Delta W = -\frac{2}{3}\,\varepsilon_F\,\frac{\Delta V}{V} \tag{9.46}$$

This energy change is called the deformation potential because it is proportional to the dilatation or deformation of the sample. It represents the interaction between a compression of the lattice and the electron gas. This interaction has the above potential, which, like any other potential energy term, can cause transitions between electron states. This compression can be generated by phonons in the metal. A phonon of wavevector q and polarization λ will induce lattice displacements of:[22]

$$\bar{u}(\bar{r}) = u_\lambda e^{i\bar{q}\cdot\bar{r}}\,\bar{e}_\lambda \tag{9.47a}$$

where u_λ is just:

$$u_\lambda = (\hbar/2\mu\Omega sq)^{1/2}\ , \tag{9.47b}$$

μ is the mass density of the crystal, Ω is the crystal volume, $\bar{e}_\lambda$ is the polarization vector, and s is the speed of sound for the mode λ. A single phonon will produce a dilatation of:

$$\nabla\cdot\bar{u}(\bar{r}) = i\bar{q}\cdot\bar{e}_\lambda\, e^{i\bar{q}\cdot\bar{r}} u_\lambda = \begin{cases} 0 & \text{if } \lambda \text{ is transverse mode} \\ iqu_\lambda\cdot\exp(i\bar{q}\cdot\bar{r}) & \text{if } \lambda \text{ is longitudinal mode} \end{cases} \tag{9.49}$$

The square of the matrix element is square of the interaction energy. Only logitudinal modes will contribute because of Eq. 9.49. Upon substituting the above results, one finds for the longitudinal modes:

$$|M|^2 = |\Delta W|^2 = \left[\frac{2}{3}\,\varepsilon_F\,\frac{\Delta V}{V}\right]^2 = \frac{\hbar q}{2\mu s\Omega}\left[\frac{2\varepsilon_F}{3}\right]^2 \tag{9.50}$$

Appendix B: The Evaluation of the Integral Expression for P_o.

The integral expression Eq. 9.12:

$$P_o(T_e) = \int_{-\infty}^{\infty} f(E_k)D_e(E_k)dE_k \int D_p(\bar{q})\varepsilon_q \frac{2\pi}{\hbar}|M|^2\delta(E_k - E_{k'} - \varepsilon_q)(1-f(E_{k'}))d^3\bar{q} \tag{9.12}$$

can be solved exactly in the limit $\varepsilon_F >> k_B T_e$. First note that the electron density of states may be removed from under the first integral, and replaced with its value at the Fermi level, because of the overlap of the Fermi function terms f(1-f). Secondly note that the term, $|M|^2$, is equal to qM_o^2/Ω, by my assumption that the electron-phonon interaction is a scalar deformation potential. Thirdly, the phonon density of states is just $D_p(q) = \Omega/(2\pi)^3$; ie. the density of states for the longitudinal acoustic branch. Fourthly, the phonon energy is just ε_q

$= \hbar sq$ for acoustic phonons. Fifthly, the delta function in the second integrand can be evaluated, although it is not entirely trivial. Recall that:

$$\int \delta(F(\bar{q}))\, d^3\bar{q} = \int dS_q / |\bar{\nabla}_q F| \qquad (9.51)$$

where $F(\bar{q})$ is a function of $\bar{q}$, and dS_q is a surface element on the surface defined by $F = 0$. For the case at hand:

$$F(\bar{q}) = E_k - E_{k'} - \varepsilon_q \qquad (9.52)$$

$$\bar{\nabla}_q F = \hbar^2(\bar{k}-\bar{q})/m - \hbar s\bar{q}/|q^2| \simeq \hbar\bar{v}_F$$

$$dS_q = 2\pi q\, dq$$

where I have used the fact that the electron wave vectors near the Fermi surface are much larger than a typical thermal phonon wave vector. Sixthly, use the relation $F = 0$, energy conservation, to replace $E_{k'}$ by $(E_k - \varepsilon_q)$.

With these substitutions, the integral becomes:

$$P_o(T_e) = \frac{D(\varepsilon_F)}{(2\pi)^3} \frac{(2\pi)^2 \hbar s\, M_o^2}{\hbar^2 v_F} \int_{-\infty}^{\infty} f(E_k)\, dE_k \int_0^{\infty} q^3 (1 - f(E_k - \varepsilon_q))\, dq \qquad (9.53)$$

The resulting integral is most easily solved by changing to reduced variables; introduce:

$$x = (E-\mu_F)/k_B T_e \qquad y = \varepsilon/k_B T_e$$

where μ is the chemical potential. One then finds:

$$P_o(T_e) = A\, T_e^5\, I_o \qquad (9.54)$$

where:

$$A = \frac{D(\varepsilon_F)}{(2\pi)} \frac{M_o^2\, k_B^5}{\hbar^5 s^3\, v_F}$$

$$I_o = \int_{-\infty}^{\infty} \frac{dx}{1 + e^x} \int_0^{\infty} \frac{y^3 dy}{1 + e^{y-x}}$$

To solve I_o, change variables to:

$$z = e^x ,$$

and rearrange:

$$I_o = \int_0^{\infty} y^3 dy \int_0^{\infty} \frac{dz}{(1+z)(e^y + z)} = \int_0^{\infty} \frac{y^4 dy}{e^y - 1} \qquad (9.55)$$

This final expression is related to the Riemann Zeta function,[23] and is:

$$I_o = \Gamma(5)\xi(5) \qquad (9.56)$$

where $\Gamma(n) = (n-1)!$ is the gamma function, and $\xi(n)$ is the Riemann Zeta function. The values of $\xi(n)$ are tabulated,[22] and $\xi(5) \simeq 1.037$. We thus have $I_o = 4 \cdot 3 \cdot 2 \cdot 1.037 \simeq 24.89$.

Substituting Eqs. 9.16, 9.17, and 9.56 into 9.54 one finds:

$$P_o = \left[\frac{6\xi(5)}{\pi^2 \xi(3)} \right] \alpha^* \gamma T_e^5 \Omega = 0.5245 \, \alpha^* \gamma T_e^5 \Omega = \Sigma \, T_e^5 \Omega \qquad (9.57)$$

where: $\Sigma \equiv A \, \Gamma(5) \, \xi(5)/\Omega = 6\xi(5)\alpha^*\gamma/\pi^2\xi(3)$

Appendix C: The Evaluation of the Integral Expression for P_1

The expression 9.13 for P_1:

$$P_1(T_e, T_p) = \int_{-\infty}^{\infty} f(E_k) D_e(E_k) dE_k \int D_p(\bar{q}) \varepsilon_q \frac{2\pi}{\hbar} |M|^2 n(\varepsilon_q)(1 - f(E_{k'})) \cdot$$

$$\cdot \left[\delta(E_k - E_{k'} - \varepsilon_q) - \delta(E_k - E_{k'} + \varepsilon_q) \right] d\bar{q}^3 \qquad (9.13)$$

can be simplified using the same substitutions as in the case of P_o. One finds:

$$P_1(T_e,T_p) = \frac{D(\varepsilon_F)}{(2\pi)}\frac{(2\pi)^2\hbar s\ M_o^2}{^3\ \hbar^2 v_F}\int_{-\infty}^{\infty} f(E_k)\ dE_k \int_o^{\infty} q^3\ n(\varepsilon_q)(f(E_k-\varepsilon_q)-f(E_k+\varepsilon_q))dq \tag{9.58}$$

I now make the change of variables:

$$x = (E_k - \mu_F)/k_BT_e \qquad\qquad y' = \varepsilon_q/k_BT_p$$

Notice that the equation for y' is with respect to T_p rather than T_e as was the case for y. The expression for P_1 then becomes:

$$P_1(T_e,T_p) = A\ T_eT_p^4\ I_1 \tag{9.59}$$

where A is the same as in Appendix B:

$$A = \frac{D(\varepsilon_F)}{(2\pi)}\frac{M_o^2\ k_B^5}{\hbar^5 s^3\ v_F} \tag{9.60}$$

and I_1 is the integral:

$$I_1 = \int_{-\infty}^{\infty} dx \int_o^{\infty} y'^3 dy'\ f(x)n(y')\ \{f(x-y'T_p/T_e) - f(x+y'T_p/T_e)\} \tag{9.61}$$

We can evaluate I_1 by expanding the f's in a Fourier series:

$$f(x-y'T_p/T_e) = f(x) - \frac{\partial f}{\partial x}\left[\frac{y'T_p}{T_e}\right] + \frac{1}{2}\frac{\partial^2 f}{\partial x^2}\left[\frac{y'T_p}{T_e}\right]^2 - \cdots$$

$$f(x+y'T_p/T_e) = f(x) + \frac{\partial f}{\partial x}\left[\frac{y'T_p}{T_e}\right] + \frac{1}{2}\frac{\partial^2 f}{\partial x^2}\left[\frac{y'T_p}{T_e}\right]^2 + \cdots$$

When substituted into I_1, only the odd partial terms survive. We can thus write I_1 in the form:

$$I_1 = -2\sum_{n=1}^{\infty}\left[\frac{T_p}{T_e}\right]^{2n-1}\frac{1}{(2n-1)!}\int_{-\infty}^{\infty} f(x)\ \frac{\partial^{2n-1} f}{\partial x^{2n-1}}\ dx \int_{-\infty}^{\infty} y'^{(3+2n-1)} n(y')dy' \tag{9.62}$$

The integral over y' is related to the Riemann Zeta function and is just:(23)

$$\Gamma(3+2n)\xi(3+2n)$$

The remaining integral over x can be done by rewriting it in the form:

$$2\int_{-\infty}^{\infty} f(x)\frac{\partial^{2n-1}f}{\partial x^{2n-1}}\,dx = 2\int_{-\infty}^{\infty}(f(x)-1/2)\frac{\partial^{2n-1}f}{\partial x^{2n-1}}\,dx + \frac{2}{2}\int_{-\infty}^{\infty}\frac{\partial^{2n-1}f}{\partial x^{2n-1}}\,dx \tag{9.63}$$

The first integral vanishes because the partial is an even function of x, and f-1/2 is an odd function of x, so the integrand is an odd function of x. The second integral is trivially:

$$\left[\frac{\partial^{2n-2}f}{\partial x^{2n-2}}(\infty) - \frac{\partial^{2n-2}f}{\partial x^{2n-2}}(-\infty)\right] = \begin{cases}-1 \text{ if } n=1\\ 0 \text{ otherwise}\end{cases} \tag{9.64}$$

Thus all terms will vanish except for the first one, and the sum over n terminates abruptly. We can then write:

$$I_1 = \left[\frac{T_p}{T_e}\right]^1 \Gamma(5)\xi(5) \tag{9.65}$$

And thus the expression for P_1 becomes:

$$P_1 = AT_p^5\Gamma(5)\xi(5) = \Sigma T_p^5 n \tag{9.66}$$

where I have used the definition of $\Sigma = A\,\Gamma(5)\xi(5)/n$ from Appendix C.

Appendix D: Approximate Calculation of Energy Loss Rate

The rate at which the electrons lose their energy can be written as:

$$P = \left|\begin{matrix}\text{\# of thermally}\\ \text{active electrons}\end{matrix}\right| \cdot \left|\begin{matrix}\text{Rate at which an}\\ \text{electron emits phonons}\end{matrix}\right| \cdot \left|\begin{matrix}\text{average energy}\\ \text{of a phonon}\end{matrix}\right|$$

(9.67)

The number of thermally active electrons is just:

$$D(\varepsilon_F)k_BT_e \tag{9.68}$$

where: Ω is the metal volume, $D(\varepsilon_F)$ is the density of states at the Fermi level, and T_e is the electron temperature. The rate at which electrons emit phonons we will take, without proof, as $\alpha^*T_e^3$. And Finally, the average energy of an emitted phonon is just the average thermal energy of the electron: k_BT_e. Putting these together, one finds:

$$P \simeq D(\varepsilon_F)k_B^2\ \alpha^*T_e^5 \tag{9.69}$$

We can identify $D(\varepsilon_F)k_B^2/\Omega \simeq \gamma$ the electronic heat capacity per unit volume. The approximate expression for the power loss thus becomes:

$$P \simeq \alpha^*\gamma\Omega T_e^5 \tag{9.70}$$

The expression from the full calculation gives:

$$P = 0.524\ \alpha^*\gamma\Omega(T_e^5-T_p^5). \tag{9.71}$$

So we see that the approximate expression has neglected phonon absorption processes, and slightly overestimated the prefactor.

Appendix E: Materials Parameters

The following table contains relevant materials parameters for the noble metals. The information for the first 7 rows is taken from a few of the numerous useful tables which can be found in C. Kittel's "Introduction to Solid State Physics",[24] and is reproduced here for the sake of completeness. The values of α^*_{calc} and Σ^*_{calc} are found from Eqs. 9.17 and 9.18 respectively. The value α^*_{GGmin} and α^*_{GGmax} are the minimum and maximum electron-phonon scattering rate constants observed experimentally in Refs. 20 and 25. The values of Σ_{GGmin} and Σ_{GGmax} are

Table 9.1 Hot electron material parameters for the noble metals.

quantity	units	Cu	Ag	Au
v_F	m/s	1.57×10^6	1.39×10^6	1.39×10^6
ε_F	eV	7.0	5.48	5.51
μ	kg/m^3	8.96×10^3	10.5×10^3	19.3×10^3
n	$\#/m^3$	8.45×10^{28}	5.85×10^{28}	5.9×10^{28}
s	m/s	4760	3650	3240
m*/m	#	1.38	1.0	1.14
γ_{mole}	$J/(Mole \cdot K^2)$	6.95×10^{-4}	6.46×10^{-4}	7.29×10^{-4}
γ	$J/(m^3 \cdot K^2)$	98.1	62.9	71.5
AW	gm/Mole	63.6	107.9	197
α^*_{calc}	$1/(s \cdot K^3)$	1.9×10^6	3.2×10^6	2.9×10^6
Σ_{calc}	$W/(K^5 m^3)$	9.8×10^7	1.1×10^8	1.1×10^8
α^*_{GGmax}	$1/(s \cdot K^3)$	2.2×10^7	6×10^7	-
α^*_{GGmin}	$1/(s \cdot K^3)$	$2. \times 10^6$	2×10^6	-
Σ_{GGmax}	$W/(K^5 m^3)$	1.1×10^9	2×10^9	-
Σ_{GGmin}	$W/(K^5 m^3)$	1.0×10^8	6.6×10^7	-

the values of the heating constants computed from Eq. 9.18, but using the experimentally determined α^*_{GGmin} and α^*_{GGmax} respectively.

References

(1) C. D. Tesche and J. Clarke, "dc SQUID: Noise and Optimization", J. Low Temp. Phys., 29, 301 (1977).

(2) J.J.P. Bruines, V.J. de Waal, and J.E. Mooij, J. Low Temp. Phys. 46, 383 (1982).

(3) V.V. Danilov, K.K. Likharev, A.B. Zorin, "Quantum Noise in SQUIDs", IEEE Trans. Magn., MAG-19, 572 (1983).

(4) R.H. Koch, D.J. Van Harlingen, and J. Clarke, "Quantum Noise Theory for the dc SQUID", Appl. Phys. Lett. 38, 380 (1981).

(5) R.T. Wakai and D.J. Van Harlingen, "Low-Frequency Noise and Discrete Charge Trapping in Small Area Tunnel Junction dc SQUIDs", Appl. Phys. Lett. 49, 593 (1986).

(6) B. Muhlfelder, M. W. Cromar, and W.W. Johnson, "Double Transformer Coupling to a Very Low Noise SQUID". IEEE Trans. Magn. Mag-19, 303 (1983); B. Muhlfelder, PhD Thesis, Univ. of Rochester, 1984; and B. Muhlfelder, M.W. Cromar, and W.W. Johnson, "Well-Coupled, Low Noise, dc SQUIDs", IEEE Trans. Magn. MAG-21, 427 (1985).

(7) See for example: C. Cosmelli, P. Carelli, M.G. Castellano, and V. Foglietti, "Long Term Operation of Low Noise dc SQUID Coupled to a High Q Gravitational Radiation Detector", IEEE Trans. Magn. Mag-23, 454 (1987).

(8) W.A. Little, "The Transport of Heat Between Dissimilar Solids at Low Temperatures", Can. J. Phys. 37, 334 (1959).

(9) See for example: S.M. Sze, "Physics of Semiconductors", Wiley Interscience, New York (1981).

(10) P. Roubeau, D. Le Fur, E.J.A. Varoquaux, third Int. Cryog. Eng. Conf., Iliffe Sci. Techn. Publ., Guildfind 315 (1970).

(11) J.C. Wheatly, R.E. Rapp, R.T. Johnson, J. of Low Temp. Phys., 4, 1 (1971).

(12) A.C. Anderson and R.E. Peterson, "The Thermal Resistance Between Electrons and Phonons in Cu", Phys. Lett., 38A, 519 (1972).

(13) M.L. Roukes, M.R. Freeman, R.S. Germain, R.C. Richardson, M. B. Ketchen, "Hot Electrons and Energy Transport in Metals at Millikelvin Temperatures", Phys. Rev. Lett., 55, 422 (1985).

(14) P.W. Anderson, E. Abrahams, and T.V. Ramakrishnan, "Phys. Rev. Lett. 43, 719 (1979).

(15) M.R. Arai, "A Fundamental Noise Limit for Biased Resistors at Low Temperatures", Appl. Phys. Lett., 42, 906 (1983).

(16) J.M. Ziman, "Principles of the Theory of Solids", Cambridge Univ. Press, Cambridge (1979).

(17) M.R. Halse, "The Fermi Surfaces of the Noble Metals",Proc. Roy. Soc. Lon., 265, 507 (1969).

(18) D. Nowak, "Anisotropy of the Electron-Phonon Interaction in Copper", Phys Rev. B, 6, 3691 (1972).

(19) V.F. Gantmakher, "The Experimental Study of Electron-Phonon Scattering in Metals", Rep. Prog. Phys. 37, 317 (1974).

(20) V.F. Gantmakher and V.A. Gasparov, "Anisotropy of the Probability of Electron Scattering by Phonons on the Fermi Surface of Copper", Sov.

Phys.-JETP, 37 864 (1973).

(21) H. Kolsky, Stress Waves in Solids, Monographs on the Physics and Chemistry of Materials, Clarendon Press, Oxford, 1953.

(22) H. Haken, "Quantum Field Theory of Solids, an Introduction", North-Holland Publ. Co., (1983).

(23) R.K. Pathria, "Statistical Mechanics", Pergamon, p 503 (1978).

(24) C. Kittel, "Introduction to Solid State Physics", 5th Edition.

(25) V.A. Gasparov; "Anisotropy of the Probability of Electron-Phonon Scattering in Silver", Sov. Phys. JETP,41, 1129 (1976).

Chapter 10: Hot Electron Experiments in Normal Metal Thin-Films

10.1 Introduction

There have been very few measurements of the hot electron effect in normal metals. The first clear demonstration of the effect was provided by the measurements of A. C. Anderson and R. E. Peterson on bulk Cu samples.[1] The only subsequent measurements, which I am aware of, were those of Roukes *et al.* on Cu thin-films.[2] In principle, it is also possible to estimate the magnitude of the hot electron effect from experimental data on the electron-phonon scattering rate. Such data has been found by using a variety of techniques, including the radio frequency size effect (RFSE)[3,4] and ultrasonic attenuation.[5] However, these techniques depend upon the electron mean free path being limited by the electron-phonon interaction, and thus require samples of high purity. The presence of a high concentration of impurity sites limits the electron mean free path by elastic collisions with the impurity sites, and in such experiments makes the effects of the electron-phonon interaction undetectable at low temperatures.

This chapter describes two seperate experiments on electron heating effects in thin normal metal films. The goal of the first experiment was to confirm, or disprove, that the hot electron effect existed in the resistor material used for the SQUIDs. The result was not a forgone conclusion. The theory of Chapter 9 was developed for pure materials with simplifying assumptions for the shape of the Fermi surface, the phonon system, and the electron-phonon interaction. On the otherhand the shunt material was a "dirty", poly-crystalline, noble metal alloy of Au

and Cu. Accordingly, the model could only serve as a rough guide for the real system under consideration, and likewise, we could not rely on any published experimental data. The experiments described in this chapter would thus be the first to study hot electron effects and the electron-phonon interaction in an alloy at low temperatures. They would also be the first experiments to confirm the results of Roukes et al. on electron heating in thin-film systems.[2]

The goal of the second experiment was to provide empirical guidelines for redesigning the SQUIDs to minimize the effect. In particular, I wanted to investigate the ability of large volume "cooling fins" to reduce the electron temperature. This is the first, although somewhat indirect, test of spatial hot electron effects in normal metals that I am aware of.

The main experimental difficulty that one faces is the determination of the electron temperature. Our investigation made use of what we call "noise thermometry". It is important to realize, at least for the purpose of this chapter, that the Nyquist noise from a resistor depends directly upon the temperature of the electrons. The temperature of the phonons enters only indirectly, in so much as it affects the electron temperature. Noise thermometry involves measuring the spectral density of the Nyquist noise in a resistor of known resistance, and then simply applying Nyquist's law to obtain the electron temperature. This approach is essentially identical to that used by Roukes et al.[2].

I should remark that the noise thermometry technique can be used quite generally as a thermometer. The noise in a resistor can easily be measured whenever one has an amplifier with a noise temperature which is comparable to or smaller than the bath temperature. For such an

application, the dc SQUID at low frequencies is an obvious choice. There are three features of the noise thermometer which make it particularly appealing. First of all it gives directly the thermodynamic temperature once the resistance is known, and provided one can measure voltage and bandwidth. Secondly, the thermometer itself does not receive any power. In the hot electron experiments, I will deliberately heat the "thermometer" by applying power. However, for use as a monitoring thermometer, no power would be applied. This makes the device rather different than, for example, a resistance thermometer, where one must be very careful to not to generate heating while measuring the resistance. Thirdly, the thermometer itself is very simple to construct. It does not matter what the material is or how it is shaped, just as long as it is normal metal and its resistance can be matched to the amplifier. In practice, this allows one to construct very small thermometers.

One problem that confronts any study of the hot electron effect is how to distinguish the observed heating from the Kapitza heating which is ordinarily encountered at low temperatures. For this problem, the use of a thin-film sample is ideal. It should be remembered from Chapter 9 that, at low temperatures in a thin film, there will be no temperature difference between the phonons in the film and the phonons in the substrate. This is because, at low temperatures, the thermal phonon wavelength becomes much larger than the sample thickness, and it is then not possible to speak of two seperate phonon systems. In practice this means that the temperature of the substrate will determine the temperature of the phonons in the metal, and there is no Kapitza resistance between the metal and the substrate.

The temperature of the substrate was estimated from published

experimental data, rather than from direct measurements. This is a shortcoming in the experiments, and was done because the expected increase in the substeate temperature should be negligible, and because a direct measurement of the substrate temperature would have required a considerably more elaborate arrangement. Such a measurement could have been made by depositing an electrically insulating layer on top of the metal film, and then depositing a second small thin film metal resistor on top. If the second film is thermally isolated from everything except the insulating layer, then its Nyquist noise will faithfully record the temperature of the phonons in the first film. This scheme would have required an additional SQUID readout system. Just such a second system was used by Roukes et al., although they made use of an adjacent resistive film rather than one placed on top of the sample.[2]

At low temperatures, the substrate temperature is determined by the substrate thermal grounding (and by the amount of power which is dissipated in the resistor), rather than by the bulk thermal conductivity of the substrate. In these experiments, the substrate loses heat through its contact with the ^{4}He bath and the phenolic canvas mount. I can obtain a conservative estimate of the substrate temperature by considering just the contact between the substrate and the ^{4}He, which obeys a Kapitza heating law of the form:

$$T_{sub} = (P/A\sigma + T_o^4)^{1/4} \qquad (10.1)$$

where P is the power dissipated in the resistor, A is the area of the substrate in contact with the ^{4}He, T_{sub} is the substrate temperature, T_o is the ^{4}He temperature, and $\sigma = 1/(4R_{Kap}AT_o^3)$ is a Kapitza heating constant for a sample with Kapitza thermal resistance R_{Kap}. Fig. 10.1 shows the result of such a calculation, where I have assumed a 5 X 5

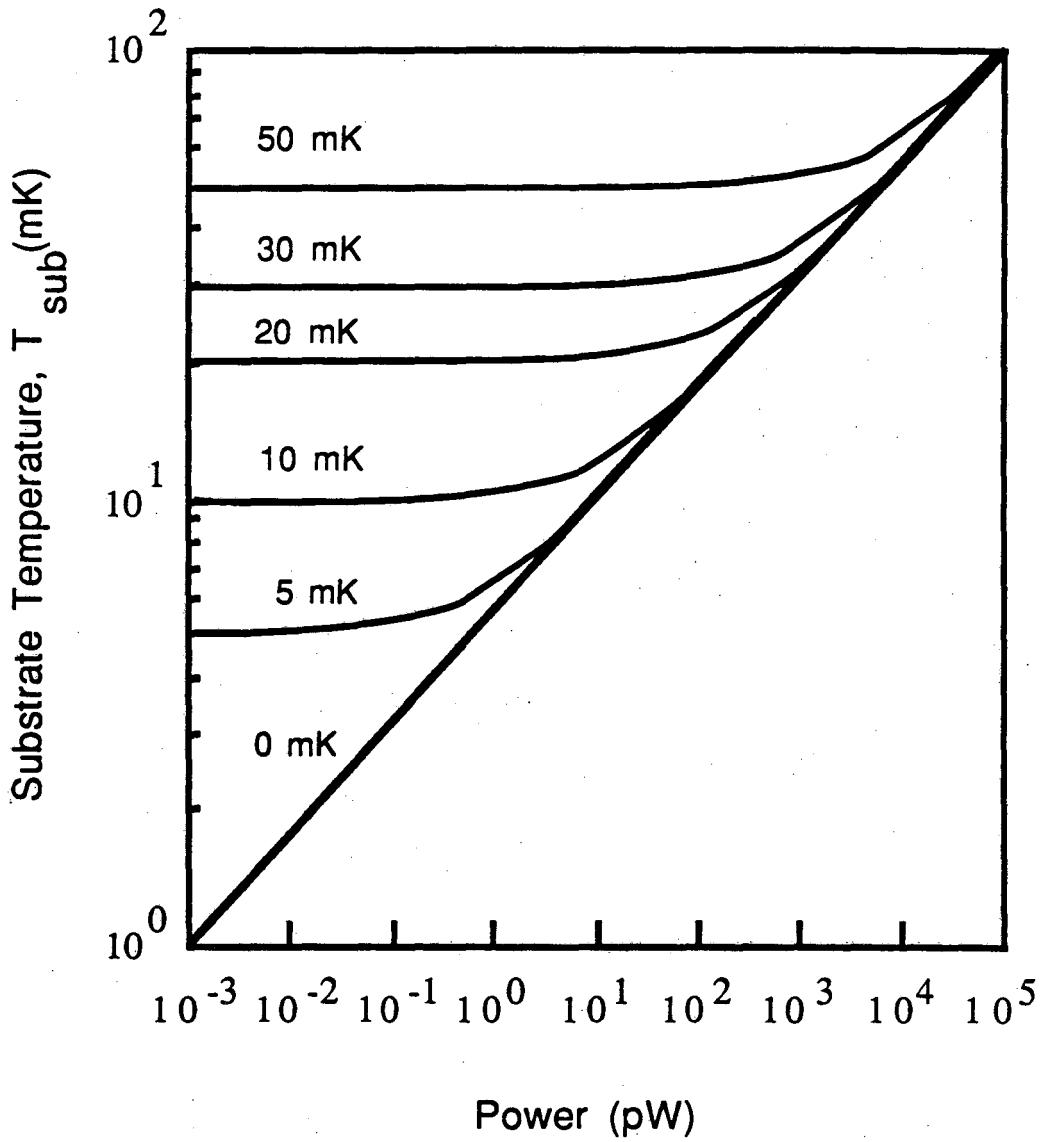

Fig. 10.1 Estimated substrate temperature vs power, the curves are labelled for different ^{4}He bath temperatures.

$(mm)^2$ chip with two sides in contact with the ^4He, and I have taken the constant σ = 20 $WK^{-4}m^{-2}$ as representative of solid to ^4He contact.(6) At a bath temperature of 20 mK and a power of 10 pW, the substrate temperature is raised to only 20.3 mK. At higher bath temperatures, the effect is negligible at this power. The reason for the smallness of this effect is that the substrate is rather large, and consequently the heating is rather small and may safely be neglected. Thus it is to be expected that the phonon temperature may be taken as the bath temperature in the low power and low temperature regime where we operate.

The above arguments notwithstanding, the fact that the phonon temperature was not measured meant that it would be more problematical to distinguish conventional phonon heating from the hot electron effect. This necessitated finding a signature for the hot electron effect other than the obvious one of the temperature difference between the electrons and the phonons. The most obvious alternative signature is the fifth root dependence of the electron temperature on the applied power, see Eq. 9.21. A secondary signature is the magnitude of the effect, although this is only roughly known for the thin-film system at hand.

10.2 Experimental Technique

The main experimental difficulty is to measure the Nyquist noise in a resistor at temperatures down to 20 mK. The experimental arrangement is shown in Fig. 10.2, and is the same as that used in the measurements of SQUID noise, except that I have replaced SQUID(1) with a thin film resistor R_{TF}. Current supply I_{b1} is used here to supply power to the

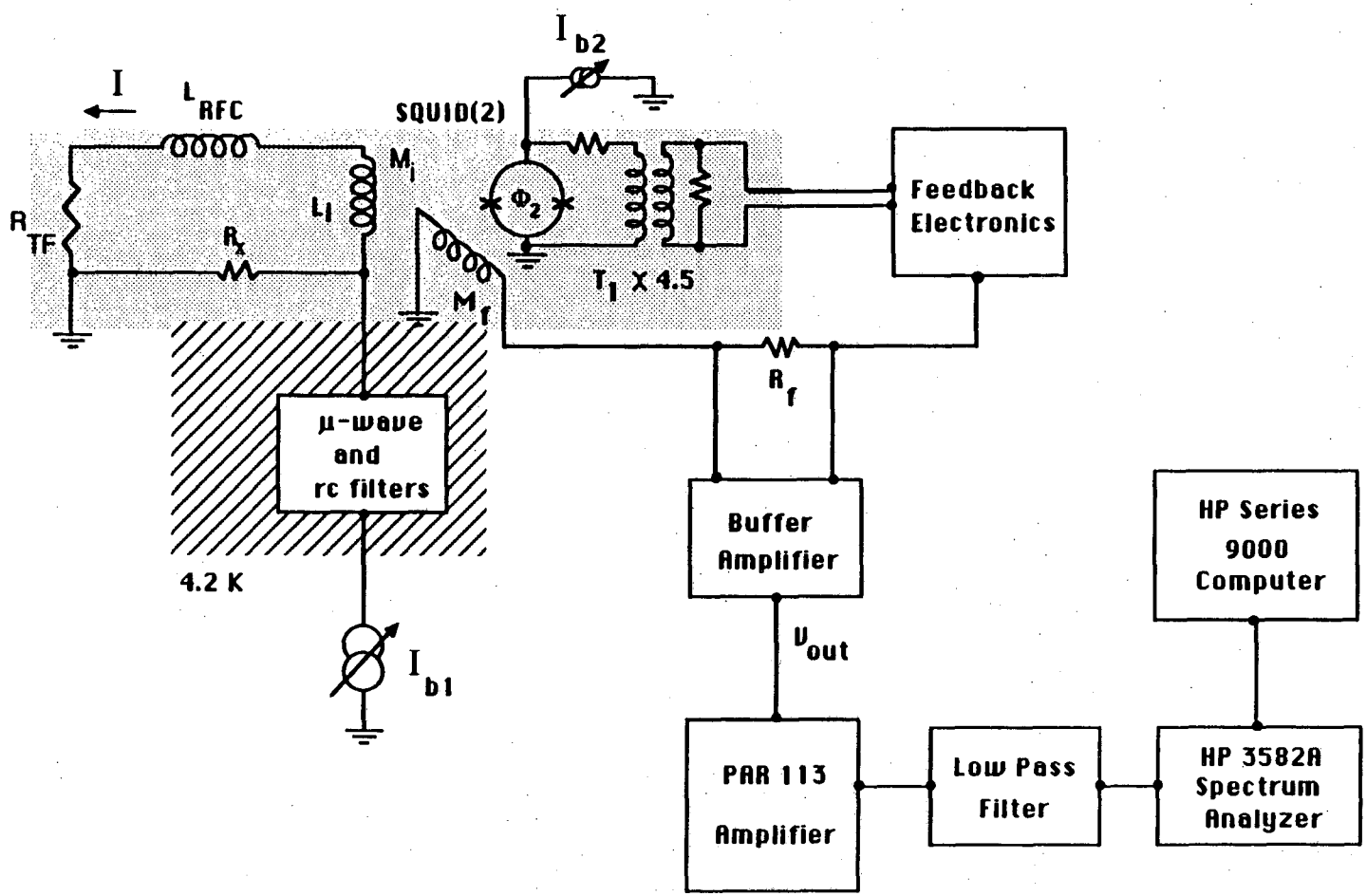

Fig. 10.2 Circuit for measuring noise in thin-film resistor R_{TF} . Shaded area is cooled by refrigerator.

resistor. The SQUID(2) measuring system monitors the noise spectrum in the usual way.

The experimental procedure is as follows. First, the refrigerator temperature is fixed at T_o, and the bias current I_{b1} is set so as to fix the power dissipation P in the thin-film resistor. The noise spectrum is then taken from the feedback output of the locked-up SQUID(2) using a Hewlett-Packard 3582A spectrum analyzer. The bias current I_{b1} is then changed, and a new noise spectrum obtained. The noise spectra and powers are stored on computer for later analysis. The analysis will produce a plot of noise magnitude versus applied current, which is easily converted into a plot of electron temperature vs power, as is discussed below.

10.3 The Bias Resistor R_x

The experimental arrangement is not ideal because of the presence of the bias resistor R_x (see Fig. 10.2). First of all, the thin-film resistance R_{TF} must have a value comparable to R_x in order for SQUID(1) to be able to detect its Nyquist noise. Secondly, the resistor R_x will also produce Nyquist noise which must be subtracted from the total noise, in order to find the noise from R_{TF}. From Nyquist's law, the voltage noise power per Hz produced by the thin film resistor will be:

$$S_{vs}(f) = 4k_B T_e R_{TF}$$

where T_e is the electron temperature in the film. The noise from the bias resistor R_x will be:

$$S_{vx}(f) = 4k_B T_x R_x$$

where T_x is the electron temperature in R_x. The total flux noise power

that is induced in SQUID(2) by the two resistors is then simply:

$$S_\Phi(f) = \frac{4k_B(T_eR_{TF} + T_XR_X)^2 M_i}{(R_{TF} + R_X)^2}$$

where: M_i is the mutual inductance between SQUID(2) and its input coil. It is thus necessary to find R_{TF}, R_X, T_X, and M_i before T_e can be estimated.

From the circuit arrangement, one can see that resistor R_X will also dissipate power and thus tend to heat up. This is undesirable, as it will add to the signal from the thin-film resistor. Electron heating in R_X was minimized by choosing a large resistor volume, and phonon heating was minimized by choosing a large area. R_X was formed from a bulk peice of manganin wire, which was glued to a fiberglass support. The wire diameter was 100 μm, and its length was 1 cm. This yielded a total volume of 7.9×10^{-11} m^3 and an area of 3.2 $(mm)^2$.

The heating in R_X can be estimated under the conservative assumption that the only thermal contact is with the ^{4}He bath. The temperature T_X of the phonons in R_X will be given by a Kapitza heating law:

$$T_X = (P/\sigma A + T_O^4)^{1/4}$$

where: $\sigma \simeq 20$ W/(K^4m^2) is a representative[6] heating constant between a solid and ^{4}He, A is the area of the resistor, and T_O is the bath temperature. Fig. 10.3 shows the result of such a calculation. The expected heating is small, but not completely negligible at a power of 10 pW.

I should here remark that, for the noise measurements on SQUIDs, noise from R_X may be neglected even if it were to heat up. The central reason is that R_X is much smaller than the SQUID dynamic resistance R_D, and thus it will induce in SQUID(2) a flux noise of only:

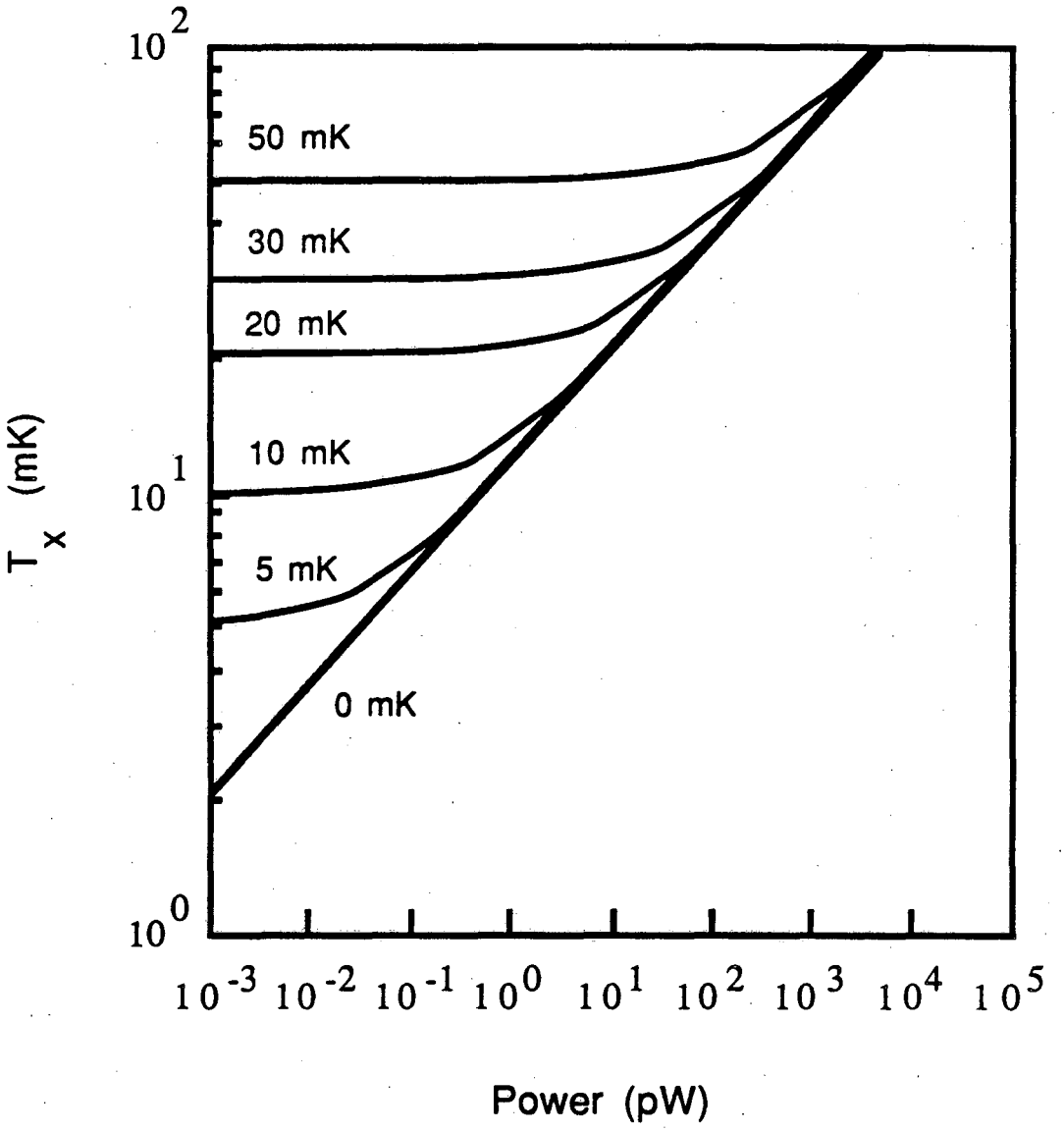

Fig. 10.3 Estimated temperature of resistor R_x vs power, the curves are labelled for different ^{4}He bath temperatures.

$$S_{\phi X} = 4k_B T_X R_X M_i^2/(R_X+R_D)^2$$

a SQUID(1) would, on the other hand, induce a flux noise in SQUID(2) of order:

$$S_{\phi} = 2k_B T_e \gamma_V R M_i^2/(R_D+R_X)^2$$

where T_e is the temperature of the SQUID shunt. For a typical one of our SQUIDs, the ratio is:

$$S_{\phi X}/S_{\phi} \simeq 2R_X T_X/(\gamma_V R T_e) < 0.003 T_X/T_e$$

I have written this as a bound because γ_V increases as the temperature is lowered. The contribution of R_X may thus be safely neglected when the SQUID is operating at low temperatures.

10.4 Data Analysis

The analysis of the data is straightforward but somewhat tedious. The first fact to contend with is that the data is in the form of flux noise power spectra taken at different applied current I_{b1}, whereas one would like electron temperature versus applied power. Also, the noise spectra represent the sum of noise powers from all noise sources, not just the hot resistor R_{TF}. In this analysis, I will assume that the noise is generated by five noise sources:

(1) SQUID(2) and the Measuring Electronics, which has a spectrum of the form white + $1/f^{2/3}$.

(2) Vibrations and Pickup, which will generate well-defined spectral peaks rather than white noise.

(3) The Thin-Film Resistor R_{TF}, which is at temperature T_e.

(4) The Bias Resistor R_X, which is at temperature T_X.

(5) The Current Bias Source, which is at room temperature.

The first step in the analysis consists of visual inspection of the spectra in order to identify frequencies where vibrational noise or pickup occur. These generally appear to be well-defined lines, and are explicitly excluded before proceeding with the remaining analysis. The frequencies chosen are excluded from all of the spectra as a set, although at the higher resistor temperatures, the peaks may not be discernable owing to the larger Nyquist signal. In addition, I explicitly exclude frequencies above 15 kHz, where the performance of the feedback system begins to deteriorate, and below 10 Hz, where the low frequency excess noise from SQUID(2) becomes large.

The noise from the last three sources will produce a Lorentzian spectrum of some height which can be denoted as A. The roll-off frequency of the Lorentzian, f_{knee}, is determined by the time constant of the input circuit, and is just:

$$f_{knee} = (R_X + R_{TF})/(2\pi(L_{RFC} + L_i))$$

Taking into account the first source, the noise spectra can then be fit to a function of the form:

$$S_\Phi = \frac{A_{2/3}}{f^{2/3}} + B + \frac{A}{1+(f/fknee)^2}$$

where: $A_{2/3}$ is a fixed constant which depends only on the temperature of SQUID(2), and has been found from independent measurements on the low frequency noise in SQUID(2). The parameters A, B, and f_{knee} are varied to produce the best χ^2 fit. The parameter B is just the white noise flux level of the measuring SQUID(2) system, and is a constant which is independent of the temperature of R_{TF}. The parameter f_{knee} is the rolloff frequency of the Lorentzian, and should likewise be a constant which is independent of the temperature of the resistor R_{TF}.

Once the coefficient A has been found, the next step in the analysis

is to subtract off the noise due to the current bias source. This is generally a small correction of order 10% or less. It is estimated from the simple construction of the current supply, the filters, and the input circuit.

The height A' of the remaining Lorentzian spectrum can then be written as the sum of the Nyquist noise from just two sources, the resistors R_{TF} and R_X. Let A_o denote the noise due to the resistors when no power is applied and both are at the same temperature T_o. The noise A' when resistor R_{TF} is at T_e and R_X is at T_X can be written in the form:

$$A' = A_o(T_X R_X + T_e R_{TF})/(T_o R_X + T_o R_{TF})$$

I can thus write:

$$T_e = A' T_o (R_X + R_{TF})/(A_o R_{TF}) - T_X R_X / R_{TF}$$

To find T_e from the above formula, I must now make the following assumptions:

(1) I will assume that the resistor R_X is at the bath temperature, ie $T_X = T_o$, for all applied power. The bath temperature is found from a calibrated Ge resistance thermometer or a calibrated carbon resistance thermometer mounted on the outside of the cell, (see Chapter 2). This non-heating of R_X is reasonable because the resistor R_X is physically much larger than the thin-film resistors, and the heating should thus be much less, as was discussed in section 10.3. I will examine the situation more closely below, for each resistor. A better way to do the experiment would be to make the bias resistor a thin film resitor as well, thereby eliminating the uncertainty, doubling the signal, and simplifying the analysis.

(2) I take A_o in Eq. 10.5 as the height of the Lorentzian when

there is no applied bias current (of course, having removed already the effect of the SQUID, vibrations, and current sources). Thus the point with no applied power is fixed at the measured power and bath temperature, and the calculated T_e and the bath temperature will accordingly agree there. The result can be checked by comparing the noise with that expected from $4k_BT_eR_{TF}$, and one finds estimates of T_e which are in close agreement.

(3) Finally, the ratio R_X/R_{TF} is found independently by sending down a known amount of current I_{b1} and seeing how much current I passes through the sample arm of the circuit. Since the remainder of the sample arm of the input circuit is superconducting, this will directly give us R_X/R_{TF}.

With the above three assumptions and independent measurements, I can find T_e at a given bias current. For a bias current I_{b1}, the power dissipated in R_{TF} is just:

$$P = I_{b1}^2 (R_X^2 R_{TF})/(R_{TF}+R_X)^2$$

The above analysis of the data is quite lengthy. Fits to the spectra can produce a Lorentzian height A which is accurate to about 1%, based upon observed χ^2 behavior for the fits. The fit for f_{knee} is no better than about 10%, but fortunately, errors in f_{knee} produce only second order corrections to the estimated height of the Lorentzian. At low temperatures, the white noise from SQUID(2) is of the same order as the Lorentzian for the large resistor, and about 1/2 as large as the Lorentzian for the small resistor. At high powers, the SQUID noise becomes quite negligible, and its estimation has little effect on the estimate of A.

10.5 The Small Resistor: Resistor 1

The main purpose of the first experiment was to determine whether or not the hot electron effect existed in our SQUID shunts. At first sight, the most obvious way to determine this would be to watch the noise in the SQUID as the bias power was varied. At higher bias voltages the shunts would be hotter, and one would expect to see more noise. By studying the dependence of the noise upon the bias voltage one could hope to verify Eq. 9.21. Unfortunately, this method turns out to be difficult for two reasons. First of all, the bias power cannot be increased greatly before, at high voltages, the SQUID begins to lose gain. On the otherhand, the temperature will only change as the 5th root of the power, so we will need to sweep the power by a large amount in order to clearly see the presence of heating. If the voltage is too large, however, the SQUID simply begins to act like a resistor. Since this resistance is rather large (say 4 Ω), the noise is rather small, and somewhat difficult to detect with the present setup. Secondly, even without the presence of heating the noise in a SQUID depends upon the bias voltage. This dependence is non-trivial even for a SQUID with a very clean I-V, and would have to be accurately accounted for before one could hope to see any additional voltage dependent heating effect.

For these reasons, it was necessary to construct a seperate test resistor, Resistor 1, which is shown schematically in Fig. 10.4. It is a small area AuCu thin-film which was chosen to have roughly the same area and volume as a pair of our typical SQUID shunts. The film is 20 μm by 30 μm, and 36 nm thick. It is contacted by two Nb strips which were 20 μm in width and 200 nm thick. In this configuration, the resistance is

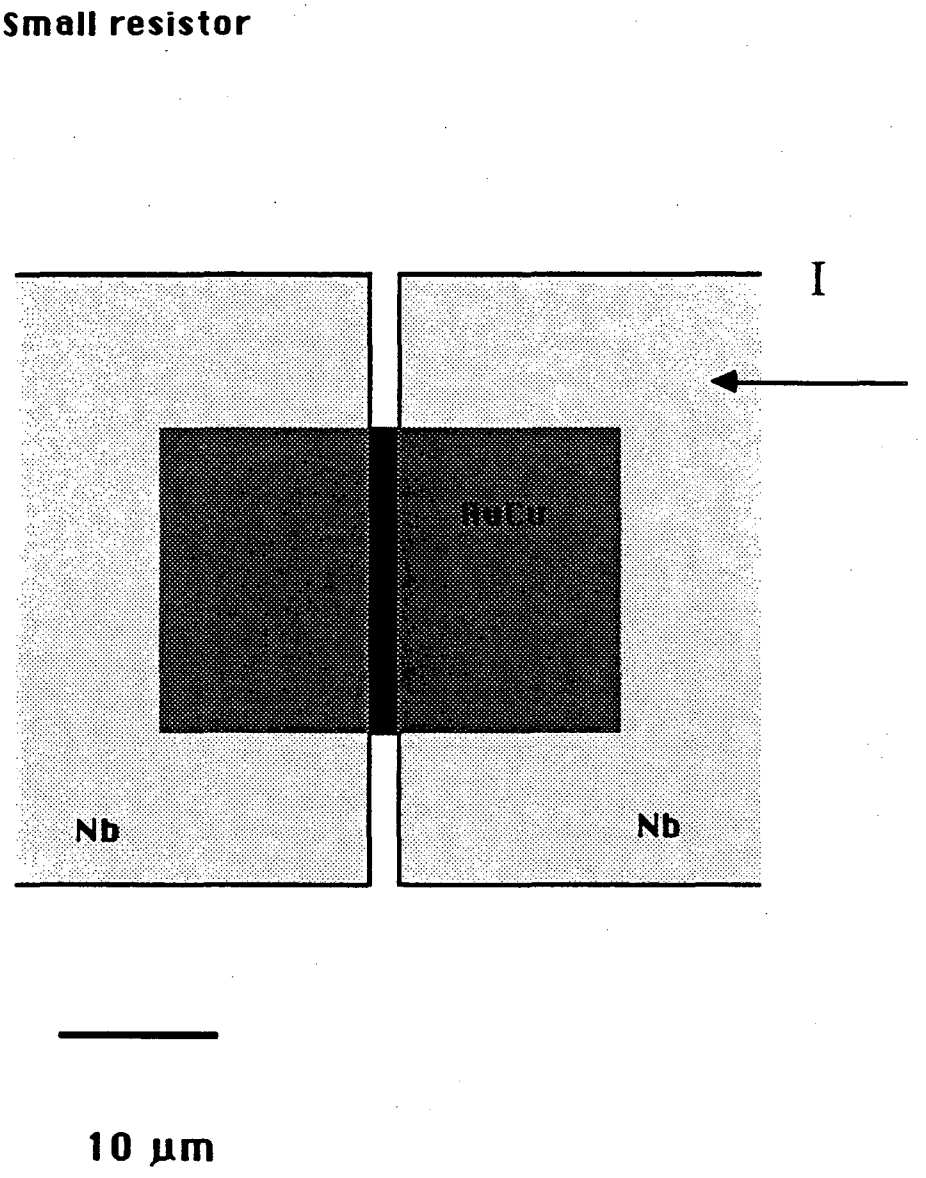

Fig. 10.4 Construction of the small thin-film test resistor R1.

determined by the narrow 2 μm gap seperating the Nb strips. This gap is bridged by the center of the AuCu film. The total volume of the AuCu was 21.6 $(\mu m)^3$, and the area was 600 $(\mu m)^2$. The bias resistor R_x was thus roughly 5000 times larger in the area and 4 X 10^6 times larger in the volume. In this case, we would expect the heating in R_x to be completely negligible compared to that in R_{TF}. Although the volume is about the same as that of the SQUID shunts, the resistance was deliberately made much smaller to increase the current noise which SQUID(2) would measure.

The AuCu was deposited and patterned using the same procedure as described in Chapter 1 for the SQUID shunts. The substrate was a Si wafer with a 1.2 μm thick layer of thermal oxide, as was used for the SQUIDs. After patterning with photoresist, 2.5 nm of Cr were evaporated, followed by the AuCu. The film was then lifted off, leaving the small AuCu region, and the wafer was cleaned in the standard way (see Chapter 1). The Nb film was then sputtered onto the AuCu, and patterned by plasma etching to form the Nb contact lines and pads. Electrical contact to the resistor was made in the usual way with pressed In pads. The resistor was mounted in the SQUID(1) stage and clamped in place with the phenolic canvas cover plate.

The resistance of the film at low temperatures was measured by applying bias current I_{b1} and watching the feedback output of the SQUID. I_{b1} divides between the two arms of the input circuit in proportion to the conductance of the arms, see Fig. 10.2. We can measure how much current I_{b1} is being sent down and we can measure how much of it is passing through the SQUID's input coil. The resitance of R_x = 0.072 Ω, and the mutual inductance of the SQUID with its input coil M_i = 6.2 nH,

were measured in separate experiments. With these parameters known, it was possible to find the resistance of the sample R_{TF} = 0.26 Ω.

10.6 The Proximity Effect

In this section I want to remark on the possible role of the proximity effect in this system. The proximity effect describes the diffusion of pairs from a superconductor into a piece of normal metal. The superconducting pair wavefunction can thus be non-zero in the normal metal, effectively turning the noraml metal into a superconductor for some distance from the normal metal-superconductor interface. De Gennes[7] first calculated this length scale, d, and found:

$$d = (\hbar v_F \ell_e / 6\pi k_B T)^{1/2}$$

where: ℓ_e is the electron mean free path in the normal metal, T is the temperature, and v_F is the Fermi velocity. For small temperature T, this length can become quite long. For the AuCu alloy used, I have estimated $\ell_e \simeq$ 20 nm from the film resistivity. The estimated length d is then about 0.7 μm at 20 mK. Thus, we might expect that the 2 μm gap between the Nb contacts and all of the AuCu under the Nb would be driven superconducting.

In fact this did not happen. The resistance of the samples was independent of temperature, was consistent with the expected resistivity of AuCu, and most certainly was not zero at even the lowest temperatures. In fact, the heating effects are consistent with the entire film being normal, even the parts overlaid with Nb. If the portions of the AuCu under the Nb were superconducting, then my estimates for the heating coefficient, Σ, would have to be increased by

an order of magnitude.

The reasons for the non-occurrence of the proximity effect are probably two-fold. First of all, the AuCu is uderlain by a Cr film about 5nm thick, some of which has probably oxidized to ferromagnetic Cr-oxide. The ferromagnetism would suppress superconductivity in the normal layer. Secondly, there was no special treatment of the AuCu surface before sputtering on the Nb contacts. The cleanliness of the interface has a strong effect on the strength of the proximity effect, as the presence of paramagnetic ions at the interface can cause a large reduction of the pair wavefunction in the normal metal. In general, some experimental care must be taken to obtain a clean interface if one is to find a strong proximity effect. I thus conclude, from experimental considerations, that the proximity effect is probably very suppressed in this system, and that all of the AuCu is normal.

10.7 Discussion of the Results: Resistor 1

The results of the data analysis for Resistor 1 are shown in Fig. 10.5. I have plotted the electron temperature in the thin-film resistor versus the power being dissipated in the film. The open squares show data from the small resistor, Resistor 1, taken at a bath temperature of 25 mK. The closed diamonds show data taken on the same resistor with the bath temperature held at 105 mK.

I first remark on the 25 mK results. At small bias powers, the electron temperature is just the bath temperature. As power is applied, the resistor begins to heat. At high powers, the plot is a straight line on a log-log plot. The slope is 1/4.87, and thus T_e is proportional to

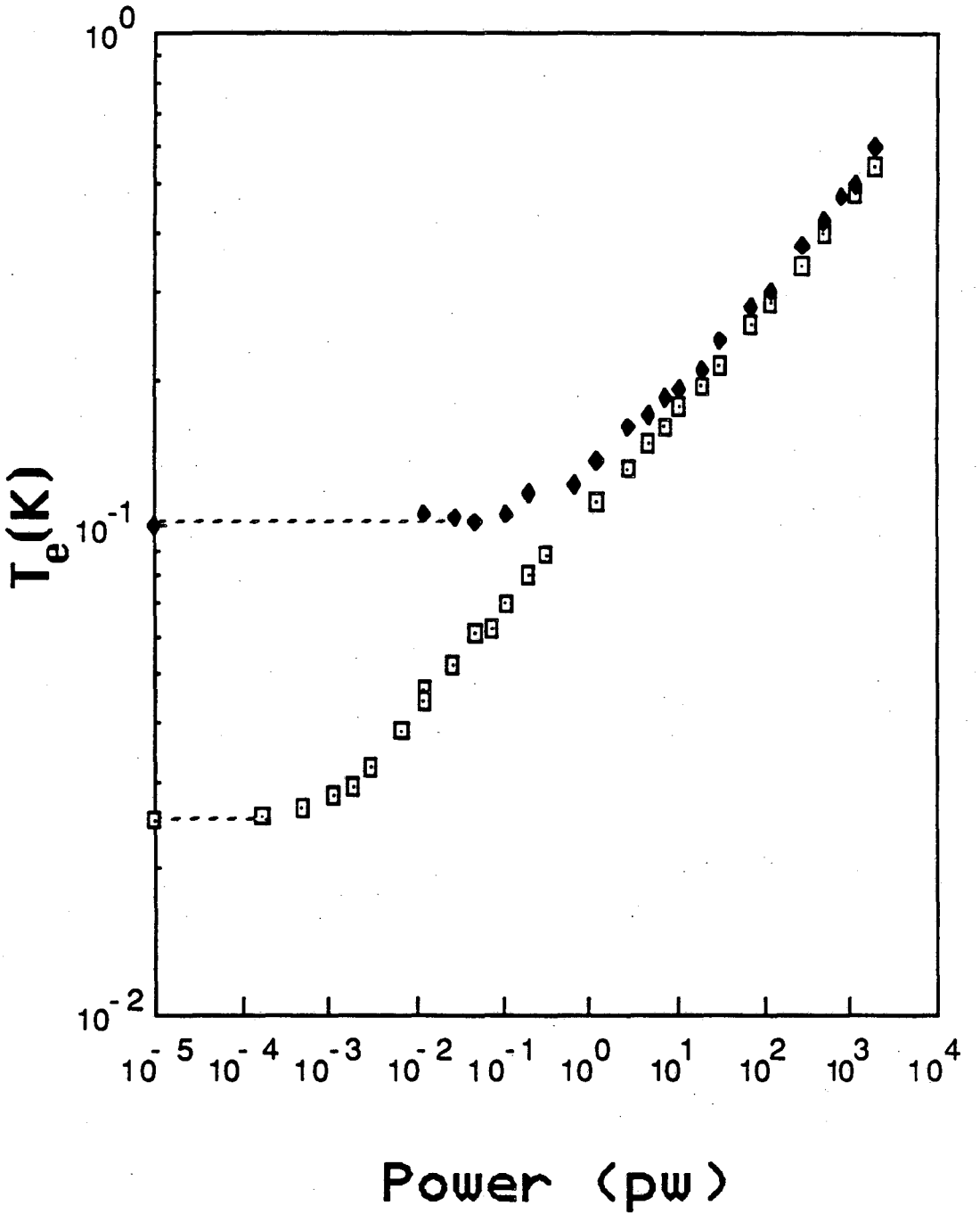

Fig. 10.5 Electron temperature vs applied power. ⊡ Resistor 1 with 25 mK bath temperature, ♦ Resistor 1 with 105 mK bath temperature.

$p^{1/4.87}$. This is very near to the 1/5 dependence expected from the electron-phonon effect, as was dicussed in Chapter 9. One startling thing about the figure is that the heating begins at quite small applied powers. When the bath temperature is 25 mK, the transition to the heating regime occurs at a power of approximately 1 fW. At a typical SQUID power of 7 pW, the electron temperature is already about 140 mK. As noted above, the small resistor has approximately the same volume as our typical SQUID shunts. From this data, we would then expect that a typical SQUID would not cool below about 140 mK. This is precisely what is observed, as will be discussed in Chapter 11.

Changing the bath temperature of the small resistor causes the transition to heating to occur at a larger power. In Fig. 10.5, the closed diamonds show the heating found in Resistor 1 when the bath temperature was held at 105 mK. At low bias power, the electron temperature is equal to the bath temperature. As the power is increased, the electrons begin to heat. Again, the transition to the heating regime is quite rapid. At high bias power, the heating again follows a 1/5 law, and falls approximately on the same curve as the data with the 20 mK bath temperature. This is to be expected, since when the electrons are much hotter than the bath temperature, the actual value of the bath temperature does not make much difference to the heating. The Ge and carbon thermometer calibrations are no better than about 5%. This produces a systematic error in T_0. Curves calculated for the same bath temperature will thus be systematically lower or higher than those for different bath temperatures if the calibration is incorrect. This uncertainty is the most likely source of the small discrepancy between the small resistor run at 105 mK compared to 25 mK at the high power

points.

The data can be fit to a heating power law of the form:

$$T_e = (P/\Sigma\Omega + T_o^n)^{1/n}$$

The solid line in Fig. 10.6 shows a chi-squared fit to the data for Resistor 1 at 25 mK, for which the data is cleanest. From the fit one finds $\Sigma \simeq 2.4 \times 10^9$ $Wm^{-3}K^{-5}$ $\pm$ (0.6×10^9) , and $n = 4.87 \pm (0.05)$. The data is good enough to categorically rule out a 1/4 dependence. The value $n = 5.0$ is about 2σ from the observed value. Thus the data is consistent with electron heating, but is inconsistent with standard phonon heating. The largest source of error in the estimation of Σ is the determination of the bath temperature; a 5% error in T_o translates into a 25% error in Σ. The transition from the bath temperature to the heating regime is very abrupt in the theory, and the data is entirely consistant with this.

The magnitude of Σ deserves some discussion. First of all, this value of Σ is somewhat larger than that which has been found in similar metallic systems. The measurements of Roukes et al.[2] on clean Cu samples can be interpreted to yield $\Sigma \simeq 1.8 \times 10^9$ $Wm^{-3}K^{-5}$. The work of Anderson and Peterson[1] on bulk Cu can be interpreted to yield a $\Sigma \simeq 1 \times 10^9$ $Wm^{-3}K^{-5}$. From the theory presented in Chapter 9, the coeficient $\Sigma \simeq 1.0 \times 10^8$ $Wm^{-3}K^{-5}$, whereas the electron-phonon scattering rate measurements of Gantmakher and Gasparov[8] can be interpreted to yield $1.1 \times 10^9 < \Sigma < 1 \times 10^8$ $Wm^{-3}K^{-5}$ in pure Cu (see Table 9.1 in Appendix E of Chapter 9). All of these values would have yielded somewhat larger heating than was observed, i.e. higher electron temperatures. Since we are mainly concerned with obtaining cooler SQUIDs, our results should be regarded as fortuitous.

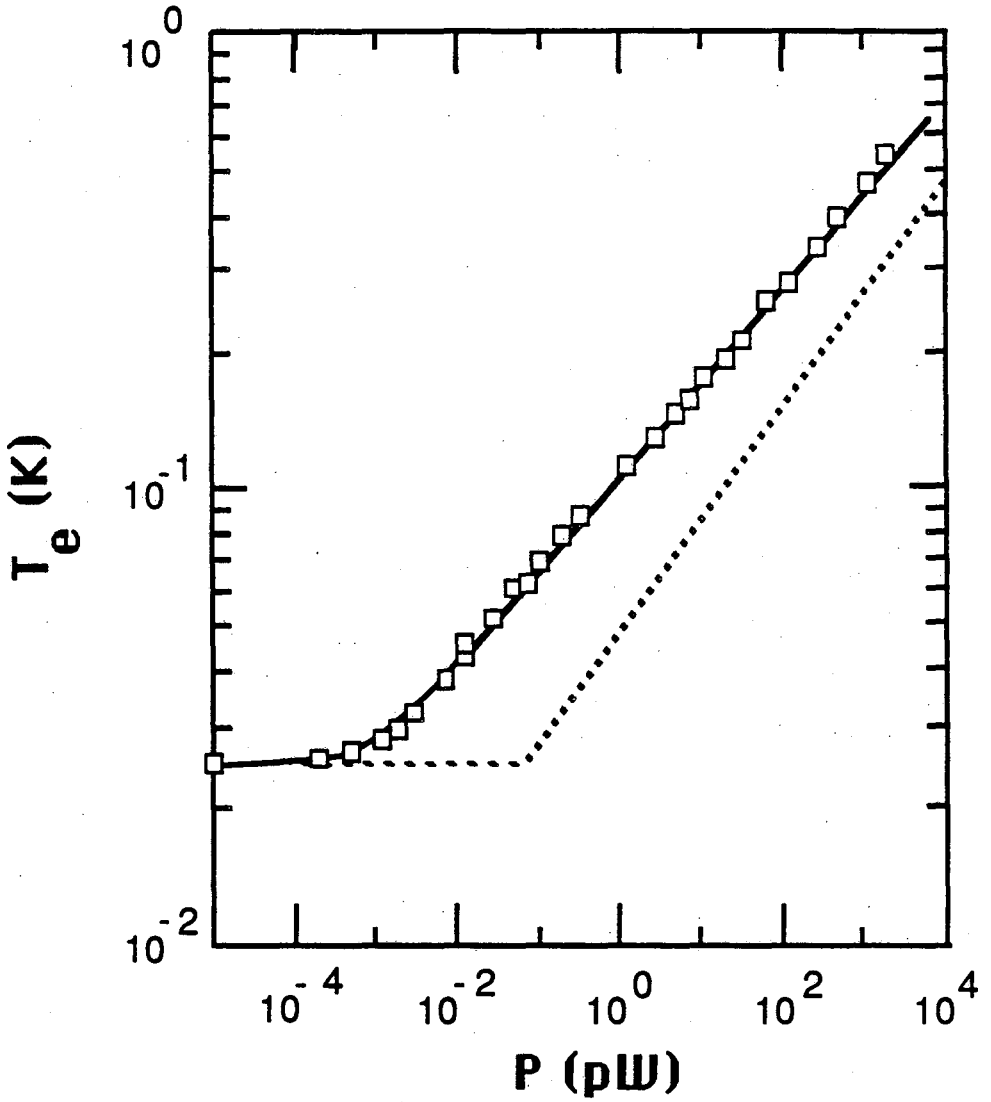

Fig. 10.6 Electron temperature T_e vs. applied power P: □ Resistor R_1 at T_0=25 mK. Solid line is fit to data, dashed line is naive estimate of phonon temperature in the metal film.

The reasons for these discrepancies are not known, however, a few remarks are in order. First of all, the other measurements were made on pure Cu, and it is not surprising that they should differ from our dirty AuCu alloy. Secondly, the model calculation of Σ does not take into account the shape of the Fermi sphere and the inclusion of transverse modes as was disscussed in Chapter 9, this means the model should considerably underestimate the scattering rate and consequently underestimate Σ. The experimental work of Gantmakher and Gasparov[8] clearly demonstrates that higher Σ can be expected due to increased scattering at the necks of the Fermi surface. Their data should, and does, yield a better estimate of Σ. Thirdly, it is interesting to note that the two thin-film experiments yield values for Σ which are within 25% of each other, depsite the different nature of the films. Finally, it is interesting to note that the two thin-film experiments yielded a value of Σ about a factor of 2 larger than the bulk experiment of Anderson and Peterson,[1] and this Σ is greater than that expected from even the highest scattering rates which were observed in Cu.[8] In general, one would expect Σ to be an average over the Fermi surface, and thus it should receive only a small contribution from the relatively small neck region, and could never exceed the highest rate. The experimentally observed large value of Σ could be a substrate effect (see section 9.7).

Finally, I note that the magnitude and form of the observed heating is inconsistent with phonon heating. If we put aside the arguments against a temperature difference between phonons in the metal and the phonons in the substrate, we can naively use Kapitza resistance arguments to estimate the temperature difference. The dased line in Fig.

10.6 shows this naive estimate for the temperature of the phonons in the metal, where I have used a representative value for the Kapitza resistance between two solids.(6) Neglecting the difference in the slopes, the curves look similar. But, at low temperatures, the power required to produce a given temperature is nearly 2 orders of magnitude greater for the naive phonons than is observed. This says that the observed thermal resistance is nearly two orders of magnitude greater than naive expectations, and this is fairly strong evidence agaist the naive phonon model. Similarly, the expected heating in R_x and the substrate are much too small to account for the observed effect.

10.8 The Large Resistor: Resistor 2

The purpose of the second thin-film experiment was to try to reduce the level of heating by increasing the volume of the film. The configuration of the second resistor, Resistor 2, is shown in Fig. 10.7, and is somewhat different than that of the the small resistor. The resistor is a composite film which was deposited in a three step process. The substrate was an oxidized Si wafer as was used for the SQUIDs. After patterning with photoresist, 2.5 nm of Cr was evaporated and a 36 nm thick Au(Cu 25Wt%) film was deposited and patterned using the same procedure as described in Chapter 1 for the SQUID shunts. The film was then lifted off and the wafer cleaned in the standard way (see Chapter 1). This procedure left a small central 60 X 60 μm^2 AuCu film. A 200 nm Nb film was then sputtered onto the AuCu with no other surface preparation, and patterned by plasma etching to form the Nb contact lines and pads. The wafer was then diced and individual chips processed

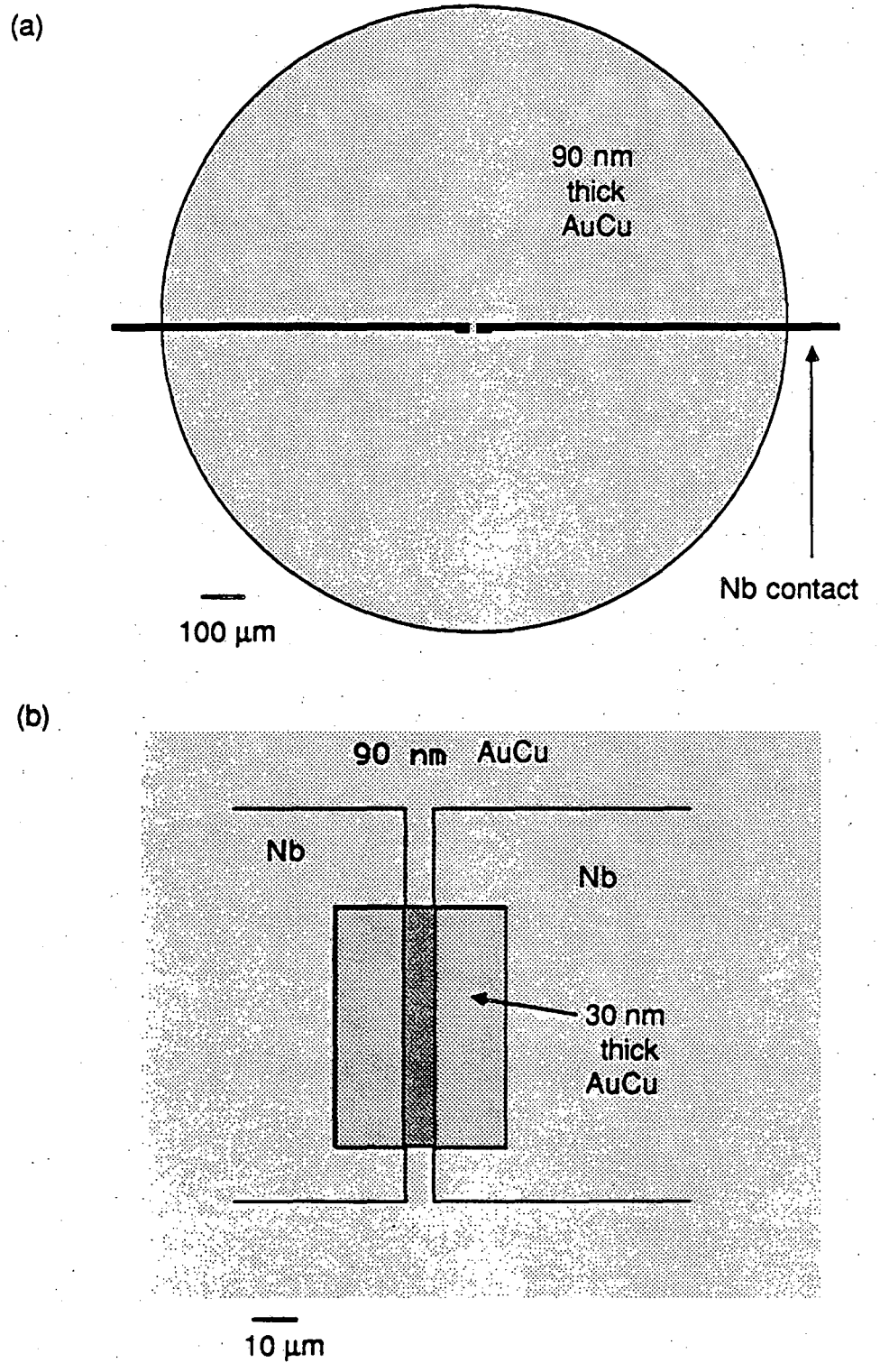

Fig. 10.7 Construction of the large resistor, R_1.
(a) Large scale, (b) detail near narrow central gap.

separately. The surfaces of the AuCu and Nb were then cleaned using an Ar ion mill as described in Chapter 1 for junction fabrication. A crude evaporation mask was then fashioned out of a piece of aluminum foil with a 1.4 mm diameter hole punched in it. The sample was removed from the vacuum evaporation chamber, the mask centered on the small gap, and system was then re-evacuated. A 90 nm thick layer of AuCu was then evaporated, leaving a 1.4 mm diameter AuCu spot covering the Nb pads. Electrical contact to the resistor was made in the usual way with pressed In pads.

The electrical configuration of Resistor 2 is somewhat unusual. The resistance is determined by the small central gap between the two Nb contacts. The resistance of the large resistor was measured in the same manner as for the small resistor, and a value of 0.076 Ω was found.

The thermal behavior of Resistor 2 is also unusual. Most of the applied current will flow through the gap region, and consequently the heating will also be greatest in the gap. On the otherhand, little bias current flows in the large surrounding region of film. Nonetheless, we expect that the surrounding film will act as a cooling fin into which hot electrons from the center can diffuse and lose energy. The total volume of the large resistor was 1.9×10^{-13} m^3, and the total area was about 1.6×10^6 $(\mu m)^2$. The bias resistor R_x was roughly 420 times larger in the volume and only about 2 times greater in the area, assuming that all of the film contributes to the cooling. In general, this will not be the case, and the effective cooling area of the film will be substantially smaller at higher temperatures.

10.9 Discussion of Results: Resistor 2

I now remark on the heating behavior of the large resistor, Resistor 2. It shows important differences from the small resistor, Resistor 1. The solid squares in Fig. 10.8 show the electron temperature as a function of applied power when the refrigerator bath temperature is held at 25 mK. Compared to Resistor 1, we can see that Resistor 2 requires about 4 orders of magnitude more power before it begins to heat above the bath temperature. At a typical SQUID power of 7 pW, the Resistor 2 has heated up to only about 30 mK, instead of the 140 mK found for Resistor 1. We thus expect to be able to operate SQUIDs down to an electron temperature of about 30 mK if the SQUID are made with such a resistor.

The results on the two resistors can be compared by plotting the electron temperature versus the power per unit volume. The result is shown in Fig. 10.9. On this plot we see that the transition to heating begins at about the same value of P/Ω for the two resistors. This is understandable if both resistors are in the 0-D limit discussed in chapter 9. The estimated inelastic mean free path at 25 mK is about 2 mm, so it is reasonable that even the large film of Resistor 2 is in this limit.

At higher power densities Resistor 2 begins to heat more rapidly than in the Resistor 1. The curve is again approximately straight on a log-log plot, although it is much more scattered at low power. The slope however is not 1/5, but 1/2.7.

The origin of this different slope is not known for certain. There are two possible explanations. First of all, this may be a spurious

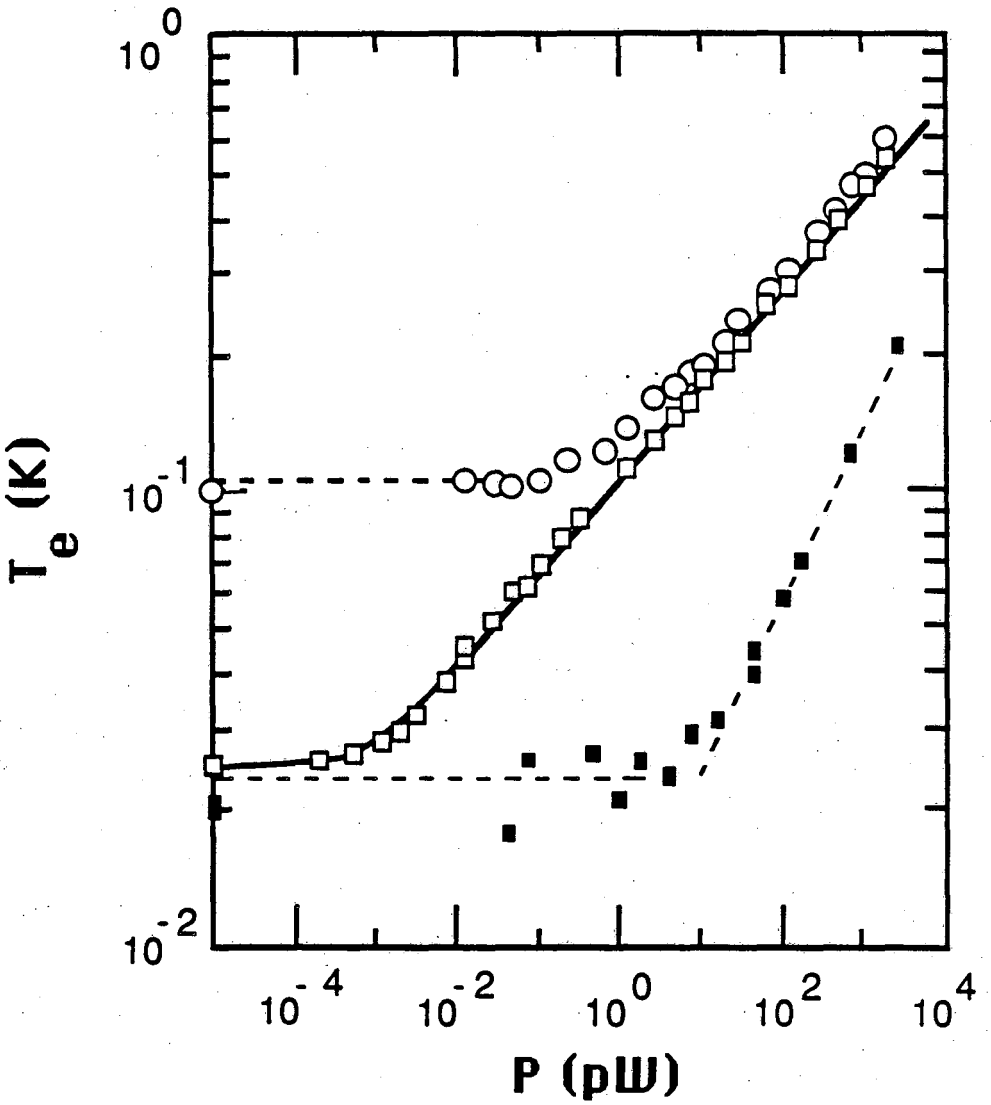

Fig. 10.8 Electron temperature T_e vs. applied power P: □ Resistor R_1 at T_0=25 mK, ○ Resistor R_1 at T_0=105 mK, ■ Resistor R_2 at T_0=25 mK. Dashed lines are to guide the eye, solid line is fit to R_1 data.

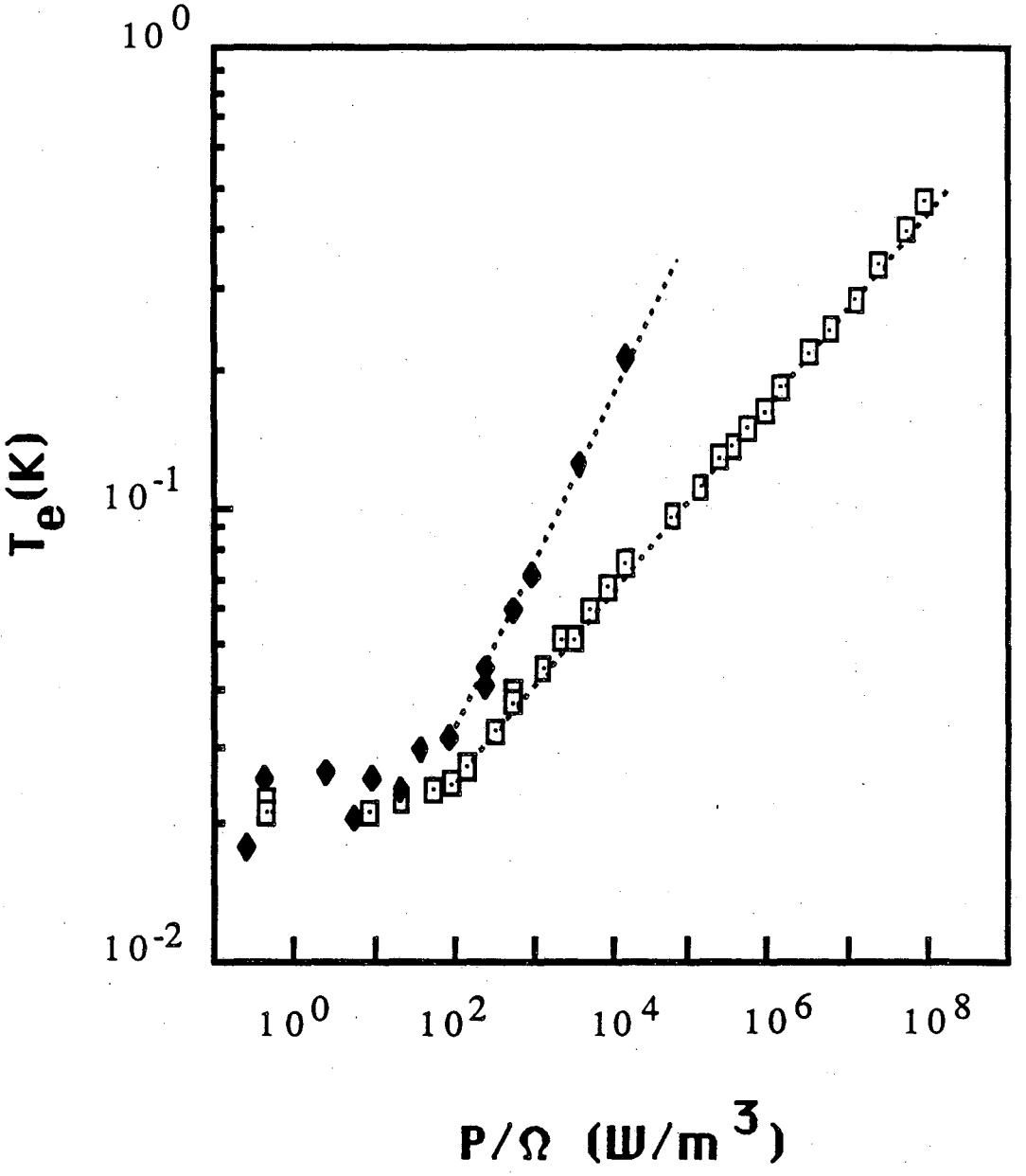

Fig. 10.9 Electron temperature vs the power per unit of volume of Resistors 1 and 2. ▫ Resistor 1 at a bath temperature of 25 mK, ♦ Resistor 2 at a bath temperature of 25 mK.

effect of phonon heating in R_X. In Fig. 10.10, the estimated heating of R_X, shown in Fig. 10.3, has been superposed on the data for Resistor 2. The two curves are uncomfortably close, especially considering the rough nature of the estimate of the heating in R_X. On the otherhand, the estimate should be a conservative bound, and at high powers, the two curves deviate considerably. The second possibility is the interpretation I presently favor. The experimental arrangement is essentially that of a 2-D film heated locally at a point. This case was discussed in Chapter 9, where I noted that the effective area of the film would decrease with increasing power because of the shortening of the inelastic mean free path with increasing temperature. A rough calculation gave a slope of 1/2 for the temperature dependence. The calculation was undoubtedly too crude to yield the exact slope, but the point here is that the slope should depend upon the heating and film geometry, and the slope should be greater than 1/5 because of the effective area reduction. The divergence of the two curves in Fig. 10.9 can then be interpreted as a measurement of the reduction in the effective volume of Resistor 2 as the electron temperature increases.

10.10 Concluding Remarks

In conclusion, I have observed a large amount of heating in small normal metal films. The level of this heating is consistent with that seen in the SQUID experiments, as will be seen in the next Chapter. The dependence of the heating on the applied power in the small volume resistor is consistent with that expected from the hot electron effect. The coefficient of the heating, Σ, is somewhat larger than that seen in

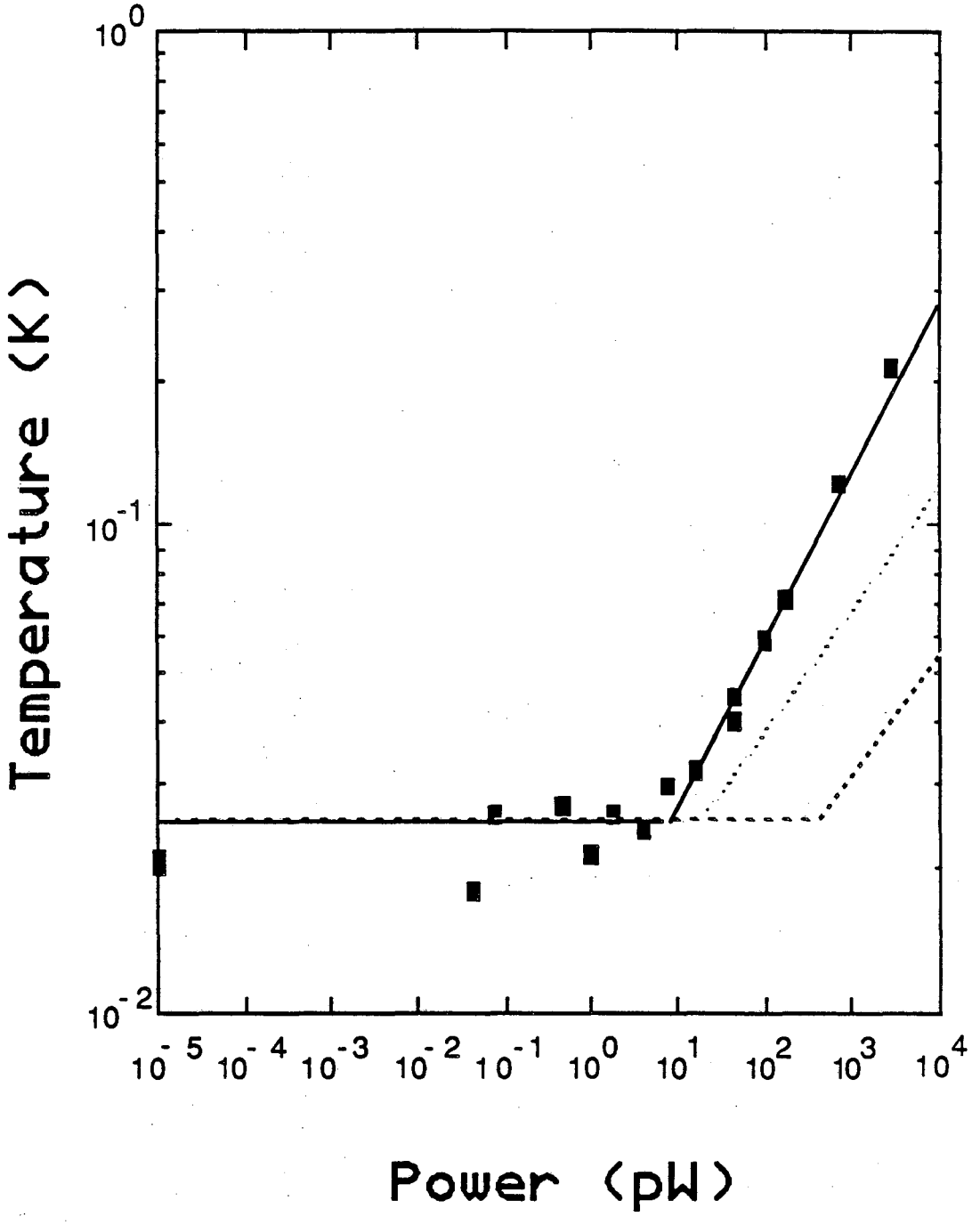

Fig. 10.10 Electron temperature vs pwer for Resistor 2 at a bath temperature of 25 mK. Dashed line shows estimate of substrate temperature, dotted line shows conservative estimate for the temperature of R_X.

other systems. Heating in the large volume resistor is substantially smaller and demonstrates that in principle the heating in the SQUID shunts could be reduced so that the effective electron temperature was 30 mK. The temperature vs power heating law is different for the large resistor, and is suggestive of the spatial hot electron effect discussed in Chapter 9.

The technique outlined above may be of interest in other experiments. The thermometer is of very small size, and in principle can be made as small as allowed by lithographic techniques. Its construction is particularly simple and robust, beig merely a thin metal film. This allows for the possibility of putting a large number of temperature sensors onto an experiment, or of packing them very close together. The small metal volumes are quite sensitive to heat and applied electrical power, and their small size would allow the construction of novel devices, such as a thin film bolometric imager. The main drawback is that the signal is very small by conventional standards, being just the thermal noise in a resistor at say 20 mK. For a well-designed SQUID measuring system however, this is actually a rather large signal, and is easily detected.

Finally, I wish to remark on the obviously incomplete nature of the experiments. Our goal was a fairly limited one. We wanted only to get the SQUIDs colder. Because of this we undoubtedtly missed a great deal of interesting and unexplored physics. There are several areas which would provide interesting experimental results. For example:

(1) What is the role of the substrate in determining the cooling rate?

(2) Is there a better choice of materials for the SQUID, ie. ones

which would yield substantially higher cooling?

(3) Are we really seeing spatial hot electron effects?

(4) What is the heating behavior in 1D, 2D, and 3D geometries?

(5) What is the ultimate limit to which a SQUID with fixed power can be cooled?

(6) Is it possible to see the hot electron effect at substantially higher temperatures in very small volumes of metal, or in a metal film which is suspended off of the substrate?

(7) Can we confirm that the electron temperature and the noise are related in the standard way in this non-equilibrium system?

There is also much theoretical work that should be finished. In particular: an explanation of why the bulk rates are so high, the development of a theory of the spatial hot electron effects, and a rigorous calculation of substrate effects. These, and many other possible investigations, would go a long way towards shedding more light on the hot electron effect. Given the ubiquity of the hot electron effect in normal metal thin-films below 1 K, and the growing development of mK techniques, the solution of these problems are of considerable general importance.

References

(1) A.C. Anderson and R.E. Peterson, "The Thermal Resistance Between Electrons and Phonons in Cu", Phys. Lett., 38A, 519 (1972).

(2) M.L. Roukes, M.R. Freeman, R.S. Germain, R.C. Richardson, M.B. Ketchen, "Hot Electrons and Energy Transport in Metals at Millikelvin

Temperatures", Phys. Rev. Lett., 55, 422 (1985).

(3) For a general review of the radio frequency size effect and related effects, the interested reader can consult: J.M. Ziman "Principles of the Theory of Solids", 2nd Ed., Cambridge Univ. Press, New York, p. 312 (1979).

(4) V.F. Gantmakher, "The Experimental Study of Electron-Phonon Scattering in Metals", Rep. Prog. Phys. 37, 317 (1974).

(5) See also ref. 1, p 287; or A.B. Bhatia, "Ultrasonic Absorption", Dover Publ. Inc., New York, 290 (1985).

(6) see Fig. 9.11 in O.V. Lounassma, "Experimental Principles and Techniques Below 1K", Academic Press Inc., N.Y., p 226 (1974).

(7) P.G. De Gennes, Rev. Mod. Phys. 36, 225 (1964); and "Superconductivity of Metals and Alloys" W.A. Benjamin Inc., New York, p. 232 (1966).

(8) V.F. Gantmakher and V.A. Gasparov, "Anisotropy of the Probability of Electron Scattering by Phonons on the Fermi Surface of Copper", Sov. Phys.-JETP, 37, 864 (1973).

Chapter 11 : Hot Electron Effects in the dc SQUID

11.1 Introduction

In the previous two Chapters, I have discussed the theory of the hot electron effect in normal metals, and presented data on two thin-film systems. In this Chapter, I will discuss the relevance of the hot electron effect to SQUID performance at low temperatures. Needless to say, this order of presentation is not the way the situation occurred historically.

Before I began work on the dilution refrigerator, Professor Clarke presented me with a list of low temperature experiments which he was interested in. This list included noise thermometry, quantum limited SQUIDs, hot electrons in metals, and I believe 1/f noise, although I cannot recall the last item for certain. He thus had an independent and early interest in the hot electron effect which predated the low temperature work on SQUIDs. Nevertheless, the choice was made to work on the SQUIDs at low temperatures first, and the hot electron experiments were put aside, presumably to be taken up when the SQUID experiments were completed. However, after two years of work on the SQUID experiments, it came as quite a surprise to me when I realized that the SQUIDs were themselves showing evidence of a hot electron effect. It was from this "SQUID perspective" that the subsequent work on the hot electron effect was undertaken.

One puzzling aspect of this history is the rather long delay between when the SQUID experiments began and the realization that the hot electron effect was important. I believe that this delay occurred for

three reasons. First of all, our first version of the experimental cell did not cool below about 100 mK because of poor thermal contact to the dilution refrigerator's mixing chamber. The hot electron effect in our typical early devices should only become significant below about 150 mK. The effect should have revealed itself as a levelling off of the linear dependence of the SQUID noise with temperature. The temperature range from 140 mK to about 100 mK is rather small, however, and the levelling off would not have looked very dramatic in the data. Secondly, in most of our early SQUIDs, the noise was greatly dominated by the low temperature excess noise, as was discussed in Chapter 8. It is very difficult to see the white noise level in most of our SQUIDs at 100 mK in the measuring bandwidth of the feedback electroncs. It was only with the discovery of the type D SQUIDs (with their $1/f^1$ noise) that the white noise became visible at the lowest temperatures. Within a few months of running the first D SQUID we began to suspect that the hot electron effect was involved. Finally, the experiments of Roukes et al.[1] on the hot electron effect were published only after the first year of SQUID experiments. In addition, it was not apparent from their work that we should see the effect in our SQUID resistors. They measured the effect in a very narrow thin-film line of high purity Cu, and much emphasis seemed to be placed on the configuration, the purity of the material, and the difficulty of seeing the effect. It was not at all apparent that the noise in our alloy resistor films should be completely dominated by the same effect. It was only after independently thinking out the problem that I became convinced that the effect depended on only a few parameters and that to first order, the cleanliness of the system would be irrelevant.

This chapter is broken up into three sections: The early SQUIDs D1 and D2 with small shunts, the SQUID M1 with large shunts, and the SQUID M2 with large thick shunts. All of these SQUIDs have a SQUID body shape which is that of the type D's (see Chapter 1), only the size and shape of the shunts differ. This choice of body shape was made because it possesses the lowest 1/f noise, from 1-10 kHz, of all of the SQUID types I tested. Although many other SQUIDs had lower noise at 1 Hz, the steeper slope of the noise in the type D and M devices more than compensated. In addition, because of their relatively large inductance, the white flux noise level in the D and M SQUIDs is larger than in most of the other SQUIDs, making it easier to detect for the same amount of excess flux noise. A few of the other SQUIDs with small shunts appear to show noise saturation at low temperatures, but all of these other devices have relatively large amounts of low temperature excess noise, and consequently the data on their white noise is not very clean.

Finally, a word of caution should be given on the energy sensitivity versus temperature plots. There are at least three possible systematic sources of error in these. First of all, the inductance is known only from the I-V behavior, as discussed in Chapter 2. An incorrect estimate of the inductance would push all of the points proportionately up or down on the graph. Secondly, all of the data has 1/f noise and measuring electronics noise subtracted out. Both of these contributions must be estimated from the spectra and the background measurements, and their relative importance increases as the temperature is lowered. Thirdly, it should be realized that the energy sensitivity is dependent on where the SQUID is biased. In general, I must search around in V and Φ until I find what appears to be the quietest point. The noise-V maps and noise-Φ

maps, which were discussed in Chapter 2, are very useful in this search. However their accuracy is limited and they are only taken at a single frequency (generally near 18kHz). A more accurate measure of the noise requires taking a detailed noise spectrum. In general, it is only possible to take high resolution spectra at a few promising looking points at any given temperature. Thus, one will tend to systematically underestimate the best ε_V, since it is difficult to be sure one has found the true minimum. Fortunately, the noise and gain of most of our SQUIDs is slowly varying with Φ and V, so it is generally possible to minimize this source of error. For devices with complicated structure, such as those with $\beta_C \simeq 1$, the search is much more difficult because the gain and the noise can be rapidly varying functions of Φ and V.

11.2 White Noise at Low Temperatures: SQUIDs with Small Shunts

SQUIDs D1 and D2 are large split SQUIDs with L ≃ 0.51 nH, and shunting resistance R = 6Ω. The details of the resistive shunt configuration are shown in Fig. 11.1(a). The shunts are slightly larger than those of a Type A SQUID, see Fig. 11.1(b). In the D devices, there are two shunts seperated by about 1 mm from each other (see Fig. 11.2a). The combined area of the shunts is 960 μm^2 and the film thickness is 30 nm, giving them a total volume of 29 μm^3. As discussed in Chapter 10, I have assumed that the AuCu under the Nb is still normal due to a suppression of the proximity effect.

As noted in Table 4.1, device D1 has β = 1.35. The I-V characteristics were very smooth at 4.2 K, with small steps appearing below 500 mK. The flux gain, $\partial I/\partial \Phi$, of the device was nearly constant

(a) Type D shunt

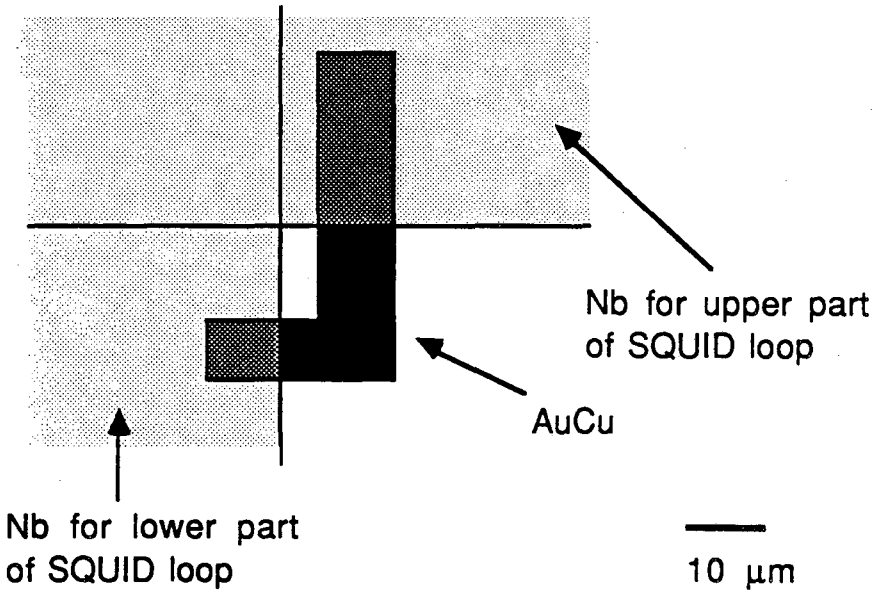

(b) Typical SQUID shunts

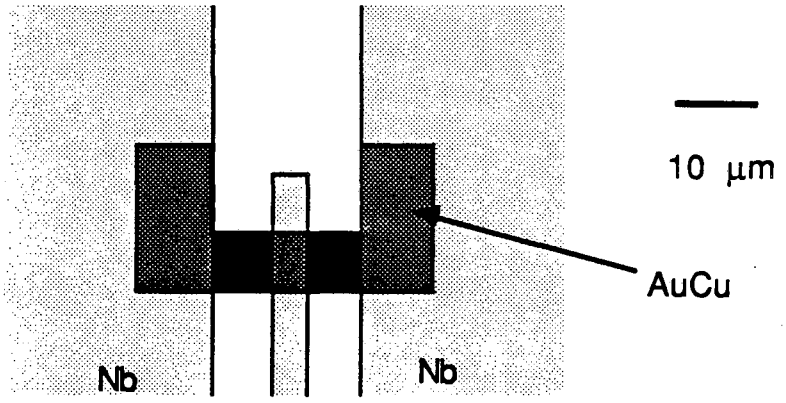

Fig. 11.1 (a) Configuration of one of the SQUID shunts for a Type D SQUID. (b) Configuration of a shunt for a typical SQUID such as a type A.

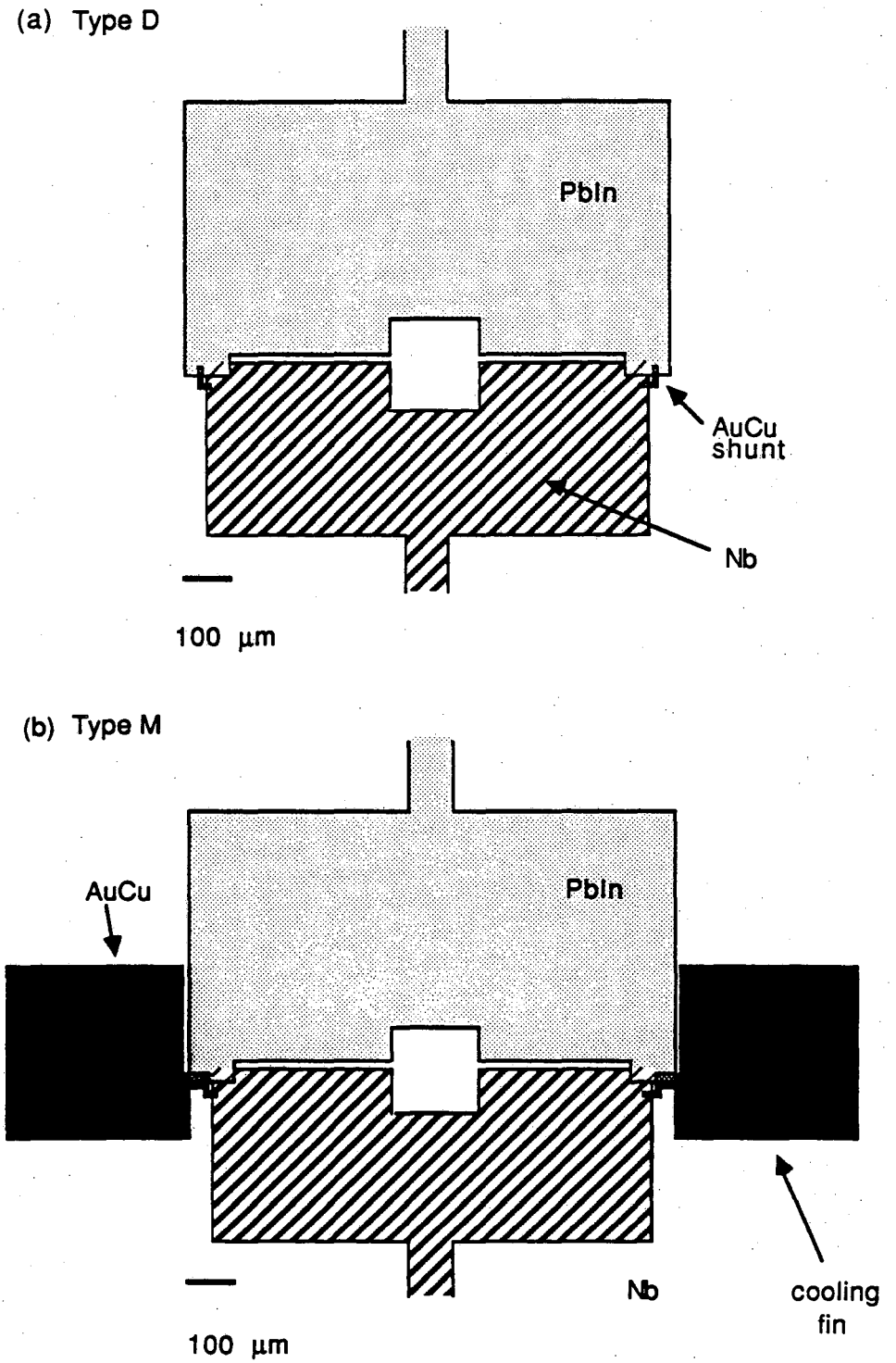

Fig. 11.2 (a) Construction of a Type D SQUID, (b) of a type M SQUID.

over the entire temperature range. From the experimental point of view, this is a nearly ideal device. SQUID D2 is very similar, and results for the I-V, I-Φ, Noise-V, and Noise-Φ are presented in Fig 4.5(a-k). The operating points for the SQUIDs are summarized in Table 11.1. I have also included the power dissipation P that this bias produces in the device, the power per unit of shunt volume Ω, and the power per unit of shunt area A.

In SQUIDs D1 and D2 at low temperatures, the low frequency noise scaled approximately as $1/f^1$ (see Fig. 8.9). As a result, I was able to measure the white noise at frequencies greater than about 2 kHz. The gains and noise spectra of devices D1 and D2 were measured as described in Chapter 2. The spectra at flux bias $\Phi_0/4$ were least square fit to a (white + $1/f^{\alpha}$) formula. The background noise from the SQUID(2) measuring

Table 11.1 Operating points for the SQUIDs D1, D2. M1, and M2. V is the voltage at which the SQUID is biased, I is the current flowing through the SQUID, P is the power dissipated in the SQUID, Ω is the shunt volume, A is the shunt area in contact with the substrate.

Device	V (μV)	I (μA)	P (pW)	P/Ω (Wm^{-3})	P/A (Wm^{-2})	$T_{min}=(P/\Sigma\Omega)^{1/5}$ (K)
D1	1.1	5	5.4	1.9×10^{5}	5.6×10^{-3}	0.151
D2	1.1	3.5	3.8	1.3×10^{5}	$4. \times 10^{-3}$	0.140
M1	1.2	4.5	5.4	1.2×10^{3}	3.5×10^{-5}	0.055
M2	4.0	5	20.	1.4×10^{2}	1.3×10^{-4}	0.036

system was measured by turning off SQUID(1), and subtracting off the Lorentzian produced by the Nyquist noise in the bias resistor R_x. The white noise and $1/f^{\alpha}$ noise due to SQUID(1) were then found by subtracting off this background.

The results of such an analysis are shown in Fig. 11.3, where I have plotted the white flux noise energy, $\varepsilon_v = S_\Phi/2L$, versus the bath temperature, where S_Φ is the white noise flux spectral density, and L is the SQUID inductance.

What is remarkable about Fig. 11.3 is that ε_v does not continue to decrease as the SQUIDs are cooled below 100 mK. Initially, as the bath temperature, T_o, was lowered to 0.2 K, the noise energy scaled with T_o, while below 0.2 K the noise dropped off less rapidly, flattening out by about 0.1 K. On analyzing the data, I found that at a bath temperature of 22 mK the SQUID D2 had an effective temperature of about 150 mK with $\varepsilon \approx 14\hbar$. This white noise energy is substantially higher than the value of $2.2\hbar$ predicted from the linear temperature dependence at higher temperatures. Device D1 showed a similar behavior over the smaller temperature range investigated, and shows evidence of a similar levelling off of the white noise at about the same temperature.

In principle, there are several possible reasons why the SQUID noise might fail to decrease below some temperature. First of all, an external source may be coupling noise into the SQUID. Secondly, limitations due to quantum mechanics are expected to produce a levelling off in the sensitivity. And finally the device may simply not be cooling as the bath temperature is decreased.

Because the levelling off occurs when there is a fairly large amount

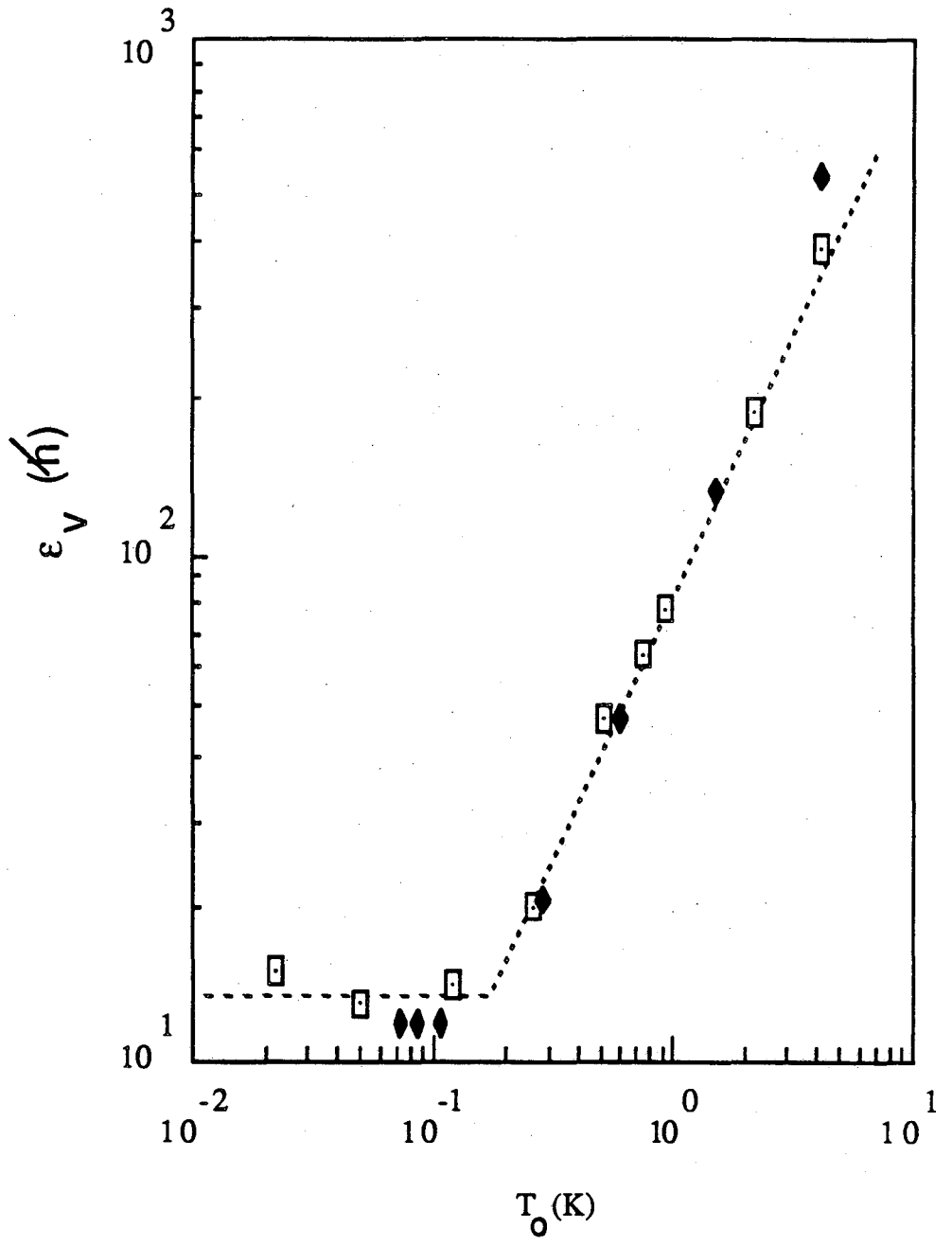

Fig. 11.3 Intrinsic energy sensitivity, ε_V, of SQUIDs D1 and D2 vs the bath temperature. The SQUIDs are biased near $\Phi_o/4$. The energy sensitivity is in units of ħ.

of noise, $\varepsilon_V \approx 14\hbar$, it cannot be due to quantum mechanical corrections. The exact value where ε_V should level off is not known, and has never been measured experimentally. Nonetheless, it is expected to be close to 1-2 $\hbar$ for typical SQUIDs, and $14\hbar$ is simply too large.

The data of Fig. 11.3 is also inconsistent with the presence of an external noise source. The observed change-over from a linear temperature dependence to a constant dependence is very abrupt. For an external noise source, one would expect that the noise in the SQUID obeys:

$$\varepsilon_V = a_o + b_o T_o \qquad (11.1)$$

where a_o and b_o are temperature independent, and T_o is the bath temperature. That is, the flux noise would be the sum of the temperature independent external noise source a_o, and the linearly dependent thermal SQUID noise $b_o T_o$. Such a functional form is quite inconsistent with the data represented in Fig. 11.3. The observed knee is much sharper than can be accounted for by Eq. 11.1 (see the dashed line in Fig. 11.4). Another way to express this is to say that the observed behavior is non-additive, ie. it is not the simple sum of a linear term plus a constant, although these are the asymptotoic limits. Now Eq. 11.1 would be expected if the thermal noise was uncorrellated with whatever source was causing the leveling off at low temperatures. The fact that this relation fails is thus evidence that the two sources are correllated or that there is really just one source which is changing its behavior with temperature.

Although the data is inconsistent with quantum effects and external noise, it is entirely consistent with the hot electron effect. Thus, the abrupt transition behavior has a natural explanation. For a fixed bath

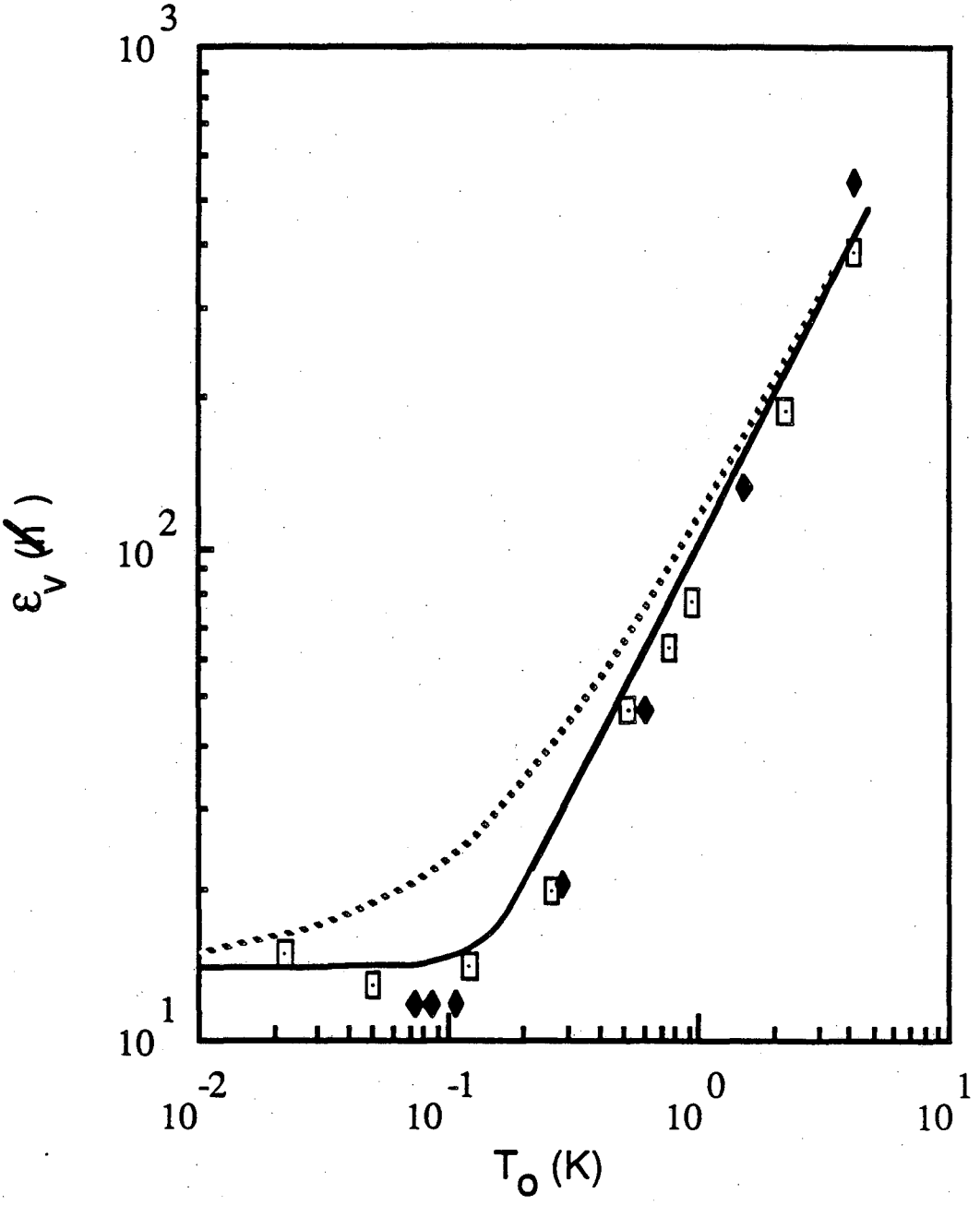

Fig. 11.4 Data points show flux noise energy vs the bath temperature for SQUIDs: ♦D1, and ⊡ D2. Solid line shows fifth power heating law, dashed line shows additive noise law.

temperature T_0, and power dissipation P in the shunts, the shunt temperature should obey:

$$T_e = (P/\Sigma\Omega + T_0^5)^{1/5} \qquad (11.2)$$

where again: T_e is the temperature of the electron gas in the shunts, Σ is the heating coefficient (see Chapters 9 and 10), and Ω is the shunt volume. The results plotted in Fig. 10.3 are for fixed power P, and since the noise in the SQUID should scale directly with the shunt temperature (neglecting quantum mechanics) we expect that Eq. 11.2 should have the same functional form as the SQUID sensitivity vs bath temperature T_0. The solid line in Fig. 11.4 shows the functional form of Eq. 11.2. The high temperature portion of the curve is the prediction of Tesche and Clarke,[2,3] while the value at which the noise levels off has been determined by the value of Σ found from the thin-film experiments of Chapter 10, and from the power dissipation in SQUID D2. The agreement is convincing, and in particular, the abrupt transition is fully in agreement with the hot electron theory. A fit to the data would yield even better agreement.

The temperature where the SQUID's white noise levels off is in good agreement with that expected from the hot electron effect. Device D2 was voltage biased at 1.1 μV with a current of 3.5 μA, so that the power dissipated was 3.8 pW. Since the shunt volume is nearly the same as that of the test resistor, Resistor 1, one can directly use Fig 11.4 to find the expected electron temperature: roughly 140 mK. This is quite close to the observed temperature where the SQUID noise stops decreasing, and represents a good agreement between the two experiments. In the last column of Table 11.1, I have also calculated $T_{min} = (P/\Sigma\Omega)^{1/5}$, the minimum temperature that the electrons can reach for a given power

level. For this calculation I have taken $\Sigma = 2.4 \times 10^9$ $Wm^{-3}K^{-5}$, the value which was found in Chapter 10 from independent measurements. This column then represents the expected temperature that the SQUID shunts will reach when the bath temperature is brought to zero. Because the transition to heating is so rapid, at any bath temperature slightly less than T_{min} the shunts will be very close to T_{min}. The minimum shunt temperatures predicted for D1 and D2, are within about 10% of the observed temperature where the levelling off occurs.

From the good agreement between the theory, the results of Chapter 10, and the data on D1 and D2, I can conclude that the sensitivity of these SQUIDs is being limited by the hot electron effect at low temperatures.

11.3 White Noise in a SQUID with Large "Cooling Fins"

Our overall goal was to produce a quantum limited SQUID, and so the levelling off of the sensitivity at low temperatures was quite disturbing. However, the solution was fairly straightforward. The basic reason the effect was so prominent was that the shunts were quite small.

The type M SQUIDs were designed to provide a large shunt volume without changing the SQUID shape. This was done by attaching a large area AuCu film to an ordinary Type D shunt. The details of the shunt structure are shown in Fig. 11.5a. The shunt and associated large film are deposited in a single evaporation, and have a thickness of just 30 nm, and a total area of 0.154 mm^2, yielding a total volume of 4.6×10^{-15} m^3. The AuCu is underlain by 2.5 nm of Cr as described in Chapter

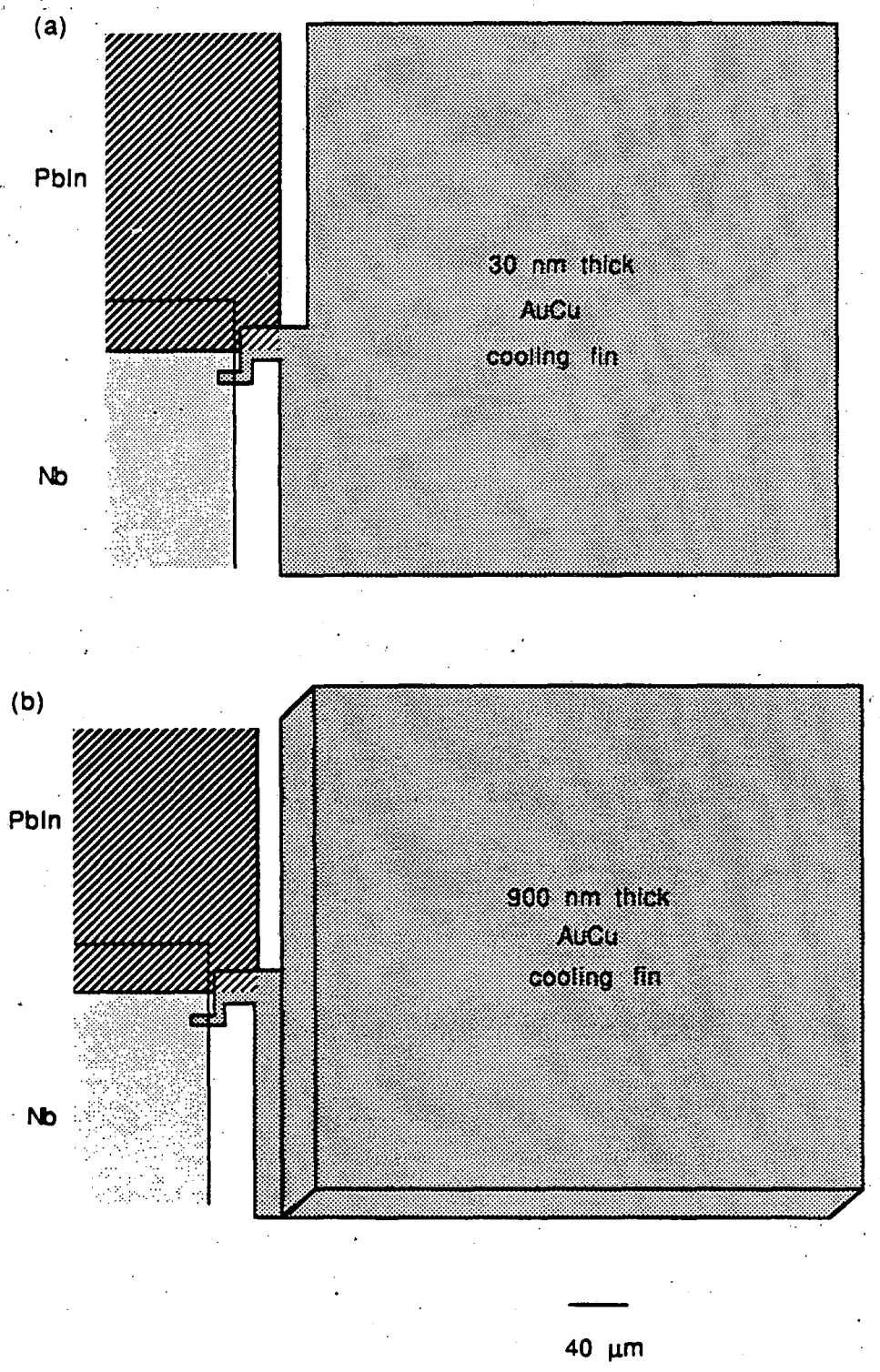

Fig. 11.5 Configuration of large SQUID shunts, (a) Type M with a thin cooling fin, (b) Type M with a thick cooling fin.

1. The cooling fin is then covered by two layers of SiO, (total thickness about 500 nm), and a layer of PbIn. This is done to screen out Nyquist currents, which flow in the normal metal film of the cooling fin, from producing extra noise in the SQUID. We expect this noise to be small in the case of the 30 nm cooling fin of device M1. But devices such as M2, as discussed below, have much thicker cooling fins and the incorporation of this screening is more important.

The behavior of the shunt structure is as follows. The shunting resistance is determined by the narrow connection between the upper and the lower portion of the SQUID body. The large attached film area contributes little to the resistance. Heating occurs locally in the narrow connection, as this is where the applied current density is greatest. Hot electrons then diffuse out into the neighboring attached film and release there energy to phonons. The large attached film area thus acts as a "cooling fin" for the hot electrons.

A few remarks about the cooling fins are in order. Their purpose is simply to increase the total volume of normal metal in the shunt, they do not contribute appreciably to the shunting resistance. This could have been accomplished simply by making the shunt much larger (keeping the same shape say), so that one had the same resitance as in the smaller shunts. Such an approach has two disadvantages. The increasing size of the shunt leads to an inductance in series with the SQUID shunting resitance, and a corresponding modification of the SQUID characteristics. Also, increases in the shunt size would necessitate changes in the SQUID geometry. This is disadvantageous because of the apparent dependence of the low temperature excess noise on the SQUID shape, as well as dependence of the inductance on the SQUID size. Thus

simply increasing the shunt size is not so straightforward. On the otherhand, by adopting cooling fins, one can seperate the electrical property, R, of the SQUID from the thermal cooling problem. I can thus keep the SQUID electrical properties fixed, while the cooling properties are improved independently.

Noise data was collected on a single SQUID with this type of shunt, SQUID M1, which had an inductance of 0.51 nH, a shunting resistance R = 6 Ω, β = 1.4, and an estimated β_C = 0.15. The I-V characteristics were very smooth from 4.2 K to 20 mK, with only very small structure visible. From the experimental point of view, this device is nearly ideal. The device was operated at 1.2 μV and a power of 5.4 pW. The gain and noise spectra of device M1 were measured as described in Chapter 2. The spectra at flux bias $\Phi_0/4$ were least square fit to a (white + $1/f^{\alpha}$) formula. The background noise from the SQUID(2) measuring system was found by turning off SQUID(1). The white noise and $1/f^{\alpha}$ noise due to M1 was then found by subtracting off the background. The results of such an analysis are shown in Fig. 11.6 for the white noise as a function of temperature. The figure also shows the earlier data on D1 and D2 for comparison.

From Fig. 11.6, we can see that the white noise scales linearly with temperature down to approximately 70 mK. Below this, the data is scattered, but appears to level off at an effective temperature of about 40 to 60 mK. This scatter arises from the need to subtract off the non-negligible contribution of the measuring electronics and the 1/f noise in the device. At high temperatures, the data from the three SQUIDs all fall on the same straight line. The solid line is the $\varepsilon_V = 8k_BTL/R$, for R=6Ω, and L=0.51nH. This is very near to the prediction of

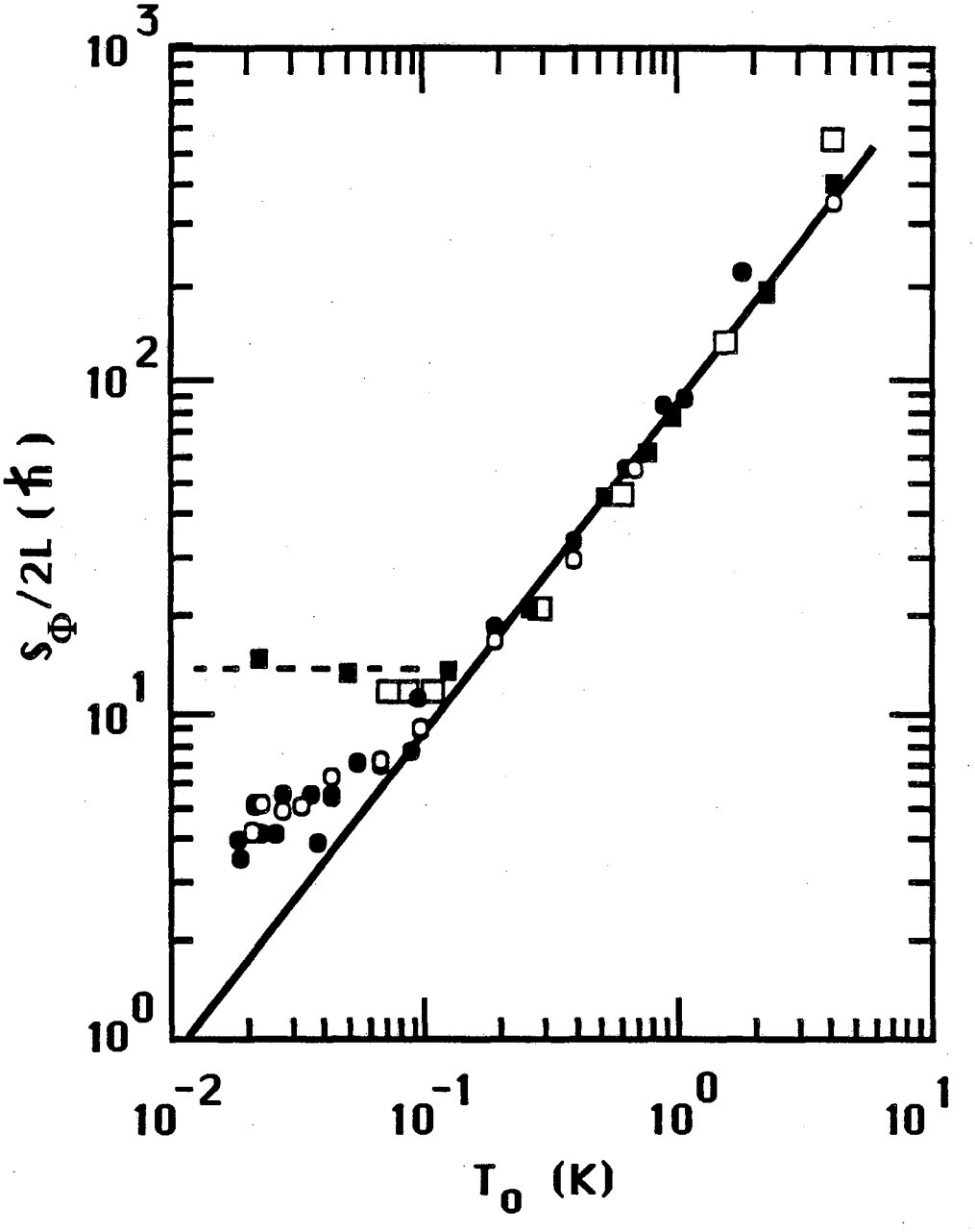

Fig. 11.6 Flux noise energy vs. T_0 for SQUIDs □ D1, ■ D2, ● M1, ○ M2. SQUIDs were biased near $\Phi_0/4$, with the operating points given in Table II. Solid line is prediction of Tesche and Clarke.[2]

Tesche and Clarke, $\varepsilon_V=(9\pm1)k_BTL/R$, which is appropriate for small β_c SQUIDs.[2-3] At the lowest temperatures, the device M1 is approximately 3 times more sensitive than the type D SQUIDs, leveling off at $\varepsilon_V\approx4$ or 5 $\hbar$. We can thus conclude that the cooling fins have produced a substantial improvement.

The fact that the white noise did decrease compared to the D devices provides a second proof that the hot electron effect was originally involved in the D devices. Had this test failed, then our conclusions about source of the noise in the D devices would have had to have been revised.

On the otherhand, the sensitivity of the device does not improve much below about 50 mK. Unfortunately the background correction from the measuring electronics is rather large. The large background correction makes it difficult to be sure that the device is actually still heating, and the transition region is not very well enough resolved. The temperature at which the sensitivity levels off is, however, quite close to the value of T_{min} predicted in Table 11.1. The expected electronic inelastic diffusion length should be about 600 μm at 50 mK, and the cooling fin should still be in the 0-D limit. This agreement is the strongest evidence that M1 is still being limited by the hot electron effect.

11.4 White Noise in a SQUID with Large Thick "Cooling Fins"

The results from SQUID M1 were encouraging, but there were two obvious difficulties. First of all the contribution from the measuring SQUID and electronics were non-negligible. Essentially, this was

happening because the noise in SQUID(1) was getting quite small. I accordingly next sought to improve the measuring electronics, and thereby lower the background. Secondly, it was evident that M1's sensitivity was levelling off at low temperature. This temperature was in agreement with the predictions of the hot electron effect, but it was considerably higher than the minimum bath temperature. Accordingly, I again increased the volume of the cooling fin in order to acheive a lower electron temperature.

At first sight, one might try to increase the shunt volume merely by increasing the area of the cooling fin still more than that in M1. This strategy will not work indefinitely, however, because the electrons only travel distances of order the inelastic mean free path before emitting a phonon. Thus, as discussed in Chapter 10, the cooling only occurs in some effective volume which lies within about the inelastic mean free path of the electrons. As noted in Chapter 11, the inelastic mean free path in the AuCu at 20 mK is expected to be of order 2 mm. The 0.4 mm sized cooling fins are thus already approaching this length scale, and it would be difficult to get much more cooling in this way, (it should be remembered that the electron temperature goes like the 1/5 root of the power per unit volume, and thus in order to lower the shunt temperature by a factor of 2 we would have to make the cooling fin nearly 6 times larger on a side, which is not only larger than the inelastic mean free path, but almost as large as the 5 mm SQUID chip). The way out of this dilemma is to increase the volume by increasing the thickness of the cooling fin.

In the case of the device M2, the thickness has been increased by a factor of about 30, to approximately 900 nm. This was accomplished by

including an additional step in the fabrication of the SQUIDs. The first step in the fabrication was to put down the resistive shunts and cooling fins exactly as was done for device M1. For the next step, a 900 nm layer of AuCu alloy was evaporated on top of the cooling fin. This made a thick cooling fin, but left the resistive connection unaffected (see Fig. 11.4b). The total area of the shunt in contact with the substrate was the same as that of device M1, about 0.154 mm^2. The total volume of metal used in the shunts was 1.4 X 10^{-13} m^3, roughly 30 times larger than in the case of device M1.

In the preceding section, I noted that the measurement of M1 was compromised at low temperatures because of the large background from the measuring SQUID and electronics. In order to improve the measurement, the measuring, SQUID(2), was replaced with a 50 turn type A device. This should have accordingly produced a factor of 2.5 improvement in the rms sensitivity. An improvement of about 2 was found, slightly less than expected because of extra noise from SQUID(2) itself. This was nonetheless a substantial improvement, and significantly improved the quality of the measurement.

The device M2 had a shunt resistance R=8Ω, β=1.6, and an estimated $\beta_c \approx 0.3$. Unfortunately, the device displayed considerable I-V structure at low temperatures, and was thus moderately non-ideal. This was probably because of M2's somewhat large β_c. This structure lead to large amounts of white noise at low biases, and necessitated operating the SQUID at the fairly high bias voltage of 4 μV. The power dissipation of 20 pW was correspondingly large.

The open circles in Fig 11.6 show ε_v vs T for SQUID M2. The noise level and temperature of saturation are not measurably different than

those found in SQUID M1. The noise still appears to begin to level off at about 50 mK. This appears to be a more gradual transition than the abrupt knee found in D1 and D2. However, the kneee is not well resolved, and there is still a fair amount of scatter in the noise data at low temperatures.

The levelling off of the noise could be due to an additive external source, however, the transition does not look soft enough. Also, it must be recognized that device M2 displayed a moderate amount of structure, and the white noise at many places on the I-V actually became much noisier as the device was cooled. It is possible that the structure also was producing extra white noise at the chosen bias point.

I note that the temperature where the data begins to level off, about 50 mK, is somewhat higher than the 36 mK expected from the hot electron effect (see Table 11.1). Although the shunt volume has increased by a factor of 30 from M1, M2 was also run at a substantially higher power. This, and the severity of the fifth root law, accounts for the rather small expected improvement for M2. Thus it is also possible that M2 is still being limited by the hot electron effect. This possibilty illustrates clearly the difficulty of avoiding the hot electron effect in thin film structures, and shows how tightly the SQUID parameters must be controlled in order to obtain a low noise device.

Perhaps the most optimistic interpretation is that the levelling off is due to quantum noise. The exact form that the noise versus temperature would take in this case is not known. The calculation of Danilov et al.[4] is in error because of the neglect of noise rounding effects. On the otherhand, Koch et al.[5] did not provide a detailed

temperature dependence for the SQUID senstivity. I have not attempted to repeat the calcultions here, although the results would be of considerable interest. Personally however, I feel that the residual level ε_v is too large for the device to be in the quantum limit.

11.5 Conclusions

In conclusion, I have measured the white noise in four large inductance dc SQUIDs down to temperatures as low as 20 mK. I have found that, at the lowest temperatures, the noise does not decrease with the bath temperature. The temperature where this levelling off occurs is consistent with the hot electron effect, and with independent measurements of electron heating in normal metal thin-films. The detailed form of the SQUID noise versus bath temperature is also consistent with the hot electron effect and is inconsistent with external noise. By attaching large volume "cooling fins" to the SQUID resistors, I have been able to reduce the heating and improve the SQUID sensitivity to a level of 4-5 $\hbar$.

References

(1) M.L. Roukes, M.R. Freeman, R.S. Germain, R.C. Richardson, M.B. Ketchen, "Hot Electrons and Energy Transport in Metals at Millikelvin Temperatures", Phys, Rev. Lett., 55, 422 (1985).

(2) C.D. Tesche and J. Clarke, "dc SQUID: Noise and Optimization", J. Low Temp. Phys., 29, 301 (1977); see also correction in ref. 3.

(3) J.J.P. Bruines, V.J. de Waal, and J.E. Mooij, J. Low Temp. Phys. 46,

383 (1982).

(4) V.V. Danilov, K.K. Likharev, A.B. Zorin, "Quantum Noise in SQUIDs", IEEE Trans. Magn., MAG-19, 572 (1983).

(5) R.H. Koch, D.J. van Harlingen, and J. Clarke, "Quantum Noise Theory for the dc SQUID", Appl. Phys. Lett. 38, 380 (1981).

CHAPTER 12: SQUID Circuit Optimization for a Current Pulse

12.1 Introduction

Several authors have worked on developing general SQUID noise and circuit optimization models.[1-3]. In addition, other work has been directed at optimizing the performance of very specific systems.[4-5] These models are all deficient in some major respect, and I note here that the results are not always consistent with each other. These different results can be attributed to the different assumptions made, although these assumptions and the ranges of their validity are usually not stated explicitly.

The noise theory of Clarke, Tesche, and Giffard[1] (CTG) was based on a number of assumptions:

(1) one neglects the effect of the SQUID dynamics on the input circuit,

(2) one works in the small α^2 limit, where α^2 is the coefficient of inductive coupling between the SQUID and the input circuit,

(3) one assumes a narrow bandwidth signal detection strategy,

(4) one minimizes the SQUID noise temperature, T_n, in order to obtain the highest sensitivity.

Each of these assumptions is independent, although the importance of the first assumption is considerably mitigated by the second assumption. The second assumption is interesting in that it is now recognized that the model fails spectacularly at large α^2; not only is the noise not predicted correctly by CTG, but the entire operating characteristics of

the SQUID change. The behavior of the SQUID for arbitrary α^2 has been analyzed by Koch,[6] Tesche,[7] and Martinis and Clarke.[8] Maritinis and Clarke,[8] and Hilbert and Clarke[9] have analyzed a few simple systems using the arbitrary coupling model and retaining the third and fourth assumptions above. In fact, even in these cases, the noise calculations were in the weak coupling limit, and have shown consistency with the earlier CTG results, except for very minor differences.

The last two assumptions are the foundations of what I will call the noise temperature formalism. The third assumption is not stated explicitly but it is implicit in the single frequency optimization presented. It is an artificial constraint which has the effect of throwing away all phase information about the signal, and any portion of the signal which lies outside of the detection bandwidth. It is a particularly subtle assumption, and appears at first sight to be quite simple and easily generalized. This is quite misleading. Its generalization requires the theory of optimal filtering and statistical prediction criterion. The validity and the utility of the fourth assumption is dependent on the earlier assumptions, and on the nature of the input signal. In particular if one relaxes the third assumption by using a wide-band detection strategy for a wide-band signal, the noise temperature is not the appropriate quantity to minimize. In addition, it is not permissible to minimize the noise temperature with respect to the resistive components of the circuit. Rather, even within the confines of the first three assumptions, for optimization with respect to some input resistance, R_i, one must minimize the expression $R_i(T+T_n)$, where T is the temperature of the resistor.

The method of optimal filtering or maximal filtering[10-13] is a

powerful and general technique that predicts the maximum sensitivity of a system, and also specifies the circuit parameters and filters which must be used to achieve this sensitivity. The point of all optimization schemes is to increase the signal-to-noise ratio, s/n. When one is trying to detect some very small effect, great care must be taken. One tries to arrange the different components of an experiment in order to have the best chance of actually seeing the effect. Clearly the more one knows about the expected effect, the more carefully the apparatus can be designed. In this sense, the optimal filter theory is a precise formulation of how best to design an experimental apparatus. For the formulation I will use here, its range of validity is all linear systems with deterministic input signals.

In order to calculate the optimum performance, however, it is necessary to know the functional form of the expected signal, the transfer functions of the circuit, and all sources of noise. Unfortunately, this means that the results will be both circuit and signal dependent. Optimization conditions for one kind of signal will not be optimum for another kind of signal. This makes it difficult to arrive at general formulas to cover all situations. In this Chapter, I will simply assume a model tuned LCR input circuit and a model pulse input signal. This choice has been made because it is the simplest and most experimentally accessible case without a trivial result. It is also interesting experimentally because it is similar to, although admittedly much simpler than, the equivalent circuit for gravity wave detection with a Weber bar and a SQUID readout. In this way I can provide some insight into the effect of strong coupling noise theory on the optimization of the bar.

For someone who is used to, and comfortable with, the noise temperature formalism, I think that the optimal filter theory comes as a bit of a shock. There are several things that he or she will probably find disturbing about the formulation:

1. The noise temperature and energy per bandwidth characterizations are not used in the formalism, except incidentally.

2. Different signals will produce different optimization conditions.

3. The sensitivity is affected by linear filters placed after the SQUID.

4. The optimization conditions and the optimum sensitivity are typically not the same as those found from the noise temperature formulation.

The following disscusion of the optimal filter results will of course answer each one of these points implicitly. I will make the following preliminary remarks however. The noise temperature and energy sensitivity are not fundamental parameters of optimization, only the s/n ratio is, and this is what the optimal filter theory works with. As a corrollary to this, the signal occurs in the numerator of the s/n ratio, and it is clearly as mathematically important as the noise in the denominator. Furthermore, the two optimization techniques (noise temperature formalism and optimal filter theory) are <u>not</u> two equivalent ways of deriving the same results. The differences are real. In particular, low frequency tuned systems show enormous differences in the predicted sensitvity and the optimum circuit parameters. For a 1 kHz resonant input circuit with a Q of 10^6, the optimal filter theory guarantees approximately a 10^6 times higher sensitvity than the noise

temperature formulation. Bluntly, this means that the T_n optimization scheme is incorrect for such systems, and its underlying assumptions must be inapplicable. More specifically, it turns out that the optimum circuits are built in such a way that they do not conform with the assumptions of the noise temperature formulation.

Corresponding to the calculational differences between the noise temprature formalism and the optimal filter theory, there are experimental differences as well. In order to obtain the sensitivity predicted by the optimal filter theory, it is necessary that the signal from the optimized SQUID circuit be sent through the optimal or matched linear filter specified by the optimal filter theory. This filter is generally only optimum for a specific signal, and different shaped signals will generally not be detected as efficiently. If one knows the expected form for the signal however, a different shaped "signal" is not a signal at all, but rather some kind of interference, and the fact that it is generally not detected as efficiently can be viewed as beneficial. Although it is possible to design systems that optimally discriminate between two known functional signals, the approach I describe below will not take such possible interference into account. Experimentally, if it is at all possible, it is best to find the source of the interference and either eliminate it or isolate the source from the system, rather than allowing the interference to get into the system in the first place.

The form of the optimal filter is discussed in Appendix D. The output of the filter essentially amounts to taking the weighted covariance of the SQUID output with the expected SQUID output if the signal were actually present. This covariance will be a maximum when the

signal is actually present, and in the statistical sense, is the best estimator of the presence of the signal. In the end, the output from the matched filter is used to find the probability that the signal was actually present at the input of the amplifier. In the presence of noise, this is the most one can hope to learn.

12.2 Optimization of an LCR Circuit Connected to a Simple Amplifier

Before analyzing the SQUID case, I will first apply the optimal filter approach to a simple LCR circuit which is connected to an ideal amplifier (which may be thought of as an op-amp). This preliminary analysis will give some insight into the optimization of the SQUID, and the circuit has been chosen to be analogous to the SQUID case.

I first specify the circuit, the input and all noise sources. The model amplifier LCR circuit is shown in Fig. 12.1, and all the parameters are defined there. A series LCR tuned circuit is coupled to an amplifier, with the amplifier connected across the inductor. I will assume that the amplifier has a frequency independent gain, G, and an infinite input impedance which does not load the input circuit. There are three effective noise sources in the circuit. I will describe the noise in the amplifier using the conventional voltage and current noise sources, e_n and i_n. I will assume that e_n, and i_n are uncorrelated white noise sources which are independent of temperature, where e_n^2 is the voltage noise power per Hertz, and i_n^2 is the current noise power per Hz generated by the amplifier. The third noise source in the circuit is the Nyquist noise in the input circuit resistor R_i, which I will denote $S_{vn}(f) = 4k_BTR_i$, the voltage noise power per Hz.

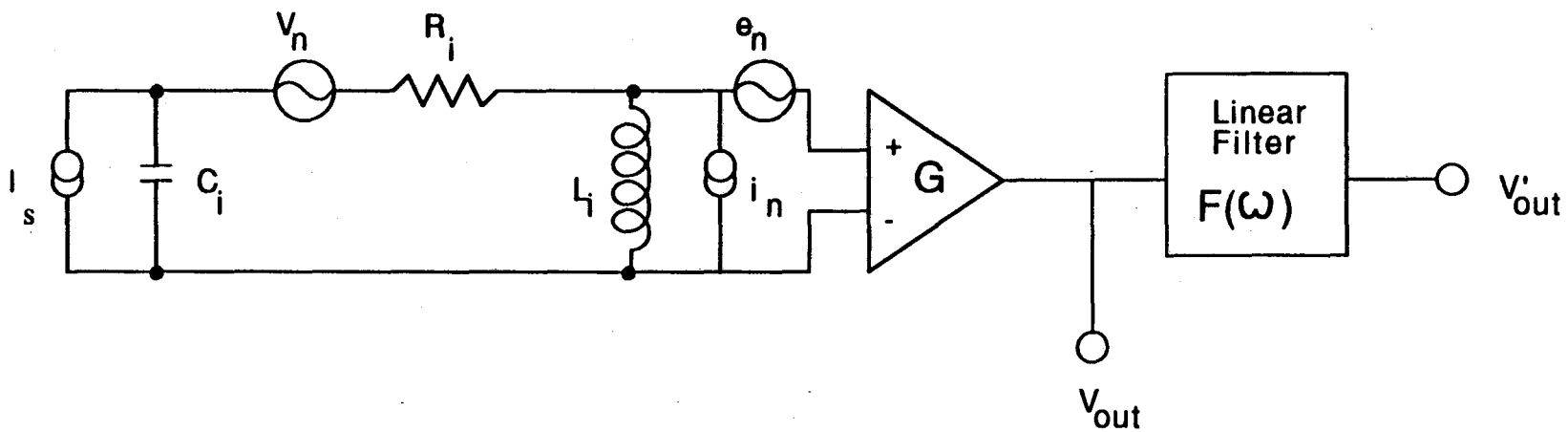

Fig. 12.1 Series resonant input circuit connected to an amplifier. I_S is the input signal current, V_n is the Nyquist noise voltage generated by resistor Ri, e_n is the voltage noise from the amplifier, i_n is the current noise from the amplifier, G is the gain of the amplifier, F is the filter.

The input for the circuit will be taken as a current source connected across the capacitor. This choice has been made as a matter of convenience and should not cause any concern because an equivalent series voltage source representation can always be constructed, (see Appendix A).

The input signal will be taken as a current pulse. This choice has been made for several reasons. First of all, the input signal is the same as will be considered in the case of the SQUID. Secondly, this is the simplest case to analyze. Thirdly, the effect of the signal on the circuit is readily understood. The pulse will suddenly place a charge q_o onto the capacitor, and thus deposit an energy $U \equiv q_o^2/2C_i$ into the input circuit. This will start the tuned circuit ringing. Thus one should expect to see a sinusoidal output from the amplifier, damped by the ringdown time of the input circuit (it is important to recognize that the output from a linear system generally is not of the same functional form as the input). Finally, the broader reason for considering this input and system is that it is analogous to the absorption of gravitational radiation by a Weber bar. The radiation from a supernova explosion and core collapse is expected to occur as a short pulse of order 1 msec. The pulse will produce a quadrapolar force field which can compress and stretch the bar. This starts the bar ringing, much as a hammer blow would, and is completely analogous to the ringing in the tank circuit. The question I wish to answer is how to choose the system parameters so as to maximize our chances of seeing the signal.

For this model calculation, I will thus take the input signal as a delta function, or pulse, in time:

$$I_s(t) = q_o\delta(t), \qquad (12.1)$$

where q_o is the charge the pulse deposits on the capacitor. I will also need the Fourier transform of the input signal $I_s(\omega)$:

$$I_s(\omega) = \int_{-\infty}^{\infty} e^{-i\omega t'} I_s(t')dt' = q_o. \tag{12.2}$$

The ouput repsonse from the amplifier will then be:

$$V_{out}(\omega) = \frac{I_s(\omega)L_i G}{C_i Z_{tot}}, \tag{12.3}$$

where Z_{tot} is the series input circuit impedance:

$$Z_{tot} \equiv R_i + i\omega L_i + \frac{1}{i\omega C_i}, \tag{12.4}$$

From elementary circuit considerations, the total noise at the output of the amplifier will be :

$$V_{out}(\omega) = G\left[e_n + i_n \frac{i\omega L_i (R_i + 1/i\omega C_i)}{Z_{tot}} + V_n \frac{i\omega L_i}{Z_{tot}} \right]. \tag{12.5}$$

Assuming no correlations between e_n, i_n, and v_n, the total voltage noise power spectral density at the amplifier output is just:

$$S_{vout} = \frac{G^2}{|Z_{tot}|^2}\left[e_n^2 |Z_{tot}|^2 + i_n^2 \omega^2 L_i^2 \left[R_i^2 + \frac{1}{\omega^2 C_i^2} \right] + \omega^2 L_i^2 V_n^2 \right]. \tag{12.6}$$

This total output noise can be thought of as being due to an effective current noise source N at the current source input. This is easily seen to be:

$$N \equiv N(f) = S_{vout} \left| \frac{i\omega C_i Z_{tot}}{i\omega L_i G} \right|^2. \tag{12.7}$$

I can write this in a more useful form by introducing the dimensionless

frequency variable $y = \omega/\omega_o$. The noise at the input thus becomes:

$$N = A(y^4 + By^2 + D)/y^2, \tag{12.8}$$

where :

$$A \equiv \frac{e_n^2}{Q^2R^2}\left[1 + \frac{R_i^2}{R_{opt}} + \frac{V_n^2}{e_n^2} \right], \tag{12.9}$$

$$B \equiv D\left[\frac{1}{Q^2} - 2 + Q_{opt}^2 \right], \tag{12.10}$$

$$D \equiv \frac{1}{1 + \left(\frac{R}{R_{opt}}\right)^2 + \left(\frac{V_n^2}{e_n^2}\right)}, \tag{12.11}$$

$$R_{opt} \equiv \frac{e_n}{i_n}, \tag{12.12}$$

$$Q_{opt} \equiv \frac{\omega_o L_i}{R_{opt}}, \qquad \omega_o = (L_iC_i)^{0.5} \tag{12.13}$$

$$Q \equiv \frac{\omega_o L_i}{R_i}. \tag{12.14}$$

The resistance R_{opt} is the optimum matching resistance that occurs in the noise temperature formalism.

I now apply the results of optimal filter theory to the circuit. The signal-to-noise ratio is written as:

$$s/n \equiv \frac{|V'_{out}(t)|^2}{\int_{-\infty}^{\infty} S_{vout}(f)\, F(\omega)\, df}, \tag{12.15}$$

where V'_{out} is the voltage at the output of the filter. This is the ratio of the output power produced by the signal at time t to the noise power at the output of the filter $F(\omega)$. As is shown in Appendix D, this integral has a maximum when the optimal filter is used, and this maximum signal-to-noise ratio, ρ, is given by:

$$\rho = \frac{1}{\pi} \int_{-\infty}^{\infty} \frac{|I_s(\omega)|^2 d\omega}{N(f)} \quad . \tag{12.16}$$

For our case, substituting for the signal and noise one finds:

$$\rho = \frac{\rho_o I_o}{\pi} \quad , \tag{12.17}$$

where:

$$\rho_o = \frac{UQ^{opt}D}{2k_B T_n} \quad , \tag{12.18}$$

$$I_o \equiv \int_{-\infty}^{\infty} \frac{y^2 dy}{y^4 + By^2 + D} \quad , \tag{12.19}$$

where I have defined the conventional noise temperature T_n of the amplifier:

$$T_n \equiv \frac{e_n i_n}{2k_B} \quad . \tag{12.20}$$

This expression for I_o can be integrated explicitly using contour integration techniques, as is shown in Appendix F. One finds for ρ:

$$\rho = \begin{cases} \dfrac{U\, Q^{opt}D}{k_B T_n (\, T_1^{1/2} + T_2^{1/2})} \quad , & \text{for } B^2/4 - D > 0, \\ \dfrac{U\, Q^{opt}D}{D^{1/4}\, k_B T_n\, 2 \sin(\theta/2)} \quad , & \text{for } B^2/4 - D < 0, \end{cases} \tag{12.21}$$

where: T_1, T_2, and $\sin(\theta/2)$ are given in Appendix F.

The behavior of the optimal s/n ratio ρ as a function of Q_{opt} for different Q is plotted in Fig. 12.2. I have taken a particular case where $T/T_n = 100$. Fig. 12.3 shows results for $T/T_n = 10^6$. As a function of Q_{opt}, the s/n ratio is a maximum for Q_{opt} about 1. In addition, as a

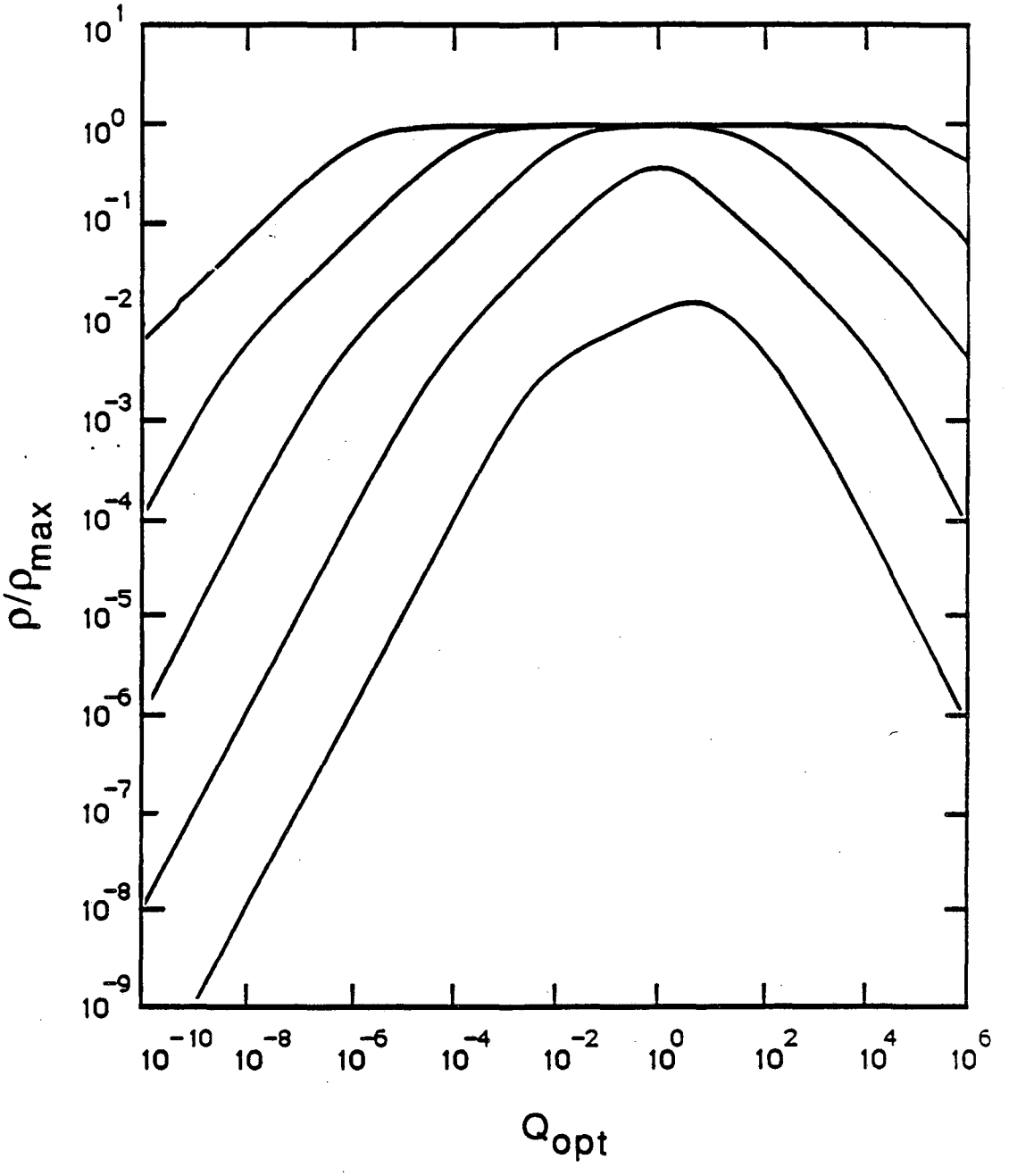

Fig. 12.2 Signal to noise ratio for the LCR-amplifier circuit of Fig 12.1, where $T/T_n = 100$. Curves are for constant Q with Q = 1, 100, ..., 10^8 , from bottom to top respectively.

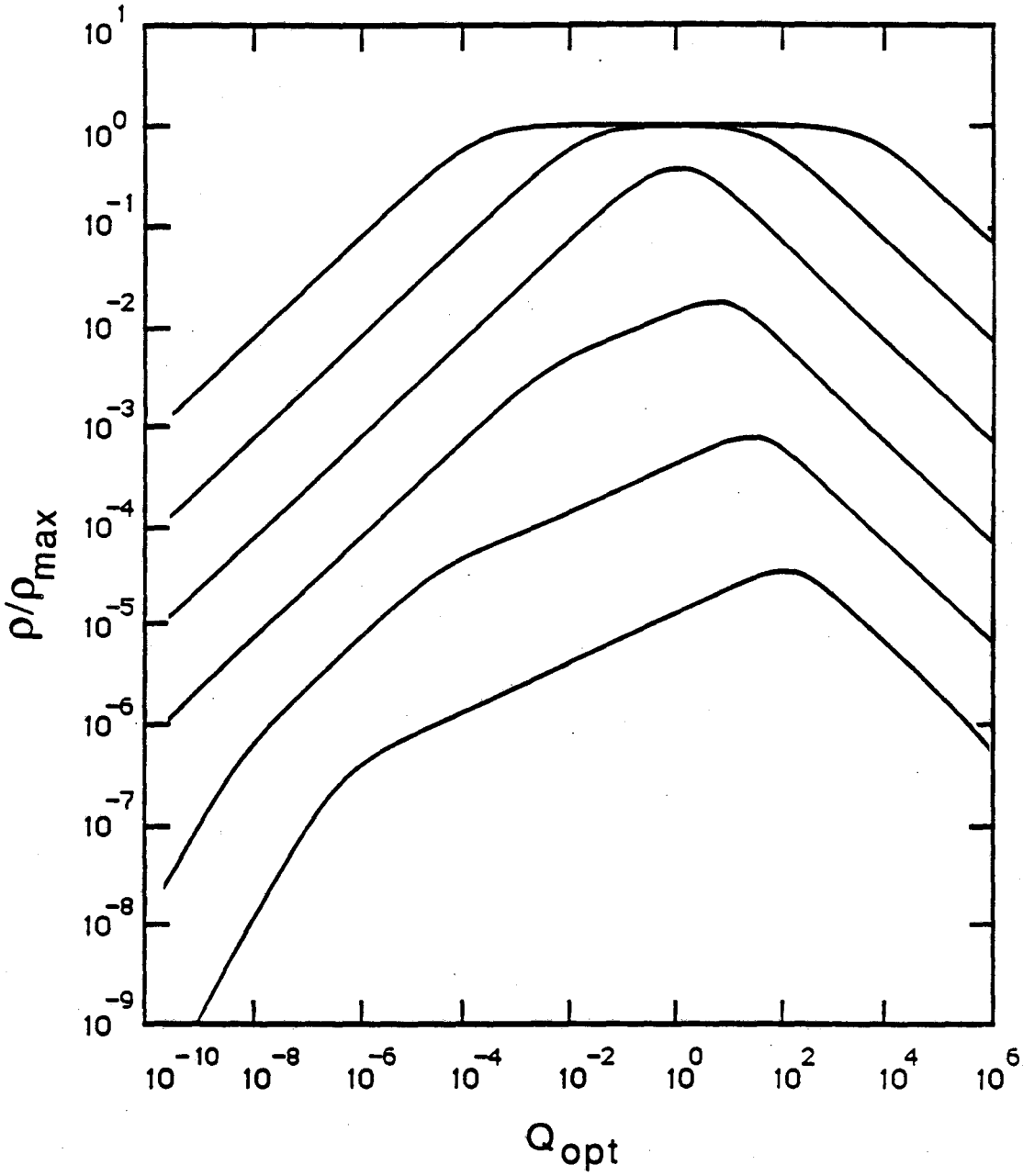

Fig. 12.3 Signal to noise ratio for the LCR-amplifier circuit of Fig 12.1, where $T/T_n = 10^6$. Curves are for constant Q with Q = 1, 100, ..., 10^{10}, from bottom to top respectively.

function of Q, the s/n ratio attains a maximum as Q ---> ∞ . This maximum s/n ratio is just $\rho_{max} = U/k_B T_n$. It is interesting to note that this maximum signal-to-noise ratio does not depend upon the temperature of the bath, and that this s/n ratio is for the system as a whole and not just for the amplifier. The point is that one needs Q to be larger than a certain number before the signal-to-noise ratio approaches the maximum value, and this value of Q must be made larger as the ratio T/T_n gets larger. In fact, one can show that Q must be larger than a value Q_{min} :

$$Q_{min} \approx T/T_n \quad ,$$

in order for ρ to approach ρ_o. This effect is often described as reducing the effective bath temperature T by the Q of the input circuit, so that the resistor looks like it is at T/Q. For Q much smaller than T/T_n, the system is limited by the Nyquist noise from the resistance R_i. When T/Q is about equal to T_n the system begins to be limited by the noise from the amplifier, and there is little subsequent improvement in sensitivity. The system noise can at best be equal to the noise from the amplifier alone, and this limit can be achieved even if the noise temperature of the amplifier is much smaller than the bath temperature.

12.3 SQUID Circuit Optimization for Current Pulse.

I now apply the optimal filter theory to a SQUID circuit. In the following formulation, I have included SQUID renormalization and dynamic input impedance effects that result from non-vanishing coupling α^2. This was done by using the theory of SQUID circuit dynamics formulated by Martinis and Clarke.[8] The model also includes the effects of

correlations between the current noise and the voltage noise.

It should be noted that the following model calculation, as well as the earlier CTG[1] calculations and the Martinis and Clarke noise theory, does not include the effects of stray capacitance between the SQUID and the coil. The effect of these stray capacitances is to alter the transfer function between the SQUID and the input circuit.[14] Given the correct transfer functions, the effect of the capacitance could readily be incorporated into the following formulation. However, it should be realized that the stray capacitance is generally distributed and dependent upon the details of the construction, which makes a general formulation difficult, and I have accordingly not attempted to include parasitic effects. Whether or not stray effects are important depends upon many experimental details. First of all, the capacitance effects can presumably be minimized by thoughtful construction and choice of materials. Secondly, it should be realized that these parasitic effects are concerned only with frequencies of order the signal frequency, not near the Josephson frequency. Since the signal frequencies are generally small, and the stray capacitance is also generally small, the impedance at the signal frequency is usually enormous. In particular, for the gravity wave experiments, a 1 pF stray capacitance that might exist between the SQUID and a coil yields an impedance of about 100 MΩ at 1 kHz. This impedance is so large compared to any other impedance in the problem that it may reasonably be neglected in any initial formulation. Finally, it should be noted that some of the effects of stray capacitance, such as capacitive feedback,[14] can be virtually eliminated by running the SQUID at constant voltage, as was done in the experiments of this thesis. Such a

configuration has other obvious advantages, as have been discussed earlier, and may well be the best way to run a SQUID for certain experiments.

12.4 Input, Circuit, and Noise Sources.

I first specify the circuit, the input and all noise sources. The model LCR circuit is shown in Fig. 12.4. All of the circuit parameters are defined in Table 12.1. The input tank circuit is coupled through a mutual inductance M_i to the SQUID. I neglect noise from any later amplifier stages which follow the SQUID, and take the SQUID voltage as the output voltage, V_{out}. The SQUID is assumed to be current biased for the purpose of this calculation. I will take the input as a current source across the capacitor. This choice is made for reasons of convenience, and it should be noted that the current source is completely equivalent to a series voltage source of strength $I_s(\omega)/i\omega C$.

12.5 The Input Signal

For this model calculation, I will take the input signal as a current delta function, or pulse, in time:

$$I_s(t) = q_o\delta(t) \ , \qquad (12.23)$$

where q_o is the charge that the current pulse deposits. The calculation is carried out in the frequency domain where:

$$I_s(\omega) = \int_{-\infty}^{\infty} e^{-i\omega t} I_s(t)\, dt = q_o \ . \qquad (12.24)$$

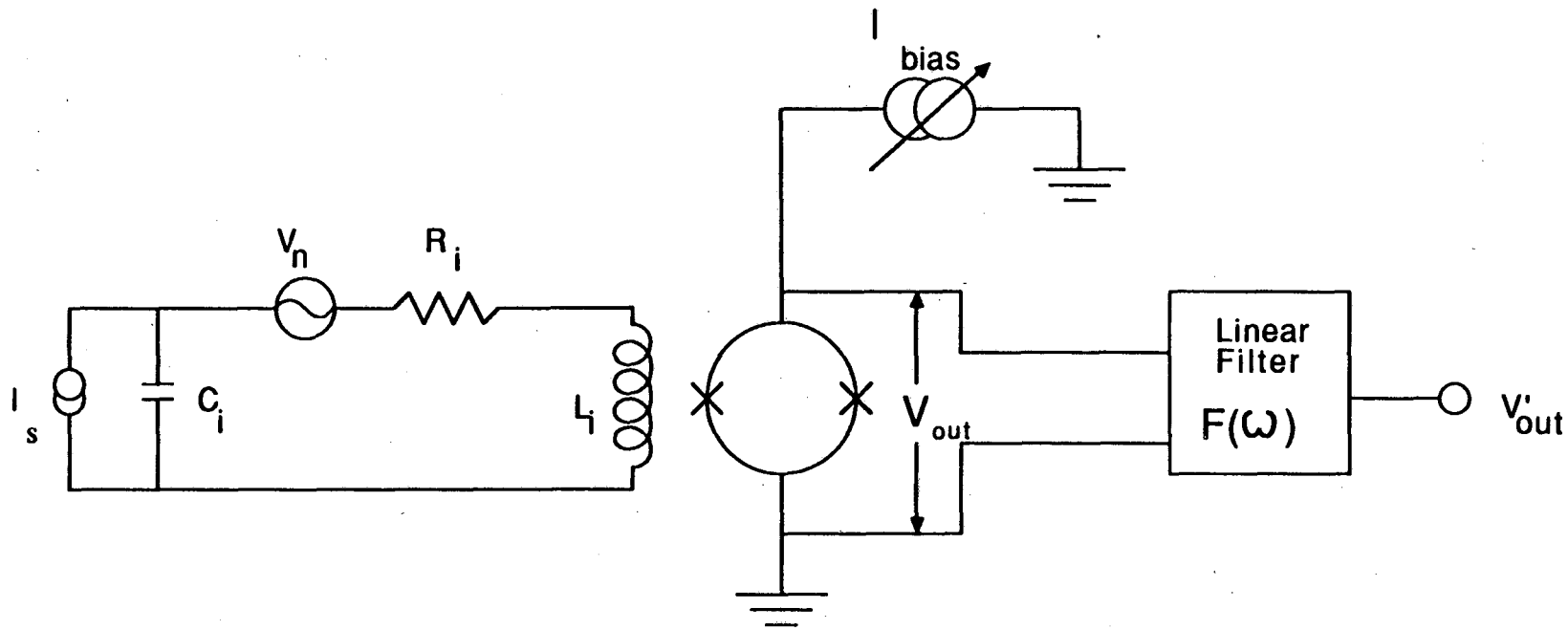

Fig. 12.4 Series LCR circuit connected to a dc SQUID. The input signal is generated by current source I_S. V_n is the voltage source for resistor R_i.

Table 12.1: The Definitions of Terms

(1) Constants

$\hbar$ = 1.054 X 10^{-34} js = Planck's constant,

Φ_0 = 2.07 X 10^{-15} Tm^2 = flux quantum,

T = temperature

(2) SQUID Parameters

(i) superscripted "r" denotes a renormalized SQUID parameter[8]

(ii) V_{out} = output voltage across SQUID, V'_{out} = voltage at filter output

L = SQUID inductance, C = single junction capacitance

R = SQUID shunt resistance, I_0 = single junction critical current

$\beta = 2LI_0/\Phi_0$ = modulation parameter

α = coupling coefficient between SQUID and input inductance

L^r = renormalized[8] SQUID inductance = $L(1-\alpha^2)$

$\mathcal{L}$ = dynamic SQUID inductance [15]

$\mathcal{L}^r$ = renormalized[8] dynamic SQUID inductance

$\mathcal{R}$ = dynamic SQUID resistance [15]

$\mathcal{R}^r$ = renormalized[8] dynamic SQUID resistance

V_Φ = SQUID flux to voltage transfer function

$V_\Phi^r = V_\Phi/(1-\alpha^2)$

S_v SQUID voltage noise spectral density

S_j SQUID current noise spectral density

S_{vj} SQUID current voltage correlation spectral density

$S_{vn} = 4k_BTR_i$ Input resistor voltage noise spectral density

$\varepsilon_v = S_v(\partial V/\partial\Phi)^{-2}/(2L)$ intrinsic energy sensitivity

$\varepsilon_j = S_jL/2$

$\varepsilon_{vj} = S_{vj}(\partial V/\partial\Phi)^{-1}/2$

$\varepsilon = (\varepsilon_v\varepsilon_j-\varepsilon_{vj}^2)^{1/2}$ total energy sensitivity

$\gamma_v = S_v/2k_BTR$

$\gamma_j = RS_j/2K_BT$

$\gamma_{vj} = S_{vj}/2K_BT$

Table 12.1 (continued)

(3) Input Circuit Parameters

(a) Circuit

L_i = input circuit inductance

R_i = input circuit resistance

C_i = input circuit capacitance

$\omega_o = (L_iC_i)^{-0.5} = 2\pi$(resonant frequency of unperturbed input circuit)

$Q = \omega_oL_i/R_i$ = quality factor of unperturbed input circuit

$Q' = \omega_oL/R^r$

$Q'' = \omega_oL/R$

I_s = input signal from input current source

V_i = equivalent series voltage produced by I_s, see Appendix A

U = work done on circuit by the signal = $q_o^2/2C_i$ for current pulse

(b) Perturbed Circuit Parameters, (see appendix B)

$$K \equiv 1 + \frac{\alpha^2 L}{L^r} + \alpha^2 \frac{\omega_o LQ}{R^r}$$

$$P \equiv 1 + \alpha^2 \frac{\omega_o L}{QR^r}$$

$$W = 1 + \alpha^2 \frac{L}{L^r}$$

$$Z_{eff} \equiv Z_T - \frac{J_\phi^r M_i^2}{L_i}\left[R_i + \frac{1}{i\omega C_i}\right] \equiv KR_i + i\omega L_i P + \frac{W}{i\omega C_i}$$

$$Z_T \equiv R_i + i\omega L_i + \frac{1}{i\omega C_i}$$

$$J_\phi^r \equiv -\left[\frac{1}{L^r} + \frac{i\omega}{R^r}\right]$$

$\omega_o' = \omega_o(W/P)^{1/2}$ = frequency at which V_{IS} is maximized

Table 12.1 (continued)

(c) Transfer Functions

$$V_{IS} \equiv \frac{\partial V_{out}(\omega)}{\partial I_s(\omega)} = \frac{M_i V_\phi^r}{i\omega C_i Z_{eff}}$$ input current to output voltage transfer function

$$V_J \equiv \frac{\partial V_{out}(\omega)}{\partial J_n^r(\omega)} = \frac{M_i^2 V_\phi^r}{L_i Z_{eff}} \left(R_i + \frac{1}{i\omega C_i} \right)$$ circulating current to output voltage transfer function

$$V_{VN} \equiv \frac{\partial V_{out}(\omega)}{\partial V_n(\omega)} = \frac{M_i V_\phi^r}{Z_{eff}}$$ input circuit series voltage to output voltage transfer function

(4) Noise Expressions (see Appendix C)

$N = N_o(y^4 + by^2 + d)$ Total noise referred to current sensing input

$b = A_1 + B_1 + C_1 + D_1$

$d = A_2 + B_2 + D_2$

$$N_o = \frac{2\varepsilon_v^r P^2 (1-\alpha^2)}{\alpha^2 L_i}$$

$$A_1 = \frac{K^2}{P^2 Q^2} - \frac{2W}{P}, \qquad A_2 = \frac{W^2}{P^2}$$

$$B_1 = \frac{\gamma_j \alpha^4 L^2 (V_\phi^r)^2}{\gamma_v R^2 Q^2 P^2}, \qquad B_2 = \frac{\gamma_j \alpha^4 L^2 (V_\phi^r)^2}{\gamma_v P^2 R^2}$$

$$C_1 = \frac{2\alpha^2 L L_i (V_\phi^r)^2}{P^2 R_i R Q^2 \gamma_v}$$

$$D_1 = \frac{2L\alpha^2 V_\phi^r \gamma_{vj}}{RP^2 \gamma_v} \left[\frac{K}{Q^2} - P \right], \qquad D_2 = \frac{2LW\alpha^2 \gamma_{vj} V_\phi^r}{RP^2 \gamma_v}$$

Table 12.1 (continued)

(5) Expression From the Noise Integrals (see Appendix F)

Region (1) occurs for $(b^2/4 - d) > 0$

Region (2) occurs for $(b^2/4 - d) < 0$

In Region (2):

$R_o = d^{1/2}$

$\cos(\theta) = -b/(2d^{1/2})$

In Region (1):

$$T_1 = \frac{b}{2} + \left[\frac{b^2}{4} - d\right]^{1/2} , \qquad T_1' = T_1^{1/2}$$

$$T_2 = \frac{b}{2} - \left[\frac{b^2}{4} - d\right]^{1/2} , \qquad T_2' = T_2^{1/2}$$

The output response from the SQUID, for this input, will be:

$$V_{out}(\omega) = V_{IS} I_s(\omega) , \qquad (12.25)$$

where V_{IS} is the input current-to-output voltage transfer function, which is calculated explicitly in Appendix B.

12.6 The Total Noise at the SQUID Output

The total noise at the SQUID output can be written as follows:

$$S_{vout} = S_v^r + V_j^2 S_j^r + V_{vn}^2 S_{vn} + (V_j + V_j^*) S_{vj}^r , \qquad (12.26)$$

where the transfer functions V_j and V_{vn} connect changes in the subscripted variables to an output voltage change, S_v^r is the spectral density of the voltage noise of the renormalized SQUID, S_j^r is the spectral density of the circulating current noise in the renormalized SQUID, S_{vj}^r is the current-voltage correlation spectrum for the renormalized SQUID, and S_{vn} is the power spectrum of the voltage noise produced by the input circuit resistor. The transfer functions must take into account the dynamic input impedance of the SQUID, and the screening or renormalization[8] of the SQUID when it is connected to the input circuit. They are calculated explicitly in Appendix B using the Martinis and Clarke[8] formulation of strong coupling SQUID noise theory.

12.7 The Total Noise Referred to the SQUID Input

The total noise referred to the current sensing input can then be written as:

$$N = S_v^r/|V_{IS}|^2 + S_j^r|V_J|^2/|V_{IS}|^2 + S_{vn}^r|V_{VN}|^2/|V_{IS}|^2 + \\ + S_{vj}^r(V_J+V_J^*)/|V_{IS}|^2 \qquad (12.27)$$

This can be put in the renormalized form:

$$N = N_o(y^4 + by^2 + d) , \qquad (12.28)$$

where $y = \omega/\omega_o$, and N_o, b, d, and ω_o are derived in Appendix C, and listed in Table 12.1.

12.8 The Best Signal-to-Noise Ratio

Using Eq. 12.23 for the signal and Eq. 12.28 for the noise, I can now use optimal filter theory to write the optimum signal-to-noise ratio

as:

$$\rho = \frac{1}{\pi} \int_{-\infty}^{\infty} \frac{|I(\omega)|^2}{N} d\omega \qquad (12.29)$$

This expression is discussed in Appendix D. Substituting for I and N, one can write:

$$\rho = \rho_0 I_1/\pi \quad , \qquad (12.30)$$

where: $\rho_0 = \omega_0 q_0^2/N_0$, (12.31)

$$I_1 = \int_{-\infty}^{\infty} \frac{dy}{y^4 + by^2 + d} \quad . \qquad (12.32)$$

Both ρ_0 and I_1 are dimensionless expressions.

12.9 The Evaluation of ρ_0

The factor ρ_0 can be put in the form :

$$\rho_0 = \frac{q_0^2}{2C_i} \cdot \frac{\alpha^2}{p^2(1-\alpha^2) \quad \varepsilon_v^r \omega_0} \quad , \qquad (12.33)$$

where p is defined in Appendix C, and $\varepsilon_v{}^r$ is the voltage energy sensitivity of the renormalized SQUID. In Appendix E, I show that $U = q_0^2/2C_i$ is the amount of energy that the pulse signal delivers to the circuit. The result is trivial, but the calculation is lengthy due to the modifying effects of the SQUID on the input circuit. With this identification, I can write:

$$\rho_0 = U\alpha^2/(\varepsilon_v{}^r \omega_0 p^2(1-\alpha^2)) \quad . \qquad (12.34)$$

I now make the following important optimization strategy: I assume that the renormalized SQUID has β=1. This can in principle always be accomplishied by adjusting I_0 so that when L is screened to $L^r=(1-\alpha^2)L$,

then I_o is adjusted to $I_o/(1-\alpha^2)$, so that $\beta=2L^rI_o^r/\Phi_o$ is equal to unity for all α^2. Of course this is not something one can easily do experimentally. One would have to build a SQUID with the correct I_o so that it achieves $\beta=1$ for a particular α^2. In this case, I can use the results of Tesche and Clarke[2] for the noise in a $\beta = 1$ SQUID, generalized to take into account the screened inductance:

$$\varepsilon_V^r = (1-\alpha^2)\varepsilon_V, \quad \text{where} \quad \varepsilon_V = 9k_BTL/R, \tag{12.35}$$

and I can thus write:

$$\rho_o = U\alpha^2/(\varepsilon_V\omega_o p^2(1-\alpha^2)2) \tag{12.36}$$

12.10 The Evaluation of I_1

The integral I_1 can be evaluated using contour integration. For different values of the coupling α^2, the poles in the integrand may be pure imaginary or complex. One finds two regions, one that occurs at low couplings, and another that occurs at high couplings. The integration is performed explicitly in Appendix F. I find:

$$I_1 = \begin{cases} \dfrac{\pi}{(T_1T_2)^{1/2}(T_1{}^{1/2}+T_2{}^{1/2})} & \text{if } b^2/4-d > 0 \\ \dfrac{\pi}{2R_o{}^{3/2}\sin(\theta/2)} & \text{if } b^2/4-d < 0 \end{cases} \tag{12.37}$$

where T_1, T_2, $\sin(\theta/2)$, and R_o are defined in Table 12.1, and are derived in Appendix F.

I thus have the following analytical formula for the optimal signal-to-noise ratio for arbitrary L_i, C_i, R_i, α^2, but only for $\beta = 1$ and input current pulses:

$$\rho = \begin{cases} \dfrac{U\alpha^2}{\varepsilon_v\omega_0 p^2(1-\alpha^2)^2(T_1T_2)^{1/2}(T_1^{1/2}+T_2^{1/2})} & \text{if } (b^2/4-d)>0 \\ \dfrac{U\alpha^2}{2\varepsilon_v\omega_0 p^2(1-\alpha^2)^2 R_0^{3/2}\sin(\theta/2)} & \text{if } (b^2/4-d)<0 \end{cases} \qquad (12.38)$$

I now will digress to mention a potentially confusing point. The above expression yields the best s/n ratio that can be achieved for a fixed set of SQUID and circuit parameters. But in what sense is this expression a maximum if the parameters are all held fixed? The point is that with a given set of parameters, one can achieve this sensitivity only with the optimal filter, and out of all possible filters this yields the highest s/n ratio. In general one would like to operate so that this ratio is also a maximum as a function of the circuit parameters, ie. one would like to build a circuit which has parameters which will yield the highest optimal signal-to-noise ratio. This is simply a matter of maximizing the above expression with respect to each of the circuit parameters.

12.11 Optimization of Circuit Parameters for Different Sources

I would like to adjust the circuit so that the above expressions for ρ, the signal-to-noise ratio, achieves its largest value. It is important to recognize however, that the optimum circuit parameters will depend on the nature of the source. To be quite specific, I can now ask the following three questions: Suppose that I vary the input circuit parameters,

(1) What is the smallest energy that the circuit can detect?

(2) What is the smallest voltage that the circuit can detect?

(3) What is the smallest current that the circuit can detect?

I will assume in each case that I am dealing with a current pulse, which produces some equivalent amount of energy U in the circuit, or some equivalent voltage V_s in the input circuit (see Appendix A). The three quantities can be written as:

$$U = q_o^2/2C_i \ , \tag{12.39}$$

$$V_s(\omega) = q_o/i\omega C_i \ , \tag{12.40}$$

$$I_s(\omega) = q_o \ . \tag{12.41}$$

In the first place, the choice of circuit parameters will be different if I want to optimally detect say a small voltage instead of a current. This can be seen by writing out the optimal signal-to-noise ratio ρ, for the three cases, in the following forms:

$$\begin{aligned} \rho &= UI/(\varepsilon_v\omega_o) \ , && \text{for energy U} \\ \rho &= C_i I\ V_s^2/(2\varepsilon_v\omega_o) \ , && \text{for input voltage } V_s \\ \rho &= q_o^2 I\ /(2\varepsilon_v\omega_o C_i) \ , && \text{for input charge } q_o \end{aligned} \tag{12.42}$$

where:

$$\begin{aligned} I &= \frac{\pi}{T_1'T_2'(T_1'+T_2')} && \text{if } (b^2/4-d)>0 \ , \\ I &= \frac{\alpha^2}{2p^2(1-\alpha^2)^2R_o^{3/2}\sin(\theta/2)} && \text{if } (b^2/4-d)<0 \end{aligned} \tag{12.43}$$

I can define the minimum detectable U, V_s, and q_o as those which will produce a signal-to-noise ratio of unity. Thus:

$$U_{min} = \varepsilon_v\omega_o/I \ , \tag{12.44}$$

$$V_{smin}^2 = 2\varepsilon_v\omega_o/(C_i I) \ , \tag{12.45}$$

$$q_{omin}^2 = 2\varepsilon_v\omega_o C_i/I \ . \tag{12.46}$$

Let us momentarily suppose, for the sake of discussion, that ω_o is held

fixed. Then, the SQUID circuit will be most sensitive to energy U when the quantity I is a maximum, to voltage when IC_i is a maximum, and to current $I_s(\omega) = q_o$ when I/C_i is a maximum. If the capacitance C_i is also assumed to be held fixed, then these three conditions are equivalent, and the best sensitivity to energy, current, and voltage will all occur for the same circuit parameters, defined by I a maximum. On the other hand, if C_i is allowed to vary, the three conditions will differ, and the optimum circuit parameters will be different in the three cases. Since I am assuming ω_o is held fixed, a variation in C_i will be equivalent to varying L_i. If I allow ω_o to vary, this is equivalent to independent variations in L_i and C_i, then it is easy to see that the three conditions will again generally differ. The optimum parmaters in each case obviously depend on the detailed form of I, which will be investigated below.

12.12 Figure of Merit for the SQUID

Now there is an important problem which I have so far avoided. How can I tell whether one SQUID is better (by which I mean more sensitive) than another? I do not mean the SQUID plus its input circuit, but just the SQUID itself. Are there some properties of a bare SQUID which can be measured which will tell us how sensitive the device will be when it is plugged into a circuit? I can pose this question somewhat differently as: What is the figure of merit or performance criterion for a SQUID? First of all, one should realize that the s/n ratio is not a good figure of merit because it depends upon the magnitude of the signal, which I have so far left arbitrary. Thus larger applied pulses may produce a

greater signal-to-noise ratio in a poor SQUID, then a small pulse in a good SQUID.

I want to construct some quantitative and objective measure of SQUID sensitivity. Suppose I wish to compare the sensitivity of two SQUIDs. Experimentally this can be done by building two identical circuits and attaching one SQUID to each. I then apply an identical signal to both SQUID circuits and compare the resulting s/n ratios. Alternatively, and equivalently, I can find the magnitudes of the input signals which makes the signal-to-noise ratio equal to unity for each SQUID circuit. The SQUID which can detect the smaller signal with a signal-to-noise ratio of unity will be the more sensitive SQUID.

Two figures of merit have already been proposed for the the SQUID, ε_v and ε (see Chapter 0). Experimentally, one generally measures the quantity ε_v, and it is used widely as a figure of merit. On the other hand it has long been recognized that this is not a good figure of merit because of the neglect of the effects of circulating current noise in the SQUID.[16-17] Instead, the quantity ε has been proposed as a figure of merit.[16-17] This proposal has been made under the assumption of weak coupling, and presumably then, this is not a good figure of merit for a SQUID at couplings near unity (how near unity has not been previously addressed).

Now in our expressions for the minimum detectable signals above, the SQUID parameters only enter into the two factors ε_v and I. Using ε_v as a figure of merit thus makes some sense because each of the above minmmum detectable quantities scales with ε_v. This is not the final answer however, for the quantity I also contains terms which depend upon the properties of the SQUID. Unfortunately, I generally depends on both the

circuit parameters and the SQUID parameters, and it is not ussually possible to separate the SQUID part from the circuit part. This means that there is in general no figure of merit for a SQUID, or equivalently, that the figure of merit will generally depend upon the input circuit parameters. In certain important limits, however, the quantity I reduces to a simple expression which is in fact independent of the input circuit (within certain limits). This case will be discussed in detail in section 12.16. In this limit, then, ε_V/I becomes the appropriate figure of merit for the SQUID.

12.13 The Minimum Detectable Energy

The minimum detectable energy, U_{min}, was defined above as the energy that the signal delivers when the signal-to-noise ratio ρ is unity. This is conventional, although somewhat arbitrary, and in general must be replaced by a more precise statistical decision criterion. I can thus write from Eq. 12.44:

$$U_{min} = \varepsilon_V \omega_o / I \ . \qquad (12.47)$$

The above expression clearly shows that I determines the minimum detectable energy. For I large, the SQUID is very sensitive, while for I small the SQUID is insensitve. I call the factor I the improvement because ε_V is the sensitivity of the SQUID in the most naive interpretations of SQUID behavior, and is generally what is measured experimentally. The true sensitivity is thus improved by a factor I from the ε_V.

The improvement is a complicated function of the SQUID and circuit parameters. Nevertheless, it can be shown that the input circuit

parameters L_i, C_i, and R_i only enter in the forms of Q, α^2, and ω_o. The SQUID parameters enter in a more complicated fashion. In particular, one has not only L and R, but also the dynamic L and R occuring in combination with ω_o. In general, for any given SQUID, not all of these parameters are well-known; usually only L, R, I_o and S_V are known. Accordingly, the potential sensitivity cannot be calculated for most SQUIDs as the characterization is incomplete. I now investigate the optimum energy sensitivity in different limits.

12.14 Minimum Detectable Energy: Optimization in The Limit $\alpha^2 << 1$

In the limit of small α^2 the maximum energy sensitivity appears to reduce to a well-known result. I say "appears" because the result at first seems to be the same as that produced by the noise temperature formulation. Although the result looks familiar, it is completely different. It is interesting to note that, it is not well known which circuit parameters are necessary to achieve the maximum sensitivity, and how seriously the performance deteriorates at other circuit parameters.

I now would like to maximize the optimal s/n ratio as a function of Q, for $\alpha^2 << 1$, and ω_o fixed. In this limit, with the constraints imposed, one finds that Q --> ∞ yields the highest sensitivty, as is shown in Appendix G. In this limit one finds a simple expression for I and U_{min}:

$$U_{min} = \varepsilon\omega_o \ , \tag{12.48}$$

$$\varepsilon = (\varepsilon_V\varepsilon_j - \varepsilon_{Vj}^2)^{1/2} \ , \tag{12.49}$$

$$I = \frac{\gamma_V^2}{(\gamma_V\gamma_j - \gamma_{Vj}^2)^{1/2}} \ , \tag{12.50}$$

where ε is the energy sensitivity.[17] Eq. (12.49) is well-known and is used in disscussing the ultimate quantum limted sensitivty of the dc SQUID. One sees here, however, that the SQUID's energy sensitivity to pulses will be given by this expression only in the limit Q --> ∞ and α^2 --> 0. The most remarkable thing about this formula, and what is difficult to appreciate initially, is that the temperature of the input circuit does not enter, and this is despite the fact that this is not the energy sensitivity of just the SQUID but the total system sensitivity. This is of course achieved by taking the limit Q --> ∞. The conventional noise temperature formulation would say that the system noise temperature is limited to T + T_n, where T is the temperature of the resistor R_i. For a low noise SQUID system, T >> T_n, and the difference between the two results is enormous. What makes the result all the more remarkable is that the noise temperature of the system can be much less than T even for finite Q, ie. when there is a non-zero resistance in the input, as will be shown below.

Tesche and Clarke[2] calculated numerically the gamma factors, γ_V, γ_V, and γ_{Vj}, and found:

$$\gamma_V \approx 8,\ \gamma_j \approx 5.5,\ \gamma_{Vj} \approx 6\ , \qquad (12.51)$$

and thus $I \approx 2.828$, and the minimum detectable energy becomes $U_{min} \approx \varepsilon_V \omega_o / 2.828$.

I am glossing over a difficult point here. The above results for the gamma factors are really only valid for $\beta = 1$ SQUIDs at $\Gamma = 2eI_o/k_BT \approx 0.05$. In Appendix C, I make plausible arguments for the temperature dependence of the gamma factors. The temperature dependence of γ_V can be found from my own experimental results, whereas there is no comparable data for the other gamma factors, and one must make assumptions. When

the temperature dependence is taken into account, one obtains different gammas at different temperatures, a fact not generally appreciated. However, the results for I and U_{min} are expected to be temperature independent due to compensating temperature variations in the SQUID transfer function V_Φ. It should be emphasized that this is not at all obvious, and that the temperature dependence of the γ_j and γ_{vj} have yet to be confirmed by detailed numerical simulations or experiment.

One should recognize that the calculations that determine the gammas are numerical simulations, and hence the gammas are not known to better than 5 or 10%. This has serious consequences when the gammas are used in Eq 14.50. In fact I becomes infinite when $\gamma_v\gamma_j = \gamma_{vj}^2$. The calculated gammas are very close to this condition, and hence a small error in any of them could alter the improvement ratio, $I = 2.828$, by a large amount. The only way out of this dilemma is a much more accurate calculation of the gammas. Until this is undertaken, the limit of 2.828 should be treated with a great deal of caution.

From the above discussion and that of section 12.11, in the limit of large Q and weak coupling α^2-->0, the figure of merit for the SQUID exists and is just $\varepsilon = \varepsilon_v/I$, as was expected.

12.15 The Minimum Detectable Energy: Optimization for Arbitrary α^2

There are two associated complications with determining the maximum sensitivity at large α^2. The first difficulty is that the signal-to-noise ratio becomes dependent not only on Q and α^2 but also on L/L^r and R/R^r. One must consider variations in a larger parameter space in order to find the optimum. The second difficulty is that one has

several choices about what is to be held fixed and what is to be varied. In particular, the resonant frequency and effective Q of the circuit will change as it is coupled to the SQUID. The most reasonable situation to consider is the case where the final renormalized resonant frequency, ω_o', is specified. The idea is that the pulse signal is at best an approximation to some real signal. Any real signal will only look like a pulse within some limited frequency range. The resonant frequency must be chosen within this range in order for this pulse approximation to be acceptable. Now if the resonant freqency of the perturbed input circuit, ω_o', is held fixed then the unperturbed resonant frequency $\omega_o = (L_i C_i)^{-1/2}$ will vary. This variation can be accomplished by varying L_i or C_i. As noted above variations of C_i will mean that the current source characterization and energy deposition characterization will not yield the same optimum parameters. It will be implicitly assumed below that I am dealing with the fixed energy source characterization, or the current source characterization with fixed C_i. It should be understood that the following sections are based on the reasonableness of the pulse approximation, and the limits of its validity are not considered here.

12.16 The Minimum Detectable Energy: Optimization for Arbitrary α^2 with ω_o Fixed

The minimum detectable energy is given by Eq. 12.48:

$$U_{min} = \varepsilon_v \omega_o / I \quad .$$

In this section, ω_o is assumed to be fixed while α^2 and Q are varied. In this case, the minimum detectable energy will occur when I is a maximum. I is sufficiently complicated that it is simplest to plot out I as a

function of Q and α^2 in order to find the maximum. These results must be treated cautiously because, as noted above, the peak system response is changing with the Q and α^2. I examine this point further below.

In Fig. 12.5, I have plotted I for Q = 10^0, 10^2,..., 10^{12}, $L/\mathcal{L}$ =+0.1 and $\omega_0 = 2\pi X10^4$ Hz. First of all, as α^2 --->0 and Q ---> ∞ , I--->2.828 ; this is the maximum that I attains for small α^2, as was discussed in section 12.14. Secondly, as Q --->0, I becomes very small. Thirdly, for any fixed Q, I increases as α^2 --->1. For Q finite, I is bounded above for all α^2. For Q--->∞ however, I --->∞ at α^2 = 1. This behavior is predominantly the result of the improvement in the sensitivity of the renormalized SQUID due to the renormalization of the SQUID inductance by screening, and implies that a SQUID can detect arbitrarily small energy pulses in this limit.

In Fig. 12.6, I is plotted for Q = 10^0, 10^2,..., 10^{12}, $\omega_0 = 2\pi$ X 10^4 and now $L/\mathcal{L}$ = -0.1. I have changed only the sign of the dynamic inductance $\mathcal{L}$, this can be accomplished experimentally by changing the SQUID flux bias from positive $\Phi_0/4$ to negative $\Phi_0/4$.[15] The resulting plots of I are qualitatively identical to those for $\mathcal{L}$ positive. In fact the only difference occurs for α^2 > 0.5, and is barely discernible to the eye as a slight upturn.

12.17 The Minimum Detectable Energy: How Large Should Q be: Qmin

It is important to realize that Q must be greater than some number, Q_{min}, before I begins to approach its maximum value for fixed α^2. From Fig. 12.5 and 12.6, it is clear that for α^2 = 0.1 and $\omega_0 = 2\pi$ X 10^4 I must have Q $\approx 10^7$ to get $I \approx 2.828$. For small α^2 it is clear that Q must

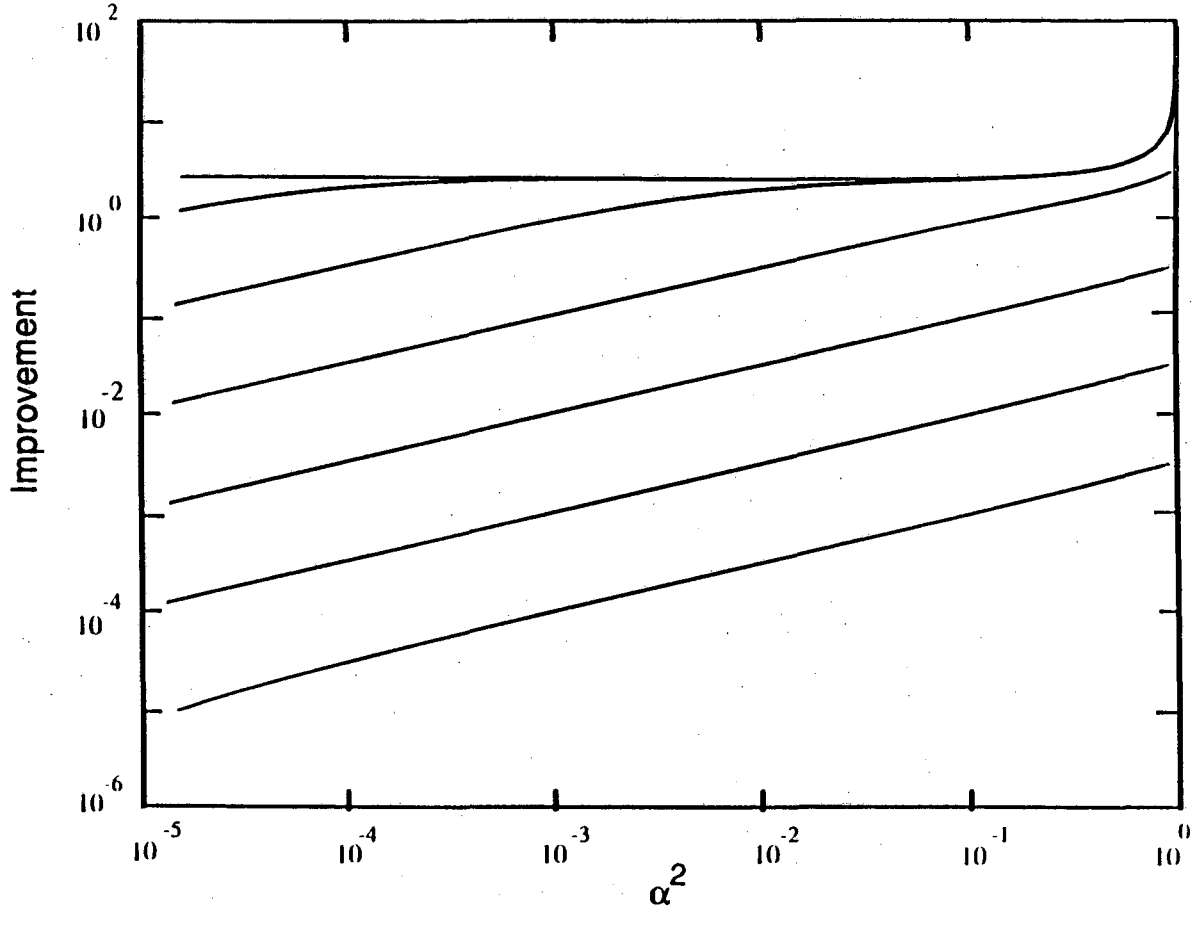

Fig. 12.5 Improvement ratio vs α^2, where $\omega_0=2\pi X10^4$, L/£ = 0.1, R=8Ω, and L=0.4nH,. Curves are for constant Q, where from bottom to top: $Q=10^0, 10^2, 10^4, ...10^{12}$.

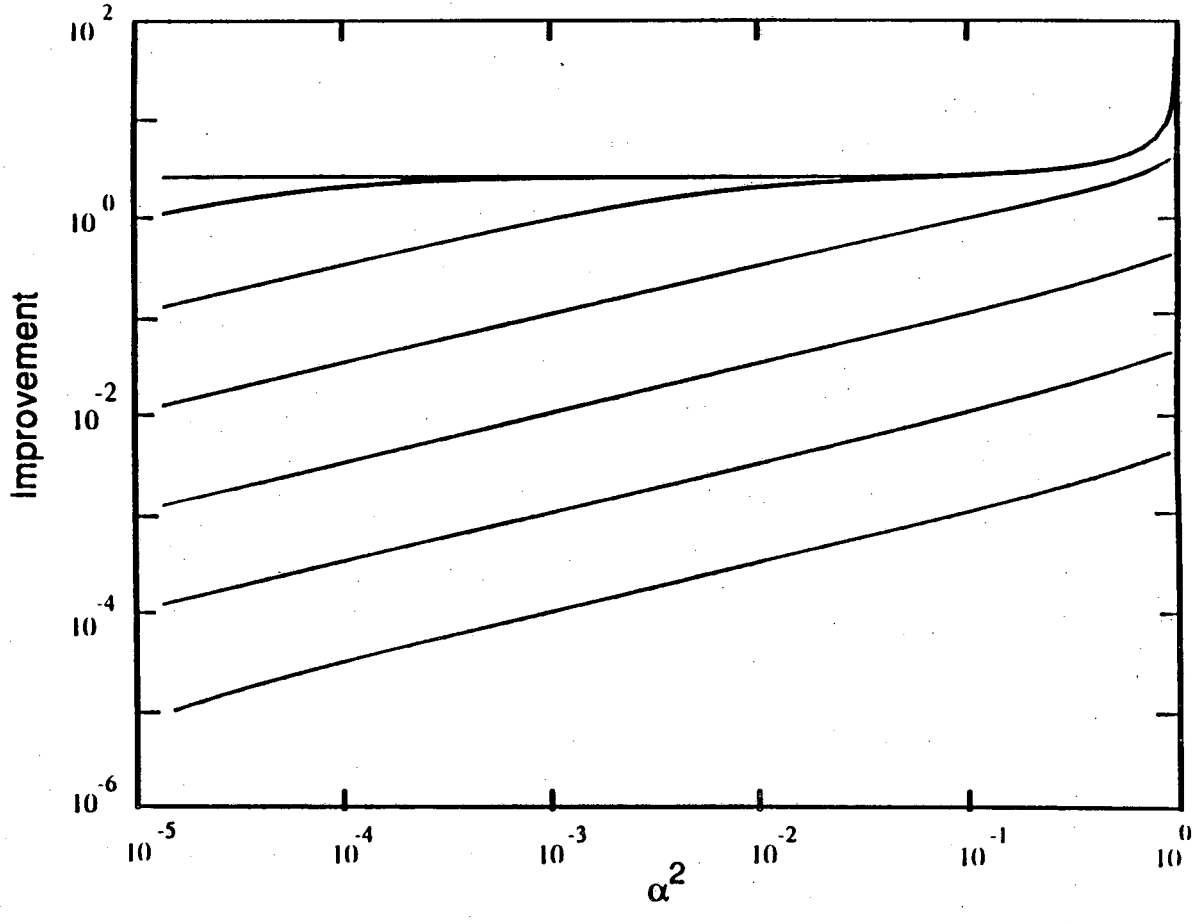

Fig. 12.6 Improvement ratio vs α^2, where $\omega_0 = 2\pi X 10^4$, L/£ = -0.1, R=8Ω, and L=0.4nH. Curves are for constant Q, where from bottom to top: $Q=10^0, 10^2, 10^4, \ldots 10^{12}$.

be larger still.

Q_{min} can be found by using the same limiting analysis as was used above to find I for small α^2. It is only necessary to retain higher order terms in 1/Q. This analysis is performed in Appendix H. The result is:

$$Q_{min} = \frac{2R\gamma_v}{\omega_o \alpha^2 L(\gamma_v\gamma_j - \gamma_{vj}^2)} , \qquad (12.52)$$

for small α^2. I note that Q_{min} is independent of T, but depends upon several SQUID parameters and ω_o. This result appears to differ from that of the ideal amplifier (see Eq. 12.22). However, the difference occurs only because the SQUID's sensitivity scales with the bath temperature, which is assumed to be the temperature of the input circuit resistance, whereas the amplifier of section 12.2 was assumed to produce a temperature independent noise.

The system will thus approach maximum sensitivity for $Q >> Q_{min}$. For $\omega_o = 2\pi \times 10^4$ and $\alpha^2 = 0.1$, one finds $Q_{min} = 4 \times 10^6$, which is consistent with the plots. For $\omega_o = 2\pi \times 30$ MHz and $\alpha^2 = 0.1$, one $Q_{min} \approx 10^3$. These optimization conditions are completely different from those found in the noise temperature formalism, which essentially predicts that the optimum performance is found for $Q\alpha^2 \approx 1$. From Fig. 12.5 or 12.6, one sees that $Q\alpha^2 = 1$ does not correspond to the best sensitivity, rather $Q \rightarrow \infty$ does. The noise temperature formalism also predicts a different sensitivity, which is limited by the bath temperature.

12.18 The Minimum Detectable Energy: Optimization for Arbitrary α^2, with ω_0' Fixed

As noted in a previous section, the optimization results for fixed ω_0 are suspect because the resonant response of the system is itself changing with Q and α^2. It can be shown that $\omega_0 \simeq \omega_0'$ for small α^2, while for large α^2, $\omega_0 \neq \omega_0'$. The distinction between the two frequencies becomes important typically for $\alpha^2 > 0.5$. I will here consider the effect of holding constant the renormalized resonant frequency, ω_0'.

The expressions for the optimal signal-to-noise ratio are unchanged, of course, it is merely a question of what is to be varied to maximize ρ. It is again easiest to present the result graphically. Analysis for fixed ω_0' shows that I is no longer a good measure of the "improvement" of the bare SQUID. Instead, I introduce a new quantity I':

$$I' = \frac{\varepsilon_V \omega_0'}{U_{min}} \quad . \tag{12.53}$$

For fixed ω_0', the SQUID will be most sensitive to energy when I' is a maximum. In Fig. 12.7, I plot I' vs α^2 for : Q = 10^0, 10^2,..., 10^{12}, $L/\mathcal{L}$ = 0.1, and $\omega_0'=2\pi X10^4$. For $\alpha^2 < 0.5$ there is little difference from Fig. 12.5 and 12.6. For larger α^2 there is a significant upturn and one finds that $I' > I$. This upturn is particularly noticeable as α^2 ---> 1. Thus, the qualitative conclusions for fixed ω_0' are the same as for fixed ω_0, although the I and I' are quantitatively distinct at large α^2.

In Fig. 12.8, I plot I' vs α^2 for: Q = 10^0, 10^2,..., 10^{12}, $L/\mathcal{L}$ =-0.1, and $\omega_0' = 2\pi X10^4$. For $\alpha^2 < 0.5$ there is little difference between Fig. 12.8, 12.7, 12.6 and 12.5. However, for larger α^2 there occurs a

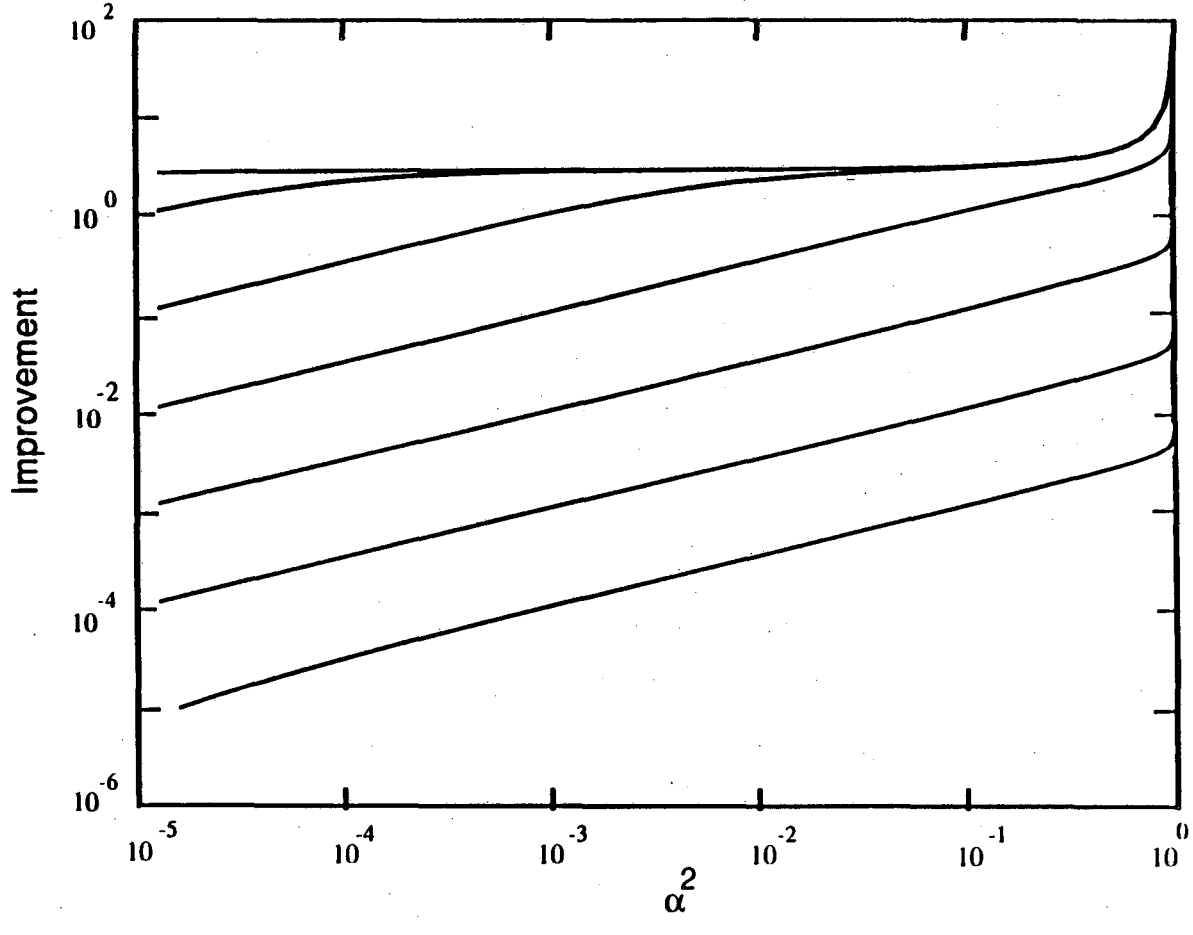

Fig. 12.7 Improvement ratio vs α^2, where $\omega_o' = 2\pi X 10^4$, L/£ = 0.1, R=8Ω, and L=0.4nH,. Curves are for constant Q, where from bottom to top: $Q=10^0; 10^2; 10^4; \ldots 10^{12}$.

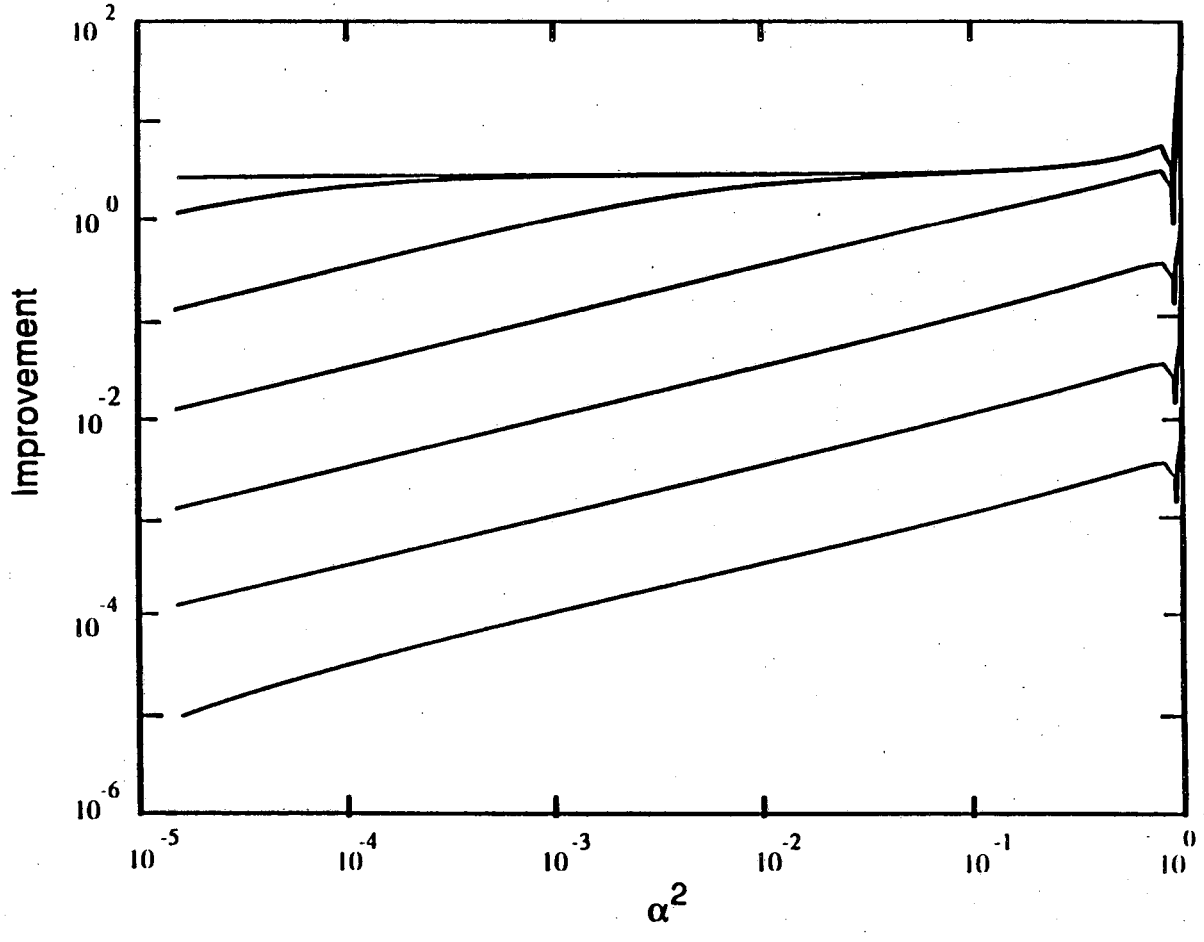

Fig. 12.8 Improvement ratio vs α^2, where $\omega_o'=2\pi X10^4$, L/£ = -0.1, R=8Ω, and L=0.4nH,. Curves are for constant Q, where from bottom to top: $Q=10^0, 10^2, 10^4, ...10^{12}$.

maximum for $\alpha^2 \approx 0.8$. In addition there is a sharp local minimum at $\alpha^2 \approx 1/1.1$, and, for $\alpha^2 > 1/1.1$, I' rapidly increases, and approaches again the result of Fig. 12.7. This rapid variation in I' near $\alpha^2 = 1/1.1$ occurs because the parameter $W = 1+\alpha^2 L/(1-\alpha^2)\mathcal{L}$ goes to zero there for $L/\mathcal{L} = -0.1$. This structure at large α^2 is highly dependent on $L/\mathcal{L}$. The parameter W controls the effective capacitance that occurs in the impedance Z_{eff}, and consequently affects the resonant frequency of the loop.

12.19 The Minimum Detectable Energy: The Optimal Filter

I have so far calculated the minimum detectable energy and the optimal parameters needed to achieve this sensitivity. Simply building such a circuit does not gaurantee that one will obtain the calculated sensitivity. The circuit must be used with the optimal filter. This filter is readily calculated from the results of Appendix D.

I should remark that it is common to call the total transfer function, from the current sensing input to the filter output, the "filter function". For our purposes here, I have factored out the frequency dependent gain of the (SQUID) X (input circuit). The filter that must be attached to the SQUID is then given explicitly, rather than the overall transfer function. I will call this the optimal attached filter.

For the case of a current pulse input, the optimal attached filter becomes, up to an arbitrary multiplicative factor:

$$F(\omega) = \frac{I^*(\omega)\ e^{-i\omega t}}{NV_{IS}} \quad . \tag{12.54}$$

This is a fairly complicated expression when written out in full. Experimentally, it is most easily implemented on a computer, after digitizing the output from the SQUID. The filter looks somewhat peculiar because of the presence of the time, t, in a frequency domain expression. The meaning is that the filter applies a time dependent phase shift to its input.

This concludes the discussion of the smallest energy pulse that the SQUID circuit can detect. In the following two sections I discuss the minimum detectable voltage and current. These sections build naturally on section 12.11 and the above discussion of the minimum detectable energy.

12.20 The Minimum Detectable Current

As was noted in section 12.11, the minimum detectable current $I_s(t) = q_o\delta(t)$ is governed by the equation:

$$\rho = q_o^2 I /(2\varepsilon_v\omega_o C_i) \quad . \tag{12.55}$$

The minimum detectable current will be the current such that $\rho = 1$. Thus:

$$q_{omin}^2 = 2\varepsilon_v\omega_o C_i/I \quad . \tag{12.56}$$

If I assume that ω_o and C_i are fixed and R_i is allowed to vary, then the best detection will occur for I a maximum. This is precisely the same condition as was discussed above for obtaining the best energy sensitivity, and thus the optimum parameters for this case are exactly those discussed above, namely $Q \to \infty$, and $\alpha^2 \to 1$. In the weak coupling limit, the best sensitivity again occurs for $Q \to \infty$. In this limit, I reduces to the simple form noted above and here yields the simple

transparent form:

$$q_{omin}^2 = 2\varepsilon\omega_o C_i \quad . \tag{12.57}$$

I again note the disappearance of the bath temperature, and that the minimum detectable current is limited by ε.

If instead, I assume that ω_o and R_i are fixed, and C_i is allowed to vary, (this is equivalent to holding ω_o and R_i fixed, and varying L_i). From the expression for q_{omin}, one can see that it is necessary to maximize I/C_i. Since ω_o and R_i are assumed fixed, this is equivalent to maximizinq QI. From the plots of I, I see that I is largest for Q-->∞ and α^2-->1, while Q-->∞ trivially makes Q largest. Again, the best performance occurs for Q-->∞ and α^2-->1.

12.21 The Minimum Detectable Voltage

The minimum detectable voltage is governed by the expression for the signal-to-noise ratio noted in section 12.11:

$$\rho = C_i I\, V_s^2/(2\varepsilon_v\omega_o) \quad . \tag{12.58}$$

The minimum detectable voltage is defined as the voltage which makes the signal-to-noise ratio unity, thus:

$$V_{smin}^2 = 2\varepsilon_v\omega_o/(IC_i) \quad . \tag{12.59}$$

If I assume that ω_o and C_i are held fixed, while R_i and α^2 are allowed to vary, then the best sensitivity again occurs for I a maximum. This is exactly the case found above, and the same optimum parameters result. In the weak coupling limit, one finds the following simple result:

$$V_{smin}^2 = 2\varepsilon\omega_o/C_i \quad . \tag{12.60}$$

Once again the result is independent of the bath temperature.

If instead, I assume that ω_o and R_i are held fixed, while C_i and α^2 are allowed to vary, (this is completely equivalent to holding ω_o and R_i fixed, and allowing L_i and α^2 to vary), then the best sensitivity will occur for IC_i a maximum. Since R_i and ω_o are held fixed, this is equivalent to maximizing I/Q. From the above discussion and plots of I, α^2-->1 maximizes I/Q for any Q, and thus α^2-->1 is the optimum for the coupling. Maximizing I/Q with respect to Q is most easily done by plotting out the function. One finds that I/Q is maximized for α^2 -->1, and Q --> 0. Since ω_o and R_i are held fixed, this implies that C_i -->∞, and L_i-->0 are the best circuit parameters.

12.22 Conclusions

In conclusion, I have presented a general technique for calculating the performance of a SQUID system using optimal filter theory and strong coupling SQUID noise theory. I have used this technique to calculate the optimum sensitivity of a model LCR circuit coupled to a SQUID when the signal was a current pulse. I have also found the circuit parameters and the optimal filter necessary to achieve this sensitivity. I have noted that this sensitivity exceeds that calculated by the noise temperature formalism, and the optimal parameters also differ greatly. I have also used a model for SQUID-circuit behavior which should be valid for arbitrary couplings α^2, and have presented results for large α where the effects of strong coupling become important. In this regime, I have noted the increased sensitivity of the SQUID. In particular one finds a greater sensitivity than $\varepsilon = (\varepsilon_v^2\varepsilon_j^2 - \varepsilon_{vj}^2)^{1/2}$.

Previous discussions of the sensitivity of the dc SQUID are valid

only at weak couplings, and even then must be used with caution as they cannot in general be expected to yield the optimum sensitivity. In particular, discussions of the quantum limit based upon the behavior of ε must be treated with suspicion in the limit of strong coupling, where ε is not a good figure of merit. The theory presented here does not take quantum corrections to the SQUID behavior into account. In particular, a real SQUID cannot be made arbitrarily sensitve by increasing the coupling coefficient α^2. At large couplings, the SQUID's behavior becomes limited by the uncertainty principle. In this respect, the theory of the optimization of the dc SQUID is still incomplete.

12.23 Appendices

Appendix A: Equivalent Voltage Source Representation

It is sometimes convenient to change from one representation to an equivalent representation. It is well-known that, given a linear network and a series voltage source, it is always possible to construct an equivalent network with a parallel current source. The two circuits we wish to consider are shown in Fig. 12A.1. In Fig. 12A.1(a) the current source is connected across a capacitor. I have replaced the SQUID and the remainder of the input coil with a linear impedance $Z(\omega)$. The result should then be valid in the small signal limit of the SQUID. I require that the current, I, which flows through the impedance $Z(\omega)$ must be the same for both circuits. For the current source:

$$I = \frac{I_s(\omega)}{1 + i\omega C_i Z(\omega)}$$

while for the voltage source one finds:

$$I = \frac{V_s(\omega)}{Z(\omega) + 1/i\omega C_i}$$

equating the two, one finds the trivial result that a current source across a capacitor has an equivalent voltage source given by:

$$V_s(\omega) = \frac{I_s(\omega)}{i\omega C_i}$$

In the time domain, this is just:

$$V_s(t) = \frac{1}{C_i}\int_{-\infty}^{t} I(t')dt'$$

For the case of a delta function current pulse one finds an equivalent

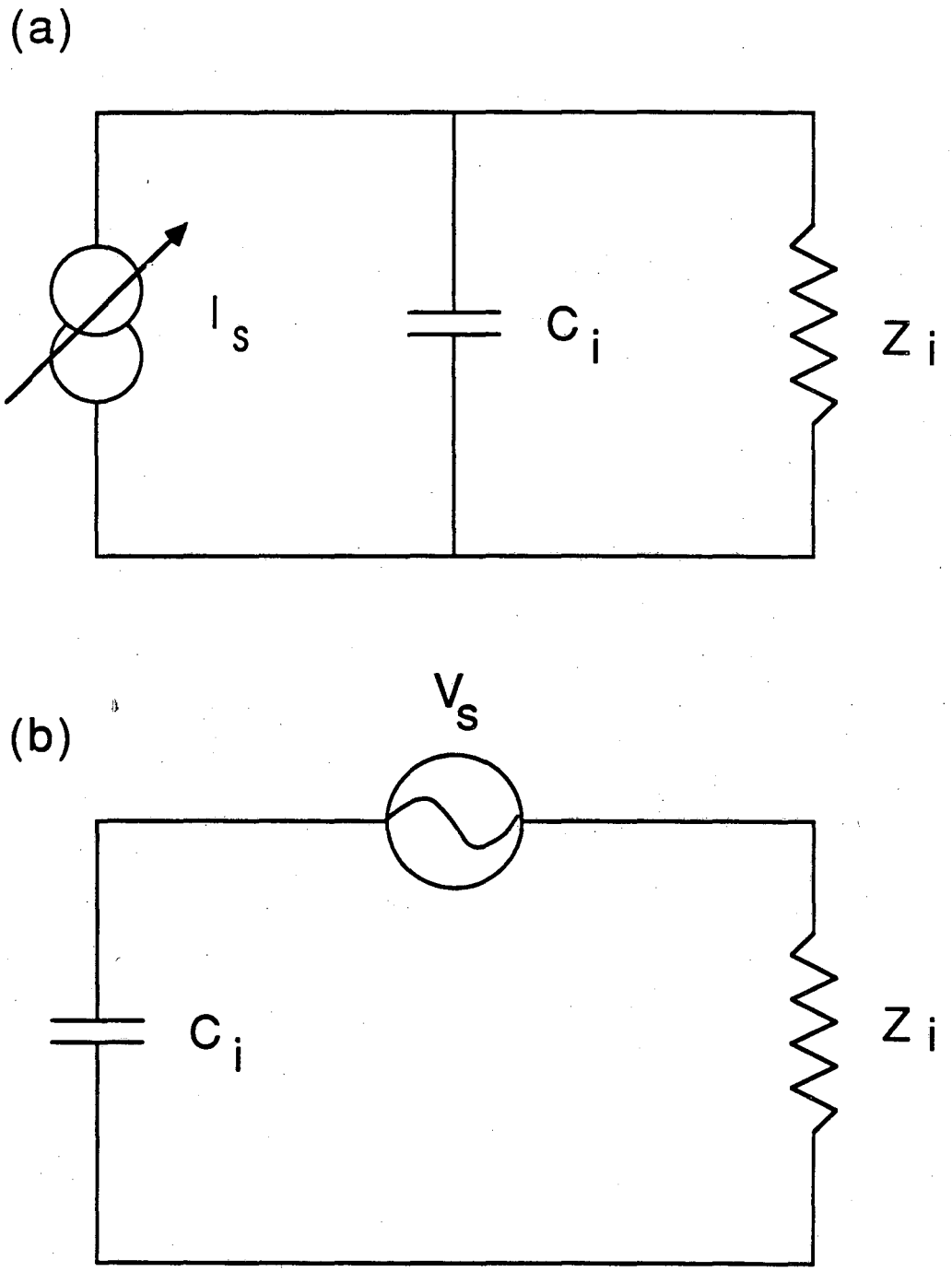

Fig 12A.1 (a) current source representation, (b) voltage source representation

step function voltage source.

Appendix B: The Transfer Functions

In order for a SQUID optimization technique to be valid at all SQUID-circuit couplings, one must use a theory of SQUID-circuit behavior which includes the effects of SQUID renormalization and dynamic input impedance. Renormalization refers to the changes in SQUID behavior that occur when the SQUID is coupled to an input circuit. The main effect is that the SQUID inductance is reduced by inductive shielding from the input circuit. The degree of renormalization depends upon the strength of the inductive coupling, α^2, between the SQUID and the input circuit. The idea of dynamic input impedance is that the SQUID is not a passive element. If one measures the impedance of a coil coupled to a SQUID, the apparent inductance will be frequency dependent, due to SQUID-circuit interaction.

Martinis and Clarke[8] have developed a self-consistent theory of SQUID noise behavior which works at arbitrary α^2. In their theory, the total output voltage can be written as:[8]

$$V_{out}(\omega) = V_{Sv}^{r}(\omega) + \frac{M^2 V_\phi^r \left(R_i + \frac{1}{i\omega C_i} \right)}{Z_{eff}\, L_i} J_n^r(\omega) + \frac{M V_\phi^r V_n(\omega)}{Z_{eff}} + \frac{M V_\phi^r V_s(\omega)}{Z_{eff}}$$

where: J_n^r is the renormalized SQUID circulating current

V_{sv}^r is the renormalized SQUID voltage noise

V_n is the Nyquist noise due to R_i

$V_s(\omega)$ is the input equivalent voltage source

$$Z_{eff} \equiv Z_T - \frac{J_\phi^r M_i^2}{L_i}\left[R_i + \frac{1}{i\omega C_i} \right] \equiv KR_i + i\omega L_i P + \frac{W}{i\omega C_i}$$

$$Z_T \equiv R_i + i\omega L_i + \frac{1}{i\omega C_i}$$

$$J_\phi^r \equiv -\left[\frac{1}{L^r} + \frac{i\omega}{R^r} \right]$$

$$K \equiv 1 + \frac{\alpha^2 L}{L^r} + \alpha^2 \frac{\omega_o L Q}{R^r}$$

$$P \equiv 1 + \alpha^2 \frac{\omega_o L}{Q R^r}$$

$$W = 1 + \alpha^2 \frac{L}{L^r}$$

Where I have introduced my own notation, and also generalized their equation to include the Nyquist noise from the input circuit resistance. Z_{eff} is what Martinis and Clarke[8] have called Z^*, a notation which I will not use because it looks like the complex conjugate of Z. It should be realized that the impedance Z_{eff} is <u>not</u> the equivalent impedance of the input circuit when the SQUID is coupled to it. Z_{eff} is merely an impedance parameter which occurs in the expressions for the transfer functions. The equivalent impedance of the input circuit will be discussed in Appendix E, and I will denote it as Z_{eq}.

I then define the transfer functions as:

$$V_{IS} \equiv \frac{\partial V_{out}(\omega)}{\partial I_s(\omega)} = \frac{M_i V_\phi^r}{i\omega C_i Z_{eff}}$$

$$V_J \equiv \frac{\partial V_{out}(\omega)}{\partial J_n^r(\omega)} = \frac{M_i^2 V_\phi^r}{L_i Z_{eff}} \left(R_i + \frac{1}{i\omega C_i} \right)$$

$$V_{VN} \equiv \frac{\partial V_{out}(\omega)}{\partial V_n^r(\omega)} = \frac{M_i V_\phi^r}{Z_{eff}}$$

The forms that appear in the noise formulation are then easily found. I define the new variables $y = \omega/\omega_o$ and $\omega_o = (L_i C_i)^{-1/2}$:

$$| V_{IS} |^{-2} = \frac{[P^2y^4 + (K^2/Q^2 - 2PW)y^2 + W^2]}{\alpha^2 L L_i V_\phi^{r2}}$$

$$\left| \frac{V_J}{V_{IS}} \right|^2 = \frac{\alpha^2 L}{L_i} \left[1 + \frac{y^2}{Q^2} \right]$$

$$\left| \frac{V_{vn}}{V_{IS}} \right|^2 = \frac{y^2}{Q^2 R_i^2}$$

$$\frac{V_J + V_J^*}{|V_{IS}|^2} = \frac{2}{V_\phi^r L_i} \left[y^2 \left(\frac{K}{Q^2} - P \right) + W \right]$$

Which concludes this section.

Appendix C: The Noise Referred to the Input

From Martinis and Clarke, the noise at the output of the SQUID can be written as:[8]

$$V_{out}(\omega) = V_{Sv}^r(\omega) + V_J J_n^r(\omega) + V_{vn} V_n(\omega)$$

where: $V_{Sv}^r(\omega)$ is the renormalized SQUID voltage noise amplitude

$J_n^r(\omega)$ is the renormalized SQUID current noise amplitude

$V_n(\omega)$ is the nyquist voltage noise amplitude from R_i

This voltage will produce a noise power spectrum given by:

$$S_{vout}(f) = S_V^r(f) + V_J^2 S_J^r(f) + V_{vn}^2 S_{vn}(f) + (V_j + V_j^*) S_{VJ}^r(f)$$

where I have used the fact that the SQUID voltage and current sources

have a real correlation. To find the equivalent noise referred to the input, N(f), one must divide by the input current-to-output voltage transfer function V_{IS}:

$$N = S_v^r|V_{IS}|^{-2} + S_j^r|V_J|^2|V_{IS}|^{-2} + S_{vn}^r|V_{VN}|^2|V_{IS}|^{-2} + S_{vj}^r(V_J+V_J^*)|V_{IS}|^{-2}$$

The transfer functions were found in Appendix B. Substituting, and collecting like powers of the dimensionless variable $y = \omega/\omega_o$, one finds:

$$N(f) = N_o(y^4 + by^2 + d)$$

where:

$$b = A_1 + B_1 + C_1 + D_1 \qquad \text{and } d = A_2 + B_2 + D_2$$

$$N_o = \frac{2\varepsilon_v^r P^2(1-\alpha^2)}{\alpha^2 L_i}$$

$$A_1 = \frac{K^2}{P^2Q^2} - \frac{2W}{P} \qquad A_2 = \frac{W^2}{P^2}$$

$$B_1 = \frac{\gamma_J^r\ \alpha^4 L^2 (V_\Phi^r)^2}{\gamma_v^r\ R^2Q^2P^2} \qquad B_2 = \frac{\gamma_J^r\ \alpha^4 L^2 (V_\Phi^r)^2}{\gamma_v^r\ P^2R^2}$$

$$C_1 = \frac{2\alpha^2 LL_i\ (V_\Phi^r)^2}{P^2R_iRQ^2\ \gamma_v^r}$$

$$D_1 = \frac{2L\alpha^2 V_\Phi^r\ \gamma_{vj}^r}{RP^2\ \gamma_v^r}\left[\frac{K}{Q^2} - P\right] \qquad D_2 = \frac{2LW\alpha^2\ \gamma_{vj}^r\ V_\Phi^r}{RP^2\ \gamma_v^r}$$

where K, P, and W are defined in Appendix B.

I now arrive at an important and not completely resolved issue. First of all, I will assume throughout the optmization that $\beta = 1$ for all α^2 (and $\beta_c << 1$, although this is not crucial). In this case I can drop the renormalized superscripts on all of the γ factors, since they depend upon the SQUID parameters only through β and β_c. There is a

remaining problem with the γ's however; they are, in general, temperature dependent. This is not a very well appreciated fact. The idea of writing the noise as Nyquist noise times some fudge factor, γ, gives no hint that the γ's are themselves dependent on the temperature. One is tempted to use:

$$\gamma_V = 8,\ \gamma_j = 5.5, \text{ and } \gamma_{Vj} = 6\ .$$

However, this is incorrect at low temperatures. The above assignments are really only "4.2 K" results for $\beta = 1$ SQUIDs with $\Gamma = 2eI_o/k_BT \simeq 0.05$. In addition, the above values of the γ's are those when the SQUID is biased at the lowest noise point, the noise will be higher at other points. As the temperature is lowered, this lowest noise bias point shifts to lower voltages. A similar problem arises for the factor V_ϕ, which is also temperature dependent. For β=1 and Γ=0.05, Tesche and Clarke[2] find $V_\phi \simeq R/L$ near the optimum bias point of the SQUID. At lower temperatures, however, V_ϕ greatly increases and this simple relation is no longer valid near the low noise bias point.

The above argument seems to suggest that the script variables $\mathcal{A}_1$, $\mathcal{B}_1$, etc. are temperature dependent. In fact, with certain reservations, I expect that the script variables are temperature independent. Accordingly, I expect that I will be left with temperature independent results which are identical to those one would find if one put in the naive Γ=0.05 assignments suggested above.

First of all, N_o contains the factor:

$$\varepsilon_V^{\Gamma} = S_\phi(f)/2L^{\Gamma} = 2k_BTR\gamma_V^{\Gamma}/(V_\phi^{\Gamma})^2$$

which is just the easily measured intrinsic energy sensitivity of a SQUID with inductance L^{Γ}. Now from the experiments discussed in Chapter 12, I have found that ε_V scales linearly with the temperature at least

down to 50 mK (I ignore the possibiltiy of quantum corrections in all of the analysis in this chapter). To a good approximation, the experiments are consistent with the predictions of Tesche and Clarke:[2]

$$\varepsilon_V = (9 \pm 1)k_B TL/R$$

If we assume that the effects of renormalization are well understood, then the experiments imply that $\gamma_V/(V_\Phi)^2$ must be temperature independent. It should be realized that $(V_\Phi)^2$ is strongly temperature dependent because of the increase in dynamic resistance as the SQUID temperature is lowered, and thus γ_V must also be temperature dependent. Nonetheless, the ratio is found to be constant. It is precisely this ratio which occurs in the scripted variables; whenever γ_V occurs, it is always divided by V_Φ^2.

Unfortunately, experimental data does not exist on the temperature dependence of γ_j and γ_{Vj}. It is possible to make simple arguments however that suggest that γ_j is approximately temperature independent, and γ_{Vj}/V_Φ is temperature independent. These arguments are based on the simple idea that it is the temperature dependence of V_Φ which makes any of the γ's containing the subscript v change with temperature.

With these assumptions, one can see that all of the scripted variables will be temperature independent, and we need only calculate there value at one temperature. Since the calculations of Tesche and Clarke[8] are available at Γ=0.05, we can use these results, and plug in these otherwise naive assignments for the γ's and V_Φ.

In conclusion, we can thus write the noise referred to the current sensing input as:

$$N = N_o(y^4 + by^2 + d)$$

where: $b = A_1 + B_1 + C_1 + D_1$ and $d = A_2 + B_2 + D_2$

$$N_o = \frac{2\varepsilon_v P^2(1-\alpha^2)}{\alpha^2 L_i}$$

$$A_1 = \frac{K^2}{P^2Q^2} - \frac{2W}{P} \qquad A_2 = \frac{W^2}{P^2}$$

$$B_1 = \frac{\gamma_J\, \alpha^4 L^2 (V_\phi)^2}{\gamma_v\, R^2Q^2P^2(1-\alpha^2)^2} \qquad B_2 = \frac{\gamma_J\, \alpha^4 L^2 (V_\phi)^2}{\gamma_v P^2R^2(1-\alpha^2)^2}$$

$$C_1 = \frac{2\alpha^2 LL_i\ (V_\phi)^2}{P^2R_iRQ^2\ \gamma_v(1-\alpha^2)^2}$$

$$D_1 = \frac{2L\alpha^2V_\phi\ \gamma_{vj}}{RP^2\ \gamma_v(1-\alpha^2)}\left[\frac{K}{Q^2} - P\right] \qquad D_2 = \frac{2LW\alpha^2\ \gamma_{vj}\ V_\phi}{RP^2\ \gamma_v(1-\alpha^2)}$$

where K, P, and W are defined in Appendix B, where it is understood that one should use the Γ=0.05 results for V_ϕ, and the γ's.

Appendix D: The Optimal Filter Theorems

I consider the general amplifier system shown in Fig. 12D.1. An input circuit is coupled to an amplifier. The output from the amplifier is fed to a filter which produces the final output $V'_{out}(t)$. All of the components are assumed to be linear. The input circuit and amplifier have associated noise sources, and the input circuit can accept signals $I_s(t)$. I will neglect noise from the output filter network and the possibility of interfering signals.

The key assumption in the optimal filter approach is that the signal-to-noise ratio is given by:

$$s/n \equiv \frac{|V'_{out}(t)|^2}{\sigma^2_{out}}$$

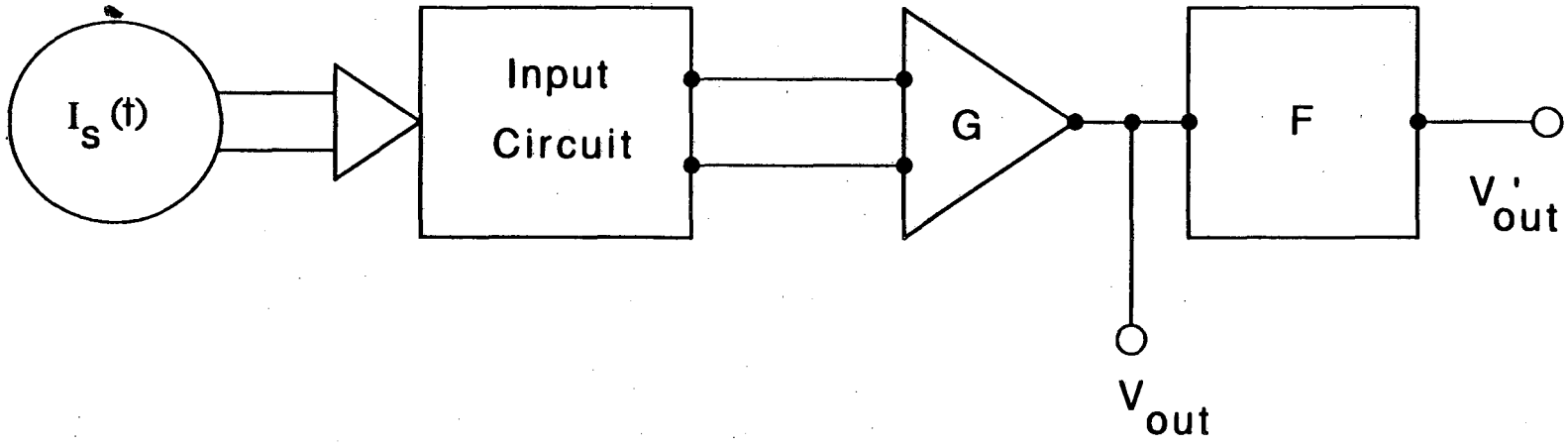

Fig. 12D.1 Signal source coupled to a linear input circuit, followed by a linear amplifier, and a linear filter.

where V'_{out} is the voltage at the output of the filter network, and σ^2_{out} is the mean square voltage noise at the output of the filter. Anyone who has looked at a small signal on a noisy oscilloscope trace can well appreciate this definition. A signal generally persists for some time, and it is obvious that smaller signals can be detected if one appropriately averages the height of the output for some time. This is the role of the post amplifier filter, and the possibilty of doing just such an operation is its function. For example, a simple average over some time to reduce the effects of noise is a linear operation which can be accomplished by a filter. Much more complicated operations are also possible, and it is the goal of the optimal filter theory to find the filter which produces the best s/n ratio.

I can rewrite the s/n ratio in the frequency domain by writing $V'_{out}(t)$ as a Fourier integral:

$$V'_{out}(t) = \frac{1}{2\pi}\int_{-\infty}^{\infty} e^{+i\omega t}\, V'_{out}(\omega)\,d\omega$$

$$V'_{out}(\omega) = \int_{-\infty}^{\infty} e^{-i\omega t}\, V'_{out}(t)\,dt$$

In addition, the mean square noise which occurs in the denominator can be written as a integral over all frequencies of the noise power per Hz at the output of the filter $N'_{out}(f)$. It is standard practice to define $N'_{out}(f)$ only for positive frequencies using the relation:

$$\sigma^2_{out} = \int_0^{\infty} N'_{out}(f)\, df$$

One can put the limits in a more symmetrical form by continuing the definition of $N'_{out}(f)$ to negative frequencies. I accordingly will define trivially:

$$N'_{out}(f) = N'_{out}(-f) \quad \text{for } f < 0$$

And thus trivially:

$$\sigma^2_{out} = \frac{1}{2}\int_{-\infty}^{\infty} N'_{out}(f)\, df$$

This can be further massaged by converting the variable of integration to $\omega = 2\pi f$:

$$\sigma^2_{out} = \frac{1}{4\pi}\int_{-\infty}^{\infty} N'_{out}(f)\, d\omega$$

I can then write the signal-to-noise ratio in the following somewhat unconventional form:

$$s/n = \frac{\left| \int_{-\infty}^{\infty} e^{+i\omega t} V'_{out}(\omega) d\omega \right|^2}{\pi \int_{-\infty}^{\infty} N'_{out}(f)\, d\omega}$$

To proceed, I now refer the noise back to the input of the circuit. This must be done using the appropriate transfer function of the system, which I will write as $H(\omega)$. Thus an input signal $I(\omega)$ will produce an output from the filter of $H(\omega)I(\omega)$, and the equivalent noise referred to the input of the circuit is $N(f) \equiv N'_{out}(f)|H(\omega)|^{-2}$, where $N(f)$ is again the conventional noise power but extended to negative frequencies. I can thus write the signal-to-noise ratio as:

$$s/n = \frac{\left| \int_{-\infty}^{\infty} e^{+i\omega t}\, H(\omega)I(\omega) d\omega \right|^2}{\pi \int_{-\infty}^{\infty} N(f)\, |H(\omega)|^2\, d\omega}$$

The idea is that we now want to find the $H(\omega)$ that maximizes this ratio. The function $H(\omega)$ contains the effect of the input circuit, the amplifier and the filter. In principle $H(\omega)$ can be any complex function since, I have left the filter arbitrary up to this point in our

discussion. In order to proceed, we factor N(f) into the form $N(f) = n(f)n^*(f)$. This is always possible because N(f) is a real positive definite quantity. I can then write:

$$s/n = \frac{\left| \int_{-\infty}^{\infty} H(\omega)n(f)\ e^{+i\omega t}\ \frac{I(\omega)}{n(f)}\ d\omega \right|^2}{\pi \int_{-\infty}^{\infty} \left| n(f)\ H(\omega) \right|^2\ d\omega}$$

This expression is of the form:

$$\Lambda = \frac{\left| \int_{-\infty}^{\infty} h\ g^*\ d\omega \right|^2}{\int_{-\infty}^{\infty} h^*h\ d\omega}$$

where $g^* = e^{i\omega t}I(\omega)/n(f)$ and $h = n(f)H(\omega)$.

Such expressions occur commonly in quantum mechanics, and are well-known in analysis. Continuous functions such as h and g can be thought of as vectors in the abstract vector space of all continuous functions. It is possible to define an inner product and a norm on this space. The inner product of two vectors g and h in this space is just:

$$\langle g,h \rangle = \int_{-\infty}^{\infty} g^*h\ d\omega$$

while the norm of a vector g is just $\langle g,g \rangle$. I can thus write the above expression for Λ in the form:

$$\Lambda = \frac{|\langle g,h \rangle|^2}{\langle h,h \rangle}$$

The Cauchy-Schwarz inequality[18] says that for any vectors g and h:

$$|\langle g,h \rangle| \leq |\langle g,g \rangle|^{1/2}\ |\langle h,h \rangle|^{1/2}$$

with the equality holding only if g is a multiple of h. And thus the

integral Λ is bounded:

$$\Lambda = \frac{|\langle g,h\rangle|^2}{\langle h,h\rangle} \leq \langle g,g\rangle$$

Expressing this in integral form:

$$\Lambda = \frac{\left| \int_{-\infty}^{\infty} h\, g^*\, d\omega \right|^2}{\int_{-\infty}^{\infty} h^* h\, d\omega} \leq \int_{-\infty}^{\infty} |g|^2\, d\omega$$

The maximum is achieved only when $g = h$, (of course up to an arbitrary multiplicative constant). The condition $g = h^*$ then implies that:

$$H(\omega) = I^*(\omega)\, e^{-i\omega t}/N(f) \equiv H_{opt}(\omega)$$

this is the optimal transfer function, and it is usually just called the optimal filter. Here however, I will call the attached filter just that part of the transfer function which is associated with the linear filter following the amplifier. If I write the transfer function of the input circuit and the amplifier as $G(\omega)$, and the attached filter transfer function as $F(\omega)$, then $H(\omega) = G(\omega)F(\omega)$, and the optimal attached filter function is then $F(\omega) = H(\omega)/G(\omega)$.

For this optimal filter the optimal signal-to-noise ratio, ρ, becomes:

$$\rho = \frac{1}{\pi} \int_{-\infty}^{\infty} \frac{|I(\omega)|^2 d\omega}{N(f)}$$

which is the required expression.

Appendix E: The Energy Deposited by a Signal

An input signal will generally do work on a circuit, and hence it

will deliver energy to the system. The magnitude of this deposited energy is an important parameter in the signal and noise analysis, and it generally turns out that the more energy that is deposited the better is the signal-to-noise ratio. It should be realized however that the optimization procedure described above does not amount to simply maximizing the deposited energy. As we will see below, many different circuit configurations will yield the same deposited energy, but only one will yield the optimum s/n ratio.

In this section I will explicitly consider a series voltage source, $V_s(t)$. The following analysis computes the deposited energy for a broad class of signals which are of the form:

$$V_s(t) = V_o\, e^{-\lambda t} \cos(\omega_a t) \qquad \text{for } t>0$$
$$= 0 \qquad \text{for } t<0$$

This is a very interesting class of signals. They occur frequently in NMR and tuned systems. Our interest here is in the limit $\omega_a \dashrightarrow 0$, and $\lambda \dashrightarrow 0$. In this limit, the free precession decay becomes a step function, which is the equivalent series voltage signal of a δ-function current pulse applied across the series capacitor (see Appendix A).

From first principles, the energy delivered is the work, U, done on the circuit:

$$U \equiv \int_{-\infty}^{\infty} V_s(t) I_i(t)\,dt = V_o \int_{0}^{\infty} e^{-\lambda t} \cos(\omega_a t) I_i(t)\,dt$$

where $I_i(t)$ is the current flowing in the input circuit at time t in response to the applied voltage. The integral is recognizable as a Laplace transform, and this is a very convenient fact which will be exploited to the utmost. I can thus write:

$$U = \frac{V_o}{2}\left[\mathcal{L}_\lambda\left(e^{i\omega_a t} I_i(t)\right) + \mathcal{L}_\lambda\left(e^{-i\omega_a t} I_i(t)\right)\right]$$

Where $\mathcal{L}_\lambda$ denotes the Laplace transform of the function in parenthesis. I can now use the elementary properties of the Laplace tansform to write this as:

$$U = \frac{V_o}{2}\left[\mathcal{L}_{\lambda - i\omega_a}\left(I_i(t)\right) + \mathcal{L}_{\lambda + i\omega_a}\left(I_i(t)\right)\right]$$

I now need to find $\mathcal{L}_s(I_i(t))$. This can be done by using the Martinis and Clarke formulation for the SQUID behavior.[8] Two coupled linear integral-differential equations are involved. In Martinis and Clarke, these are written in the frequency domain. The equivalent differential equations to their Eqs. 2.7 and 2.8 are:

$$\text{(i)}\quad V_i(t) = R_i I_i(t) + L_i \frac{dI_i}{dt} + M_i \frac{dJ}{dt} + \frac{1}{C_i}\int_{-\infty}^{t} I_i(t')dt'$$

$$\text{(ii)}\quad -\left[\frac{M_i V_i(t)}{L^r} + \frac{M_i}{R^r}\frac{dV_i}{dt}\right] = \left[1 + \alpha^2 \frac{L}{L^r}\right]\left[R_i J(t) + L_i \frac{dJ}{dt} + \frac{1}{C_i}\int_{-\infty}^{t} J(t')dt'\right] + \\ + L_i \frac{dJ}{dt} - \frac{M_i^2}{L^r}\frac{dJ}{dt} + \frac{\alpha^2 L}{R^r}\left[R_i \frac{dJ}{dt} + \frac{J(t)}{C_i}\right]$$

Where J is the circulating current in the SQUID, V_i is the equivalent series input voltage source, and I_i is the current flowing in the input circuit. This is precisely the kind of systems of equations that the Laplace transform is best suited to solve. I can apply a Laplace transform to both sides of these equations. I will take the initial conditions as $I_i(0) = J(0) = V_i(0) = 0$, corresponding to the signal not started yet, and neglecting the effect of noise on the energy deposition. The result can be put in the form:

$$\mathcal{L}_s(V_i) = Z_{tot}(s)\mathcal{L}_s(I_i) + sM_i\mathcal{L}_s(J)$$

and:

$$-\left[\frac{M_i}{L^r} + \frac{sM_i}{R_i}\right]\mathcal{L}(V_i) = \left[1 + \alpha^2\frac{L}{L^r}\right]Z_{tot}(s)\mathcal{L}_s(J) + -s\mathcal{L}_s(J)\frac{M_i^2}{L^r} + \frac{\alpha^2 L}{R^r}\left[R_i s + \frac{1}{C_i}\right]\mathcal{L}_s(J)$$

This system of equations is completely equivalent to Martinis and Clarke's Eqs. 2.7 and 2.8, which can be found by taking $s = i\omega$. The equations can be solved for $\mathcal{L}_s(J(t))$ in terms of the Laplace transform of the input voltage $\mathcal{L}_s(V_i(t))$:

$$\mathcal{L}_s(J) = -\frac{M_i\left[\frac{1}{L^r} + \frac{s}{R^r}\right]}{Z_{eff}(s)}\,\mathcal{L}_s(V_i)$$

$$\mathcal{L}_s(I_i(t)) = \frac{\mathcal{L}_s(V_i(t))}{Z_{eq}(s)}$$

where:

$$Z_{eq}(s) \equiv \frac{Z_{eff}(s)}{\left[1 + \alpha^2\frac{L}{L^r} + s\,\alpha^2\frac{L}{R^r}\right]}$$

$$Z_{eff}(s) = KR_i + sPL_i + \frac{W}{sC_i}$$

If one takes $s = i\omega$, then Z_{eff} is just the effective impedance which arises in the transfer functions. Furthermore, I can recognize Z_{eq} as the equivalent impedance of the input circuit with the SQUID attached. That is, the applied voltage divided by the induced current is just the impedance that the voltage source sees.

It is a simple matter to find the Laplace transform of the input signal.

$$\mathcal{L}_s(V_i(t)) = \int_0^\infty e^{-st}\,V_i(t)dt = V_o\,\frac{s+\lambda}{(s+\lambda)^2 + \omega_a{}^2}$$

And thus, the deposited energy is:

$$U = \frac{V_o^2}{2Z_{eq}(\lambda)}\left[\left| \frac{s+\lambda}{(s+\lambda)^2+\omega_a^2} \right|_{s=\lambda-i\omega_a} + \left| \frac{s+\lambda}{(s+\lambda)^2+\omega_a^2} \right|_{s=\lambda+i\omega_a} \right]$$

I want to explicitly consider the current pulse case. This corresponds to a step function in $V_i(t)$. Setting $\omega_a = 0$, and then taking the limit $\lambda \dashrightarrow 0$, I find the simple result:

$$U = C_i V_o^2/2 = q_o^2/2C_i.$$

It should be realized that I have neglected the effect of noise on the amount of energy deposited. For very small energy depositions, this can be serious. One finds that energy may be added to, or extracted from, the system, depending upon whether the noise is in phase or out of phase with the signal. One thus expects a statistical distribution for the deposited energy, even for a fixed input signal strength. A more complete treatment which takes this effect into account would be of interest.

Appendix F: The Contour Integrations

In this appendix I evaluate the two related integrals I_1 and I_o, where:

$$I_o = \int_{-\infty}^{\infty} \frac{y^2\,dy}{y^4 + By^2 + D}$$

$$I_1 = \int_{-\infty}^{\infty} \frac{dy}{y^4 + by^2 + d}$$

This is most easily done using contour integration techniques.

The Evaluation of I_1

I must first locate the four poles of the integrand. It is impossible for the noise to vanish at a real frequency y, and hence all four poles must be either pure imaginary or complex. Also, since N(f) = N(-f), two poles must lie above the real axis, and two below. I can find the poles by applying the quadratic equation twice to y^4. The first application results in:

$$y^2 = \frac{-b}{2} \pm \left[\frac{b^2}{4} - d \right]^{1/2}$$

The second application generates solutions which are either pure imaginary (Region 1) or complex (Region 2), depending upon whether $(b^2/4-d)$ is positive or negative.

Region (1): $(b^2/4-d)>0$

Then:

$$y^2 = \frac{-b}{2} + \left[\frac{b^2}{4} - d \right]^{1/2}$$

must be real and less than zero, or else one would find the noise going to zero at real frequencies. Thus the poles occur at:

$$y = \pm i \left[\frac{-b}{2} + \left[\frac{b^2}{4} - d \right]^{1/2} \right]^{1/2}$$

I can thus write the four poles as:

$$z_1 = i(T_1)^{1/2} \qquad z_3 = -i(T_1)^{1/2}$$

$$z_2 = i(T_2)^{1/2} \qquad z_4 = -i(T_2)^{1/2}$$

where:

$$T_1 = \frac{b}{2} + \left[\frac{b^2}{4} - d \right]^{1/2} \qquad T_1' = T_1^{1/2}$$

$$T_2 = \frac{b}{2} - \left[\frac{b^2}{4} - d\right]^{1/2} \qquad T_2' = T_2^{1/2}$$

The contour integration can be taken over the path shown in Fig. 12F.1(a). The integral vanishes along the upper arc, and the two poles z_1 and z_2 are enclosed. I can then use the Cauchy residue theorem to write the integral as:

$$I_1 = 2\pi i\left[\frac{1}{(iT_1'+iT_2')(iT_1'-iT_2')(2iT_1')} + \frac{1}{(iT_1'+iT_2')(iT_2'-iT_1')(2iT_2')}\right]$$

Rearranging this one finds:

$$I_1 = \frac{\pi}{T_1'T_2'(T_1'+T_2')}$$

Region (2): $(b^2/4-d) < 0$

Then:

$$y^2 = \frac{-b}{2} \pm \left[\frac{b^2}{4} - d\right]^{1/2} = R_o\, e^{\pm i\theta}$$

must be complex. Where:

$$R_o = d^{1/2} \qquad \text{and} \qquad \cos(\theta) = -b/(2d^{1/2})$$

Thus the poles occur at:

$$y = \pm R_o^{1/2} e^{\pm i\theta/2} = \pm R_o^{1/2}\cos(\theta/2) \pm iR_o^{1/2}\sin(\theta/2)$$

I can write the four poles as:

$$z_1 = R_o{}^{1/2}\, e^{i\theta/2} \qquad z_3 = R_o{}^{1/2}\, e^{-i\theta/2} = z_1{}^*$$

$$z_2 = -R_o{}^{1/2}\, e^{-i\theta/2} = -z_1{}^* \qquad z_4 = -R_o{}^{1/2}\, e^{i\theta/2} = -z_1$$

The contour integration can be taken over the path shown in Fig. 12F.1(b). The integral vanishes along the upper arc, and the path encloses the two poles z_1 and z_2. I can now apply the Cauchy residue theorem to write the integral as:

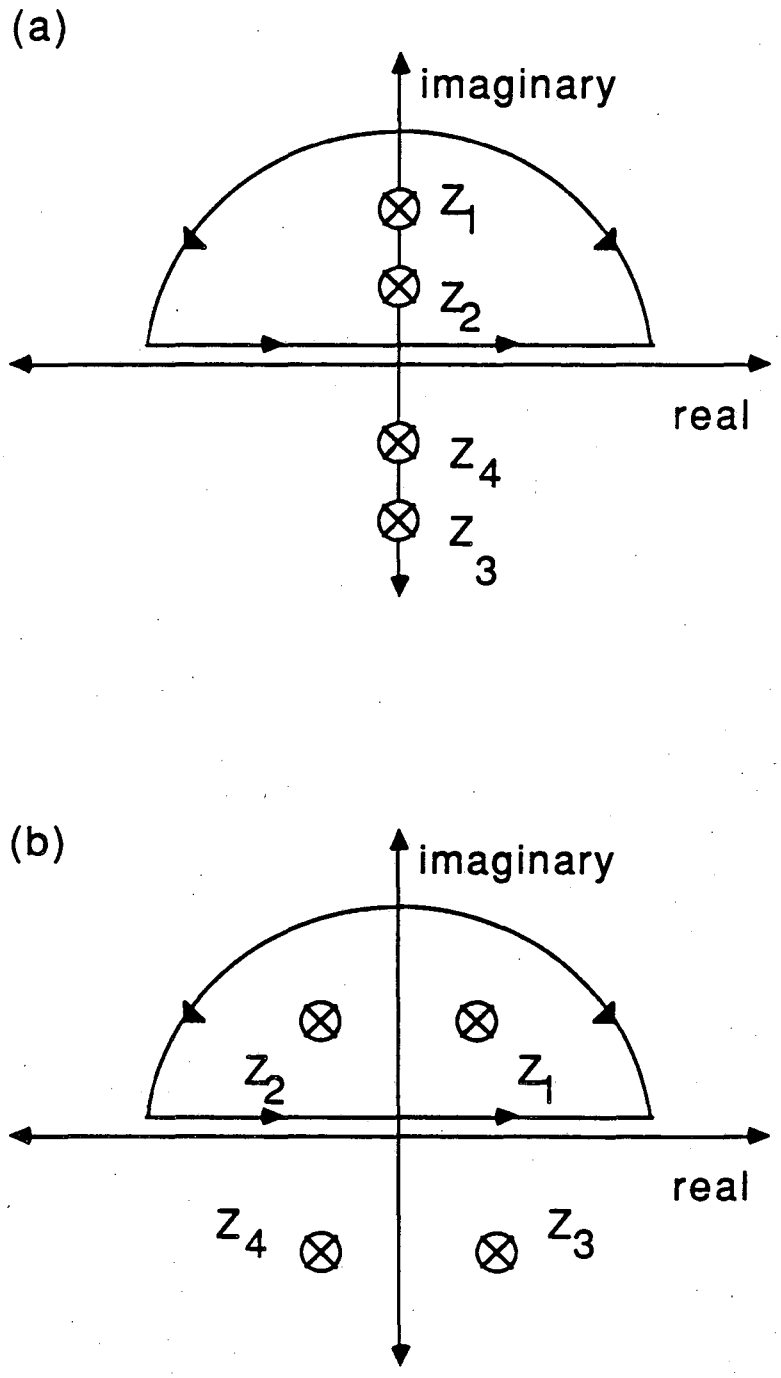

Fig. 12F.1 Poles and integration path for the integral I_1, (a) region 1, (b) region 2.

$$I_1 = 2\pi i\left[\frac{1}{(z_1+z_1^*)(z_1-z_1^*)(2z_1)} + \frac{1}{(-z_1^*+z_1)(-z_1^*-z_1)(-2z_1^*)}\right]$$

This can be put in the form:

$$I_1 = \frac{\pi}{2R_o^{3/2}(1/2 + b/(4R_o))^{1/2}} = \frac{\pi}{2R_o^{3/2}\sin(\theta/2)}$$

The Integral I_o

The related integral expression for I_o may be treated in a very similar manner. If one makes the identification b <--> B, and d <--> D, the poles are the same as for I_1, and again there occur two regions. Substituting for the residues one finds, in region 1: $(B^2/4-D) > 0$:

$$I_o = 2\pi i\left[\frac{(iT_1')^2}{(iT_1'+iT_2')(iT_1'-iT_2')(2iT_1')} + \frac{(iT_2')^2}{(iT_1'+iT_2')(iT_2'-iT_1')(2iT_2')}\right]$$

$$I_o = \frac{\pi}{(T_1'+T_2')}$$

Where T_1' and T_2' are the same as for I_1 above, except that b has been replaced by B, and d has been replaced by D. Similarly in region 2: $(B^2/4-D) < 0$:

$$I_o = 2\pi i\left[\frac{z_1^2}{(z_1+z_1^*)(z_1-z_1^*)(2z_1)} + \frac{(z_1^*)^2}{(-z_1^*+z_1)(-z_1^*-z_1)(-2z_1^*)}\right]$$

Upon substituting for z_1, this can be put in the form:

$$I_o = \frac{\pi}{2R_o^{1/2}(1/2 + b/(4R_o))^{1/2}}$$

where again, the terms R_o and b are found from the I_1 expressions by replacing b with B, and d with D.

Appendix G: Optimization for α^2 -->0

When α^2 is small compared to 1, the plots of ρ vs α^2 for different Q show that the highest sensitivity is obtained when Q --> ∞. That Q-->∞ gives the best ρ for small α^2 and large Q is shown analytically in Appendix H. In this section I will show that for α^2 small, and Q -->∞, the minimum detectable energy reduces to a simple form.

I first take the limit Q -->∞. In this limit one finds that:

$A_1 = -2$ $\qquad$ $A_2 = 1$

$B_1 = 0$ $\qquad$ $B_2 = \alpha^4 \gamma^r{}_j / \gamma^r{}_v$

$C_1 = 0$

$D_1 = -2\alpha^2 \gamma^r{}_{vj} / \gamma^r{}_v$ $\qquad$ $D_2 = 2\alpha^2 \gamma^r{}_{vj} / \gamma^r{}_v$

This is correct to all orders in α^2, provided Q is strictly infinte, $W \neq 0$, and $\alpha^2 \neq 1$. The $W \neq 0$ condition can only fail at isolated points for relatively large α^2.

I can then write $N = N_0(y^4 + by^2 + d)$, where:

$$b = A_1+B_1+C_1+D_1 = -2 \left[1 + \alpha^2 \frac{\gamma^r_{vjo}}{\gamma^r_v}\right]$$

$$d = A_2+B_2+D_2 = 1 + 2\alpha^2 \frac{\gamma^r_{vj}}{\gamma^r_v} + \alpha^2 \frac{\gamma^r_j}{\gamma^r_v}$$

I can drop the renormalized labels on the γ's as noted in Appendix C. The poles of the integrand for the optimum signal-to-noise ratio will occur at the zeros of N(y). A check shows that the zeros with respect to y^2 are complex, and thus the zeros with respect to y are of the form (this is in region 2, see Appendix F):

$$y = \pm R_0{}^{1/2} (\cos(\theta/2) + i\sin(\theta/2))$$

and the optimum signal-to-noise ratio becomes:

$$\rho = \rho_0 \frac{1}{2R_0^{3/2}\sin(\theta/2)}$$

where:

$$\rho_0 = \frac{U\,\alpha^2}{\varepsilon_v\omega_0(1-\alpha^2)2p2}$$

$$R_0 = \left[\left[1 + \alpha^2 \frac{\gamma_{vjo}}{\gamma_{vo}}\right]^2 + \alpha^4\left[\frac{\gamma_v\gamma_j - \gamma_{vj}}{\gamma_v^2}\right]\right]^{1/2}$$

$$\sin(\theta) = \frac{\alpha^2}{R_0}\left[\frac{\gamma_v\gamma_j - \gamma_{vj}^2}{\gamma_v^2}\right]^{1/2}$$

I now explicitly take the small α^2 limit, $\alpha^2 \rightarrow 0$. One finds that $P \rightarrow 1$, $(1-\alpha^2) \rightarrow 1$, $R_0 \rightarrow 1$, and $\sin(\theta/2) \cong \theta/2 \cong \sin(\theta)/2$, and thus the optimal signal-to-noise ratio is:

$$\rho = \frac{U}{\varepsilon_v\omega_0}\left[\frac{\gamma_v^2}{\gamma_v\gamma_j - \gamma_{vj}^2}\right]^{1/2}$$

The minimum detectable energy, U_{min}, is the energy which makes the ratio $\rho=1$. Thus: $U_{min} = \omega_0(\varepsilon_v\varepsilon_j - \varepsilon_{vj}^2)^{1/2} = \omega_0\varepsilon$, where I have used the definitions of the ε's. This is precisely the result Danilov et al.[17] find for the energy sensitivity of the SQUID. It is interesting to note however, that from our analysis we can see it only describes the SQUID sensitivity at small coupling α^2, and is only achievable in the large Q limit. Nonetheless, this is the total system noise, and not just the SQUID noise temperature part which arises in the noise temperature formalism.

From the above result, and the considerations of Appendix C on the behavior of the γ's, the SQUID improvement ratio is just:

$$I = \left[\frac{U_{min}}{\varepsilon_v \omega_o} \right]^{-1} = \frac{\gamma_v^2}{[\gamma_v \gamma_j - \gamma_{vj}^2]^{1/2}}$$

where it is here understood that the γ's are to be taken for Γ=0.05. From the numerical simulations of Tesche and Clarke[2], the gammas are roughly:

$$\gamma_v \simeq 8 \qquad \gamma_j \simeq 5.5 \qquad \gamma_{vj} \simeq 6$$

and thus $I \simeq 8^{1/2} \simeq 2.828$. I note in caution that the improvement I is a very sensitive function of the γ's and therefore this number is not well known. If γ_{vj} were to increase to 6.633, the improvement would become infinite, which is physically unreasonable.

Appendix H: How large must Q Be

I want to know how large Q must be for I to approach its maximum value. This will be done only for small α^2. I follow the technique of Appendix G, except that we will now retain terms to first order in 1/Q.

For small α^2, we are always in Region (2), where $b^2/4-d < 0$. Thus from Appendix F:

$$I_1 = \frac{\pi}{2d^{3/4}\left[\frac{1}{2} + \frac{b}{4(d)^{1/2}} \right]}$$

I wish to make an expansion for I_1 in the large Q limit. I thus make a series axpansion in powers of 1/Q and retain only the first order term:

$$I_1(Q) \simeq I_1(Q=\infty) + c/Q$$

I will determine the coefficient c of the 1/Q term to lowest order in α^2.

In the small α^2 limit, retaining terms only to first order in 1/Q,

and dropping the renormalized superscripts, one finds for the various scripted coefficients:

$$A_1 = A_1^{\infty} + \frac{2\alpha^2 Q'}{Q} \qquad A_2 = A_2^{\infty} + \frac{2\alpha^6 \omega_o L \gamma_j}{QR\gamma_v}$$

$$B_1 = B_1^{\infty} = 0 \qquad B_2 = B_2^{\infty} + \frac{2\alpha^2 \omega_o L}{QR}$$

$$C_1 = C_1^{\infty} + \frac{2\alpha^2}{QQ''\gamma_v}$$

$$D_1 = D_1^{\infty} + \frac{2\alpha^4 \omega_o L \gamma_{vj}}{RQ\gamma_v} \qquad D_2 = D_2^{\infty} + \frac{4\alpha^4 \omega_o L \gamma_{vj}}{QR\gamma_v}$$

where: $Q = \omega_o L_i/R_i$, $Q' = \omega_o L_i/R$, $Q'' = \omega_o L/R^{\Gamma}$, and the (∞) superscripted variables are just the values for the scripted variables found in Appendix G when $Q \rightarrow \infty$:

$$A_1^{\infty} = -2 \qquad A_2^{\infty} = 1$$

$$B_1^{\infty} = 0 \qquad B_2^{\infty} = \alpha^4 \gamma_j/\gamma_v$$

$$C_1^{\infty} = 0$$

$$D_1^{\infty} = -2\alpha^2 \gamma_{vj}/\gamma_v \qquad D_2^{\infty} = 2\alpha^2 \gamma_{vj}/\gamma_v$$

In these expressions I have also taken the Γ=0.05 result $V_{\phi} = R/L$, as discussed in Appendix C. Thus to order 1/Q I can write:

$$b = b^{\infty} + \Delta b, \text{ and } d = d^{\infty} + \Delta d,$$

where:

$$b^{\infty} = A_1^{\infty} + B_1^{\infty} + C_1^{\infty} + D_1^{\infty} \qquad d^{\infty} = A_2^{\infty} + B_2^{\infty} + D_2^{\infty}$$

$$\Delta b = \frac{1}{Q}\left[2\alpha^2 Q' + \frac{2\alpha^2}{Q''\gamma_v} + \frac{2\gamma_{vj}\omega_o L}{\gamma_v R^{\Gamma}} \right]$$

$$\Delta d = \frac{2\alpha^2 \omega_o L}{QR^{\Gamma}}\left[\frac{\alpha^4 \gamma_j}{\gamma_v} + 1 + \frac{2\alpha^2 \gamma_{vj}}{\gamma_v} \right]$$

Most SQUID measurements occur at $\omega_o << R/L$, and thus $Q'' << 1$, and $Q' << 1$.

For relatively large Q, one finds then that only the middle term in Δb and Δd is important. Furthermore, the Δd term is of order $\alpha^2 Q'/Q$ and will be much smaller than the Δb term. For the following, I will take the typical case where $Q' << 1$. The Δd term may then be neglected, and one finds:

$$\Delta b = 2\alpha^2/(QQ''\gamma_v) \qquad \Delta d = 0$$

I can thus write for I_1, to lowest order in $1/Q$ and α^2:

$$I_1(Q) = I_1(Q=\infty) - I_1(Q=\infty)\,\frac{\Delta b}{4(d^\infty)^{1/2}\left[\frac{1}{2} + \frac{b^\infty}{4(d^\infty)^{1/2}}\right]}$$

Since $d^\infty \simeq 1$, the correction term only becomes appreciable when the numerator is of order the denominator. Thus the high Q limit of Appendix G will be reached only for:

$$\Delta b << 2(d^\infty)^{1/2} + b^\infty$$

Upon substituting for Δb and rearranging, I find that the high Q limit occurs for:

$$Q >> Q_{min} \equiv \frac{1}{\alpha^2} \cdot \left[\frac{R}{\omega_o L}\right] \cdot \left[\frac{2\gamma_v}{\gamma_v\gamma_j - \gamma_{vj}^2}\right]$$

For $Q=Q_{min}$, the improvement will be reduced by a factor of 1.414 from the $Q \rightarrow \infty$ value. As noted above, this result is valid only in the large Q limit, and only for $Q' = \omega_o L/R << 1$.

References

(1) J. Clarke, C.D. Tesche, and R.P. Giffard, "Optimization of dc SQUID Voltmeter and Magnetometer Circuits", J. Low Temp. Phys. 37, 405 (1979).

(2) C.D. Tesche and J. Clarke, "dc SQUID : Noise and Optimization", J. Low Temp. Phys. 29, 301 (1977); "dc SQUID: Current Noise", J. Low Temp. Phys., 37, 397 (1979); and an important correction by J.J.P. Bruines, V.J. de Waal, and J.E. Mooij, "Comment on: "dc SQUID: Noise and optimization" by Tesche and Clarke", J. Low Temp Phys. 46, 383 (1982).

(3) R.P. Giffard, "Fundamentals for SQUID Applications", SQUID'80, W. de Gruyter and Co., New York, 445 (1985).

(4) J. Knuutila, M. Kajola, H. Seppa, R. Mutikainen, J. Salmi, "Design, Optimization, and Construction of a dc SQUID with Complete Flux Transformer Circuits", Report TKK-F-A619, Helsinki University of Technology, Low Temperature Laboratory, Otaniemi (1987).

(5) P.F. Michelson and R.C. Taber, "Sensitivity Analysis of a Resonant Mass Gravitaional Wave Antenna with Resonant Transducer", J. Appl. Phys. 52, 4313 (1981).

(6) R.H. Koch, U.C.B. Physics PhD thesis.

(7) C.D. Tesche, Appl. Phys. Lett. 41, 490 (1982), and IEEE Trans. Magn., MAG-19, 458..

(8) J.M. Martinis, and J. Clarke, "Signal and Noise Theory for a dc SQUID Amplifier", J. Low Temp. Phys. 61, 227 (1985).

(9) C. Hilbert and J. Clarke, "dc SQUIDs as Radiofrequency Amplifiers", J. Low Temp. Phys. 61, 263 (1985).

(10) S.I. Baskakov, Signals and Circuits, Mir Publishers, Moscow, 487 (1987).

(11) C.W. Helstrom, Statistical Theory of Signal Detection, Pergamon Press (1960).

(12) L.S. Schwartz, Principles of Coding Filtering and Information Theory, Spartan Books Inc., Baltimore (1963).

(13) see ref. 5.

(14) C. Hilbert and J. Clarke, "Input Impedance of an Amplifier Based on a dc Superconducting Quantum Interference Device", Appl. Phys. Lett. 45, 799 (1984).

(15) C. Hilbert and J. Clarke, "Measurement of the Dynamic Input Impedance of a dc SQUID", J. Low Temp. Phys., 61, 237 (1985).

(16) R.H. Koch, D.J. Van Harlingen, J. Clarke, "Quantum Noise Theory for the dc SQUID", Appl. Phys. Lett., 38, 380 (1981).

(17) V.V. Danilov, K.K. Likharev, A.B. Zorin, "Quantum Noise in SQUIDs", IEEE Trans. Magn. Mag-19, 572 (1983).

(18) J.E. Marsden, Elementary Classical Analysis, W. H. Freeman & Co. (1974), p 337.

LAWRENCE BERKELEY LABORATORY
TECHNICAL INFORMATION DEPARTMENT
1 CYCLOTRON ROAD
BERKELEY, CALIFORNIA 94720